Imperial College London

Sensory perception in model and pathogenic fungi: Engineering misappropriation of response

Margherita Bertuzzi

A thesis submitted to fulfill the requirements for a Doctor of Philosophy degree from Imperial College London, Faculty of Medicine

November 2010

Department of Microbiology
Imperial College London

To my mum and dad, for loving me so much and having always encouraged me to follow my dreams

ABSTRACT

The research described characterises pH signalling in the human pathogen *Aspergillus fumigatus*. Normal functioning of this regulatory system in *Aspergillus* species requires the integrity of seven genes, including the DNA binding transcription factor PacC, which responds to an alkaline pH signal transmitted by PalA, B, C, F, H and I. Two protein complexes are proposed to sense and transmit the pH signal, the first of which is plasma membrane-localised and composed of two putative pH signal receptors, PalH and PalI, plus a cytoplasmic non-metazoan member of the arrestin family, PalF. Using *A. fumigatus* transcriptional profiling, *Saccharomyces cerevisiae* phenotypic screening and the split-ubiquitin MYTH technology, *A. fumigatus* functions, likely to moderate, or be moderated by the PacC transcription factor, were sought.

Two independent *A. fumigatus* Δ*pacC* strains have been phenotypically characterised and assessed for virulence in a neutropenic murine model of pulmonary aspergillosis. Of the two, one mutant was further characterised using transcriptional profiling in order to elucidate functions under PacC control during murine infection. The results of this analysis underline the physiological importance of alkaline adaptation during initiation of infection, especially with respect to impacts upon cellular homeostasis, transport and nutrient availability.

A *S. cerevisiae* membrane two-hybrid system has been developed to investigate *A. fumigatus* plasma membrane protein-protein interactions. Applying the technology, the network of interactions between the components of the *A. fumigatus* plasma membrane pH signalling complex was explored, and the interaction between the pH-sensing PalH protein and the cytoplasmic arrestin PalF and likely the homodimerisation of PalH were identified. A screen for novel interactors of PalH was also performed, providing 5 candidates for further validation.

The *S. cerevisiae* Δ*rim101* null mutant and another 80 cation-sensitive null mutants were analysed. An epistacy screen to address the impact of activated Rim101p upon cation sensitivity was performed supporting the identification of putative novel Rim101p/PacC regulators. In parallel the activity of a synthetic Rim101p-regulatable promoter was examined identifying 10 mutants suffering aberrant Rim101p processing and/or transcriptional activity.

Finally two *A. fumigatus* strains have been constructed to functionally express the firefly luciferase gene. Preliminary tests indicate this as a powerful resource to follow murine infection in real time with bioluminescence assays.

DECLARATION

I certify that the work described within this
thesis is entirely my own, unless otherwise stated.

Margherita Bertuzzi

ACKNOWLEDGMENTS/RINGRAZIAMENTI

These three years have been such an intense experience both from a scientific and a personal point of view and there are a lot of people I want to thank to for their help and support.

First of all, a special thank you goes to my supervisor Dr. Elaine Bignell for being a constant source of inspiration and for always giving me support and advice. Thanks to Prof. Ken Haynes for always reminding me of my priorities and for the jokes about italians, and to Prof Herb Arst for the precious advice during my project.

Thanks to Markus Schrettl and Hubertus Haas for the two *A. fumigatus* Δ*pacC* mutants, to Charlie Cairns and Laura Alcazar Fuoli for the help with the mice experiments, to the JCVI team and in particular to Bill Nierman, Natalie Federova and John Varga, for the experimental support and discussion and for performing the microarray hybridisations; to Andy McDonagh and Geraint Barton for the precious help and support with the microarray analysis; to Igor Stagljar for the help with the split-ubiquitin MYTH system; to Ana Maria Calcagno-Pizarelli for supplying the split-ubiquitin plasmids for *A. nidulans* bait and preys; to Sven Krappmann for providing the plasmid pSK379 and to Siouxsie Wiles for the help with the luciferase experiments.

Thanks to all the previous and current members of the Fifth Floor crew, for the good time we had together working in an enjoyable and friendly environment. I'm really grateful for this experience which allowed me to meet so many special people, most of which became not only colleagues but dear friends. Above all, Charlie, who shared with me every moment of success, fun and difficulty through our PhDs and taught me proper English and proper English manners. Thanks mate!

To all the old and new friends, who have been supportive during the writing up, thanks for understanding that I needed your patience, quiet and time to focus on my thesis. In particular thanks to the Girls, Lauren, Mel, and Nino for all the laughs, smiles and girly nights. Muchas Gracias a las chicas Jime y Laura.

Before I started writing up my thesis, I was joking about how a citation in the acknowledgment has to be deserved, probably underestimating the stressful time I was going to go through. Now, seven months after, I have to admit that the most deserved acknowledgement goes to the person that joke

was addressed to in the first place. My Jonny Boy has been so patient with me and to be honest I don't know if I would have made it without him showing me everyday his love, support and a bit of that "Worboys" attitude. Jonathan, Rydw i yn dy garu di, grazie amore!

Now I apologise to the English speakers but there are really important people I need to thank in my native language. E' difficile esprimere tutta la gratitudine che provo per le persone a me care senza pensare alle mancanze che sono sicura di aver compiuto in questi anni perche' intenta nel perseguire i miei obbiettivi. Innanzitutto, vorrei ringraziare Chiara, per avermi sempre capito e supportato in questi anni ed essere stata una amica speciale attraverso gioie e dolori, film, concerti, gare culinarie e chiacchierate interminabili. Vorrei anche ringraziare Ana Maria, per essere sempre stata così buona con me e avermi accolto fin da subito a braccia aperte come un membro della sua famiglia. L'ultimo ringraziamento, ma di sicuro il piu' importante va alla mia famiglia. Un pensiero va di sicuro ai miei nonni, che credevano così tanto nel valore dell'istruzione e che spero di aver reso orgogliosi nel mio tentativo di far buon uso della familiare caparbietà. Un ringraziamento speciale anche ai miei zii Nella e Paolo, per essermi sempre stati vicini e aver creduto in me. E infine, non ci sono abbastanza parole per esprimere l'amore e la gratitudine che nutro nei confronti dei miei genitori. Nonostante le soddisfazioni, sono stati tre anni duri, abituarsi alla lontananza per noi che abbiamo sempre avuto un rapporto speciale e a non curarsi del parere delle persone che non hanno mai capito la mia scelta. Mi ritengo estremamente fortunata, perchè ho i migliori genitori al mondo, che mi hanno sempre supportato, capito e incoraggiato. Grazie mamma e papà!

La mia tesi finalmente ultimata non presenta semplicemente i risultati del lavoro di questi tre anni ma rappresenta il frutto tangibile di tutto l'amore e il sostegno che le persone citate mi hanno dato e senza l'aiuto delle quali non sarei riuscita ad arrivare fino a qui. Perciò spero che questi ringraziamenti siano almeno in parte riusciti ad esprimere tutto l'amore che io nutro per loro.

TABLE OF CONTENTS

Title 1

Abstract 3

Declaration 4

Acknowledgments/Ringraziamenti 5

Table of Contents 7

List of Abbreviations and Acronyms 14

List of Figures 18

List of Tables 25

Chapter I – Introduction 29

1.1 Invasive aspergillosis 30

1.1.1 Clinical symptoms and diagnosis of respiratory aspergillosis 30

1.1.2 Host defence mechanisms against *Aspergillus* species and role of immunosuppression in the development of IPA 32

1.1.3 Current treatment available for IPA 33

1.1.4 Murine models of invasive aspergillosis 35

1.2 *Aspergillus fumigatus* 36

1.2.1 Morphology and reproductive cycle 37

1.2.2 Genome 39

1.2.3 Putative virulence factors 39

1.3 The PacC/Rim101p signalling pathway for adaptation to environmental pH stress 43

1.3.1 pH regulation in *Aspergillus nidulans* 45

1.3.2 What is known about pH signalling in the other fungal species and its role in fungal virulence? 51

1.4 Fungal DNA microarray studies 53

1.4.1 Review of the relevant fungal DNA microarray studies 54

1.5 *Saccharomyces cerevisiae*: a model organism for fungal research 56

1.5.1 pH regulation in *S. cerevisiae* 57

1.6 Membrane protein-protein interactions: biological roles, limits of available detention techniques and a new innovative investigative approach 62

1.6.1 The split-ubiquitin Membrane Yeast Two Hybrid (MYTH): an innovative system to investigate membrane protein-protein interactions 64

1.7 *In vivo* bioluminescence imaging (BLI) 66

1.7.1 Definition of bioluminescence and i*n vivo* bioluminescence imaging (BLI) 66
1.7.2 Interesting applications of BLI for the detection of fungal pathogens 68
1.8 Objectives of this study 69
Chapter II – Material and methods 71
2.1 Chemicals, reagents and enzymes 71
2.2 Bacterial and fungal strains 71
2.3 Media 71
2.3.1 Bacterial cultures 71
2.3.2 Fungal cultures 72
2.3.3 Fungal phenotypic assays 73
2.4 Oligonucleotide primer synthesis 73
2.5 Plasmids 73
2.6 General molecular techniques 73
2.6.1 Preparation of competent cells 73
2.6.2 Bacterial transformation 74
2.6.3 Plasmid DNA extraction 74
2.6.4 Separation of DNA fragments by electrophoresis 74
2.6.5 Nucleic acid quantification 75
2.6.6 Dephosphorylation of vector 75
2.6.7 Restriction enzyme digests 75
2.6.8 Polymerase chain reaction (PCR) 76
2.6.9 Treatment of PCR products 76
2.6.10 Ligation 76
2.6.11 Sequencing 77
2.6.12 Western blotting analysis 77
2.6.13 Southern blotting analysis 78
2.7 *Aspergillus fumigatus* techniques 79
2.7.1 *A. fumigatus* genomic DNA extraction 79
2.7.2 Transformation of *A. fumigatus* 80
2.8 *Saccharomyces cerevisiae* techniques 80
2.8.1 DNA extraction 80
2.8.2 Protein extraction 81
2.8.3 Yeast transformation 81
Lithium acetate protocol 81

Lithium acetate protocol for 96-wells plate 82
Split-ubiquitin modified lithium acetate protocol 82
2.8.4 Quantitative β-galactosidase assay 82
2.9 *In vivo* virulence analysis 83
2.10 DNA microarray techniques 84
2.10.1 Fungal RNA extraction from BALFs 84
2.10.2 Reverse transcription and fluorescent labelling of RNA 84
2.10.3 Data capture for cDNA microarrays 84
2.10.4 Manipulation and analysis of microarray data 85
Chapter III – Physiological requirement for pH signaling during *A. fumigatus* stress adaptation and virulence 86
3.1 Overview 86
3.2 Methods 87
3.2.1 *A. fumigatus* strains 87
3.2.2 *A. fumigatus* phenotypic testing 88
3.2.3 Murine infections 89
3.3 Results 89
3.3.1 Phenotypic characterisation of *A. fumigatus* Δ*pacC* mutants 89
3.3.2 Effect of *pacC* deletion on *A. fumigatus* virulence in a neutropenic murine model of infection 92
3.3.3 Histopathological analysis of *A. fumigatus* ATCC46645 Δ*pacC* mutant in neutropenic mice 95
3.4 Discussion 96
3.4.1 *pacC* deletion prevents *A. fumigatus* adaptation to alkaline stress *in vitro* 98
3.4.2 *A. fumigatus* Δ*pacC* mutants are attenuated for virulence 101
Chapter IV – Transcriptional profiling of *A. fumigatus* ATCC46645 *pacC* null mutant during initiation of murine infection 105
4.1 Overview 105
4.2 Methods 106
4.2.1 *A. fumigatus* strains 106
4.2.2 Murine infection 106
4.3 Results 108
4.3.1 Microarray analysis of alkaline pH adaptation in *A. fumigatus* early stages of infection in a neutropenic murine model 108

4.3.2 *A. fumigatus* ATCC46645 transcriptional profile during initiation of murine infection 110
4.3.3 *A. fumigatus* ATCC46645 Δ*pacC* mutant transcriptional profile during initiation of murine infection 152
4.3.4 Directly comparative analysis of *A. fumigatus* ATCC46645 and ATCC46645 Δ*pacC* transcription during initiation of murine infection 185
4.4 Discussion 211
4.4.1 The *A. fumigatus* ATCC46645 transcriptional profile during initiation of murine infection highlighted crucial trends for the adaptation to the host niche and the establishment of infection 211
4.4.2 The *A. fumigatus* ATCC46645 Δ*pacC* mutant transcriptional profile during initiation of murine infection reveals possible involvement of epigenetic mechanisms to effect PacC-mediated gene regulation 217
Chapter V - Characterisation of an *A. fumigatus* membrane protein complex involved in pH perception using the split-ubiquitin Membrane Yeast Two-Hybrid (MYTH) system 224
5.1 Overview 224
5.2 Methods 227
5.2.1 *S. cerevisiae* strains 227
5.2.2 Plasmids 227
Bait plasmids: pPR3-STE (x-Cub), pPR3-SUC (x-Cub) and pBT3-N (Cub-X) 228
Prey plasmids: pPR3-N (x-NubG) and pPR3-STE (NubG-X) 229
Control plasmids: pCCW-Alg5, pAL-Alg5 and pDL-Alg5 230
5.2.3 MYTH system 231
5.3 Results 231
5.3.1 Construction of a panel of *A. fumigatus* baits and preys to test pH-sensing protein interactions 231
5.3.2 Expression of *A. fumigatus* pH sensing bait and prey fusion proteins 234
5.3.3 Testing of *A. fumigatus* bait functionality for split-ubiquitin reconstitution 236
5.3.4 Use of *A. fumigatus* PalH bait to investigate the interaction network between the components of the plasma membrane signalling complex 239
5.4 Discussion 245
5.4.1 Split-ubiquitin MYTH analysis confirms *in silico* topological predictions for *A. fumigatus* PalH and PalI 246
5.4.2 *A. fumigatus* PalH baits are expressed and functional in the MYTH system 248

5.4.3 MYTH analysis identifies *A. fumigatus* PalH and PalF interaction, and PalH homodimerisation 250
5.4.5 The MYTH is a versatile and powerful approach to test in yeast *A. fumigatus* protein-protein interactions 255
Chapter VI - Isolation of novel protein interactors for *A. fumigatus* PalH 257
6.1 Overview 257
6.2 Methods 257
6.2.1 The full length *A. fumigatus* cDNA prey library 257
6.2.2 Large scale and high-efficiency lithium acetate transformation protocol for library screenings 260
6.2.3 Optimisation of *A. fumigatus* cDNA prey library screening 261
6.3 Results 263
6.3.1 Optimisation of the screening conditions for *A. fumigatus* PalH baits 263
6.3.2 *A. fumigatus* cDNA prey library transformation to select for putative interactors of *A. fumigatus* PalH 265
6.3.3 Bait-dependency assay for positive interactors of *A. fumigatus* PalH 267
6.4 Discussion 270
6.4.1 The MYTH system was adapted for the high-throughput screening of the full-length *A. fumigatus* cDNA prey library 270
6.4.2 Bioinformatic validation of PalH putative interactors 273
Chapter VII - Identification of novel *rim101* regulators by genetic screening in *S. cerevisiae* 279
7.1 Overview 279
7.2 Methods 282
7.2.1 The Euroscarf *S. cerevisiae* ORF deletion library 282
7.2.2 Plasmids 282
pWL86URA 282
pAED39 283
7.2.3 *S. cerevisiae* phenotypic testing 283
7.2.4 Assessment of yeast growth in liquid media 284
7.2.5 ß-galactosidase assay 284
7.3 Results 285
7.3.1 Confirmation of Δ*rim101*-like phenotypes for 80 mutants from the Euroscarf *S. cerevisiae* ORF deletion library 285

7.3.2 Epistacy screen of the *S. cerevisiae* Δ*rim101*-like mutants 295
7.3.3 Use of a synthetic Rim101p promoter to identify novel regulators of Rim101p processing and/or transcriptional activity 304
7.3.4 Analysis of the Δ*rim101*-like null mutants using a synthetic Rim101p-regulated promoter 306
7.4 Discussion 308
7.4.1 Δ*rim101*-like phenotypes 309
7.4.2 For several null mutants, the Δ*rim101*-like phenotype depends on whether the assessment is performed on solid media or in liquid culture 311
7.4.3 Identification of putative novel regulators of Rim101p 312
7.4.4 Diverse functional classes of proteins govern Rim101p functionality 313
The multivesicular body (MVB) pathway 313
The cell wall integrity (CWI) pathway 316
The calcineurin pathway 318
7.4.5 Novel regulators of Rim101p functionality 319
Transport 319
Chromatin modification, architecture and transcription 319
Cell cycle 320
Structure 321
7.4.6 Use of a synthetic Rim101p-regulated promoter for identification of null mutants suffering aberrant Rim101p processing and/or transcriptional activity 321
Chapter VIII - Construction of an *A. fumigatus* strain expressing luciferase for bioluminescence detection purposes 323
8.1 Overview 323
8.2 Methods 324
8.2.1 *A. fumigatus* strains 324
8.2.2 Plasmid pSK379 for the construction of the bioluminescent *A. fumigatus* CEA10 and Δ*ku80* strains 324
8.2.3 Verification of the bioluminescent *A. fumigatus* CEA10 strains 326
8.2.4 *In vitro* bioluminescence imaging of *A. fumigatus* CEA10 strains 326
8.3 Results 327
8.3.1 Development of the bioluminescent *A. fumigatus* CEA10 strains 327
8.3.2 Preliminary testing of the bioluminescent *A. fumigatus* CEA10 strains 330
8.4 Discussion 333

8.4.1 The *A. fumigatus* strain expressing firefly luciferase represents a promising tool for *A. fumigatus* bioluminescence detection purposes 334
8.4.2 Future perspectives and applications for BLI 335
Chapter IX – Summary and conclusions 338
Appendix A – Strains 347
Appendix B – Oligonucleotide primer sequences 348
Appendix C – Plasmids for the split-ubiquitin MYTH system 351
Appendix D – List of genes differentially expressed in the microarray datasets (also Supplementary materials CD) 360
AD.1 *A. fumigatus* ATCC46645 transcript profile during initiation of murine infection 360
AD.2 *A. fumigatus* ATCC46645 Δ*pacC* mutant transcript profile during initiation of murine infection 367
AD.3 *A. fumigatus* ATCC46645 Δ*pacC*/ATCC46645 $\log_2$ ratio comparison during initiation of murine infection 374
Appendix E – Optimisation of the split-ubiquitin MYTH system using pBT3-STE *A. nidulans* PalH bait 375
Appendix F – *In silico* studies of *A. fumigatus* PacC/Rim101p pathway members 384
AF.1 Alignments of *A. nidulans* and *A. fumigatus* PacC/Rim101p pathway members 385
AF.2 *In silico* prediction topology for *A. fumigatus* PalH and PalI 389
References 392

LIST OF ABBREVIATIONS AND ACRONYMS

3-AT	3-aminotriazole
µg	Microgram
µl	Microlitre
µm	Micrometre
µM	Micromolar
A260/280	Absorbance at 260 nm/absorbance at 280 nm
A260/230	Absorbance at 260 nm/absorbance at 230 nm
aa	Amino acid
ABPA	Allergic bronchopulmonary aspergillosis
ACM	*Aspergillus* complete media
AIDS	Acquired immune deficiency syndrome
AMM	*Aspergillus* minimum media
ATP	Adenosine triphosphate
ATCC	American type culture collection
BALs	Bronchoalveolar lavages
BALFs	BAL fluids
BCA	Bicinchoninic acid
BLAST	Basic local alignment search tool
BLI	Bioluminescence imaging
bp	Base pair
BRET	Bioluminescent Resonance Energy Transfer
CAT	Chloramphenicol resistance gene
CCD	Charge-coupled device
CDK	Cyclin dependant kinase
cDNA	Complementary DNA
CDREs	Calcineurin-dependent responsive elements
CIP	Calf Intestinal Alkaline Phosphatase
CFU	Colony-forming unit
CGD	Chronic granulomatous disease
CRET	Chemioluminescence Resonance Energy Transfert
CT	Computerised tomography
Cub	C-terminal ubiquitin
CWI	Cell wall integrity
CZA	Czapek dox
DBD	DNA binding domain
dH2O	Distilled water
DNA	Deoxyribonucleic acid
ECL	Enhanced chemiluminescence
EDTA	Ethylenediaminetetraacetic acid
EGF	Epidermal growth factor
ER	Endoplasmic reticulum
ESCRT	Endosomal sorting complex required for transport
ESTs	Expressed sequence tags
F	Faraday
Fig.	Figure
FRET	Fluorescence Resonance Energy Transfer
FLuc	Firefly luciferase
G	Growth

GABA	*γ*-Amino-*n*-butyric acid
gDNA	genomic DNA
GFP	Green fluorescent protein
GLP-1	Glucagon-like peptide 1
GLuc	Gaussia luciferase
GMS	Grocott's methanamine staining
GO	Gene ontology
GPI	Glycosylphosphoinositol
GPCRs	G-protein coupled receptors
GPR	GenePix Results
GRKs	G protein-coupled receptor kinases
GTP	Guanosine-5'-triphosphate
g/l	Grams per litre
h(r)	Hour
H & E	Haemotoxylin and eosin
HDACs	Histone acetyltransferases and deacetylases
HOG	High osmolarity glycerol
IC	Infection clusters
Ig	Immunoglobulin
iMYTH	integrated MYTH
IPA	Invasive pulmonary aspergillosis
IPTG	Isopropyl-beta-D-thiogalactopyranoside
JCVI	J. Craig Venter Institute
Kb	Kilobase
KDa	Kilodalton
kg	Kilogram
KO	Knock-out
kV	kilovolts
L or l	Litre
LB	Luria Bertani
LINEs	Long interspersed nuclear elements
LOWESS	Locally-weighted scatter plot smoothing
LRET	Luminescence Resonance Energy Transfer
LTRs	long terminal repeats
M	Molar
MA	Microarray
MAPK	Mitogen-activated protein kinase
Mb	Megabase
MDR	Multidrug resistance
MES	2-(N-morpholino)ethanesulfonic acid hemisodium salt
MFS	Major facilitator superfamily
mg	Milligram
mg/L	Milligram per litre
ml	Millilitre
mM	millimolar
MIPS	Munich Information Center for Protein Sequences
MIT	Microtubule interacting and transport
mRNA	messenger RNA
MS	Mass spectrometry
MVB	Multivesicular body
mw	Molecular weight

MYTH	Membrane Yeast Two Hybrid
n	number
ng	nanogram
NG	No growth
nm	nanometre
Nub	N-terminal ubiquitin
OD	Optical Density
OHM	Ohms
ORF	Open reading frame
p	P-value
PAGE	PolyAcrylamide Gel Electrophoresis
PBS	Phosphate buffered saline
PCR	Polymerase chain reaction
PEG	Polyethylene glycol
PHO	Phosphate signal transduction (pathway)
PKA	Protein Kinase A
PKS/NRPS	Polyketide synthase-non-ribosomal peptide synthetase
PM	Plasma membrane
PMN	Polymorphonuclear cells
PMT	Photomultiplier tube
PNK	Polynucleotide Kinase
PT	Prototrophic transformants
PTR	Pyrithiamine
RIA	Reductive iron assimilation
RLuc	Renilla luciferase
RNA	Ribonucleic acid
rRNA	Ribosomal RNA
ROI	Region of interest
rpm	revolutions per minute
s	Second
S	Sensitive
SD	Synthetic Drop-out (media)
SDS	Sodium dodecyl sulfate
SECMET	secondary metabolite genes
SGD	Saccharomyces genome database
SINEs	Short interspersed nuclear elements
SS	Super sensitive
STEM	Short Time-series Expression Miner
tRNA	Transport RNA
TCA	Trichloroacetic acid
T_{hyb}	Optimal temperature of hybridisation of probe to target in DIG Easy Hyb
TF	Transcription Factor
TE	Tris EDTA buffer
TEs	Transposable elements
Tm	Melting Temperature
TMD	Trans-membrane domain
TT	Total transformants
Ub	Ubiquitin
UBPs	Ubiquitin-specific proteases
UPR	Unfolded protein response
UV	Ultraviolet

V	Volts
v/cm	volts per centimeter
v/v	volume/volume
VPS	Vacuolar protein sorting
WIP	Wiskott-Aldrich syndrome protein (WASP)-interacting protein
WT	Wild type
w/v	weight/volume
YKO	Yeast knock out
YNB	Yeast nitrogen base
YPAD	Yeast extract peptone adenine dextrose
YPD	Yeast extract peptone dextrose

LIST OF FIGURES

Fig. 1.1: Infectious life cycle of *A. fumigatus* 33
Fig. 1.2: Morphological features of *A.fumigatus* 37
Fig. 1.3: Schematic representation of pH regulation in *A. nidulans* 46
Fig. 1.4: Histological analysis to compare the growth of *A.nidulans* wild type strain (*pacC*$^{+}$), *pacC*$^{-}$, *palB*$^{-}$, and *pacC*^{c} mutants in the neutropenic murine lung 53
Fig. 1.5: Schematic representation of pH regulation in *S. cerevisiae* 59
Fig. 1.6: The split-ubiquitin Membrane Yeast Two-Hybrid (MYTH) system 65
Fig. 3.1: Verification of Δ*pacC* mutant in the *A. fumigatus* CEA10 genetic background by PCR and Southern blotting 90
Fig. 3.2: Phenotypic analysis of the *A. fumigatus* Δ*pacC* 92
Fig. 3.3: Comparative survival of neutropenic mice infected with ATCC46645 and ATCC46645 Δ*pacC* 93
Fig. 3.4: Comparative survival of neutropenic mice infected with CEA10 and CEA10 Δ*pacC* 94
Fig. 3.5: Survival of neutropenic mice infected with low dose CEA10 Δ*pacC* 95
Fig. 3.6: Comparative lung histopathology in neutropenic mice infected with ATCC46645 and ATCC46645 Δ*pacC* 96
Fig. 4.1: Schematic representation of hybridisations performed to analyse *pac*C-mediated virulence functions in *A. fumigatus* 109
Fig. 4.2: Schematic representation of the hybridisations performed to analyse *A. fumigatus* ATCC46645 transcription during initiation of murine infection 110
Fig. 4.3: Data normalisation plot for the ATCC46645 4 hrs *in vivo* versus dormant spores analysis 111
Fig. 4.4: Data normalisation plot for the ATCC46645 8 hrs *in vivo* versus dormant spores analysis 112
Fig. 4.5: Data normalisation plot for the ATCC46645 16 hrs *in vivo* versus dormant spores analysis 112
Fig. 4.6: Three-way Venn diagrams depicting temporal aspects of differential gene expression in the ATCC46645 time course experiment during initiation of murine infection 114
Fig. 4.7: STEM clustering analysis of differentially expressed genes in the ATCC46645 time course during initiation of murine infection 141
Figure 4.8: Venn diagrams illustrating commonalities between cohorts of differentially expressed genes during initiation of murine infection by *A. fumigatus* ATCC46645 and Af293 strains 147

Fig. 4.9: Selection of STEM clustering analyses of the differentially expressed genes in the ATCC46645 time course during initiation of murine infection, ordered on the basis of containing Af293 infection cluster genes 148
Fig. 4.10: STEM clustering analysis of the differentially expressed genes in the ATCC46645 time course during initiation of murine infection ordered on the basis of the subtelomeric location 148
Fig. 4.11: STEM clustering analysis of the differentially expressed genes in the ATCC46645 time course during initiation of murine infection ordered on the basis of the involvement on secondary metabolite production 149
Fig. 4.12: Venn diagrams illustrating the proportions of alkaline-responsive *A. fumigatus* genes during initiation of murine infection by ATCC46645 150
Fig. 4.13: STEM clustering analysis of the differentially expressed genes in the ATCC46645 time course during initiation of murine infection ordered on the basis of containing genes also up-regulated in response to an alkaline pH shift 151
Fig. 4.14: STEM clustering analysis of the differentially expressed genes in the ATCC46645 time course during initiation of murine infection ordered on the basis of the *in vitro* down-regulated genes in response to an alkaline pH shift 151
Fig. 4.15: Schematic representation of hybridisations performed to analyse the *A. fumigatus* ATCC46645 Δ*pacC* transcriptome during initiation of murine infection 152
Fig. 4.16: Data normalisation plot for the ATCC46645 Δ*pacC* 4 hrs *in vivo* versus dormant spores analysis 153
Fig. 4.17: Data normalisation plot for the ATCC46645 Δ*pacC* 8 hrs *in vivo* versus dormant spores analysis 153
Fig. 4.18: Data normalisation plot for the ATCC46645 Δ*pacC* 16 hrs *in vivo* versus dormant spores analysis 154
Fig. 4.19: Three-way Venn diagrams depicting temporal aspects of differential gene expression in the ATCC46645 Δ*pacC* time course experiment during initiation of murine infection 156
Fig. 4.20: STEM clustering analysis of differentially expressed genes in the ATCC46645 Δ*pacC* time course during initiation of murine infection 173
Fig. 4.21: Selection of STEM clustering analysis of differentially expressed genes in the ATCC46645 Δ*pacC* time course during initiation of murine infection ordered on the basis of the Af293 infection clusters 177
Fig. 4.22: Selection of STEM clustering analysis of the differentially expressed genes in the ATCC46645 Δ*pacC* time course during initiation of murine infection ordered on the basis of the subtelomeric gene inclusion 177

Fig. 4.23: Selection of STEM clustering analysis of the differentially expressed genes in the ATCC46645 Δ*pacC* time course during initiation of murine infection ordered on the basis of secondary metabolism gene inclusion 178
Fig. 4.24: Selection of STEM clustering analysis of the differentially expressed genes in the ATCC46645 Δ*pacC* time course during initiation of murine infection ordered on the basis of *in vitro* alkaline-responsive gene inclusion 179
Fig. 4.25: Selection of STEM clustering analysis of the differentially expressed genes in the ATCC46645 Δ*pacC* time course during initiation of murine infection ordered on the basis of *in vitro* alkaline down-regulated gene inclusion 179
Fig. 4.26: Selection of STEM clustering analysis of the differentially expressed genes in the ATCC46645 Δ*pacC* time course during initiation of murine infection ordered on the basis of transposition gene inclusion 180
Fig. 4.27: Genome-wide comparison of transcripton in the *A. fumigatus* ATCC46645 Δ*pacC* and respective parental strain during initiation of murine infection 181
Fig. 4.28: Venn diagrams comparing datasets of differentially expressed genes during initiation of murine infection for the wild type ATCC46645 and the ATCC46645 Δ*pacC* mutant 183
Fig. 4.29: Comparison of the ATCC46645 and ATCC46645 Δ*pacC* time course datasets 185
Fig. 4.30: Schematic representation of the hybridisations performed to directly compare *A. fumigatus* ATCC46645 and ATCC46645 Δ*pacC* host adapting transcriptional profiles 186
Fig. 4.31: Data normalisation plot for the ATCC46645 Δ*pacC*/ATCC46645 4 hrs analysis 187
Fig. 4.32: Data normalisation plot for theATCC46645 Δ*pacC*/ATCC46645 8 hrs analysis 187
Fig. 4.33: Data normalisation plot for the ATCC46645 Δ*pacC*/ATCC46645 16 hrs analysis 188
Fig. 4.34: Three-ways Venn diagram depicting temporal aspects of differential gene expression in the ATCC46645 Δ*pacC*/ATCC466645 comparison during initiation of murine infection 189
Fig. 5.1: Principle of the split-ubiquitin Membrane Yeast Two-Hybrid (MYTH) system 226
Fig. 5.2: Bait plasmids 228
Fig. 5.3: Prey plasmids 229
Fig. 5.4: Control plasmids 230

Fig. 5.5: Scheme representing the plasmids constructed to test every possible interaction between the three components of the plasma membrane pH signalling complex of *A. fumigatus* 232
Fig. 5.6: Experimental procedure for testing *A. fumigatus* membrane protein-protein interactions using the split-ubiquitin MYTH system 234
Fig. 5.7: Western blotting analysis to verify the expression of bait and prey proteins 236
Fig. 5.8: Verification of the expression and functionality of pH-sensing baits constructed by co-transformation with control preys in yeast 238
Fig. 5.9: Test to detect interactions between PalH, expressed as bait in the pBT3-SUC vector in the MYTH system, and the members of the membrane signalling complex PalH, PalI and PalF 240
Fig. 5.10: Panel showing the optimisation of the 3-AT concentration used in SD-leu-trp-his-ade to discriminate between positive interactors and false positives 242
Fig. 5.11: Graphical representation of the results for the co-transformations to test the interaction between PalH, expressed as bait in the pBT3-SUC vector in the MYTH system, and the members of the membrane signalling complex PalH, PalI and PalF 245
Fig. 5.12: PalH and PalI topology in the *A. fumigatus* plasma membrane, as demonstrated by western blot and interaction assays 248
Fig. 6.1: Invitrogen Gateway adaptation of the DUALmembrane vector pPR3-N to generate pPR3-N GW 258
Fig. 6.2: Experimental procedure for the screening of the full length *A. fumigatus* cDNA prey library using the MYTH system 262
Fig. 6.3: Panel showing the results of the pilot screen for the baits PalH pBT3-STE and PalH pBT3-SUC 264
Fig. 6.4: Graphical representation of the results for the co-transformations to test the interaction between PalH, expressed as bait in the pBT3-SUC vector in the MYTH system, and the 6 putative interactors from the screening of the preys *A. fumigatus* library 270
Fig. 7.1: Epistacy screen of 80 *S. cerevisiae* Δ*rim101p*-like mutants to identify novel regulators of Rim101p 281
Fig. 7.2: Use of a synthetic Rim101p promoter to identify mutants in Rim101p processing and/or transcriptional activity 282
Fig. 7.3: Phenotypes of Δ*rim101* and Δ*rim101*-like mutants on YPD pH 8 (100 mM Tris-HCl) 287
Fig. 7.4: Phenotypes of Δ*rim101* and Δ*rim101*-like mutants on YPD pH 4 (100 mM glycolic acid) 288
Fig. 7.5: Phenotypes of Δ*rim101* and Δ*rim101*-like mutants on YPD pH 4 (100 mM glycolic acid) 200 mM LiCl 289

Fig. 7.6: Phenotypes of Δ*rim101* and Δ*rim101*-like mutants on YPD 100 mM LiCl 290
Fig. 7.7: Phenotypes of Δ*rim101* and Δ*rim101*-like mutants on YPD 200 mM LiCl 291
Fig. 7.8: Phenotypes of Δ*rim101* and Δ*rim101*-like mutants on YPD pH 4.5 (100 mM glycolic acid) 800 mM NaCl 292
Fig. 7.9: Phenotypes of Δ*rim101* and Δ*rim101*-like mutants on YPD pH 7.4 (100 mM Tris-HCl) 200 mM LiCl 293
Fig. 7.10: Lithium sensitivity phenotype on solid media for BY4741, (A) Δ*rim101* (B), Δ*rim8* (C), Δ*rim9* (D) and Δ*rim13* (E) and resulting pWL86URA transformants 296
Fig. 7.11: Experimental scheme for assessment of cation sensitivity in liquid media 297
Fig. 7.12: OD_{600} adjustments for comparative cation sensitivity analyses of BY4741 and Δ*rim101* in liquid culture 298
Fig. 7.13: Cation sensitivity profiles of Δ*rim101* and other previously characterised Rim pathway mutants in YPD pH 7.4 200 mM LiCl 229
Fig. 7.14: Relative cation hypersensitivity of BY4741 and Rim pathway mutants following pWL86URA transformation 230
Fig. 7.15: Relative cation hypersensitivity of BY4741 and Δ*rim101*-like mutants following pWL86URA transformation 302
Fig. 7.16: Experimental scheme for assessment of β-galactosidase activity in a 96-well plate format 305
Fig. 7.17: β-galactosidase activity in BY4741 and Δ*rim101* strains expressing a synthetic Rim101p-regulated promoter 306
Fig. 7.18: β-galactosidase activity in BY4741 and Δ*rim101-like* mutants expressing a synthetic Rim101p regulated promoter 307
Fig. 7.19: Summary of β-galactosidase activity in BY4741 and Δ*rim101-like* mutants highlighting mutants showing derepression of *lac*Z gene expression 308
Fig. 8.1: pSK379 325
Fig. 8.2: pSK379Luc 326
Fig. 8.3: *In vitro* bioluminescence imaging of purified *A. fumigatus* CEA10 strains producing firefly luciferase 328
Fig. 8.4: Scheme representing the predicted mode of integration of pSK379Luc in the targeted genomic locus 329
Fig. 8.5: *In vitro* bioluminescence imaging of purified *A. fumigatus* CEA10 strains producing firefly luciferase 331
Fig. 8.6: *In vitro* bioluminescence imaging of purified *A. fumigatus* strains producing firefly luciferase 332
Fig. AC.1: pBT3-SUC 352
Fig. AC.2 pBT3-STE 353

Fig. AC.3: pBT3-N 354
Fig. AC.4: pPR3-N 355
Fig. AC.5: pPR3-STE 356
Fig. AC.6: pCCW-Alg5 357
Fig. AC.7: pAL-Alg5 358
Fig. AC.8: pDL-Alg5 359
Fig. AD.1.1: STEM clustering analysis of the differentially expressed genes in the ATCC46645 time course during initiation of murine infection ordered on the basis of the Af293 infection clusters 362
Fig. AD.1.2: STEM clustering analysis of the differentially expressed genes in the ATCC46645 time course during initiation of murine infection ordered on the basis of the subtelomeric location 363
Fig. AD.1.3: STEM clustering analysis of the differentially expressed genes in the ATCC46645 time course during initiation of murine infection ordered on the basis of the involvement on secondary metabolite production 364
Fig. AD.1.4: STEM clustering analysis of the differentially expressed genes in the ATCC46645 time course during initiation of murine infection ordered on the basis of the *in vitro* up-regulated genes in response to an alkaline pH shift 365
Fig. AD.1.5: STEM clustering analysis of the differentially expressed genes in the ATCC46645 time course during initiation of murine infection ordered on the basis of the *in vitro* down-regulated genes in response to an alkaline pH shift 366
Fig. AD.2.1: STEM clustering analysis of the differentially expressed genes in the ATCC46645 Δ*pacC* time course during initiation of murine infection ordered on the basis of the Af293 infection clusters 368
Fig. AD.2.2: STEM clustering analysis of the differentially expressed genes in the ATCC46645 Δ*pacC* time course during initiation of murine infection ordered on the basis of the subtelomeric location 369
Fig. AD.2.3: STEM clustering analysis of the differentially expressed genes in the ATCC46645 Δ*pacC* time course during initiation of murine infection ordered on the basis of the involvement on secondary metabolite production 370
Fig. AD.2.4: STEM clustering analysis of the differentially expressed genes in the ATCC46645 Δ*pacC* time course during initiation of murine infection ordered on the basis of the *in vitro* up-regulated genes in response to an alkaline pH shift 371
Fig. AD.2.5: STEM clustering analysis of the differentially expressed genes in the ATCC46645 Δ*pacC* time course during initiation of murine infection ordered on the basis of the *in vitro* down-regulated genes in response to an alkaline pH shift 372

Fig. AD.2.6: STEM clustering analysis of the differentially expressed genes in the ATCC46645 Δ*pacC* time course during initiation of murine infection ordered on the basis of the involvement in transposition 373
Fig. AE.1: Western blotting analysis to verify the expression of *A. nidulans* bait and preys 376
Fig. AE.2: Verification of the expression and functionality of *A. nidulans* PalH bait (pBT3-STE) by co-transformation with the control preys in yeast 377
Fig. AE.3: Co-transformation of the expression-verified *A. nidulans* PalH pBT3-STE bait with *A. fumigatus* PalI pPR3-STE (A) and *A. fumigatus* PalF pPR3-N (B) preys to test direct interactions 378
Fig. AE.4: Scheme showing the preliminary analysis of 85 of the 200 putative interactors identified by the screening of the full length *A. fumigatus* cDNA library with *A. nidulans* PalH bait 380
Fig. AE.5: Scheme showing the composition of the 107 E. *coli* clones containing an *A. fumigatus* gene in frame with the NubG of the library vector identified by the preliminary analysis of 85 of the 200 putative interactors obtained by the screening of the full-length *A. fumigatus* cDNA library with *A. nidulans* PalH bait 381
Fig. AF.1: Alignment between *A. nidulans* PacC (AN2855) and *A. fumigatus* PacC (Afu3g11970) 384
Fig. AF.2: Alignment between *A. nidulans* PalH (AN6886) and *A. fumigatus* PalH (Afu5g13270) 385
Fig. AF.3: Alignment between *A. nidulans* PalI (AN4853) and *A. fumigatus* PalI (Afu3g07530) 386
Fig. AF.4: Alignment between *A. nidulans* PalF (AN1844) and *A. fumigatus* PalF (Afu4g09650) 387
Fig. AF.5: TMpred prediction for the topology of the *A. fumigatus* plasma membrane PalH (Afu5g13270) 389
Fig. AF.6: Signal P3.0 prediction for the presence of a signal peptide in the *A. fumigatus* plasma membrane PalH (Afu5g13270) 390
Fig. AF.7: TMpred prediction for the topology of the *A. fumigatus* plasma membrane PalI (Afu3g07530) 390
Fig. AF.8: Signal P3.0 prediction for the presence of a signal peptide in the *A. fumigatus* plasma membrane PalI (Afu3g07530) 391

LIST OF TABLES

Table 3.1: Media and buffers used for *A. fumigatus* phenotypic screening 88
Table 4.1: Summary statistics for the ATCC46645 time course during initiation of murine infection 113
Table 4.2: Number of differentially expressed genes in the ATCC46645 time course during initiation of murine infection 113
Table 4.3: 100 ORFs with the highest $\log_2$ values between the up-regulated genes in common for the 3 time points (4, 8 and 16 hrs) of the ATCC46645 time course 116
Table 4.4: 100 ORFs with the lowest $\log_2$ values between the down-regulated genes in common for the 3 time points (4, 8 and 16 hrs) of the ATCC46645 time course 124
Table 4.5: Significant GO terms among the up-regulated genes in the ATCC46645 time course 134
Table 4.6: Significant GO terms among the down-regulated genes in the ATCC46645 time course 136
Table 4.7: Significant GO terms among the profiles 0, 12, 1, 9, 49, 48, 42, 47, and 29 in the ATCC46645 time course experiment 142
Table 4.8: Summary statistics for the ATCC46645 Δ*pacC* time course during initiation of murine infection 154
Table 4.9: Number of differentially expressed genes in the ATCC46645 Δ*pacC* time course during initiation of murine infection 155
Table 4.10: 100 ORFs having the highest $\log_2$ values among up-regulated genes across the 3 time points (4, 8 and 16 hrs) of the ATCC46645 158
Table 4.11: 100 ORFs with the lowest $\log_2$ values among down-regulated genes common to all 3 time points (4, 8 and 16 hrs) of the ATCC46645 Δ*pacC* time course 163
Table 4.12: Significant GO terms among the up-regulated genes in the ATCC46645 Δ*pacC* time course 167
Table 4.13: Significant GO terms among the down-regulated genes in the ATCC46645 Δ*pacC* time course 172
Table 4.14: Significant GO terms among profiles 0, 12, 1, 9, 49, 48, 42, 47, 29 in the ATCC46645 Δ*pacC* time course experiment 174
Table 4.15: Summary statistics for the ATCC46645 Δ*pacC*/ATCC46645 comparison *in vivo* 188
Table 4.16: Number of differentially expressed genes in the ATCC46645 Δ*pacC*/ATCC46645 comparison 189
Table 4.17: 68 up-regulated ORFs in common for the 3 time points (4 hrs, 8 hrs and 16 hrs) of the ATCC46645 Δ*pacC*/ATCC46645 comparison 191

Table 4.18: 74 down-regulated ORFs in common for the 3 time points (4 hrs, 8 hrs and 16 hrs) of the ATCC46645 Δ*pacC*/ATCC46645 comparison 194
Table 4.19: Significant GO terms among the up-regulated genes of the ATCC46645 Δ*pacC*/ATCC466645 comparison 199
Table 4.20: Significant GO terms among the down-regulated genes of the ATCC46645 Δ*pacC*/ATCC466645 comparison 201
Table 4.21: Functional classification of selected genes having increased abundance in the ATCC46645 Δ*pacC* mutant relative to the parental isolate ATCC46645 during initiation of murine infection 205
Table 4.22: Functional classification of selected genes having decreased abundance in the ATCC46645 Δ*pacC* mutant relative to the parental isolate ATCC46645 during initiation of murine infection 206
Table 5.1: Summary of bait vector properties 228
Table 5.2: Summary of prey vector properties 229
Table 5.3: Summary of control vector properties 230
Table 5.4: Results for co-transformations testing the interaction between PalH, expressed as bait in the pBT3-SUC vector in the MYTH system, and the members of the membrane signalling complex PalH, PalI and PalF 243
Table 6.1: Summary of the characteristics of the full-length *A. fumigatus* cDNA library 259
Table 6.2: Summary statistics of the two screenings of the full-length *A. fumigatus* cDNA prey library with the *A. fumigatus* PalH pBT3-SUC bait 265
Table 6.3: Summary of the putative interactors identified from the analysis of 40 random candidates obtained in the high throughput screening of the full-length *A. fumigatus* cDNA prey library with the *A. fumigatus* PalH pBR3-SUC bait 266
Table 6.4: Results for co-transformations testing the interaction between PalH, expressed as bait in the pBT3-SUC vector in the MYTH system, and the 6 putative interactors from the screening of the preys *A. fumigatus* library. 268
Table 7.1: Buffers used for pH-buffered media in the *S. cerevisiae* phenotypic screening 284
Table 7.2: Buffers used for pH-buffered media 285
Table 7.3: Phenotypes of Δ*rim101* and Δ*rim101*-like mutants 294
Table 7.4: Summary of cation sensitivity data from epistacy screen of Δ*rim101*-like mutants 303
Table AA.1: Strains used for this study 347
Table AB.1: Oligonucleotides used in this study 348
Table AC.1: Plasmids used in this study for the split-ubiquitin MYTH system 351

Table AD.1.1: List of up-regulated genes in the ATCC46645 time course 360
Table AD.1.2: 30 ORFs with the highest log_2 values between the up-regulated genes unique to the 4 hrs time point of the ATCC46645 time course 360
Table AD.1.3: 30 ORFs with the highest log_2 values between the up-regulated genes unique to the 8 hrs time point of the ATCC46645 time course 360
Table AD.1.4: 30 ORFs with the highest log_2 values between the up-regulated genes unique to the 16 hrs time point of the ATCC46645 time course 360
Table AD.1.5: List of down-regulated genes in the ATCC46645 time course 360
Table AD.1.6: 30 ORFs with the lowest log_2 values between the down-regulated genes unique to the 4 hrs time point of the ATCC46645 time course 361
Table AD.1.7: 30 ORFs with the lowest log_2 values between the down-regulated genes unique to the 8 hrs time point of the ATCC46645 time course 361
Table AD.1.8: 30 ORFs with the lowest log_2 values between the down-regulated genes unique to the 16 hrs time point of the ATCC46645 time course 367
Table AD.2.1: List of up-regulated genes in the ATCC46645 Δ*pacC* time course 367
Table AD.2.2: 30 ORFs having the highest log_2 among up-regulated genes unique to the 4 hrs time point of the ATCC46645 Δ*pacC* time course 367
Table AD.2.3: 30 ORFs with the highest log_2 values between the up-regulated genes unique to the 8 hrs time point of the ATCC46645 Δ*pacC* time course 367
Table AD.2.4: 30 ORFs with the highest log_2 values among up-regulated genes unique to the 16 hrs time point of the ATCC46645 Δ*pacC* time course 367
Table AD.2.5: List of down-regulated genes in the ATCC46645 Δ*pacC* time course 367
Table AD.2.6: 30 ORFs with the lowest log_2 values among down-regulated genes unique to the 4 hrs time point of the ATCC46645 Δ*pacC* time course 367
Table AD.2.7: 30 ORFs with the lowest log_2 values among down-regulated genes unique to the 8 hrs time point of the ATCC46645 Δ*pacC* time course 367
Table AD.2.8: 30 ORFs with the lowest log_2 values between the down-regulated genes unique to the 16 hrs time point of the ATCC46645 Δ*pacC* time course 367
Table AD.3.1: List of up-regulated genes in the ATCC46645 Δ*pacC*/ATCC46645 dataset 374
Table AD.3.2: 30 ORFs with the highest log_2 values between the up-regulated genes unique to the 4 hrs time point of the ATCC46645 Δ*pacC*/ATCC46645 comparison 374
Table AD.3.3: 23 up-regulated ORFs unique to the 8 hrs time point of the ATCC46645 Δ*pacC*/ATCC46645 comparison 374
Table AD. 3.4: 30 ORFs with the highest log_2 values between the up-regulated genes unique to the 16 hrs time point of the ATCC46645 Δ*pacC*/ATCC46645 comparison 374
Table AD.3.5: List of down-regulated genes in the ATCC46645 Δ*pacC*/ATCC46645 dataset

374
Table AD.3.6: 30 ORFs with the lowest log_2 values between the down-regulated genes unique to the 4 hrs time point of the ATCC46645 Δ*pacC*/ATCC46645 374
Table AD.3.7: 11 down-regulated ORFs unique to the 8 hrs time point of the ATCC46645 Δ*pacC*/ATCC46645 comparison 374
Table AD.3.8: 30 ORFs with the lowest log_2 values between the down-regulated genes unique to the 16 hrs time point of the ATCC46645 Δ*pacC*/ATCC46645 comparison 375
Table AE.1: Summary of the clones identified as putative interactors of *A. nidulans* PalH because containing an *A. fumigatus* gene in frame with the NubG domain of the library vector to allow the expression of a functional fusion protein 381

CHAPTER I

INTRODUCTION

A significant change in the epidemiology of invasive fungal infection has occurred in the past 30 years due to the increasing practice of transplantation as a remedy to organ dysfunction, the intensification of chemotherapy for cancer and the sudden outbreak of Acquired Immune Deficiency Syndrome (AIDS). All of these conditions involve acute immunosuppressive states, either induced by, or as a consequence of the infection, exposing the patients to a broad range of invasive mycoses. Only two hundred of the estimated thousands of fungal species present in the environment have been identified as causative agents of disease in humans (Samson and Varga, 2009). Twenty of these belong to the genus *Aspergillus*, which remains the most common cause of mould infections in humans, although recent increases in infections have been observed due to other moulds, for example *Scedosporium apiospermum*, *Fusarium* species and various zygomycetes such as *Rhizopus* and *Mucor* (Kauffman, 2006). Epidemiological data indeed shows a dramatic change from the beginning of the century when *Aspergillus* infections in humans were defined as "so rare as to be of a little practical importance" (Henrici, 1939). A detailed understanding of *Aspergillus* biology, particularly of mechanisms involved in pathogenicity, is therefore crucial to the development of novel and more effective therapies.

Environmental adaptation is particularly interesting, considering it is crucial for all microbes, but especially for those inhabiting mammalian niches during infection. pH is a negative logarithmic measurement of hydrogen ion activity. In all circumstances where metabolism is active, a steady flux of protons goes in and out of the cytoplasm of the cells, which have therefore evolved several mechanisms to maintain ion balance and guarantee optimal activity of major metabolic pathways, whose function would be otherwise damaged by large deviations of intracellular pH. One aspect of this adaptation is the ability to appropriately express genes involving functions at the cell surface or in the environment. Among these genes, there are permeases, secreted enzymes, enzymes involved in synthesis of exported metabolites (i.e. toxins and antibiotics) and enzymes post-translationally modifying secreted proteins. The genetic regulatory system involved in ambient pH regulation is widespread in the fungal kingdom and depends on the transcription factor Rim101p/PacC. Since its first discovery more than 20 years ago (Caddick *et al.*, 1986c), ambient pH regulation of gene expression has been extensively studied, especially in the model

ascomycete *Aspergillus nidulans* (Caddick and Arst, 1986; Caddick *et al.*, 1986a; Caddick *et al.*, 1986b; Arst, 2003; Arst Jr and Peñalva, 2003; Penalva and Arst Jr, 2002; Peñalva and Arst Jr, 2004; Peñalva *et al.*, 2008). Appropriate response to ambient pH is fundamental for fungal virulence in plants, insects and animals, as initially demonstrated in *Candida albicans* (Davis, 2003; Davis *et al.*, 2000a) and recently in *Aspergillus* (Bignell *et al.*, 2005). In *A. nidulans*, PacC activates genes expressed preferentially at alkaline ambient pH and represses genes expressed preferentially at acidic pH (Caddick *et al.*, 1986c). The discovery that murine aspergillosis requires functionality of *A. nidulans pacC* has given new insights into the importance of this crucial regulatory pathway (Bignell *et al.*, 2005). Alkaline adaptation, a mechanism not essential for *Aspergillus* viability, but critical for its virulence, might provide a useful target for prevention of fungal growth *in vivo*.

1.1 Invasive aspergillosis

Aspergillosis includes a broad range of diseases caused by members of the *Aspergillus* genus, affecting almost any organ or system principally in immunocompromised individuals, the most high-risk category of patients (Baddley, 2010). Non-respiratory infections are infrequent, but other sites of infections, either in immunocompetent or immunocompromised individuals, have been described, i.e. the skin, peritoneum, kidneys, bones, eyes and gastrointestinal tract (Denning, 1998).

1.1.1 Clinical symptoms and diagnosis of respiratory aspergillosis

Due to the small diameter of spores, the major portal of entry and site of infection for *Aspergillus* is the respiratory tract. Inhalation of conidiospores can lead to several types of pulmonary aspergillosis, classified according to the site of the disease within the respiratory tract and the presence and extent of mycelial colonisation (Bodey and Vartivarian, 1989; Dixon and Walsh, 1992), which are all conditions influenced by the immune status of the patient. Asthma and allergic sinusitis occur without mycelial colonisation as a consequence of the repeated exposure to conidia or *Aspergillus* antigens. On the contrary, there are several diseases involving mycelial growth that usually require therapeutic treatment.

Allergic Bronchopulmonary Aspergillosis (ABPA) represents the most severe hypersensitivity reaction caused by *Aspergillus* species and it is usually seen in patients with long-standing asthma (1-2%) or cystic fibrosis (7-35%), particularly in patients taking oral corticosteroids for a long period (Basich *et al.*, 1981; Knutsen and Slavin, 1992; Knutsen and

Slavin, 1991; Krasnick *et al.*, 1995). Commencing as classic asthma with transient pulmonary infiltrates, ABPA is typified by the unique T-cell mediated cellular immune response that could lead to the fatal destruction of the lungs. The disease is therefore very difficult to diagnose in the early stages and if not treated can eventually progress to pulmonary fibrosis and respiratory failure (Greenberger and Patterson, 1987; Wardlaw and Geddes, 1992). Diagnosis is based on patient history, imaging tests, immediate skin reactivity to *Aspergillus* antigenic extracts and the measurement of IgE levels and *Aspergillus*-specific antibodies. Treatment consists of corticosteroids or itraconazole (Lazarus *et al.*, 2008).

Pulmonary aspergilloma (mycetoma) refers to the mass formed when fungal spores settle into or colonize pre-existing pulmonary cavities originated as a consequence of previous diseases (10-15% of patients), such as tuberculosis and prior pneumonia (Addrizzo-Harris *et al.*, 1997; Israel *et al.*, 1982; Kirsten *et al.*, 1992; Wollschlager and Khan, 1984). Aspergillomas are detected by chest radiography, appearing as spherical masses surrounded by a radiolucent corona. Patients are usually asymptomatic but they present a high level of *Aspergillus*-specific antibodies. At present, there is no established consensus therapy, but recent evidence has demonstrated amphotericin B as an effective candidate against aspergillomas, if administered subcutaneously (Zmeili and Soubani, 2007).

Invasive Pulmonary Aspergillosis (IPA) refers to rare cases in which the fungus spreads from the lungs throughout the body via the blood stream and invades other organs, particularly the lungs, heart and kidneys. With an associated mortality of 70-90% (Denning, 1998), IPA is recognised as the most serious type of *Aspergillus* infection. This is principally due to the difficulty of diagnosing IPA, especially in the early stages of infection, when the symptoms, such as fever, a cough, chest pain or breathlessness, are usually not specific enough to exclude many other illnesses. There is no established consensus diagnosis but the principal methods include a positive CT (computerised tomography) scan, culture and/or microscopic evidence of the disease and detection of *Aspergillus* antigens in serum. Fungal pathogens of humans are classified either as primary pathogens, if able to cause infection in an immunocompetent host, or as secondary (or opportunistic) pathogens, if some defects (often in the immune system) are required for the establishment of the infection (Casadevall and Pirofski, 1999). IPA occurs mostly in immunocompromised or critically ill patients (Patterson, 2005) and it is therefore classified as an opportunistic infection.

1.1.2 Host defence mechanisms against *Aspergillus* species and the role of immunosuppression in the development of IPA

Between the severely immunocompromised patients, the categories at highest risk include individuals with haematological malignancies (such as leukaemia), solid-organ and hematopoietic stem cell transplant patients, patients on prolonged corticosteroid therapy, individuals with genetic immunodeficiencies (such as chronic granulomatous disease, CGD) and AIDS patients (Denning, 1998; Marr *et al.*, 2002; Mikulska *et al.*, 2009; Pagano *et al.*, 2001; Post *et al.*, 2007; Wiederhold *et al.*, 2003). Aspergillosis is estimated to afflict 10-15% of patients with solid or allogeneic hematopoietic stem cells transplants and with leukaemia. Also it is not an uncommon infection for advanced AIDS, affecting 3% of the patients (Baddley, 2010; Denning, 1998). For these patients the overall mortality when developing aspergillosis varies between 45-90%, depending on factors such as the host immune status, the site of infection and the treatment regimen (Lin *et al.*, 2001). Among the human pathogenic species of *Aspergillus*, *A. fumigatus* is responsible for 90% of human infections (Kauffman, 2006), followed by *A. flavus*, *A.terreus*, *A. niger* and the model organism *A. nidulans* (Denning, 1998). *A. fumigatus* has become the most important airborne fungal pathogen worldwide, resulting in a significant increase in fatal IPA, a disease which was quite unknown 30 years ago.

Every day, as indicated by environmental surveys, most humans inhale at least several hundred *A. fumigatus* conidia, but inhalation of conidia in immunocompetent persons rarely has negative effects because the conidia are efficiently eliminated by the innate immune system (Chazalet *et al.*, 1998; Hospenthal *et al.*, 1998). In immunocompetent individuals, inhaled airborne conidia are either removed through the ciliary action of the mucous epithelium or encounter epithelial cells and alveolar macrophages. Alveolar macrophages represent the primary resident phagocytes of the lungs and are not only responsible for the elimination of *Aspergillus* conidia, but also of the initiation of the pro-inflammatory response, recruiting neutrophils to the infection site. If the macrophages are unable to clear the inhaled conidia, these germinate to produce hyphae, the elimination of which requires infiltrating neutrophils, a type of polymorphonuclear cell (PMN). The risk of developing IPA is therefore correlated with a dysfunction of one of these two lines in the host defence system and the pattern of pulmonary injury and the outcome of the infection are strictly related to the form of immunosuppression involved, either corticosteroid-induced immunosuppression or neutropenia, as shown in Fig. 1.1 (Dagenais and Keller, 2009; Ibrahim-Granet *et al.*, 2003; Philippe *et al.*, 2003).

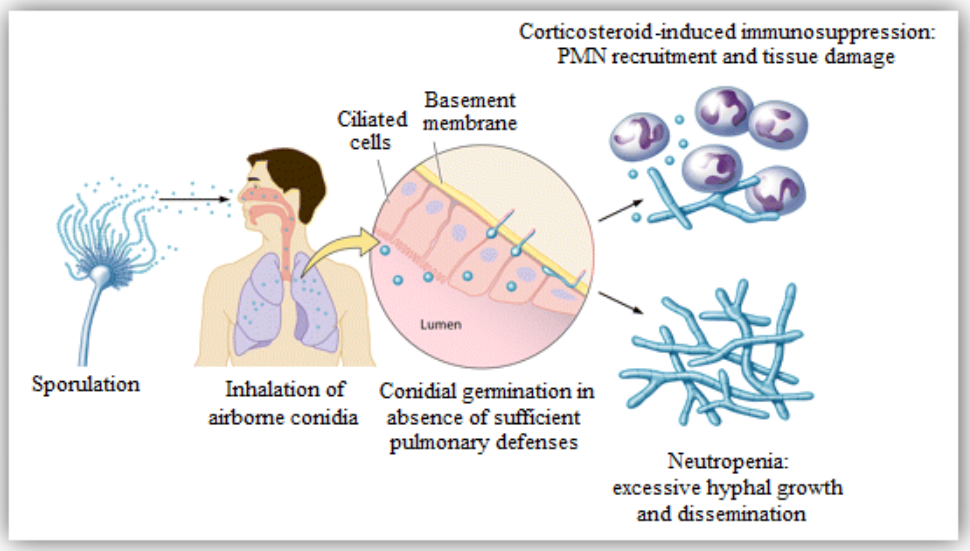


Fig. 1.1: Infectious life cycle of *A. fumigatus.* In immunosuppressed patients, the inhalation of conidia and their establishment and germination in the lung is followed by a specific outcome depending on the immune state of the host. In corticosteroid-induced immunosuppression, the infection is characterised by PMN-mediated fungal control with significant inflammation, whereas in a neutropenic scenario, uncontrolled hyphal growth with a lack of PMN infiltrates may lead, in severe cases, to dissemination. From Dagenais and Keller, 2009.

Corticosteroid therapy is generally used in allogenic transplant patients and significantly impairs macrophages functional abilities such as phagocytosis, phagocyte oxidative burst, production and secretion of cytokines and chemokines and cellular migration (Lionakis and Kontoyiannis, 2003). IPA in these patients is characterised by limited fungal development, but excessive inflammation and tissue necrosis as a consequence of the massive recruitment of neutrophils *in situ*. Neutropenia is often caused by highly cytotoxic therapies such as cyclophosphamide, a DNA alkylating agent, used for haematological diseases or transplants. Cyclophosphamide binds to DNA, interfering with cellular replication and depleting circulating white blood cells. In these patients, IPA is characterised by low levels of inflammation, thrombosis and haemorrhages result from the rapid and extensive invasive hyphal growth (Chiang *et al.*, 2008; Stergiopoulou *et al.*, 2007).

1.1.3 Current treatment available for IPA

Once established, invasive fungal infections are extremely difficult to cure and, as a result, the associated death rate is extremely high and although systemic antifungals have been available for more than 50 years, the drugs initially available for the treatment of aspergillosis were characterised by several limitations (as reviewed in Ghannoum and Rice, 1999; Ostrosky-Zeichner *et al.*, 2010). Initially only Amphotericin B and early formulations

of triazoles were available to treat aspergillosis but these drugs showed low efficacy *in vivo*, despite their activity *in vitro* (Denning, 1995; Denning, 1996a; Denning, 1996b; Denning, 1998; De Pauw, 1997; Gallis *et al.*, 1990; Kauffman, 2006). Antifungal treatments were unable to kill *A. fumigatus* rapidly and without toxicity for patients. Moreover, they had a limited spectra of activity and sometimes cross-react with other treatments (Kauffman, 2006). There was also a problem of emerging resistance (Chryssanthou, 1997; Denning *et al.*, 1997a; Denning *et al.*, 1997b; Verweij *et al.*, 1998).

Amphotericin B has represented for more than 30 years the standard antifungal therapy for IPA (Brajtburg and Bolard, 1996). The antifungal action of amphotericin B is due to its ability to differentially bind fungal and human membrane sterols, targeting preferentially ergosterol in the fungal membrane rather than cholesterol found in mammalian membranes. As a consequence of this binding, transmembrane channels are formed in the membranes and its permeability to monovalent cations is increased (Bolard, 1986). Other effects of amphotericin B are the inhibition of proton ATPase pumps, decreasing cellular energy reserves, and the promotion of lipid peroxidation, increasing membrane fragility and causing Ca^{2+} leakage (Brajtburg *et al.*, 1985; Ramos *et al.*, 1989; Surarit and Shepherd, 1987). The disadvantages of the use of amphotericin B include its insolubility in water and the severe side effects, such as nephrotoxicity (Clements and Peacock, 1990; Pathak *et al.*, 1998; Patterson, 1998). The reformulation of amphotericin B with lipid compounds in the 1990s considerably overcame these limitations, reducing renal toxicity and improving bioavailability (Juliano *et al.*, 1987; Payne *et al.*, 1987).

Another category of antifungal agents used against *Aspergillus* is triazoles, initially developed in the 1980s and further developed in the 1990s, with compounds such as fluconazole, voriconazole and itraconazole. The mechanism of action of triazoles is based on the competition for oxygen between the free azole nitrogen in these molecules and the catalytic heme iron atom of cytochrome P-450 enzymes (De Beule, 1996; Vanden Bossche *et al.*, 1980; Vanden Bossche *et al.*, 1983; Vanden Bossche *et al.*, 1988; Vanden Bossche *et al.*, 1989; Vanden Bossche *et al.*, 1990). Inhibition of the cytochrome P-450 enzymes prevents the synthesis of ergosterol in fungal membranes, whose fluidity is therefore increased, and causes the cytosolic accumulation of other membrane components, like phospholipids and unsaturated fatty acids. Itraconazole is the most frequently used of the triazoles, because it binds only weakly to mammalian cytochrome P-450 and this reduces drastically its toxicity in humans. Unfortunately, there is no intravenous preparation available and absorption of itraconazole varies between patients. A new generation of triazoles (posaconazoles, isavuconazole, ravuconazole and albaconazole) is characterised by a broad spectrum of

activity and is thought to represent the future therapeutic alternative to overcome resistance (De Sarro *et al.*, 2008).

For decades, amphotericin B has been the standard therapy for IPA, even if responses were less than 40% in severely immunosuppresed patients (Denning, 1998; Stevens and Forgac, 1997; Patterson, 1998). In a non-comparative study, voriconazole has shown a 48% response rate among patients with IPA. An open, randomised trial comparing the efficacy, safety, and tolerability of amphotericin B and voriconazole to treat IPA in almost 400 immunocompromised patients has shown 60% and 71% survival rate respectively for patients at 12 weeks of therapy (Herbrecht, 2002; Herbrecht *et al.*, 2002). The underlying condition for the selection of patients with IPA for the trials was allogeneic hematopoietic-cell transplantation, acute leukemia, or other hematologic diseases and the study demostrated that in these, initial therapy with voriconazole yield better responses and improved survival, with less severe side effects than the standard therapy with amphotericin B.

In addition, new antifungal treatments have been recently approved to proceed to clinical trials or have become available. As an alternative to the traditional therapies, caspofungin has now been approved for IPA treatment (Letscher-Bru and Herbrecht, 2003). Caspofungin belongs to the echinocandins, a new family of antifungal molecules acting on the fungal cell wall by inhibiting glucan synthesis, and more specifically it blocks the synthesis of β-(1,3)-D-glucan, by non-competitive inhibition of the enzyme β-(1,3)-D-glucan synthase. Caspofungin potential has been demonstrated in several trials with patients refractory or intolerant to previuos therapy, with a favourable response rate of 45% of 83 patients and infrequent drug-related nephrotoxicity and hepatotoxicity (Maertens *et al.*, 2004). Also in a comparative clinical trial involving over 1000 patients with persistent fever and neutropenia, caspofungin has been demonstrated to be as effective and generally better tolerated in comparison with liposomal amphotericin B (Walsh *et al.*, 2004).

Despite the advances in therapy, there is a critical and urgent need for the development of new antifungal therapeutic agents. Infection burden remains high because of the difficulty to diagnose *Aspergillus* infections especially in the early stages of infection.

1.1.4 Murine models of invasive aspergillosis

Immunosuppressive regimens differentially impact fungal development and host response (Balloy *et al.*, 2005), highlighting the importance of studying *Aspergillus fumigatus* pathogenesis in multiple relevant contexts of host immune status. For this reason, there are several different models of invasive fungal infection in use, but even considering the

heterogeneity in the animal models in use, it has been shown that there is a direct correlation between the dosage of conidia and the lethality observed, as for other fungal pathogens. Also, following the typical pattern in humans, different immunosuppressive regimens in animal models result in a different development and different characteristics of infection (Stephens-Romero *et al.*, 2005). The most commonly used animal models of IPA involve induction of neutropenia or corticosteroid-induced immunosuppression to reproduce the pre-existing conditions necessary for the development of the infection in humans. To explain the importance of the use of different immunosuppressive drugs, the most appropriate example is the case of the gliotoxin null mutant, which shows a completely different outcome of infection in different host immune status scenarios (Bok *et al.*, 2006; Spikes *et al.*, 2008; Sugui *et al.*, 2007b; Dagenais and Keller, 2009). This mutant is characterised by wild type virulence in a neutropenic model, but reduced virulence in a non-neutropenic model, identifying gliotoxin as an important *A. fumigatus* virulence factor in the context of non neutropenic hosts. Other variables, which have been established as crucial in the context of the application of animal models, are the amount of spores inoculated, the route of infection and the type of analysis to perform (Dixon *et al.*, 1989). Fungal infection may be performed following different routes such as intratracheally, intravenously or via inhalation chamber but the intranasal inoculation is commonly used as it mimics human infection (Sheppard *et al.*, 2004; Steinbach *et al.*, 2004). Possible applications of animal models include survival analysis, organ pathology or histology examination, fungal burden quantification or measurement of host cellular response.

The murine model of infection in use at Imperial College and utilised in this study has been extensively used for over 15 years (Smith *et al.*, 1994). CD1 male mice are immunosuppresed by intraperitoneal injections of cyclophosphamide and by a single subcutaneous dose of hydrocortisone acetate. This treatment causes neutropenia in mice, closely mimicking the condition required to develop IPA in humans (Schrettl *et al.*, 2004). Also *A. fumigatus* conidia are inoculated intranasally to mimic the natural route of infection. The resulting IPA has a clinical pattern and outcome similar to what is observed in humans, with a mortality greater than 80%.

1.2 *Aspergillus fumigatus*

A. fumigatus belongs to the genus *Aspergillus* (phylum *Ascomycota*) comprising almost 200 species of ubiquitous, saprophytic fungi. *Aspergillus* species are primarily

involved in global carbon and nitrogen recycling, and their typical niche is soil, food, decaying vegetation and air vents. They produce small, hydrophobic conidia, dispersed into the air and able to survive a wide range of environmental conditions. For this reason, the impact of these species on public health is of enormous importance. Several *Aspergillus* species are used in industry for the production of food and pharmaceuticals, such as *A. niger*, *A. terreus* and *A.oryzae*. Other species, particularly *A. flavus* and *A. parasiticus* are well known as contaminants of crops, for their production of aflatoxin, a highly toxic carcinogen with immunosuppressive properties (Wild, 2007). Among the human pathogenic species of *Aspergillus*, *A. fumigatus* is responsible for 90% of human infections, followed by *A. flavus*, *A. terreus*, *A. niger* and the model organism *A. nidulans* (Denning, 1998; Morgan *et al.*, 2005). Species are differentiated on the basis of formation, colour, shape and texture of the spores. In the last 30 years, *A. fumigatus* has emerged as one of the most important causes of infection related death in immunocompromised patients (Wiederhold *et al.*, 2003). Its first description however appeared in 1863 in the book '*Nova plantarum genera juxta Tournafortii methodum disposita*' by the Italian priest and biologist Pier Antonio Micheli, who named the species after the instrument used for the dispersion of holy water in catholic churches, called aspergillum, for the similarity in shape with the fungus.

1.2.1 Morphology and reproductive cycle

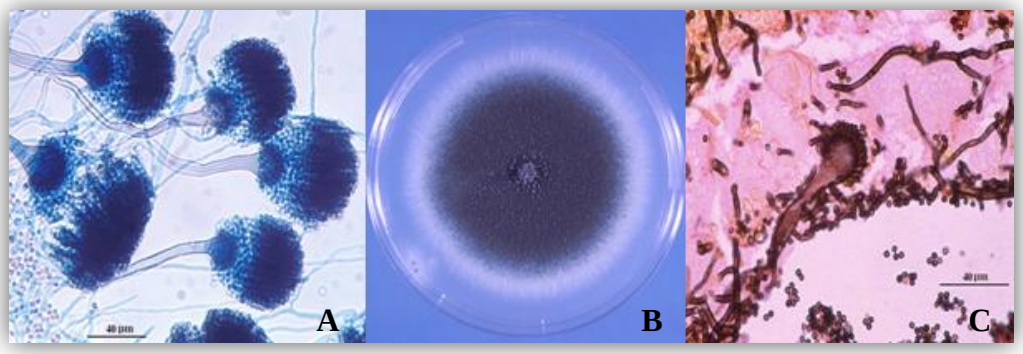


Fig. 1.2: Morphological features of *A.fumigatus* (A) Microscopic morphology of *Aspergillus fumigatus*. (B) On Czapek dox agar showing typical blue-green surface pigmentation with a suede-like surface consisting of a dense felt of conidiophores. (C) Grocott's methenamine silver (GMS) stained tissue sections showing *Aspergillus fumigatus* in lung tissue, note conidial heads forming in an alveolus. From www.mycology.adelaide.edu.au.

A. fumigatus (Fig. 1.2) is a cosmopolitan and saprophytic fungus, essential for recycling of environmental carbon and nitrogen. The organism survives and grows on organic debris. Identification of *A. fumigatus* is based predominantly upon the morphology of the conidia and conidiophores. The green echinulate conidia are produced in chains basipetally

from green phialides about 6 to 8 µm. Conidia are simply released in the air and they have a diameter small enough (2-3 µm) to reach the lung alveoli. A few pigmentless isolates of *A. fumigatus* producing white conidia have been discovered (Latge, 1999). The chains of conidia originate directly from broadly clavate vesicles (20 to 30 µm in diameter) in the absence of metulae. *A. fumigatus* grows fast and the colonies can reach 4 ± 1 cm within a week when grown on Czapek dox agar (CZA) at 25°C (Raper, 1965). The species is thermophilic and capable of growth at 37°C (human body temperature), but growth occurs at temperatures as high as 55°C and survival is maintained at temperatures up to 70°C (Samson, 1994). Differently to the original classification describing *A. fumigatus* as a single homogenous species (Raper, 1965), strains have been demonstrated to differ in cultural conditions and micro-morphologic characteristics, such as branched conidiophores, elongate or septate phialides and size or shape difference in conidia (Leslie *et al.*, 1988; Rinyu *et al.*, 1995).

Conidial germination starts in the presence of water, carbon, phosphate and nitrate sources, and oxygen (Fortwendel *et al.*, 2004), whereas it is inhibited under anaerobic conditions (Taubitz *et al.*, 2007). Water uptake, with rehydration and growth of the cell wall, determines a first stage of swelling or isotropic growth. Subsequently, in preparation for DNA replication and mitosis, nuclear decondensation occurs and polar growth starts with the formation of a germ tube (Momany and Taylor, 2000). These initial steps are the same in the case of development in soil or within the host.

A. fumigatus has a stable haploid genome and it sporulates abundantly, with every conidial head generating thousands of conidia. For many years *A. fumigatus* was thought to only reproduce asexually, because neither mating nor meiosis had ever been observed. However, there were various lines of evidence to support the possible occurrence of sexual reproduction (Dyer and Paoletti, 2005; Paoletti *et al.*, 2005). Population genetic analyses had revealed a high degree of genetic variation within natural population of *A. fumigatus*, possibly as a result of sexual reproduction and recombination (Chazalet *et al.*, 1998; Paoletti *et al.*, 2005; Pringle *et al.*, 2005; Rydholm *et al.*, 2006). The sequencing of *A. fumigatus* clinical isolate Af293 and successive studies had demonstrated the presence and expression of apparently functional genes required for sexual development in other ascomycete fungi (Galagan *et al.*, 2005; Nierman *et al.*, 2005; Paoletti *et al.*, 2005). Mating types, whose role as transcriptional activators is crucial in governing the mating process in ascomycete fungi, had also been identified (Paoletti *et al.*, 2005; Casselton, 2002; Galagan *et al.*, 2005) and shown to be distributed in a homogenous 1:1 ratio of *MAT1-1* and *MAT1-2* in geographic areas (O'Gorman *et al.*, 2009). In 2008 it was finally demonstrated that *A. fumigatus* possesses a fully functional sexual reproductive cycle (O'Gorman *et al.*, 2009).

1.2.2 Genome

The sequencing of the *A. fumigatus* genome represents a crucial milestone for the fungal community. The project for the whole genome shotgun sequence analysis of the *A. fumigatus* Af293 wild type isolate was started in the late 90's as a collaboration between the Sanger Institute at the University of Cambridge (www.sanger.ac.uk) and the Institute of Genome Research (TIGR) (www.jcvi.org). The genome sequence was finished and published in 2005 (Nierman *et al.*, 2005), together with a comprehensive comparative analysis with the *A. nidulans* strain FGSC A4 and the *A. oryzae* RIB40 (Galagan *et al.*, 2005; Machida *et al.*, 2005). The Af293 wild type isolate contains eight chromosomes, whose sizes vary from 1.8 to 4.9 Mb for a total of 29.4 Mb with a 49.9% G + C content. The comparison with *A. nidulans* and *A. oryzae* indicates about 500 genes as unique to *A. fumigatus* (Galagan *et al*., 2005). Initially, the number of predicted protein-coding genes was estimated to be 9926 and one third of these, 3288, had an unknown function (Ronning *et al.*, 2005). According to the last version available from February 2008, the genome of *A. fumigatus* contains 9630 genes. More recently the genome sequence of the strain A1163, a derivative of the *A. fumigatus* wild-type CEA17, has been published by TIGR, showing 99.8% identity, at the nucleotide level, with the Af293 wild type isolate (Fedorova *et al.*, 2008). Currently the genomes of seven of the closest phylogenetic relatives of *A. fumigatus* have been sequenced, permitting in more detail the determination of *A. fumigatus* specific and non specific genes and families. The sequenced genomes include *A. flavus* (12,587 genes), *A. oryzae* (12,063 genes), *A. terreus* (10,406 genes), *A. niger* (8,592 genes), *Neosartorya fisheri* (10,407 genes), *A. clavatus* (9,124 genes) and *A. nidulans* (10,701 genes) (Nierman *et al.*, 2005; Baker, 2006; Galagan *et al.*, 2005; Machida *et al.*, 2005; Payne *et al.*, 2006). Between these species, about 2% of each genome is specific to the *Aspergillus* species and there is a variability ranging from 4 to 11% for species-specific genes.

1.2.3 Putative virulence factors

A. fumigatus virulence has been defined as a polygenic trait (Askew, 2008; Hohl and Feldmesser, 2007), being due to the unique combination of multiple contributing basic traits. IPA pathogenesis depends on the equilibrium between the ability of the host to overcome fungal invasion and the various ways by which the fungus can inactivate or escape the host's defence systems. Infection is facilitated because of the versatile nature of this organism that can withstand the nutritional, oxidative and other physiological stresses exerted by the host

niche. *A. fumigatus* relies on the combined and coordinated expression of genes involved in fungal growth, such as conidial germination, cell wall assembly, hyphal growth, nutrient acquisition and resistance to host-imposed stresses (Askew, 2008; Hohl and Feldmesser, 2007).

One aspect of this adaptation is *A. fumigatus* thermotolerance. Deletion of the *cgrA*[1] gene, encoding a nucleolar protein involved in ribosome biogenesis, results in the impairment of growth at 37°C and in the attenuation of virulence in a murine model of IPA (Bhabhra *et al.*, 2004).

Following inhalation, *A. fumigatus* needs to adhere to and penetrate the human respiratory epithelia and overcome surrounding cells response, in particular from phagocytic cells. The conidial surface contains protrusions, called rodlets, essential to maintain conidial hydrophobicity (Thau *et al.*, 1994), but also sialic acid residues. Sialidase treatment causes spore agglutination and for this reason sialic acid residues exposed on the conidial surface are thought to be important for the dispersion of conidia and pulmonary colonisation (Warwas *et al.*, 2007; Wasylnka and Moore, 2000). Accordingly, it has been shown that pathogenic species of *Aspergillus*, including *A. fumigatus*, contain more sialic acid residues on the conidia surface than other non-pathogenic species (Wasylnka and Moore, 2000). The cell wall in *A. fumigatus* is composed predominantly of α-(1,3) glucan, β-(1,3) glucan, some of which contains β-(1,6) branches, linear β-(1,3), β-(1,4) glucan, chitin and galactomannan (Latge *et al.*, 2005). Fungal cell wall composition has also been demonstrated to play a crucial role in *A. fumigatus* virulence in immunocompromised mice (Hohl and Feldmesser, 2007), as gene deletions for fungal cell wall components causing an increased growth rate yield hypervirulent *Aspergillus* strains (Beauvais *et al.*, 2005; Chabane *et al.*, 2006; Maubon *et al.*, 2006; Romano *et al.*, 2006). Cell wall maintenance and homeostasis are ensured through the redundancy of proteins involved in the synthesis of structural polysaccharides. In addition, like many other fungi, the *A. fumigatus* cell wall contains melanin, a protective barrier against UV radiation. In the context of the infection, pigment biosynthesis is useful in resisting phagocytosis and increasing resistance to reactive oxygen species (Brakhage and Liebmann, 2005). *A. fumigatus* wild type strains deficient in pigment production have been demonstrated to be less pathogenic than strains with green conidia (Latge, 1999).

[1]Following *A. nidulans* nomenclature, *A. fumigatus* gene names are italicized; complete, partial loss-of-function and gain-of-function (constitutive) mutants using superscripts and proteins non-italicized starting with an upper case letter.

A. fumigatus relies on crucial biosynthetic pathways evolved to counter hostility in ecological niches, in particular by the production of several toxic secondary metabolites (Cui *et al.*, 1996a; Cui *et al.*, 1996b; Frisvad *et al.*, 2009). As introduced previously, gliotoxin is the most extensively studied secondary metabolite, especially after the elucidation of its role as a crucial *A. fumigatus* virulence factor in the context of non-neutropenic hosts. Gliotoxin, a metabolite of the epipolythiodioxopiperazine family (Mullbacher and Eichner, 1984; Mullbacher *et al.*, 1985), is acutely toxic and has immunosuppressive properties, blocking phagocytosis (Waring *et al.*, 1988) and the release of inflammatory mediators by leukocytes (Pahl *et al.*, 1996), and inducing the apoptosis of neutrophils and monocytes (Frame and Carlton, 1988; Waring *et al.*, 1988; Stanzani *et al.*, 2005). Environmental *A. fumigatus* strains defective in the production of gliotoxin have been demonstrated to be less virulent than strains producing this secondary metabolite efficiently (Sutton *et al.*, 1996). Deletion of gliotoxin differentially affects *A. fumigatus* virulence depending on the immunosuppressive regimen of the host, in particular the gliotoxin mutant is characterised by wild type virulence in a neutropenic model, but reduced virulence in a non-neutropenic model. Other secondary metabolites are fumagillin, helvolic acid and verruculogen, able, at higher concentrations, to damage human respiratory epithelial cells and slow ciliary beat frequency (Amitani *et al.*, 1995a; Amitani *et al.*, 1995b; Botterel *et al.*, 2002; Cody *et al.*, 1997; Khoufache *et al.*, 2007). Secondary metabolite production is strongly affected by the disruption of the predicted methyltransferase LeaA (Bok *et al.*, 2005). LaeA regulates 10% of the *A. fumigatus* genome and deletion results in the attenuation of the mutant strain in mice (Sugui *et al.*, 2007a; Perrin *et al.*, 2007).

Once overcame the resident pulmonary defences, *A. fumigatus* germination and hyphal growth ensues depending upon regulatory pathways sensing and responding to stress conditions, nutrient availability and other environmental conditions within the host. *A. fumigatus* can express a broad range of degradative enzymes, such as elastases and proteases, for the invasion of host and nutrient acquisition. For example, since elastin and collagen constitute major components of lung tissues, a direct correlation has been described between elastase production in *A. fumigatus* strains and their virulence, because strains not producing elastase showed few germinated spores and no destruction of alveoli in murine lungs (Kothary *et al.*, 1984). In general, *A. fumigatus* produces and secretes a series of catabolic enzymes, especially peptidases, to degrade macromolecular complexes and derive nutrients (Alp and Arikan, 2008). Acquisition of essential nutrients within the host environment, such as calcium, iron, zinc and nitrogen, is necessary to support sufficient growth and is therefore required for invasive growth.

Calcium (Ca^{2+}) is an ubiquitous second messenger involved in many signal transduction pathways in eukaryotic cells (Carafoli, 2005; Cyert, 2003). In particular, in filamentous fungi, Ca^{2+} is important for hyphal morphogenesis (Fox and Heitman, 2002). Two mediators, the Ca^{2+}- binding protein calmodulin and the Ca^{2+}-calmodulin-activated protein phosphatase calcineurin, are involved in calcium signalling: (Carafoli, 2005). Calcineurin consists of a catalytic subunit A and a Ca^{2+}-calmodulin binding domain and the association between these two domains is essential for functioning (da Silva Ferreira *et al.*, 2007; Steinbach *et al.*, 2006; Fox and Heitman, 2002). Deletion of *cnaA*, the catalytic subunit of calcineurin, determines the attenuation of virulence in mutant strains (Steinbach *et al.*, 2006; da Silva Ferreira *et al.*, 2007). As well, mutants lacking the calcineurin-dependent transcription factor CrzA are attenuated for virulence (Soriani *et al.*, 2008).

Iron is involved in many biosynthetic pathways, acting as a cofactor in many enzymatic reactions, and as a catalyst in electron transport systems. Its availability in the host environment is limited, because of the instability and toxicity of free iron and its retention as chelates to deprive microbes. *A. fumigatus*, as many other pathogens, possesses systems able to ensure iron acquisition in the host, the storage and the detoxification of iron, and these systems are crucial and necessary virulence determinants. *A fumigatus* utilizes two different mechanisms for iron acquisition: siderophore-mediated iron uptake and reductive iron assimilation (Schrettl *et al.*, 2004). Siderophores are small ferric-iron-specific chelators and *A. fumigatus* produces four known siderophores. Fusaricine C and triacetylfusaricine C are secreted and responsible for chelation of extracellular iron, whereas ferricrocin and hydroxyferricrocin permit the intracellular storage of iron in hyphae and conidia, respectively (Eisendle *et al.*, 2004; Haas *et al.*, 2008). Multiple genes involved in *A. fumigatus* siderophore biosynthesis have been identified and characterised (Hissen *et al.*, 2005; Schrettl *et al.*, 2004), establishing the requirement for both the extracellular and intracellular siderophores for the acquisition and the storage of iron during infection (Schrettl *et al.*, 2007).

It has been estimated that over 300 enzymes use zinc as a catalytic or structural component. Zinc has also a limited bio-availability *in vivo.* Zinc uptake is mediated by the zinc-responsive transcriptional activator ZafA (Vicentefranqueira *et al.*, 2005) and the regulation of zinc homeostasis has been shown to be essential for *A. fumigatus* pathogenicity in a murine model of IPA (Moreno *et al.*, 2007). Interestingly, the interplay between iron and zinc metabolism in *A. fumigatus* has been demonstrated recently, whereby the expression of various genes involved in zinc homeostatic maintenance is increased as a consequence of iron starvation (Schrettl *et al.*, 2008; Yasmin *et al.*, 2009). Zinc availability is also influenced by pH, because the solubility of zinc decreases gradually with neutral pH.

Aspergillus species can use a variety of nitrogen sources and are actively involved in global nitrogen recycling by nitrate assimilation. In this process, environmental nitrate is converted into ammonium and subsequently to glutamine and glutamate. The transcription factor responsible for nitrate transport and assimilation is AreA. Differences in growth rate are evident between *areA* mutants and wild type strains on poor nitrogen media, and for *areA* mutants delayed growth is also observed in host tissue, although virulence is similar to that one of the wild type strains (Hensel *et al.*, 1998; Krappmann *et al.*, 2004; Krappmann and Braus, 2005).

Recently, the transcriptional analysis of *A. fumigatus* in the early stages of infection in a neutropenic murine model of IPA has been performed to identify genes preferentially expressed during adaptation to the mammalian host niche (McDonagh *et al.*, 2008a). This analysis permitted the measurement of more than 9,000 *A. fumigatus* genes and identified iron limitation, nitrogen limitation and alkaline stress as prominent stresses imposed by the host in the early stages of infection. In addition, it demonstrated the physical clustering of genes involved in infection and their preferential localisation near the chromosomes termini, in the telomeres. As a crucial component of this study, alkaline stress will be described in detail in the following paragraphs but it represents one of the host-imposed stresses *A. fumigatus* must face to adapt to the host niche, together with temperature (discussed previously) and oxygen limitation.

Several genes have been shown to be involved in *A. fumigatus* oxidative stress tolerance, such as catalases (*catA*, *cat1* and *cat2*) (Calera *et al.*, 1997; Paris *et al.*, 2003), the PKA regulatory subunit PkaR (Zhao *et al.*, 2006), the MAPK pathway (Ma *et al.*, 2008; Valiante *et al.*, 2008) and two transcription factors Yap1 and Skn7 (Lessing *et al.*, 2007). The role of anti-oxidant mechanisms in *A. fumigatus* pathogenicity is still debated because only some null mutants of the aforementioned genes have shown an attenuation of virulence. Also, in the previously cited study of *A. fumigatus* adaptation in a murine model of IPA, it was not possible to demonstrate a significant overlap between genes differentially expressed *in vivo* in the early-stages of infection and *in vitro* in anaerobic conditions (McDonagh *et al.*, 2008a).

1.3 The PacC/Rim101p signalling pathway for adaptation to environmental pH stress

All microorganisms, in particular those inhabiting mammalian niches during infection, need to be able to adapt to the pH of the surrounding environment. Especially for organisms

growing over a wide pH range, adaptation implies the maintenance of internal pH homeostasis but also the appropriate expression of genes involving functions at the cell surface or in the environment. These genes include permeases, secreted enzymes, enzymes involved in synthesis of exported metabolites (i.e. toxins and antibiotics) and enzymes post-translationally modifying secreted proteins. The main genetic regulatory system involved in ambient pH regulation is widespread in the fungal kingdom and was first recognised more than 20 years ago (Caddick *et al.*, 1986c). Since then, ambient pH regulation of gene expression has been extensively studied (Caddick and Arst, 1986; Caddick *et al.*, 1986a; Caddick *et al.*, 1986b; Arst, 2003; Arst Jr and Peñalva, 2003; Penalva and Arst Jr, 2002; Peñalva and Arst Jr, 2004; Peñalva *et al.*, 2008), especially in the ascomycete *A. nidulans*, where genetic manipulations are easily achievable (Pontecorvo *et al.*, 1953; Dorn, 1965b; Dorn, 1965a; Arst, 1967; Arst *et al.*, 1980; Arst *et al.*, 1994), in contrast to *A. fumigatus*.

The system for the regulation of gene expression according to environmental pH is an essential requisite for microorganisms growing over a broad range pH. *A. nidulans*, which grows over a range of pH from 2.5 to 9.0, is the fungal species where the pH regulatory system was identified in the first instance (Caddick *et al.*, 1986c). In 1965, some *A. nidulans* mutants defective in the production of phosphatases were isolated (Dorn, 1965b; Dorn, 1965a). Some of these mutants were called *pal* and other *pac*, missing respectively alkaline phosphatase or acid phosphatase activities. The link between these mutants and the regulation of gene expression by ambient pH was not demonstrated until 1986, when the mutations in the *pal* and *pac* genes were attributed to a defective regulation of gene expression by pH (Caddick *et al.*, 1986c). In the same study, it was also shown that pH regulation is not only limited to phosphatase genes, but it is important for other genes and activities such as γ-amino-*n*-butyric acid (GABA) uptake by the GABA permease gene, *gabA*, and sensitivity to neomycin and molybdate (Caddick *et al.*, 1986c). Mutations affecting pH regulation were categorised mainly into two categories, according to their phenotypic effects: alkalinity-mimicking and acidity-mimicking mutations. The alkalinity-mimicking mutations, irrespective of ambient pH, show a pattern of gene expression similar to the wild type growing under alkaline conditions, for example with the reduction of GABA transport and acid phosphatase levels, the increase of alkaline phosphatase, molybdate resistance and neomycin hypersensitivity. The opposite phenotype, with the prevention or the reduction of growth at alkaline pH, the increase of GABA transport and acid phosphatase levels, the decrease of alkaline phosphatase, molybdate hypersensitivity and neomycin resistance, is shown by the acidity-mimicking mutations. These mutations lead, irrespective of ambient pH,

to a pattern of gene expression similar to the wild type growing under acidic conditions (Caddick *et al.*, 1986c; Mingot *et al.*, 1999; Tilburn *et al.*, 1995).

The genes involved in pH regulation were named *pacC* and *palA*, *palB*, *palC*, *palF*, *palH* and *palI*; *pacC* was proposed to encode a transcriptional regulatory factor, activator of alkaline-expressed genes and repressor of acid-expressed genes (Caddick *et al.*, 1986c; Tilburn *et al.*, 1995).

1.3.1 pH regulation in *Aspergillus nidulans*

In the model developed in *A. nidulans*, seven genes are involved in pH regulation (Fig. 1.3): *pacC*, encoding a transcription factor which activates genes expressed in alkaline conditions and represses those expressed in acid conditions, and *palA, palB*, *palC, palF*, *palH* and *palI*, whose products transmit the alkaline ambient pH signal to PacC (Arst *et al.*, 1994; Caddick *et al.*, 1986c; Denison *et al.*, 1995; Denison *et al.*, 1998; Fernández-Martinez *et al.*, 2003; Maccheroni *et al.*, 1997; Negrete-Urtasun *et al.*, 1997; Negrete-Urtasun *et al.*, 1999; Tilburn *et al.*, 1995). Normal functioning of the *A. nidulans* pH regulatory system requires the integrity of all these genes, as confirmed by phenotypic consequences of loss-of-function mutations. Null mutations in any of the *pal* genes of the pH signal transduction pathway, and in some *pacC* mutants, have an acidity-mimicking phenotype (Arst *et al.*, 1994; Caddick *et al.*, 1986c; Denison *et al.*, 1995; Denison *et al.*, 1998; Fernández-Martinez *et al.*, 2003; Maccheroni *et al.*, 1997; Negrete-Urtasun *et al.*, 1997; Negrete-Urtasun *et al.*, 1999; Tilburn *et al.*, 1995).

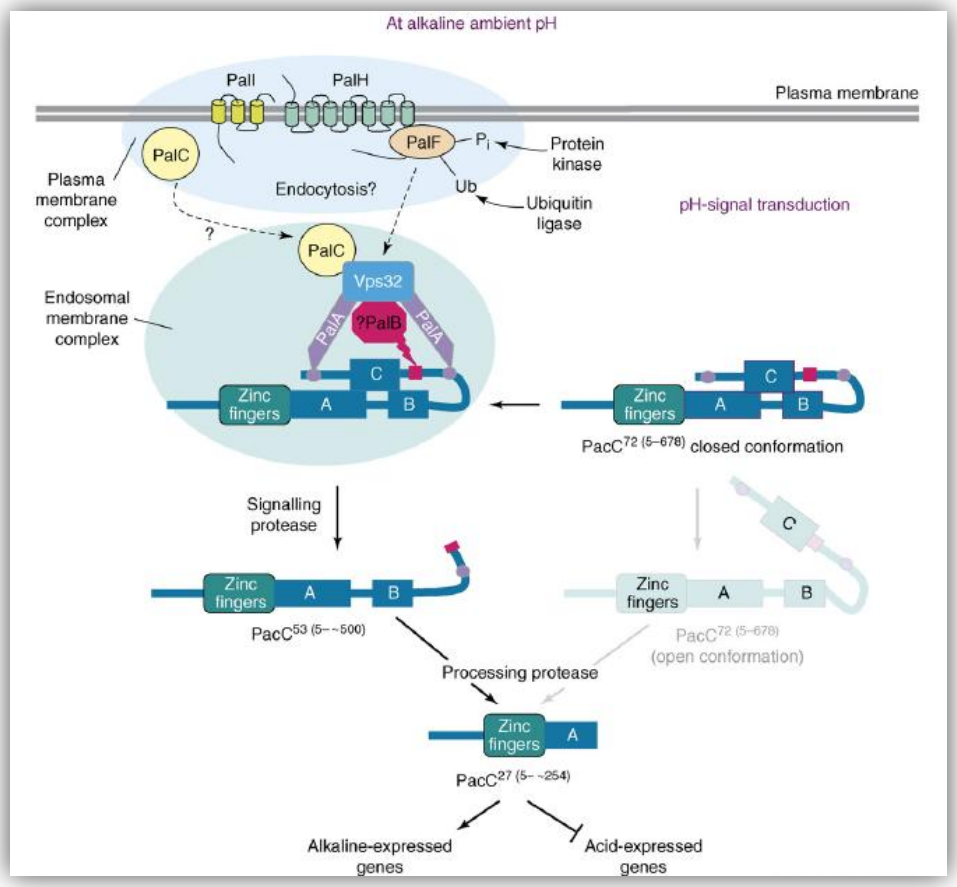


Fig. 1.3: **Schematic representation of pH regulation in *A. nidulans*.** The shift to alkaline pH causes the signal for PacC processing to be transmitted from the plasma membrane to the endosomal membrane complex involving the endocytosis of PalH and/or PalF and the participation of PalC. The full-lenght PacC protein ($PacC^{72}$), bound by PalA, undergoes signalling proteolysis by the cysteine protease PalB, which removes the negatively acting C-terminus to form the intermediate-lenght ($PacC^{53}$). $PacC^{53}$ conformation is recognised by the pH-independent processing protease, likely the proteasome, which forms $PacC^{27}$. This form of PacC is the activator of alkaline-expressed genes and repressor of acid-expressed genes. Modified from Peñalva *et al*., 2008.

The 72-kD translation product $PacC^{72}$ contains 674 amino acids (Mingot *et al.*, 1999; Tilburn *et al.*, 1995). Translation starts at the Methionine codon 5 of the open reading frame (Mingot *et al.*, 1999), but residues are counted from the first Met codon 1 to avoid inconsistency between the publications. This 674-residue full-length form of PacC ($PacC^{72}$) is predominant at acidic conditions. Three interacting regions keep $PacC^{72}$ in an apparently inert "closed" form, preventing proteolytic processing (Espeso *et al.*, 2000). In neutral-to-alkaline conditions, $PacC^{72}$ is processed by two successive proteolytic cleavages, although the formation of a small amount of the processed form occurs independently of pH signal. The first (signalling) proteolysis is dependent on pH-signal transduction and occurs within the conserved 24-residue "signalling protease box" removing ~180 C-terminal residues and

yielding the intermediate $PacC^{53}$ (Diez *et al.*, 2002). The second (processing) proteolysis is pH-independent and catalysed by the proteasome (Hervas-Aguilar *et al.*, 2007), removing further ~245 C-terminal residues; this cleavage leaves the zinc-finger region intact and yields the processed $PacC^{27}$ form, repressor of acid-expressed genes and activator of alkaline-expressed genes (Diez *et al.*, 2002; Orejas *et al.*, 1995; Mingot *et al.*, 1999). Within the $PacC^{27}$ processed form lies the DNA binding domain (DBD) composed of three Cys_2His_2 zinc fingers; among these only the second and the third contact the DNA-binding site (consensus 5' –GCCARG) (Espeso *et al.*, 1997; Fernández-Martinez *et al.*, 2003; Tilburn *et al.*, 1995). A nuclear localisation signal overlaps with the third zinc finger (Fernández-Martinez *et al.*, 2003) and both $PacC^{27}$ and $PacC^{53}$, but not $PacC^{72}$, are preferentially localised in the nucleus (Mingot *et al.*, 1999; Fernández-Martinez *et al.*, 2003).

Acidity-, alkalinity- and neutrality-mimicking mutations have been isolated for *pacC* (Arst *et al.*, 1994; Caddick *et al.*, 1986c; Diez *et al.*, 2002; Espeso *et al.*, 1997; Espeso *et al.*, 2000; Fernández-Martinez *et al.*, 2003; Mingot *et al.*, 1999; Orejas *et al.*, 1995; Tilburn *et al.*, 1995; Vincent *et al.*, 2003). Alkaline-mimicking $pacC^{c}$ (PacC constitutive) mutations remove or inactivate, by amino acid(s) substitution, one or more of the interacting regions, leading to PacC processing independently of ambient pH. Acidity-mimicking $pacC^{-}$ mutations include frameshift and polypeptide chain termination mutations truncating PacC upstream of, or within, the DBD or single amino acids substitutions preventing DNA binding, or gene replacement removing the entire coding region (Espeso and Penalva, 1996; Espeso *et al.*, 2000; Vincent *et al.*, 2003). $pacC^{-}$ mutations also demonstrate cryosensitivity, poor growth and reduced conidiation at permissive temperatures (Tilburn *et al.*, 1995).

In the model established for *A. nidulans*, establishment of the ambient pH signal involves the connection between two complexes, the first one of which comprises the two plasma membrane proteins PalH and PalI and an arrestin-like protein PalF and the other is composed of PacC, a cysteine protease PalB, a scaffold PalA, PalC and endosomal components (Peñalva *et al.*, 2008).

The plasma membrane signalling complex contains a seven-transmembrane domain (TMD) protein PalH, the arrestin PalF and, very likely, the three-TMD protein PalI (Calcagno-Pizarelli *et al.*, 2007; Herranz *et al.*, 2005; Negrete-Urtasun *et al.*, 1999).

palH encodes the predicted transmembrane protein PalH, candidate for sensor protein of ambient pH. PalH contains seven transmembrane domains and a long, hydrophilic C-terminus located in the cytosol. These analogies have raised the possibility of the involvement in pH signalling of G-protein coupled receptors (GPCRs) (Herranz *et al.*, 2005), a group of transmembrane receptors involved in transmitting outside stimuli inside the cells.

palF encodes the non-metazoan arrestin protein PalF, representing the first of its kind identified in fungi (Herranz *et al.*, 2005). Metazoan arrestins are known to down-regulate or facilitate the signalling from seven-TMD receptors to downstream regulatory proteins (Lefkowitz and Shenoy, 2005). The hydrophilic C-terminal part of PalH interacts strongly with the arrestin-like protein PalF. *palF* and *palH* mutations preventing this interaction prevent pH signalling as well (Herranz *et al.*, 2005). These findings strongly indicate PalH as one, perhaps the only, essential component of a plasma membrane receptor.

palI encodes the predicted transmembrane protein PalI, as well candidate for sensor protein of ambient pH, which contains three putative membrane-spanning domains with an N-terminal signal peptide and the basic C-terminus facing the cytosol (Calcagno-Pizarelli *et al.*, 2007). Unlike the null mutants of other *pal* genes, null *palI* mutants grow, though poorly, at alkaline pH (Denison *et al.*, 1995), suggesting an important, but not essential role for PalI in pH signalling. The function of PalI is suggested as assisting the plasma membrane localisation of PalH (Calcagno-Pizarelli *et al.*, 2007) by three possible mechanisms, which are still under investigation, namely down-regulation of PalH endocytosis, up-regulation of PalH recycling or assistance of PalH exit from the Golgi. Co-overexpression of PalI redirects GFP-tagged PalH (PalH-GFP) to the plasma membrane which otherwise, when overexpressed, it is predominantly assembled in internal punctate structures (Calcagno-Pizarelli *et al.*, 2007). Overexpression of PalH also allows almost wild type growth of *palI* mutants at alkaline pH, as expected if in these mutants the physiological quantity of PalH is unable to populate sufficiently the plasma membrane without the assistance of PalI (Calcagno-Pizarelli *et al.*, 2007). Each of the three possibilities could require an interaction between PalH and PalI, either direct or indirect, but this has not been investigated (Peñalva *et al.*, 2008).

Recent work has shown an unexpected role in pH signal transduction for most, but not all, the components of the multivesicular body pathway cargo-sorting protein complexes. Endocytosis is a process, occurring in every eukaryotic cell, by which cells internalize portions of their lipid membrane with embedded proteins. After the internalisation in endocytic vesicles, membrane proteins (e.g. plasma membrane receptors, ion channels or nutrient uptake systems) are recycled from endosomal compartments to the plasma membrane, or sent to the vacuole, the fungal equivalent of the metazoan cell lysosome, for proteolytic degradation. Initially this mechanism was associated with the down-regulation of plasma membrane receptors, but plasma membrane receptors do not always reach the vacuole but instead stay in the endosome suggesting this association could promote, rather than prevent, signalling, as shown by a growing number of examples. Among these, there is the pH-signalling pathway, where the positive-acting association between endocytosis and

signalling putatively connects two spatially separated complexes, located at the plasma membrane and on endosomal membranes (Di Fiore PP, 2001; Katzmann *et al.*, 2002).

The proposed endosomal membrane complex comprises PacC, a cysteine protease of the calpain family PalB (Denison *et al.*, 1995), a scaffold PalA (Peñalva and Arst Jr, 2004) and endosomal components. *palB* encodes the protease PalB, showing similarity to calpains (Denison *et al.*, 1995). Calpains are calcium-activated cysteine proteases, catalysing the modifications of substrates, such as transcription factors (Hirai *et al.*, 1991). Although it shows no similarities with other domains in conventional calpains (Sorimachi *et al.*, 1997), at the time of its discovery, PalB was the first example of a calpain involved in a specific signal transduction pathway. *palA* encodes the protein PalA, whose mammalian homologue AIP1/Alix interacts with the apoptosis-linked protein ALG-2, recognising the protein-protein binding motif called YPXL/I (Vincent *et al.*, 2003). PacC contains two of these motifs next to the signalling protease cleavage site (Vincent *et al.*, 2003). *palC* encodes the protein PalC, the last component of the ambient pH signalling pathway to be characterised (Galindo *et al.*, 2007). PalC is distantly related to *Saccharomyces cerevisiae* pheripheral endosomal sorting complexes required for transport III (ESCRT-III) protein Bro1p.

pH signal transduction, culminating with PacC cleavage by the signalling protease, requires the binding of PalA to the two YPXL/I motifs at either side of the signalling box in $PacC^{72}$ (Vincent *et al.*, 2003). The Bro1 domain-containing protein PalA, like its mammalian homologue AIP1/Alix, interacts also with Vps32p/Snf7p[2], a component of the endosomal complex required at a late stage in the multivesicular body pathway (Vincent *et al.*, 2003). Work with *S. cerevisiae* suggests a role for this protein in the pH signal transduction pathway. PalA might serve as an adapter to link PacC to a multiprotein complex on the cytosolic side of the endosomal membrane (Xu and Mitchell, 2001; Xu *et al.*, 2004). PalB is a cysteine protease of the calpain family, most likely the signalling protease, which removes the negatively acting C-terminus to form $PacC^{53}$ (Mingot *et al.*, 1999; Denison *et al.*, 1995; Sorimachi *et al.*, 1997). PalB has been excluded as the protease effecting the second (processing) proteolysis of PacC, since a $palB^-$ mutant is not able to prevent the processing of a $pacC^-$ mutant lacking the 214 C-terminal residues (Denison *et al.*, 1995). In *S. cerevisiae*, a demonstrated interaction between Vps32p and the yeast PalB homologue Rim13p suggests

[2] Following *S. cerevisiae* nomenclature, *S. cerevisiae* gene names are instead italicized and in upper case, loss-of-function mutants in lower case and italicized and proteins non-italicized, starting with an upper case letter and ending with 'p'.

that Vps32p might act like a scaffold in the protein complex in which Rim20p/PalA recruit the protease Rim13p/PalB to its Rim101/PacC substrate (Ito *et al.*, 2001).

Understanding the links between the two complexes has been possible with the recent works on PalF and PalC, until then the most enigmatic of the pH-signalling proteins (Herranz *et al.*, 2005; Galindo *et al.*, 2007). PalF is phosphorylated and multi-ubiquitinated depending on alkaline ambient pH in a PalH- and partially PalI- but not PalA-, PalB-, PalC-dependent manner (Herranz *et al.*, 2005). The participation of the arrestin-like protein PalF in this pathway strongly supports the involvement of endocytosis for pH-signal transduction, because mammalian arrestins specifically bind to the seven-TMD receptors promoting their endocytosis (Lefkowitz and Shenoy, 2005). As demonstrated by PalC-GFP localisation experiments, in alkaline conditions PalC is recruited and assembled in puntate structures associated with the plasma membrane; these cortical punctuate structures have been shown to depend on the presence of PalH but not of PalA and therefore hypothesised to be the sites of PalH-PalF signal-dependent interactions (Galindo *et al.*, 2007). PalC is therefore likely to act later in the pH signalling pathway than PalH but earlier, or concomitant with PalA action. As shown by two-hybrid interaction assays, PalC contains a Bro1-like domain supporting its interaction with Vps32 and this interaction has been demonstrated to be essential for pH signalling (Tilburn *et al.*, 1995; Galindo *et al.*, 2007). Given its ability to localize in cortical puntate structures and to bind to Vps32, PalC has the expected characteristics required to link the two complexes involved in pH regulation. As recently suggested in Peñalva *et al.*, 2008, an attractive hypothesis is that, after PalF-mediated internalisation, the plasma membrane complex recruits PalC, which functions as a guide to the endosomal membranes containing PalA and PalB.

PacC^{27} binds to target sites in the promoter of genes expressed preferentially at alkaline ambient pH to activate their expression and to target sites of those genes preferentially expressed at acidic ambient pH to prevent their expression (Espeso and Penalva, 1996; Espeso and Arst Jr, 2000; Tilburn *et al.*, 1995). The main categories in which identified ambient pH-regulated *A. nidulans* genes are classified are three: those encoding secreted enzymes (*pacA, xlnA, xlnB, abfB*), those encoding permeases (*gabA*), and those encoding enzymes involved in the synthesis of exported metabolites (*ipnA*) (Penalva and Arst Jr, 2002; Peñalva and Arst Jr, 2004). Two new categories have been added recently: enzymes involved in transcriptional modification of secreted enzymes and enzymes catalysing reactions to yield energy (Peñalva *et al.*, 2008). Each of these genes contains multiple consensus sites in the promoter region for the recognition by PacC. The regulation of the genes *ipnA* and *gabA* has been studied extensively in *A. nidulans*, demonstrating the ability of

PacC of acting either as an activator or a repressor of gene expression. *ipnA* encodes the isopenicillin N synthetase, whose expression is directly activated by PacC in alkaline conditions (Espeso and Penalva, 1996). *gabA* encodes the GABA permease, whose expression is instead repressed by PacC as consequence of the competitive binding for overlapping target sites with the transcription factor IntA, positive regulator of the expression of ω-amino acids (Espeso and Arst Jr, 2000).

Significantly, *pacC* is itself preferentially expressed at alkaline pH, following a mechanism of positive feedback that amplifies the response to alkaline conditions (Tilburn *et al.*, 1995). Recent works include also genes involved in the siderophore biosynthesis pathway (Eisendle *et al.*, 2004). The expression of the genes *sidA*, *mirA* and *mirB*, involved in siderophore biosynthesis and iron uptake, has been demonstrated to depend both on iron and pH control. The consensus sites for PacC and SreA, the iron regulator, do not overlap in these genes, indicating the independence of the two regulatory pathways, because the two transcription factor do not compete for the same binding site (Eisendle *et al.*, 2004).

1.3.2 What is known about pH signalling in the other fungal species and its role in fungal virulence?

Homologues of *A. nidulans pacC* have been identified in numerous filamentous ascomycetes, such as *A. niger* (MacCabe et al., 1996), *A. oryzae* (Machida *et al.*, 2005), *A. fumigatus* (Nierman *et al.*, 2005), *Penicillum chrysogenum* (Suarez and Penalva, 1996), *Acremonium chrysogenum* (Schmitt et al., 2001) and *Sclerotinia sclerotiorum* (Rollins and Dickman, 2001). The regulatory system has also been demonstrated to be present in the budding yeast *S. cerevisiae* (Su and Mitchell, 1993a; Su and Mitchell, 1993b) and in the two dimorphic yeast *Candida albicans* (Davis *et al.*, 2000b) and *Yarrowia lipolytica* (Lambert *et al.*, 1997), where *pacC* homologue is called *RIM101*. In fungi, one of the main conserved transduction pathway involved in adaptation to environmental pH is focused on the proteolytical activation of PacC/Rim101p. Fungal pathogens share the necessity to respond to chemical and physical stresses to accomplish infection and the appropriate response to ambient pH is fundamental for fungal virulence in plants, insects and animals.

Initially, the importance of pH adaptation during mammalian infection was shown in *C. albicans* (De Bernardis et al., 1998; Davis et al., 2000a; Davis, 2003). It was demonstrated that *C. albicans* virulence is attenuated according to the pH of the host niche (systemic or vaginal colonisation are possible) in the absence of the pH regulated cell surface glycoproteins Phr1 and Phr2, which are functionally redundant but essential for growth (De

Bernardis *et al.*, 1998). For this opportunistic pathogen, the ability to shift between the two different morphological forms is essential for virulence and environmental pH has been demonstrated to function as a powerful signal for morphological differentiation. Yeast growth is favoured at acidic pH, whereas hyphal growth is favoured in alkaline or neutral conditions (Davis, 2003). Highlighting the role of *CaRIM101* in *C. albicans* pathogenesis, the Δ*rim101* mutant shows significant reduction in virulence in a mouse model of systemic candidiasis and impaired kidney damage compared to the wild type. Since this pathway is not present in mammals, it could represent not only an important contribution to fungal virulence but also a novel target for the development of antifungal therapies. To support the targeting of pH adaptation aiming to inhibit fungal growth in the host, studies in *S. cerevisiae* have shown that the perturbation of the pH regulatory system determines the hypersensitivity to fluconazole (Parsons *et al.*, 2004).

As previously introduced, *Aspergillus* pathogenicity is the result of a multitude of attributes that the causative fungi possess to deal successfully with the physical conditions within the host and its defences. A significant role is likely played by adaptation to physiological pH, over the wide range of changes infections *Aspergillus* species have to face, not only within the pulmonary niche but also as a result of phagocytosis by macrophages or ingestion by neutrophils and exposure to their vacuole contents (Ibrahim-Granet *et al.*, 2003; Levitz *et al.*, 1999; Newman, 1999; Reeves *et al.*, 2002). First evidence of the coupling of virulence and pH signal transduction was provided by studies of murine intraperitoneal administration of *A. nidulans*, marking the correlation between the production of alkaline phosphatase and virulence (Purnell and Martin, 1971). This species is of clinical importance for patients with CGD, an inherited condition characterised by the inability of the phagocytes to generate reactive antimicrobial oxidants (Dotis *et al.*, 2003; Dotis and Roilides, 2004; Johnston, 2001; Segal *et al.*, 1998). Recently it has been demonstrated that murine aspergillosis requires integrity of *A. nidulans pacC* (Fig. 1.4): elimination of *A. nidulans* PacC strongly attenuates virulence in neutropenic mice (Bignell *et al.*, 2005). Not only the presence of *A. nidulans pacC*, but also its proteolytic processing and the upstream Pal proteins mediating pH-sensing are essential for murine pathogenicity. Mutants where the ambient pH signal transduction pathway is blocked or PacC proteolytic processing is prevented are attenuated for virulence and the infection in neutropenic mice is characterised by reduced growth *in vivo* and reduction of inflammatory infiltrate (Bignell *et al.*, 2005). On the contrary, constitutive activation of PacC determines extensive tissue invasion by the fungal mycelia, leading to an increased murine mortality (Bignell *et al.*, 2005).

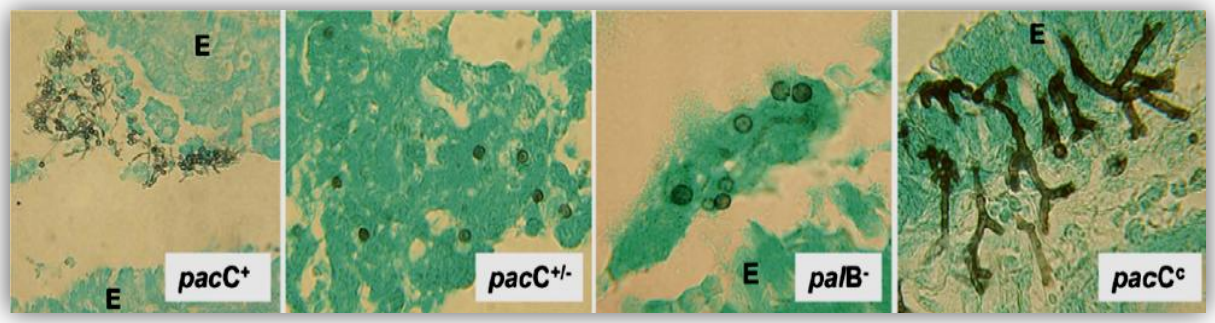


Fig. 1.4: Histological analysis to compare the growth of *A. nidulans* wild type strain (*pacC*$^{+}$), *pacC*$^{-}$, *palB*$^{-}$, and *pacC*^{c} mutants in the neutropenic murine lung. Murine lung sections sampled at 40 h post-infection, paraffin-embedded and stained with Grocott's Methenamine Silver. (E) bronchiolar epithelium. From Peñalva *et al*., 2008.

The components for alkaline adaptation in *A. nidulans* are highly conserved in *A. fumigatus* (Arst, 2003; Bignell *et al.*, 2005; Peñalva and Arst Jr, 2004). However, the mechanism leading to the activation of this regulatory pathway has not yet been characterised extensively in *A. fumigatus* and especially the elucidation of its role during infection is still unexplored by the current literature. Because of the conserved nature of the pathway throughout the fungal kingdom, proteins involved in pH adaptation in *A. fumigatus* might indeed represent novel targets for the development of antifungal drugs, in particular if localised in the plasma membrane or involved in plasma membrane protein-protein interactions.

1.4 Fungal DNA microarray studies

Microarrays are a powerful instrument to monitor relative expression levels for a multitude of genes at the same time and permit therefore the characterisation of various processes. Thus, the development of microarray represents one of the most important and innovative scientific invention in the 1990s (Schena *et al.*, 1995; Shalon *et al.*, 1996). DNA microarrays consist of grids of nucleic acids (probes), synthesised and immobilised on a solid substrate (slide) as discrete features or spots. Each slide is therefore composed of tens of thousands of spots, each containing tens of millions of identical DNA molecules. According to the microarray terminology, the target is the sequence of interest, fluorescently labelled and hybridised to the probe slide. The hybridisation results in an increase in fluorescence over the background level measured by a fluorescent scanner (Miller and Tang, 2009). Microarrays

differ according to the nature of the probe, the support used and the method for hybridisation and detection. mRNA level detection relies upon the hybridisation of two complementary single-stranded nucleic acid molecules (either DNA or RNA). In the microarray analysis, this principle is applied on a large scale permitting the analysis of thousands of gene transcripts in parallel. DNA microarrays have been utilised for a variety of applications, including quantitative (gene expression) and qualitative (diagnostic) ones. The most popular use is probably for the comparison of gene expression levels in two different samples or the same sample in two different conditions via differential labelling (usually with the fluorochromes Cy3 and Cy5) and competitive hybridisation to the same slide.

DNA microarray analysis is in general a complicated process, articulated in multiple stages, all requiring a high level of organisation, skills and time to assure the best results in measuring, comparing and interpreting gene expression levels properly. A typical DNA experiment consists of two major stages: material processing and data collection, and information processing. The first stage involves the array preparation, the sample extraction and labelling, the hybridisation of the labelled extracts to the array, and the image acquisition. The second stage is basically the interpretation of the results, with the conversion of the image(s) in quantitative measurements of fluorescent intensities, the data normalisation and integration, and the analysis.

1.4.1 Review of the relevant fungal DNA microarray studies

Since the development of DNA microarrays, multiple studies in filamentous fungi have been based on the comparison of gene expression levels. In 2007 the number of these studies was estimated to be fifty (Breakspear and Momany, 2007), but further studies are now frequent due to the recent completion of several fungal genomes. The first reported application of DNA microarrays for the fungal kingdom was for the budding yeast *S. cerevisiae* (DeRisi *et al.*, 1997; Lashkari *et al.*, 1997), but since then studies in filamentous fungi have covered a variety of biological processes, such as metabolism and secretion of secondary metabolites, development and pathogenesis (Breakspear and Momany, 2007).

Within the context of *A. fumigatus* biology and pathogenicity, some interesting studies have focused on the mechanisms of adaptation to the physical conditions within the host and its defences. For example, as already mentioned, the secretion of secondary metabolites is an important virulence factor for the *Aspergillus* species. Because of its crucial role in the regulation of secondary metabolite production (Bok *et al.*, 2005), LaeA has been the subject of multiple DNA microarray studies. The transcriptional profiles of the Δ*laeA* mutant in

comparison with the respective wild type have been studied both *in vitro* (Perrin *et al.*, 2007) and *in vivo* using a neutropenic murine model of IPA (Cairns *et al.*, unpublished). In particular, the *in vitro* transcriptional profiling analysis has indicated that LaeA influences the expression of at least 9.5% of *A. fumigatus* genome and between 20 and 40% of the genes involved in secondary metabolite production (Perrin *et al.*, 2007). Among other aspects crucial for *A. fumigatus* adaptation to the host, thermotolerance has also been investigated, comparing *A. fumigatus* transcriptional profiling for temperatures typical of pathogenic (37°C) and non-pathogenic (30°C and 48°C) environments (Do *et al.*, 2009; Nierman *et al.*, 2005). Host temperature has been excluded as the only determinant of virulence-related genes expression, as no genes previously identified as necessary for virulence were demonstrated to be up-regulated at 37°C (Nierman *et al.*, 2005). Interestingly, an inverse correlation between heat-shock and central metabolic pathway genes has been revealed, i.e. regulation of metabolic genes by heat shock proteins appear stronger at 37°C than at 48°C, suggesting a feed-forward loop of regulation by the first category on the second one (Do *et al.*, 2009). Accordingly, exit from dormancy was associated with the change from fermentative to respiratory metabolism (Lamarre *et al.*, 2008). Finally, an interesting DNA microarray analysis focused on *A. fumigatus* response to the attack by host cells, comparing gene expression from conidia and hyphae exposed to neutrophils, both from healthy donors and from patients with CGD and identifying oxidative stress, reductive iron assimilation and metabolic reprogramming as crucial in the context of adaptation to and surviving host attack (Sugui *et al.*, 2008). DNA microarray analyses of *A. fumigatus* during murine infection are emerging as a consequence of overcoming the difficulties in obtaining RNA from the sites of infection in sufficient quantity. The most interesting application for the purpose of this study is the previously cited transcriptional analysis of *A. fumigatus* in the early stages of infection in a neutropenic murine model of IPA (McDonagh *et al.*, 2008a). Measuring more than 9,000 *A. fumigatus* genes, this study identified iron limitation, nitrogen limitation and alkalinity as prominent stresses imposed by the host in the early stages of infection and it has showed the preferential clustering of genes involved in infection and their preferential localisation in the telomeres.

Adaptation to environmental pH for fungal species and the role of this pathway in virulence have been extensively studied via DNA microarrays especially in *S. cerevisiae* and *C. albicans*. Time course analyses have followed temporal scale gene expression during transitions from normal pH to mid-alkaline (pH 7.6) (Serrano *et al.*, 2002) and alkaline conditions (pH 7.9-8.0) (Causton *et al.*, 2001) in *S. cerevisiae* and from normal pH to alkaline (pH 7.9-8.0) (Bensen *et al.*, 2004) conditions in *C. albicans*. Several genes involved in pH

homeostasis were up-regulated, but also genes involved in cell wall biogenesis and in the uptake, mobilisation and utilisation of important ions such as calcium, iron and copper, to counter the limited bioavailability of nutrients. Recently, a similar study has been performed in *A. fumigatus*, delineating the temporal response of this species to an alkaline shift *in vitro* and comparing it to high concentration of Ca^{2+} (Loss *et al*., unpublished).

1.5 *Saccharomyces cerevisiae*: a model organism for fungal research

The yeast *S. cerevisiae* has been largely used as a model system to investigate biological processes such as cell cycle, signalling, DNA replication and protein translation. In the context of this study, it has been also demonstrated to be an important tool for the investigation of protein-protein interactions.

The ascomycete *S. cerevisiae* was first described by Hansen in 1883 and is commonly isolated from human, mammals, birds, wine, beer, fruits, trees, plants and soil. The name "*Saccharomyces*" from Latinised Greek combines the words "*saccharo*" for sugar and "*myces*" for fungus and means "sugar mold" or "sugar fungus", whereas *cerevisiae* comes from Latin and means "of beer". This microorganism conducts the most common type of fermentation and for this reason has been, since ancient time, the most useful yeast because of its application in baking and brewing. Thus, it is also known as "baker's" or "brewer's" yeast. The shape of *S. cerevisiae* cells is round to ovoid and the diameter varies from 5 to 10 µm. *S. cerevisiae* can exist in the haploid or diploid form, with one or two copies of the genome respectively. In either case, it reproduces by forming buds by mitosis and from this derives the denomination "budding yeast". In the haploid form, cells can occur in two different mating types (a or α) and the type depends on the expression of genes in the active mating type locus. Haploid cells can survive indefinitely in this form. However, in case of contact with cells of opposite mating types, haploid cells can fuse to enter the diploid phase of the cell cycle. Diploid cells are more resistant to stressful conditions or nutrient starvation and undergo meiosis with the formation of four haploid spores contained in asci. In more favourable conditions, the germination of the spores generates four haploid yeast cells, two for each mating type.

S. cerevisiae possesses several traits required for a good model organism, such as small size, short generation time, easy of manipulation and genetics, and conservation of mechanisms with higher organisms. In addition, *S. cerevisiae* can be easily cultured on defined media at low cost. In its haploid form, *S. cerevisiae* is small and has a short

generation time (doubling time 1.5–2 hours at 30°C). The simple life cycle is ideal for classical genetic analysis; detailed genetic maps of the haploid set of sixteen chromosomes are therefore available. *S. cerevisiae* was the first eukaryotic organism whose genome was completely sequenced (Goffeau *et al.*, 1996). The genomic sequence was released on April 24, 1996 and since then continuously updated in the *Saccharomyces* Genome Database (SGD). This database is highly annotated and cross-referenced and represents an important resource for the scientific community. Another important *S. cerevisiae* database is held by the Munich Information Center for Protein Sequences (MIPS). *S. cerevisiae* genome is one of the smallest among well studied eukaryotes; it is composed of about 12.2 Mb, encoded on 16 chromosomes. The 16 chromosomes contain 6,275 genes but only about 5,800 of these are believed to be functional genes. The percentage of homology with human genes is estimated to be about 23%, therefore many proteins important in human biology were first discovered by studying their homologues in yeast. Interestingly, it can be transformed permitting the addition or deletion of genes of interest through homologous recombination. An interesting example of the easy genetic manipulation achievable in *S. cerevisiae* is the construction of multiple genome-wide gene knock out (KO) collections (Winzeler *et al.*, 1999; Winzeler *et al.*, 2000). Of particular interest for this study is the *Saccharomyces* Genome Deletion Project (SGDP) knockout library that contains 4811 disruption mutants for most of the non-essential *S. cerevisiae* genes. Furthermore, *S. cerevisiae* presents the same complex internal cell structure of plants and animals but without the high percentage of non-coding DNA typical in higher eukaryotes.

S. cerevisiae has also been the organism of choice for methods that detect novel protein-protein interactions. Indeed, for the purpose of this study, *S. cerevisiae* is confirmed as a crucial model organism for studying conserved features of fungal pH regulatory pathway. As introduced in the previous paragraphs, important contributions to the understanding of the pH regulation were achieved by studies in *S. cerevisiae*. Among these, there is the first demonstration of a PalA family member to interact with a PacC family member and the first evidence of the involvement of the endocytic pathway in pH transduction and in particular of Vps32p/Snf7p (Arst, 2003; Xu and Mitchell, 2001; Xu *et al.*, 2004; Hayashi *et al.*, 2005).

1.5.1 pH regulation in *S. cerevisiae*

Rim101p, formerly known as Rim1p (regulator of Ime2p) is the *S. cerevisiae* homologue of PacC and has been demonstrated to be a positive regulator of sporulation, invasive growth, ion tolerance and acquisition, alkaline pH adaptation and certain cell wall

characteristics (Denison, 2000; Hayashi *et al.*, 1998; Lamb *et al.*, 2001; Lamb and Mitchell, 2003; Li and Mitchell, 1997). Rim101p was first discovered as a positive regulator of meiosis, via stimulation of the transcription of Ime1p. *IME1* encodes a positive-acting transcription factor, which activates numerous meiotic genes, such as the kinase-encoding gene *IME2* (Su and Mitchell, 1993a; Su and Mitchell, 1993b). Like its *A. nidulans* homologue, Rim101p contains three zinc fingers (Su and Mitchell, 1993b). Similarly to the PacC regulatory pathway, in *S. cerevisiae* the gene products are called Rim13p (the *S. cerevisiae* calpain-like protease) (Futai *et al.*, 1999; Su and Mitchell, 1993a), Rim20p (the protease scaffold) (Xu and Mitchell, 2001), Rim9p and Rim21p (the putative transmembrane proteins PalI and PalH) (Denison *et al.*, 1998; Li and Mitchell, 1997) and Rim8p (the arrestin-like protein)(Su and Mitchell, 1993a). Recently a PalC homolog has been identified in yeast, likely to be YGR122wp (Barwell *et al.*, 2005; Rothfels *et al.*, 2005). Deletion of *RIM101*, *RIM13* or *RIM20* impairs growth at alkaline pH, confirming the essential role of this pathway in yeast alkaline adaptation (Futai *et al.*, 1999; Lamb *et al.*, 2001; Xu and Mitchell, 2001). *rim101*, *rim8*, *rim9* and *rim13* mutations exhibit the same phenotype at neutral conditions, characterised by reduced expression of Ime1p and Ime2p and therefore poor sporulation, poor growth at low temperature and altered colony morphology with smooth colonies (Su and Mitchell, 1993a; Su and Mitchell, 1993b). In addition the same mutants, together with *rim20*, prevented haploid invasive growth (Li and Mitchell, 1997; Xu and Mitchell, 2001).

Rim101p-mediated pH regulation shows some notable differences from the PacC system (Fig. 1.5). First, the proteolytic activation of PacC ortholog Rim101p is mediated by a single cleavage. The processing is executed by the signalling protease Rim13p and eliminates approximately 100 residues from the C-terminus of the protein (Diez *et al.*, 2002; Xu and Mitchell, 2001). As in *A. nidulans*, mutations in the Pal homologues, *RIM8*, *RIM9*, *RIM13* and *RIM20* prevent the activation of Rim101p, whereas if Rim101p is truncated a constitutive phenotype results which is epistatic to mutations in *RIM8*, *RIM9* and *RIM13* (Lamb *et al.*, 2001; Li and Mitchell, 1997; Xu and Mitchell, 2001). In addition to Rim9p and Rim21p, in *S. cerevisiae* another transmembrane protein is involved in pH signalling. Dfg16p is predicted to be a seven transmembrane domain protein with a hydrophilic C-terminus and it has been hypothesised to be a GPCR (Barwell *et al.*, 2005). The activation of Rim101p is suggested to occur by Rim8-directed endocytosis either of Dfg16p or Rim21p or of both (Boysen and Mitchell, 2006). Recent findings in *S. cerevisiae* indicate the intersection between the Rim101p and the ESCRT pathways. Eight ESCRT subunits (Snf7p/Vps32p, Vps20p, Snf8p/Vps22p, Vps25p, Vps36p, Vps23p, Vps28p and Vps37p) participate in Rim101 processing. In particular Vps32p has been demonstrated to interact both with Rim20p and

Rim13p and for this reason hypothesised to act as a scaffold, bringing in close proximity all of the components required for Rim101p cleavage (Barwell *et al.*, 2005).

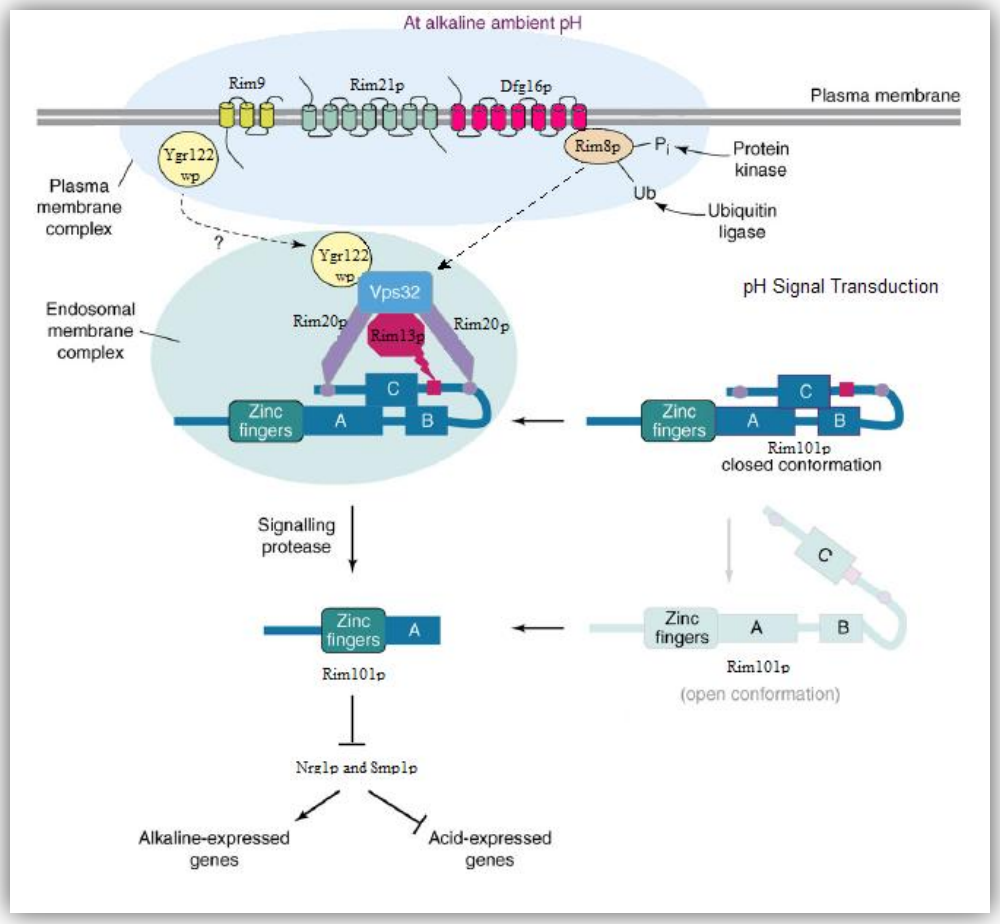


Fig. 1.5: Schematic representation of pH regulation in *S. cerevisiae*. The components for alkaline adaptation in *A. nidulans* are highly conserved in *S. cerevisiae*. However, some differences between the two microorganisms have been demonstrated. The signal for the activation of Rim101p is transmitted from the plasma membrane to the endosomal membrane complex by a process probably involving the Rim8-directed endocytosis of Rim21 and/or Dfg16p and the participation of the product of the gene *YGR122W*, only recently identified as *palC* homologue in *S. cerevisiae*. At alkaline pH, Rim101p is activated by a one step C-terminal proteolytic cleavage corresponding to the first step in PacC processing. Modified from Peñalva *et al.*, 2008.

Environmental pH not only influences *S. cerevisiae* growth, but also its differentiation, invasive growth and meiotic sporulation. The main effect of external alkalinity is the disruption of membrane proton gradients supplying energy for transmembrane transport and the consequent nutrient and ion limitation. Rim101p is therefore principally required for general ion homeostasis. Yeast cells grow faster at acidic than neutral or alkaline pH (Lamb *et al.*, 2001) and in alkaline conditions the maintenance of homeostasis is ensured by the expression of *PMA1*, which encodes a plasma membrane H^+-ATPase, which hydrolyses ATP

to exclude protons and thereby neutralize the cytoplasm (van der Rest *et al.*, 1995). The proton gradient is necessary for acquisition of solutes from the environment and for the transport of amino acids, nucleotide bases, phosphate and other molecules in symport reactions. The Na^+-ATPase Ena1p, also called Pmr2p, expels Na^+ to generate a gradient utilised for the uptake of other cations (Rodriguez-Navarro *et al.*, 1994). Ena1p is a Na^+-ATPase responsible of the efflux of Na^+, Li^+ and K^+ by exchange with proton and is crucial for environmental pH adaptation as demonstrated by the high increase of its expression in response to lithium, saline and alkaline pH stress (Ruiz and Arino, 2007) and by the phenotype of the *ena1* mutants. These mutants are sensitive to Na^+ and Li^+ cations and show impaired growth at alkaline pH (Garciadeblas *et al.*, 1993; Haro *et al.*, 1991). Finally the vacuolar H^+-ATPase Vma4p is necessary for vacuolar acidification (Stevens and Forgac, 1997). The essential role of these homeostatic mechanisms is highlighted by the inability of null mutants lacking these pumps to grow in alkaline conditions and/or in presence of high concentrations of extracellular cations (Lamb and Mitchell, 2003). Coherent with the necessity for pH homeostasis, a new role for the Rim101p pathway has been identified in *S. cerevisiae* i.e. the tolerance to weak acid-induced stress at constant pH (pH 4.0) (Mira *et al.*, 2008), where the analysis of genes susceptible to inhibitory concentrations of propionic acid has revealed a correlation between the resistance to propionic acid and other weak acid, and Rim101p processing; the deletion of each of the genes participating to Rim101p processing leads to strains sensitive to propionic acid.

RIM101p directs the adaptation to environmental pH in *S. cerevisiae*, via a conserved regulatory pathway homologous to that described for PacC in *A. nidulans*. Whereas PacC acts both as a transcriptional activator for alkaline-expressed genes (Tilburn *et al.*, 1995) and as a transcriptional repressor for acidic-expressed genes (Espeso and Arst Jr, 2000), Rim101p appears to function only as a repressor, acting in an indirect manner by repressing the expression of genes encoding transcriptional repressors, particularly *NRG1* and *SMP1* (Lamb *et al.*, 2001; Lamb and Mitchell, 2003). The action of Rim101p on the two repressors is demonstrated by the ability of *nrg1*$^-$ mutations to rescue the sensitivity to alkaline pH, NaCl and LiCl of the *rim101*$^-$ mutant, as well as *smp*$^-$ mutations to rescue the sporulation and invasion phenotype in the *rim101*$^-$ mutant (Lamb and Mitchell, 2003). In particular, Nrg1p is a repressor involved in the control of the expression of several glucose-repressed genes and invasive growth (Vyas *et al.*, 2005). The rescue of the alkaline-, NaCl- and LiCl- sensitive phenotype in the *nrg1*$^-$ *rim101*$^-$ mutant has been hypothesised as due to the de-repression of the sodium pump ENA1p (Haro *et al.*, 1991; Tenney and Glover, 1999), whose expression levels are increased in *nrg1*$^-$ mutants, even in absence of stress (Lamb and Mitchell, 2003).

Confirming the link between Rim101p, Nrg1p and Ena1p, several binding sites have been identified in the promoter region of the Ena1p, in particular two for Ngr1p and one for Rim101p (Ruiz and Arino, 2007). Rim101p has been therefore demonstrated as a regulator of pump expression and the reduction of ion pump activity may explain the phenotype observed for *rim101*$^{-}$ in neutral conditions (Lamb *et al.*, 2001). As demonstrated by the evidence that *ENA1* expression is also induced by NaCl, the regulation the Na^{+}-ATPase is not only Rim101p mediated but it involves other pathways such as the HOG (high osmolarity glycerol) osmoresponsive pathway and the calcium-calcineurin-Crz1p-mediated pathway (Ruiz and Arino, 2007).

An interesting study using open reading frame macroarray hybridisation identified 71 genes whose transcripts were at least 2.1-fold more abundant when cells were shifted from neutral to alkaline pH rather than to acidic pH (Lamb *et al.*, 2001). Among these, several genes are involved in phosphate, iron or copper uptake and utilisation (*CTR3*, *FRE1*, *PHO11*/12, *PHO84*, *ARN4*/*ENB1*) and significantly the two ion pump genes *ENA1* and *VMA1*, confirming the correlation between ion homeostasis and alkaline adaptation. *CTR3* and *FRE1* are targets of the copper-responsive transcription factor Mac1p (Jungmann *et al.*, 1993; Pena *et al.*, 1998); *PHO11/PHO12* and *PHO84* are targets of the phosphate-responsive transcription factor Pho4p (Ogawa *et al.*, 1995a; Ogawa *et al.*, 1995b). In general, these genes were classified according to their transcriptional dependence upon *RIM101*, to demonstrate that in yeast alkaline adaptation is not only mediated by the PacC homologue, but by other mechanisms such as the calcium-calcineurin-Crz1p-mediated response (Lamb and Mitchell, 2003; Serrano *et al.*, 2002). Three classes of alkaline response genes have been identified: genes independent of the Rim101p pathway (*PHO11*/*12*, *PHO84*, *CTR3*, *FRE1* and *TIS11*), weakly dependent on Rim101p (*ENA1* and *NRG1*) and strictly dependent on Rim101p (*ARN4*, *YAR068W*/ *YHR214W*, *YOL154W* and *WMA4*) (Lamb *et al.*, 2001). Arn4p is involved in iron uptake and in particular imports a bacterial siderophores-iron complex, facilitating competition with bacteria in alkaline conditions (Heymann *et al.*, 2000; Lamb *et al.*, 2001). *YOR154W* is a target of the zinc-responsive transcription factor Zap1p (Lyons *et al.*, 2000).

Unlike *pacC*, *RIM101* does not seem to be alkaline-expressed (Lamb and Mitchell, 2003). To avoid an increasing response to alkaline pH, *S. cerevisiae Rim8* expression is subjected to a negative-feedback loop by the processed form of Rim101p (Lamb and Mitchell, 2003), as recently demonstrated for *A. nidulans palF* (Munera-Huertas, PhD thesis).

1.6 Membrane protein-protein interactions: biological roles, limits of available detention techniques and a new innovative investigative approach

Protein-protein interactions are intrinsic to and crucial for almost every cellular process within a cell and the formation of most cellular structures result from complex interactions between many different proteins. Crucial membrane proteins are pumps, channels, pores and transporters involved in exchange of membrane-impermeable molecules between the cellular compartments and the extracellular environment. Transmembrane receptors are involved in the sensing of environmental changes to activate specific cellular adaptation responses, usually via intermediate intracellular proteins. Thus, membrane protein-protein interactions are hugely involved in the organisation of living cells. Often identification of interacting partners permits inference of function of the protein itself. Because of their essential role and accessibility as potential drug targets, membrane protein-protein interactions have been among the most difficult aspects of biology to be investigated. It was estimated that around 50% (500) of the current known drug targets are either membrane receptors or ion channels (Reiss, 2001).

Genome analyses surprisingly revealed that approximately a third of the predicted proteins of an organism are localised or anchored to the plasma membrane (Auerbach *et al.*, 2002; Goffeau *et al.*, 1996). Many biological issues can be addressed by studying protein-protein interactions, such as the identification and characterisation of novel gene products or the discovery of structural and functional motifs. Traditionally, the tools available to analyze protein-protein interactions in multicellular organisms have been restricted to biochemical approaches. Much has been learned through biochemical methods, such as coimmunoprecipitation, and cross-linking proteins and thereafter cofractionation by chromatography. However, these approaches can be difficult to set up and time-consuming to carry out, generally requiring extensive optimisation. In addition they are characterised by some limitations i.e. they are destructive methods and consequently do not give live-cell dynamics. Besides membrane proteins are very unsuitable for biochemical studies due to their hydrophobic nature, which makes protein isolation difficult and so complicates the determination of protein complex composition. Several interacting proteomic techniques have been developed in the recent years to detect membrane protein-protein interactions, such as Fluorescence Resonance Energy Transfer (FRET) (Miyawaki *et al.*, 1997), β-lactamase protein fragment complementation assay (Galarneau *et al.*, 2002) and β-galactosidase complementation assay (Rossi *et al.*, 1997). In addition, the combination of conventional

affinity tagging methods and mass spectrometry (MS) has been demonstrated to be adaptable to the high-throughput analysis of yeast protein complexes (Gavin *et al.*, 2002; Ho *et al.*, 2002).

The limits of biochemical methods have been partially circumvented with the development of protein library screening techniques such the yeast two-hybrid system (Fields and Song, 1989). The analysis of protein-protein interactions through genetic selection in yeast has several important advantages. First, no optimisation of binding or washing conditions is required, because the interactions are detected *in vivo*. In addition, proteins of interest do not need to be purified. But more interestingly for the purposes of this study, novel protein-protein interactions can be relatively easily selected from a pool of potential interaction partners (e.g. a cDNA expression library) and genetic screening systems yield not only information on the interaction itself but also directly provide the cDNA encoding the novel interaction partner (e.g. they give information on the region of the protein specifically involved in the exposed interaction). Genetic selection for protein-protein interactions in yeast was initially developed by Fields and Song (1989) with the yeast two-hybrid system (Fields and Song, 1989). To test for protein interactions, this method employs the modular nature of transcription factors that can be separated into a DNA-binding domain and a transcriptional activation domain. If two interacting proteins are fused to these separated domains, the protein interaction will bring the two portions of the transcription factor together and hence reconstitute its activity. The interaction between the two proteins takes the transcription factor to a specific sequence of DNA upstream of a reporter gene, whose expression is therefore activated. Since its invention, this method has rapidly become the choice for identifying novel protein-protein interactions. However, the limitation of the two-hybrid technique is that the set of detectable protein interactions only occur in the nucleus, near to the reporter gene, so the method is not useful for the study of membrane proteins (Fields and Song, 1989). The features that make membrane proteins unsuitable for the two-hybrid system include not only their propensity to aggregate if not in the lipid bilayer, but also the presence of either specific post-translational modification (such as glycosylation and disulfide bond formation) or intra-membraneous ligand-binding pockets and the possibility of oligomerisation. To overcome the limitation in the yeast two-hybrid assay, a wide range of similar screening systems have followed and one of them is the split-ubiquitin Membrane Yeast Two Hybrid (MYTH), also commercially called DUALmembrane system (Johnsson and Varshavsky, 1994).

1.6.1 The split-ubiquitin Membrane Yeast Two Hybrid (MYTH): an innovative system to investigate membrane protein-protein interactions

As previously described, an intense network of protein-protein interactions is established in fungi for pH sensing and adaptation (for a review Peñalva *et al.*, 2008). These interactions, in particular those taking place in the plasma membrane, might be required for the initial contact between host and fungus and therefore could provide a way to interfere with the first stages of fungal growth. For example, in the absence of either PalH or PalI pH signalling is blocked and PacC is not proteolytically processed (Denison *et al.*, 1998; Negrete-Urtasun *et al.*, 1999).

The split-ubiquitin Membrane Yeast Two Hybrid (MYTH) is based on the complementation between separable domains of ubiquitin (Ub) (Fetchko and Stagljar, 2004; Johnsson and Varshavsky, 1994; Stagljar *et al.*, 1998). This assay has been applied successfully in various studies i.e. to investigate how mutations affect the assembly of fragments of presenilin in the development of the Alzheimer disease (Cervantes *et al.*, 2001) or the interaction between the two yeast proteins α1,2-mannosidase Mns1p and Rer1p in the endoplasmic reticulum (Massaad and Herscovics, 2001) or the intra- and intermolecular interactions between plant sucrose transporters (Reinders *et al.*, 2002). Recently the approach has also been extended to the screening of libraries of NubG-fused inserts to identify novel protein–protein interactions for specific membrane proteins both of yeast and mammalian origin (Snider *et al.*, 2010b; Thaminy *et al.*, 2003).

Ub is a conserved protein of 76 residues that is present in cells both free and covalently linked to other proteins and plays a role in many processes, primarily through protein degradation (Hershko and Ciechanover, 1992), whereby it is usually attached to the N-terminus of proteins as a signal for their degradation by the 26S proteosome. While the target protein is degraded by the 26S proteosome, the ubiquitin motifs are saved from degradation by cellular ubiquitin-specific proteases (UBPs), which cleave ubiquitin from the target protein after the C-terminal residue (Gly76), hence recycling the ubiquitin back to the cytoplasm. The inventors of this system (Fig. 1.6) found that yeast ubiquitin can be divided into two halves, called Nub (for N-terminal ubiquitin) and Cub (for C-terminal ubiquitin) and that their strong affinity can be abolished by a single amino acid exchange in the N-terminal portion (mutated Nub is termed NubG) (Fetchko and Stagljar, 2004; Johnsson and Varshavsky, 1994; Stagljar *et al.*, 1998).

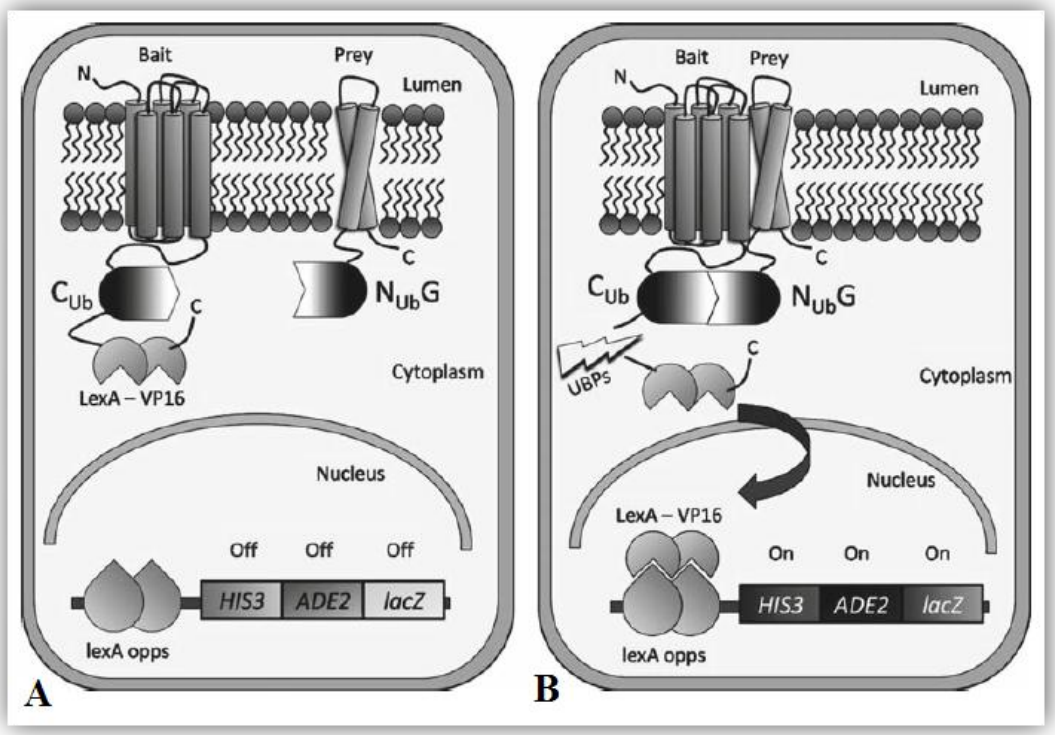


Fig. 1.6: **The split-ubiquitin Membrane Yeast Two-Hybrid (MYTH) system.** (A) A point mutation in the N-terminal part, therefore called NubG from the amino acidic substitution obtained, completely abolishes the affinity between the two halves of the ubiquitin. A membrane protein of interest X is fused to Cub and the hybrid transcriptional factor LexA-VP16, whereas another protein Y, either membrane or cytoplasmic, is fused to the NubG moiety. (B) If interaction occurs between X and Y, split-ubiquitin is reconstituted and the hybrid transcription factor LexA-VP16 is released. From Kittanakom *et al.*, 2009.

A membrane protein of interest, termed the bait, is fused to the C-terminal half of Ub, Cub. A second protein of interest, termed the prey, is fused to the mutated N-terminal half of ubiquitin, NubG. If the two proteins are in sufficiently close proximity, NubG and Cub are forced to reconstitute split-ubiquitin, which is immediately recognised by the UBPs. The polypeptide chain is therefore cleaved between Cub and the reporter protein LexA-VP16, the latter being released from the membrane and translocated to the nucleus where it binds the LexA operators situated upstream of reporter genes. The reporter protein LexA-VP16 is a hybrid transcription factor, composed of the bacterial LexA protein and the *Herpes simplex* VP16 transactivator protein. Thus, the reconstitution of the split-ubiquitin converts the protein interaction into a transcriptional output.

As well as for small-scale and specific membrane protein-protein interaction studies, the methodology can be adapted for high-throughput screening of cDNA prey libraries, as recently demonstrated (Gisler *et al.*, 2008; Lissanu Deribe *et al.*, 2009; Scheper *et al.*, 2003b; Thaminy *et al.*, 2003; Paumi *et al.*, 2007).

1.7 *In vivo* bioluminescence imaging (BLI)

The Split-ubiquitin MYTH assay cannot inform on the dynamics of protein interactions in the native organism *A. fumigatus*, or on the relevance of tested interactions during infection. Bioluminescence imaging (BLI) can allow the *in vivo* study of establishment and manifestation of infection, providing information on its inception and progress in real time. BLI has been successfully applied to a multitude of microorganisms, including several bacteria species (Glomski *et al.*, 2007; Karsi and Lawrence, 2007; Sjolinder and Jonsson, 2007), viruses (Hutchens and Luker, 2007) and eukaryotic parasites like *Toxoplasma*, *Leishmania*, and *Plasmodium* species (Dellacasa-Lindberg *et al.*, 2007; Franke-Fayard *et al.*, 2006; Hutchens and Luker, 2007; Saeij *et al.*, 2005). Successful imaging of fungal species during infection provides real time data on location and distribution of infectious particles, which is currently unobtainable. In addition, repetitive imaging of single mice dramatically reduces the number of animals required for experimentation.

1.7.1 Definition of bioluminescence and i*n vivo* bioluminescence imaging (BLI)

The application of an internal biological source of light, called luciferase, as a marker for cells, pathogens or genes, represents a resourceful approach to gain biological information *in vivo*, but externally in a non-invasive way (Doyle *et al.*, 2004). In the case of animal models of infectious disease, BLI gives not only insights into the establishment and the development of the disease, but also about the means by which pathogens avoid host defences during the infection. Bioluminescence is a naturally occurring enzyme reaction whereby light is produced by enzyme-mediated chemical conversion of a substrate usually through an intermediate highly energised state. This process occurs in multiple organisms from different genera and for various aims, such as to facilitate location of food or for identifying mates (Hastings, 1996). Independent evolution has originated different luciferases and substrates with different colours of emission but in general, these enzymes require energy, oxygen and a specific substrate (commonly known as luciferin) and may also require cofactors for light production. Briefly, to monitor infectious diseases in animal models by BLI, cells are engineered to express a bioluminescent marker; after the induction of light emission through the administration of the appropriate substrates, the bioluminescent photons emitted are able to pass through the tissues and to be detected on the surface of the animal. This provides indication of spatial and temporal localisation, because the signal is detectable

externally using sensitive proton detectors, such as cooled or intensified charge-coupled device (CCD) cameras (Rice *et al.*, 2001).

The first application of bioluminescence to quantify pathogen loads in a non-invasive way was conducted with the bacteria *Salmonella enterica* and the lux operator, which does not require the addition of any substrate (Contag *et al.*, 1995). Subsequently, multiple studies reported the use of luciferase genes from *Photinus pyralis* and *Renilla reniformis*, the latter of which has however been demonstrated to be effective only for cells near to the surface of the animals in analysis (Bhaumik and Gambhir, 2002; Contag *et al.*, 2000; Contag and Stevenson, 2001; Rice *et al.*, 2001; Zhang *et al.*, 2001). Respect to fluorescent markers such as GFP or near-infra red fluorescent dyes, bioluminescence drastically reduces the background due to the intrinsic fluorescence of the animal tissues (Becker *et al.*, 2001; Chishima *et al.*, 1997; Rudin and Weissleder, 2003; Weissleder *et al.*, 1999; Yang *et al.*, 2000).

Photinus pyralis (Firefly) is one of the most well-recognised bioluminescent organisms: the male uses bioluminescence as a way to attract potential mates (Wood *et al.*, 1989). The firefly luciferase (FLuc) is a single polypeptide (550 aa; 62 kDa) and uses the benzothiazole luciferin as substrate along with ATP as energy source and oxygen and Mg^{2+} as cofactor (de Wet *et al.*, 1985; de Wet *et al.*, 1987). Light emission for cells expressing this enzyme and provided with luciferin is yellow-green with an emission peak at 560 nm. Luciferin can be administered to the animal before imaging via intraperitoneal or intravenous injection or oral delivery and it is able to passively diffuse into cells, to spread quickly in the body (Contag *et al.*, 1997), to cross the blood-brain (Rehemtulla *et al.*, 2000; Rehemtulla *et al.*, 2002) and placental barriers (Lipshutz *et al.*, 2001) with no adverse reactions for the animals. Other bioluminescent markers recently tested are the luciferase from the sea pansy *Renilla reniformis* and the marine copepod *Gaussia princeps*. Renilla luciferase (RLuc) derives from the sea pansy (*Renilla reniformis*) and is a monomeric, bioluminescent protein (311 aa, 34 kDa) emitting blue light with a peak at 480 nm, using coelenterazine as substrate and not requiring ATP as energy source (Bhaumik and Gambhir, 2002; Grentzmann *et al.*, 1998; Lorenz *et al.*, 1996; Stables *et al.*, 1999). However, the emission colour is not suitable for its application *in vivo* (Contag and Bachmann, 2002). Gaussia luciferase (GLuc) from the marine copepod *Gaussia princeps* is the smallest luciferase known (185 aa, 19.9 kDa); it emits blue light at a broad peak extending from 480 to 600 nm, uses coelenterazine as substrate and is secreted, therefore does not require ATP as energy source (Tannous *et al.*, 2005; Verhaegent and Christopoulos, 2002).

1.7.2 Interesting applications of BLI for the detection of fungal pathogens

Within the fungal kingdom, BLI was firstly applied to the pathogenic yeast *C. albicans*, to study the difference between vaginal and systemic infection (Doyle *et al.*, 2006). In particular *C. albicans* cells were engineered to express the firefly luciferase by its stable integration in a transcriptionally silent region of the genome, to generate strains with identical pathogenicity and growth rate to the parental isolates (Doyle *et al.*, 2004). The substrate was supplied externally, by virtue of the ability of *C. albicans* cells to uptake luciferin without any treatment and the presence of enough intracellular ATP to catalyze light emission. However, luciferin availability in the cytoplasm is a limiting factor for the BLI, because hyphal cells are less able to absorb the substrate and therefore when *C. albicans* switches to the hyphal form (e.g. during systemic infection) light emission is significantly reduced (Doyle *et al.*, 2006). Because luciferin is thought to enter the cells via passive diffusion, this difference may be a consequence of changes in the cell wall composition. In contrast with the application of GFP for *C. albicans* imaging (Cormack *et al.*, 1997), firefly luciferase was demonstrated to be detectable within an hour after the addition of the substrate and to have a relatively short half-time (3 hours in mammalian cells). In addition, the study included the use of the Renilla luciferase and has revealed the instability of the substrate coelenterazine in aqueous solution and a significant level of background (Doyle *et al.*, 2004).

In concomitance with our study, BLI has been developed for *A. fumigatus*, using the firefly luciferase under the control of the glyceraldehde-3-phosphate dehydrogenase gene (*gpdA*) promoter. The *gpdA* promoter was chosen because it is constitutively active, with some variations depending on the carbon source, but is actively expressed when the mycelium is growing invasively in the host tissue. In contrast to observation in *C. albicans*, the bioluminescent signal generated by the *A. fumigatus* engineered strain during infection shows a good correlation with fungal biomass, permitting the evaluation of the fungal burden in infected tissues and providing a means to test antifungal treatments for efficiency. Light emission can be directly correlated with the copies of luciferase gene present in the engineered strain (Brock *et al.*, 2008). The same study demonstrated that the *A. fumigatus* strain expressing firefly luciferase is a powerful tool for drug efficiency testing and *in vivo* monitoring of IPA, allowing the assessment of infection parameters such as the levels of tissue colonisation and invasion (Brock *et al.*, 2008). In addition, the *A. fumigatus* strain expressing firefly luciferase has been used to monitor fungal progression and location during the infection in mice with different types of immunosuppressive regimens, affecting either macrophages or neutrophils functions. In particular bioluminescent imaging of infected mice

and histopathologic analysis have correlated light emission and fungal invasion for the cyclophosphamide-treated murine model, where neutrophil function is depleted (Ibrahim-Granet *et al.*, 2010). Instead, in murine models where the neutrophil function is not depleted, there is no correlation between light emission and fungal invasion, because of the extensive tissue damage and consequent tissue hypoxia occurring in the other murine model of infection as a consequence of the action of neutrophils. Firefly luciferase requires oxygen as substrate for light emission and it has been demonstrated that oxygen saturation below 5% decreases significantly the efficiency of the reaction (Robertson *et al.*, 2008). Under conditions of high inflammation, therefore, the intensity of bioluminescent signal reflects properly only the early stages of infection, because at later stages it declines as a consequence of the progressive hypoxia (Ibrahim-Granet *et al.*, 2010). This study demonstrated the applicability of BLI for *A. fumigatus* to monitor fungal germination, tissue invasion and inflammatory response.

1.8 Objectives of this study

Environmental-sensing proteins are particularly interesting from a therapeutic perspective because they are important at the earliest stage of the development of the fungus in the host and they are more accessible to inhibitory agents due to their membrane localisation. Alkaline adaptation, a mechanism not essential for *Aspergillus* viability, but critical for its virulence, might therefore provide a useful target for prevention of fungal growth *in vivo*. Using *A. fumigatus* transcriptional profiling during murine infection, phenotypic screening in *S. cerevisiae*, and a yeast-based *A. fumigatus* split-ubiquitin screen, novel virulence-essential *A. fumigatus* functions acting upstream of the transcription factor PacC, central regulator of *Aspergillus* virulence, have been investigated.

The mechanism leading to the activation of PacC regulatory pathway has not yet been characterised extensively in *A. fumigatus* and especially the elucidation of its role during infection is still unexplored by the current literature. This study presents therefore the characterisation of an *A. fumigatus* Δ*pacC* mutant in terms of phenotype, virulence and tissue invasion to determine the physiological requirement for pH signaling during *A. fumigatus* virulence (Chapter III). In addition, transcriptional profiling of the *A. fumigatus* Δ*pacC* in comparison with the respective parental isolate was performed to identify functions under PacC transcriptional control during murine infection (Chapter IV).

An intense network of protein-protein interactions has been demonstrated to be established in fungi for pH sensing and adaptation. These interactions, in particular those

taking place in the plasma membrane, are required during initial contact between host and fungus and therefore could provide a way to interfere with the first stages of fungal growth.The innovative split-ubiquitin Membrane Yeast Two-Hybrid (MYTH) system was applied to characterise *A. fumigatus* membrane protein interactions involved in pH perception (Chapter V).In addition, the system was optimised and adapted to a high-throughput format to discover novel protein interactors for *A. fumigatus* PalH from a full-length *A. fumigatus* cDNA prey library (Chapter VI).

In virtue of the conservation of the PacC/Rim101 pathway between the *Aspergillus* species and *S. cerevisiae*, novel upstream components of the Rim101 regulatory pathway were identified in yeast through an epistacy screen using *S. cerevisiae* null mutants, having Δ*rim101*-like phenotype and showing cation hypersensitivity as the *rim101* mutant (Chapter VII). The epistacy screen was based upon the reversal of lithium toxicity by an activated *RIM101* allele, which would strongly suggest a PacC regulating role for these genes. In addition, a synthetic Rim101p promoter fused to a lacZ reporter was used to isolate mutants suffering aberrant Rim101p processing and transcriptional activity among the *S. cerevisiae* Δ*rim101*-like mutants (Chapter VII);

Finally, for the ultimate purpose of transposing protein interaction assays into tissue cultures and murine models of infection, an *A. fumigatus* strain expressing firefly luciferase under the control of the glyceraldehde-3-phosphate dehydrogenase gene (*gpdA*) promoter has been constructed and tested for its potential use in the murine model (Chapter VIII).

CHAPTER II

MATERIAL AND METHODS

2.1 Chemicals, reagents and enzymes

Chemicals and reagents were purchased from Sigma UK or Fisher Chemicals unless otherwise stated. Restriction enzymes, ligases, phosphatases, kinases and other modifying enzymes were purchased from New England Biolabs (USA). Taq DNA polymerase enzymes were purchased from KAPABiosystems (UK), Bioline (UK) and Invitrogen (UK) unless otherwise stated.

2.2 Bacterial and fungal strains

All bacterial and fungal strains used in this study are listed in the respective Chapters and in Appendix A.

2.3 Media

Unless otherwise stated, all ingredients were purchased from Oxoid Ltd (UK), BDH (UK), or Sigma (UK). All media were sterilised by autoclaving at 121°C for 15 minutes.

2.3.1 Bacterial cultures

XL-10 *Escherichia coli* [F- *mcr*A Δ(*mrr-hsd*RMS-*mcr*BC) Φ80*lacZ*ΔM15 Δ*lac*X74 *rec*A1 *ara*D139 Δ(*araleu*) 7697 *gal*U *gal*K *rps*L (StrR) *end*A1 *nup*G] (Stratagene) were grown in Luria Bertani (LB) medium (1% (w/v) tryptone, 0.5% (w/v) yeast extract, 1% (w/v) NaCl) at 37°C, 180 rpm. Solid LB was produced by addition of 2% (w/v) agar prior to autoclaving. When required, after autoclaving the media was supplemented with 100 μg/ml ampicillin or 30 μg/ml kanamycin or, for β-galactosidase assays, 0.5 mM IPTG and 80 μg/ml X-Gal. Strains were stored for up to 1 week at 4°C. For longer term storage, strains were stored in 25% (w/v) glycerol at -80°C.

2.3.2 Fungal cultures

S. cerevisiae strains, constructed in the genetic background BY4741 [MATa *his3_1 leu2_0 met15_0 ura3_0*], were grown in yeast extract peptone dextrose (YPD) media (1% (w/v) yeast extract, 2% (w/v) peptone, 2% (w/v) glucose), or in appropriate synthetic drop-out (SD) media (0.17% (w/v) yeast nitrogen base (YNB) without amino acids, 2% (w/v) glucose and 0.08% (w/v) drop out mix [Formedium, UK]) according to specific nutritional or experimental requirements. *S. cerevisiae* strains, constructed in the genetic background NMY51 [MATa *his3delta200 trp1-901 leu2-3,112 ade2 LYS2::(lexAop)4-HIS3 ura3::(lexAop)8-lacZ (lexAop)8-ADE2 GAL4*] were grown in yeast extract peptone adenine dextrose (YPAD) media (1% (w/v) yeast extract, 2% (w/v) peptone, 2% (w/v) glucose, 0.004% adenine sulfate), or in appropriate SD media as previously described. Solid YPD, YPAD or SD media was produced by addition of 2% (w/v) agar prior to autoclaving. Liquid cultures were agitated by orbital shaking at 180 rpm unless otherwise specified. *S. cerevisiae* strains were cultured for 2-3 days at 30°C. Strains were either stored at 4°C for up to 4 weeks on solid agar plates or for long term storage in 25% (w/v) glycerol at -80°C.

A. fumigatus strains used in this study were the wild type strain CEA10, a clinical isolate, obtained at a Paris hospital in 1989 (D'Enfert *et al.*, 1996), the wild type strain ATCC46645 (Hearn and Mackenzie, 1980) and the PyrG Δ*ku80* which has a non-homologous end joining deficiency (da Silva Ferreira *et al.*, 2006). Recipes for solid and liquid media were identical, save the addition of 1% (w/v) agar to solid media. Liquid cultures were agitated by orbital shaking at 150 rpm unless otherwise specified. *A. fumigatus* strains were cultured at 37°C in *Aspergillus* Minimal Media (AMM) (20 ml/l *Aspergillus* salt solution [26 g/l KCl, 26 g/l $MgSO_4.7H_2O$, 76 g/l KH_2PO_4], 10 ml/l vitamin solution [400 mg/l 4-aminobenzoic acid, 50 mg/l aneurin, 1 mg/l biotin, 24 g/l mesoinositol, 100 mg/l nicotinic acid, 200 mg/l DL-pantothenic acid (hemicalcium salt), 250 mg/l pyridoxine monohydrochloride, 100 mg/l riboflavin, 1.4 mg/l choline chloride], 20 ml/l 50% glucose, 10 ml/l 500 mM ammonium tartrate) or *Aspergillus* Complete Media (ACM) (1% (w/v) glucose, 0.1% (w/v) yeast extract, 0.1% (w/v) casamino acids, 0.2% (w/v) peptone, 75 mg/l adenine, 20 ml/l A*spergillus* salt solution, 10 ml/l vitamin solution). The pH of ACM was adjusted to 6.5 using 10 M NaOH, whereas AMM was buffered using 100 mM MES (2-(N-Morpholino) ethanesulfonic acid hemisodium salt) pH 6.5. Strains were either stored at 4°C for up to 4 weeks on solid agar plates or for long term storage in 20% (w/v) glycerol at -20°C.

2.3.3 Fungal phenotypic assays

Media conditions used for fungal phenotypic assays in this study are listed in the respective chapters.

S. cerevisiae cell density was calculated by assessing OD_{600} using an UltroSpec II (Biochrom, LRB) spectrophotomer and assuming that an OD_{600} equivalent to 1.0 corresponds to 3.0 x 10^7 cells/ml. Serial dilutions of $1.0x10^6$, $1.0x10^5$, $1.0x10^4$ and $1.0x10^3$ cells were plated in the test conditions. Plates were incubated for 2-4 days at 30°C and photographed without magnification using a Nikon Coolpix 990 digital camera.

A. fumigatus conidia were harvested in sterile H_2O and filtered on MIRACLOTH (Calbiochem). Spores were counted using a haemocytometer and resuspended at a concentration of 2 x 10^6 cfu/ml in sterile H_2O prior to serial dilutions of $1x10^4$, $1x10^3$, $1x10^2$, $1x10^1$ spores. Each serial dilution was plated 3 times and plates were incubated for 2 days at 37°C. Plates were photographed without magnification using a Nikon Coolpix 990 digital camera. For counting, *Aspergillus* spores were visualised using a Nikon Eclipse 80i microscope.

2.4 Oligonucleotide primer synthesis

All primers used in this study are summarised in the respective Chapters and in Appendix B. Oligonucleotides were purchased from Sigma-Genosys and designed to contain, where necessary, an appropriate restriction site for cloning.

2.5 Plasmids

Full details regarding plasmids used during this study are given in the respective Chapters.

2.6 General molecular techniques

2.6.1 Preparation of competent cells

E. coli XL10 cells were grown in 15 ml of LB media overnight at 37°C. The following day 5 ml of the culture was inoculated in 100 ml of LB (pre-warmed to 37°C) and grown at

37°C until the A_{550} of the culture reached 0.48. The culture was subsequently transferred to 50 ml falcon tubes, chilled for 5 minutes on ice and then centrifuged in a Sorvall centrifuge at 3660 rpm for 10 minutes at 4°C. Cells were resuspended in 40 ml ice-cold TfbI (30 mM KAc, 100 mM KCl, 10 mM $CaCl_2$, 50 mM $MnCl_2$, Glycerol 15%, pH 5.8 with 0.2 M acetic acid), chilled on ice for 5 minutes and centrifuged as before. Finally cells were resuspended in 4 ml ice-cold TfbII (10 mM MOPs or PIPES, 10 mM $CaCl_2$, 10 mM KCl, Glycerol 15%, pH to 6.5 with 3 M KOH), left on ice for 15 minutes and aliquoted into cryotubes to be stored at -80°C.

2.6.2 Bacterial Transformation

Bacterial transformation was performed using the $CaCl_2$ heat shock method (Mandel and Higa, 1970). 50 µl of *E. coli* XL-10 competent cells were mixed with 10-100 ng of plasmid DNA. The suspension was left on ice for 30 minutes and then heat-shocked in a 42°C H_2O bath for 40 seconds. Cells were resuspended in 500 µl of LB without any selective drug and left at 37°C for 45 minutes to allow cells to express drug resistance. Cells were subsequently plated on LB plates containing the selective antibiotic and incubated overnight at 37°C. The day after, single colonies were transferred to 3 ml of LB broth supplemented with the appropriate antibiotic to be grown overnight at 37°C, 180 rpm.

2.6.3 Plasmid DNA extraction

According to the manufacturer's instructions, plasmids were extracted from 3 ml overnight *E. coli* LB culture (supplemented with the appropriate antibiotic) with the commercial kit NucleoSpin Plasmid (Macherey-Negen, Germany), specifically designed to extract plasmid DNA for a variety of routine applications (i.e. restriction enzyme digestion, sequencing, ligation and transformation). The procedure is based on alkaline lysis of bacterial cells followed by adsorption of DNA onto silica in the presence of high salt.

2.6.4 Separation of DNA fragments by electrophoresis

DNA fragments were visualised by electrophoretic separation on 1% agarose gel (w/v) (Electran). In order to facilitate sample loading and to visualize the migration of the samples, 6X Loading Dye Solution (10mM Tris-HCl (pH 7.6), 0.03% bromophenol blue, 60% glycerol, 60mM EDTA) was added to the DNA in a ratio 1:5. To prepare and run the gel, TBE 1X buffer (Tris-borate 0.09 M, EDTA 1 mM, pH 8.0) was used and 4 µl of the dye

SYBR Safe DNA gel stain (Invitrogen) was added to each 50 ml gel for DNA vizualisation using the UV transilluminator AlphaImager (Alpha Innotech, USA). To define the size of DNA fragments, 500 ng of various molecular ladders (Marker λ, Marker 1Kb and Marker 100 bp, New England Biolabs) were used.

For specific applications, the DNA was purified directly after the electrophoretic separation by excising the DNA band of interest from the agarose gel with a clean, sharp scalpel and using the commercial kit QIAquick Gel extraction Kit (QIAGEN) according to the manufacturer's instructions.

2.6.5 Nucleic acid quantification

Nucleic acid concentration and purity were assayed with a Nanodrop ND-1000 Spectrophotometer (Nanodrop, Wilmington, USA).

2.6.6 Dephosphorylation of vector

To prevent re-ligation of digested vectors, dephosphorylation was achieved using enzyme calf intestinal alkaline phosphatase (CIP) (New England BioLabs) that catalyzes the removal of 5' phosphate groups from DNA, RNA, ribo- and deoxyribonucleoside triphosphates. 0.1-10 µg of DNA was mixed with 3 µl of NEBuffer 3 and 2 µl of enzyme to a final volume of 30 µl and the reaction was incubated for 3 h at 37°C.

After this treatment, the samples were purified according to the manufacturer's specifications with the commercial kit QIAquick PCR purification Kit (QIAGEN), designed for rapid cleanup of DNA from amplification reactions and other enzymatic reactions such as treatment with alkaline phosphatase and restriction digestions to avoid interference with subsequent downstream applications.

2.6.7 Restriction enzyme digests

Restriction digestion of DNA was performed using restriction enzymes purchased from New England Biolabs and according to the manufacturer's specifications. The appropriate NEBuffer was used at a final concentration of 1X and when needed, bovine serum albumin (BSA) was supplied at the final concentration of 100 µg/ml. To remove the enzymes and buffer following restriction digests, the QIAquick PCR Purification Kit (QIAGEN) was

used according to the manufacturer's specifications.

2.6.8 Polymerase chain reaction (PCR)

PCRs were performed following standard procedures described by manufacturers and using one of three enzymes: BIO-X-ACT-Long (Bioline), BD-ADVANCED (BD Advantage™ 2 Polymerase Mix, Takara) and Platinum Taq DNA Polymerase High Fidelity (Invitrogen). For colony PCR initial incubation at 95 °C was extended to 10 minutes. PCR amplification of probes for digoxigenin-labelled Southern analysis was performed following the manufacturer's instructions (Roche Diagnostics Ltd, UK). PCR products were purified with QIAquick PCR purification kit (QIAGEN) according to the manufacturer's specifications.

2.6.9 Treatment of PCR products

DNA Polymerase I, Large (Klenow) Fragment (New England BioLabs) was used to fill-in 5' overhangs to form blunt ends. 0.1-5 µg of DNA was mixed with 4 µl of NEBuffer 2, 13 µl of dNTPs (100 µM) and 3 µl of enzyme and the reaction was incubated for 30 minutes at 37°C.

T4 Polynucleotide Kinase (PNK) (New England BioLabs) was used for the addition of 5´-phosphates to oligonucleotides to allow subsequent ligation. 0.1-5 µg of DNA was mixed with 4 µl of T4 DNA ligase buffer in a total volume of 21 µl. The reaction was incubated for 5 minutes at 70°C and immediately cooled on ice. Subsequently 1.5 µl of enzyme was added and the reaction was incubated for 30 minutes at 37°C.

To purify DNA after each of these treatments the QIAquick PCR Purification Kit (QIAGEN) was used according to the manufacturer's specifications.

2.6.10 Ligation

The ligations were performed using T4 DNA Ligase (New England BioLabs), catalyzing the formation of a phosphodiester bond between juxtaposed 5' phosphate and 3' hydroxyl termini in duplex DNA joining blunt end and cohesive end termini. The overall concentration of vector + insert was between 1-10 µg/ml for efficient ligation. The volume of DNA to use for each reaction was determined by comparison with the molecular ladder in a 1% agarose gel and Nanodrop quantification. A ratio 1 : 3 of vector : insert was routinely used

to avoid self-ligation of the vectors. The total volume used was 10 µl using 1 µl of the enzyme (400000 units/ml) and the reaction was incubated overnight at 16°C.

2.6.11 Sequencing

Every plasmid obtained was verified by sequencing with the Sanger's method using a 3730 capillarity electrophoresis sequencer (Applied Biosystems Warrington Cheshire). For each reaction, the mix was comprised of 200-500 ng of the plasmid to sequence, 2 µl of the primer (20 µM) in a final volume of 10 µl. DNA sequencing was performed at the DNA Core Laboratory, Medical Research Council, Imperial College London. The oligonucleotides used to sequence (listed in the respective Chapters and in Appendix B) were purchased from Sigma-Genosys and appropriately co-ordinated for maximal coverage of the region of interest.

2.6.12 Western blotting analysis

To assay for the expression of fusion proteins by western blotting (Towbin *et al.*, 1979), *S. cerevisiae* strains were inoculated in liquid SD medium and grown overnight to prepare total extracts as described in Section 2.10.

Protein samples were run on 8% SDS-PAGE gels in a XCell-SureLock Mini Cell electrophoresis tank (Invitrogen) with SDS-PAGE running buffer (25 mM Tris-HCl, 192 mM glycine, 0.1 % (v/v) SDS) at 150V until samples reached the end of the gel. Gels were transferred to nitrocellulose membrane (Amersham) in transfer buffer (25mM Tris base, 192mM glycine, 20% (v/v) methanol) using Invitrogen's XCell-SureLock Mini Cell XII Blot module. Membranes were blocked overnight in 5 % (w/v) milk (Marvel) PBS-Tween (137 mM NaCl, 1.47 mM KH_2PO_4, 2.68 mM KCl, 8.1 mM $Na_2HPO_4.12H_2O$, 0.001 % (v/v) Tween-20) and incubated for 4 hours with primary antibody in 1 % (w/v) milk PBS-Tween. Membranes were washed 3 x 10 minutes with PBS-Tween, incubated with secondary antibody in 1 % (w/v) milk PBS-Tween for an hour and washed 3 x 10 minutes with PBS-Tween. Membranes were developed using the ECL solution (Amersham) and exposed onto Hyper film from Kodax. During all incubations and washings, the membrane was maintained in continuous agitation.

2.6.13 Southern blotting analysis

Southern analysis was performed by using a slightly modified version of the original one (Southern, 1975). Briefly, 20 µg of *A. fumigatus* genomic DNA was digested with the appropriate restriction enzyme and digested DNA was separated on a 1% (w/v) agarose gel, stained for 30 minutes in 100 ml TBE with 20 µl of SYBR Safe DNA gel stain (Invitrogen), and photographed. Following depurination (250 mM HCl), denaturation (0.5 M NaOH, 1.5 M NaCl), neutralisation (0.5 M Tris-HCl, pH 7.5, 1.5 M NaCl) and equilibration in 20 x SSC (3 M NaCl, 300 mM sodium citrate, pH 7), the gel was blotted overnight onto a positively charged nylon membrane (Roche Diagnostics). After transfer, the DNA was fixed to the membrane using the autocrosslink function on a Stratagene UV Stratalinker 1800. The DIG Easy Hyb solution, hybridisation solution for nucleic acid blots with digoxigenin-labeled probes (Roche) was pre-warmed to the hybridisation temperature (T_{hyb}) of the probe. T_{hyb} was calculated using the following equations:

$$Tm = 49.82 + 0.41\ (\%\ G+C) - 600/l$$

$$T_{hyb} = Tm - (20°C \text{ to } 25°C)$$

where Tm = melting point of probe-target hybrid, % (G+C) = % of G and C residues in probe sequence, T_{hyb} = optimal temperature of hybridisation of probe to target in DIG Easy Hyb and l = length of the probe in base pairs. The membrane was pre-hybridised at the T_{hyb} in DIG Easy Hyb solution for 1-3 hours with gentle agitation. The probes were generated using the PCR DIG Probe Synthesis Kit (Roche) for production of highly sensitive probes labeled with DIG-dUTP (alkali-labile) according to the manufacturer's instructions. 50 ng of the probe was denatured in a final volume of 50 µl of H_20 at 100°C for 5 minutes before chilling immediately on ice. The probe was added to 10 ml pre-warmed DIG Easy Hyb solution, mixed and the membrane was incubated overnight at the T_{hyb} with agitation. The membrane was then washed in low stringency buffer (2 x SSC, 0.1% (w/v) SDS) at 25°C, high stringency buffer (0.5 x SSC, 0.1 % (w/v) SDS) at 65°C and washing buffer (0.1 M maleic acid, 0.15 M NaCl (pH 7.5), 0.3% (v/v) Tween 20). The membrane was blocked in blocking solution (1% (w/v) blocking powder [Roche Diagnostics] in 0.1 M maleic acid, 0.15 M NaCl, pH 7.5) for 1-3 hours at 25°C. The antibody, Anti-Digoxigenin-AP Fab fragments (Roche), was centrifuged at 10000 rpm for 5 minutes and used at a dilution of 1 in 10000 in 30 ml blocking solution for an incubation of 30 minutes with gentle agitation. The membrane was washed in washing buffer and equilibrated in detection buffer (0.1 M Tris-HCl, 0.1 M NaCl, pH 9.5) for 3 minutes. CDP-Star (Roche) was added to the membrane and incubated for 5 minutes before the membrane was exposed onto Hyper film (Kodax).

2.7 *Aspergillus fumigatus* techniques

2.7.1 *A. fumigatus* genomic DNA extraction

DNA was extracted from *A. fumigatus* following two different protocols according to the requirements of the planned experiment.

For colony PCR, spores were picked from a colony using a loop and mixed in 200 µl of breaking buffer (2% Triton X-100, 1% SDS, 100 mM NaCl, 10 mM Tris-HCl pH 8.0, 1 mM EDTA pH 8.0). After the addition of 300 mg of glass beads (0.4-0.6 mm diameter, Sartorius UK), samples were incubated for 30 minutes at 70°C, vortexing every 10 minutes. 200 µl phenol:chloroform:isoamyl alcohol 25:24:1 was added and the samples were vortexed for 5 minutes and subsequently centrifugated for 8 minutes at 13000 rpm. The supernatant was precipitated by adding an equal volume of isopropanol and incubated for 1 hour at 4°C. After centrifugation at 13000 rpm for 10 minutes, the pellet was washed in 70 % (v/v) ethanol and air-dried before resuspension in 20 µl of sterile H_2O.

For large scale genomic DNA preparations, *A. fumigatus* genomic DNA was extracted from mycelia following the modified method of Raeder and Broda (Raeder and Broda, 2008). Mycelia from an overnight culture in ACM (37°C, 180 rpm) were harvested, frozen in liquid nitrogen and ground with a mortar and pestle. Then, 1.5 ml of *Aspergillus* extraction buffer (300 mM Tris-HCl, 375 mM NaCl, 37.5 mM EDTA, 2% (v/v) sarkosyl) was added to 300 mg of mycelia reduced to a fine powder. Following addition of a half volume of phenol and a half volume of chloroform:isoamyl alcohol 24:1 (Sigma), tubes were mixed on a tube rotator for 15 minutes at room temperature and then centrifuged at 13000 rpm for 1 hour. The supernatant was transferred to a microcentrifuge tube containing 400 µl of chloroform, centrifuged for 15 minutes, and the aqueous phase transferred to a new eppendorf tube where 400 µl of chloroform was added. After 15 minutes of centrifugation, the aqueous phase was mixed with an equal volume of isopropanol. The tube was left at 4°C for 1 hour, centrifuged at 13000 rpm for 10 minutes and the pellet was washed in 70 % (v/v) ethanol and air-dried. Finally, the pellet was resuspended in 50 µl of TE containing RNace-It ribonuclease cocktail (Stratagene).

2.7.2 Transformation of *A. fumigatus*

Transformation of DNA into *A. fumigatus* was conducted by electroporation. Electrocompetent spores were made according to the Sanchez and Aguirre protocol (Sanchez and Aguirre, 1996). *Aspergillus* spores were plated on ACM and incubated for 5 days, then harvested in sterile H_2O and filtered through Miracloth (Calbiochem). Spores were centrifuged for 10 minutes at 4000 g, washed 5 times with H_2O and counted. 250 ml YG broth (0.5% Yeast Extract, 2% Glucose) was inoculated with 5 x 10^9 spores and grown at 37°C for 2-4 hours. Spores were then centrifuged for 10 minutes at 4000 g, washed in cold H_2O, and resuspended in 20 ml YED (1% Yeast Extract, 1% Glucose, 20 mM Hepes, pH 8 with NaOH). Spores were grown at 30°C for 1 hour, and then resuspended in cold EB (10 mM Tris HCl pH 7.5, 270 mM Sucrose, 1 mM LiAc).

For the transformation, 2 μg of DNA was mixed with 50 μl of electrocompetent spores and incubated on ice for 15 minutes. Electroporation was then performed by application of a pulse of 1 kV, 400 OHM and 25 F. After incubation on ice for 15 minutes in presence of YED, spores were incubated at 30°C for 90 minutes. Resulting transformant spores were plated on AMM (- aneurin) supplemented with the optimal concentration of 0.5 μg/ml Pyrithiamine (Takara), as selective agent, and then incubated for 3 days at 37°C.

2.8 *Saccharomyces cerevisiae* techniques

2.8.1 DNA extraction

Plasmid DNA extraction was performed using a modification of the standard protocol described previously (Sambrook and Russell, 2001). Plasmids were extracted from 10 ml overnight yeast SD cultures with the commercial kit NucleoSpin Plasmid (Macherey-Negen, Germany) but an additional step was introduced to disrupt yeast cells with acid-washed glass beads (425-600 μm diameter, Sigma). After resuspension of yeast cells according to the manufacturer's instructions, 300 mg of glass beads were added and the mixture was vigorously agitated for 30 minutes.

2.8.2 Protein extraction

S. cerevisiae strains were inoculated in 10 ml of liquid SD medium supplemented with the appropriate drop-out mixture and grown overnight at 30°C, 180 rpm. Cells were then centrifuged at 700 g for 5 minutes and the pellets were washed once in 1 mM EDTA/water. 200 µl of 2 M NaOH was added to cells and the mixture was transferred to eppendorf tubes to be incubated on ice for 10 minutes. Following the addition of 200 µl of 50 % TCA and 2 hours of incubation on ice, cells were centrifuged at 14000 g for 20 minutes at 4°C. The supernatant was discarded and 200 µl ice-cold acetone was added to the pellet, gently broken up using a pipette tip. Samples were centrifuged at 14000 g for 20 minutes at 4°C and the supernatants were discarded. 200 µl of 5 % SDS was added to the pellet to resuspend and later an equal volume of 2X SDS Loading Buffer (65.5M Tris-HCl (pH 6.8), 2% (w/v) SDS, 5% (v/v) β-mercaptoethanol, 6 M Urea and bromophenol blue in distilled/deionized water).

was added. If the colour of the sample was yellow several drops of 2 M Tris-Cl pH 9 were added until the colour changed from yellow to blue. Samples were stored at -20°C and prior to western blotting analysis they were incubated at 37°C for 15 minutes and then centrifuged at 14000 g for 5 minutes.

Total protein quantification of the samples was performed using the Bicinchoninic Acid Protein Assay Kit (Sigma) according to the manufacturer's instructions. The principle of the bicinchoninic acid (BCA) assay relies on the formation of a Cu^{2+}-protein complex under alkaline conditions, followed by reduction of the Cu^{2+} to Cu^{1+}, where the amount of reduction is proportional to the protein present. Unless otherwise stated, 30 µg of protein extract was loaded on 8% SDS-PAGE gels.

2.8.3 Yeast transformation

Lithium acetate protocol

S. cerevisiae cells were transformed using a modification of the lithium acetate protocol described by Gietz and Woods (Gietz *et al.*, 1992). Briefly, yeast cells were grown at 30°C overnight in 5 ml of YPD and then centrifuged, washed once with 1 ml of H_2O and incubated for 15 minutes at 30°C in 1 ml 100 mM lithium acetate. After centrifugation, 360 µl of transformation mix (33% (w/v) polyethylene glycol (PEG) 3350, 0.1 M LiAc, 0.3 mg/ml boiled and chilled salmon sperm DNA, 200-500 ng DNA per transformation) was added. Following the incubation for 30 minutes at 30°C and heat-shock at 42°C for 20 minutes, cells

were centrifuged and 400 µl of H_2O was added. After an incubation of 5 minutes at room temperature, cells were resuspended, spread onto SD plates and incubated for 3 days at 30°C.

Lithium acetate protocol for 96-wells plate

The lithium acetate transformation method (Gietz *et al.*, 1992) was adapted to the 96-well plate format as follows: *S. cerevisiae* cells were grown at 30°C overnight in 100 µl of YPD. Cells were centrifuged, washed once with 150 µl of H_2O and incubated for 15 minutes at 30°C in 150 µl 100 mM lithium acetate. Cells were then centrifuged and 20 µl of mix 1 (9 µl TE buffer, 10.5 µl of 2 mg/ml boiled and chilled salmon sperm DNA, 5 µl of 180 ng/µl plasmid) was added. After mixing, 55 µl of mix 2 (48 µl 50% (w/v) PEG 3350, 7 µl 1 M lithium acetate) was added. After incubation for 30 minutes at 30°C followed by 30 minutes of incubation at 42°C, cells were centrifuged and 100 µl of H_2O was added. After incubation for 5 minutes at room temperature, cells were resuspended in H_2O, spread onto SD plates and incubated for 3 days at 30°C. For each strain, three transformants were selected, and cultured in 150 µl of SD in a 96-wells plate overnight at 30°C.

Split-ubiquitin modified lithium acetate protocol

Another modified version of the lithium acetate transformation method (Gietz *et al.*, 1992) was utilised for split-ubiquitin experiments. 50 ml of YPAD was inoculated with several colonies of NMY51 taken from a fresh plate and grown overnight at 30°C with shaking. The OD_{546} of the culture was measured and the yeast cells were diluted to OD_{546} = 0.2 and re-grown to OD_{546} = 0.6. 50 ml of culture was centrifuged for 5 minutes at 2500 g and resuspended in 2.5 ml of H_2O. PEG/LiOAc mix (sufficient for 5 reactions) was prepared with 1.2 ml 50 % PEG 3350, 180 µl 1 M LiOAc and 125 µl of boiled and chilled salmon sperm DNA and added to 1.5 µg of the transforming plasmid. After vigorous shaking, 100 µl of resuspended yeast cells was added, followed by vortexing for 1 min. Samples were incubated in a 42°C water bath for 45 minutes and centrifuged for 5 minutes at 700 g. Each pellet was dissolved in 150 µl 0.9 % NaCl and spread onto SD plates. Plates were incubated for 4 days at 30°C.

2.8.4 Quantitative β-galactosidase assay

The β-galactosidase activity of *S. cerevisiae* strains was measured using the non-stop protocol for 96-well plate recommended by the yeast β-galactosidase assay kit (Pierce) manufacturers. Briefly, overnight broth cultures were diluted (1/10) and grown to an OD_{660} of approximately 0.6. The OD_{660} was then recorded and 100 µl of working solution (50 µl 2X ONPG and 50 µl Y-PER Reagent) was added to each well. After 20-30 minutes the absorbance at 420 nm was measured and the β-galactosidase activity was calculated applying the following formula:

$$(1000 \times A_{420})/ T \times V \times OD_{660} = \beta\text{-galactosidase activity}$$

where T = reaction time= 20 min, V = total volume= 200 µl and A420 = Absorbance at 420 nm.

2.9 *In vivo* virulence analysis

Murine infections were conducted under UK Home Office Project Licence PPL/70/6487 in a dedicated facility at Imperial College London, where individually vented cages with free access to food and H_2O were used to house outbred male mice (strain CD1, 18 – 22 g, Harlan Ortech). H_2O was supplemented with 1 g/l tetracycline hydrochloride and 64 mg/L ciprofloxacin as prophylaxis against bacterial infection. For a neutropenic model of infection, immunosuppression of mice was performed by intraperitoneal injections of cyclophosphamide (150 mg/kg) on days –3, –1, +2, and subsequently every third day for the duration of the experiment and by a single subcutaneous dose of hydrocortisone acetate (112.5 mg/kg) on day –1 (Schrettl *et al.*, 2004). *A. fumigatus* spores were grown on ACM, supplemented with 1 % (w/v) glucose and 5 mM ammonium tartrate, for 5 days prior to harvesting the conidia using sterile saline (Baxter Healthcare Ltd, UK) and filtering them through MIRACLOTH.

For survival analysis, conidial suspensions were centrifuged for 5 minutes at 5000 rpm, washed twice with sterile saline, counted using a haemocytometer and resuspended at a concentration of $1.25x10^6$-$1.5x10^7$ (respectively for low and high dose) cfu/ml. The determination of viable counts for the administered inocula was performed by serial dilution on ACM plates supplemented with 1 % (w/v) glucose and 5 mM ammonium tartrate and incubated for 3 days at 37°C. Mice were anaesthetised by isofluorane inhalation and infected by intranasal instillation of $5.0x10^4$-$6.0x10^5$ (respectively for low and high dose) conidia in 40

µl of saline solution. Mice were weighed every 24 hours from day -3 and inspected twice daily. For survival analysis, in the majority of instances, the end of the experimentation corresponded to a 20% reduction in body weight measured from the day 0, at which point mice were culled.

For the transcriptional time course comparison between ATCC466645 Δ*pacC* and the respective parental isolate throughout murine infection, spores, prepared as before, were resuspended at a concentration of $2.5x10^9$ cfu/ml and mice, anaesthetised by isofluorane inhalation, were infected by intranasal instillation of $1x10^8$ conidia in 40 µl of saline solution. Groups of infected mice were culled and processed collectively during a 2 hour window corresponding to time points 4, 8 and 16 hours post-infection. Bronchoalveolar lavages (BALs) were performed using three 0.5 ml aliquots of sterile saline. BAL fluids (BALFs) were snap frozen immediately following harvesting using liquid nitrogen.

Lungs were removed immediately after sacrifice or after BALFs were obtained and fixed in 4 % (w/v) formaldehyde (Sigma) for histological sectioning. Lungs were embedded in paraffin prior to being sectioned and stained with hemotoxylin and eosin (H&E) or light green and Grocott's Methenamine Silver (GMS).

2.10 DNA microarray techniques

2.10.1 Fungal RNA extraction from BALFs

BALF samples were centrifuged at 14000 rpm for 5 minutes and the pellet was washed with 500 µl ice cold H_2O to lyse host cells. Seven BALFs were pooled, resuspended in 450 µl ME-RLC buffer (QIAGEN) and ground in liquid nitrogen with a pestle and mortar. RNA was then extracted using RNeasy® Kit (QIAGEN). Quality of RNA used for microarray analysis was checked by Nanodrop ND-1000 Spectrophotometer (Nanodrop, Wilmington, USA). Only RNA with an $A_{260/280}$ and an $A_{260/230}$ ratio > 1.9 was used for the experiments.

2.10.2 Reverse transcription and fluorescent labelling of RNA

Labelled cDNA samples were synthesised at the J. Craig Venter Institute (JCVI), Rockville, Maryland, USA, as described previously (McDonagh *et al.*, 2008a). Protocols for direct labelling and hybridisation of cDNA probes can be found on the JCVI website (pfgrc.jcvi.org/index.php/microarray/protocols.html).

2.10.3 Data capture for cDNA microarrays

The GenePix 4000b (Axon Instruments, Foster City, CA) semiconfocal microarray scanner was used to measure the intensities of hybridised probes. Fluorescence was measured with the associated GenPix Pro 3.0 software, setting pixel size at 10 μm and lines to average at 2. The photomultiplier tube (PMT) voltage for each channel (532 nm and 635 nm) was adjusted to give an overall intensity ratio across each slide of around 1, a background intensity at 532 nm of around 100, and a maximal intensity at around saturation (65536 or 216 i.e. 16 bit scanning resolution). Datasets were exported as GenePix Results (GPR) files. Images were saved as .TIF files and TIGR Spotfinder (Saeed *et al.*, 2003) was used to quantify fluorescence intensities. Poor quality spots were identified manually and flagged.

2.10.4 Manipulation and analysis of microarray data

After Spotfinder analysis, results were exported as TIGR software-compatible MEV files. Data normalisation was performed with TIGR TM4 freeware (www.tm4.org/) for locally-weighted scatter plot smoothing (LOWESS). After LOWESS normalisation, the flip dye pairs were analysed in a consistency check to remove any outlier spots (defined as those falling beyond the standard deviation of the array-wide average $\log_2$ ratio of the fluorescence values for spot intensity). The resulting data was averaged taking a total of 6 intensity data points for each gene (triplicate copies of the genes printed on each array and the duplicate flip-dye arrays for each experiment). The phase- or strain-specific comparative analysis of gene expression datasets was conducted in Genespring GX 11.02 (Aligent). Normalised $\log_2$ expression ratios were filtered on expression level and differentially regulated transcripts were defined as having $\log_2$ (Cy5/Cy3) greater than the arbitrary thresholds of ± 1.5 or ±2, as appropriate. Clustering was performed using the software STEM (Short Time-series Expression Miner), designed for clustering, comparing, and visualizing gene expression data from short time series microarray experiments (Ernst and Bar-Joseph, 2006).

CHAPTER III

PHYSIOLOGICAL REQUIREMENT FOR pH SIGNALING DURING *A. FUMIGATUS* STRESS ADAPTATION AND VIRULENCE

3.1 Overview

A. fumigatus virulence has been defined as a polygenic trait (Askew, 2008; Hohl and Feldmesser, 2007), originating from a combination of several contributing basic traits, which allows the fungus to inactivate or escape host defence systems and to withstand the nutritional, oxidative and other physiological stresses exerted by the host niche. The mammalian immune system is usually depicted as the primary impediment to fungal colonisation and subsequently infection, but in this context it is also necessary to consider the dramatic differences between a saprophytic lifestyle in the natural environment and a parasitic lifestyle as a mammalian pathogen (Cooney and Klein, 2008). Host-related abiotic stresses include elevated temperature, heightened ambient pH, and low availability of metal ions, usually sequestered by the host to support its own metabolism. Accordingly, transcriptional profiling of *A. fumigatus* in the early stages of infection identifies differentially expressed genes involved in environmental pH adaptation and in iron uptake, utilisation and mobilisation in a neutropenic murine model of IPA (McDonagh *et al.*, 2008a). This study demonstrated that, together with various types of other stresses such as iron and nitrogen limitation and temperature, alkaline stress is indeed one of the host-imposed stresses *A. fumigatus* must face to adapt to the host niche. All microorganisms, but in particular those inhabiting mammalian niches during infection, must adapt to the pH of the surrounding environment. In fact, within a human or murine host, the pH shifts to slightly alkaline; adaptation to which requires therefore, not only the maintenance of internal pH homeostasis but also the appropriate expression of genes involving functions at the cell surface or in the extracellular environment, especially to ensure supply of the necessary nutrients, whose bioavailability is altered as a function of ambient pH.

The conserved PacC/Rim101p signal transduction pathway mediates fungal pH adaptation. Due to the easy genetic manipulation achievable in *A. nidulans* (Pontecorvo *et al.*, 1953), this model ascomycete has represented the organism of choice for the extensive

characterisation of the PacC/Rim101p pathway, since its first discovery more than 20 years ago (Caddick *et al.*, 1986c). Findings that murine aspergillosis requires functionality of *A. nidulans pacC* highlights the importance of fungal PacC-mediated alkaline adaptation in the pathogenesis of murine pulmonary aspergillosis (Bignell *et al.*, 2005). For murine pathogenicity, *A. nidulans* PacC must be present, and proteolytically processed via pH-sensing Pal proteins (Bignell *et al.*, 2005). The mechanism leading to the activation of this regulatory pathway has not yet been characterised extensively in *A. fumigatus* and its precise role during infection is still unexplored by the current literature. In this study two *A. fumigatus* Δ*pacC* mutants, constructed in different genetic backgrounds, were characterised in terms of phenotype, virulence and tissue invasion. Concordant with studies in *A. nidulans,* these findings underline the physiological requirement for PacC-mediated pH signaling during *A. fumigatus* alkaline stress adaptation.

3.2 Methods

3.2.1 *A. fumigatus* strains

Two *A. fumigatus* strains, the clinical isolates CEA10 and ATCC46645 (see Appendix A), were used for Δ*pacC* mutant construction. Both mutants were constructed by gene replacement using a split-marker strategy by a collaborator Markus Schrettl (Hubertus Haas laboratory at Innsbruck Medical University). To propagate Δ*pacC* mutants, AMM (- aneurin) was supplemented with 0.5 μg/ml Pyrithiamine (PTR, Takara) as selective agent. PTR is thiamine antagonist, inhibiting thiamine pyrophosphorylation and therefore inducing thiamine deficiency (Liu *et al.*, 2006). Hence, the use of PTR in culturing media requires omission of aneurin.

Gene replacement was confirmed by PCR and by Southern Blotting for both mutants. In the case of the ATCC46645 Δ*pacC* mutant, this was conducted in the Haas laboratory. For the CEA10 Δ*pacC* mutant, the integrity of the *pacC* coding region was tested in 3 independent transformants, supplied by Markus Schrettl, using the oligonucleotides pF-PacCint1 and pR-PacCint1 (see Appendix B), designed to amplify a region of 1100 bp of the *pacC* gene (nucleotides +543 to +1593 with respect to the ATG). Clones from which the *pacC* genetic locus could not be amplified were further analysed by Southern blotting using two DIG probes. A *pacC*-specific probe, obtained by PCR with the oligonucleotides PacCSB1 and PacCSB2 (see Appendix B), which amplify a region of 1250 bp of the 5' flanking region of

pacC gene (nucleotides -1266 to -24 with respect to the ATG) was used to differentiate between wild type and mutant *pac*C genetic loci. A second *ptrA*-specific probe, obtained by PCR using the oligos LucPtrAF and LucPtrAR (see Appendix B), which amplify a region of 580 bp of the *ptrA* gene (nucleotides +638 to +1137 with respect to the ATG) was used to determine between single and multiple insertions of the gene replacement cassette. Genomic DNA was extracted from the mycelia and digested overnight with the enzyme SalI.

3.2.2 *A. fumigatus* phenotypic testing

As summarised in Table 3.1, the phenotype of the *A. fumigatus* Δ*pacC* mutants was examined in AMM pH 6.5, AMM pH 8.0 (buffered with 100 mM Tris-HCl pH 8.0) and AMM pH 7.2 (buffered with 100 mM Tris-HCl pH 7.2).

Media	Test Condition	Comments
AMM pH 6.5	Neutral pH	Buffered with 100 mM MES pH 6.5
AMM pH 7.2	Physiological (host) pH	Buffered with 100 mM Tris-HCl pH 7.2
AMM pH 8.0	Alkaline stress	Buffered with 100 mM Tris-HCl pH 8.0

Table 3.1: Media and buffers used for *A. fumigatus* phenotypic screening. The composition of the media is described in Section 2.3.2.

An alternative buffering system, using phosphate, was also used to test the response to alkaline conditions and was composed of 2.7 mM NaH_2PO_4, 50 mM Na_2HPO_4, and 20 ml/ phosphate-free salt solution (26 g/l KCl, 26 g/l $MgSO_4$, 40 mg/l $Na_2B_4O_7.10H_2O$, 400 mg/l $CuCl_2.5H_2O$, 800 mg/l $FeCl_3.H_2O$, 800 mg/l $MnSO_4.4H_2O$, 800 mg/l $Na_2MoO_4.2H_2O$, 8 g/l $ZnSO_4.7H_2O$).

A. fumigatus was cultured for 4 days on ACM at 37°C. Spores were harvested from a single plate and serially diluted prior to plating ($1x10^4$, $1x10^3$, $1x10^2$, $1x10^1$ spores). Each dilution of $1x10^4$, $1x10^3$, $1x10^2$, $1x10^1$ spores was plated in triplicate as individual spots on the same plate. Plates were incubated for 2 days at 37°C. Plates were photographed without magnification using a Nikon Coolpix 990 digital camera. *Aspergillus* spores were visualised using a Nikon Eclipse 80i microscope.

3.2.3 Murine infections

Murine infections were performed under UK Home Office project Licence PPL/70/6487 in dedicated facilities at Imperial College London. Outbred male mice (strain CD1, 18-22 g, Harlan Ortech) were housed in individually vented cages. Mice were immunosuppressed as previously described (Schrettl *et al.*, 2004). *A. fumigatus* spores for inoculation were grown on ACM for 5 days prior to infection. Conidia were freshly harvested using sterile saline (Baxter Healthcare) and filtered through Miracloth (Calbiochem, UK) and conidial suspensions were spun for 10 min at 3,000 rpm, washed twice with sterile saline and counted using a hemocytometer.

For the high dose-survival analysis, conidia were resuspended at a concentration of $1.5x10^7$ cfu/ml and viable counts from administered inocula were determined by serial dilutions on ACM plates incubated for 3 days at 37ºC. Mice were anaesthetised by isofluorane inhalation and infected by intranasal instillation of $6.0x10^5$ conidia in 40 µl of saline. For the low dose-survival analysis, conidia were resuspended at a concentration of $1.25x10^6$ cfu/ml and viable counts from administered inocula were determined by serial dilutions on ACM plates incubated for 3 days at 37ºC. Mice were infected by intranasal instillation of $5.0x10^4$ conidia in 40 µl of saline. Mice were weighed every 24 hours from the day of infection and visual inspection was made twice daily. In the majority of cases, the end point for survival experimentation was a 20% reduction in body weight measured from day of infection, at which point mice were sacrificed.

Histological analysis was performed on samples obtained during infections for transcriptional analysis of the ATCC46645 Δ*pacC* mutant and the respective parental isolate. Mice were culled and processed at 4, 8 and 16 hours post-infection. Lungs were removed immediately after sacrifice and fixed in 4% (w/v) formaldehyde (Sigma). Lungs were embedded in paraffin prior to being sectioned and stained with hemotoxylin and eosin (H&E) or light green and Grocott's Methenamine Silver (GMS).

3.3 Results

3.3.1 Phenotypic characterisation of *A. fumigatus* Δ*pacC* mutants

The two *A. fumigatus* Δ*pacC* mutants (ATCC46645 and CEA10 genetic backgrounds) provided by Markus Schrettl (Hubertus Haas's laboratory) were analysed to verify gene

replacement by PCR and by Southern Blotting. In the case of the ATCC46645 Δ*pacC* mutant, this was conducted in the Haas laboratory.

For the CEA10 Δ*pacC* mutant, the integrity of the *pacC* coding region was initially tested in three independent transformants using the oligonucleotides pF-PacCint1 and pR-PacCint1 (see Appendix B). Because these oligonucleotides were designed to amplify a region of 1100 bp of the *pacC* gene, no PCR product was expected if the *pacC* gene had been efficiently deleted and substituted with the split-pyrithiamine cassette. Using this approach, no amplification product resulted for the clone represented in Fig. 3.1A, which was therefore further analysed by Southern blotting using two DIG probes (Fig.3.1B). A *pacC*-specific probe, obtained by PCR with the oligonucleotides PacCSB1 and PacCSB2 (see Appendix B) was used to differentiate between wild type and mutant *pac*C genetic loci. The expected signals were 7883 bp for the wild type and 3355 bp for the Δ*pacC* mutant. A second *ptrA*-specific probe, obtained by PCR using the oligos LucPtrAF and LucPtrAR (see Appendix B) was used to determine between single and multiple insertions of the gene replacement cassette. No signal was expected for the wild type, whereas for a single, homologous integration of the deletion cassette the expected signal was 3355 bp.

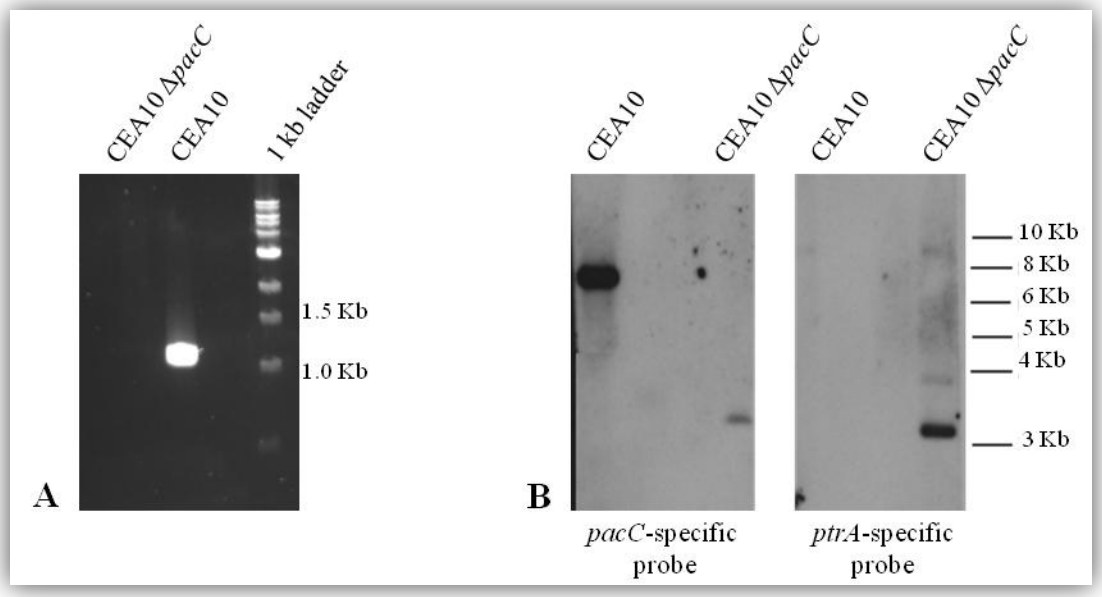


Fig. 3.1: Verification of Δ*pacC* mutant in the *A. fumigatus* CEA10 genetic background by PCR and Southern blotting. (A) PCR results showing the CEA10 Δ*pacC* mutant in comparison to the CEA10 wild type. 1 Kb DNA ladder (10.0, 8.0, 6.0, 5.0, 4.0, 3.0, 2.0, 1.5, 1.0 and 0.5 Kb). (B) Southern Blotting results showing the CEA10 Δ*pacC* mutant in comparison to the CEA10 wild type for *pac*C-specific and *ptrA*-specific probes.

The phenotype of Δ*pacC* mutants in the *A. fumigatus* ATCC46645 and CEA10 genetic backgrounds were analysed and compared to those of the respective parental strains at neutral (pH 6.5), host physiological pH (pH 7.4: supposed murine lung pH) and alkaline conditions (pH 8.0). Each strain was tested in serial dilutions of $1x10^4$, $1x10^3$, $1x10^2$, $1x10^1$ spores. Tests were performed in triplicate (data not shown). Fig. 3.2 shows the results of the phenotypic test for *A. fumigatus* Δ*pacC* mutants and the respective parental strains. In addition to a morphological defect and poor conidiation at pH 6.5, *A. fumigatus* Δ*pacC* mutants exhibit reduced or complete prevention of growth at pH 8.0 compared to the wild type. Significantly, the growth of *A. fumigatus* ATCC46645 Δ*pacC* is prevented at pH 7.2, the physiological conditions expected in mouse lungs. Alkaline sensitivity was less extreme in the case of CEA10 Δ*pacC*.

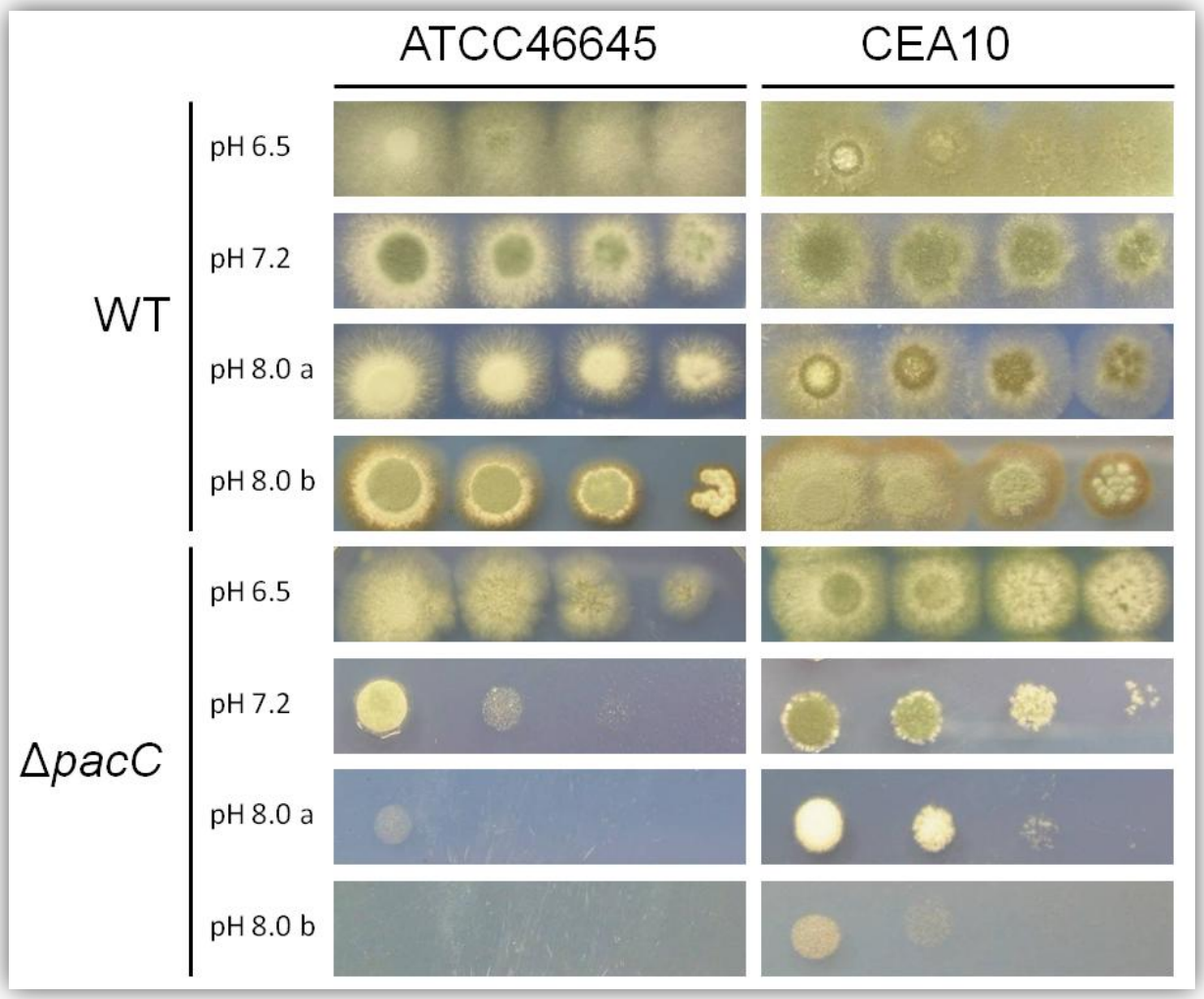


Fig. 3.2: Phenotypic analysis of the *A. fumigatus* Δ*pacC.* *A. fumigatus* Δ*pacC* mutants in the ATCC46645 (bottom left) and CEA10 genetic backgrounds (bottom right) compared to respective parental isolates ATCC46645 (top right) and CEA10 (top left). Each strain was plated in serial dilutions of $1x10^4$, $1x10^3$, $1x10^2$ and $1x10^1$ spores from left to right. For each strain, the conditions tested were AMM 6.5, AMM 7.2, AMM pH 8.0 (pH 8.0 a) and phosphate-buffered pH 8.0 media (pH 8.0 b). Plates were incubated for 2 days at 37°C.

3.3.2 Effect of *pacC* deletion on *A. fumigatus* virulence in a neutropenic murine model of infection

The virulence of *A. fumigatus* Δ*pacC* mutants was compared to that of the parental wild type strains using a neutropenic murine model of invasive pulmonary aspergillosis. For the neutropenic model of infection, immunosuppression of mice was performed by intraperitoneal injections of cyclophosphamide (150 mg/kg) on days –3, –1, +2, and subsequently every third day for the duration of the experiment and by a single subcutaneous dose of hydrocortisone acetate (112.5 mg/kg) on day –1 (Schrettl *et al.*, 2004). Initially four groups of 8 neutropenic male mice were inoculated intranasally with $6x10^5$ spores of the

ATCC46645 Δ*pacC* and CEA10 Δ*pacC* mutants and the respective parental isolates. To verify the administered inocula in mice, the determination of viable counts was performed using serial dilution on solid ACM culture. Mice were weighed daily and inspected regularly. For survival analysis, in the majority of instances, the end of the experimentation corresponded to a 20% reduction in body weight measured from the day of the infection, at which point mice were culled. As shown in Fig. 3.3, infection with ATCC46645 Δ*pacC* mutant resulted in 50% mortality within 13.5 days compared to infection with the wild type ATCC46645 strain which resulted in 50% mortality within 5 days ($p<0.0001$, Kaplan-Meier log rank analysis). This demonstrates that, in comparison with the wild type strain, *A. fumigatus* ATCC46645 Δ*pacC* is attenuated in a murine model of pulmonary aspergillosis.

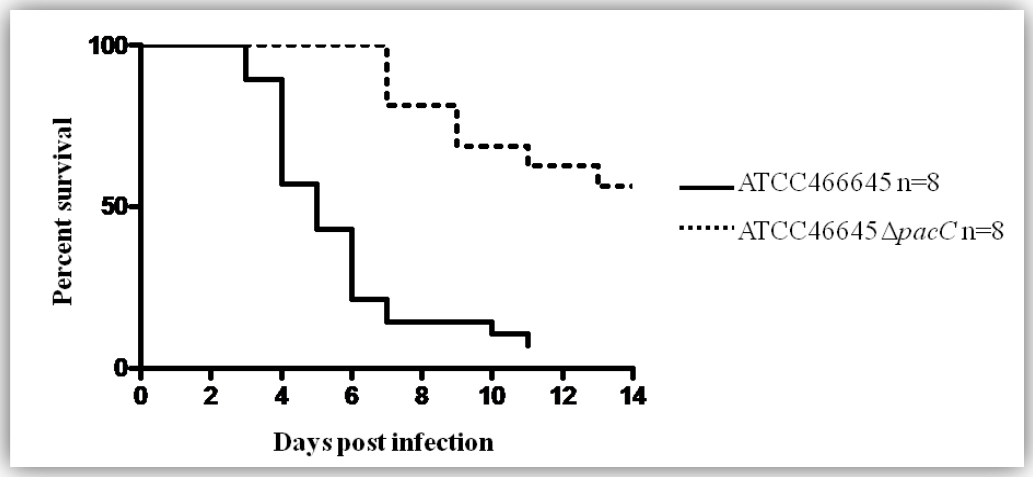


Fig. 3.3: Comparative survival of neutropenic mice infected with ATCC46645 and ATCC46645 Δ*pacC*. Mice were inoculated with $6x10^5$ spores for each strain (n=8). Median survival was 5 and 13.5 days for ATCC46645 and ATCC46645 Δ*pacC* respectively. A Kaplan-Meier survival curve and a log rank test were used to compare survival levels among the strain groups, demonstrating significant difference between the survival curves for ATCC46645 and ATCC46645 Δ*pacC* ($p<0.0001$).

A different result was observed following infection with an *A. fumigatus* CEA10 Δ*pacC* mutant. As shown in Fig. 3.4, infection with CEA10 Δ*pacC* and the wild type CEA10 strain resulted, in both cases, in 50% mortality within 5 days ($p=0.3774$, Kaplan-Meier log rank analysis). This suggests that, in comparison with the wild type strain, the *A. fumigatus* CEA10 Δ*pacC* mutant is not attenuated in a murine model of pulmonary aspergillosis.

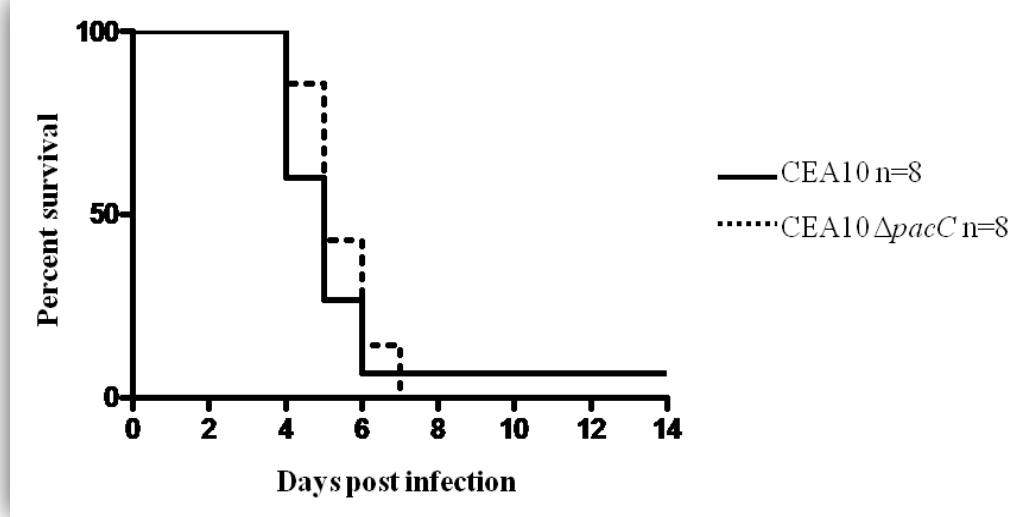


Fig. 3.4: Comparative survival of neutropenic mice infected with CEA10 and CEA10 Δ*pacC*. Mice were inoculated with $6x10^5$ spores for each strain (n=8). Median survival was, for both strains, 5 days. A Kaplan-Meier survival curve and a log rank test were used to compare survival levels among the strain groups, showing no significant difference between the survival curves for CEA10 and CEA10 Δ*pacC* (p=0.3774).

The differential virulence observed for the ATCC46645 Δ*pacC* and CEA10 Δ*pacC* mutants correlates with the observed differential alkaline pH sensitivity of the strains (Fig. 3.2). At pH 7.2, ATCC46645 Δ*pacC* is almost unable to grow, whereas CEA10 Δ*pacC* is reduced for growth but not entirely impaired, possibly explaining the differential virulence data obtained in the murine model. Relating the phenotypic data to those obtained in model infections, an inoculum of 10^4 is ten times lower than the concentration usually used to infect a single mouse.

Hypothesising that the infectious dose of $6x10^5$ spores masked a possible virulence defect, the experiment was repeated with a lower infectious dose. Two groups of 8 neutropenic male mice were inoculated with $5x10^4$ spores of CEA10 Δ*pacC* and CEA10 reconstituted via ectopic insertion of the *pacC* gene. As before, the determination of viable counts was performed using serial dilution on solid ACM culture to verify the administered inocula in mice. Mice were weighed daily and inspected regularly. For survival analysis, in the majority of instances, the end of the experimentation corresponded to a 20% reduction in body weight measured from the day of the inoculum, at which point mice were sacrificed. As shown in Fig. 3.5, infection with low doses of CEA10 Δ*pacC* resulted in 50% mortality within 17 days, compared to 50% mortality within 4 days for the reconstituted CEA10 strains. This demonstrates that, in comparison with the respective wild type strain, *A. fumigatus* CEA10 Δ*pacC* is attenuated in a low-dose murine model of pulmonary aspergillosis ($p<0.0001$, Kaplan-Meier log rank analysis).

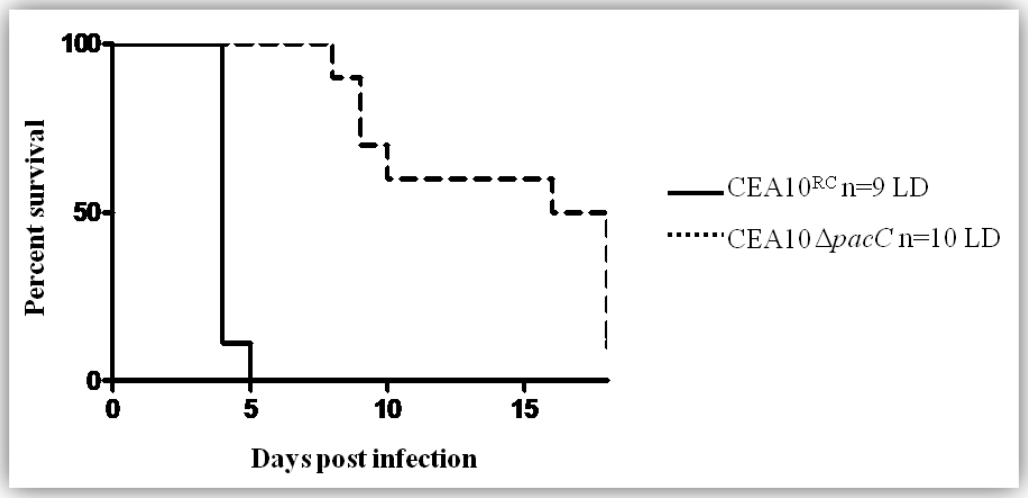


Fig. 3.5: Survival of neutropenic mice infected with low dose CEA10 Δ*pacC*. Mice were inoculated with $5.0x10^4$ spores for the CEA10 Δ*pacC* strain and ectopically reconstituted CEA10. Median survival was 17 and 4 days for CEA10 Δ*pacC* and reconstituted CEA10 ($CEA10^{RC}$) respectively. A Kaplan-Meier survival curve and a log rank test were used to compare survival levels among the strain groups, demonstrating a significant difference between survival curves ($p < 0.0001$).

3.3.3 Histopathological analysis of *A. fumigatus* ATCC46645 Δ*pacC* mutant in neutropenic mice

To examine comparative growth of the highly attenuated ATCC46645 Δ*pacC* mutant, and a fully virulent parental strain, tissues were recovered from a further murine infection experiment, which explored the *A. fumigatus* transcriptome during initiation of infection (Chapter IV). Fig. 3.6 shows a time course of histological samples (4, 8 and 16 hrs) for the wild type strain ATCC46645 (top row) and the ATCC46645 Δ*pacC* mutant (bottom row). Minimal differences between the wild type and mutant isolates are visible in the earlier stages, corresponding to 4 and 8 hrs, of infection (Fig 3.5A, B, D and E). Although, at 8 hours post infection, wild type spores are visibly swollen and beginning to germinate (Fig. 3.5B). In addition, some slight differences in the level of inflammation were associated with the wild type infection, as visible from the comparison between panels B and E in Fig. 3.6. The difference becomes clearly visible from the comparison at 16 hours between the wild type strain and the ATCC46645 Δ*pacC*, as shown in panels C and F of Fig. 3.6. The Δ*pacC* mutant seems unable to progress beyond primary hyphal morphotypes, whereas the parental isolate revealed extensively branched invasive growth.

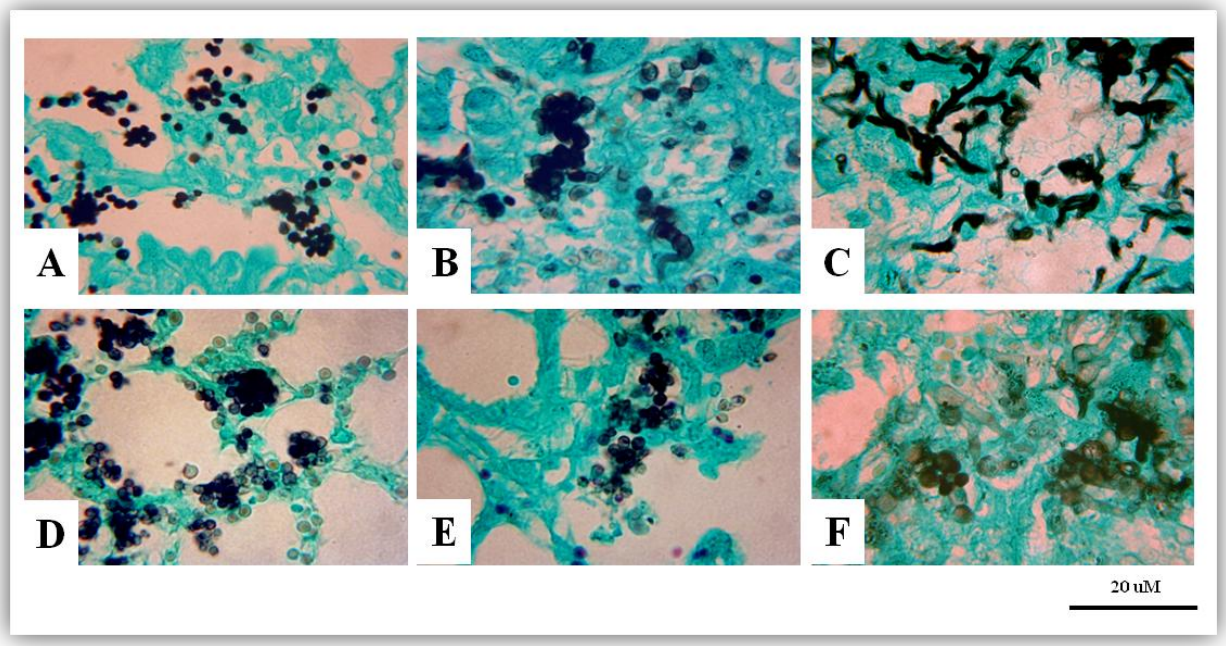


Fig. 3.6: Comparative lung histopathology in neutropenic mice infected with ATCC46645 and ATCC46645 Δ*pacC*. Mice were infected with $1x10^8$ *A. fumigatus* spores. Lung sections were stained with Grocott's Methenamine silver and light green. Host tissue stains green and fungal material stains black. Pictures were taken with 50x magnification. **(A)** ATCC466645, 4 hours; **(B)** ATCC466645, 8 hours; **(C)** ATCC466645, 16 hours; **(D)** ATCC466645 Δ*pacC*, 4 hours; **(E)** ATCC466645 Δ*pacC*, 8 hours; **(F)** ATCC466645 Δ*pacC*, 16 hours.

3.4 Discussion

The role of the Rim101p/PacC family members in virulence has been extensively studied, highlighting how this regulatory pathway is able to affect, in different ways, the success of fungal pathogens in their host niche. In mice, *C. albicans* Rim101p (Davis *et al.*, 2000a) and *A. nidulans* PacC (Bignell *et al.*, 2005) are necessary for the establishment of disseminated candidiasis and IPA respectively. In plants, the homologue of PacC in *Sclerotinia sclerotiorum* (Pac1) (Rollins, 2003) and *Colletotrichum acutatum* (Klap2) (You *et al.*, 2007) are also required for virulence; however, no specific role in plant infection has been identified for *Ustilago maydis* Rim101 (Arechiga-Carvajal and Ruiz-Herrera, 2005). On the contrary, in the plant pathogen *Fusarium oxysporum* PacC has been demonstrated to act as a negative regulator of virulence (Caracuel *et al.*, 2003b). Certain components required for alkaline adaptation of *Aspergillus* species are highly conserved between *A. nidulans* and *A. fumigatus*, as shown by the alignments presented in Appendix F. Due to the existence of

sexual and parasexual stages in the *A. nidulans* life cycle, this organism has been widely used as a model for *A. fumigatus*.

The recent development of new molecular tools for *A. fumigatus* genetic manipulation, and considerable progress in the comprehension of its genetic and molecular biology (Brakhage and Langfelder, 2002), have facilitated investigation of the pH regulatory mechanism directly in this pathogen. Pertinent publications are extremely recent (Amich *et al.*, 2009; Amich *et al.*, 2010), representing the first experimental studies on *A. fumigatus* PacC. The construction and phenotypical characterisation of *A. fumigatus* PacC mutants confirmed strong parallels with PacC function in *A. nidulans* (Amich et al., 2009) and revealed the role of the transcription factor in repressing, under neutral, zinc-limiting conditions, the ZfrA and ZfrB transporters. As in *A. nidulans*, growth of the *pacC*$^{+/-}$ mutant was almost identical to that of the wild type at acid pH, but impaired as a consequence of pH increase. Growth of the *pacC*^{c} mutant was impaired at acid pH, but not at alkaline pH, where the growth was identical to the wild type. The behaviour of the two mutants therefore reflects that expected on the basis of experimental evidence in *A. nidulans* for acidity- (*pacC*$^{+/-}$) and alkalinity-mimicking (*pacC*^{c}) phenotypes. In addition, similarly to *A. nidulans* (Tilburn *et al.*, 1995), *pacC* gene expression is slightly increased as a consequence of alkalinisation. *A. fumigatus* PacC has been demonstrated to be involved in regulation of zinc uptake, in particular by repressing under neutral, zinc-limiting conditions the ZfrA and ZfrB transporters, in order to economise cellular resources. Considering the proximity between the PacC consensus site and the TATA box in *zfrB*, the mechanism by which PacC is hypothesised to repress *zfrB* transcription involves the physical blockage of efficient RNA polymerase binding. The link between pH regulation and zinc homeostasis is crucial, considering zinc solubility decreases around neutral pH. *A. fumigatus* PacC has also been linked to the regulation of expression of two other genes required for fungal growth in alkaline and extreme zinc-limiting conditions *zrfC* and *asp2* (Amich et al., 2010). Interestingly, in this case, the mode of action of PacC contrasts with the accepted model of PacC function, which supposes that in alkaline conditions PacC activates the transcription of alkaline-expressed genes and represses the expression of acid-expressed genes. In fact, PacC derepresses the transcription of the *zrfC* and *asp2* at alkaline pH but represses it at acidic pH.

The zinc studies extensively focused on the role of *A. fumigatus* PacC on zinc uptake but no biological clues were provided on its role during infection, which is still unreported in the current literature. The analysis of phenotype, virulence and tissue invasion of the *A. fumigatus* Δ*pacC* mutants presented in this study has highlighted (as for numerous fungal

species such as *A. nidulans*, *S. cerevisiae* and *C. albicans*), the importance of PacC for *A. fumigatus* virulence and its requirement for pH tolerance in alkaline environments.

3.4.1 *pacC* deletion prevents *A. fumigatus* adaptation to alkaline stress *in vitro*

Our collaborators at Innsbruck Medical University generated two Δ*pacC* mutants using a split-pyrithiamine marker in the *A. fumigatus* ATCC46645 genetic background and in the sequenced *A. fumigatus* isolate CEA10. The choice of these genetic backgrounds align with other mutant constructions in the Bignell laboratory which had previously used both backgrounds and with the previous cited publications from Amich *et al.*, 2009 where the *pacC*$^{+/-}$ mutant was constructed in CEA17, the auxotrophic *pyrG*$^{-}$ version of CEA10. These genetic backgrounds are also routinely used for collaborations with the Haas laboratory, which has extensively characterised the role of siderophores in fungal physiology and virulence (for a comprehensive review see Haas *et al.*, 2008; Haas, 2003).

These Δ*pacC* mutants were verified for the correct and single insertion of the split-pyrithiamine marker in the *pacC* genomic locus and subsequently their phenotypes were analysed and compared to that of the respective parental strains at pH 6.5, 7.2 and 8.0. Specific phenotypes are associated with *pacC* null mutants in *A. nidulans* which extend beyond growth defects in alkaline conditions. The phenotype of *A. nidulans pacC* deletants includes cryosensitivity of growth in neutral conditions, a low growth rate at the permissive temperature, poor conidiation and overproduction of a brown pigment, presumed to be melanin (Tilburn *et al.*, 1995). The same phenotypic alterations were revealed for the two *A. fumigatus* Δ*pacC* mutants in the ATCC46645 and CEA10 backgrounds (Fig. 3.2). In neutral conditions, *A. fumigatus* Δ*pacC* mutants in both backgrounds show morphological defects, i.e. poor conidiation (Fig. 3.2). As reported for *A. nidulans pacC* null mutations (Tilburn *et al.*, 1995), the *A. fumigatus* Δ*pacC* mutants also exhibit reduced, or lack of growth, compared to the wild type when pH is increased. These findings align with the characterisation of the *A. fumigatus pacC*$^{+/-}$ mutant recently presented by Amich *et al.*, 2009 which shows an acidity-mimicking phenotype whereby growth of the *pacC*$^{+/-}$ mutant impaired gradually as a consequence of increasing pH. However, in neutral conditions only minor defects was associated with this mutant, which was constructed by replacing the *pacC* ORF with a truncated version deleted for residues L471 to H556, therefore leading to the inability of PacC to undergo proteolytic processing (similarly to the *A. nidulans pacC*$^{+/-}$ *20205* mutant presented in Mingot *et al.*, 1999). The difference in phenotype at neutral pH between the Δ*pacC* mutants characterised in this study and the *pacC*$^{+/-}$ mutant presented by Amich *et al.*,

2009 probably derives from the salt composition of the media itself, which slightly differ in iron concentration. The importance of the salt composition was confirmed in the present study, where two different alkaline media were used to assess fungal growth. In fact, alkaline media buffered with phosphate-free solution affects significantly more the growth of Δ*pacC* mutants (Fig. 3.2).

pH is a negative logarithmic measure of hydrogen ion activity (Sörensen, 1909), used to express the wide variation in H^+ concentration occurring in aqueous solution. According to an established scale, the term acidity is associated with pH from 1 to 6.9 and the term alkalinity with pH from 7.1 to 14. As a consequence of active metabolism, there is always a movement of protons inside and outside the cytoplasm of cells. Cells have therefore evolved several mechanisms to maintain ion balance and guarantee optimal activity of major metabolic pathways, whose functioning would be otherwise damaged by large deviations of intracellular pH. In fact, proteins have an optimal pH at which their activity is maintained and outside this range their functioning is strongly impaired. In addition, most cellular nutrients uptake systems are driven by the electrochemical gradient. As a consequence of *pacC* deletion, many, as opposed to few, functions are likely to be impaired, including the control of the synthesis of secreted proteins (mainly enzymes), permeases and (intracellular) enzymes involved in the synthesis of exported metabolites (Arst, 2003; Peñalva and Arst Jr, 2004) to the synthesis of enzymes implicated in post-translational modifications of secreted enzymes and enzymes catalyzing energy-yielding reactions. Accordingly, it is not surprising that a specific phenotype is associated with *pacC* deletion not only in alkaline, but also in neutral conditions, as observed in previous studies for *A. nidulans* and in this study for *A. fumigatus*.

Transcriptional expression is likely to be profoundly modified in *pacC* mutants, as extensively studied in the budding yeast *S. cerevisiae*, where Rim101p has been associated with a multitude of biological processes, other than alkaline pH adaptation, such as sporulation, invasive growth, ion tolerance and acquisition, and certain cell wall characteristics (Denison, 2000; Hayashi *et al.*, 1998; Lamb *et al.*, 2001; Lamb and Mitchell, 2003; Li and Mitchell, 1997). As for *A. nidulans* and *A. fumigatus*, Δ*rim101* mutants exhibit specific phenotypes in neutral conditions including reduced growth, poor sporulation, poor growth at low temperature and altered colony morphology (Su and Mitchell, 1993a; Su and Mitchell, 1993b) and defective haploid invasive growth (Li and Mitchell, 1997; Xu and Mitchell, 2001). The predicted immediate effect of the alkalinisation of the external environment is the disruption of membrane proton gradients supplying energy for transmembrane transport and consequent nutrient and ion limitation (Lamb and Mitchell, 2003). Rim101p has been associated principally with general ion homeostasis, through

control of the transcriptional expression of a series of protein pumps. The essential role of these transporters at alkaline pH is evidenced by phenotypes of null mutants lacking these pumps, which are unable to grow in alkaline conditions and/or cation sensitivity (Lamb and Mitchell, 2003). The plasma membrane pump Pma1p neutralises the cytoplasm by pumping protons out of the cell in an ATP-dependent manner (van der Rest *et al.*, 1995). The proton gradient generated from its action is utilised to support symport activitites acquiring solutes from the extracellular environment, such as amino acids, nucleotide bases, phosphate and other molecules. The plasma membrane-localised Ena1p sodium/H^+ ATPase expels Na^+ from the cytoplasm to generate a gradient utilised for the uptake of other cations (Rodriguez-Navarro *et al.*, 1994) and the vacuolar H^+ ATPase Vma4p is necessary for vacuolar acidification (Stevens and Forgac, 1997). Reduction of such ion pump activity may clearly explain the phenotype observed for *rim101*$^-$ in neutral conditions (Lamb *et al.*, 2001). A similar set of targets for the regulatory action of PacC might be hypothesised for the *Aspergillus* species, but currently only a limited number of PacC-dependent genes have been identified and anyway mostly for *A. nidulans* (Espeso and Penalva, 1996*;* Tilburn *et al*., 1995).

In the context of adaptation to the host niche and its relationship with virulence, it is important to remember that the pH of different cellular compartments, body fluids, and organs is usually tightly regulated by the acid-base homeostatic process. In humans, the pH of blood is usually slightly basic with a value of pH 7.4, often referred to as physiological pH. Other pH values in human body fluids range from pH 1 for the gastric acid to pH 8.1 for pancreas secretions, through pH 6 for urine. Within the mammalian cell, different pHs are represented too, ranging from pH 4.5 in the lysosomes to pH 7.2 in the cytosol and pH 7.5 in the mitochondrial matrix. Enzymes and other proteins have an optimum pH range and can become inactivated or denatured outside this range. The most common disorder in acid-base homeostasis is acidosis, an acid overload in the body which is generally defined by pH falling below pH 7.35. Physiological pH of murine lungs has been defined as pH 7.2 (Song *et al.*, 2003) and interestingly, the *A. fumigatus* Δ*pacC* mutants already exhibit reduced or prevented growth, compared to the wild type, when pH is increased to this slightly-alkaline value.

An unexpected and significant difference was found between the mutants constructed in two different *A. fumigatus* genetic backgrounds whereby *pacC* deletion in the ATCC46645 genetic background was more sensitive to alkaline pH than in the CEA10 background. However, from our phenotypic analysis, a different growth rate was visible already when comparing the two wild type isolates. Considering ATCC46645 and CEA10 in neutral conditions, it looks likely that the CEA10 wild type strain produces slightly more conidia or

sporulates earlier and it would be therefore interesting to quantitatively assess radial growth and conidiation rate for the two different wild type strains. The differential response to alkalinisation of the media might be due to an altered modification of the media pH as a consequence of fungal growth. Originally *A. fumigatus* had been defined as a single homogenous species (Raper, 1965); however, different strains have been demonstrated to differ in growth requirements and micromorphology, having branched conidiophores, elongate or septate phialides and size or shape differences in conidia (Leslie *et al.*, 1988; Rinyu *et al.*, 1995). At present, the morphological and molecular differences between the numerous *A. fumigatus* strains are poorly understood: in the literature, there are few occurrences where mutants have been constructed and characterised at the same time and in the same differential genetic backgrounds used in this study. A Δ*sidA* mutant was constructed in both the *A. fumigatus* ATCC46645 and the CEA10 genetic backgrounds (Schrettl *et al.*, 2004), to study the siderophore biosynthetic pathway in *A. fumigatus*. *sid*A encodes the L-ornithine-N^5-monooxygenase, which catalyzes the first step of the hydroxamate-type siderophore biosynthesis (Haas, 2003; Haas *et al.*, 2008). The phenotypic tests performed and the additional quantitative analysis of radial growth and conidiation of the strains did not show any significant difference between *A. fumigatus* genetic backgrounds. The phenotypic difference between the *A. fumigatus* Δ*pacC* mutants in two different genetic backgrounds might indicate a differential regulation of a function(s) under PacC regulatory control, which supports alkaline adaptation *in vitro*, for instance of certain pumps or transporters. Unfortunately, only for the CEA10 strain the sequence is publicly available (Nierman *et al.*, 2005), so it is not possible to infer which PacC-related function(s) might differ between the strains. Another explanation might be the redundancy of genes encoding for specific functions. An example is the Ena1p transporters: *S. cerevisiae* S288c has three *ENA*, but this number varies in other yeasts strains. According to the redundancy of a function in a specific strain and the extent by which this function is regulated by PacC, *pacC* deletion in different genetic backgrounds could differentially affect alkaline adaptation. However, a growth difference was notable also in the wild type strains on alkaline medium suggesting loss of a PacC-independent function, which may be worsened in the absence of PacC-mediated alkaline adaptation.

3.4.2 *A. fumigatus* Δ*pacC* mutants are attenuated for virulence

One of the most important applications of the study of ambient pH regulation in fungi is derived from its impact on fungal virulence, especially for the most prominent airborne

pathogen *A. fumigatus* (Latge, 1999). The importance of the *A. nidulans* PacC-mediated pH response in the pathogenesis of pulmonary aspergillosis was firstly shown using mutational analysis to demonstrate that, in neutropenic mice, the virulence is acutely attenuated when eliminating the *A. nidulans* transcription factor PacC, blocking the ambient pH signal transduction pathway or preventing PacC proteolytic processing (Bignell *et al.*, 2005). *pacC* and *palB* loss of function mutants are attenuated for virulence in a respiratory model of murine infection, indicating that *A. nidulans* Pal-mediated pH signalling and PacC-regulated gene expression are essential for the development of infection in the host. In stark contrast, constitutive activation of PacC leads to increased mortality, even in a *palB* loss of function mutant. These data (Bignell *et al.*, 2005) link *A. nidulans* pathogenicity with PacC action, which is required for, and able to, enhance virulence.

Similar results were observed for *A. fumigatus*, when comparing the virulence of *A. fumigatus* Δ*pacC* null mutants in the ATCC46645 and the CEA10 genetic backgrounds to the respective wild type strains using a neutropenic murine model of invasive pulmonary aspergillosis. Following the high dose-survival protocol routinely used in our laboratory, *A. fumigatus* ATCC46645 Δ*pacC* virulence was attenuated in a murine model of pulmonary aspergillosis, in comparison with the respective wild type strain. The outcomes of the infection with ATCC46645 Δ*pacC* mutant and ATCC46645 wild type strain were significantly different, with associated medial survival of 13.5 days and 5 days respectively ($p<0.0001$, Kaplan-Meier log rank analysis). According to the same protocol, a different result was observed for the *A. fumigatus* CEA10 Δ*pacC* mutant where median survival following infection with either *A. fumigatus* CEA10 Δ*pacC* or CEA10 wild type strain corresponded to 5 days ($p=0.3774$, Kaplan-Meier log rank analysis). The differential virulence observed for the ATCC46645 Δ*pacC* and CEA10 Δ*pacC* mutants was attributed to the differential pH sensitivity between the strains, which had been demonstrated to behave differently with the progressive alkalinisation of the pH media. This difference was evident in slightly alkaline conditions *in vitro*, where the ATCC46645 Δ*pacC* mutant was almost unable to grow, whereas CEA10 Δ*pacC* mutant was only reduced for growth (Fig. 3.2). A difference between the two *A. fumigatus* Δ*pacC* mutants was observed at a concentration of 10^4 cells concentration at pH 8.0 *in vitro* (Fig. 3.2). This concentration is ten times lower than the concentration usually used to infect a single mice. This link between phenotypic and virulence data was further maintained in comparing the virulence of the *A. fumigatus* CEA10 Δ*pacC* mutant to the respective reconstituted strain using a low dose-survival protocol in a neutropenic murine model of invasive pulmonary aspergillosis. Inoculating a concentration of spores ten times lower than that used in the standard high dose-survival protocol, *A. fumigatus*

CEA10 Δ*pacC* was demonstrated to be attenuated in comparison with the respective reconstituted strain (Fig. 3.5).

In the *A. nidulans* study, demonstrating the importance of PacC-mediated pH responses in the pathogenesis of pulmonary aspergillosis, a specific pathology was associated with infection caused by the Δ*pacC* mutant. Not only was the virulence acutely attenuated as a consequence of eliminating *A. nidulans* PacC, blocking of the ambient pH signal transduction pathway or preventing PacC proteolytic processing (Bignell *et al.*, 2005), but in addition the infection resulting from alkaline-sensitive mutants was characterised by limited fungal growth in mice and a reduction of inflammatory cell infiltration. In stark contrast, the constitutive activation of PacC led to increased mortality and extensive fungal invasive growth. A similar pathology was identified in this study for the *A. fumigatus* ATCC466645 Δ*pacC* mutant in comparison to the respective parental isolate throughout early stages of murine infection in a neutropenic model. The histological time course analysis (4, 8 and 16 hrs) for ATCC46645 wild type strain and the ATCC46645 Δ*pacC* mutant revealed a dramatic impairment in hyphal growth, as a consequence of *pacC* deletion. Minimal differences were visible in the earliest studied stages of infection; however, at 8 hours post infection, the ATCC46645 wild type spores appear swollen and begin to germinate. Also, some slight differences in the level of inflammation were associated with the wild type infection (Fig. 3.6).

From the evidence presented here, it is clear that the PacC pathway plays a crucial role in *A. fumigatus* virulence. However, this provides only limited indications of the mechanisms involved and more detailed information will follow in Chapter IV, where the transcriptional profiling of an *A. fumigatus* Δ*pac*C mutant and the respective parental isolate is described. Several hypotheses can be formulated at this stage, considering the demonstrated links of the PacC pathway with several other biological pathways, and will be validated by evidence obtained in subsequent chapters.

In the first instance, PacC/Rim101p has been demonstrated to be involved in the regulation of the transport across the plasma membrane of essential nutrients (Amich *et al.*, 2009; Arino *et al.*, 2010a; Caracuel *et al.*, 2003a), among which iron is essential for virulence of pathogenic fungi, and specifically of *A. fumigatus* (Haas, 2003; Haas *et al.*, 2008; Schrettl *et al.*, 2004; Schrettl *et al.*, 2007). Siderophore biosynthesis but not reductive iron assimilation is essential for *A. fumigatus* virulence (Schrettl *et al.*, 2004). Elimination of both intra- and extracellular siderophores causes the attenuation of *A. fumigatus* virulence in a murine model of invasive aspergillosis, indicating the importance of iron acquisition for *A. fumigatus* virulence, as also supported by the transcriptional profiling of *A. fumigatus* during initiation

of murine infection (McDonagh *et al.*, 2008a), which highlighted the abundant upregulation of genes involved in siderophore biosynthesis relative to a laboratory culture.

Increasing evidence suggests PacC/Rim101p might mediate pathogenic interaction through cell wall functions (Nobile *et al.*, 2008; O'Meara *et al.*, 2010; Villar *et al.*, 2007). For *C. albicans*, several hypothesised PacC-mediated virulence strategies collaborate for the establishment of colonisation and tissue invasion of mucosal tissues (for a recent rewiew see Davis, 2009), such as the degradation of E-cadherin in epithelial adherens junctions mediated by Sap5, a secreted aspartyl proteinase (Villar *et al.*, 2007). *C. albicans rim101*$^{-}$*/rim101*$^{-}$ mutant was found unable to invade the mucosal tissues as a consequence of its inability to degrade E-cadherin, therefore suggesting the possible involvement of Rim101p in the regulation of the Sap proteases, which was confirmed by reverse transcription-PCR data (Villar *et al.*, 2007). Nobile *et al.*, 2008 also demonstrated that Rim101p-dependent cell wall alterations affect *C. albicans* pathogenic interaction with oral epithelial cells using an over-expression rescue approach. The over-expression of four genes, the functions of which are related to cell wall structure, were identified as Rim101p targets, being able to partially restore the pathogenic interactions of a *C. albicans rim101*Δ/Δ mutant with the oral epithelial cells (Nobile *et al.*, 2008). Finally, in *Cryptococcus neoformans*, the *rim101*Δ mutant (which is slightly more virulent than the wild-type) is characterised by major defects in the polysaccharide capsule (O'Meara *et al.*, 2010), an important virulence factor for this species (Granger *et al.*, 1985). However, few genes involved in capsule biosynthesis were transcriptionally regulated by Rim101p, suggesting the phenotype observed was more likely due to defects in the attachment of the capsule to the cell wall (O'Meara *et al.*, 2010). Interestingly, transcriptional profiling of the *C. neoformans rim101*Δ mutant also revealed the Rim101p-mediated regulation of *ENA1* and various genes involved in iron homeostasis.

CHAPTER IV

TRANSCRIPTIONAL PROFILING OF *A. FUMIGATUS* ATCC46645 AND AN ISOGENIC Δ*pacC* MUTANT DURING INITIATION OF MURINE INFECTION

4.1 Overview

The characterisation of *A. fumigatus* Δ*pacC* mutants, and associated pathogenicity presented in Chapter III, has validated a fundamental role for PacC in *A. fumigatus* adaptation to environmental pH and virulence in the murine host. The profound defects of growth *in vitro* at alkaline pH and the impairment of virulence in a murine model of IPA, are likely to be due to aberrant transcriptional regulation in *A. fumigatus* Δ*pacC* mutants. In addition to alkaline adaptation, *S. cerevisiae* Rim101p has been demonstrated as involved in a variety of other biological processes, such as sporulation, invasive growth, ion tolerance and acquisition, and cell wall structure and modification (Denison, 2000; Hayashi *et al.*, 1998; Lamb *et al.*, 2001; Lamb and Mitchell, 2003; Li and Mitchell, 1997). Considering the high level of conservation of PacC/Rim101p pathway components within the fungal kingdom, a similar set of targets for the regulatory action of PacC might be hypothesised for the *Aspergillus* species, but currently only a limited number of PacC-dependent genes have been identified, mostly in *A. nidulans* (for a recent review please refer to Peñalva *et al.*, 2008).

DNA microarray technology is a powerful tool for analysis of gene expression and fungal adaptation to environmental pH (Bensen *et al.*, 2004; Causton *et al.*, 2001; Serrano *et al.*, 2002; Viladevall *et al.*, 2004) as well as adaptation to the murine host (McDonagh *et al.*, 2008a) have been extensively studied using this methodology. In *S. cerevisiae* and *C. albicans*, genes whose expression is up-regulated in alkaline conditions include those encoding functions with direct relevance to pH homeostasis and also those involved in cell wall biogenesis and in the uptake, mobilisation and utilisation of essential ions such as calcium, iron and copper (Bensen *et al.*, 2004; Causton *et al.*, 2001; Serrano *et al.*, 2002; Viladevall *et al.*, 2004). To elucidate the transcriptional response to alkaline conditions, a microarray study performed by our research group has recently delineated the temporal response of *A. fumigatus* to an alkaline shift *in vitro* and compared it to that induced by high

extracellular concentrations of Ca^{2+} (Loss *et al.*, unpublished). However, beyond this unpublished dataset there are no available pH-responsive transcriptome data for *Aspergillus* species. Besides, PacC is highly responsive to the extracellular environment and as such *in vitro* investigations of its function can not be directly extrapolated to the murine niche.

DNA microarray analyses of *A. fumigatus* transcriptional profiling during murine infection have been limited by the difficulty in obtaining RNA from the sites of infection in sufficient quantity. Our research group recently performed transcriptional profiling analysis during initiation of murine infection, identifying many genes whose expression is up-regulated or down-regulated with respect to a laboratory culture (McDonagh *et al.*, 2008a). This analysis identified pH, oxygen, iron and nitrogen limitation as host-imposed combinatorial stresses during early-stage *A. fumigatus* infection and revealed a biased distribution of induced genes (relative to a laboratory culture) in subtelomeric regions of chromosomes (McDonagh *et al.*, 2008a).

To identify functions under PacC transcriptional control during murine infection, the transcriptional profiling comparison between an *A. fumigatus* Δ*pac*C mutant and the respective parental isolate was performed. The Δ*pacC* mutant in the ATCC46645 genetic background, having the most severely pH-sensitive phenotype (Chapter III, Fig. 3.2), was used for the analysis.

4.2 Methods

4.2.1 *A. fumigatus* strains

A. fumigatus strains used in this chapter are the wild type isolates ATCC46645 and the ATCC46645 Δ*pacC* mutant (see Appendix A), obtained using a split-pyrithiamine marker and kindly provided from our collaborator Markus Schrettl (Hubertus Haas's laboratory at Innsbruck Medical University). To propagate the ATCC46645 Δ*pacC* mutant, AMM was supplemented with 0.5 μg/ml Pyrithiamine (Takara).

4.2.2 Murine infection

Murine infections were conducted under UK Home Office Project Licence PPL/70/6487 in a dedicated facility at Imperial College London, where individually vented cages, providing free access to food and H_2O were used to house outbred male mice (strain CD1, 18 – 22 g, Harlan Ortech). H_2O was supplemented with 1 g/l tetracycline hydrochloride

and 64 mg/L ciprofloxacin as prophylaxis against bacterial infection. For a neutropenic model of infection, immunosuppression of mice was performed by intraperitoneal injections of cyclophosphamide (150 mg/kg) on days –3, –1, +2, and subsequently every third day for the whole time of the experiment and by a single subcutaneous dose of hydrocortisone acetate (112.5 mg/kg) on day –1 (Schrettl *et al.*, 2004). *A. fumigatus* spores were grown on ACM, supplemented with 1 % (w/v) glucose and 5 mM ammonium tartrate, for 5 days prior to infection. Spores were harvested on the day of infection, using sterile saline (Baxter Healthcare Ltd, UK), and filtered through MIRACLOTH. Conidial suspensions were centrifuged for 5 minutes at 5000 rpm, washed twice with sterile saline, counted using a haemocytometer and resuspended at a concentration of $2.5x10^9$ cfu/ml. Mice were anaesthetised by isofluorane inhalation and infected by intranasal instillation of $1x10^8$ conidia in 40 μl of saline solution. The determination of viable counts for the administered inocula was performed using serial dilution on ACM plates supplemented with 1 % (w/v) glucose and 5 mM ammonium tartrate and incubated for 3 days at 37°C.

For the transcriptional time course comparison between ATCC466645 Δ*pacC* and the respective parental isolate during murine infection, groups of infected mice were culled and processed, as previously described (McDonagh *et al.*, 2008a) at time points corresponding to 4, 8 and 16 hours post-infection. Bronchoalveolar lavage (BAL) was performed using three 0.5 ml aliquots of sterile saline per mouse. Once collected, BAL fluids (BALFs) were snap frozen immediately in liquid nitrogen. Lung samples for histological analysis were protected from BAL by suturing. These were removed subsequent to BALF, and snap frozen.

For *A. fumigatus* RNA extraction, mRNA amplification and hybridisation of fluorescently labelled cDNA to DNA microarray and microarray data capture, normalisation and analysis please consult Chapter 2.10.

4.3 Results

4.3.1 Microarray analysis of *A. fumigatus* during early stages of infection in a neutropenic murine model

Six groups of 8 neutropenic male mice were inoculated intranasally with $1x10^8$ spores of ATCC46645 Δ*pacC* and the respective parental isolate. One group of infected mice for each strain were culled and processed for each of three time points (4, 8 and 16 hours post-infection) to harvest BALF and tissue for histological analysis. Fungal RNA extracted from the BALF samples was sent to the J. Craig Venter Institute (JCVI), Rockville, Maryland, USA, for amplification and labelling as described previously (McDonagh *et al.*, 2008a).

Three sets of hybridisations were performed to obtain the greatest amount of biological information as possible from the experiment, as displayed in Fig. 4.1. To investigate the biological functions crucial for *A. fumigatus* ATCC46645 wild type virulence, the transcriptional profile of the strain during initiation of murine infection was performed comparing the three time points (4, 8 and 16 hrs) to a common reference of RNA extracted from ATCC46645 spores (Fig. 4.1A). To analyse which virulence functions are affected by *pacC* deletion, the *A. fumigatus* ATCC46645 Δ*pacC* mutant transcriptional profile during initiation of murine infection was performed comparing the three time points (4, 8 and 16 hrs) to a common reference of RNA extracted from ATCC46645 Δ*pacC* spores (Fig. 4.1B). Finally, to directly compare gene expression of the two strains at each time point of infection a comparative analysis of *A. fumigatus* ATCC46645 Δ*pacC* mutant transcript profile relative to the parental isolate ATCC46645 was also performed (Fig. 4.1C).

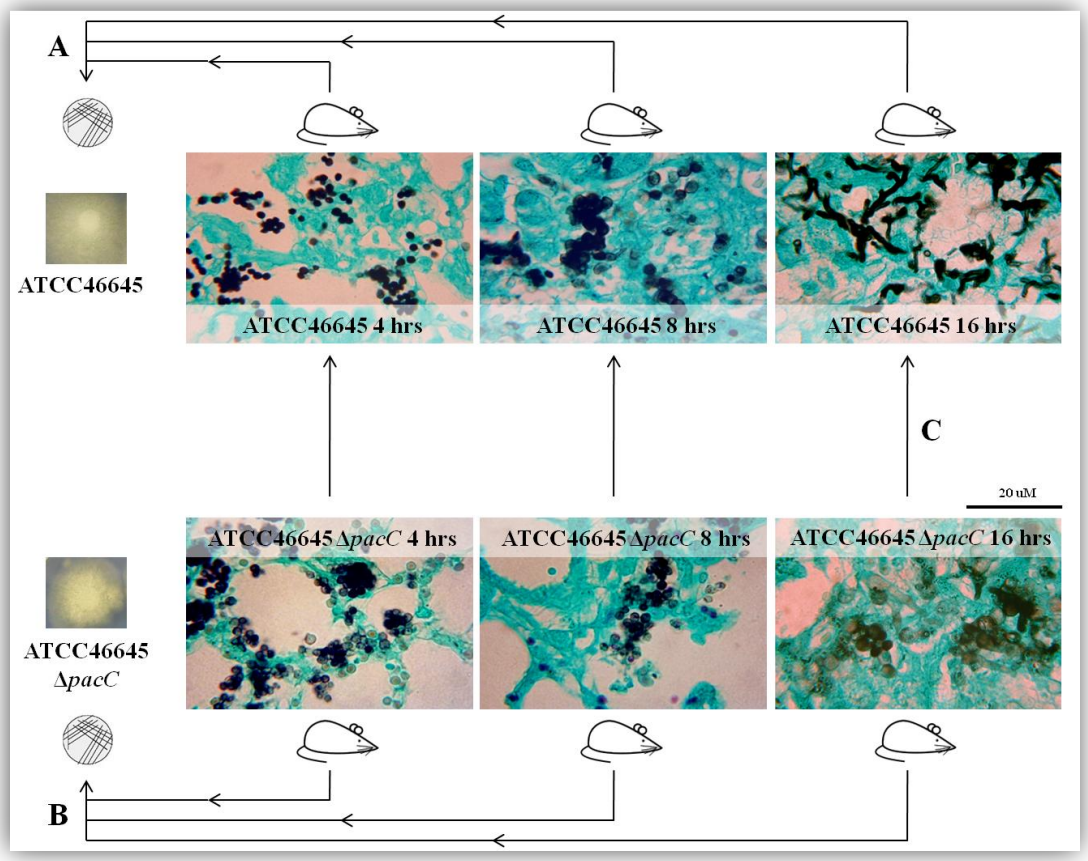


Fig. 4.1: Schematic representation of hybridisations performed to analyse *pac*C-mediated virulence functions in *A. fumigatus*. (A) *A. fumigatus* ATCC46645 transcriptional profile during initiation of murine infection compares three time points (4, 8 and 16 hrs) to a common reference of RNA extracted from ATCC46645 spores. (B) *A. fumigatus* ATCC46645 Δ*pacC* transcriptional profile during initiation of murine infection compares three time points (4, 8 and 16 hrs) to a common reference of RNA extracted from ATCC46645 Δ*pacC* spores. (C) *A. fumigatus* ATCC46645 Δ*pacC* transcript profile relative to the parental isolate ATCC46645 during initiation of murine infection compares transcript abundance between ATCC46645 Δ*pacC* and the parental isolate ATCC46645 for each time point (4, 8 and 16 hrs) of infection.

For each of the analyses, a total of two microarray hybridisations were included for significance testing, including a dye swapped technical replicate. Data were normalised with TIGR TM4 freeware (www.tm4.org/) for locally-weighted scatter plot smoothing (LOWESS) and standard deviation regularisation and subsequently analysed using MeV software (www.tm4.org/).

4.3.2 *A. fumigatus* ATCC46645 transcriptional profile during initiation of murine infection

A. fumigatus ATCC46645 transcriptional profiling during initiation of murine infection was performed by hybridising doubly amplified fungal RNA, extracted from BALFs harvested at each of the 3 time points (4, 8 and 16 hrs) of murine infection, against a common reference of *in vitro*-cultured ATCC46645 spores, as shown in Fig. 4.2.

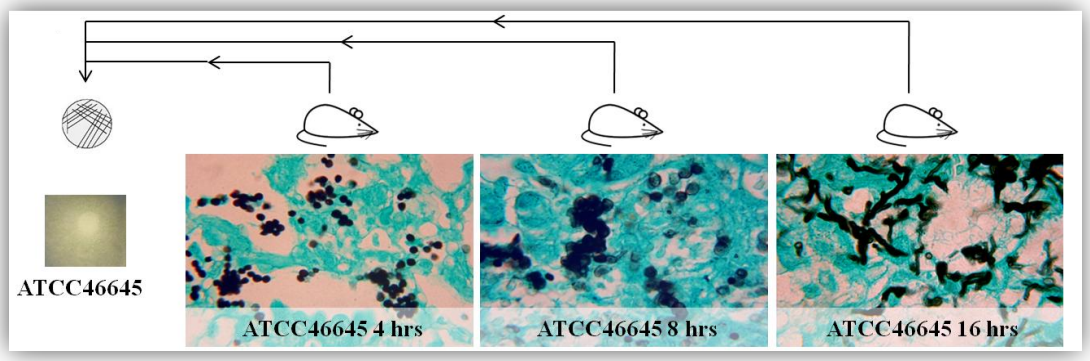


Fig. 4.2: Schematic representation of the hybridisations performed to analyse *A. fumigatus* ATCC46645 transcription during initiation of murine infection. *A. fumigatus* ATCC46645 transcriptional profile during initiation of murine infection was performed comparing the three time points (4, 8 and 16 hrs) to a common reference of RNA extracted from ATCC46645 spores.

Poor quality spots were manually flagged when the background subtracted intensity was less than an arbitrary threshold of 1000. Normalisation was performed by locally-weighted scatter plot smoothing (LOWESS) and standard deviation regularisation using TIGR TM4 freeware (www.tm4.org/). After LOWESS normalisation, the flip dye pairs were combined in a consistency check to remove spot values, from either of the two slides, that outlie the specific deviation of the array-wide average $\log_2$ ratio. Finally, the resulting data was derived as the average of six values for each gene (triplicate copies of the genes printed on each array and the duplicate flip-dye arrays for each experiment).

Fig. 4.3, 4.4 and 4.5 show microarray (MA) and box plots of the datasets for each of the three time points studied, both before and after normalisation. The MA plots for each time point (A) show the distribution of data before (UN-NORMALISED) and after (NORMALISED) LOWESS normalisation thereby depicting the dataset adjustments implemented by normalisation. In MA plots the $\log_2$ ratio between red and green channels (Y-axis) is plotted against the sum of red and green channels (X-axis). Normalisation adjusts for the higher measured spot intensities associated with the green dye (Cy3). Box plots (B) also

show dataset $\log_2$ ratio distributions for each time point, both before (UN-NORMALISED) and after LOWESS normalisation (NORMALISED), but on a slide specific basis. On the X-axis, each box represents a distinct set of spots printed by a given pin. In the case of this JCVI amplicon array (http://pfgrc.jcvi.org/index.php/microarray/protocols.html) having ~29,952 spots, each block consists of 624 spots arranged in a 24x26 grid and these blocks are arranged in 4 columns with 12 rows. The arrays are printed by a machine that has 48 metal pins arranged in 4 columns of 12 rows. When the robot prints the array, it drops those pins into a 384 well plate then touches the glass slide, making 48 spots on the array. The pins get rinsed off and the robot then dips the pins into the 384 well plate again (moving 1 well over) and places another set of 48 spots adjacent to the first 48. The process is repeated for all ~9500 genes present on the array and then repeated twice to achieve triplicate printing for all spots on the array. After normalisation the median values obtained for all blocks are set to zero and the standard deviation is regularised.

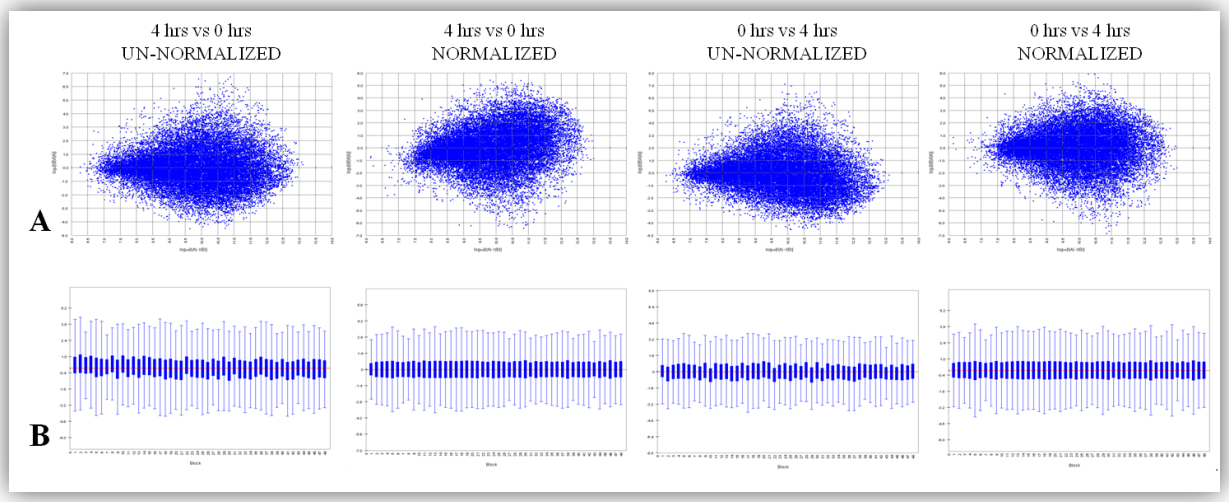


Fig. 4.3: Data normalisation plot for the ATCC46645 4 hrs *in vivo* versus dormant spores analysis. Pairwise MA (A) and box plots (B) for the 4 hour time point of ATCC46645 (mouse) versus ATCC46645 (dormant spores) RNA. Datasets plotted before (UN-NORMALISED) and after (NORMALISED) LOWESS normalisation are shown.

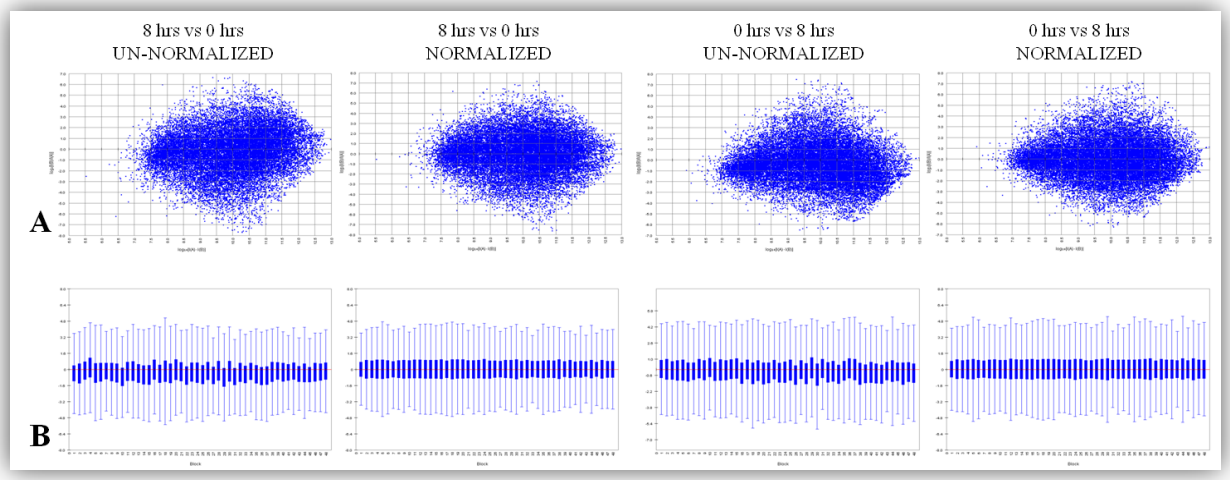


Fig. 4.4: Data normalisation plot for the ATCC46645 8 hrs *in vivo* versus dormant spores analysis. Pairwise MA (A) and box plots (B) for the 8 hour time point of ATCC46645 (mouse) versus ATCC46645 (dormant spores) RNA. Datasets plotted before (UN-UN-NORMALISED) and after (UN-NORMALISED) LOWESS normalisation are shown.

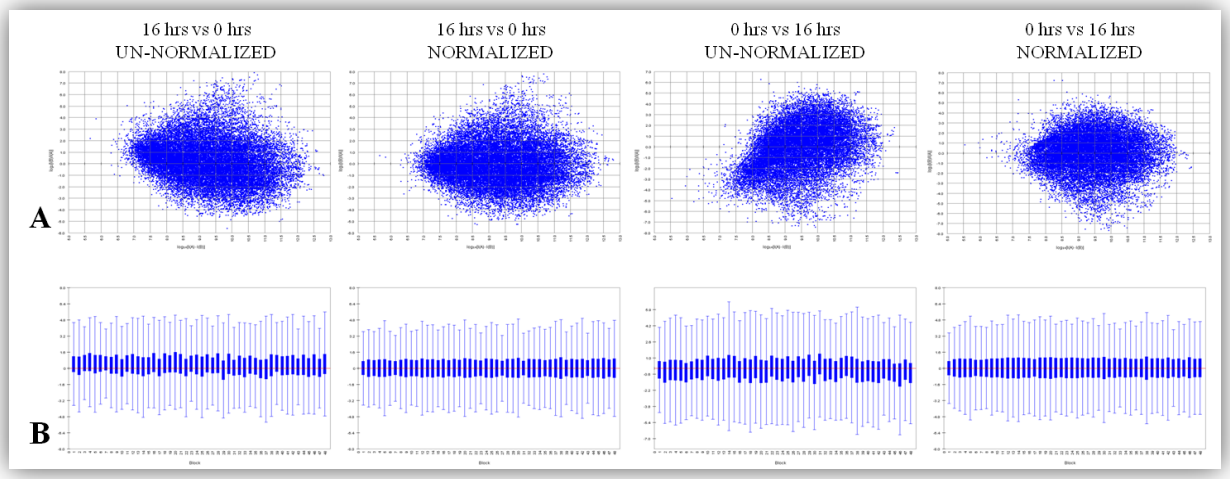


Fig. 4.5: Data normalisation plot for the ATCC46645 16 hrs *in vivo* versus dormant spores analysis. Pairwise MA (A) and box plots (B) for the 16 hour time point of ATCC46645 (mouse) versus ATCC46645 (dormant spores) RNA. Datasets plotted before (UN-UN-NORMALISED) and after (UN-NORMALISED) LOWESS normalisation are shown.

As summarised in the summary statistics for the ATCC46645 time course during initiation of murine infection reported in Table 4.1, among a total of 8243 genes in the slides, signals were detected for 8217, 8157 and 7164 genes, for the 4, 8 and 16 hr time points, respectively.

	4 hrs vs 0 hrs	8 hrs vs 0 hrs	16 hrs vs 0 hrs
Observations	8217	8157	7164
Missing observations	26	86	1079
Minimum value	-4.65	-6.66	-4.78
Maximum value	6.66	7.25	7.57
Mean	0.0173	0.0211	-9.0731E-5
Median	-0.05	-0.08	-0.13
Standard deviation	1.4964	1.8908	1.8854
Outliers	179	118	112

Table 4.1: Summary statistics for the ATCC46645 time course during initiation of murine infection.

The analysis of temporal gene expression *in vivo* for the ATCC46645 strain was conducted in Genespring GX 11.02. Normalised $\log_2$ expression ratios were filtered on expression level and differentially regulated transcripts were defined as having averaged $\log_2$ (Cy5/Cy3) ratios less or greater than the arbitrary thresholds of ±2. The numbers and classifications of differentially expressed genes are shown in Table 4.2. Among a total of 2663 (26.8% of *A. fumigatus* genome, Nierman *et al.*, 2005) differentially expressed genes across the entire time course, 1364 (13.7%) were up-regulated and 1299 (13.1%) were down-regulated in at least one time point. The complete lists of differentially expressed genes are attached in the Supplementary Data CD, as listed in Appendix D.

	Up-regulated	Down-regulated	Differentially expressed
TOTAL	1364	1299	2663
4 hrs	787	682	1469
8 hrs	1178	1088	2266
16 hrs	999	974	1973

Table 4.2: Number of differentially expressed genes in the ATCC46645 time course during initiation of murine infection.

A. fumigatus genome sequences have been published relatively recently (Nierman *et al.*, 2005), as well as new techniques for *A. fumigatus* manipulation (Brakhage and Langfelder, 2002). However, the status of functional genomic understanding is primitive when compared to better-characterised microorganisms such as *S. cerevisiae* where a detailed gene annotation is available. Often the function of *A. fumigatus* genes is predicted upon the basis of finding orthologues in *S. cerevisiae* by BLAST analysis, and subsequent use of gene

ontology (GO) tools (www.yeastgenome.org/GOContents.html) whereby, according to the annotation available for *S. cerevisiae*, differentially expressed *A. fumigatus* genes can be partially functionally characterised.

The temporal basis of gene regulation in the ATCC46645 time course experiment is simply depicted in a 3-way Venn diagram in Fig. 4.6 for both up-regulated (Fig. 4.6A) and down-regulated (Fig. 4.6B) genes. In addition, the complex pattern of differentially expressed genes in the ATCC46645 time course is shown in a detailed heat map attached in the Supplementary Data CD, as listed in Appendix D.

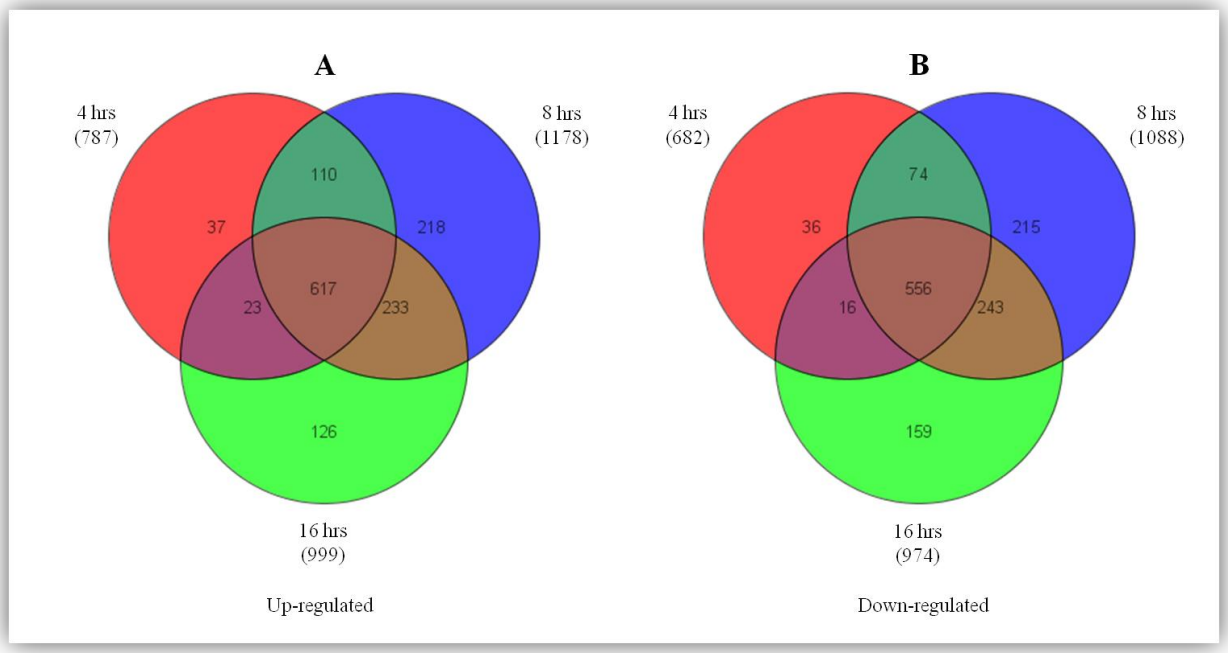


Fig. 4.6: Three-way Venn diagrams depicting temporal aspects of differential gene expression in the ATCC46645 time course experiment during initiation of murine infection. Up-regulated (A) and down-regulated genes (B) have been identified using a fold change cut off of ±2 on a $\log_2$ scale. Analysis performed using Genespring GX 11.02.

Among a total of 1364 up-regulated genes (13.7% of *A. fumigatus* genome), 617 (6.2%) were similarly differentially regulated at all three time points. Among these, one hundred genes, having the highest $\log_2$ ratios are reported in Table 4.3. Across all time points, multiple genes involved in the uptake, mobilisation and utilisation of crucial ions and nutrients are up-regulated. These include at least five genes, involved in siderophore biosynthesis for extracellular iron acquisition (Afu3g03440, Afu3g03390, Afu7g04730, Afu2g07680, and Afu6g13750), several sugar permeases (Afu3g3700, Afu4g00800 and Afu7g05100), and also transporters for a variety of other elements, such as phosphate (Afu3g03010 and Afu8g01850), sodium (Afu2g01320), ammonium (Afu1g10930), choline

(Afu8g00840 and Afu5g02940), urea (Afu6g03200) and amino acids (Afu7g0190). In addition, several up-regulated genes represent functions involved cell wall biogenesis and organisation (Afu7g05450, Afu1g16250, Afu4g10150 and Afu2g00640). Other genes commonly associated with *A. fumigatus* pathogenicity are also up-regulated in the ATCC46645 time course experiment, such as a secreted peptidase (Afu4g09320) and genes involved in response to stress (Afu3g02280), more specifically oxidative stress (Afu1g14550 and Afu3g07150). In addition, Tables AD.1.2-AD.1.4 in Appendix D list thirty ORFs, having the highest $\log_2$ ratios for each time point. Each of the categories contains up-regulated genes involved in transport (Afu8g0210, Afu4g14670 at 4 hrs, Afu3g01670, Afu2g03730 Afu1g17160 at 8 hrs, Afu3g14670, Afu4g00830 at 16 hrs). Whereas the role of transport in *A. fumigatus* ATCC46645 adaptation to the murine niche is highlighted across the entire ACTT46645 time course, it is possible to extrapolate several phase-specific trends for the up-regulated genes, such as the abundance of genes with oxidoreductase activity at 4 hrs post-infection (Afu2g02810, Afu2g04560, Afu2g04060 and Afu5g02490) and of transcriptional regulators at 16 hrs post-infection (Afu6g12150, Afu1g02860, Afu5g13020 and Afu6g03800). Interestingly, the regulator of second metabolite synthesis LaeA is uniquely up-regulated at 8 hrs post-infection.

Of a total of 1299 down-regulated genes (13.1% of *A. fumigatus* genome), 556 (5.6%) were similarly differentially regulated at all three time points, among these, one hundred genes having the greatest down-regulation are reported in Table 4.4. Among the down-regulated genes, several ORFs are involved in the regulation of transcription (Afu5g02880, Afu7g02620, Afu5g06140, Afu3g11330, Afu3g10120, Afu1g17360, Afu4g12390, Afu1g14750, Afu2g10550). In addition, to aid evaluation of phase-specific, down-regulated genes across the ACTT46645 time course, Tables AD.1.6-AD.1.8 in Appendix D list the thirty ORFs subject to the greatest degree of down-regulation at each of 4, 8 and 16 hrs time points. The functional trend of transcriptional repression is particularly emphasised at 4 (Afu8g02750, Afu3g08580) and 8 hrs (Afu7g08500, Afu3g03070) post-infection.

Table 4.3: 100 ORFs with the highest log_2 values between the up-regulated genes in common for the 3 time points (4, 8 and 16 hrs) of the ATCC46645 time course.

ORF	T4 vs T0	T8 vs T0	T16 vs T0	Annotation	Functional classification	Predicted Function (Assigned from literature)
Afu3g03410	6.66	7.19	7.13	enoyl-CoA hydratase/isomerase family protein		Fatty acid degradation in mitochondria
Afu1g17180	6.58	7.25	7.49	pyridine nucleotide-disulphide oxidoreductase, putative	electron carrier activity///nucleus///mitochondrion///DNA fragmentation involved in apoptosis	Oxidative metabolism of fatty acids, mitochondria
Afu3g03440	6.22	7.18	7.57	MFS family siderophore transporter, putative	siderophore-iron transport///siderophore-iron (ferrioxamine) uptake transmembrane transporter activity///integral to membrane///cellular iron ion homeostasis	Transport (Iron acquisition)
Afu7g05450	6.18	7.17	7.06	SUN domain protein (Uth1), putative	autophagic cell death///cell wall organisation///barrier septum formation///fungal-type cell wall///response to oxidative stress///beta-glucosidase activity///mitochondrion organisation///mitochondrial outer membrane///apoptosis	Cell wall biogenesis/CWI/mitochondrial association
Afu3g02940	6.08	6.55	6.01	allergen, putative		Immunoreactive
Afu1g14550	5.98	6.76	6.71	Mn superoxide dismutase MnSOD	manganese superoxide dismutase activity///oxygen and reactive oxygen species metabolic process///mitochondrial matrix///mitochondrion	Antioxidant/mitochondrial
Afu3g03010	5.87	6.67	7.2	phosphate-repressible phosphate permease	sodium:inorganic phosphate symporter activity///plasma membrane///phosphate transport	Phosphate transport
Afu7g06380	5.75	6.06	5.58	maltase	cellular component unknown///alpha-glucosidase activity///maltose catabolic process	Polysaccharide hydrolysis
Afu3g03420	5.71	6.25	7.32	hypothetical protein		
Afu1g16250	5.68	6.62	5.96	alpha-glucosidase B	alpha-glucosidase activity///fungal-type cell wall biogenesis///endoplasmic reticulum	Polysaccharide hydrolysis
Afu3g03860	5.65	5.4	4.84	3-hydroxyacyl-CoA		Oxidative metabolism of fatty acids,

				dehydrogenase, putative		mitochondria
Afu8g01710	5.44	5.63	6.64	antigenic thaumatin domain protein, putative		
Afu3g03820	5.39	4.61	5.29	MFS transporter, putative	nicotinamide mononucleotide transport///nicotinamide mononucleotide permease activity///integral to plasma membrane	Transport
Afu3g03390	5.37	5.8	5.76	siderophore biosynthesis lipase/esterase, putative		Iron acquisition
Afu3g03430	5.35	5.94	6.67	ABC multidrug transporter SitT, putative	ATP-binding cassette (ABC) transporter activity///ATP binding///transport	Transport
Afu3g03700	5.29	5.74	5.68	Sugar transporter subfamily	mannose transmembrane transporter activity///hexose transport///fructose transmembrane transporter activity///plasma membrane///glucose transmembrane transporter activity	Transport
Afu6g13750	5.26	6.73	6.51	ferric-chelate reductase, putative	ferric-chelate reductase activity///transition metal ion transport///integral to membrane	Iron acquisition
Afu4g09320	5.2	5.25	6.29	antigenic dipeptidyl-peptidase Dpp4	proteolysis///serine-type peptidase activity///aminopeptidase activity	Secreted proteinase
Afu1g10780	5.18	5.42	5.95	glycine cleavage system T protein	glycine metabolic process///mitochondrion///one-carbon metabolic process///glycine dehydrogenase (decarboxylating) activity	One-carbon metabolism, mitochondrion
Afu8g07090	5.16	5.81	6.98	extracellular proline-serine rich protein		Extracellular protein
Afu3g00900	5.1	5.73	6.07	alpha-amylase AmyA		Polysaccharide hydrolysis
Afu3g07910	5.05	6.29	6.15	UDP-glucose 4-epimerase, putative	cellular component unknown///UDP-glucose 4-epimerase activity///galactose metabolic process	Galactose metabolism

Afu1g17170	4.99	6.79	6.42	alpha-ketoglutarate-dependent taurine dioxygenase	cellular component unknown///sulfur metabolic process///sulfonate dioxygenase activity///"oxidoreductase activity, acting on paired donors, with incorporation or reduction of molecular oxygen, 2-oxoglutarate as one donor, and incorporation of one atom each of oxygen into both donors"	Utilization of taurine as sulphur source
Afu1g11480	4.97	5.52	5.29	hypothetical protein		
Afu1g14390	4.9	5.75	5.88	zinc binding dehydrogenase family protein	cellular component unknown///L-iditol 2-dehydrogenase activity///fructose metabolic process///zinc ion binding///mannose metabolic process	
Afu4g01140	4.87	4.48	5.4	MFS multidrug transporter, putative	drug transport///drug transporter activity///integral to membrane	Transport
Afu5g10290	4.86	4.71	4.04	fructose-bisphosphate aldolase, putative	fructose-bisphosphate aldolase activity///glycolysis	Glycolysis
Afu8g00850	4.86	5.36	5.49	dihydroorotase, homodimeric type	dihydroorotase activity///pyrimidine nucleotide biosynthetic process///cytoplasm///nucleus	Pyrimidine biosynthesis
Afu3g03400	4.82	5.95	6.06	siderophore biosynthesis acetylase AceI, putative		Iron acquisition
Afu8g05610	4.78	5.88	6.1	cell wall glucanase (Scw11), putative	hydrolase activity, hydrolyzing O-glycosyl compounds///cellular glucan metabolic process///fungal-type cell wall///"cytokinesis, completion of separation"	Cell wall assembly
Afu6g03420	4.72	3.44	3.32	trehalose synthase, putative		Trehalose synthesis
Afu4g10150	4.7	5.91	4.27	alpha-glucosidase	alpha-glucosidase activity///fungal-type cell wall biogenesis///endoplasmic reticulum	Glucosidase
Afu6g03190	4.7	5.36	5.55	hypothetical protein		
Afu2g05800	4.64	5.43	5.23	IdgA domain protein		

Afu1g17200	4.63	5	5.55	nonribosomal peptide synthase, putative	nonribosomal peptide biosynthetic process///catalytic activity///amino acid adenylylation by nonribosomal peptide synthase	NRPS secondary metabolism
Afu3g07150	4.63	5.49	5.43	succinate-semialdehyde dehydrogenase, putative	response to oxidative stress///succinate-semialdehyde dehydrogenase [NAD(P)+] activity///cytoplasm///glutamate catabolic process	Mitochondrial succinate production
Afu2g04570	4.63	4.75	4.86	BNR/Asp-box repeat domain protein		
Afu3g07870	4.61	5.52	5.69	extracellular serine-rich protein		Extracellular enzyme
Afu5g14680	4.6	5.25	6.14	hypothetical protein		
Afu8g01850	4.6	4.08	5.24	phosphate-repressible phosphate permease	sodium:inorganic phosphate symporter activity///plasma membrane///phosphate transport	Transport
Afu3g02280	4.6	4.78	4.45	alpha,alpha-trehalose glucohydrolase, putative	fungal-type vacuole///trehalose catabolic process///"alpha,alpha-trehalase activity"///response to stress	Trehalase
Afu8g02450	4.6	5.06	5.84	hypothetical protein		
Afu7g01090	4.57	4.87	5.67	proline permease	plasma membrane///neutral amino acid transmembrane transporter activity///neutral amino acid transport///amino acid permease activity	Transport
Afu7g05070	4.56	4.14	4.38	FAD dependent oxidoreductase, putative	cytoplasm///metabolic process///fumarate reductase (NADH) activity	
Afu4g00800	4.56	4.43	4.96	MFS monosaccharide transporter, putative	response to glucose stimulus///plasma membrane///glucose transmembrane transporter activity///signal transduction///glucose binding///receptor activity	Transport
Afu3g07140	4.52	4.71	5.06	developmental regulator FluG		Regulation of development
Afu1g10930	4.51	3.79	2.39	ammonium transporter	pseudohyphal growth///plasma membrane///ammoniu	Transport

					m transport///ammonium transmembrane transporter activity	
Afu7g06080	4.5	4.79	4.69	ubiE/COQ5 methyltransferase, putative	methyltransferase activity///metabolic process	Respiratory chain
Afu1g15330	4.48	4.95	4.94	T10O22.24		
Afu1g17190	4.47	5.67	5.98	long-chain-fatty-acid-CoA ligase, putative	peroxisomal membrane///peroxisomal matrix///cytoplasm///AMP binding	Bioactivation of fatty acids
Afu2g01320	4.47	5.26	5.12	P-type ATPase, putative	sodium ion transport///plasma membrane///"ATPase activity, coupled to transmembrane movement of ions, phosphorylative mechanism"	Transport
Afu4g09580	4.45	6.36	6.99	major allergen Asp F2	biological process unknown///molecular function unknown	Immunoreactive and zinc transport
Afu3g01370	4.43	5.55	6.08	MFS transporter, putative	pantothenate transport///plasma membrane///transporter activity	Transport
Afu5g07620	4.37	5.06	5.68	DUF1212 domain membrane protein	conjugation with cellular fusion///molecular function unknown///integral to membrane	
Afu1g16480	4.36	4.16	4.45	acid phosphatase, putative		Phosphate acquisition
Afu8g02440	4.36	5.98	6.61	C-4 methyl sterol oxidase, putative	plasma membrane///ergosterol biosynthetic process///endoplasmic reticulum membrane///C-4 methylsterol oxidase activity	Erg25
Afu7g00700	4.36	3.99	4.32	aldo-keto reductase (AKR13), puatative	aldo-keto reductase activity///cytoplasm///nucleus///cellular aldehyde metabolic process	Oxidoreductase
Afu6g02260	4.35	4.79	4.7	hypothetical protein		
Afu8g06470	4.34	5.86	6.03	N,N-dimethylglycine oxidase	aminomethyltransferase activity	Osmostabilisation
Afu5g11850	4.33	4.45	4.04	mitochondrial carrier protein (Pet8), putative	S-adenosylmethionine transmembrane transporter activity///mitochondrial inner membrane///S-adenosylmethionine transport///mitochondrion	Biotin biosynthesis and respiratory growth, mitochondrial

Afu3g11480	4.33	4.53	3.91	mitochondrial methylglutaconyl-CoA hydratase (Auh), putative	endocytosis///3-hydroxyisobutyryl-CoA hydrolase activity///mitochondrion///fatty acid beta-oxidation	Enoyl coA activity
Afu6g12240	4.32	5.32	4.84	Glycerophosphoryl diester phosphodiesterase family family		
Afu8g00840	4.27	4.42	4.6	amino acid permease, putative	plasma membrane///choline transport///choline transmembrane transporter activity	Transport
Afu7g06390	4.25	4.69	4.29	maltose permease	alpha-glucoside:hydrogen symporter activity///membrane fraction///alpha-glucoside transport	Transport
Afu5g02940	4.19	3.14	3.67	choline transport protein Ctr, putative	plasma membrane///choline transport///choline transmembrane transporter activity	Transport
Afu1g02890	4.18	4.82	5.29	dUTPase (Dut), putaive	pyrimidine deoxyribonucleoside triphosphate catabolic process///dUTP diphosphatase activity///cytoplasm///nucleus	
Afu6g03200	4.16	4.84	5.59	solute symporter family transporter	plasma membrane///urea transport///urea transmembrane transporter activity	Transport
Afu5g09400	4.16	4.8	3.96	carbonyl reductase, putative	oxidoreductase activity///metabolic process	
Afu2g01280	4.15	3.59	4.04	D-mandelate dehydrogenase, putative	NAD or NADH binding///cytoplasm///nucleus///metabolic process///"oxidoreductase activity, acting on the CH-OH group of donors, NAD or NADP as acceptor"	
Afu6g10090	4.15	4.1	4.11	D-isomer specific 2-hydroxyacid dehydrogenase family protein	formate catabolic process///formate dehydrogenase activity///NADH regeneration///cytosol	
Afu5g13810	4.14	4.83	4	transulfuration enzyme family protein, putative	sulfur metabolic process///cytoplasm///cystathionine beta-lyase activity	
Afu2g07680	4.13	4.69	5.01	L-ornithine N5-oxygenase SidA	pathogenesis	Siderophore biosynthesis
Afu2g00770	4.13	3.87	5.12	salicylate hydroxylase		Oxidoreductase

Afu4g11400	4.12	4.29	4.23	cell surface receptor/MFS transporter (FLVCR), putative	transporter activity///transport	Transport
Afu1g05940	4.11	4.32	4.92	conserved hypothetical protein	mediator complex///RNA polymerase II transcription mediator activity///transcription from RNA polymerase II promoter	
Afu5g06910	4.1	5.31	5.58	DUF636 domain protein		
Afu4g06860	4.09	4.92	5.45	conserved hypothetical protein		
Afu1g10800	4.09	3.83	3.72	thioesterase family protein	CoA hydrolase activity///fatty acid metabolic process///mitochondrion	Mitochondrion
Afu1g03550	4.09	3.94	2.73	mitochondrial dihydroxy acid dehydratase, putative	dihydroxy-acid dehydratase activity///branched chain family amino acid biosynthetic process///mitochondrion	Mitochondrion
Afu6g14330	4.08	4.5	3.95	5-oxo-L-prolinase, putative	5-oxoprolinase (ATP-hydrolyzing) activity///cytoplasm///biological process unknown	
Afu3g14030	4.05	4.52	5.11	alkaline phosphatase		Phosphate acquisition
Afu3g11640	4.04	4.3	2.85	homoserine dehydrogenase	homoserine biosynthetic process///cytoplasm///nucleus///methionine metabolic process///threonine metabolic process///homoserine dehydrogenase activity	Glycine, serine, threonine metabolism
Afu6g00620	4.03	4.74	4.29	GPI anchored hypothetical protein		
Afu2g00640	4.03	5.32	4.43	beta-N-hexosaminidase, putative	fungal-type cell wall///cell wall chitin metabolic process///beta-N-acetylhexosaminidase activity	Cell wall assembly/degradation
Afu6g04920	4	4.66	3.41	NAD-dependent formate dehydrogenase	formate catabolic process///acetate metabolic process///formate dehydrogenase activity///NADH regeneration///cytosol	
Afu1g04300	3.99	4.1	5.14	hypothetical		

				protein		
Afu2g04590	3.98	3.64	3.35	alcohol dehydrogenase, putative	cytoplasm///fermentation///zinc ion binding///alcohol dehydrogenase (NAD) activity///ethanol metabolic process	
Afu5g09140	3.97	3.41	3.41	amidase, putative	aerobic respiration///amidase activity///mitochondrion	
Afu2g07810	3.96	4.17	4.41	cytosolic hydroxymethyltransferase, putative	glycine hydroxymethyltransferase activity///mitochondrion///one-carbon metabolic process	One-carbon metabolism, mitochondrion
Afu6g08630	3.94	4.62	4.35	hypothetical protein	mitochondrion///biological process unknown///molecular function unknown	
Afu2g11010	3.93	4.22	4.16	dihydroorotate reductase PyrE, putative	pyrimidine ribonucleotide biosynthetic process///dihydroorotate oxidase activity	Pyrimidine biosynthesis
Afu1g12290	3.93	4.46	4.54	possible NADH-ubiquinone oxidoreductase		
Afu6g02470	3.92	3.68	4.21	fumarate hydratase, putative	tricarboxylic acid cycle///fumarate hydratase activity///fumarate metabolic process///cytosol///mitochondrial matrix	
Afu7g02340	3.92	4.74	4.97	L-PSP endoribonuclease family protein (Hmf1), putative	cytoplasm///cytosol///nucleus///biological process unknown///molecular function unknown	
Afu7g04730	3.92	4.43	4.76	siderochrome-iron transporter, putative	endosome///siderophore-iron transport///cytoplasmic membrane-bounded vesicle///siderophore-iron (ferrioxamine) uptake transmembrane transporter activity///cellular iron ion homeostasis	Iron acquisition
Afu6g08640	3.92	4	4.12	metallopeptidase Mip1	metallopeptidase activity///mitochondrion///mitochondrial protein processing during import///cellular iron ion homeostasis	Mitochondrial respiration
Afu7g05100	3.92	3.82	3.22	hexose transporter protein	mannose transmembrane transporter activity///hexose transport///fructose	Transport

					transmembrane transporter activity///plasma membrane///glucose transmembrane transporter activity	
Afu6g10080	3.9	4.45	4.97	conserved hypothetical protein		
Afu2g01040	3.9	4.52	3.84	formaldehyde dehydrogenase	formaldehyde dehydrogenase (glutathione) activity///cytoplasm///formaldehyde assimilation	
Afu1g13500	3.89	4.14	3.55	transketolase TktA	cytoplasm///pentose-phosphate shunt///transketolase activity	Pentose-phosphate pathway

Table 4.4: 100 ORFs with the lowest log_2 values between the down-regulated genes in common for the 3 time points (4, 8 and 16 hrs) of the ATCC46645 time course.

ORF	T4 vs T0	T8 vs T0	T16 vs T0	Annotation	Functional classification	Predicted Function (Assigned from literature)
Afu6g00770	-4.65	-6.66	-4.74	extracellular arabinanase, putative	hydrolase activity, hydrolyzing N-glycosyl compounds///metabolic process	Secreted enzyme
Afu1g10950	-4.56	-5.45	-4.78	conserved hypothetical protein	extrinsic to membrane///cytoplasmic membrane-bounded vesicle///vesicle-mediated transport///molecular function unknown///negative regulation of gluconeogenesis	
Afu5g02880	-4.49	-5.59	-4.51	C6 transcription factor, putative	transcription factor activity///regulation of transcription	Transcription
Afu7g06840	-4.43	-5.85	-4.75	class III aminotransferase	arginine catabolic process///cytoplasm///nucleus///ornithine-oxo-acid transaminase activity	
Afu8g05120	-4.41	-5.51	-4.77	hypothetical protein		
Afu7g04930	-4.4	-5.37	-4.34	alkaline serine protease (PR1), putative	protein catabolic process///cellular component unknown///peptidase activity	Proteinase
Afu2g00200	-4.35	-6.14	-4.73	catalase, putative	oxygen and reactive oxygen species metabolic process///peroxisomal	Oxidative stress

					matrix///response to oxidative stress///catalase activity	
Afu3g00810	-4.35	-4.68	-3.87	cholestenol delta-isomerase, putative		
Afu2g06290	-4.21	-4.35	-3.95	nuclear division rft1 protein	protein amino acid N-linked glycosylation///oligosaccharide transmembrane transporter activity///oligosaccharide transport///endoplasmic reticulum membrane	Protein N-glycosylation
Afu1g06350	-4.21	-4.85	-3.52	virulence related protein (Cap20), putative		
Afu1g06190	-4.2	-5.69	-4.59	hnrnp arginine n-methyltransferase	mRNA export from nucleus///peptidyl-arginine modification///nucleus///protein-arginine N-methyltransferase activity	Protein arginine methylation
Afu2g14330	-4.16	-5.06	-3.97	hypothetical protein		
Afu8g02290	-4.13	-5.48	-4.08	conserved hypothetical protein		
Afu6g04390	-4.09	-5.44	-4.66	conserved hypothetical protein	chromatin silencing at telomere///ubiquitin-protein ligase activity///histone ubiquitination///protein monoubiquitination///nucleus///histone methylation	Chromatin silencing
Afu2g03950	-4.02	-5.31	-4.66	serine/threonine protein phosphatase, putative	cellular component unknown///cellular sodium ion homeostasis///protein serine/threonine phosphatase activity	
Afu7g05500	-4.01	-4.8	-3.78	theta class glutathione S-transferase	regulation of nitrogen utilisation///soluble fraction///transcription corepressor activity	
Afu7g05490	-3.95	-5.16	-2.76	hypothetical protein		
Afu8g02270	-3.94	-4.84	-4.01	dihydrodipicolinate synthetase family protein		
Afu4g11960	-3.91	-4.37	-3.34	Iron only hydrogenase large subunit, C-terminal domain	cellular component unknown///iron hydrogenase activity///biological process unknown	

				containing protein		
Afu5g00800	-3.89	-4.29	-3.98	conserved hypothetical protein		
Afu3g06770	-3.89	-4.76	-4.08	zinc knuckle domain protein	pre-mRNA splicing factor activity///spliceosomal complex///"nuclear mRNA splicing, via spliceosome"///protein binding	
Afu7g06890	-3.88	-4.72	-3.51	Dyp-type peroxidase family protein		
Afu5g12630	-3.86	-3.95	-3.71	hypothetical protein		
Afu5g05610	-3.85	-4.78	-3.74	cell cycle control protein Cwf14, putative	nucleus///cellular bud site selection///molecular function unknown	Cell cycle control
Afu4g14630	-3.85	-5.52	-3.51	FAD binding domain protein		
Afu4g11480	-3.83	-4.35	-3.66	C2H2 finger domain protein, putative	DNA binding///nucleus///zinc ion binding	Transcription
Afu7g06260	-3.81	-3.22	-3.02	alcohol dehydrogenase, zinc-containing	oxidoreductase activity///zinc ion binding///metabolic process	
Afu5g05480	-3.8	-4.37	-3.88	Rheb GTPase RhbA	detection of nutrient///extrinsic to plasma membrane///pathogenesis///nitrogen utilisation///RHEB small monomeric GTPase activity	Nitrogen utilisation
Afu2g13850	-3.77	-5.46	-4.17	protein phosphatase regulatory subunit (Gac1), putative		Glycogen synthesis
Afu6g10150	-3.76	-4.03	-3.35	hypothetical protein		
Afu7g00270	-3.75	-4.64	-3.95	FAD binding monooxygenase, putative	cellular aromatic compound metabolic process///monooxygenase activity	
Afu8g06040	-3.75	-5.08	-3.52	hypothetical protein		
Afu3g14550	-3.73	-4.27	-3.71	DNA repair protein (Rex1), putative		
Afu6g10790	-3.73	-4.55	-4.06	MFS amine transporter, putative		Transport
Afu5g02400	-3.72	-4.71	-4.36	catabolite	cytoplasm///nucleus///	

				degradation protein, putative	molecular function unknown///negative regulation of gluconeogenesis	
Afu5g12150	-3.72	-4.16	-3.87	PH domain protein		
Afu7g02620	-3.7	-4.17	-4.24	DNA-directed RNA polymerases N/8 kDa subunit superfamily	DNA-directed RNA polymerase III complex///DNA-directed RNA polymerase I complex///transcription from RNA polymerase II promoter///transcription from RNA polymerase III promoter///DNA-directed RNA polymerase activity///transcription from RNA polymerase I promoter///"DNA-directed RNA polymerase II, core complex"	Transcription
Afu6g03370	-3.7	-5.45	-4.29	oxidoreductase, short-chain dehydrogenase/reductase family	lipid particle///cytoplasm///endoplasmic reticulum///acylglycerone-phosphate reductase activity///phosphatidic acid biosynthetic process	
Afu3g10530	-3.68	-5.16	-4.49	protein serine/threonine kinase (Ran1), putative	protein serine/threonine kinase activity///G1/S transition of mitotic cell cycle///cytoplasm///protein amino acid phosphorylation///protein kinase activity	
Afu5g11520	-3.66	-4.49	-3.91	serine/threonine protein kinase (Nrc-2), putative	cytoplasm///protein kinase activity	
Afu5g06140	-3.65	-4.41	-3.56	histone acetyltransferase, putative	DNA-directed RNA polymerase II, holoenzyme///transcription elongation factor complex///RNA polymerase II transcription elongation factor activity///regulation of transcription from RNA polymerase II promoter///histone acetyltransferase activity	
Afu7g03770	-3.65	-5.22	-3.43	hypothetical protein		

Afu3g02550	-3.64	-3.29	-4.02	conserved hypothetical protein		
Afu6g02020	-3.63	-4.7	-4.27	hypothetical protein		
Afu3g12530	-3.63	-4.74	-3.74	sensor histidine kinase/response regulator, putative	protein histidine kinase activity///plasma membrane///protein amino acid phosphorylation///two-component sensor activity	Signalling
Afu2g14110	-3.63	-3.81	-3.24	sulfur metabolite repression control protein SconB, putative	SCF ubiquitin ligase complex///protein ubiquitination///sulfur metabolic process///ubiquitin-dependent protein catabolic process///cell cycle///protein binding///nuclear ubiquitin ligase complex	Sulphur metabolism
Afu5g04260	-3.6	-4.88	-3.9	arginine transporter, putative	basic amino acid transmembrane transporter activity///arginine permease activity///lysine permease activity///basic amino acid transport///plasma membrane	Transporter
Afu4g11710	-3.6	-5.55	-4.61	oxidoreductase, zinc-binding dehydrogenase family superfamily	cellular component unknown///biological process unknown///molecular function unknown	
Afu3g11330	-3.59	-4.73	-4.26	bZIP transcription factor (AtfA), putative	RNA polymerase II transcription factor activity///negative regulation of transcription from RNA polymerase II promoter///cytosol///nucleus	Transcription: Response to oxidative and osmotic stress
Afu6g02640	-3.59	-3.86	-3.96	hypothetical protein		
Afu5g14350	-3.57	-3.87	-4.04	c-24(28) sterol reductase	delta24(24-1) sterol reductase activity///endoplasmic reticulum///ergosterol biosynthetic process	Erg4 homologue (which catalyses final step in ergosterol biosynthesis)
Afu5g12100	-3.57	-4.04	-3.16	pmt2 methyltransferase	RNA methyltransferase activity///nucleolus///rRNA processing///nucleus	
Afu2g09510	-3.54	-4.35	-3.82	hypothetical protein		
Afu3g00500	-3.51	-5.18	-4	integral membrane protein		

Afu6g02680	-3.49	-4.81	-3.84	ankyrin repeat and BTB/POZ domain protein	cytoplasm///biological process unknown///molecular function unknown	
Afu3g13470	-3.49	-3.56	-3.22	sulfate transporter, putative	endoplasmic reticulum	
Afu4g05870	-3.48	-4.55	-3.55	oxidoreductase, short-chain dehydrogenase/reductase family	cytoplasm///biological process unknown///molecular function unknown	
Afu2g02390	-3.46	-3.89	-3.51	hypothetical protein		
Afu1g00910	-3.45	-4.16	-2.98	conserved hypothetical protein		
Afu5g11690	-3.45	-4.44	-3.89	related to protein tyrosine phosphatase PPS1	cellular component unknown///regulation of S phase of mitotic cell cycle///vitamin B12 reduction///protein tyrosine/threonine phosphatase activity	
Afu3g10120	-3.45	-5.43	-4.53	TATA-box binding protein	DNA binding///RNA polymerase I transcription factor activity///transcription initiation from RNA polymerase II promoter///RNA polymerase I transcription factor complex///general RNA polymerase II transcription factor activity///nucleus///transcription factor TFIIIB complex///transcription factor TFIID complex///transcription initiation from RNA polymerase III promoter///transcription from RNA polymerase I promoter///RNA polymerase III transcription factor activity	Transcription
Afu6g10500	-3.44	-4.36	-2.72	conserved hypothetical protein		
Afu3g03040	-3.43	-4.95	-3.86	conserved hypothetical protein		
Afu3g13160	-3.43	-4.11	-3.08	hypothetical protein		
Afu8g01340	-3.43	-3.9	-4.13	MFS sugar transporter, putative	alpha-glucoside:hydrogen symporter	Transport

					activity///membrane fraction///alpha-glucoside transport	
Afu3g06400	-3.42	-4.28	-3.98	hypothetical protein		
Afu3g02140	-3.42	-3.9	-2.89	large conductance mechanosensitive channel, putative	nonselective channel activity///ion channel activity///transport	Transport
Afu5g10590	-3.42	-3.21	-2.13	stress response RCI peptide, putative	cytoplasm///response to stress///molecular function unknown///integral to membrane	
Afu7g01850	-3.41	-3.56	-3.66	RNA polymerase Rpc34 subunit superfamily		
Afu1g16570	-3.39	-3.59	-3.38	G4P04 protein	chromosome segregation	
Afu8g02260	-3.39	-4.4	-3	neutral amino acid permease		Transport
Afu3g06540	-3.36	-4.71	-3.99	3'-phosphoadenosine-5'-phosphosulfate reductase	intracellular///phosphoadenylyl-sulfate reductase (thioredoxin) activity///sulfate assimilation///methionine metabolic process	
Afu1g11720	-3.36	-3.83	-3.61	conserved hypothetical protein		
Afu1g11930	-3.36	-3.81	-3.13	protein kinase, putative	proteolysis///cytoplasm///protein kinase activity	
Afu1g16450	-3.35	-4.15	-2.92	hypothetical protein		
Afu4g06260	-3.35	-3.83	-3.35	mating-type switch/DNA repair protein Swi10, putative	double-strand break repair via single-strand annealing, removal of nonhomologous ends///nucleotide-excision repair factor 1 complex///"nucleotide-excision repair, DNA incision, 5'-to lesion"///removal of nonhomologous ends///single-stranded DNA specific endodeoxyribonuclease activity	Cell cycle control
Afu3g04310	-3.35	-4.07	-4.04	snoRNA binding protein, putative	nucleus///maturation of SSU-rRNA///snoRNA binding	
Afu2g16180	-3.34	-4.07	-3.57	hypothetical protein		
Afu5g06060	-3.31	-3.35	-3.91	sulfur metabolism regulator SkpA, putative	SCF ubiquitin ligase complex///ubiquitin-dependent protein catabolic	Sulphur metabolism

					process///ubiquitin-protein ligase activity///G1/S transition of mitotic cell cycle///cytoplasm///regulation of sulfur metabolic process///protein binding///nucleus///nuclear ubiquitin ligase complex///G2/M transition of mitotic cell cycle///kinetochore	
Afu2g10980	-3.3	-3.57	-3.68	ADP-ribosylation factor, putative	soluble fraction///vesicle-mediated transport///protein targeting to vacuole///small monomeric GTPase activity	
Afu5g10910	-3.3	-3.22	-4.02	hypothetical protein		
Afu5g13870	-3.3	-4.34	-4.05	mlo3 protein		mRNA export, mitotic chromosome segregation
Afu1g17360	-3.29	-4.38	-3.26	bZIP transcription factor (BACH2), putative	transcription///transcription factor activity///nucleus	
Afu4g08780	-3.28	-4.16	-3.29	hypothetical protein		
Afu3g10150	-3.27	-4.48	-4.27	hypothetical protein		
Afu2g05250	-3.27	-4.4	-3.49	RfeD		
Afu6g06390	-3.26	-2.45	-3.14	hypothetical protein		
Afu1g12900	-3.26	-3.67	-3.98	Leucine Rich Repeat domain protein	negative regulation of microtubule depolymerisation///cell wall organisation///microtubule///structural constituent of cytoskeleton	
Afu4g12390	-3.25	-4	-2.83	cell differentiation protein (Rcd1), putative	regulation of transcription from RNA polymerase II promoter///CCR4-NOT complex///molecular function unknown	Regulator of nitrogen starvation-induced sexual differentiation
Afu5g05600	-3.25	-3.44	-2.75	forkhead transcription factor (Sep1), putative	spindle organisation///transcription initiation from RNA polymerase II promoter///specific RNA polymerase II transcription factor activity///nucleus	Mitotic gene transcription

Afu1g14750	-3.24	-4.27	-3.89	C2H2 transcription factor (Sfp1), putative	regulation of transcription, DNA-dependent///transcription factor activity///nucleus///zinc ion binding///regulation of cell size	Transcription factor: Integration of nutrient and stress signals for down regulation of protein synthesis
Afu6g02810	-3.24	-2.61	-3.01	Ctr copper transporter family family		Transport
Afu3g06690	-3.24	-4.12	-3.73	Rho GTPase Rho3	actin filament organisation///intracellular///signal transducer activity///Rho small monomeric GTPase activity///small GTPase mediated signal transduction///exocytosis	Bud formation and exocytosis
Afu2g10550	-3.23	-4.15	-3.19	C2H2 transcription factor (RfeC), putative	regulation of transcription, DNA-dependent///transcription factor activity///nucleus///zinc ion binding	Transcription factor
Afu4g10110	-3.23	-3.57	-3.65	homeobox transcription factor, putative	cellular copper ion homeostasis///transcription initiation from RNA polymerase II promoter///specific RNA polymerase II transcription factor activity///nucleus	Transcription factor
Afu5g00810	-3.23	-5.02	-4.03	hypothetical protein		
Afu3g01300	-3.23	-4.24	-3.39	hypothetical protein		
Afu2g11180	-3.22	-3.74	-3.94	developmental regulator FlbA	regulation of sporulation resulting in formation of a cellular spore///pheromone-dependent signal transduction involved in conjugation with cellular fusion///response to pheromone during conjugation with cellular fusion///response to stress	Developmental regulator upstream of FluG
Afu4g07490	-3.22	-4.35	-3.98	hypothetical protein		
Afu1g04230	-3.22	-2.75	-2.55	mitoribosomal protein YmL27	structural constituent of ribosome///translation///mitochondrial large ribosomal subunit	Essential for mitochondrial function

To identify biological categories enriched, in a stage-specific manner among the total population of differentially expressed genes (fold change cut off of ±2 on a $\log_2$ scale) in the ATCC46645 time course experiment, GO analysis was performed using Genespring GX 11.02. Table 4.5 and Table 4.6 show the GO terms, which satisfy an arbitrarily imposed p-value cut-off of 0.05 with respect to their occurrence in the *A. fumigatus* genome. Significant GO terms among total up-regulated genes included catalytic and oxidoreductase activities, and metabolism. Additionally, phase-specific GO analysis of the up-regulated genes partitioned functional categories according to time point of infection, revealing increased significance of transport functions as infection progresses. Significant GO terms among the down-regulated genes in the ATCC46645 time course included several members involved in transcription and transcriptional regulation.

Total up-regulated genes in the ATCC46645 time course							
GO ACCESSION	**GO Term**	**p-value**	**corrected p-value**	**Count in Selection**	**% Count in Selection**	**Count in Total**	**% Count in Total**
GO:0003824	catalytic activity	2.6329286E-13	4.504941E-9	47	36.71875	2044	45.462635
GO:0016491	oxidoreductase activity	6.042038E-12	5.1689636E-8	38	29.6875	472	10.49822
GO:0006082	organic acid metabolic process	1.9514832E-9	4.7699823E-6	6	4.6875	309	6.872776
GO:0019752	carboxylic acid metabolic process	1.9514832E-9	4.7699823E-6	6	4.6875	309	6.872776
GO:0042180	cellular ketone metabolic process	1.0381139E-9	4.7699823E-6	6	4.6875	319	7.095196
GO:0043436	oxoacid metabolic process	1.9514832E-9	4.7699823E-6	6	4.6875	309	6.872776
GO:0044281	small molecule metabolic process	1.5245785E-9	4.7699823E-6	1	0.78125	483	10.742883
GO:0022857|GO:0005386|GO:0015646	transmembrane transporter activity	1.6942975E-7	2.8989432E-4	1	0.78125	354	7.8736653
GO:0006811	ion transport	2.3700125E-6	0.003119301	1	0.78125	132	2.9359431
GO:0005886|GO:0005904	plasma membrane	1.4934758E-5	0.012776686	53	41.40625	315	7.006228
GO:0032787	monocarboxylic acid metabolic process	1.4664228E-5	0.012776686	5	3.90625	115	2.5578291
GO:0044242	cellular lipid catabolic process	1.5870719E-5	0.012930858	5	3.90625	32	0.7117438
GO:0016042|GO:0006724	lipid catabolic process	2.6027752E-5	0.019362384	5	3.90625	33	0.7339858
GO:0016616	oxidoreductase activity, acting on the CH-OH group of donors, NAD or NADP as acceptor	2.981266E-5	0.021253943	4	3.125	114	2.535587
GO:0006753	nucleoside phosphate metabolic process	6.2342755E-5	0.028829312	1	0.78125	80	1.7793595
GO:0009062	fatty acid catabolic process	5.984095E-5	0.028829312	5	3.90625	25	0.5560498
GO:0009117	nucleotide metabolic process	6.2342755E-5	0.028829312	1	0.78125	80	1.7793595
GO:0016614	oxidoreductase activity, acting on CH-OH group of donors	4.6860412E-5	0.028829312	4	3.125	129	2.8692172
GO:0016054	organic acid catabolic process	7.5876196E-5	0.03245604	6	4.6875	61	1.3567616
GO:0046395	carboxylic acid catabolic process	7.5876196E-5	0.03245604	6	4.6875	61	1.3567616
GO:0005215|GO:0005478	transporter activity	1.1932882E-4	0.04640264	24	18.75	525	11.677046
4 hrs up-regulated genes in the ATCC46645 time course							
GO ACCESSION	**GO Term**	**p-value**	**corrected p-value**	**Count in Selection**	**% Count in Selection**	**Count in Total**	**% Count in Total**
GO:0042180	cellular ketone metabolic process	8.861405E-12	6.27341E-8	6	3.0456853	319	7.095196
GO:0044281	small molecule metabolic process	4.8981244E-12	6.27341E-8	1	0.5076142	483	10.742883
GO:0016491	oxidoreductase activity	1.8180478E-11	8.58055E-8	27	13.705584	472	10.49822
GO:0006082	organic acid metabolic process	4.053666E-11	9.565943E-8	6	3.0456853	309	6.872776
GO:0019752	carboxylic acid metabolic process	4.053666E-11	9.565943E-8	6	3.0456853	309	6.872776
GO:0043436	oxoacid metabolic process	4.053666E-11	9.565943E-8	6	3.0456853	309	6.872776
GO:0003824	catalytic activity	5.8614547E-10	1.0374007E-6	34	17.258883	2044	45.462635
GO:0022857|GO:0005386|	transmembrane transporter activity	2.8638493E-7	3.1191617E-4	1	0.5076142	354	7.8736653

GO:0015646							
GO:0005737	cytoplasm	9.120414E-7	6.456775E-4	146	74.11167	2039	45.351425
GO:0006753	nucleoside phosphate metabolic process	4.487924E-6	0.0024440114	1	0.5076142	80	1.7793595
GO:0009117	nucleotide metabolic process	4.487924E-6	0.0024440114	1	0.5076142	80	1.7793595
GO:0044242	cellular lipid catabolic process	9.112341E-6	0.0047785626	5	2.5380712	32	0.7117438
GO:0016042|GO:0006724	lipid catabolic process	1.3607678E-5	0.0066438084	5	2.5380712	33	0.7339858
GO:0032787	monocarboxylic acid metabolic process	1.454998E-5	0.006867082	6	3.0456853	115	2.5578291
GO:0008152	metabolic process	2.50623E-5	0.011446963	60	30.456852	2366	52.624554
GO:0005739	mitochondrion	3.7388872E-5	0.015570212	46	23.350254	435	9.675267
GO:0044444	cytoplasmic part	5.4811295E-5	0.02080657	46	23.350254	1294	28.78114
GO:0006457|GO:0007022| GO:0007024|GO:0007025	protein folding	7.3481424E-5	0.026010498	13	6.5989847	48	1.0676156
GO:0006811	ion transport	8.0210826E-5	0.027040506	1	0.5076142	132	2.9359431
GO:0016616	oxidoreductase activity, acting on the CH-OH group of donors, NAD or NADP as acceptor	9.7396965E-5	0.03134179	3	1.5228426	114	2.535587
GO:0009062	fatty acid catabolic process	1.1876168E-4	0.036299374	5	2.5380712	25	0.5560498
GO:0016054	organic acid catabolic process	1.2305783E-4	0.036299374	5	2.5380712	61	1.3567616
GO:0046395	carboxylic acid catabolic process	1.2305783E-4	0.036299374	5	2.5380712	61	1.3567616
GO:0016614	oxidoreductase activity, acting on CH-OH group of donors	1.3296878E-4	0.03842242	3	1.5228426	129	2.8692172
GO:0055086	nucleobase, nucleoside and nucleotide metabolic process	1.73719E-4	0.04858762	1	0.5076142	105	2.3354092

8 hrs up-regulated genes in the ATCC46645 time course

GO ACCESSION	GO Term	p-value	corrected p-value	Count in Selection	% Count in Selection	Count in Total	% Count in Total
GO:0003824	catalytic activity	1.7023827E-11	2.774999E-7	37	40.217392	2044	45.462635
GO:0016491	oxidoreductase activity	3.622693E-9	2.9526173E-5	28	30.434782	472	10.49822
GO:0044281	small molecule metabolic process	5.97662E-8	2.4355738E-4	1	1.0869565	483	10.742883
GO:0022857|GO:0005386| GO:0015646	transmembrane transporter activity	3.155829E-7	8.573691E-4	1	1.0869565	354	7.8736653
GO:0006811	ion transport	7.8666125E-7	0.001831873	1	1.0869565	132	2.9359431
GO:0042180	cellular ketone metabolic process	9.0772875E-7	0.001849574	5	5.4347825	319	7.095196
GO:0006082	organic acid metabolic process	2.0390244E-6	0.0030215888	5	5.4347825	309	6.872776
GO:0019752	carboxylic acid metabolic process	2.0390244E-6	0.0030215888	5	5.4347825	309	6.872776
GO:0043436	oxoacid metabolic process	2.0390244E-6	0.0030215888	5	5.4347825	309	6.872776
GO:0006753	nucleoside phosphate metabolic process	1.150689E-5	0.011765132	1	1.0869565	80	1.7793595
GO:0009062	fatty acid catabolic process	1.1548116E-5	0.011765132	5	5.4347825	25	0.5560498
GO:0009117	nucleotide metabolic process	1.150689E-5	0.011765132	1	1.0869565	80	1.7793595
GO:0044242	cellular lipid catabolic process	1.2443318E-5	0.011931441	5	5.4347825	32	0.7117438

GO:0005886|GO:0005904	plasma membrane	1.6725186E-5	0.015146213	48	52.173912	315	7.006228
GO:0016042|GO:0006724	lipid catabolic process	1.9778961E-5	0.016120521	5	5.4347825	33	0.7339858
GO:0032787	monocarboxylic acid metabolic process	2.2823499E-5	0.016910838	5	5.4347825	115	2.5578291
GO:0016054	organic acid catabolic process	7.7985234E-5	0.045400433	5	5.4347825	61	1.3567616
GO:0046395	carboxylic acid catabolic process	7.7985234E-5	0.045400433	5	5.4347825	61	1.3567616
16 hrs up-regulated genes in the ATCC46645 time course							
GO ACCESSION	**GO Term**	**p-value**	**corrected p-value**	**Count in Selection**	**% Count in Selection**	**Count in Total**	**% Count in Total**
GO:0003824	catalytic activity	2.0177418E-9	2.8934535E-5	3	4.83871	2044	45.462635
GO:0022891	substrate-specific transmembrane transporter activity	2.6887168E-8	1.927818E-4	1	1.6129032	317	7.0507116
GO:0022857|GO:0005386|GO:0015646	transmembrane transporter activity	1.3589522E-7	3.8974907E-4	2	3.2258065	354	7.8736653
GO:0022892	substrate-specific transporter activity	1.9675623E-7	4.0333378E-4	1	1.6129032	357	7.9403915
GO:0006811	ion transport	9.644869E-6	0.0138308	1	1.6129032	132	2.9359431
GO:0005342	organic acid transmembrane transporter activity	3.5586836E-5	0.03925518	1	1.6129032	59	1.3122776
GO:0005215|GO:0005478	transporter activity	4.0179137E-5	0.039597526	19	30.64516	525	11.677046
GO:0005886|GO:0005904	plasma membrane	4.1419837E-5	0.039597526	42	67.741936	315	7.006228

Table 4.5: Significant GO terms among the up-regulated genes in the ATCC46645 time course. p-value represents the probability of obtaining the GO term from a list of random entities, corrected p-value derived from Bonferroni testing of multiple comparisons. Analysis performed using Genespring GX 11.02.

Total down-regulated genes in the ATCC46645 time course							
GO ACCESSION	**GO Term**	**p-value**	**corrected p-value**	**Count in Selection**	**% Count in Selection**	**Count in Total**	**% Count in Total**
GO:0005634	nucleus	5.5901533E-10	9.502934E-6	154	79.38145	1124	25.0
GO:0006350	transcription	1.4846413E-9	1.2619017E-5	35	18.041237	120	2.6690392
GO:0044428	nuclear part	3.2058924E-8	1.8166099E-4	6	3.0927835	464	10.320285
GO:0031981	nuclear lumen	5.2097686E-8	2.2140756E-4	6	3.0927835	238	5.2935944
GO:0016070	RNA metabolic process	1.0409707E-7	3.539179E-4	21	10.824742	372	8.274021
GO:0044260|GO:0034960	cellular macromolecule metabolic process	3.2913212E-7	9.3250896E-4	35	18.041237	1075	23.910143
GO:0006351	transcription, DNA-dependent	1.4624209E-6	0.0035514713	21	10.824742	87	1.9350533
GO:0003702	RNA polymerase II transcription factor activity	2.3201442E-6	0.004323292	7	3.6082475	65	1.4457295
GO:0032774	RNA biosynthetic process	2.5432005E-6	0.004323292	21	10.824742	93	2.0685053
GO:0043170|GO:0043283	macromolecule metabolic process	2.4108556E-6	0.004323292	35	18.041237	1199	26.66815
GO:0010467	gene expression	2.8524491E-6	0.004408179	35	18.041237	571	12.700178
GO:0005488	binding	3.9904253E-6	0.0054627666	5	2.5773196	867	19.283808

GO:0005654	nucleoplasm	4.3250748E-6	0.0054627666	6	3.0927835	138	3.069395
GO:0006357	regulation of transcription from RNA polymerase II promoter	4.734825E-6	0.0054627666	13	6.7010307	83	1.8460854
GO:0050789|GO:0050791	regulation of biological process	4.820254E-6	0.0054627666	43	22.164948	512	11.3879
GO:0003676	nucleic acid binding	5.3128256E-6	0.005644683	5	2.5773196	439	9.764235
GO:0050794|GO:0051244	regulation of cellular process	6.974342E-6	0.006974102	39	20.103092	489	10.876334
GO:0006366	transcription from RNA polymerase II promoter	8.355536E-6	0.007891068	21	10.824742	65	1.4457295
GO:0044451	nucleoplasm part	1.0704729E-5	0.009577586	2	1.0309278	129	2.8692172
GO:0019222	regulation of metabolic process	1.4490729E-5	0.012316696	43	22.164948	339	7.5400357
GO:0016591	DNA-directed RNA polymerase II, holoenzyme	1.5400934E-5	0.012466994	1	0.5154639	37	0.82295376
GO:0065007	biological regulation	1.8282262E-5	0.014126717	43	22.164948	618	13.745552
GO:0043233	organelle lumen	2.69467E-5	0.018323125	6	3.0927835	365	8.118327
GO:0070013	intracellular organelle lumen	2.69467E-5	0.018323125	6	3.0927835	365	8.118327
GO:0080090	regulation of primary metabolic process	2.5067759E-5	0.018323125	43	22.164948	318	7.0729537
GO:0006355	regulation of transcription, DNA-dependent	3.8250757E-5	0.02500925	25	12.886598	168	3.7366548
GO:0032991	macromolecular complex	4.5281955E-5	0.02749167	5	2.5773196	774	17.215303
GO:0051252	regulation of RNA metabolic process	4.5101173E-5	0.02749167	25	12.886598	169	3.7588968
GO:0031326	regulation of cellular biosynthetic process	5.4806183E-5	0.031055769	39	20.103092	299	6.650356
GO:0000151	ubiquitin ligase complex	5.9944836E-5	0.0318446	3	1.5463917	23	0.51156586
GO:0006109	regulation of carbohydrate metabolic process	5.899354E-5	0.0318446	4	2.0618556	14	0.3113879
GO:0030528	transcription regulator activity	6.48235E-5	0.033392776	8	4.123711	280	6.227758
GO:0009889	regulation of biosynthetic process	6.930231E-5	0.03464996	39	20.103092	301	6.69484
GO:0031323	regulation of cellular metabolic process	7.23957E-5	0.035162415	39	20.103092	322	7.1619215
GO:0005667	transcription factor complex	7.806755E-5	0.036863964	1	0.5154639	41	0.9119217
GO:0006367	transcription initiation from RNA polymerase II promoter	8.660711E-5	0.03979109	13	6.7010307	27	0.6005338
GO:0006139	nucleobase, nucleoside, nucleotide and nucleic acid metabolic process	9.365904E-5	0.041898653	35	18.041237	660	14.679715
4 hrs down-regulated genes in the ATCC46645 time course							
GO ACCESSION	**GO Term**	**p-value**	**corrected p-value**	**Count in Selection**	**% Count in Selection**	**Count in Total**	**% Count in Total**
GO:0005634	nucleus	1.4105173E-6	0.008881466	83	98.809525	1124	25.0
GO:0006350	transcription	1.3111768E-6	0.008881466	10	11.904762	120	2.6690392
8 hrs down-regulated genes in the ATCC46645 time course							
GO ACCESSION	**GO Term**	**p-value**	**corrected p-value**	**Count in Selection**	**% Count in Selection**	**Count in Total**	**% Count in Total**
GO:0006350	transcription	6.2399946E-10	9.384578E-6	33	19.298246	120	2.6690392
GO:0005634	nucleus	1.2679399E-9	9.534528E-6	147	85.96491	1124	25.0
GO:0031981	nuclear lumen	9.829524E-8	4.9276714E-4	27	15.789474	238	5.2935944

GO:0016070	RNA metabolic process	1.7188285E-7	6.4625376E-4	20	11.695907	372	8.274021
GO:0006351	transcription, DNA-dependent	9.879598E-7	0.002476387	20	11.695907	87	1.9350533
GO:0044428	nuclear part	8.6203045E-7	0.002476387	27	15.789474	464	10.320285
GO:0032774	RNA biosynthetic process	1.4132655E-6	0.0030363807	20	11.695907	93	2.0685053
GO:0010467	gene expression	3.1244708E-6	0.005873771	33	19.298246	571	12.700178
GO:0003702	RNA polymerase II transcription factor activity	4.209757E-6	0.0070346915	5	2.9239767	65	1.4457295
GO:0005634	nucleus	1.4105173E-6	0.008881466	83	98.809525	1124	25.0
GO:0006350	transcription	1.3111768E-6	0.008881466	10	11.904762	120	2.6690392
GO:0016591	DNA-directed RNA polymerase II, holoenzyme	6.470116E-6	0.009730667	1	0.5847953	37	0.82295376
GO:0005488	binding	1.4964731E-5	0.01664453	5	2.9239767	867	19.283808
GO:0006366	transcription from RNA polymerase II promoter	1.5494197E-5	0.01664453	20	11.695907	65	1.4457295
GO:0003676	nucleic acid binding	1.8162524E-5	0.01821023	5	2.9239767	439	9.764235
GO:0005654	nucleoplasm	3.0831856E-5	0.025549265	4	2.3391812	138	3.069395
GO:0005730	nucleolus	3.1949843E-5	0.025549265	24	14.035088	112	2.4911032
GO:0030528	transcription regulator activity	3.2443582E-5	0.025549265	5	2.9239767	280	6.227758
GO:0043233	organelle lumen	3.397644E-5	0.025549265	27	15.789474	365	8.118327
GO:0070013	intracellular organelle lumen	3.397644E-5	0.025549265	27	15.789474	365	8.118327
GO:0044451	nucleoplasm part	4.0753133E-5	0.02918584	1	0.5847953	129	2.8692172
GO:0006367	transcription initiation from RNA polymerase II promoter	6.870035E-5	0.044922266	12	7.017544	27	0.6005338

16 hrs down-regulated genes in the ATCC46645 time course

GO ACCESSION	GO Term	p-value	corrected p-value	Count in Selection	% Count in Selection	Count in Total	% Count in Total
GO:0005634	nucleus	8.61132E-9	1.3784424E-4	124	78.48101	1124	25.0
GO:0006350	transcription	3.4257312E-7	0.0018278938	29	18.354431	120	2.6690392
GO:0044260|GO:0034960	cellular macromolecule metabolic process	2.2965533E-7	0.0018278938	29	18.354431	1075	23.910143
GO:0044428	nuclear part	4.764217E-7	0.0019065599	4	2.5316455	464	10.320285
GO:0043170|GO:0043283	macromolecule metabolic process	7.557978E-7	0.0024196613	29	18.354431	1199	26.66815
GO:0016070	RNA metabolic process	1.1366951E-6	0.0030325758	19	12.025316	372	8.274021
GO:0031981	nuclear lumen	1.8273149E-6	0.0041786334	4	2.5316455	238	5.2935944
GO:0006366	transcription from RNA polymerase II promoter	2.1125286E-6	0.0042269933	19	12.025316	65	1.4457295
GO:0005488	binding	3.4334078E-6	0.0061066328	3	1.8987342	867	19.283808
GO:0005622	intracellular	5.202852E-6	0.008328378	130	82.27848	2921	64.968864
GO:0000151	ubiquitin ligase complex	5.8427418E-6	0.008502427	3	1.8987342	23	0.51156586
GO:0003702	RNA polymerase II transcription factor activity	8.137292E-6	0.010854694	6	3.7974684	65	1.4457295
GO:0044424	intracellular part	9.518359E-6	0.01172027	126	79.74683	2899	64.47954
GO:0003676	nucleic acid binding	1.2039269E-5	0.013603866	3	1.8987342	439	9.764235
GO:0050789|GO:0050791	regulation of biological process	1.3597636E-5	0.013603866	31	19.620253	512	11.3879
GO:0065007	biological regulation	1.3079437E-5	0.013603866	31	19.620253	618	13.745552

GO:0006351	transcription, DNA-dependent	1.6304955E-5	0.015352872	19	12.025316	87	1.9350533
GO:0050794|GO:0051244	regulation of cellular process	1.8027062E-5	0.016031398	31	19.620253	489	10.876334
GO:0016591	DNA-directed RNA polymerase II, holoenzyme	1.9954921E-5	0.016148277	1	0.6329114	37	0.82295376
GO:0032774	RNA biosynthetic process	2.0176101E-5	0.016148277	19	12.025316	93	2.0685053
GO:0010467	gene expression	2.215825E-5	0.016890211	29	18.354431	571	12.700178
GO:0006367	transcription initiation from RNA polymerase II promoter	4.6177567E-5	0.033599075	12	7.594937	27	0.6005338
GO:0006357	regulation of transcription from RNA polymerase II promoter	6.25143E-5	0.043508135	12	7.594937	83	1.8460854
GO:0043227	membrane-bounded organelle	7.410959E-5	0.047451865	124	78.48101	2057	45.751778
GO:0043231	intracellular membrane-bounded organelle	7.410959E-5	0.047451865	124	78.48101	2057	45.751778
GO:0005654	nucleoplasm	7.931446E-5	0.04883126	4	2.5316455	138	3.069395

Table 4.6: Significant GO terms among the down-regulated genes in the ATCC46645 time course. p-value represents the probability of obtaining the GO term from a list of random entities, corrected p-value derived from Bonferroni testing of multiple comparisons. Analysis performed using Genespring GX 11.02.

Differentially expressed genes in the ATCC46645 transcriptome during initiation of murine were also analysed using the STEM (Short Time-series Expression Miner) software, designed for clustering, comparing, and visualizing gene expression data from short time series microarray experiments (Ernst and Bar-Joseph, 2006). This software utilises a novel method for clustering short time series expression data, differentiating between real and random patterns and is also integrated with the GO for a biological interpretation of the results. The software generates a set of distinct and representative models corresponding to possible patterns of gene expression over time. The expression profiles from the geneset of interest are then assigned to the most closely matching model profile based on correlation coefficient. Significant model profiles are those having a statistically significant number of genes assigned to them, as compared to that expected by chance. The number of genes expected to be assigned by chance to a profile is calculated by repeating a large number of random permutations, which renormalise the genes' expression values and then assign the genes to their most closely matching model profiles. After these permutations, the average number of genes assigned to a model profile is used as the number of genes expected to be assigned by chance. Statistical significance is calculated on the basis of the number of genes assigned to each profile versus the number randomly expected by the permutations. The biological significance of the set of genes assigned to the same profile or the same cluster of profiles can then be assessed using a GO enrichment analysis.

Fig. 4.7 shows the STEM output profiles for the ATCC46645 time course experiment. Each box is a different model temporal expression profile, having a unique profile number (top left hand corner). The box is coloured when a statistically significant number of genes were assigned to the model expression profile. Model profiles of the same colour are similar in temporal expression characteristics and can be considered as a cluster. Model profiles can be ordered by various parameters, such as significance or number of genes assigned. In the following examples the model profiles are ordered by default to list models by similarity, thereby grouping similar temporal profiles together. The significance of, and the number of genes associated to each model profiles is indicated in the legend. As summarised in Fig 4.7, STEM allocated the differentially expressed genes (fold change cut off of ±2 on a $\log_2$ scale) of the ATCC46645 time course dataset into nine model profiles, belonging to four different clusters. Among these, four model profiles (0, 12, 1, 9) contain genes whose expression is down-regulated across the ATCC46645 time course and five (49, 48, 42, 47 and 29) contain genes whose expression is up-regulated across the ATCC46645 time course.

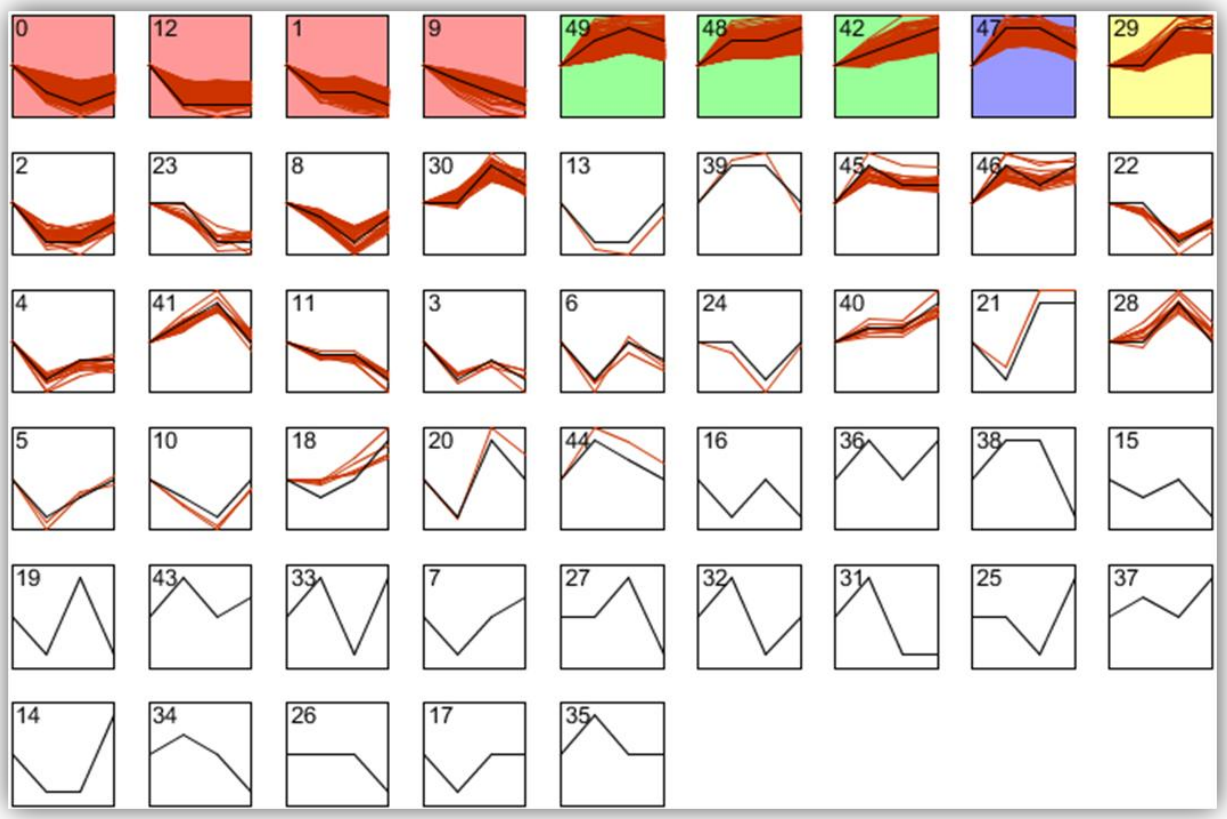


Fig. 4.7: STEM clustering analysis of differentially expressed genes in the ATCC46645 time course during initiation of murine infection. Statistically significant model profiles are coloured. Clustered model profiles are similarly coloured. Profile 0, n = 395 (1e-201), Profile 12, n = 444 (2e-119), Profile 1, n = 197 (7e-59), Profile 9, n = 85, (4e-25), Profile 49, n = 479 (6e-180), Profile 48, n = 398 (1e-142), Profile 42, n = 114, (1e-44), Profile 47, n=122 (6e-21), Profile 29, n = 75 (2e-36). All analysed genes are indicated in red.

Functional classification of the genes assigned to each model profile was performed by using a GO enrichment analysis. For GO analysis in STEM, the *A. fumigatus* annotation used elsewhere in this study (produced by the JCVI) was extended to include additional categories of interest, extrapolated from the literature or from the research performed in our laboratory. These categories include those located in clusters of physically-linked genes, termed by us as infections clusters (ICs) which were identified as differentially expressed at a single timepoint of *A. fumigatus* virulence (Af293, 14 hours) relative to laboratory culture (McDonagh *et al.*, 2008a), and genes having subtelomeric (300 kb from telomeres) and semi-subtelomeric locations (300-600 kb from telomeres). Genes specific to *A. fumigatus*, *A. fisheri* and *A. clavatus* lineage (AFFC-specific) were also collectively analysed as the latter two species are phylogenetically the closest (based upon sequenced *Aspergillus* genomes) to *A. fumigatus* and may be used as indicators of recently evolved function. In addition, genes specific to *A. fumigatus* only (AFU-SPECIFIC) were annotated. Genes involved in secondary metabolite

production (as predicted from *in silico* analyses) by Perrin *et al.*, 2007 (SECMET) and genes putatively involved in transposition were additional functional classifications. Genes differentially regulated during shift from low (pH=5) to high (pH=8.0) pH were also included (Loss *et al.*, unpublished).

The GO enrichment analysis for each profile is shown in Table 4.7. For each model profile, only GO terms with corrected p-value <0.05 are included, where the p-value, initially based on a hypergeometric distribution, was corrected by the software using a Bonferonni correction for multiple GO categories being tested simultaneously. This corrected p-value is the original p-value divided by the number of GO categories in which the number of genes on the array is above the GO analysis minimum number of genes parameter.

Broadly speaking the STEM analysis confirmed the enrichment for transport and cell wall functions among up-regulated genes, whereby profiles 48 and 49 were significantly enriched for such terms. In addition, profiles 0, 12 and 1, representing down-regulated genes were significantly enriched in GO terms associated with the functional category transcription.

Significant GO terms for Profile 0 (n = 395)						
Category ID	**Genes in Category**	**Count Genes**	**Genes Expected**	**Genes Enriched**	**p-value**	**Corrected p-value**
Semi-subT	438	71.0	9.1	+61.9	2.5E-40	6.2E-38
nucleus	221	46.0	4.6	+41.4	1.1E-31	2.8E-29
cytoplasm	286	36.0	6.0	+30.0	1.4E-17	3.5E-15
molecular function unknown	186	29.0	3.9	+25.1	5.7E-17	1.4E-14
In vitro pH response genes	282	34.5	5.9	+28.6	6.1E-17	1.5E-14
zinc ion binding	68	19.0	1.4	+17.6	1.5E-16	3.7E-14
Subtelomeric	373	39.0	7.8	+31.2	3.9E-16	9.5E-14
AFU-SPECIFIC	70	16.0	1.5	+14.5	1.1E-12	2.7E-10
DNA binding	33	11.0	0.7	+10.3	4.2E-11	1.0E-8
regulation of transcription	40	11.0	0.8	+10.2	4.4E-10	1.1E-7
transcription factor activity	44	11.0	0.9	+10.1	1.3E-9	3.3E-7
cellular component unknown	97	15.0	2.0	+13.0	1.9E-9	4.7E-7
biological process unknown	151	18.0	3.2	+14.8	3.7E-9	9.0E-7
SECMET	81	13.0	1.7	+11.3	1.4E-8	3.5E-6
mitochondrial matrix	17	7.0	0.4	+6.6	2.8E-8	6.8E-6
nuclear mRNA splicing	13	6.0	0.3	+5.7	1.3E-7	3.1E-5
via spliceosome	13	6.0	0.3	+5.7	1.3E-7	3.1E-5
IC	279	20.5	5.8	+14.7	6.2E-7	1.5E-4
transcription	17	6.0	0.4	+5.6	8.4E-7	2.1E-4
endoplasmic reticulum	50	9.0	1.0	+8.0	8.7E-7	2.1E-4
negative regulation of transcription from RNA polymerase II promoter	10	5.0	0.2	+4.8	9.2E-7	2.2E-4
general RNA polymerase II transcription factor activity	11	5.0	0.2	+4.8	1.7E-6	4.0E-4
protein serine/threonine kinase activity	11	5.0	0.2	+4.8	1.7E-6	4.0E-4
nucleolus	29	7.0	0.6	+6.4	1.8E-6	4.4E-4
protein amino acid phosphorylation	30	7.0	0.6	+6.4	2.3E-6	5.6E-4

transcription initiation from RNA polymerase II promoter	13	5.0	0.3	+4.7	4.4E-6	0.001
response to stress	23	6.0	0.5	+5.5	6.2E-6	0.002
pathogenesis	23	6.0	0.5	+5.5	6.2E-6	0.002
protein kinase activity	15	5.0	0.3	+4.7	1.0E-5	0.002
integral to plasma membrane	39	6.5	0.8	+5.7	1.5E-5	0.004
DNA-dependent	17	5.0	0.4	+4.6	2.0E-5	0.005
AFFC specific	42	7.0	0.9	+6.1	2.5E-5	0.006
mitochondrion	79	9.0	1.7	+7.3	4.2E-5	0.010
transport	49	6.5	1.0	+5.5	6.9E-5	0.017
plasma membrane	74	8.0	1.5	+6.5	1.6E-4	0.039
Significant GO terms for Profile 12 (n = 444)						
Category ID	**Genes in Category**	**Count Genes**	**Genes Expected**	**Genes Enriched**	**p-value**	**Corrected p-value**
nucleus	221	59.0	10.2	+48.8	3.2E-28	7.8E-26
molecular function unknown	186	47.0	8.6	+38.4	1.0E-21	2.5E-19
cytoplasm	286	52.0	13.3	+38.7	4.0E-17	9.8E-15
biological process unknown	151	32.0	7.0	+25.0	5.2E-13	1.3E-10
Semi-subT	438	58.0	20.3	+37.7	1.2E-12	3.0E-10
protein binding	36	15.0	1.7	+13.3	2.2E-11	5.3E-9
nucleolus	29	12.0	1.3	+10.7	2.4E-9	6.0E-7
35S primary transcript processing	16	9.0	0.7	+8.3	8.4E-9	2.1E-6
zinc ion binding	68	16.0	3.2	+12.8	6.7E-8	1.6E-5
In vitro pH response genes	282	34.0	13.1	+20.9	4.5E-7	1.1E-4
rRNA modification	6	5.0	0.3	+4.7	1.2E-6	3.0E-4
cellular component unknown	97	16.0	4.5	+11.5	1.0E-5	0.002
signal transducer activity	8	5.0	0.4	+4.6	1.1E-5	0.003
regulation of transcription	40	10.0	1.9	+8.1	1.1E-5	0.003
ubiquitin-dependent protein catabolic process	20	7.0	0.9	+6.1	2.1E-5	0.005
transcription factor activity	44	10.0	2.0	+8.0	2.7E-5	0.007
Subtelomeric	373	36.0	17.3	+18.7	3.4E-5	0.008
nucleotide-excision repair	11	5.0	0.5	+4.5	7.8E-5	0.019
AFU-SPECIFIC	70	12.0	3.2	+8.8	8.5E-5	0.021
endoplasmic reticulum	50	10.0	2.3	+7.7	8.6E-5	0.021
proteolysis	13	5.0	0.6	+4.4	2.0E-4	0.049
transcription initiation from RNA polymerase II promoter	13	5.0	0.6	+4.4	2.0E-4	0.049
Significant GO terms for Profile 1 (n = 197)						
Category ID	**Genes in Category**	**Count Genes**	**Genes Expected**	**Genes Enriched**	**p-value**	**Corrected p-value**
Semi-subT	438	36.0	8.1	+27.9	1.8E-13	4.4E-11
ubiquitin-dependent protein catabolic process	20	10.0	0.4	+9.6	6.9E-13	1.7E-10
nucleus	221	22.0	4.1	+17.9	2.2E-10	5.4E-8
cytoplasm	286	25.0	5.3	+19.7	2.2E-10	5.4E-8
biological process unknown	151	17.0	2.8	+14.2	3.7E-9	9.0E-7
protein binding	36	9.0	0.7	+8.3	1.4E-8	3.5E-6
molecular function unknown	186	17.0	3.4	+13.6	8.3E-8	2.0E-5
ATPase activity	19	6.0	0.3	+5.7	8.5E-7	2.1E-4
translational initiation	11	5.0	0.2	+4.8	8.8E-7	2.2E-4
translation initiation factor activity	11	5.0	0.2	+4.8	8.8E-7	2.2E-4
regulation of transcription from RNA polymerase II promoter	14	5.0	0.3	+4.7	3.7E-6	8.9E-4
zinc ion binding	68	8.0	1.3	+6.7	3.6E-5	0.009
cellular component unknown	97	9.0	1.8	+7.2	8.0E-5	0.019

Significant GO terms for Profile 9 (n = 85)						
Category ID	**Genes in Category**	**Count Genes**	**Genes Expected**	**Genes Enriched**	**p-value**	**Corrected p-value**
protein amino acid phosphorylation	30	6.0	0.2	+5.8	1.5E-7	3.6E-5
cytoplasm	286	13.0	2.3	+10.7	9.5E-7	2.3E-4
nucleus	221	10.0	1.8	+8.2	1.7E-5	0.004
Significant GO terms for Profile 49 (n = 479)						
Category ID	**Genes in Category**	**Count Genes**	**Genes Expected**	**Genes Enriched**	**p-value**	**Corrected p-value**
Subtelomeric	373	84.5	13.8	+70.7	1.6E-41	3.8E-39
Semi-subT	438	86.5	16.2	+70.3	1.5E-37	3.7E-35
IC	279	63.0	10.3	+52.7	5.5E-31	1.3E-28
biological process unknown	151	34.0	5.6	+28.4	2.0E-17	4.8E-15
cytoplasm	286	45.0	10.6	+34.4	3.6E-16	8.7E-14
molecular function unknown	186	33.0	6.9	+26.1	8.7E-14	2.1E-11
In vitro pH response genes	282	37.0	10.4	+26.6	3.6E-11	8.7E-9
cellular component unknown	97	21.0	3.6	+17.4	5.4E-11	1.3E-8
mitochondrion	79	19.0	2.9	+16.1	6.2E-11	1.5E-8
fungal-type vacuole	19	9.0	0.7	+8.3	8.4E-9	2.0E-6
plasma membrane	74	16.0	2.7	+13.3	1.0E-8	2.5E-6
spindle pole body	11	7.0	0.4	+6.6	2.7E-8	6.6E-6
SECMET	81	16.0	3.0	+13.0	4.0E-8	9.9E-6
oxidoreductase activity	55	13.0	2.0	+11.0	8.0E-8	1.9E-5
metabolic process	75	15.0	2.8	+12.2	8.9E-8	2.2E-5
microsome	9	6.0	0.3	+5.7	1.9E-7	4.7E-5
fatty acid beta-oxidation	9	6.0	0.3	+5.7	1.9E-7	4.7E-5
nucleus	221	26.0	8.2	+17.8	2.4E-7	5.9E-5
structural constituent of cytoskeleton	10	6.0	0.4	+5.6	4.7E-7	1.1E-4
cytosol	44	10.0	1.6	+8.4	3.7E-6	9.0E-4
endoplasmic reticulum	50	10.0	1.8	+8.2	1.2E-5	0.003
ergosterol biosynthetic process	17	6.0	0.6	+5.4	2.2E-5	0.005
glucose transmembrane transporter activity	14	5.0	0.5	+4.5	1.0E-4	0.025
fungal-type cell wall	15	5.0	0.6	+4.4	1.5E-4	0.037
Significant GO terms for Profile 48 (n = 398)						
Category ID	**Genes in Category**	**Count Genes**	**Genes Expected**	**Genes Enriched**	**p-value**	**Corrected p-value**
In vitro pH response genes	282	57.0	9.0	+48.0	9.2E-29	2.2E-26
Semi-subT	438	67.5	13.9	+53.6	8.0E-27	2.0E-24
IC	279	54.0	8.9	+45.1	2.3E-26	5.5E-24
Subtelomeric	373	58.5	11.9	+46.6	6.4E-24	1.6E-21
cytoplasm	286	50.0	9.1	+40.9	1.8E-22	4.3E-20
plasma membrane	74	17.0	2.4	+14.6	1.4E-10	3.5E-8
mitochondrion	79	16.0	2.5	+13.5	3.5E-9	8.6E-7
metabolic process	75	15.0	2.4	+12.6	1.3E-8	3.1E-6
nucleus	221	25.0	7.0	+18.0	5.5E-8	1.3E-5
arginine biosynthetic process	6	5.0	0.2	+4.8	1.9E-7	4.6E-5
hydrolase activity	24	8.0	0.8	+7.2	4.9E-7	1.2E-4
molecular function unknown	186	21.0	5.9	+15.1	6.3E-7	1.5E-4
cytosol	44	10.0	1.4	+8.6	9.7E-7	2.4E-4
oxidoreductase activity	55	11.0	1.7	+9.3	1.1E-6	2.7E-4
transporter activity	32	8.0	1.0	+7.0	5.6E-6	0.001
biological process unknown	151	17.0	4.8	+12.2	7.4E-6	0.002
cellular component unknown	97	13.0	3.1	+9.9	1.3E-5	0.003
AFFC specific	42	8.0	1.3	+6.7	4.7E-5	0.011
cell wall organisation	23	6.0	0.7	+5.3	6.6E-5	0.016

membrane	24	6.0	0.8	+5.2	8.5E-5	0.021
transport	49	8.0	1.6	+6.4	1.5E-4	0.036
integral to plasma membrane	39	7.0	1.2	+5.8	2.1E-4	0.050
SECMET	81	9.0	2.6	+6.4	1.1E-3	0.269
integral to membrane	38	6.0	1.2	+4.8	1.2E-3	0.291
endoplasmic reticulum	50	6.0	1.6	+4.4	5.0E-3	1.000
transcription factor activity	44	5.0	1.4	+3.6	0.01	1.000
zinc ion binding	68	5.0	2.2	+2.8	0.07	1.000
Significant GO terms for Profile 42 (n = 122)						
Category ID	**Genes in Category**	**Count Genes**	**Genes Expected**	**Genes Enriched**	**p-value**	**Corrected p-value**
IC	279	33.0	2.3	+30.7	1.4E-27	3.5E-25
Subtelomeric	373	30.0	3.0	+27.0	2.5E-20	6.0E-18
In vitro pH response genes	282	23.0	2.3	+20.7	4.4E-16	1.1E-13
SECMET	81	11.0	0.7	+10.3	7.7E-11	1.9E-8
Semi-subT	438	21.0	3.6	+17.4	2.0E-10	4.8E-8
integral to plasma membrane	39	5.0	0.3	+4.7	1.7E-5	0.004
cellular component unknown	97	6.0	0.8	+5.2	1.6E-4	0.038
Significant GO terms for Profile 47 (n = 122)						
Category ID	**Genes in Category**	**Count Genes**	**Genes Expected**	**Genes Enriched**	**p-value**	**Corrected p-value**
cytoplasm	286	26.0	5.0	+21.0	1.2E-11	3.0E-9
ATP synthesis coupled proton transport	6	5.0	0.1	+4.9	9.3E-9	2.3E-6
metabolic process	75	11.0	1.3	+9.7	7.6E-8	1.9E-5
rotational mechanism	8	5.0	0.1	+4.9	8.5E-8	2.1E-5
oxidoreductase activity	55	9.0	1.0	+8.0	4.4E-7	1.1E-4
mitochondrion	79	8.5	1.4	+7.1	9.9E-6	0.002
Semi-subT	438	21.0	7.6	+13.4	3.8E-5	0.009
Significant GO terms for Profile 29 (n = 75)						
Category ID	**Genes in Category**	**Count Genes**	**Genes Expected**	**Genes Enriched**	**p-value**	**Corrected p-value**
IC	279	31.0	1.2	+29.8	1.3E-33	3.1E-31
Subtelomeric	373	30.0	1.6	+28.4	2.3E-28	5.7E-26
In vitro pH response genes	282	25.0	1.2	+23.8	6.0E-25	1.5E-22
N-acetyltransferase activity	12	5.0	0.1	+4.9	1.0E-9	2.5E-7
Semi-subT	438	15.0	1.9	+13.1	1.1E-9	2.8E-7
SECMET	81	8.0	0.3	+7.7	2.5E-9	6.1E-7
metabolic process	75	6.0	0.3	+5.7	8.9E-7	2.2E-4

Table 4.7: Significant GO terms among the profiles 0, 12, 1, 9, 49, 48, 42, 47, and 29 in the ATCC46645 time course experiment. Table details the GO terms, whose corrected p-value based on the expected number of genes assigned to the profile satisfy the cut-off of <0.05.

Significant model profiles can be ordered according to the enrichment of a specific GO term, whereby the output can offer an indication of how many ORFs associated with that GO term are present within a profile, and if that profile is significantly enriched for a specific GO term. This study, which represents the first documentation of stage-specific gene expression profiling during early aspergillosis was analysed in this manner to probe the activity of certain gene sets of interest and provide an indication of concordance with previous studies.

McDonagh *et. al.* (2008) studied transcription during adaptation of a clinical isolate Af293 to the murine host niche, finding a total of 2180 genes (22.6% of the *A. fumigatus* genome) as differentially expressed, having a fold-change in $\log_2$ intensity ratio of 2 or greater. Among these, 1281 were up-regulated and 897 were down-regulated, relative to developmentally-matched, laboratory-culterd germlings. In contrast to the present study which analysed ATCC46645 adaptation to the murine niche across a time course composed of three time points, the McDonagh study considered only one (i.e. 14 hours post-infection) Another difference between the studies relates to the reference samples used for the hybridations whereby McDonagh used lab cultured germlings (YPD) as opposed to dormant conidia (this study).

Fig. 4.8 illustrates commonalities between cohorts of differentially expressed genes during initiation of murine infection by *A. fumigatus* ATCC46645 and Af293 strains. Among a total of 1364 and 1136 genes up-regulated, respectively, in the ATCC46645 time course and in the Af293 study, the overlap consists of 504 genes (Fig. 4.8A) having phase-specific variations as indicated (A.1, A.2, A.3). Among a total of 1299 and 726 genes down-regulated, respectively, in the ATCC46645 time course and in the Af293 study, the overlap consists of 276 genes (Fig. 4.8B) having phase-specific variations as indicated (B.1, B.2, B.3).

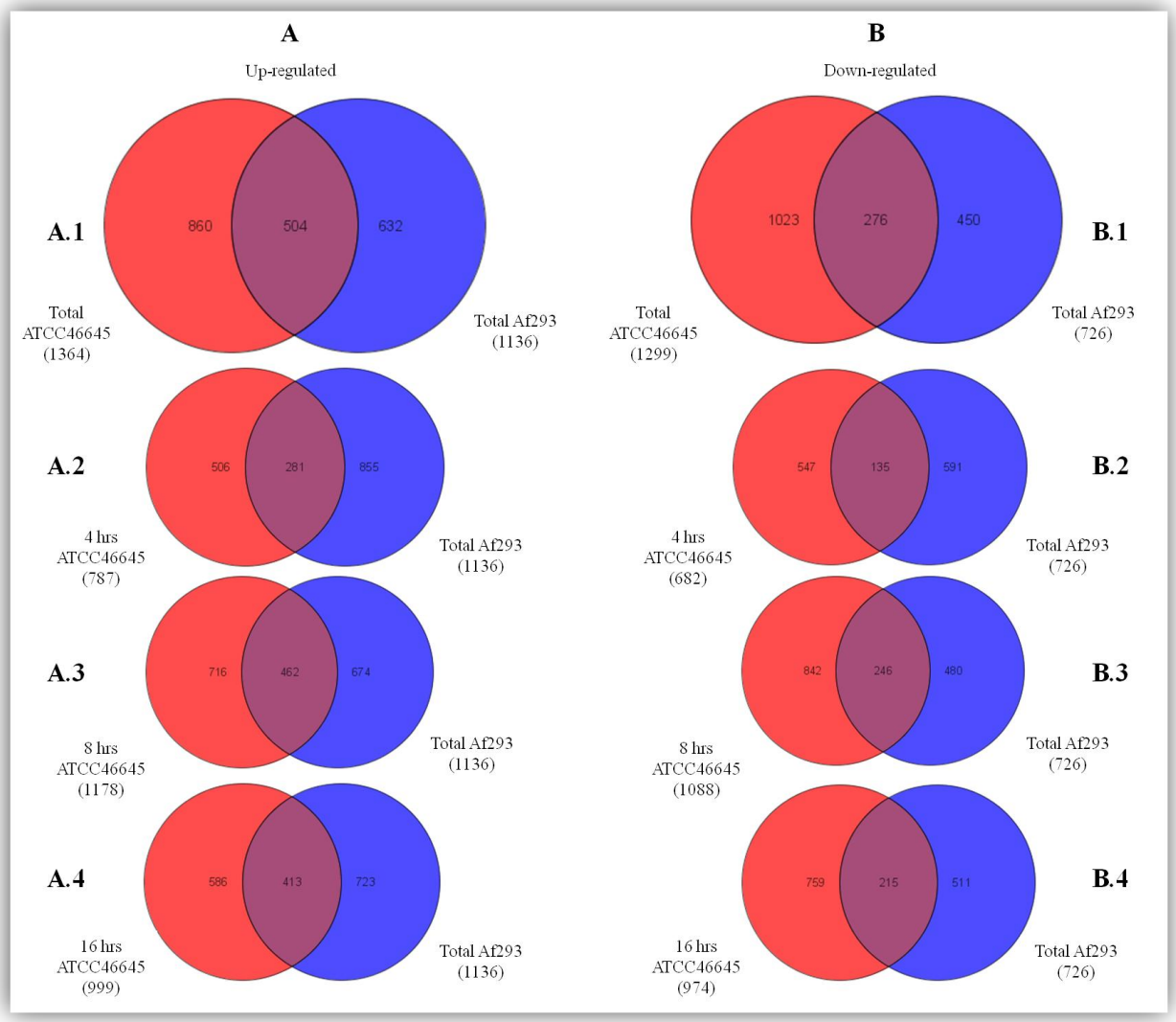


Fig. 4.8: Venn diagrams illustrating commonalities between cohorts of differentially expressed genes during initiation of murine infection by *A. fumigatus* ATCC46645 and Af293 strains. Total up-regulated genes (n=1136) for the Af293 strain (McDonagh *et. al.* 2009) (blue) compared to the up-regulated genes for the ATCC45546 (red) strain (A=total up-regulated, A.1=4 hours, A.2=8 hours and A.3=16 hours). Total down-regulated genes (n=726) for the Af293 strain (McDonagh *et. al.* 2009) (blue) compared to the down-regulated genes for the ATCC45546 (red) strain (A=total down-regulated, A.1=4 hours, A.2=8 hours and A.3=16 hours). Analysis performed using Genespring GX 11.02.

The previous Af293 analysis (McDonagh *et al.*, 2008a) had revealed that many up-regulated genes required for *A. fumigatus* adaptation to the murine niche and were located in contiguous chromosome locations (ICs). We therefore asked whether these gene clusters were also significant during initiation of murine infection by ATCC46645. This was addressed by STEM clustering analysis of the differentially expressed genes in the ATCC46645 time course during initiation of murine infection, ordered on the basis of the previously identified (McDonagh *et al.*, 2008a) Af293 infection clusters (Fig. 4.9) (the unabridged output of this

analysis is reported in Appendix D). Model profiles remain coloured according to significance in the initial analysis, however, red traces now correspond to genes in the dataset specifically annotated as residing in infection clusters.

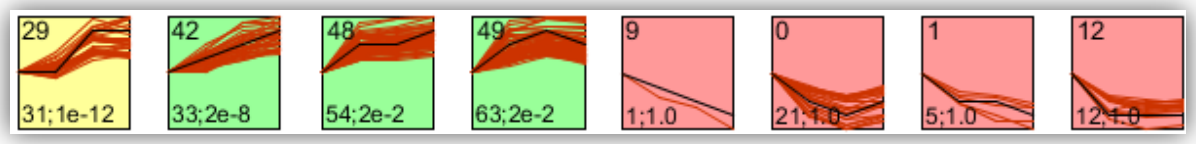


Fig. 4.9: Selection of STEM clustering analyses of the differentially expressed genes in the ATCC46645 time course during initiation of murine infection, ordered on the basis of containing Af293 infection cluster genes (McDonagh *et al.*, 2008a). Values at the bottom of each profile indicate the number of genes (in this case genes previously identified in the Af293 infection clusters) and the significance of the intersect size, based upon the hypergeometric distribution of dataset genes in the respective model profiles.

McDonagh *et al.*, 2008a also reported that 29% of the transcripts having increased abundance during initiation of murine infection, relative to a laboratory culture, are localised in the subtelomeric region of the chromosomes. In contrast, only 11% of the down-regulated genes are localised within 300 kb from the telomeres. We therefore asked how many subtelomeric genes were differentially expressed in the ATCC46645 time course (Fig. 4.10), (the unabridged STEM output is reported in Appendix D). In this instance red gene profiles correspond to genes having subtelomerics locations.

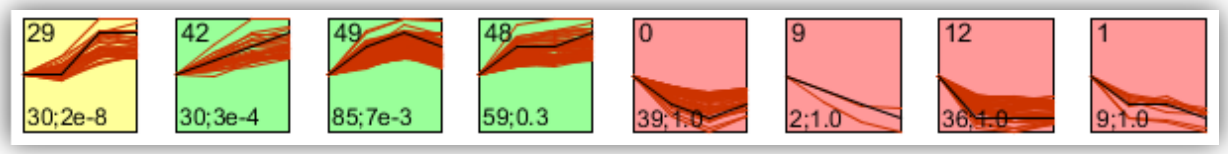


Fig. 4.10: STEM clustering analysis of the differentially expressed genes in the ATCC46645 time course during initiation of murine infection ordered on the basis of the subtelomeric location (McDonagh *et al.*, 2008a). The two values at the bottom of each profile indicate how many specific genes (in this case genes with subtelomeric location) are present in the profile and the significance of the intersect size, based upon the hypergeometric distribution of dataset genes in the respective model profiles.

Our *A. fumigatus* annotation was also extended for genes involved in the production of secondary metabolites (based on Perrin *et al.*, 2007) and STEM model profiles were also ordered depending upon the enrichment of this category. STEM clustering analysis of the secondary metabolite genes in the ATCC46645 time course are represented in Fig. 4.11 (the unabridged output is reported in Appendix D).



Fig. 4.11: STEM clustering analysis of the differentially expressed genes in the ATCC46645 time course during initiation of murine infection ordered on the basis of the involvement on secondary metabolite production (Perrin *et al.*, 2007). The two values at the bottom of each profile indicate how many specific genes (in this case genes involved on secondary metabolite production) and the significance of the intersect size, based upon the hypergeometric distribution of dataset genes in the respective model profiles.

To elucidate the transcriptional response to alkaline conditions, a microarray study performed by our research group has recently delineated the temporal response of *A. fumigatus* to an alkaline shift *in vitro* and compared it to that induced by high concentration of Ca^{2+} (Loss *et al.*, unpublished). Specifically, this study investigated the transcriptional profile of *A. fumigatus* mycelia grown for 14 hours in AMM pH 5.0 and subsequently shifted to pH 8.0 for 60 minutes. Samples were taken for RNA extraction after 5, 15, 30, 45 and 60 minutes, the common reference being a sample shifted to pH 5.0 media. According to the resultant dataset, Fig. 4.12 illustrates the representation of alkaline-responsive *A. fumigatus* genes among those in the ATCC46645 host-responsive transcriptome. Among a total of 1364 and 433 genes up-regulated, respectively, in the murine time course and in the *in vitro* study, the overlap consists of 127 genes (Fig. 4.12A) having phase-specific variations (A.1, A.2, A.3) as indicated. Among a total of 1299 and 141 genes down-regulated, respectively, in the murine time course and in the *in vitro* study, the overlap consists of 30 genes (Fig. 4.12B) with phase-specific variations as shown (B.1, B.2, B.3).

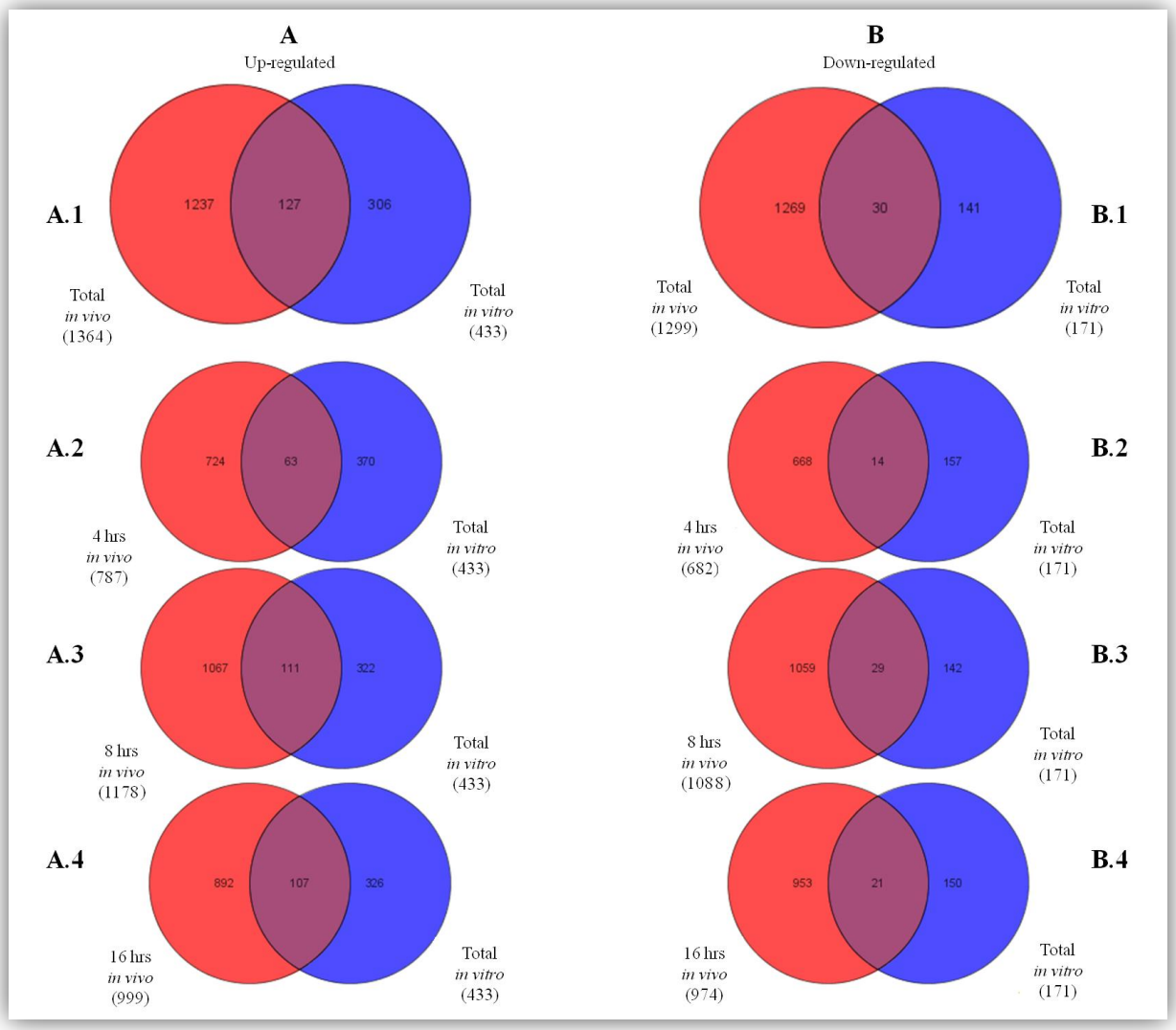


Fig. 4.12: Venn diagrams illustrating the proportions of alkaline-responsive *A. fumigatus* genes during initiation of murine infection by ATCC46645. Total up-regulated genes (n=433) following the *in vitro* shift to alkaline pH (blue) are compared to the up-regulated genes for the ATCC45546 (red) strain (A=total up-regulated, A.1=4 hours, A.2=8 hours and A.3=16 hours). Total down-regulated genes (n=171) following the *in vitro* shift to alkaline pH (blue) are compared to the down-regulated genes for the ATCC45546 (red) strain (B=total down-regulated, B.1=4 hours, B.2=8 hours and B.3=16 hours). Analysis performed using Genespring GX 11.02.

STEM clustering analyses of alkaline-responsive genes, also differentially regulated in the ATCC46645 time course during initiation of murine infection are shown in Fig. 4.13 and Fig. 4.14 (unabridged output is reported in Appendix D). As illustrated in Fig. 4.13, only model profiles containing up-regulated (as opposed to down-regulated) genes across the ATCC46645 time course (29, 48 and 42) are significantly enriched in alkaline-responsive genes. The comparison with down-regulated *in vitro* pH response genes (Fig. 4.14) revealed several genes in differential behaviour between the murine and *in vitro* niches including five

genes in cluster 29, which are instead up-regulated *in vivo*. Interestingly, among these genes are two ORFs involved in cell wall organisation (Afu3g08110 encoding a putative cell wall protein and Afu2g14490 encoding an endoglucanase). Additionally, profile 45 revealed the co-ordinate behaviour of three genes in the ATCC46645 time course experiment, which are up-regulated *in vivo* but down-regulated *in vitro*. Two of them (Afu4g06620 and Afu1g07380) have been linked to secondary metabolite production.



Fig. 4.13: STEM clustering analysis of the differentially expressed genes in the ATCC46645 time course during initiation of murine infection ordered on the basis of containing genes also up-regulated in response to an alkaline pH shift (Loss, unpublished). The two values at the bottom of each profile indicate how many specific genes (in this case up-regulated genes in response to an alkaline pH shift) are present in the profile and the significance of the intersect size, based upon the hypergeometric distribution of dataset genes in the respective model profiles.

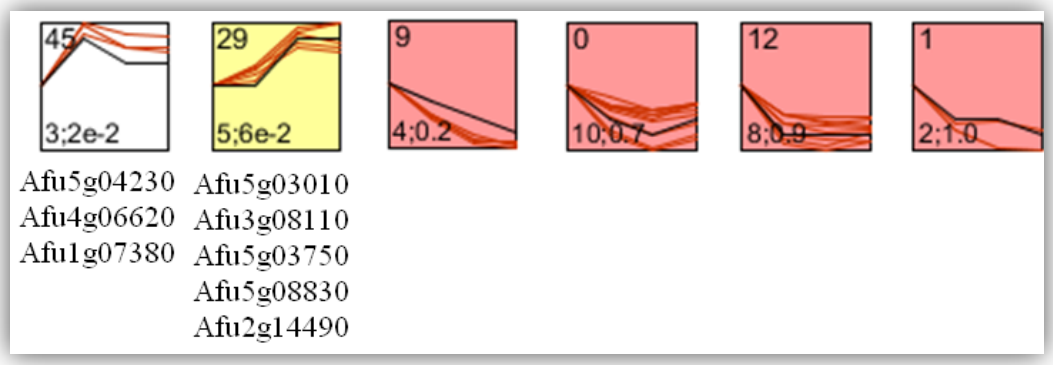


Fig. 4.14: STEM clustering analysis of the differentially expressed genes in the ATCC46645 time course during initiation of murine infection ordered on the basis of the *in vitro* down-regulated genes in response to an alkaline pH shift (Loss, unpublished). Values at the bottom of each profile indicate how many genes (in this case down-regulated genes in response to an alkaline pH shift) are present in the profile and the significance of the intersect size, based upon the hypergeometric distribution of dataset genes in the respective model profiles.

4.3.3 *A. fumigatus* ATCC46645 Δ*pacC* mutant transcriptional profile during initiation of murine infection

The *A. fumigatus* ATCC46645 Δ*pacC* transcriptional profile during initiation of murine infection was performed by hybridising doubly amplified fungal RNA, extracted from

BALFs harvested at each of 3 time points (4, 8 and 16 hrs) post-infection against a common reference of RNA extracted from *in vitro*-cultured dormant ATCC46645 Δ*pacC* spores, as shown in Fig. 4.15.

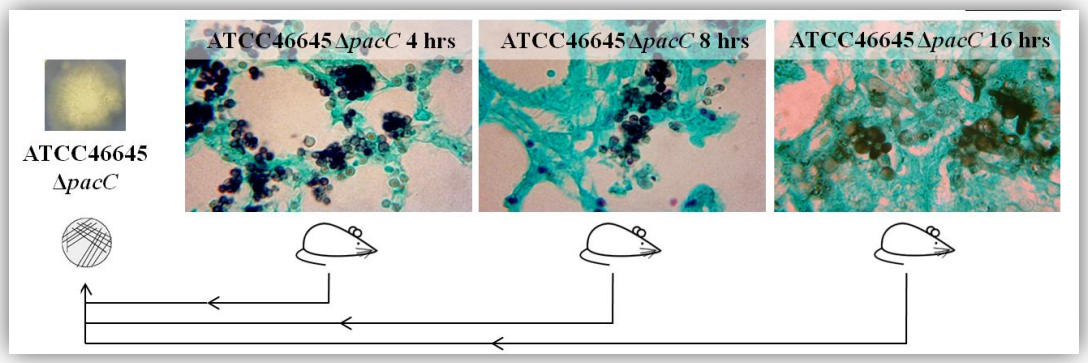


Fig. 4.15: Schematic representation of hybridisations performed to analyse the *A. fumigatus* ATCC46645 Δ*pacC* transcriptome during initiation of murine infection. Characterisation of the *A. fumigatus* ATCC46645 Δ*pacC* transcriptional profile during initiation of murine infection was performed by comparing transcript abundance at three time points (4, 8 and 16 hrs) to that of a common reference of dormant ATCC46645 Δ*pacC* spores.

Fig. 4.16, 4.17 and 4.18 show MA and box plots of the datasets for each of the three time points studied, both before and after normalisation. The MA plots for each time point (A) show the distribution of the data before (UN-NORMALISED) and after the LOWESS normalisation (NORMALISED), therefore depicting the dataset adjustments implemented by normalisation. In MA plots the $\log_2$ ratio between red and green channels (Y-axis) is plotted against the sum of red and green channels (X-axis). Normalisation adjusts for the higher measured spot intensities associated with the green dye (Cy3). Box plots (B) also show dataset $\log_2$ ratio distributions for each time point before (UN-NORMALISED) and after LOWESS normalisation (NORMALISED) but on a slide specific basis. After normalisation the medians of the blocks are all equal to zero and the standard deviation is regularised.

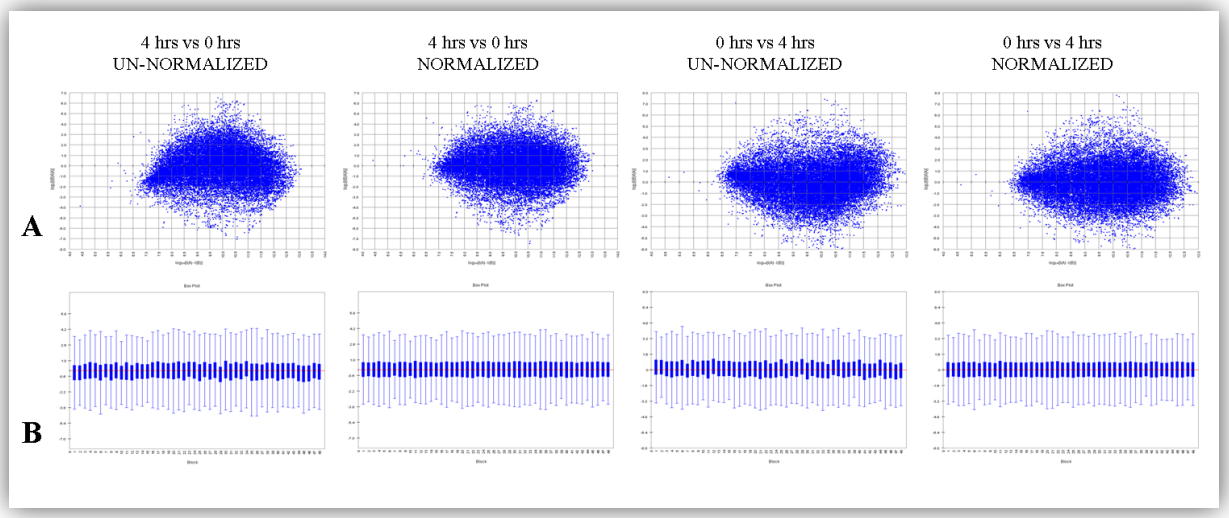


Fig. 4.16: Data normalisation plot for the ATCC46645 Δ*pacC* 4 hrs *in vivo* versus dormant spores analysis. Pairwise MA (A) and box plots (B) for the 4 hour time point of ATCC46645 Δ*pacC* (mouse) versus ATCC46645 Δ*pacC* (dormant spores) RNA. Datasets plotted before (UN-NORMALISED) and after (NORMALISED) LOWESS normalisation are shown.

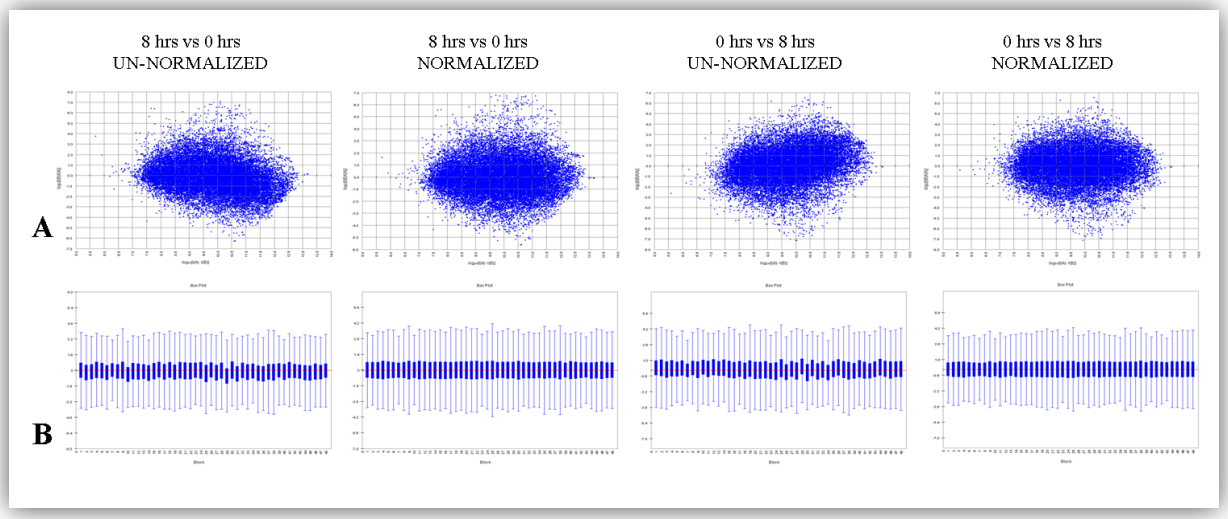


Fig. 4.17: Data normalisation plot for the ATCC46645 Δ*pacC* 8 hrs *in vivo* versus dormant spores analysis. Pairwise MA (A) and box plots (B) for the 8 hour time point of ATCC46645 Δ*pacC* (mouse) versus ATCC46645 Δ*pacC* (dormant spores) RNA. Datasets plotted before (UN-NORMALISED) and after (NORMALISED) LOWESS normalisation are shown.

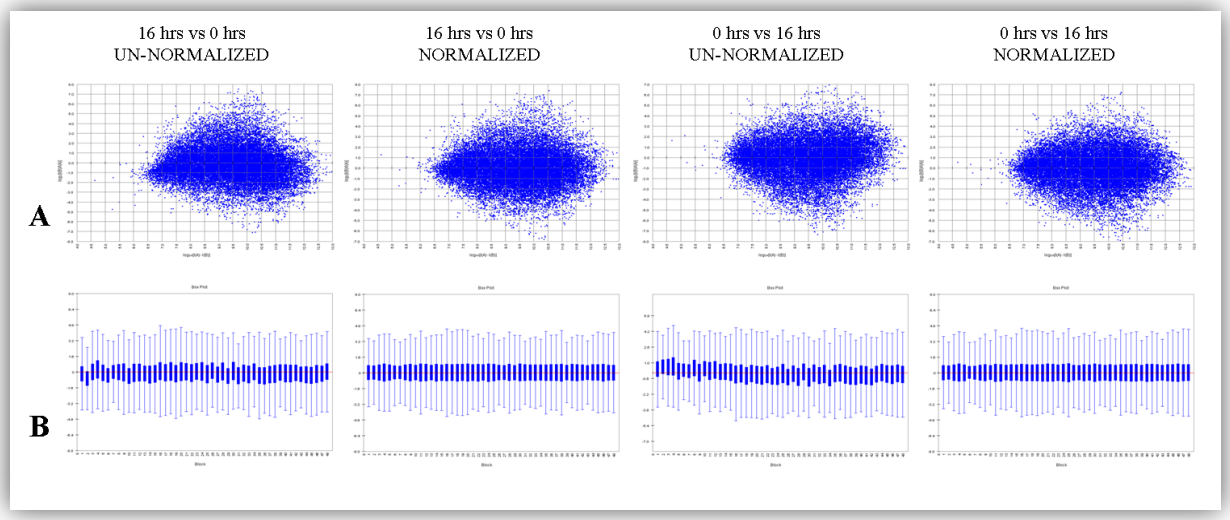


Fig. 4.18: Data normalisation plot for the ATCC46645 Δ*pacC* 16 hrs *in vivo* versus dormant spores analysis. Pairwise MA (A) and box plots (B) for the 16 hour timepoint of ATCC46645 Δ*pacC* (mouse) versus ATCC46645 Δ*pacC* (dormant spores) RNA. Datasets plotted before (UN-NORMALISED) and after (NORMALISED) LOWESS normalisation are shown.

The summary statistics for the ATCC46645 Δ*pacC* time course dataset (Table 4.8) report that among a total of 8243 genes represented on the slides, 8222, 7993 and 8200, returned signal, for the 4, 8 and 16 hrs time points respectively.

	4 hrs vs 0 hrs	8 hrs vs 0 hrs	16 hrs vs 0 hrs
Observations	8222	7993	8200
Missing observations	21	250	43
Minimum value	-7.28	-5.74	-6.99
Maximum value	5.85	7.05	6.94
Mean	0.0392	0.0162	0.0333
Median	0.06	-0.05	-0.04
Standard deviation	1.4328	1.5441	1.5858
Outliers	175	160	182

Table 4.8: Summary statistics for the ATCC46645 Δ*pacC* time course during initiation of murine infection.

The analysis of temporal gene expression for the ATCC46645 Δ*pacC* strain was conducted in Genespring GX 11.02. Normalised $\log_2$ expression ratios were filtered on expression level and differentially regulated transcripts were defined as having average $\log_2$ (Cy5/Cy3) ratios less or greater than the arbitrary thresholds of ±2. The numbers and

classifications of differentially expressed genes are shown in Table 4.9. Among a total of 2515 (25.3% of *A. fumigatus* genome, Nierman *et al.*, 2005) differentially expressed genes across the entire time course, 1198 were up-regulated and 1317 were down-regulated in at least in one time point of the dataset. The complete lists of differentially expressed genes are attached in the Supplementary Data CD, as listed in Appendix D.

	Up-regulated	Down-regulated	Differentially expressed
TOTAL	1198	1317	2515
4 hrs	788	741	1529
8 hrs	788	654	1442
16 hrs	969	874	1843

Table 4.9: Number of differentially expressed genes in the ATCC46645 Δ*pacC* time course during initiation of murine infection.

The temporal basis of gene regulation in the ATCC46645 Δ*pacC* time course experiment is simply depicted in a 3-way Venn diagram in Fig. 4.19 for both up-regulated (Fig. 4.19A) and down-regulated (Fig. 4.19B) genes. In addition, the complex pattern of differentially expressed genes in the ATCC46645 Δ*pacC* time course is shown in a detailed heat map attached in the Supplementary Data CD, as listed in Appendix D.

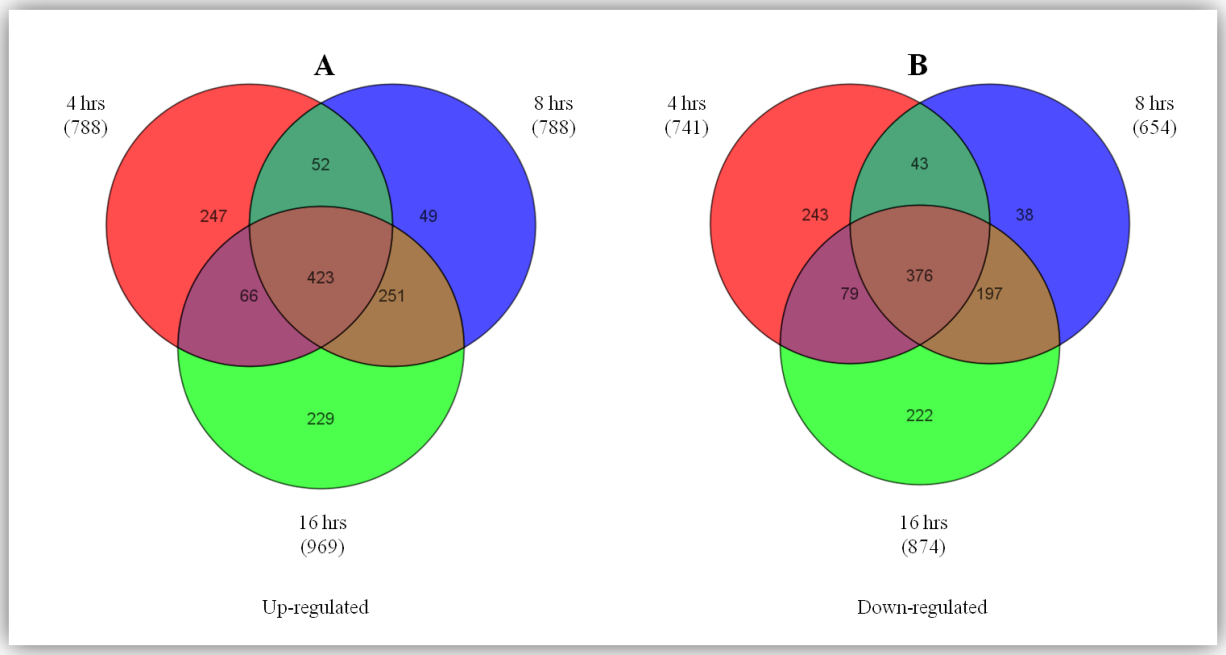


Fig. 4.19: Three-way Venn diagrams depicting temporal aspects of differential gene expression in the ATCC46645 Δ*pacC* time course experiment during initiation of murine infection. Up-regulated (A) and down-regulated genes (B) have been identified using a fold change cut off of ±2 on a $\log_2$ scale. Analysis performed using Genespring GX 11.02.

Among a total of 1198 up-regulated genes (12.1% of *A. fumigatus* genome), 423 were similarly differentially regulated across all 3 time points. Among these, one hundred up-regulated genes, having the greatest fold change relative to dormant spores, are reported in Table 4.10. As observed for the relative parental strain, across the ATCC46645 Δ*pacC* time course experiment, several genes involved in the uptake, mobilisation and utilisation of crucial ion and nutrients are up-regulated. At least three genes are involved in siderophore biosynthesis for the uptake of extracellular iron (Afu3g03440, Afu3g03430 and Afu7g04730) and were also identified as up-regulated in the ATCC46645 time course (Table 4.3). Likewise, several sugar permeases are included (Afu3g3700, Afu6g04270, Afu4g00800 and Afu2g14590), but few other transporters are up-regulated, and notable omissions, relative to the parental strain include Afu5g02940 and Afu1g15300 for choline and Afu4g00150 for maltose transport. Several up-regulated genes represent functions involved cell wall biogenesis and organisation, Afu7g05370, Afu8g05610, Afu1g16250 and Afu4g10150, the two latter of were also identified as up-regulated in the ATCC46645 time course (Table 4.3). To aid the evaluation of phase-specific up-regulated genes across the ACTT46645 Δ*pacC* time course, Tables AD.2.2-AD.2.4 in Appendix D list the thirty ORFs with the greatest $\log_2$ ratios for the up-regulated genes at 4, 8 and 16 hrs post-infection respectively.

Of a total of 1317 down-regulated genes (13.3% of *A. fumigatus* genome), 376 were similarly differentially regulated at all 3 time points. Among these, one hundred genes having the greatest fold changes are reported in Table 4.11. Among the down-regulated genes, there are several ORFs are involved in the regulation of transcription (Afu5g02880 and Afu2g15680), however the most striking difference noted between the Δ*pacC* and parental profiles the abundance of ORFs putatively involved in transposition (Afu4g00820, Afu8g01040, Afu4g14870, Afu2g18080, Afu6g09470, Afu8g00310, Afu6g00780, Afu6g14660, Afu8g06290, Afu3g15370, Afu3g09430) in the Δ*pacC* profile. All of the aforementioned genes were already highly down-regulated at early stages of infection (4 hrs post-infection). To aid the evaluation of phase-specific down-regulated genes across the ACTT46645 Δ*pacC* time course, Tables AD.2.6-AD.2.8 in Appendix D list the thirty ORFs having lowest $\log_2$ ratios for 4, 8 and 16 hrs post-infection respectively.

According to expanded *A. fumigatus* annotation utilised for analysis of the ATCC46645 analyses outlined earlier in this chapter, GO analysis of the differentially expressed genes in the ATCC46645 Δ*pacC* time course (fold change cut off of ±2 on a $\log_2$ scale) was performed using Genespring GX 11.02. Table 4.12 and Table 4.13 show the GO terms, which satisfy an imposed p-value cut-off of 0.05, respectively, among the up-regulated and down-regulated genes, with respect to their occurrence in the *A. fumigatus* genome. Aiming to identify functional categories arsing in a stage-specific manner GO analyses on the total set of differentially expressed genes and also on the single time points (4, 8 and 16 hrs) of the analysis are reported. Significant GO terms among the up-regulated genes in the ATCC46645 Δ*pacC* time course included several members correlated with transport, uptake and mobilisation of crucial nutrients, especially glucose and fructose, and with lipid metabolism. Significant GO terms among the down-regulated genes in the ATCC46645 Δ*pacC* time course include several members involved in transcription and its regulation.

Table 4.10: 100 ORFs having the highest log_2 values among up-regulated genes across the 3 time points (4, 8 and 16 hrs) of the ATCC46645.

ORFs	T4 vs T0	T8 vs T0	T16 vs T0	Annotation	Functional classification
Afu3g03440	5.85	6.29	6.55	MFS family siderophore transporter, putative	siderophore-iron transport///siderophore-iron (ferrioxamine) uptake transmembrane transporter activity///integral to membrane///cellular iron ion homeostasis
Afu7g06380	5.81	7.05	6.43	Maltase	cellular component unknown///alpha-glucosidase activity///maltose catabolic process
Afu7g04730	5.74	6.46	6.78	siderochrome-iron transporter, putative	endosome///siderophore-iron transport///cytoplasmic membrane-bounded vesicle///siderophore-iron (ferrioxamine) uptake transmembrane transporter activity///cellular iron ion homeostasis
Afu1g17180	5.7	6.51	6.73	pyridine nucleotide-disulphide oxidoreductase, putative	electron carrier activity///nucleus///mitochondrion///DNA fragmentation involved in apoptosis
Afu6g00260	5.59	4.13	5.19	phosphatidylserine decarboxylase family protein	phosphatidylserine decarboxylase activity///phosphatidylserine catabolic process
Afu3g03390	5.34	5.37	5.87	siderophore biosynthesis lipase/esterase, putative	
Afu1g14550	5.29	6.65	6.03	Mn superoxide dismutase MnSOD	manganese superoxide dismutase activity///oxygen and reactive oxygen species metabolic process///mitochondrial matrix///mitochondrion
Afu1g10930	5.28	3.26	2.04	ammonium transporter	pseudohyphal growth///plasma membrane///ammonium transport///ammonium transmembrane transporter activity
Afu3g03700	5.21	6.69	6.7	Sugar transporter subfamily	mannose transmembrane transporter activity///hexose transport///fructose transmembrane transporter activity///plasma membrane///glucose transmembrane transporter activity
Afu3g03410	5.2	6.21	6.25	enoyl-CoA hydratase/isomerise family protein	
Afu6g00630	5.07	5.49	6.15	MFS transporter, putative	transporter activity///transport///integral to membrane
Afu3g02940	5.04	5.54	5.48	allergen, putative	
Afu5g00290	5.04	4.97	5.13	C6 transcription factor, putative	
Afu5g13300	5	6.42	6.94	aspartic endopeptidase Pep1	protein catabolic process///aspartic-type endopeptidase activity///extracellular region///pathogenesis
Afu5g00300	4.94	4.59	4.18	zinc-binding oxidoreductase, putative	oxidoreductase activity///cellular component unknown///zinc ion binding///metabolic process
Afu4g10150	4.91	6.35	5.88	alpha-glucosidase	alpha-glucosidase activity///fungal-type cell wall biogenesis///endoplasmic reticulum
Afu3g03400	4.88	5.58	5.49	siderophore biosynthesis acetylase	

				AceI, putative	
Afu4g00800	4.81	4.53	4.35	MFS monosaccharide transporter, putative	response to glucose stimulus///plasma membrane///glucose transmembrane transporter activity///signal transduction///glucose binding///receptor activity
Afu5g09400	4.78	4.97	4.73	carbonyl reductase, putative	oxidoreductase activity///metabolic process
Afu3g03660	4.77	2.49	3.8	esterase superfamily protein	hydrolase activity, acting on ester bonds
Afu1g12690	4.75	4.03	4.06	ABC multidrug transporter Mdr4	response to drug///xenobiotic-transporting ATPase activity///ABC-type efflux porter activity///multidrug transport///integral to plasma membrane///multidrug efflux pump activity
Afu7g04910	4.74	6.5	5.6	phosphatidylglycerol specific phospholipase C, putative	
Afu1g03570	4.61	5.22	5.61	acid phosphatase PHOa	
Afu2g17320	4.59	5.29	5.74	conserved hypothetical protein	
Afu1g11250	4.5	3.8	4.37	amidohydrolase, putative	proteolysis///carboxypeptidase activity
Afu6g12670	4.46	3.37	3.74	beta-alanine synthase, putative	
Afu1g13500	4.44	3.73	2.11	transketolase TktA	cytoplasm///pentose-phosphate shunt///transketolase activity
Afu2g07680	4.44	4.31	4.65	L-ornithine N5-oxygenase SidA	pathogenesis
Afu3g03420	4.42	6.45	6.07	hypothetical protein	
Afu6g04270	4.39	2.49	2.59	fructose symporter	membrane///myo-inositol transport///myo-inositol transmembrane transporter activity
Afu3g03430	4.32	5.73	5.71	ABC multidrug transporter SitT, putative	ATP-binding cassette (ABC) transporter activity///ATP binding///transport
Afu1g12920	4.32	3.23	3.24	glycogen phosphorylase 1; possible glycogen phosphorylase	cytoplasm///glycogen phosphorylase activity///glycogen catabolic process
Afu7g05150	4.25	3.67	4.97	hypothetical protein	
Afu5g11240	4.23	3.84	4.06	oxidoreductase, short chain dehydrogenase/reductase family	L-serine metabolic process///cytoplasm///nucleus///"oxidoreductase activity, acting on the aldehyde or oxo group of donors, NAD or NADP as acceptor"
Afu3g06530	4.2	3.4	3.43	ATP sulphurylase	cytoplasm///sulfate assimilation///methionine metabolic process///sulfate adenylyltransferase (ATP) activity
Afu6g00640	4.19	4.5	5.41	integral membrane protein	
Afu7g06390	4.16	5.05	5.54	maltose permease	alpha-glucoside:hydrogen symporter activity///membrane fraction///alpha-glucoside transport
Afu3g00900	4.13	4.86	4.97	alpha-amylase AmyA	
Afu1g17170	4.13	4.7	5.17	alpha-ketoglutarate-dependent taurine dioxygenase	cellular component unknown///sulfur metabolic process///sulfonate dioxygenase activity///"oxidoreductase activity, acting on paired donors, with incorporation or reduction of molecular

					oxygen, 2-oxoglutarate as one donor, and incorporation of one atom each of oxygen into both donors"
Afu3g00740	4.12	3.88	4.14	2-dehydropantoate 2-reductase, putative	2-dehydropantoate 2-reductase activity///cytoplasm///nucleus///FAD binding
Afu1g10910	4.09	3.87	3.92	tubulin beta, putative	kinetochore microtubule///spindle pole body///cytoplasmic microtubule///nuclear migration during conjugation with cellular fusion///mitotic sister chromatid segregation///nuclear microtubule///polar microtubule///homologous chromosome segregation///structural constituent of cytoskeleton
Afu4g11550	4.05	3.21	2.51	hypothetical protein	
Afu6g10660	4.05	2.85	2.64	ATP-citrat-lyase	
Afu1g17190	4.02	4.52	4.4	long-chain-fatty-acid-CoA ligase, putative	peroxisomal membrane///peroxisomal matrix///cytoplasm///AMP binding
Afu1g11480	4.02	5.08	4.81	hypothetical protein	
Afu4g08710	4.02	3.93	4.39	short chain dehydrogenase, putative	fatty acid catabolic process
Afu2g02950	4.02	3.28	3.01	aldehyde reductase, putative	cellular component unknown///aldo-keto reductase activity///cellular aldehyde metabolic process
Afu1g07130	4.02	3.55	3.53	dienelactone hydrolase family protein	aromatic compound catabolic process///cytoplasm///carboxymethylene butenolidase activity
Afu4g07690	4.01	2.73	2.58	phosphoribosylaminoimidazolecarboxamide formyltransferase/IMP cyclohydrolase	'de novo' IMP biosynthetic process///phosphoribosylaminoimidazole carboxamide formyltransferase activity///cytosol///IMP cyclohydrolase activity
Afu3g02280	4	4.74	4.77	alpha,alpha-trehalose glucohydrolase, putative	fungal-type vacuole///trehalose catabolic process///"alpha,alpha-trehalase activity"///response to stress
Afu7g05450	3.96	5.03	5.08	SUN domain protein (Uth1), putative	autophagic cell death///cell wall organisation///barrier septum formation///fungal-type cell wall///response to oxidative stress///beta-glucosidase activity///mitochondrion organisation///mitochondrial outer membrane///apoptosis
Afu5g12480	3.95	3.5	3.74	short chain dehydrogenase/reductase family	
Afu5g02940	3.94	3.71	2.71	choline transport protein Ctr, putative	plasma membrane///choline transport///choline transmembrane transporter activity
Afu2g02590	3.94	2.67	2.07	aspartyl-tRNA synthetase	translation///cytoplasm///aspartate-tRNA ligase activity
Afu4g13900	3.93	2.78	2.37	MFS transporter, putative	nicotinamide mononucleotide transport///nicotinamide mononucleotide permease activity///integral to plasma membrane
Afu7g06810	3.93	5.21	5.51	L-amino acid oxidase LaoA, putative	
Afu4g00150	3.93	4.5	4.84	MFS maltose transporter, putative	carbohydrate transmembrane transporter activity///carbohydrate transport///plasma membrane///maltose porter activity

Afu3g08290	3.9	2.73	2.24	aspartyl aminopeptidase	cytoplasm///biological process unknown///molecular function unknown
Afu1g17700	3.89	4.32	4.52	short chain dehydrogenase, putative	oxidoreductase activity///metabolic process
Afu1g16250	3.87	5.94	5.07	alpha-glucosidase B	alpha-glucosidase activity///fungal-type cell wall biogenesis///endoplasmic reticulum
Afu6g11340	3.86	3	3.75	peroxisomal AMP binding enzyme, putative	peroxisomal membrane///peroxisomal matrix///cytoplasm///biological process unknown///AMP binding
Afu1g02550	3.85	3.76	3.39	tubulin alpha-1 subunit	kinetochore microtubule///spindle pole body///cytoplasmic microtubule///nuclear migration (sensu Saccharomyces)///nuclear migration during conjugation with cellular fusion///mitotic sister chromatid segregation///nuclear microtubule///polar microtubule///homologous chromosome segregation///structural constituent of cytoskeleton
Afu3g03670	3.85	3.34	4.08	ABC multidrug transporter, putative	ATP-binding cassette (ABC) transporter activity///ATP binding///transport
Afu2g11540	3.83	2.18	2.48	ketoreductase, putative	endoplasmic reticulum///ketoreductase activity///fatty acid elongation///integral to membrane
Afu3g03860	3.82	3.43	4.91	3-hydroxyacyl-CoA dehydrogenase, putative	
Afu6g07490	3.81	2.55	2.69	WD repeat protein	cytoplasm///biological process unknown///molecular function unknown
Afu8g01710	3.8	4.74	5.37	antigenic thaumatin domain protein, putative	
Afu1g02880	3.8	2.84	3.5	Phosphotransferase enzyme family domain protein	transferase activity, transferring phosphorus-containing groups
Afu1g17200	3.76	4.16	4.37	nonribosomal peptide synthase, putative	nonribosomal peptide biosynthetic process///catalytic activity///amino acid adenylylation by nonribosomal peptide synthase
Afu7g05550	3.76	3.81	4.43	sugar transporter family protein	lactate transmembrane transporter activity///lactate transport///plasma membrane
Afu2g03830	3.74	3.92	4.19	allergen Asp F4	pathogenesis
Afu6g14440	3.73	5.03	5.13	MFS monosaccharide transporter, putative	response to glucose stimulus///plasma membrane///glucose transmembrane transporter activity///signal transduction///glucose binding///receptor activity
Afu2g08300	3.7	3.07	2.66	DnaJ domain protein, putative	endoplasmic reticulum lumen///co-chaperone activity///protein folding
Afu5g09140	3.7	3.91	3.71	amidase, putative	aerobic respiration///amidase activity///mitochondrion
Afu5g04250	3.67	3.38	2.73	homocysteine synthase, putative	cysteine synthase activity///O-acetylhomoserine aminocarboxypropyltransferase activity///cytoplasm///methionine metabolic process
Afu3g11640	3.66	3.56	4.17	homoserine dehydrogenase	homoserine biosynthetic process///cytoplasm///nucleus///methionine metabolic process///threonine

					metabolic process///homoserine dehydrogenase activity
Afu3g03820	3.66	4.09	5.47	MFS transporter, putative	nicotinamide mononucleotide transport///nicotinamide mononucleotide permease activity///integral to plasma membrane
Afu1g10020	3.65	4.68	3.93	reverse transcriptase, RNaseH	
Afu8g01580	3.63	4.33	4.68	aminotransferase, classes I and II family	arylformamidase activity///cytoplasm///mitochondrion///NAD biosynthetic process
Afu6g06770	3.62	2.67	2.26	enolase	phosphopyruvate hydratase complex///cytoplasm///pathogenesis///phosphopyruvate hydratase activity///gluconeogenesis///glycolysis
Afu5g02850	3.62	4.17	4.49	conserved hypothetical protein	
Afu5g13170	3.61	2.42	2.6	MATE efflux family protein subfamily, putative	cellular component unknown///biological process unknown///molecular function unknown
Afu3g00680	3.6	3.18	3.39	copper amine oxidase	
Afu1g03630	3.6	5.62	5.83	GPI anchored serine-threonine rich protein	
Afu5g10320	3.59	2.33	3.94	toxin biosynthesis protein (GliH), putative	
Afu5g10020	3.59	3.7	4.82	sensor histidine kinase/response regulator, putative	
Afu1g15300	3.58	3.3	3.17	choline transport protein, putative	plasma membrane///choline transport///choline transmembrane transporter activity
Afu2g09810	3.58	3.56	2.81	mandelate racemase/muconate lactonizing enzyme family protein	
Afu5g03550	3.55	2.57	2.87	plasma membrane H(+)ATPase, putative	hydrogen-exporting ATPase activity, phosphorylative mechanism///regulation of pH///plasma membrane///fungal-type vacuole///endoplasmic reticulum///proton transport
Afu2g14590	3.54	2.54	2.22	MFS monosaccharide transporter, putative	response to glucose stimulus///plasma membrane///glucose transmembrane transporter activity///signal transduction///glucose binding///receptor activity
Afu6g00620	3.53	4.82	4.95	GPI anchored hypothetical protein	
Afu6g02600	3.53	2.93	3.09	phosphoglycerate mutase family protein	cytoplasm///nucleus///biological process unknown///molecular function unknown
Afu7g05370	3.52	2.83	2.35	septin AspB	cell wall organisation///prospore membrane///axial cellular bud site selection///phosphatidylinositol binding///cytokinesis///structural constituent of cytoskeleton///mating projection///ascospore wall///cell morphogenesis
Afu1g03550	3.52	2.75	2.52	mitochondrial dihydroxy acid dehydratase, putative	dihydroxy-acid dehydratase activity///branched chain family amino acid biosynthetic process///mitochondrion
Afu4g13580	3.51	3.91	3.44	gamma-	

				glutamyltranspeptidase	
Afu6g03060	3.5	4.2	4.15	monosaccharide transporter	response to glucose stimulus///plasma membrane///glucose transmembrane transporter activity///signal transduction///glucose binding///receptor activity
Afu8g05610	3.5	4.71	4.51	cell wall glucanase (Scw11), putative	hydrolase activity, hydrolyzing O-glycosyl compounds///cellular glucan metabolic process///fungal-type cell wall///"cytokinesis, completion of separation"
Afu5g11850	3.49	3.48	3.83	mitochondrial carrier protein (Pet8), putative	S-adenosylmethionine transmembrane transporter activity///mitochondrial inner membrane///S-adenosylmethionine transport///mitochondrion
Afu7g04500	3.48	3.46	3.84	ATP phosphoribosyltransferase	cell///ATP phosphoribosyltransferase activity///histidine biosynthetic process

Table 4.11: 100 ORFs with the lowest log_2 values among down-regulated genes common to all 3 time points (4, 8 and 16 hrs) of the ATCC46645 Δ*pacC* time course.

ORFs	T4 vs T0	T8 vs T0	T16 vs T0	Annotation	Functional classification
Afu5g02880	-7.28	-5.53	-6.46	C6 transcription factor, putative	transcription factor activity///regulation of transcription
Afu5g00810	-6.76	-5.33	-6.4	hypothetical protein	
Afu2g10130	-6.69	-4.64	-5.2	phase-specific adhesin, putative	
Afu3g00810	-6.16	-4.5	-6.19	cholestenol delta-isomerase, putative	
Afu4g00820	-6.07	-2.45	-4.18	reverse transcriptase, RNaseH	
Afu8g01040	-6.05	-2.92	-4.56	reverse transcriptase, RNaseH	
Afu5g00790	-5.99	-4.5	-5.44	ABC multidrug transporter, putative	ATP-binding cassette (ABC) transporter activity///ATP binding///transport
Afu2g14330	-5.97	-4.81	-5.97	hypothetical protein	
Afu3g03040	-5.97	-3.53	-4.34	conserved hypothetical protein	
Afu4g14870	-5.9	-2.83	-4.46	LINE-1 class reverse transcriptase, RNaseH, putative	
Afu3g01300	-5.81	-4.65	-5.26	hypothetical protein	
Afu2g00200	-5.8	-5.74	-6.99	catalase, putative	oxygen and reactive oxygen species metabolic process///peroxisomal matrix///response to oxidative stress///catalase activity
Afu2g18080	-5.78	-2.7	-4.36	LINE-1 class reverse transcriptase, RNaseH, putative	
Afu4g14760	-5.77	-3.33	-4.46	ABC multidrug transporter, putative	
Afu6g09470	-5.73	-2.67	-3.9	reverse transcriptase, RNaseH, putative	
Afu3g11880	-5.7	-2.28	-2.24	hypothetical protein	
Afu3g02140	-5.63	-4.47	-4.52	large conductance mechanosensitive channel, putative	nonselective channel activity///ion channel activity///transport
Afu3g01400	-5.59	-3.77	-4.06	ABC multidrug transporter, putative	response to drug///xenobiotic-transporting ATPase activity///plasma membrane
Afu8g00310	-5.54	-2.6	-4.08	LINE-1 class reverse	

				transcriptase, RNaseH, putative	
Afu2g13060	-5.54	-3.22	-3.54	calcineurin binding protein, putative	
Afu1g14000	-5.49	-3.48	-3.71	hypothetical protein	
Afu6g00780	-5.48	-2.79	-4.18	LINE-1 class reverse transcriptase, RNaseH, putative	
Afu4g11710	-5.43	-4.92	-5.94	oxidoreductase, zinc-binding dehydrogenase family superfamily	cellular component unknown///biological process unknown///molecular function unknown
Afu6g14660	-5.41	-2.64	-3.95	reverse transcriptase, RNaseH	
Afu7g06840	-5.4	-5.39	-5.98	class III aminotransferase	arginine catabolic process///cytoplasm///nucleus///ornithine-oxo-acid transaminase activity
Afu8g06290	-5.39	-2.74	-4.07	LINE-1 class reverse transcriptase, RNaseH, putative	
Afu3g15370	-5.37	-2.77	-4.01	LINE-1 class reverse transcriptase, RNaseH, putative	
Afu1g16450	-5.36	-3.33	-4.18	hypothetical protein	
Afu7g05490	-5.31	-4.11	-5.03	hypothetical protein	
Afu3g09430	-5.3	-2.82	-4.23	LINE-1 class reverse transcriptase, RNaseH, putative	
Afu3g12000	-5.26	-3.57	-3.18	hypothetical protein	
Afu4g00730	-5.14	-5.1	-6.21	HHE domain protein	
Afu6g03210	-5.13	-3.77	-5.61	conidiation-specific protein 10	
Afu7g04930	-5.13	-4.92	-4.84	alkaline serine protease (PR1), putative	protein catabolic process///cellular component unknown///peptidase activity
Afu3g14620	-5.12	-3.67	-3.7	extracellular endo-1,5-alpha-L-arabinase, putative	hydrolase activity, hydrolyzing N-glycosyl compounds///metabolic process
Afu1g00170	-4.99	-3.59	-4.58	hypothetical protein	
Afu8g01400	-4.96	-3.57	-3.66	mitochondrial carrier protein (Pet8), putative	S-adenosylmethionine transmembrane transporter activity///mitochondrial inner membrane///S-adenosylmethionine transport///mitochondrion
Afu2g03150	-4.87	-2.81	-2.04	kinesin family protein	kinesin complex///microtubule motor activity///establishment of mitotic spindle orientation///cytoplasmic microtubule///microtubule depolymerisation///nuclear microtubule
Afu8g05770	-4.79	-3.91	-4.06	hypothetical protein	
Afu4g00180	-4.79	-3.96	-4.37	fatty acid oxygenase, putative	
Afu8g02290	-4.77	-3.78	-3.97	conserved hypothetical protein	
Afu3g10690	-4.73	-3.19	-4.59	calcium-translocating P-type ATPase(PMCA-type),putative	calcium ion transport///cellular calcium ion homeostasis///calcium-transporting ATPase activity
Afu2g06290	-4.71	-4.55	-4.99	nuclear division rft1 protein	protein amino acid N-linked glycosylation///oligosaccharide transmembrane transporter activity///oligosaccharide transport///endoplasmic reticulum membrane
Afu1g00910	-4.67	-3.73	-3.92	conserved hypothetical protein	

Afu5g04040	-4.66	-2.16	-3	conserved hypothetical protein	
Afu5g01930	-4.66	-3.51	-3.84	hypothetical protein	
Afu3g00500	-4.63	-4.41	-5	integral membrane protein	
Afu7g00400	-4.61	-3.35	-3.33	hypothetical protein	
Afu7g00410	-4.57	-3.16	-2.56	C6 transcription factor, putative	DNA binding///zinc ion binding
Afu4g00860	-4.56	-4.64	-5.36	conserved hypothetical protein	
Afu4g12490	-4.51	-2.92	-3.94	guanine nucleotide exchange factor VPS9, putative	ubiquitin binding///cytosol///protein targeting to vacuole///guanyl-nucleotide exchange factor activity
Afu3g08920	-4.47	-4.65	-4.54	hypothetical protein	
Afu8g01570	-4.46	-3.41	-4.26	ADP-ribosylglycohydrolase family protein	
Afu2g15270	-4.41	-3.57	-3.79	conserved hypothetical protein	
Afu5g10270	-4.4	-3.02	-2.9	heat shock protein, HSP20 family	
Afu3g14550	-4.37	-2.71	-3.21	DNA repair protein (Rex1), putative	
Afu8g05880	-4.37	-2.35	-2.23	10 kDa chaperonin (GroES/Cpn10), putative	protein folding///chaperone regulator activity///chaperone binding
Afu3g01410	-4.36	-3.01	-3.23	polyketide synthase, putative	3-oxoacyl-[acyl-carrier-protein] synthase activity///polyketide synthase activity
Afu4g14770	-4.35	-2.81	-2.17	squalene-hopene-cyclase, putative	lipid particle///plasma membrane///endoplasmic reticulum///ergosterol biosynthetic process///lanosterol synthase activity
Afu6g03140	-4.34	-3.78	-3.75	isp4 protein, putative	oligopeptide transporter activity///integral to plasma membrane///oligopeptide transport
Afu2g09510	-4.33	-3.84	-4.29	hypothetical protein	
Afu1g01180	-4.33	-2.72	-2.66	isoamyl alcohol oxidase	FAD binding
Afu4g00740	-4.29	-5.6	-6.02	hypothetical protein	
Afu1g14330	-4.28	-4.3	-5.29	ABC transporter, putative	ATP-binding cassette (ABC) transporter activity///transport///integral to membrane
Afu8g01330	-4.25	-4.21	-4.46	hypothetical protein	
Afu2g15680	-4.19	-2.34	-3.81	transcription initiation factor iia small chain	transcription factor TFIIA complex///transcription initiation from RNA polymerase II promoter///general RNA polymerase II transcription factor activity
Afu2g04880	-4.17	-3.45	-4.54	DUF77 domain protein	cell wall organisation///cytoplasm///nucleus///molecular function unknown
Afu5g00800	-4.17	-3.28	-4.73	conserved hypothetical protein	
Afu1g17290	-4.15	-3.48	-3.35	conserved hypothetical protein	
Afu6g03130	-4.14	-3.76	-4.22	hypothetical protein	
Afu3g14870	-4.14	-4.02	-4.18	hypothetical protein	
Afu6g04470	-4.13	-2.82	-3.11	hypothetical protein	
Afu2g15130	-4.12	-3.08	-2.61	ABC multidrug transporter,	response to drug///drug

				putative	transport///xenobiotic-transporting ATPase activity///plasma membrane
Afu1g17370	-4.11	-2.26	-3.32	chaperone/heat shock protein Hsp9, putative	response to desiccation///response to heat///response to oxidative stress///cytoplasm///nucleus///cell adhesion///hyperosmotic response///heat shock protein activity
Afu6g10790	-4.09	-3.78	-4.12	MFS amine transporter, putative	
Afu6g13220	-4.08	-3.45	-3.11	hypothetical protein	
Afu1g04860	-4.07	-2.47	-3.33	hypothetical protein	
Afu2g00160	-4.03	-3.12	-2.56	hypothetical protein	
Afu5g02300	-4.03	-3.43	-3.57	peroxidase, putative	
Afu3g14810	-4.02	-3.41	-2.61	pathogenicity associated protein PEP2, putative	
Afu5g05480	-4.02	-4.33	-5.24	Rheb GTPase RhbA	detection of nutrient///extrinsic to plasma membrane///pathogenesis///nitrogen utilisation///RHEB small monomeric GTPase activity
Afu5g00160	-4.01	-3.92	-4.57	MFS polyamine transporter, putative	drug transport///drug transporter activity///integral to membrane
Afu7g08410	-4.01	-3.07	-3.87	Tc1-mariner transposase, putative	
Afu2g05060	-4.01	-2.35	-2.05	alternative oxidase	
Afu1g01500	-4	-3.36	-3.32	short-chain dehydrogenase/reductase family protein, putative	
Afu3g12270	-3.98	-2.2	-3.42	glutathione peroxidase family protein	intracellular///response to oxidative stress///thiol peroxidase activity///glutathione peroxidase activity
Afu1g11560	-3.97	-3.42	-3.99	4-hydroxyphenylpyruvate dioxygenase, putative	
Afu5g14350	-3.96	-4.67	-4.92	c-24(28) sterol reductase	delta24(24-1) sterol reductase activity///endoplasmic reticulum///ergosterol biosynthetic process
Afu2g00170	-3.92	-3.29	-3.55	glutathione-dependent formaldehyde dehydrogenase	cellular component unknown///D-xylulose reductase activity///monosaccharide metabolic process
Afu6g02580	-3.92	-3.55	-3.82	hypothetical protein	
Afu5g07940	-3.91	-3.79	-4.33	hypothetical protein	
Afu6g10840	-3.91	-2.92	-3.34	hypothetical protein	
Afu3g00820	-3.9	-3.36	-4.15	putative exported protein	
Afu6g03080	-3.86	-3.11	-3.54	ABC multidrug transporter, putative	ATP-binding cassette (ABC) transporter activity///ATP binding///transport
Afu6g09340	-3.81	-2.23	-3.15	hypothetical protein	
Afu5g09440	-3.81	-2.78	-2.12	amino acid permease, putative	
Afu4g13230	-3.81	-3.47	-3.65	regulatory protein weta	

Total up-regulated genes in the ATCC46645 Δ*pacC* time course							
GO ACCESSION	**GO Term**	**p-value**	**corrected p-value**	**Count in Selection**	**% Count in Selection**	**Count in Total**	**% Count in Total**
GO:0044281	small molecule metabolic process	6.63651E-15	1.2072986E-10	25	12.315271	483	10.742883
GO:0016491	oxidoreductase activity	5.785961E-14	5.262843E-10	50	24.630543	472	10.49822
GO:0022891	substrate-specific transmembrane transporter activity	1.1653739E-11	7.066737E-8	21	10.344828	317	7.0507116
GO:0022857|GO:0005386|GO:0015646	transmembrane transporter activity	5.0577924E-11	2.3002548E-7	23	11.3300495	354	7.8736653
GO:0022892	substrate-specific transporter activity	9.059585E-11	3.2961975E-7	21	10.344828	357	7.9403915
GO:0003824	catalytic activity	2.9774658E-10	9.027562E-7	57	28.078817	2044	45.462635
GO:0005215|GO:0005478	transporter activity	5.084814E-10	1.3214537E-6	53	26.108374	525	11.677046
GO:0005886|GO:0005904	plasma membrane	1.4289192E-9	3.249321E-6	66	32.512314	315	7.006228
GO:0051119	sugar transmembrane transporter activity	4.3564534E-9	8.805732E-6	20	9.852217	47	1.0453737
GO:0006091	generation of precursor metabolites and energy	1.0009635E-8	1.8209295E-5	18	8.866995	98	2.1797154
GO:0006066	alcohol metabolic process	4.602692E-8	7.611919E-5	15	7.3891625	176	3.9145908
GO:0015144	carbohydrate transmembrane transporter activity	7.047467E-8	1.0683824E-4	21	10.344828	52	1.1565837
GO:0006082	organic acid metabolic process	1.1781765E-7	1.4288742E-4	17	8.374384	309	6.872776
GO:0019752	carboxylic acid metabolic process	1.1781765E-7	1.4288742E-4	17	8.374384	309	6.872776
GO:0043436	oxoacid metabolic process	1.1781765E-7	1.4288742E-4	17	8.374384	309	6.872776
GO:0042180	cellular ketone metabolic process	1.4006086E-7	1.5924718E-4	17	8.374384	319	7.095196
GO:0005355|GO:0015579	glucose transmembrane transporter activity	2.3727443E-7	2.2718114E-4	19	9.359606	33	0.7339858
GO:0015145	monosaccharide transmembrane transporter activity	2.3727443E-7	2.2718114E-4	19	9.359606	33	0.7339858
GO:0015149	hexose transmembrane transporter activity	2.3727443E-7	2.2718114E-4	19	9.359606	33	0.7339858
GO:0016052|GO:0006095	carbohydrate catabolic process	4.342581E-7	3.5908743E-4	9	4.4334974	66	1.4679716
GO:0016614	oxidoreductase activity, acting on CH-OH group of donors	4.1676213E-7	3.5908743E-4	13	6.4039407	129	2.8692172
GO:0044283	small molecule biosynthetic process	4.1528762E-7	3.5908743E-4	8	3.9408867	157	3.491993
GO:0016020	membrane	1.1899675E-6	9.412006E-4	85	41.87192	816	18.149466
GO:0006096|GO:0019641|GO:0019642	glycolysis	1.2537006E-6	9.50293E-4	9	4.4334974	10	0.22241993
GO:0016616	oxidoreductase activity, acting on the CH-OH group of donors, NAD or NADP as acceptor	1.3907705E-6	0.0010120231	13	6.4039407	114	2.535587
GO:0034641	cellular nitrogen compound metabolic process	1.4911448E-6	0.0010433292	8	3.9408867	298	6.6281137
GO:0044275	cellular carbohydrate catabolic process	3.4398627E-6	0.0023176735	9	4.4334974	44	0.9786477
GO:0016903	oxidoreductase activity, acting on the aldehyde or oxo group of donors	4.231417E-6	0.0027491772	2	0.9852217	38	0.8451957
GO:0006811	ion transport	5.975443E-6	0.0037484097	1	0.49261084	132	2.9359431
GO:0006113	fermentation	8.235532E-6	0.0048328675	9	4.4334974	16	0.3558719
GO:0006753	nucleoside phosphate metabolic process	1.4288173E-5	0.00787658	2	0.9852217	80	1.7793595

GO:0009117	nucleotide metabolic process	1.4288173E-5	0.00787658	2	0.9852217	80	1.7793595
GO:0019318	hexose metabolic process	1.939019E-5	0.01037476	12	5.91133	66	1.4679716
GO:0016620	oxidoreductase activity, acting on the aldehyde or oxo group of donors, NAD or NADP as acceptor	2.2327078E-5	0.01160483	2	0.9852217	35	0.77846974
GO:0009309	amine biosynthetic process	3.3054006E-5	0.016703079	8	3.9408867	111	2.468861
GO:0006810|GO:0015457|GO:0015460	transport	3.8006103E-5	0.018686438	53	26.108374	774	17.215303
GO:0006007	glucose catabolic process	4.258342E-5	0.019863276	9	4.4334974	18	0.40035588
GO:0019320	hexose catabolic process	4.258342E-5	0.019863276	9	4.4334974	18	0.40035588
GO:0006090	pyruvate metabolic process	4.9155457E-5	0.021810358	4	1.9704434	24	0.5338078
GO:0008643|GO:0006861|GO:0008644	carbohydrate transport	4.84225E-5	0.021810358	15	7.3891625	47	1.0453737
GO:0051234	establishment of localisation	5.569749E-5	0.024124663	53	26.108374	784	17.437723
GO:0044271	cellular nitrogen compound biosynthetic process	6.461863E-5	0.027337842	8	3.9408867	161	3.5809608
GO:0005353|GO:0015585|GO:0019192	fructose transmembrane transporter activity	8.018974E-5	0.02861234	14	6.8965516	28	0.6227758
GO:0006519	cellular amino acid and derivative metabolic process	8.0213715E-5	0.02861234	8	3.9408867	225	5.0044484
GO:0008645	hexose transport	8.018974E-5	0.02861234	14	6.8965516	28	0.6227758
GO:0009308	amine metabolic process	7.6350596E-5	0.02861234	8	3.9408867	243	5.404804
GO:0015578|GO:0015589	mannose transmembrane transporter activity	8.018974E-5	0.02861234	14	6.8965516	28	0.6227758
GO:0015749	monosaccharide transport	8.018974E-5	0.02861234	14	6.8965516	28	0.6227758
GO:0032787	monocarboxylic acid metabolic process	7.832624E-5	0.02861234	9	4.4334974	115	2.5578291
GO:0006526	arginine biosynthetic process	8.551552E-5	0.02902297	8	3.9408867	11	0.24466193
GO:0009062	fatty acid catabolic process	8.615107E-5	0.02902297	5	2.4630542	25	0.5560498
GO:0051179	localisation	9.239746E-5	0.030561332	53	26.108374	801	17.815836
GO:0005975	carbohydrate metabolic process	1.0310591E-4	0.033494264	20	9.852217	292	6.494662
GO:0044242	cellular lipid catabolic process	1.1437101E-4	0.036501944	5	2.4630542	32	0.7117438
GO:0044106	cellular amine metabolic process	1.1960411E-4	0.03751397	8	3.9408867	205	4.5596085
GO:0004022	alcohol dehydrogenase (NAD) activity	1.2755851E-4	0.039330762	6	2.955665	9	0.20017794
GO:0005529	sugar binding	1.6262209E-4	0.042875122	5	2.4630542	5	0.111209966
GO:0005536	glucose binding	1.6262209E-4	0.042875122	5	2.4630542	5	0.111209966
GO:0005996	monosaccharide metabolic process	1.473509E-4	0.042875122	12	5.91133	81	1.8016014
GO:0009746	response to hexose stimulus	1.6262209E-4	0.042875122	5	2.4630542	5	0.111209966
GO:0009749	response to glucose stimulus	1.6262209E-4	0.042875122	5	2.4630542	5	0.111209966
GO:0015980	energy derivation by oxidation of organic compounds	1.4673773E-4	0.042875122	9	4.4334974	77	1.7126335
GO:0034284	response to monosaccharide stimulus	1.6262209E-4	0.042875122	5	2.4630542	5	0.111209966
GO:0048029	monosaccharide binding	1.6262209E-4	0.042875122	5	2.4630542	5	0.111209966
GO:0016042|GO:0006724	lipid catabolic process	1.7621237E-4	0.0451495	5	2.4630542	33	0.7339858
4 hrs up-regulated genes in the ATCC46645 Δ*pacC* time course							

GO ACCESSION	GO Term	p-value	corrected p-value	Count in Selection	% Count in Selection	Count in Total	% Count in Total
GO:0044281	small molecule metabolic process	3.7342728E-14	6.0288985E-10	11	6.111111	483	10.742883
GO:0016491	oxidoreductase activity	7.343491E-11	5.9279495E-7	25	13.888889	472	10.49822
GO:0006082	organic acid metabolic process	8.269015E-9	2.0108255E-5	4	2.2222223	309	6.872776
GO:0019752	carboxylic acid metabolic process	8.269015E-9	2.0108255E-5	4	2.2222223	309	6.872776
GO:0043436	oxoacid metabolic process	8.269015E-9	2.0108255E-5	4	2.2222223	309	6.872776
GO:0042180	cellular ketone metabolic process	1.4123668E-8	2.8502925E-5	4	2.2222223	319	7.095196
GO:0044275	cellular carbohydrate catabolic process	6.2424937E-7	8.398637E-4	7	3.8888888	44	0.9786477
GO:0016614	oxidoreductase activity, acting on CH-OH group of donors	7.302754E-7	8.4215216E-4	6	3.3333333	129	2.8692172
GO:0003824	catalytic activity	8.9877665E-7	8.6225814E-4	29	16.11111	2044	45.462635
GO:0006066	alcohol metabolic process	9.290171E-7	8.6225814E-4	11	6.111111	176	3.9145908
GO:0006091	generation of precursor metabolites and energy	9.613419E-7	8.6225814E-4	7	3.8888888	98	2.1797154
GO:0005737	cytoplasm	2.6871924E-6	0.0021692056	129	71.666664	2039	45.351425
GO:0022891	substrate-specific transmembrane transporter activity	3.2259588E-6	0.0024801127	1	0.5555556	317	7.0507116
GO:0022892	substrate-specific transporter activity	6.524553E-6	0.004579888	1	0.5555556	357	7.9403915
GO:0005215|GO:0005478	transporter activity	7.013951E-6	0.0047182767	20	11.111111	525	11.677046
GO:0016052|GO:0006095	carbohydrate catabolic process	8.912103E-6	0.005620392	7	3.8888888	66	1.4679716
GO:0016616	oxidoreductase activity, acting on the CH-OH group of donors, NAD or NADP as acceptor	9.051239E-6	0.005620392	6	3.3333333	114	2.535587
GO:0022857|GO:0005386|GO:0015646	transmembrane transporter activity	9.568086E-6	0.005682468	2	1.1111112	354	7.8736653
GO:0006096|GO:0019641|GO:0019642	glycolysis	2.3987086E-5	0.012908868	7	3.8888888	10	0.22241993
GO:0006090	pyruvate metabolic process	2.816085E-5	0.014666145	4	2.2222223	24	0.5338078
GO:0051119	sugar transmembrane transporter activity	4.1540137E-5	0.02032291	1	0.5555556	47	1.0453737
GO:0006007	glucose catabolic process	6.62467E-5	0.030531187	7	3.8888888	18	0.40035588
GO:0019320	hexose catabolic process	6.62467E-5	0.030531187	7	3.8888888	18	0.40035588
GO:0044282	small molecule catabolic process	7.657155E-5	0.03341163	7	3.8888888	75	1.6681495
GO:0019318	hexose metabolic process	1.1145624E-4	0.043967117	9	5.0	66	1.4679716

8 hrs up-regulated genes in the ATCC46645 Δ*pacC* time course

GO ACCESSION	GO Term	p-value	corrected p-value	Count in Selection	% Count in Selection	Count in Total	% Count in Total
GO:0005886|GO:0005904	plasma membrane	7.637119E-12	1.03925835E-7	50	42.016808	315	7.006228
GO:0022892	substrate-specific transporter activity	7.765989E-11	5.283975E-7	17	14.285714	357	7.9403915
GO:0022891	substrate-specific transmembrane transporter activity	2.3831545E-10	1.080998E-6	17	14.285714	317	7.0507116
GO:0016491	oxidoreductase activity	1.3308146E-9	4.5274273E-6	24	20.168068	472	10.49822
GO:0005215|GO:0005478	transporter activity	7.1044024E-9	1.4498662E-5	35	29.411764	525	11.677046

GO:0022857|GO:0005386|GO:0015646	transmembrane transporter activity	5.818035E-9	1.4498662E-5	17	14.285714	354	7.8736653
GO:0051119	sugar transmembrane transporter activity	7.458166E-9	1.4498662E-5	16	13.445378	47	1.0453737
GO:0015144	carbohydrate transmembrane transporter activity	5.8931413E-8	1.0024225E-4	17	14.285714	52	1.1565837
GO:0005355|GO:0015579	glucose transmembrane transporter activity	2.05277E-7	2.4286375E-4	15	12.605042	33	0.7339858
GO:0015145	monosaccharide transmembrane transporter activity	2.05277E-7	2.4286375E-4	15	12.605042	33	0.7339858
GO:0015149	hexose transmembrane transporter activity	2.05277E-7	2.4286375E-4	15	12.605042	33	0.7339858
GO:0044281	small molecule metabolic process	2.1416574E-7	2.4286375E-4	5	4.2016807	483	10.742883
GO:0016614	oxidoreductase activity, acting on CH-OH group of donors	3.5052767E-7	3.6692127E-4	5	4.2016807	129	2.8692172
GO:0006811	ion transport	6.232896E-7	5.727891E-4	1	0.84033614	132	2.9359431
GO:0016616	oxidoreductase activity, acting on the CH-OH group of donors, NAD or NADP as acceptor	6.3138185E-7	5.727891E-4	5	4.2016807	114	2.535587
GO:0016020	membrane	1.6291028E-6	0.0013855508	62	52.10084	816	18.149466
GO:0003824	catalytic activity	3.8398152E-6	0.0030736567	34	28.571428	2044	45.462635
GO:0044242	cellular lipid catabolic process	6.369742E-6	0.0045620725	5	4.2016807	32	0.7117438
GO:0005529	sugar binding	1.0993901E-5	0.004986829	5	4.2016807	5	0.111209966
GO:0005536	glucose binding	1.0993901E-5	0.004986829	5	4.2016807	5	0.111209966
GO:0006753	nucleoside phosphate metabolic process	9.483033E-6	0.004986829	2	1.6806723	80	1.7793595
GO:0009117	nucleotide metabolic process	9.483033E-6	0.004986829	2	1.6806723	80	1.7793595
GO:0009746	response to hexose stimulus	1.0993901E-5	0.004986829	5	4.2016807	5	0.111209966
GO:0009749	response to glucose stimulus	1.0993901E-5	0.004986829	5	4.2016807	5	0.111209966
GO:0016042|GO:0006724	lipid catabolic process	9.544039E-6	0.004986829	5	4.2016807	33	0.7339858
GO:0034284	response to monosaccharide stimulus	1.0993901E-5	0.004986829	5	4.2016807	5	0.111209966
GO:0048029	monosaccharide binding	1.0993901E-5	0.004986829	5	4.2016807	5	0.111209966
GO:0009062	fatty acid catabolic process	1.343512E-5	0.0058975792	5	4.2016807	25	0.5560498
GO:0005975	carbohydrate metabolic process	1.45814865E-5	0.006200772	6	5.042017	292	6.494662
GO:0006810|GO:0015457|GO:0015460	transport	2.5284562E-5	0.010119766	25	21.008404	774	17.215303
GO:0051234	establishment of localisation	4.579353E-5	0.01730994	25	21.008404	784	17.437723
GO:0006066	alcohol metabolic process	6.80319E-5	0.025021007	3	2.5210085	176	3.9145908
GO:0051179	localisation	7.401006E-5	0.025823796	25	21.008404	801	17.815836
GO:0004553|GO:0016800	hydrolase activity, hydrolyzing O-glycosyl compounds	8.374581E-5	0.0284903	4	3.3613446	91	2.0240214
GO:0016798	hydrolase activity, acting on glycosyl bonds	1.13699854E-4	0.037737224	6	5.042017	112	2.4911032
GO:0008643|GO:0006861|GO:0008644	carbohydrate transport	1.6033494E-4	0.049587183	1	0.84033614	47	1.0453737
16 hrs up-regulated genes in the ATCC46645 Δ*pacC* time course							
GO ACCESSION	**GO Term**	**p-value**	**corrected p-**	**Count in**	**% Count in**	**Count in**	**% Count in**

			value	Selection	Selection	Total	Total
GO:0005886|GO:0005904	plasma membrane	2.841722E-15	3.8772603E-11	85	50.898205	315	7.006228
GO:0005215|GO:0005478	transporter activity	1.08944395E-14	6.138478E-11	48	28.742516	525	11.677046
GO:0022891	substrate-specific transmembrane transporter activity	1.3497041E-14	6.138478E-11	20	11.9760475	317	7.0507116
GO:0022892	substrate-specific transporter activity	4.870091E-14	1.6611944E-10	20	11.9760475	357	7.9403915
GO:0022857|GO:0005386 |GO:0015646	transmembrane transporter activity	8.0102334E-14	2.1858407E-10	21	12.57485	354	7.8736653
GO:0016491	oxidoreductase activity	2.394451E-13	5.4450017E-10	37	22.15569	472	10.49822
GO:0051119	sugar transmembrane transporter activity	9.279857E-12	1.8087833E-8	19	11.377246	47	1.0453737
GO:0015144	carbohydrate transmembrane transporter activity	1.6450498E-10	2.8056428E-7	20	11.9760475	52	1.1565837
GO:0016020	membrane	2.1066484E-9	3.1936909E-6	101	60.479042	816	18.149466
GO:0005355|GO:0015579	glucose transmembrane transporter activity	4.8021573E-9	5.460073E-6	18	10.778443	33	0.7339858
GO:0015145	monosaccharide transmembrane transporter activity	4.8021573E-9	5.460073E-6	18	10.778443	33	0.7339858
GO:0015149	hexose transmembrane transporter activity	4.8021573E-9	5.460073E-6	18	10.778443	33	0.7339858
GO:0006811	ion transport	1.5215225E-8	1.4828379E-5	1	0.5988024	132	2.9359431
GO:0016614	oxidoreductase activity, acting on CH-OH group of donors	8.2171574E-8	7.418002E-5	6	3.5928144	129	2.8692172
GO:0016616	oxidoreductase activity, acting on the CH-OH group of donors, NAD or NADP as acceptor	8.6988855E-8	7.418002E-5	6	3.5928144	114	2.535587
GO:0003824	catalytic activity	1.3094343E-7	1.05094055E-4	42	25.1497	2044	45.462635
GO:0006810|GO:0015457 |GO:0015460	transport	1.620457E-7	1.228311E-4	47	28.143713	774	17.215303
GO:0051234	establishment of localisation	2.0719052E-7	1.4878517E-4	47	28.143713	784	17.437723
GO:0051179	localisation	4.617725E-7	3.1502236E-4	47	28.143713	801	17.815836
GO:0008643|GO:0006861 |GO:0008644	carbohydrate transport	8.1487195E-7	5.0537067E-4	14	8.383233	47	1.0453737
GO:0016620	oxidoreductase activity, acting on the aldehyde or oxo group of donors, NAD or NADP as acceptor	5.0529648E-6	0.0029975176	2	1.1976048	35	0.77846974
GO:0005353|GO:0015585 |GO:0019192	fructose transmembrane transporter activity	7.4749823E-6	0.0037773717	13	7.784431	28	0.6227758
GO:0008645	hexose transport	7.4749823E-6	0.0037773717	13	7.784431	28	0.6227758
GO:0015578|GO:0015589	mannose transmembrane transporter activity	7.4749823E-6	0.0037773717	13	7.784431	28	0.6227758
GO:0015749	monosaccharide transport	7.4749823E-6	0.0037773717	13	7.784431	28	0.6227758
GO:0031226	intrinsic to plasma membrane	1.3524271E-5	0.0065902085	24	14.371258	95	2.1129894
GO:0016903	oxidoreductase activity, acting on the aldehyde or oxo group of donors	1.693006E-5	0.007965332	2	1.1976048	38	0.8451957
GO:0005529	sugar binding	2.647224E-5	0.009761853	5	2.9940119	5	0.111209966
GO:0005536	glucose binding	2.647224E-5	0.009761853	5	2.9940119	5	0.111209966
GO:0005887	integral to plasma membrane	2.294872E-5	0.009761853	24	14.371258	87	1.9350533

GO:0009746	response to hexose stimulus	2.647224E-5	0.009761853	5	2.9940119	5	0.111209966
GO:0009749	response to glucose stimulus	2.647224E-5	0.009761853	5	2.9940119	5	0.111209966
GO:0034284	response to monosaccharide stimulus	2.647224E-5	0.009761853	5	2.9940119	5	0.111209966
GO:0048029	monosaccharide binding	2.647224E-5	0.009761853	5	2.9940119	5	0.111209966
GO:0006113	fermentation	2.8851056E-5	0.010359086	8	4.790419	16	0.3558719
GO:0044242	cellular lipid catabolic process	4.3537024E-5	0.015231317	5	2.9940119	32	0.7117438
GO:0016042|GO:0006724	lipid catabolic process	6.395591E-5	0.021815442	5	2.9940119	33	0.7339858
GO:0006091	generation of precursor metabolites and energy	7.1965354E-5	0.023378545	8	4.790419	98	2.1797154
GO:0009062	fatty acid catabolic process	7.123115E-5	0.023378545	5	2.9940119	25	0.5560498

Table 4.12: Significant GO terms among the up-regulated genes in the ATCC46645 Δ*pacC* time course. p-value represents the probability of obtaining the GO term from a list of random entities, corrected p-value derived from Bonferroni testing of multiple comparisons. Analysis performed using Genespring GX 11.02.

Total down-regulated genes in the ATCC46645 Δ*pacC* time course							
GO ACCESSION	**GO Term**	**p-value**	**corrected p-value**	**Count in Selection**	**% Count in Selection**	**Count in Total**	**% Count in Total**
GO:0005634	nucleus	4.52213E-6	0.02259516	126	99.2126	1124	25.0
GO:0006350	transcription	3.4448162E-6	0.02259516	10	7.874016	120	2.6690392
GO:0016591	DNA-directed RNA polymerase II, holoenzyme	1.1784711E-5	0.041981492	1	0.78740156	37	0.82295376
GO:0030528	transcription regulator activity	4.75705E-6	0.02259516	2	1.5748031	280	6.227758

Table 4.13: Significant GO terms among the down-regulated genes in the ATCC46645 Δ*pacC* time course. p-value represents the probability of obtaining the GO term from a list of random entities, corrected p-value derived from Bonferroni testing of multiple comparisons. Analysis performed using Genespring GX 11.02.

Genes differentially expressed in the ATCC46645 Δ*pacC* time course were clustered using the STEM software (Fig. 4.20) which allocated differentially expressed genes to twelve model profiles. Among these, five model profiles (12, 1, 9, 4 and 3) contain genes whose expression is down-regulated across the ATCC46645 Δ*pacC* time course and seven (48, 42, 49, 45, 46, 29 and 47) contain genes whose expression is up-regulated across the ATCC46645 Δ*pacC* time course.

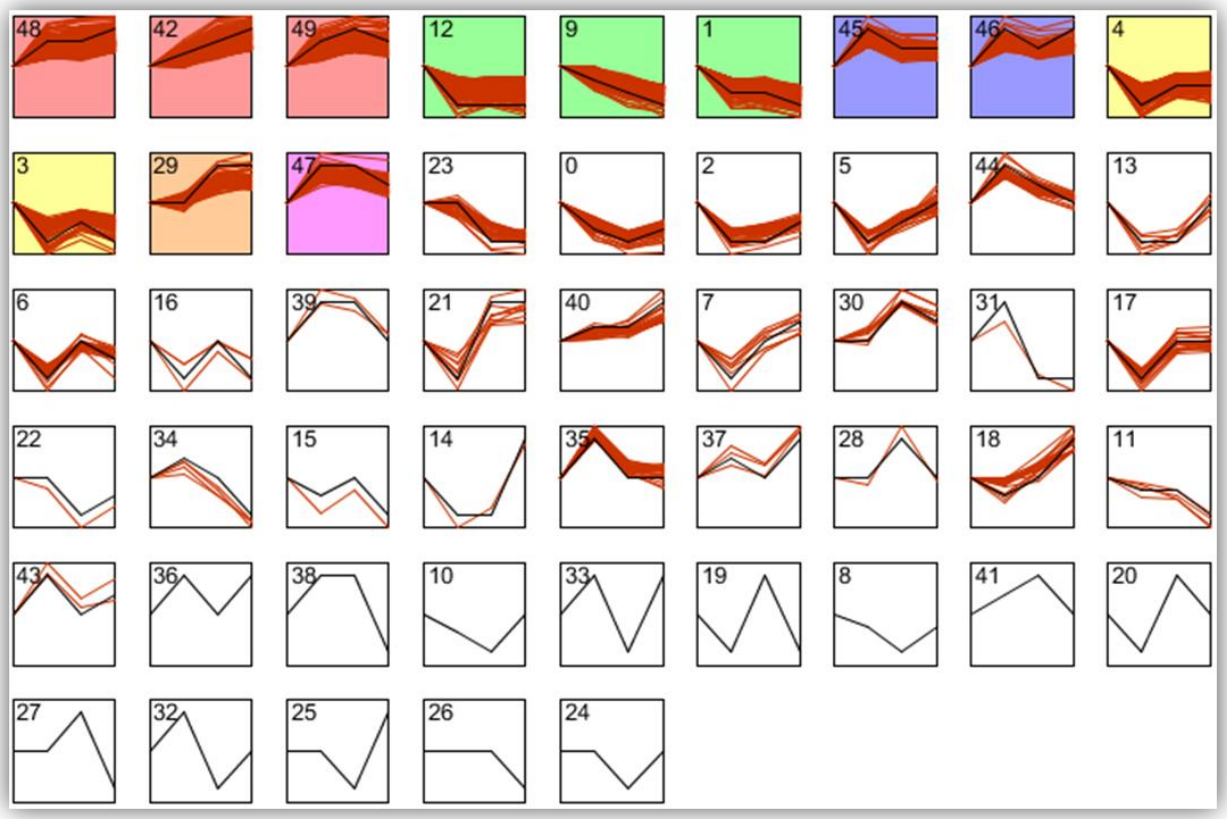


Fig. 4.20: STEM clustering analysis of differentially expressed genes in the ATCC46645 Δ*pacC* time course during initiation of murine infection. Statistically significant model profiles are coloured, similarly coloured profiles cluster according to the similar temporal nature of gene expression profiles assigned Profile 48, n = 351 (2e-132), Profile 42, n = 229 (1e-110), Profile 49, n = 159 (1e-11), Profile 12, n = 332 (2e-98), Profile 9, n = 202 (5e-88), Profile 1, n = 194 (3e-64), Profile 45, n = 185 (3e-44), Profile 46, n = 95 (3e-10), Profile 4, n = 163 (1e-38), Profile 3, n = 76 (2e-8), Profile 29, n = 75 (4e-20), Profile 47, n = 70 (9e-4). Analysis performed using STEM. Red lines represent all analysed gene expression profiles in the dataset.

GO analysis in STEM (Table 4.14) of the ATCC46645 Δ*pacC* time course experiment followed the protocol described earlier for ATCC46645, using the expanded *A. fumigatus* gene annotation created for this study. GO terms with corrected p-value <0.05 are included, where the p-value, initially based on an hypergeometric distribution, was corrected by the software using a Bonferonni correction for multiple GO categories being tested

simultaneously. This corrected p-value is the original p-value divided by the number of GO categories for which the number of genes on the array is above the GO analysis minimum number of genes parameter. Profile 48, containing upregulated genes across the ATCC46645 Δ*pacC* time course, was significantly enriched in GO terms associated with the functional categories of transport and cell wall. Profile 12, containing OFRs whose expression was decreased across the ATCC46645 Δ*pacC* time course, was significantly enriched in GO terms associated with the functional category of transcription.

Significant GO terms for Profile 48 (n = 351)						
Category ID	**Genes in Category**	**Count Genes**	**Genes Expected**	**Genes Enriched**	**p-value**	**Corrected p-value**
IC	284	66.0	8.0	+58.0	3.5E-40	7.3E-38
Subtelomeric	430	71.0	12.1	+58.9	6.8E-33	1.4E-30
cytoplasm	276	43.0	7.7	+35.3	1.4E-19	2.9E-17
In vitro pH response genes	254	37.0	7.1	+29.9	4.2E-16	8.7E-14
oxidoreductase activity	68	20.0	1.9	+18.1	2.1E-15	4.3E-13
transporter activity	42	16.0	1.2	+14.8	1.2E-14	2.6E-12
transport	55	17.0	1.5	+15.5	1.0E-13	2.1E-11
metabolic process	82	19.0	2.3	+16.7	1.2E-12	2.5E-10
Semi-subT	403	41.0	11.3	+29.7	2.5E-12	5.2E-10
plasma membrane	91	19.0	2.6	+16.4	8.5E-12	1.8E-9
cellular component unknown	75	17.0	2.1	+14.9	2.6E-11	5.4E-9
membrane	23	9.0	0.6	+8.4	6.2E-9	1.3E-6
SECMET	96	15.0	2.7	+12.3	8.0E-8	1.7E-5
integral to plasma membrane	39	10.0	1.1	+8.9	9.1E-8	1.9E-5
biological process unknown	127	17.0	3.6	+13.4	1.2E-7	2.4E-5
molecular function unknown	143	18.0	4.0	+14.0	1.3E-7	2.7E-5
nucleus	211	22.0	5.9	+16.1	1.7E-7	3.5E-5
mitochondrion	74	12.0	2.1	+9.9	1.0E-6	2.2E-4
cell wall organisation	30	7.0	0.8	+6.2	1.6E-5	0.003
membrane fraction	21	6.0	0.6	+5.4	1.8E-5	0.004
AFU-SPECIFIC	112	12.0	3.1	+8.9	7.8E-5	0.016
Significant GO terms for Profile 42 (n = 229)						
Category ID	**Genes in Category**	**Count Genes**	**Genes Expected**	**Genes Enriched**	**p-value**	**Corrected p-value**
Subtelomeric	430	71.0	5.8	+65.2	4.5E-53	9.3E-51
IC	284	60.0	3.8	+56.2	9.2E-52	1.9E-49
Semi-subT	403	45.0	5.5	+39.5	8.2E-27	1.7E-24
In vitro pH response genes	254	37.0	3.4	+33.6	1.9E-26	3.9E-24
plasma membrane	91	19.0	1.2	+17.8	2.3E-17	4.8E-15
SECMET	96	17.0	1.3	+15.7	2.0E-14	4.1E-12
AFFC specific	52	8.0	0.7	+7.3	5.0E-7	1.0E-4
metabolic process	82	9.0	1.1	+7.9	1.8E-6	3.9E-4
cellular component unknown	75	8.0	1.0	+7.0	8.5E-6	0.002
hydrolase activity	27	5.0	0.4	+4.6	2.9E-5	0.006
nucleus	211	12.0	2.9	+9.1	3.8E-5	0.008
integral to plasma membrane	39	5.0	0.5	+4.5	1.8E-4	0.037
Significant GO terms for Profile 49 (n =159)						

Category ID	Genes in Category	Count Genes	Genes Expected	Genes Enriched	p-value	Corrected p-value
In vitro pH response genes	254	23.0	9.1	+13.9	5.2E-5	0.011
Significant GO terms for Profile 12 (n =332)						
Category ID	**Genes in Category**	**Count Genes**	**Genes Expected**	**Genes Enriched**	**p-value**	**Corrected p-value**
nucleus	211	41.0	7.1	+33.9	1.1E-19	2.2E-17
Semi-subT	403	54.0	13.5	+40.5	9.6E-18	2.0E-15
AFU-SPECIFIC	112	28.0	3.7	+24.3	6.0E-17	1.3E-14
Subtelomeric	430	46.0	14.4	+31.6	8.1E-12	1.7E-9
regulation of transcription	46	15.0	1.5	+13.5	1.4E-11	2.9E-9
zinc ion binding	61	16.0	2.0	+14.0	1.2E-10	2.5E-8
molecular function unknown	143	21.0	4.8	+16.2	1.5E-8	3.2E-6
transcription factor activity	46	12.0	1.5	+10.5	2.6E-8	5.5E-6
In vitro pH response genes	254	27.0	8.5	+18.5	1.7E-7	3.5E-5
DNA-dependent	20	7.0	0.7	+6.3	2.5E-6	5.2E-4
DNA binding	30	8.0	1.0	+7.0	4.7E-6	9.9E-4
cellular component unknown	75	12.0	2.5	+9.5	7.2E-6	0.002
ATP-binding cassette (ABC) transporter activity	13	5.0	0.4	+4.6	4.3E-5	0.009
Significant GO terms for Profile 9 (n =202)						
Category ID	**Genes in Category**	**Count Genes**	**Genes Expected**	**Genes Enriched**	**p-value**	**Corrected p-value**
cytoplasm	276	34.0	3.7	+30.3	4.9E-22	1.0E-19
nucleus	211	27.0	2.9	+24.1	3.0E-18	6.2E-16
molecular function unknown	143	23.0	1.9	+21.1	5.0E-18	1.0E-15
biological process unknown	127	20.0	1.7	+18.3	1.1E-15	2.3E-13
Semi-subT	403	25.0	5.5	+19.5	5.8E-10	1.2E-7
cellular component unknown	75	9.0	1.0	+8.0	8.6E-7	1.8E-4
transcription factor activity	46	7.0	0.6	+6.4	2.8E-6	5.9E-4
endoplasmic reticulum	48	7.0	0.7	+6.3	3.8E-6	7.9E-4
mitochondrion	74	7.0	1.0	+6.0	6.8E-5	0.014
Significant GO terms for Profile 1 (n =194)						
Category ID	**Genes in Category**	**Count Genes**	**Genes Expected**	**Genes Enriched**	**p-value**	**Corrected p-value**
Semi-subT	403	33.0	7.0	+26.0	5.0E-13	1.0E-10
nucleus	211	24.0	3.7	+20.3	6.9E-13	1.4E-10
In vitro pH response genes	254	21.0	4.4	+16.6	6.5E-9	1.4E-6
cytoplasm	276	20.0	4.8	+15.2	1.3E-7	2.7E-5
protein binding	26	7.0	0.5	+6.5	2.4E-7	5.1E-5
transcription initiation from RNA polymerase II promoter	10	5.0	0.2	+4.8	3.8E-7	7.9E-5
Subtelomeric	430	24.0	7.5	+16.5	9.4E-7	2.0E-4
molecular function unknown	143	11.0	2.5	+8.5	4.8E-5	0.010
DNA binding	30	5.0	0.5	+4.5	1.6E-4	0.034
Significant GO terms for Profile 45 (n =185)						
Category ID	**Genes in Category**	**Count Genes**	**Genes Expected**	**Genes Enriched**	**p-value**	**Corrected p-value**
cytoplasm	276	40.0	6.1	+33.9	8.8E-21	1.8E-18
cytosol	45	13.0	1.0	+12.0	1.1E-11	2.3E-9
mitochondrion	74	14.0	1.6	+12.4	8.5E-10	1.8E-7
Semi-subT	403	30.0	8.9	+21.1	1.2E-8	2.5E-6
In vitro pH response genes	254	22.0	5.6	+16.4	7.4E-8	1.5E-5

biological process unknown	127	14.0	2.8	+11.2	9.6E-7	2.0E-4
translation	19	6.0	0.4	+5.6	2.4E-6	5.1E-4
nucleus	211	17.0	4.7	+12.3	5.7E-6	0.001
structural constituent of ribosome	15	5.0	0.3	+4.7	1.3E-5	0.003
Significant GO terms for Profile 46 (n =95)						
Category ID	**Genes in Category**	**Count Genes**	**Genes Expected**	**Genes Enriched**	**p-value**	**Corrected p-value**
cytoplasm	276	17.0	5.1	+11.9	2.2E-5	0.005
membrane fraction	21	5.0	0.4	+4.6	3.6E-5	0.007
Significant GO terms for Profile 4 (n =163)						
Category ID	**Genes in Category**	**Count Genes**	**Genes Expected**	**Genes Enriched**	**p-value**	**Corrected p-value**
AFU-SPECIFIC	112	20.0	2.2	+17.8	7.8E-14	1.6E-11
Semi-subT	403	25.0	7.9	+17.1	6.3E-7	1.3E-4
SECMET	96	11.0	1.9	+9.1	3.1E-6	6.4E-4
structural constituent of ribosome	15	5.0	0.3	+4.7	7.3E-6	0.002
In vitro pH response genes	254	17.0	5.0	+12.0	1.4E-5	0.003
AFFC specific	52	7.0	1.0	+6.0	6.8E-5	0.014
Subtelomeric	430	21.0	8.4	+12.6	1.5E-4	0.032
Significant GO terms for Profile 3 (n =76)						
Category ID	**Genes in Category**	**Count Genes**	**Genes Expected**	**Genes Enriched**	**p-value**	**Corrected p-value**
Transposition	20	9.0	0.3	+8.7	5.3E-12	1.1E-9
Significant GO terms for Profile 29 (n =75)						
Category ID	**Genes in Category**	**Count Genes**	**Genes Expected**	**Genes Enriched**	**p-value**	**Corrected p-value**
Subtelomeric	430	29.0	3.6	+25.4	2.3E-17	4.7E-15
IC	284	19.0	2.4	+16.6	7.6E-12	1.6E-9
In vitro pH response genes	254	18.0	2.1	+15.9	1.0E-11	2.1E-9
SECMET	96	8.0	0.8	+7.2	1.7E-6	3.5E-4
Semi-subT	403	13.0	3.4	+9.6	4.8E-5	0.010
Significant GO terms for Profile 47 (n =70)						
Category ID	**Genes in Category**	**Count Genes**	**Genes Expected**	**Genes Enriched**	**p-value**	**Corrected p-value**
molecular function unknown	143	12.0	2.7	+9.3	1.8E-5	0.004

Table 4.14: Significant GO terms among profiles 0, 12, 1, 9, 49, 48, 42, 47, 29 in the ATCC46645 Δ*pacC* time course experiment. For each significant profile identified by STEM, corrected p-values based on the expected number of genes assigned to the profile, and satisfying the cut-off of <0.05.

The model profiles from the ATCC46645 STEM analysis were ordered according to the significance of IC enrichment, and other functional classifications (Section 4.3.2). Likewise (Fig. 4.21), a STEM clustering analysis was performed on the ATCC46645 Δ*pacC* dataset to interrogate the presence of Af293 infection cluster genes in the dataset (McDonagh *et al.*, 2008a) (unabridged output is reported in Appendix D). Model profiles are coloured according to significance in the initial analysis, however, red profiles now indicate IC gene profiles.

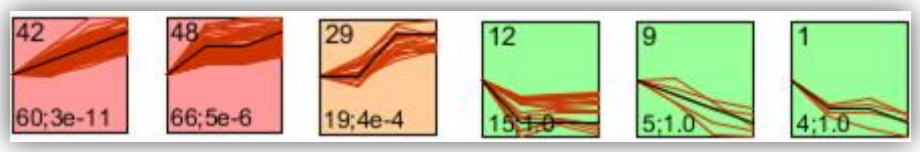


Fig. 4.21: Selection of STEM clustering analysis of differentially expressed genes in the ATCC46645 Δ*pacC* time course during initiation of murine infection ordered on the basis of the Af293 infection clusters (McDonagh *et al.*, 2008a). The two values at the bottom of each profile indicate the number of specific genes (in this case genes previously identified in the Af293 infection clusters) are present in the profile and the significance of the intersect size, based upon the hypergeometric distribution of dataset genes in the respective model profiles.

The whereabouts of subtelomeric genes within the ATCC46645 Δ*pacC* time course dataset was also examined (Fig. 4.22) (unabridged output is reported in Appendix D).



Fig. 4.22: Selection of STEM clustering analysis of the differentially expressed genes in the ATCC46645 Δ*pacC* time course during initiation of murine infection ordered on the basis of the subtelomeric gene inclusion. For each profile indicate are indicated the number of genes (in this case genes with subtelomeric location) and the significance of the intersect size, based upon the hypergeometric distribution of dataset genes in the respective model profiles.

A. fumigatus annotation was also extended for genes involved in the production of secondary metabolites, using predictions made by Perrin *et al.*, 2007 and STEM model profiles were ordered by enrichment for this functional category to examine the effect of *pac*C deletion upon secondary metabolism genes (Fig. 4.23) (unabridged output is reported in Appendix D). In contrast to results obtained in the ATCC46645 analysis, where only model profiles containing up-regulated genes (42 and 29) were significantly enriched in genes predicted to be involved in secondary metabolism, profile 4, to which down-regulated genes are assigned, contains eleven ORFs identified by Perrin *et al.*, 2007 as involved in secondary metabolite production.

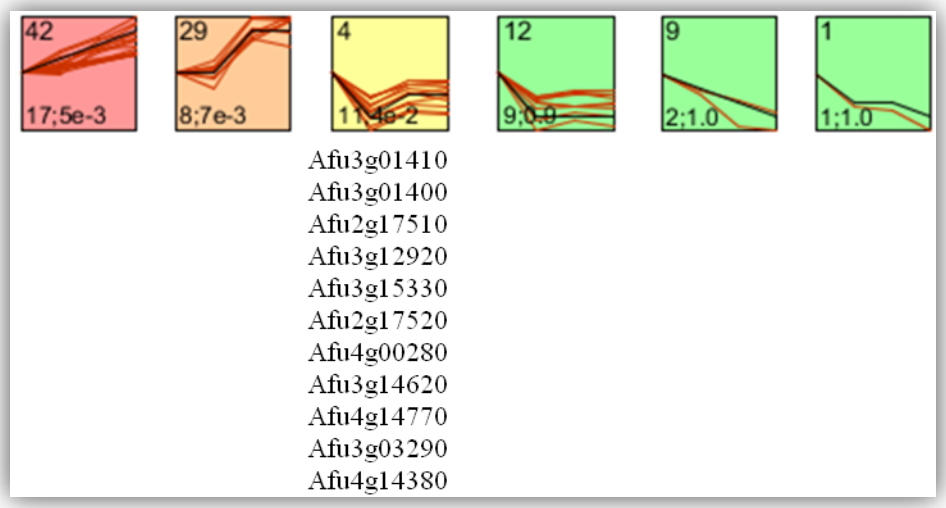


Fig. 4.23: Selection of STEM clustering analysis of the differentially expressed genes in the ATCC46645 Δ*pacC* time course during initiation of murine infection ordered on the basis of secondary metabolism gene inclusion. For each profile the number of assigned genes (in this case genes involved in secondary metabolite production) are indicated as well as the significance of the intersect size, based upon the hypergeometric distribution of dataset genes in the respective model profiles.

Given the role of PacC in regulating pH-dependent gene expression, the inclusion of alkaline-responsive genes among those differentially expressed genes in the ATCC46645 Δ*pacC* time course was intriguing. This was addressed by STEM analysis (Fig. 4.24 and Fig. 4.25) (unabridged output is reported in Appendix D). As illustrated in Fig. 4.24, only model profiles containing up-regulated genes across the ATCC46645 Δ*pacC* time course (29, 48 and 42) were significantly enriched in genes annotated as up-regulated *in vitro* at high pH and must correspond to alkaline-responsive genes regulated independently of PacC regulation. As illustrated in Fig. 4.25, comparison with the down-regulated *in vitro* pH response genes, revealed a differential behaviour in murine and *in vitro* experimentation for several genes in profiles 49 and 45, which are instead up-regulated *in vivo* in ATCC46645 Δ*pacC* during initiation of murine infection. Only three of these genes (Afu5g04230, Afu1g07380, and Afu5g03750) were found to behave in an opposite manner *in vivo* and *in vitro* when analysing the ATCC46645 transcriptional profile. The remainder may correspond to PacC-repressible functions.



Fig. 4.24: Selection of STEM clustering analysis of the differentially expressed genes in the ATCC46645 Δ*pacC* time course during initiation of murine infection ordered on the basis of *in vitro* alkaline-responsive gene inclusion. For each profile the number of assigned genes (in this case up-regulated genes in response to an alkaline pH shift) are indicated, as well as the significance of the intersect size, based upon the hypergeometric distribution of dataset genes in the respective model profiles.

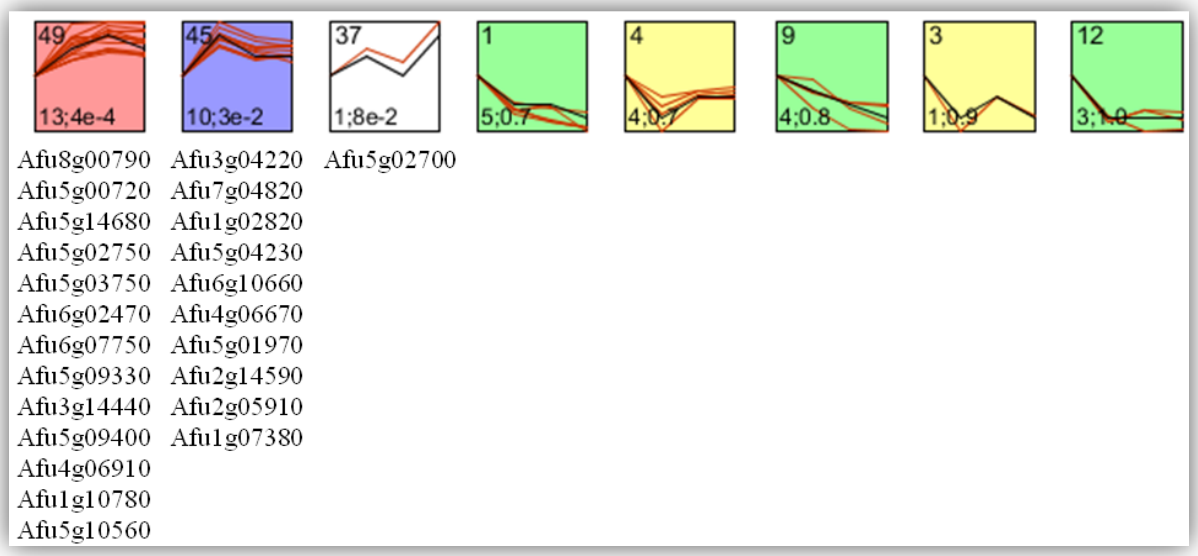


Fig. 4.25: Selection of STEM clustering analysis of the differentially expressed genes in the ATCC46645 Δ*pacC* time course during initiation of murine infection ordered on the basis of *in vitro* alkaline-down-regulated gene inclusion. For each profile the number of genes assigned (in this case down-regulated genes in response to an alkaline pH shift) are indicated, as well as the significance of the intersect size, based upon the hypergeometric distribution of dataset genes in the respective model profiles.

A. fumigatus STEM analysis was also selectively extended to genes putatively involved in transposition. (Fig. 4.26) (unabridged output is reported in Appendix D). In this analysis only model profiles containing down-regulated genes across the ATCC46645 Δ*pacC* time course (3 and 4) were significantly enriched in genes involved in transposition, confirming the trend observed in the GO analysis (Table 4.11).

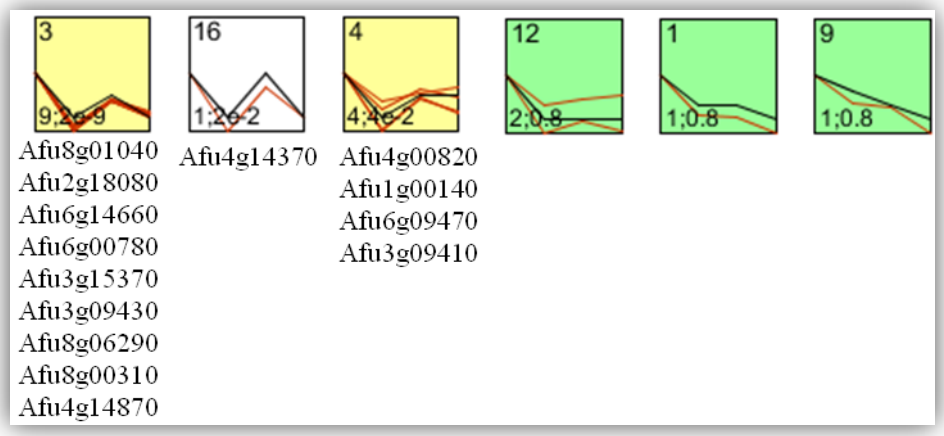
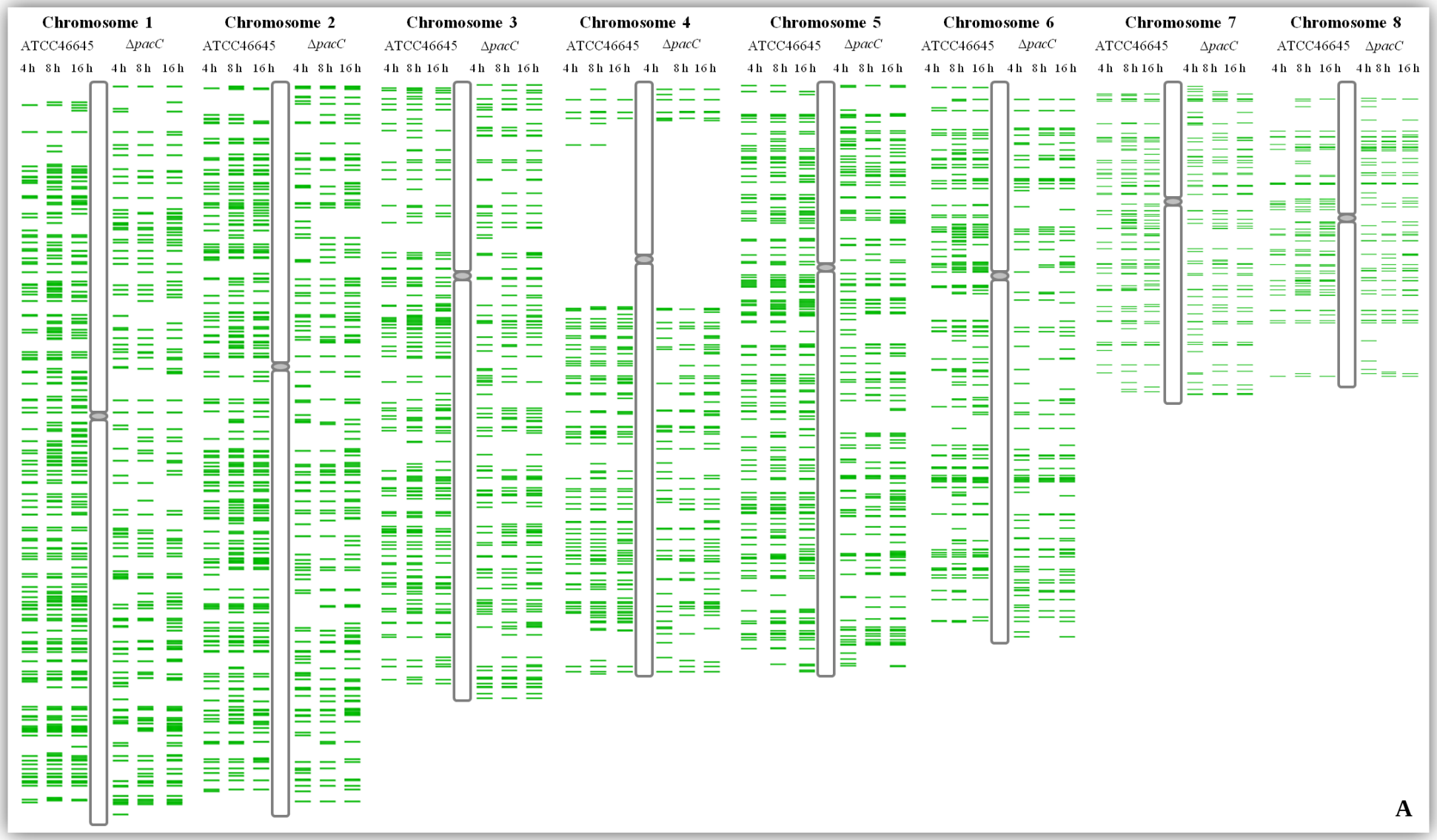


Fig. 4.26: Selection of STEM clustering analysis of the differentially expressed genes in the ATCC46645 Δ*pacC* time course during initiation of murine infection ordered on the basis of transposition gene inclusion. For each profile the number of assigned genes is indicated (in this case genes involved in transposition) as well as the significance of the intersect size, based upon the hypergeometric distribution of dataset genes in the respective model profiles.

To identify general trends crucial for *A. fumigatus* infection and affected by PacC deletion, a genome-wide comparison between the two sets of differentially expressed genes in the ATCC46645 and ATCC46645 Δ*pacC* time courses during initiation of murine infection was performed utilising the genome browser function of Genespring GX 11.02. This comparison is graphically represented in Figure 4.27, which aligns the up-regulated (A) and down-regulated genes (B) genes (fold change cut off of ±2 on a $\log_2$ scale) for the wild type and ATCC46645 Δ*pacC* time course (4, 8 and 16 hours post-infection) experiments according to chromosomal locus.


Chromosome 1
Chromosome 2
Chromosome 3
Chromosome 4
Chromosome 5
Chromosome 6
Chromosome 7
Chromosome 8
ATCC46645
ΔpacC
4h 8h 16h 4h 8h 16h
A


Chromosome 1
Chromosome 2
Chromosome 3
Chromosome 4
Chromosome 5
Chromosome 6
Chromosome 7
Chromosome 8
ATCC46645
ΔpacC
4h 8h 16h
B

Fig. 4.27: Genome-wide comparison of transcriptome in the *A. fumigatus* ATCC46645 Δ*pacC* and respective parental strain during initiation of murine infection. According to their location on the eight *A. fumigatus* chromosomes, green (A) and red (B) lines correspond respectively to down- and up-regulated genes for the three time points (4 hrs, 8 hrs and 16 hrs) studied.

As shown in Fig. 4.28, the overlap between the ATCC46645 and ATCC46645 Δ*pacC* datasets extends to 1573 genes (A), of which 816 are up-regulated (A.1) and 719 are down-regulated (A.2).

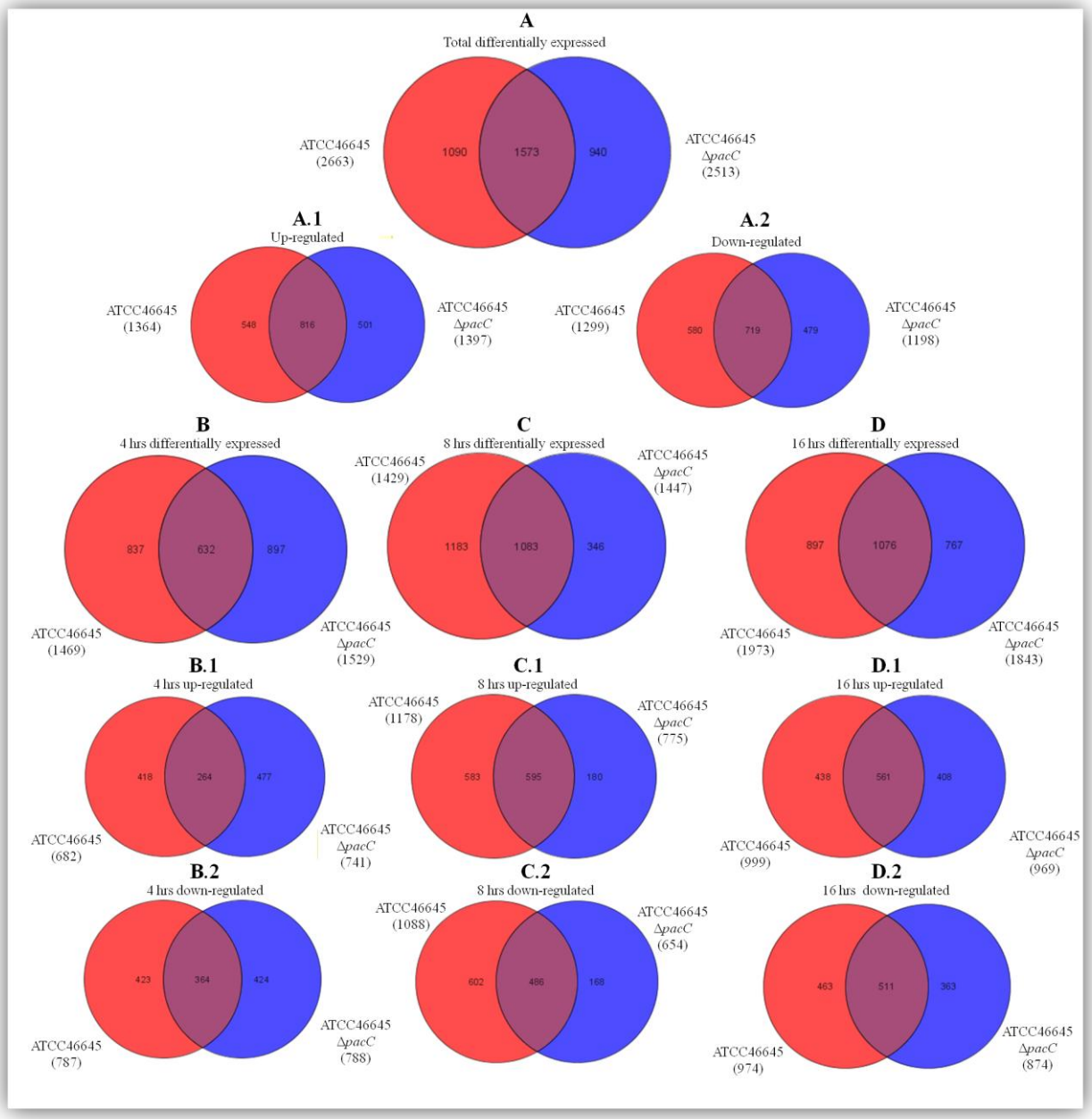


Fig. 4.28: Venn diagrams comparing datasets of differentially expressed genes during initiation of murine infection for the wild type ATCC46645 and the ATCC46645 Δ*pacC* mutant. Analysis performed using Genespring GX 11.02.

STEM permits the comparison of gene expression data sets from two different experimental conditions, allowing the identification of genes which are co-expressed under both experimental conditions. STEM pairs model profiles from two experiments identifying intersecting gene sets which are coexpressed in both experiments, implicating commonality of function. Using STEM gene expression time courses for the wild type ATCC46645 and the ATCC46645 Δ*pacC* mutant were compared to identify statistically significant sets of genes which were co-expressed in both experiments. The maximum uncorrected intersection p-value set to 0.05 and the minimum number of genes in the intersection of the set of genes assigned to two profiles to 5 (Fig. 4.29). Output data are ordered according to correlation between matched profiles (test set and comparison set organised to the left and the right, respectively) of the yellow bar. For intersections in which temporal expression of co-expressed genes differs between the two datasets (based upon an arbitrary cut-off of correlation coefficient equal to 0.7 or less) GO enrichment analysis was performed. The number of intersecting genes, and the significance of the intersection are indicated in bottom left hand corners of every model profile returned from the comparison.

Profile 3 of the ATCC46645 Δ*pacC* dataset and profile 8 of the ATCC46645 dataset contain a set of 10 intersecting co-expressed genes having an altered temporal expression profile in the Δ*pacC* mutant, relative to the wild type (correlation coefficient=0.2). This revealed a specific trend of down-regulation for these 10 genes in the ATCC46645 Δ*pacC* mutant in the murine niche. GO enrichment analysis revealed 8 of these genes are putatively involved in transposition, thereby indicating similarity of function for these genes and suggesting the existence of a common regulatory mechanism for them.

Profiles 48 and 46 of the ATCC46645 Δ*pacC* dataset have intersections containing co-expressed genes (22 and 14 genes, and correlation co-efficients of 0.62 and 0.64 respectively) with profile 47 of the ATCC46645 dataset. Although the three profiles contain up-regulated genes, a deviation in temporal gene expression is observable at 16 hrs post-infection, whereby a decrease in gene expression in the wild type strain is not observed in the mutant. GO enrichment analysis revealed 5 of the 22 genes in the ATCC46645 Δ*pacC* profile 48 intersection as belonging to infection clusters identified in Af293 (McDonagh *et al.*, 2008a). Among 14 co-expressed genes in the ATCC46645 Δ*pacC* profile 46, six of them are located in subtelomeric regions of the genome.

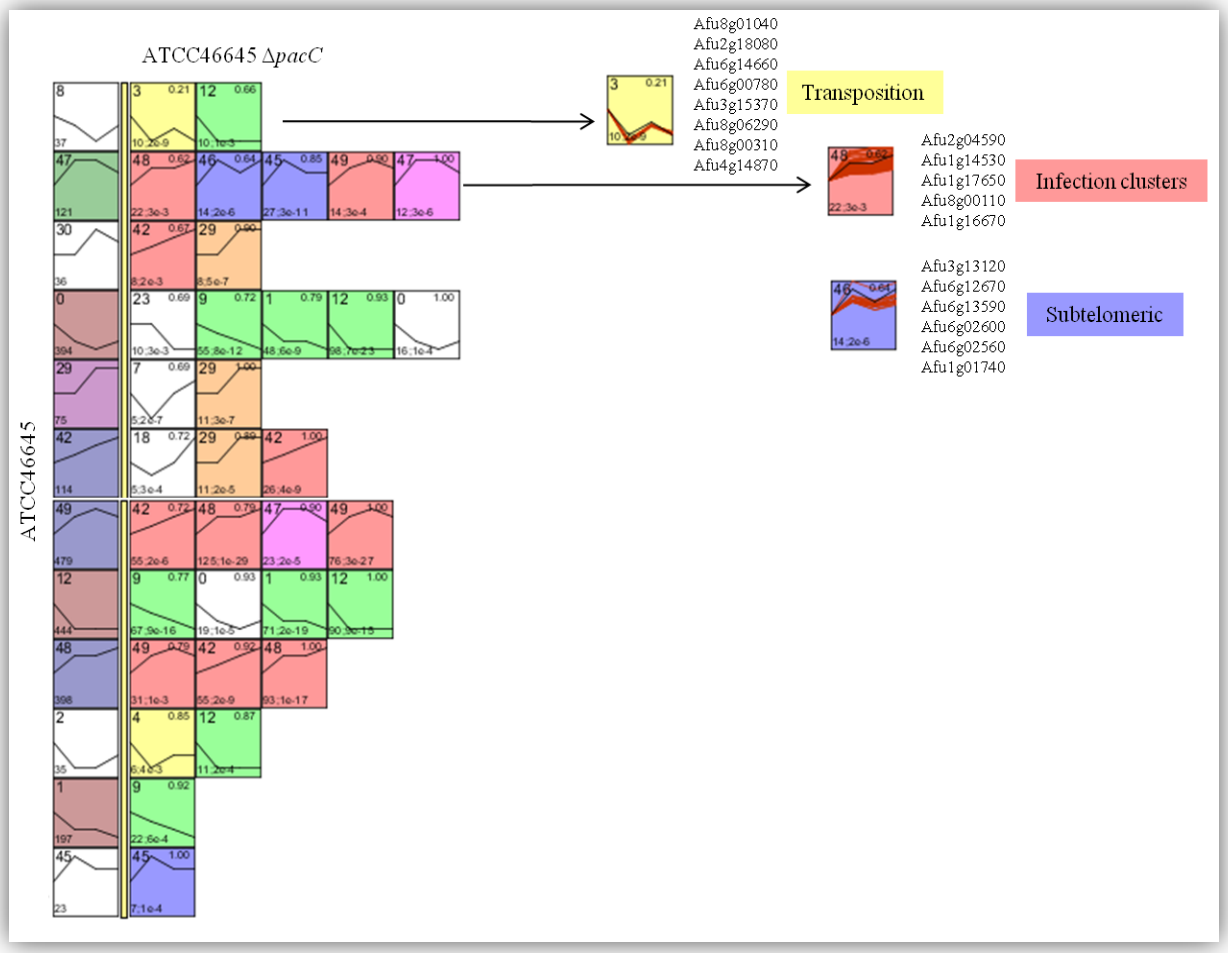


Fig. 4.29: Comparison of the ATCC46645 and ATCC46645 Δ*pacC* time course datasets. The immediate left of the vertical yellow bar contains the "Original set profiles", in this case from the ATCC46645 time course, whereas to the right of the yellow bars are reported the "Comparison Set Profiles", in this case from the ATCC46645 Δ*pacC* time course. A profile appears to the right of the yellow bar if the intersection satisfies the minimum size of 5 and p-value not greater than 0.05 (reported in bottom left of each profile intersection). Profiles which cluster with respect to similar temporal expression profiles are similarly coloured. Analysis performed using STEM.

4.3.4 Directly comparative analysis of *A. fumigatus* ATCC46645 and ATCC46645 Δ*pacC* transcription during initiation of murine infection

A directly comparative study of transcription was performed by hybridising doubly amplified fungal RNA, extracted from BALFs harvested, for each strain, at 3 time points (4, 8 and 16 hrs) as shown in Fig. 4.30.

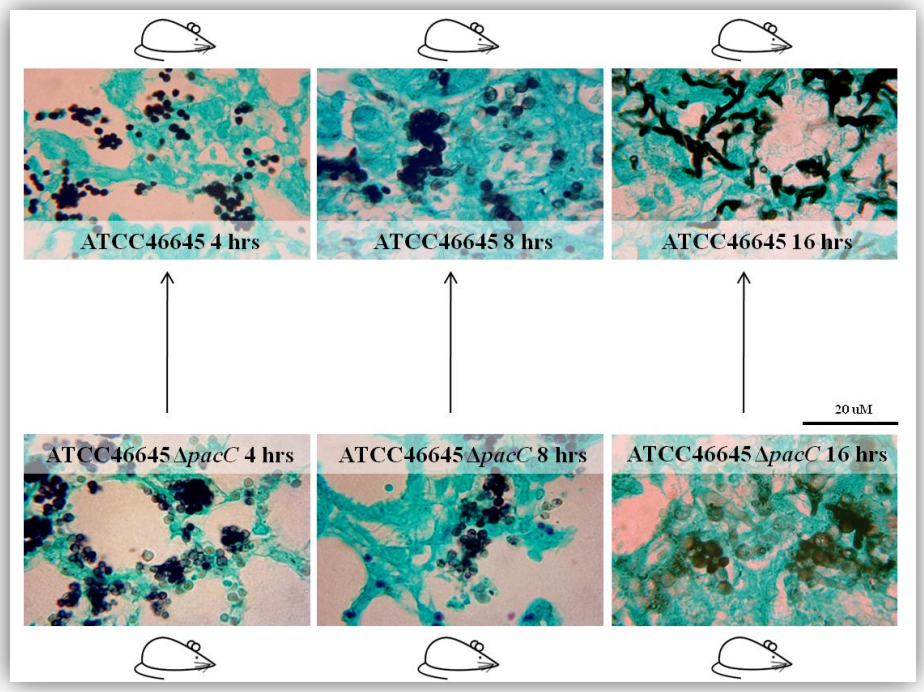


Fig. 4.30: Schematic representation of the hybridisations performed to directly compare *A. fumigatus* ATCC46645 and ATCC46645 Δ*pacC* host adapting transcriptional profiles.

Fig. 4.31, 4.32 and 4.33 show microarray (MA) and box plots of the datasets for each of the three time points studied, both before and after normalisation. The MA plots for each time point (A) show the distribution of data before (UN-NORMALISED) and after (NORMALISED) LOWESS normalisation thereby depicting the dataset adjustments implemented by normalisation. In MA plots the $\log_2$ ratio between red and green channels (Y-axis) is plotted against the sum of red and green channels (X-axis). Normalisation adjusts for the higher measured spot intensities associated with the green dye (Cy3). Box plots (B) also show dataset $\log_2$ ratio distributions for each time point before (UN-NORMALISED) and after LOWESS normalisation (NORMALISED) but on a slide specific basis. After normalisation the medians of the blocks are all equal to zero and the standard deviation is regularised.

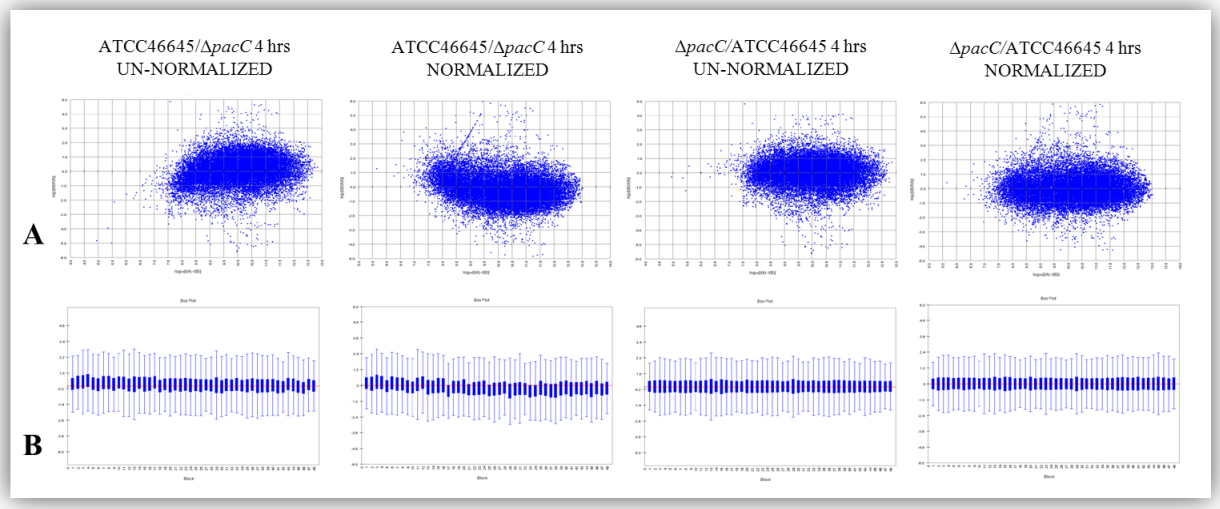


Fig. 4.31: Data normalisation plot for the ATCC46645 Δ*pacC*/ATCC46645 4 hrs analysis. Pairwise MA (A) and box plots (B) for the 4 hour time point of ATCC46645 Δ*pacC* versus ATCC46645 RNA. Datasets plotted before (UN-NORMALISED) and after (NORMALISED) LOWESS normalisation are shown.

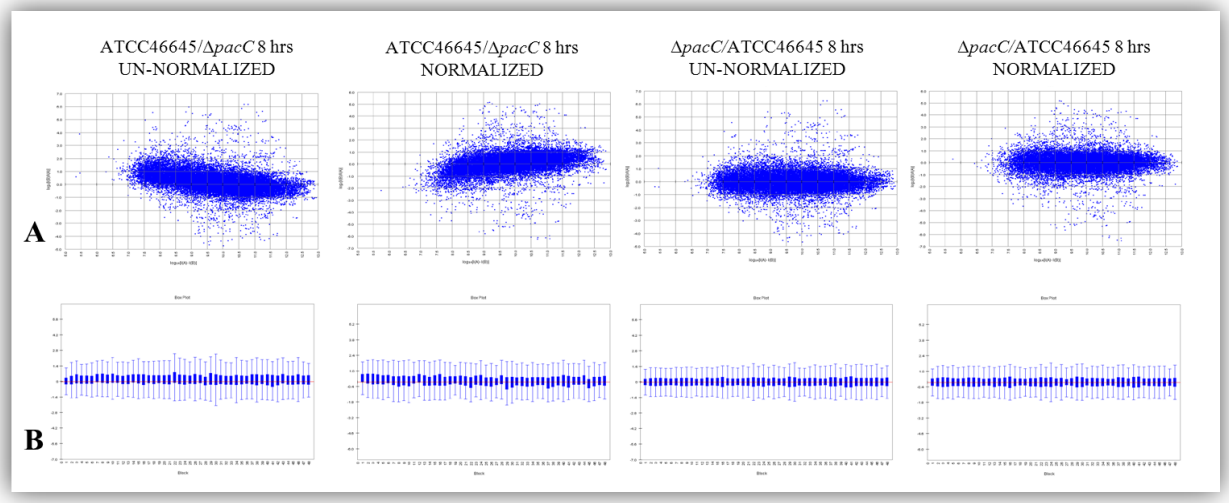


Fig. 4.32: Data normalisation plot for theATCC46645 Δ*pacC*/ATCC46645 8 hrs analysis. Pairwise MA (A) and box plots (B) for the 8 hour time point of ATCC46645 Δ*pacC* versus ATCC46645 RNA. Datasets plotted before (UN-NORMALISED) and after (NORMALISED) LOWESS normalisation are shown.

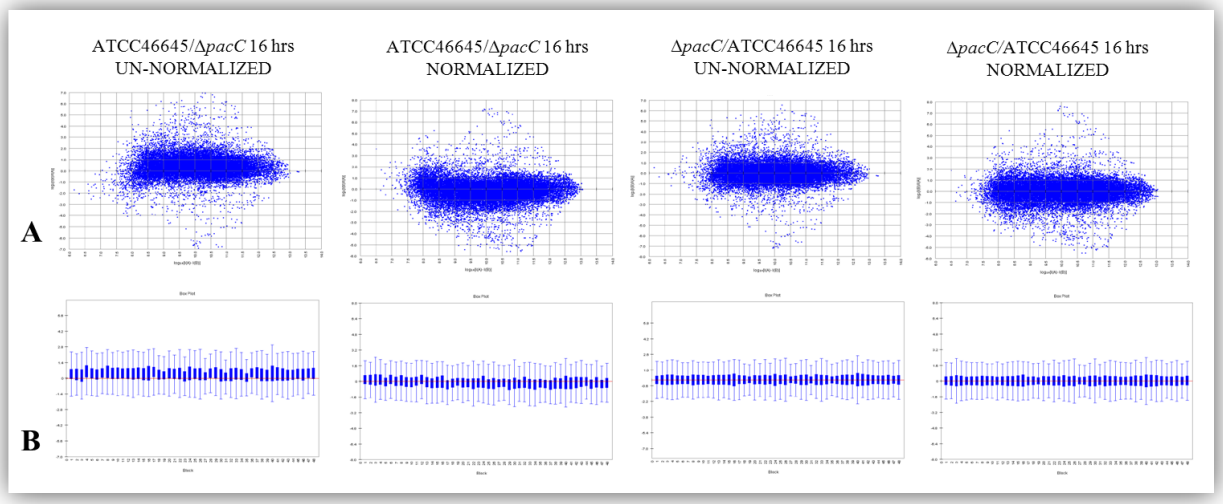


Fig. 4.33: Data normalisation plot for the ATCC46645 Δ*pacC*/ATCC46645 16 hrs analysis. (A) Pairwise MA (A) and box plots (B) for the 16 hour time point of ATCC46645 Δ*pacC* versus ATCC46645 RNA. Datasets plotted before (UN-NORMALISED) and after (NORMALISED) LOWESS normalisation are shown.

Among a total of 8243 genes represented on the slides, 8034, 7915 and 7442, returned detectable signals for the 4, 8 and 16 hrs time points, respectively (Table 4.15).

	ATCC46645 Δ*pacC* vs ATCC46645 4 hrs	ATCC46645 Δ*pacC* vs ATCC46645 8 hrs	ATCC46645 Δ*pacC* vs ATCC46645 16 hrs
Observations	8034	7915	7442
Missing observations	210	320	802
Minimum value	-5.70	-4.85	-7.37
Maximum value	4.18	6.32	5.71
Mean	0.0119	-0.0053	0.0079
Median	0.06	-0.03	-0.02
Standard deviation	0.8784	0.7167	0.9574
Outliers	226	365	340

Table 4.15: Summary statistics for the ATCC46645 Δ*pacC*/ATCC46645 comparison *in vivo*.

Bioinformatic analysis of the dataset was conducted in Genespring GX 11.02 where normalised $\log_2$ expression ratios were filtered on expression level and differentially regulated transcripts were defined as having $\log_2$ (Cy5/Cy3) greater than the arbitrary threshold of ±1.5. The numbers of genes identified following these criteria as up-regulated, down-regulated or in general differentially regulated for each of the 3 time points in the ATCC46645

Δ*pacC*/ATCC466645 comparison are shown in Table 4.16. Among a total of 1491 (15.0% of *A. fumigatus* genome, Nierman *et al.*, 2005) differentially expressed genes across the entire comparison, 729 were up-regulated and 762 were down-regulated in at least one time point of the dataset. The complete lists of the differentially expressed genes are attached in the Supplementary Data CD, as listed in Appendix D.

	Up-regulated	Down-regulated	Differentially expressed
TOTAL	729	762	1491
4 hrs	217	385	602
8 hrs	161	134	295
16 hrs	351	243	594

Table 4.16: Number of differentially expressed genes in the ATCC46645 Δ*pacC*/ATCC46645 comparison.

The temporal basis of gene regulation in the ATCC46645 Δ*pacC* time course relative to the parental strain ATCC46645 is simply depicted in 3-way Venn diagrams in Fig 4.34. In addition, the entire dataset of differentially expressed genes is detailed in a heat map attached in the Supplementary Data CD, as listed in Appendix D.

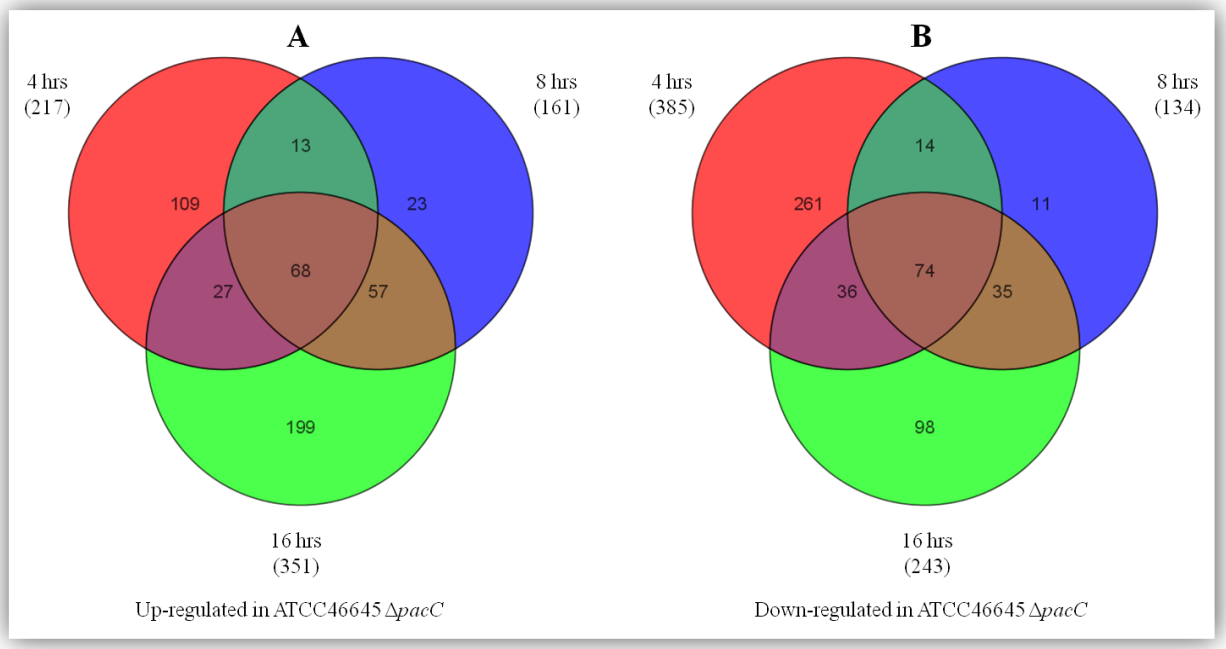


Fig. 4.34: Three-ways Venn diagrams depicting temporal aspects of differential gene expression in the ATCC46645 Δ*pacC*/ATCC466645 comparison during initiation of murine infection. Up-regulated (A) and down-regulated genes (B) have been identified using a fold change cut off of ±1.5 on a $\log_2$ scale. Analysis performed using Genespring GX 11.02.

Among a total of 729 up-regulated genes, 68 were similarly differentially expressed at all 3 time points, as listed in Table 4.17. Several of these genes are involved in the transport of various nutrients across the plasma membrane, such as sugars (Afu7g05550, Afu6g04270, Afu8g06870), amino acids (Afu2g17790), cytosine (Afu2g09860), zinc (Afu2g03860) and phosphate (Afu2g10690). Several transporters belong to the major facilitator superfamily (MFS), a group of multidrug resistance (MDR) transporter, whose substrates are still poorly characterised (Sa-Correia *et al.*, 2009). Multiple ORFs are involved in cell wall biogenesis and organisation (Afu3g02040, Afu1g15440, Afu4g10150). Interestingly, the sexual development protein EsdC (Afu7g01930) is up-regulated in the ATCC46645 Δ*pacC* relative to the parental strain ATCC466645 during initiation of murine infection. To aid the evaluation of phase-specific up-regulated genes Tables AD.3.2-AD.3.4 in Appendix D list thirty ORFs having the greatest fold changes among up-regulated genes specific to each of the 4, 8 and 16 hrs time points.

Among a total of 762 down-regulated genes, 74 were similarly differentially expressed at all 3 time points, as listed in Table 4.18. These genes can be assigned to similar functional categories as those in the corresponding up-regulated geneset (Table 4.17) which likely reflects the role of PacC as both a repressor and activator of pH-responsive genes. Several of these genes are involved in the transport of various nutrients across the plasma membrane, such as sugars (Afu6g14500), zinc (Afu6g00470, Afu4g09560) and phosphate (Afu8g01850). However, transporters of elements such as iron (Afu6g13750), calcium (Afu7g01030 and Afu3g10690) and sodium (Afu2g01320, Afu4g09440) are uniquely found among the down-regulated genes relative to the parental strain ATCC466645. Several ORFs involved in cell wall biogenesis and organisation (Afu7g05610, Afu2g14490, Afu6g11390, Afu2g14540) are also present. To aid the evaluation of phase-specific down-regulated genes in the ATCC46645 Δ*pacC*/ATCC46645 comparison, Tables AD.3.6-AD.3.8 in Appendix D list the thirty ORFs having greatest fold changes at each of the three time points. Among genes specifically down-regulated at 4 and 16 hrs post infection an enrichment for ORFs putatively involved in transposition (Afu6g14660, Afu4g00820, Afu4g14870, Afu2g18080, afu6g09470, Afu6g00780, Afu8g06290, Afu8g00310, Afu8g01040) is observable. At 8 hours these genes are moderately up-regulated (with the sole exception of Afu8g06290) with respect to the wild type.

Table 4.17: 68 up-regulated ORFs in common for the 3 time points (4 hrs, 8 hrs and 16 hrs) of the ATCC46645 Δ*pacC*/ATCC46645 comparison.

ORFs	T4	T8	T16	Annotation	Functional classification
Afu7g05550	4.175793	6.317348	5.587271	sugar transporter family protein	lactate transmembrane transporter activity///lactate transport///plasma membrane
Afu7g04950	3.926574	2.624316	2.603744	lipase, putative	
Afu7g04910	3.91836	6.050162	5.280204	phosphatidylglycerol specific phospholipase C, putative	
Afu2g17790	3.896936	5.420857	5.166142	amino acid transporter, putative	
Afu3g02040	3.746189	5.254534	4.7594	glycosyl hydrolase, putative	membrane fraction///fungal-type cell wall biogenesis///anchored to plasma membrane///molecular function unknown
Afu8g02060	3.723205	5.266514	5.04937	glycan biosynthesis protein (PigL), putative	endoplasmic reticulum///hydrolase activity
Afu1g03570	3.698552	5.100834	5.093108	acid phosphatase PHOa	
Afu4g14000	3.526856	4.978075	5.625625	tripeptidyl peptidase A	protein catabolic process///serine-type endopeptidase activity
Afu8g01260	3.473357	4.504778	3.936613	hypothetical protein	
Afu6g03360	3.413945	2.829504	2.309741	oxidoreductase, zinc-binding	cytoplasm///nucleus///biological process unknown///alcohol dehydrogenase (NADP+) activity
Afu2g09860	3.364603	4.368039	4.333609	purine-cytosine permease	purine transport///cytosine transport///cytosine-purine permease activity///plasma membrane
Afu8g02070	3.188502	4.379067	4.185896	glycosyl transferase, putative	fungal-type vacuole///"transferase activity, transferring glycosyl groups"///biological process unknown
Afu6g04270	3.104719	3.231792	4.351751	fructose symporter	membrane///myo-inositol transport///myo-inositol transmembrane transporter activity
Afu7g04930	3.081243	2.018681	3.62872	alkaline serine protease (PR1), putative	protein catabolic process///cellular component unknown///peptidase activity
Afu1g11250	3.064082	1.525513	2.960487	amidohydrolase, putative	proteolysis///carboxypeptidase activity
Afu2g03860	2.981831	3.334712	4.044913	plasma membrane low affinity zinc ion transporter, putative	low-affinity zinc ion transmembrane transporter activity///low-affinity zinc ion transport///plasma membrane
Afu8g02050	2.965567	4.341667	4.125514	hypothetical protein	
Afu8g01970	2.876005	4.263019	3.673103	extracellular endo-polygalacturonase, putative	pectin catabolic process///pseudohyphal growth///extracellular region///polygalacturonase activity
Afu2g17800	2.68522	4.326293	3.936312	C6 transcription factor, putative	
Afu1g03490	2.614601	1.831615	1.826264	conserved hypothetical protein	
Afu5g13300	2.601901	4.370506	5.717124	aspartic endopeptidase Pep1	protein catabolic process///aspartic-type endopeptidase activity///extracellular region///pathogenesis
Afu8g02090	2.597404	4.356246	4.31544	nucleotide-sugar	integral to plasma membrane

				transporter family protein	
Afu8g02040	2.543908	3.958048	4.145863	glycosyl transferase, putative	N-linked glycoprotein maturation///"transferase activity, transferring glycosyl groups"
Afu2g16860	2.542182	3.395212	3.139038	membrane transporter	drug transport///drug transporter activity///integral to membrane
Afu7g08540	2.507654	2.19692	2.047114	ankyrin repeat protein	
Afu5g03750	2.502965	2.641063	3.028794	WW domain protein	
Afu6g00230	2.489269	1.7238	1.918675	isoflavone reductase family protein	
Afu1g15440	2.430342	2.289956	1.816144	alpha-1,3-glucan synthase, putative	cellular glucan metabolic process///fungal-type cell wall biogenesis///plasma membrane///pathogenesis///"alpha-1,3-glucan synthase activity"///cell morphogenesis
Afu1g01730	2.429553	2.12989	2.352826	glycosyl hydrolase, putative	membrane fraction///fungal-type cell wall biogenesis///anchored to plasma membrane
Afu1g12240	2.384094	4.672033	4.825639	MFS peptide transporter, putaitve	peptide transporter activity///plasma membrane///peptide transport
Afu2g17780	2.379672	1.973376	2.608322	hypothetical protein	
Afu7g01930	2.362303	2.264808	2.883049	sexual development protein EsdC, putative	GTP binding
Afu7g01490	2.343722	3.670149	4.50575	MFS peptide transporter, putative	peptide transporter activity///plasma membrane///peptide transport
Afu6g03230	2.301067	3.139545	1.81531	cell wall glucanase, putative	hydrolase activity, hydrolyzing O-glycosyl compounds///cellular glucan metabolic process///fungal-type cell wall
Afu5g06290	2.300585	1.57533	2.879125	MFS transporter, putative	nicotinamide mononucleotide transport///nicotinamide mononucleotide permease activity///integral to plasma membrane///transporter activity///transport
Afu6g00160	2.287963	1.612811	2.412885	Ser/Thr protein phosphatase family protein	phosphate metabolic process///phosphoric ester hydrolase activity///fungal-type vacuole
Afu6g14440	2.28792	3.410211	4.332058	MFS monosaccharide transporter, putative	response to glucose stimulus///plasma membrane///glucose transmembrane transporter activity///signal transduction///glucose binding///receptor activity
Afu8g02130	2.28665	3.44073	2.971659	1,3-beta-glucanosyltransferase, putative	cell wall organisation///cellular glucan metabolic process///"1,3-beta-glucanosyltransferase activity"///anchored to plasma membrane
Afu6g00430	2.283747	2.252905	3.478899	IgE-binding protein	
Afu5g07250	2.237775	1.718106	1.650559	DUF300 domain protein, putative	
Afu6g13710	2.232682	2.269822	2.409657	hypothetical protein	
Afu1g15940	2.10417	1.667671	1.754036	Auxin Efflux Carrier superfamily	endoplasmic reticulum///biological process unknown///molecular

					function unknown
Afu6g03260	2.095991	1.834628	2.978108	aspartic endopeptidase (AP1), putative	aspartic-type endopeptidase activity///protein metabolic process
Afu2g03510	2.095412	2.601344	3.272029	pheromone processing carboxypeptidase (Sxa2), putative	trans-Golgi network///carboxypeptidase D activity///protein processing///pheromone-dependent signal transduction involved in conjugation with cellular fusion
Afu1g11060	2.093834	1.898946	2.105986	ubiquitin domain protein, putative	protein tagging activity
Afu2g17480	2.075763	2.844162	1.691341	amino acid transporter, putative	
Afu5g10320	2.041693	2.750266	2.635519	toxin biosynthesis protein (GliH), putative	
Afu4g10150	2.007181	2.48935	3.190924	alpha-glucosidase	alpha-glucosidase activity///fungal-type cell wall biogenesis///endoplasmic reticulum
Afu8g06560	1.984356	2.355302	3.511185	DUF895 domain membrane protein	
Afu6g07750	1.912118	1.993151	2.4586	MFS phospholipid transporter (Git1), putative	phospholipid transporter activity///phospholipid transport///plasma membrane
Afu5g10350	1.886612	3.16846	3.590186	conserved hypothetical protein	
Afu1g02730	1.885592	1.826359	1.82254	mitochondrial phosphate carrier protein (Ptp), putative	mitochondrial envelope///inorganic phosphate transmembrane transporter activity///mitochondrion///phosphate transport
Afu3g08990	1.872484	2.080799	2.092822	hypothetical protein	
Afu2g15240	1.823145	3.90622	5.275664	small oligopeptide transporter, OPT family	sulfur metabolic process///oligopeptide transporter activity///integral to plasma membrane///endoplasmic reticulum
Afu5g10340	1.819392	2.310857	2.194829	MFS transporter, putative	membrane///transporter activity///transport
Afu3g00470	1.781531	4.620455	5.052703	endo-1,4-beta-xylanase, putative	xylan metabolic process
Afu8g06870	1.758739	2.950008	3.317154	MFS sugar transporter, putative	mannose transmembrane transporter activity///hexose transport///fructose transmembrane transporter activity///plasma membrane///glucose transmembrane transporter activity
Afu3g00560	1.748148	2.19679	1.513076	conserved hypothetical protein	
Afu6g14020	1.714603	2.277314	2.925721	conserved hypothetical protein	
Afu6g00220	1.694713	2.450534	2.411222	fungal specific transcription factor, putative	transcription factor activity///nucleus///regulation of transcription
Afu2g17730	1.668651	2.508534	3.165124	MFS multidrug transporter, putative	integral to plasma membrane///multidrug transporter activity///response to toxin
Afu2g00180	1.651918	2.351271	2.351043	neutral amino acid permease	
Afu3g02970	1.635816	4.987893	4.891337	aspergillopepsin, putative	
Afu5g06670	1.592823	2.238361	2.820534	related to L-fucose	

				permease, putative	
Afu2g10690	1.583959	2.539124	3.414005	MFS phosphate transporter, putative	integral to plasma membrane///inorganic phosphate transmembrane transporter activity///phosphate transport
Afu6g10160	1.57446	3.416952	2.119306	hypothetical protein	
Afu3g13640	1.560996	2.265358	2.088059	extracellular serine-rich protein	
Afu2g17770	1.503121	3.490145	3.710501	conserved hypothetical protein	

Table 4.18: 74 down-regulated ORFs in common for the 3 time points (4 hrs, 8 hrs and 16 hrs) of the ATCC46645 Δ*pacC*/ATCC46645 comparison.

ORFs	T4	T8	T16	Description	Annotation
Afu4g09320	-5.70488	-3.6869	-6.06983	antigenic dipeptidyl-peptidase Dpp4	proteolysis///serine-type peptidase activity///aminopeptidase activity
Afu8g02550	-5.63989	-3.67786	-2.73562	Ptr2-like MFS peptide transporter, putative	peptide transporter activity///plasma membrane///peptide transport
Afu8g01850	-5.48612	-2.47323	-3.55294	phosphate-repressible phosphate permease	sodium:inorganic phosphate symporter activity///plasma membrane///phosphate transport
Afu6g13750	-5.45038	-4.1642	-5.5474	ferric-chelate reductase, putative	ferric-chelate reductase activity///transition metal ion transport///integral to membrane
Afu3g03010	-5.35211	-2.98665	-2.88884	phosphate-repressible phosphate permease	sodium:inorganic phosphate symporter activity///plasma membrane///phosphate transport
Afu8g02450	-5.13943	-3.62022	-4.96588	hypothetical protein	
Afu6g12240	-4.95213	-4.27884	-5.18859	Glycerophosphoryl diester phosphodiesterase family family	
Afu5g01580	-4.89919	-1.80796	-3.66114	oxidoreductase, short chain dehydrogenase/reductase family	
Afu3g14030	-4.81041	-3.75299	-3.91879	alkaline phosphatase	
Afu6g13840	-4.18974	-1.79254	-1.62686	conserved hypothetical protein	
Afu2g09450	-4.14543	-4.46141	-4.48151	carboxylic acid transport protein	lactate transmembrane transporter activity///lactate transport///plasma membrane
Afu6g14500	-4.11452	-3.69359	-2.59179	MFS sugar transporter, putative	mannose transmembrane transporter activity///hexose transport///fructose transmembrane transporter activity///plasma membrane///glucose transmembrane transporter activity
Afu1g16250	-3.98608	-1.86471	-1.9136	alpha-glucosidase B	alpha-glucosidase activity///fungal-type cell wall biogenesis///endoplasmic reticulum
Afu3g11970	-3.9454	-2.86591	-3.86937	C2H2 transcription factor PacC, putative	negative regulation of transcription from RNA polymerase II promoter///specific

					transcriptional repressor activity///cytoplasm///nucleus///response to pH
Afu4g00930	-3.89543	-2.73872	-3.68476	CorA family metal ion transporter, putative	di-, tri-valent inorganic cation transmembrane transporter activity///plasma membrane///"di-, tri-valent inorganic cation transport"///magnesium ion transport
Afu3g07910	-3.87473	-2.69264	-3.09276	UDP-glucose 4-epimerase, putative	cellular component unknown///UDP-glucose 4-epimerase activity///galactose metabolic process
Afu6g00470	-3.8478	-2.43813	-3.05478	plasma membrane zinc ion transporter, putative	high-affinity zinc ion transport///integral to plasma membrane///high affinity zinc uptake transmembrane transporter activity
Afu7g00580	-3.83554	-3.25568	-4.67765	conserved hypothetical protein	
Afu7g00450	-3.53704	-2.76433	-3.10848	GPI anchored protein, putative	
Afu8g07080	-3.50607	-4.1299	-7.06079	elastinolytic metalloproteinase Mep	pathogenesis///endopeptidase activity
Afu3g00490	-3.43907	-2.56088	-3.98654	C6 finger domain protein, putative	
Afu4g09990	-3.33982	-3.09717	-3.52317	Nucleoside transporter family	nucleoside transport///intracellular///nucleoside transmembrane transporter activity///membrane
Afu5g01570	-3.30705	-2.19541	-3.33579	hypothetical protein	
Afu3g07870	-3.2583	-2.58044	-3.08684	extracellular serine-rich protein	
Afu4g09580	-3.21865	-2.25343	-2.20607	major allergen Asp F2	biological process unknown///molecular function unknown
Afu2g07840	-3.18255	-1.80366	-2.73814	competence/damage-inducible protein CinA, putative	
Afu3g03000	-3.03972	-1.69699	-2.63717	phosphatidylethanolamine-binding protein, putative	
Afu8g06880	-2.98178	-2.70623	-2.9835	pectin methylesterase, putative	pectin catabolic process///pectinesterase activity
Afu8g00980	-2.91964	-2.04418	-2.34145	hypothetical protein	
Afu4g09560	-2.88717	-2.23687	-2.91824	ZIP Zinc transporter, putative	low-affinity zinc ion transmembrane transporter activity///low-affinity zinc ion transport///plasma membrane
Afu2g01320	-2.85971	-2.44687	-2.62818	P-type ATPase, putative	sodium ion transport///plasma membrane///"ATPase activity, coupled to transmembrane movement of ions, phosphorylative mechanism"
Afu4g00750	-2.82259	-2.86946	-3.5066	hypothetical protein	
Afu2g00720	-2.8001	-2.92199	-2.97175	aldehyde dehydrogenase, putative	aldehyde dehydrogenase (NAD) activity///fermentation///mitochondrion
Afu7g01030	-2.78931	-1.68384	-1.60965	Calcium-transporting ATPase 1 (PMC1),	calcium ion transport///fungal-type vacuole membrane///cellular

				putative	calcium ion homeostasis///calcium-transporting ATPase activity
Afu3g10690	-2.76171	-2.36651	-3.77666	calcium-translocating P-type ATPase(PMCA-type),putative	calcium ion transport///cellular calcium ion homeostasis///calcium-transporting ATPase activity
Afu5g10250	-2.74254	-1.60641	-3.38493	hypothetical protein	
Afu4g09440	-2.7356	-2.04896	-1.70613	sodium P-type ATPase, putative	sodium ion transport///plasma membrane///"ATPase activity, coupled to transmembrane movement of ions, phosphorylative mechanism"
Afu2g09030	-2.7325	-2.51411	-3.13085	secreted dipeptidyl peptidase	proteolysis///serine-type peptidase activity
Afu7g06160	-2.6903	-2.23403	-1.68728	hypothetical protein	
Afu7g05610	-2.65728	-2.40367	-2.88316	glucanase, putative	
Afu6g13760	-2.5832	-2.2536	-2.55726	alpha-1,2-mannosidase, putative subfamily	
Afu4g01560	-2.56994	-3.05494	-4.91541	MFS myo-inositol transporter, putative	membrane///myo-inositol transport///myo-inositol transmembrane transporter activity
Afu5g00870	-2.53523	-1.90113	-3.24655	hypothetical protein	
Afu8g01030	-2.53032	-2.9141	-2.53425	hypothetical protein	
Afu4g09310	-2.5043	-2.76968	-3.89044	hypothetical protein	
Afu8g06960	-2.47942	-2.85947	-3.43666	hypothetical protein	
Afu4g06650	-2.44872	-2.23717	-2.72098	hypothetical protein	
Afu6g03350	-2.40852	-3.59946	-4.50725	acetyltransferase, GNAT family, putative	N-acetyltransferase activity///metabolic process
Afu1g10460	-2.40156	-1.50526	-2.15278	hypothetical protein	
Afu5g00790	-2.39026	-2.76225	-3.68673	ABC multidrug transporter, putative	ATP-binding cassette (ABC) transporter activity///ATP binding///transport
Afu8g01400	-2.37446	-1.96089	-1.59242	mitochondrial carrier protein (Pet8), putative	S-adenosylmethionine transmembrane transporter activity///mitochondrial inner membrane///S-adenosylmethionine transport///mitochondrion
Afu3g07900	-2.35902	-1.77246	-2.56435	conserved hypothetical protein	
Afu4g08840	-2.25856	-2.9668	-2.17697	RING finger domain protein, putative	zinc ion binding
Afu6g03460	-2.24279	-1.65175	-3.10588	hypothetical protein	
Afu2g14490	-2.22677	-4.64428	-4.74212	endoglucanase, putative	
Afu3g08130	-2.19257	-1.96609	-2.49794	hypothetical protein	
Afu7g00440	-2.17307	-2.4214	-2.77414	GABA permease, putative	plasma membrane///choline transport///choline transmembrane transporter activity
Afu6g11390	-2.10708	-2.45351	-3.3174	1,3-beta-glucanosyltransferase Gel2	cell wall organisation///fungal-type cell wall///"1,3-beta-glucanosyltransferase activity"
Afu3g13600	-2.07268	-1.86632	-2.05877	C6 transcription factor, putative	transcription factor activity///nucleus///zinc ion binding///regulation of transcription
Afu4g13760	-2.04993	-2.0473	-3.66204	hypothetical protein	

Afu8g07340	-2.04659	-2.61429	-2.69408	HET domain protein	
Afu3g00770	-2.03269	-2.90049	-2.9231	hypothetical protein	
Afu4g08850	-1.95902	-1.88833	-1.92419	hypothetical protein	
Afu2g14540	-1.94557	-2.0974	-1.81869	endoglucanase, putative	
Afu8g02660	-1.93589	-2.39552	-2.72212	chromate ion transporter, putative	chromate transport///chromate transmembrane transporter activity
Afu6g00140	-1.89921	-2.3289	-2.24832	hypothetical protein	
Afu3g10500	-1.86875	-2.1834	-2.772	hypothetical protein	
Afu5g11190	-1.7936	-1.76659	-2.89347	hypothetical protein	
Afu8g02440	-1.7788	-2.02111	-2.56518	C-4 methyl sterol oxidase, putative	plasma membrane///ergosterol biosynthetic process///endoplasmic reticulum membrane///C-4 methylsterol oxidase activity
Afu5g02990	-1.73048	-2.01029	-2.89557	aromatic amino acid aminotransferase, putative	aromatic amino acid family metabolic process///cytoplasm///aromatic-amino-acid:2-oxoglutarate aminotransferase activity
Afu8g02670	-1.67504	-1.7847	-2.06379	conserved hypothetical protein	
Afu2g07910	-1.67143	-1.62151	-1.65005	myo-inositol transporter	membrane///myo-inositol transport///myo-inositol transmembrane transporter activity
Afu2g12680	-1.58025	-3.39852	-4.33782	conserved hypothetical protein	
Afu1g17150	-1.51031	-2.19274	-2.08193	C6 transcription factor, putative	carbohydrate metabolic process///"regulation of transcription, DNA-dependent"///transcription factor activity///nucleus

According to the expanded functional classifications generated for this study, GO analysis of the differentially expressed genes (fold change cut off of ±1.5 on a $\log_2$ scale) was performed using Genespring GX 11.02. Table 4.19 and Table 4.20 show the GO terms, which satisfy an imposed p-value cut-off of 0.05 respectively among the up-regulated and down-regulated genes, with respect to their occurrence in the *A. fumigatus* genome. Aiming to identify the phase-specific biological categories enriched among the differentially expressed genes, GO terms are reported for both the entire differentially expressed geneset and on the genesets for each of the single time points (4, 8 and 16 hrs). Transport across the plasma membrane is strikingly affected by *pacC* deletion and many transporters are therefore differentially expressed on the in the ATCC46645 Δ*pacC* relative to the parental strain ATCC466645 during initiation of murine infection. While sugar transporters predominate among genes upregulated in the ATCC46645 Δ*pacC* mutant relative to the parental strain, metal ion transporters predominate among down-regulated genes, such as those transporting iron, calcium and sodium.

Total up-regulated genes in the ATCC46645 Δ*pacC* /ATCC46645 analysis							
GO ACCESSION	**GO Term**	**p-value**	**corrected p-value**	**Count in Selection**	**% Count in Selection**	**Count in Total**	**% Count in Total**
GO:0005215|GO:0005478	transporter activity	2.556894E-13	2.617588E-9	20	25.974026	525	11.677046
GO:0005886|GO:0005904	plasma membrane	3.1958737E-12	1.6358676E-8	48	62.33766	315	7.006228
GO:0022857|GO:0005386 |GO:0015646	transmembrane transporter activity	8.949631E-9	3.054024E-5	1	1.2987013	354	7.8736653
GO:0016020	membrane	1.1439736E-7	2.9278212E-4	60	77.92208	816	18.149466
GO:0031226	intrinsic to plasma membrane	1.7446146E-7	3.5720543E-4	17	22.077923	95	2.1129894
GO:0044459	plasma membrane part	1.081094E-6	0.0013834452	17	22.077923	114	2.535587
GO:0004553|GO:0016800	hydrolase activity, hydrolyzing O-glycosyl compounds	1.7424368E-6	0.0019819974	8	10.38961	91	2.0240214
GO:0005975	carbohydrate metabolic process	1.3817783E-5	0.01414578	6	7.7922077	292	6.494662
GO:0005887	integral to plasma membrane	1.5841506E-5	0.014743219	17	22.077923	87	1.9350533
GO:0016798	hydrolase activity, acting on glycosyl bonds	4.1193092E-5	0.03514242	9	11.688312	112	2.4911032
GO:0005529	sugar binding	6.715382E-5	0.038193263	4	5.194805	5	0.111209966
GO:0005536	glucose binding	6.715382E-5	0.038193263	4	5.194805	5	0.111209966
GO:0009746	response to hexose stimulus	6.715382E-5	0.038193263	4	5.194805	5	0.111209966
GO:0009749	response to glucose stimulus	6.715382E-5	0.038193263	4	5.194805	5	0.111209966
GO:0034284	response to monosaccharide stimulus	6.715382E-5	0.038193263	4	5.194805	5	0.111209966
GO:0048029	monosaccharide binding	6.715382E-5	0.038193263	4	5.194805	5	0.111209966
4 hrs up-regulated genes in the ATCC46645 Δ*pacC* /ATCC46645 analysis							
GO ACCESSION	**GO Term**	**p-value**	**corrected p-value**	**Count in Selection**	**% Count in Selection**	**Count in Total**	**% Count in Total**
GO:0005886|GO:0005904	plasma membrane	3.2131474E-8	2.1500605E-4	15	100.0	315	7.006228
8 hrs up-regulated genes in the ATCC46645 Δ*pacC* /ATCC46645 analysis							
GO ACCESSION	**GO Term**	**p-value**	**corrected p-value**	**Count in Selection**	**% Count in Selection**	**Count in Total**	**% Count in Total**
GO:0005886|GO:0005904	plasma membrane	2.7505406E-11	1.0179134E-7	27	57.446808	315	7.006228
GO:0005215|GO:0005478	transporter activity	9.147836E-11	1.6927045E-7	10	21.276596	525	11.677046
GO:0022892	substrate-specific transporter activity	6.1910434E-8	7.637221E-5	3	6.382979	357	7.9403915
GO:0022857|GO:0005386 |GO:0015646	transmembrane transporter activity	2.3556998E-7	2.1794793E-4	3	6.382979	354	7.8736653
GO:0022891	substrate-specific transmembrane transporter activity	6.477588E-7	4.79442E-4	3	6.382979	317	7.0507116
GO:0031226	intrinsic to plasma membrane	2.1938467E-6	0.0013531558	11	23.404255	95	2.1129894
GO:0016020	membrane	7.2993053E-6	0.003859013	29	61.70213	816	18.149466
GO:0000322	storage vacuole	1.559729E-5	0.004123005	9	19.148935	95	2.1129894
GO:0000323	lytic vacuole	1.559729E-5	0.004123005	9	19.148935	95	2.1129894
GO:0000324	fungal-type vacuole	1.559729E-5	0.004123005	9	19.148935	95	2.1129894

GO:0005976	polysaccharide metabolic process	1.4402617E-5	0.004123005	2	4.255319	115	2.5578291
GO:0006811	ion transport	9.650219E-6	0.004123005	4	8.510638	132	2.9359431
GO:0015082	di-, tri-valent inorganic cation transmembrane transporter activity	1.1094846E-5	0.004123005	3	6.382979	40	0.88967973
GO:0044459	plasma membrane part	1.3240378E-5	0.004123005	11	23.404255	114	2.535587
GO:0046873	metal ion transmembrane transporter activity	3.8471688E-5	0.009491673	2	4.255319	48	1.0676156
GO:0006810|GO:0015457|GO:0015460	transport	5.109021E-5	0.011817088	12	25.531916	774	17.215303
GO:0015085	calcium ion transmembrane transporter activity	6.576237E-5	0.01355278	2	4.255319	12	0.2669039
GO:0051234	establishment of localisation	6.591862E-5	0.01355278	12	25.531916	784	17.437723
GO:0004553|GO:0016800	hydrolase activity, hydrolyzing O-glycosyl compounds	7.032721E-5	0.013698169	5	10.638298	91	2.0240214
GO:0051179	localisation	1.0037675E-4	0.018573591	12	25.531916	801	17.815836
GO:0005773	vacuole	1.1074471E-4	0.019516254	9	19.148935	119	2.6467972
GO:0015674	di-, tri-valent inorganic cation transport	1.2081563E-4	0.020323252	4	8.510638	40	0.88967973
GO:0006816	calcium ion transport	1.289598E-4	0.020750057	4	8.510638	14	0.3113879
GO:0004180	carboxypeptidase activity	2.5621933E-4	0.03792841	1	2.1276596	7	0.15569395
GO:0005887	integral to plasma membrane	3.023021E-4	0.043028932	8	17.021276	87	1.9350533
GO:0016798	hydrolase activity, acting on glycosyl bonds	3.4942618E-4	0.04789437	5	10.638298	112	2.4911032
GO:0004339	glucan 1,4-alpha-glucosidase activity	3.9634787E-4	0.049839173	2	4.255319	2	0.044483986
GO:0031225	anchored to membrane	4.040167E-4	0.049839173	3	6.382979	8	0.17793594
GO:0046658	anchored to plasma membrane	4.040167E-4	0.049839173	3	6.382979	8	0.17793594

16 hrs up-regulated genes in the ATCC46645 Δ*pacC* /ATCC46645 analysis

GO ACCESSION	GO Term	p-value	corrected p-value	Count in Selection	% Count in Selection	Count in Total	% Count in Total
GO:0005215|GO:0005478	transporter activity	3.3751432E-15	2.6466893E-11	25	40.322582	525	11.677046
GO:0005886|GO:0005904	plasma membrane	7.858818E-13	3.0813283E-9	40	64.51613	315	7.006228
GO:0022857|GO:0005386|GO:0015646	transmembrane transporter activity	6.496924E-10	1.6982331E-6	9	14.5161295	354	7.8736653
GO:0022892	substrate-specific transporter activity	2.9585399E-9	5.8000023E-6	9	14.5161295	357	7.9403915
GO:0022891	substrate-specific transmembrane transporter activity	1.3164447E-8	2.0646354E-5	9	14.5161295	317	7.0507116
GO:0031226	intrinsic to plasma membrane	7.909516E-8	1.0337354E-4	14	22.580645	95	2.1129894
GO:0016020	membrane	1.4121808E-7	1.5819875E-4	49	79.03226	816	18.149466
GO:0004553|GO:0016800	hydrolase activity, hydrolyzing O-glycosyl compounds	2.2975897E-7	2.2521288E-4	6	9.67742	91	2.0240214
GO:0044459	plasma membrane part	1.3735781E-6	0.0011968	14	22.580645	114	2.535587
GO:0016798	hydrolase activity, acting on glycosyl bonds	4.790316E-6	0.0037564265	7	11.290322	112	2.4911032
GO:0005887	integral to plasma membrane	1.7249293E-5	0.010404918	14	22.580645	87	1.9350533
GO:0005975	carbohydrate metabolic process	1.6606062E-5	0.010404918	5	8.064516	292	6.494662

GO:0006810|GO:0015457|GO:0015460	transport	1.5189253E-5	0.010404918	16	25.806452	774	17.215303
GO:0051179	localisation	2.0952391E-5	0.0117358975	16	25.806452	801	17.815836
GO:0051234	establishment of localisation	2.255319E-5	0.011790371	16	25.806452	784	17.437723
GO:0005355|GO:0015579	glucose transmembrane transporter activity	5.9088194E-5	0.025741803	8	12.903226	33	0.7339858
GO:0015145	monosaccharide transmembrane transporter activity	5.9088194E-5	0.025741803	8	12.903226	33	0.7339858
GO:0015149	hexose transmembrane transporter activity	5.9088194E-5	0.025741803	8	12.903226	33	0.7339858
GO:0031224	intrinsic to membrane	6.44668E-5	0.02660684	14	22.580645	251	5.5827403
GO:0005976	polysaccharide metabolic process	1.0928889E-4	0.040810082	2	3.2258065	115	2.5578291

Table 4.19: Significant GO terms among the up-regulated genes of the ATCC46645 Δ*pacC*/ATCC466645 comparison. p-value represents the probability of obtaining the GO term from a list of random entities, corrected p-value derived from Bonferroni testing of multiple comparisons. Analysis performed using Genespring GX 11.02.

Total down-regulated genes in the ATCC46645 Δ*pacC* /ATCC46645 analysis							
GO ACCESSION	**GO Term**	**p-value**	**corrected p-value**	**Count in Selection**	**% Count in Selection**	**Count in Total**	**% Count in Total**
GO:0005215|GO:0005478	transporter activity	2.5311437E-9	1.9870076E-5	15	29.411764	525	11.677046
GO:0005886|GO:0005904	plasma membrane	9.274286E-9	3.640267E-5	26	50.980392	315	7.006228
GO:0006810|GO:0015457|GO:0015460	transport	8.783157E-8	1.1407305E-4	17	33.333332	774	17.215303
GO:0051234	establishment of localisation	6.156969E-8	1.1407305E-4	17	33.333332	784	17.437723
GO:0051179	localisation	1.4760494E-7	1.448417E-4	17	33.333332	801	17.815836
GO:0016020	membrane	5.949372E-5	0.038919978	33	64.70588	816	18.149466
GO:0019184	nonribosomal peptide biosynthetic process	7.958824E-5	0.048060495	5	9.803922	11	0.24466193
4 hrs down-regulated genes in the ATCC46645 Δ*pacC* /ATCC46645 analysis							
GO ACCESSION	**GO Term**	**p-value**	**corrected p-value**	**Count in Selection**	**% Count in Selection**	**Count in Total**	**% Count in Total**
GO:0005215|GO:0005478	transporter activity	2.7621502E-7	4.5917497E-4	7	26.923077	525	11.677046
GO:0005886|GO:0005904	plasma membrane	2.9486916E-6	0.0031683843	19	73.07692	315	7.006228
GO:0006810|GO:0015457|GO:0015460	transport	3.55948E-6	0.0031683843	8	30.76923	774	17.215303
GO:0051179	localisation	3.8118599E-6	0.0031683843	8	30.76923	801	17.815836
GO:0051234	establishment of localisation	2.0431485E-6	0.0027171953	8	30.76923	784	17.437723
8 hrs down-regulated genes in the ATCC46645 Δ*pacC* /ATCC46645 analysis							
GO ACCESSION	**GO Term**	**p-value**	**corrected p-value**	**Count in Selection**	**% Count in Selection**	**Count in Total**	**% Count in Total**

GO:0000041	transition metal ion transport	1.18887285E-4	0.026356254	2	8.695652	51	1.1343416
GO:0005215|GO:0005478	transporter activity	1.964337E-6	7.257934E-4	7	30.434782	525	11.677046
GO:0005436	sodium:phosphate symporter activity	2.3899628E-4	0.04182896	2	8.695652	2	0.044483986
GO:0005886|GO:0005904	plasma membrane	1.7641414E-5	0.0048886808	15	65.21739	315	7.006228
GO:0006810|GO:0015457 |GO:0015460	transport	1.348755E-6	6.4072927E-4	6	26.086956	774	17.215303
GO:0006811	ion transport	7.912988E-11	2.631359E-7	2	8.695652	132	2.9359431
GO:0006812|GO:0006819	cation transport	5.356705E-8	3.5626017E-5	2	8.695652	106	2.3576512
GO:0015075	ion transmembrane transporter activity	1.4707778E-5	0.004446251	5	21.73913	149	3.3140569
GO:0015082	di-, tri-valent inorganic cation transmembrane transporter activity	2.8995273E-5	0.007416917	1	4.347826	40	0.88967973
GO:0015296	anion:cation symporter activity	2.3899628E-4	0.04182896	2	8.695652	2	0.044483986
GO:0015319	sodium:inorganic phosphate symporter activity	2.3899628E-4	0.04182896	2	8.695652	2	0.044483986
GO:0015662	ATPase activity, coupled to transmembrane movement of ions, phosphorylative mechanism	1.7512009E-4	0.036396157	2	8.695652	19	0.42259786
GO:0016020	membrane	4.153547E-5	0.009865763	19	82.608696	816	18.149466
GO:0022857|GO:0005386 |GO:0015646	transmembrane transporter activity	2.0520172E-7	1.137285E-4	5	21.73913	354	7.8736653
GO:0022891	substrate-specific transmembrane transporter activity	3.216616E-8	3.5626017E-5	5	21.73913	317	7.0507116
GO:0022892	substrate-specific transporter activity	4.555204E-8	3.5626017E-5	5	21.73913	357	7.9403915
GO:0030001	metal ion transport	7.107388E-9	1.1817336E-5	2	8.695652	71	1.5791816
GO:0051179	localisation	2.7942067E-6	9.2917617E-4	6	26.086956	801	17.815836
GO:0051234	establishment of localisation	1.7740875E-6	7.257934E-4	6	26.086956	784	17.437723
16 hrs down-regulated genes in the ATCC46645 Δ*pacC* /ATCC46645 analysis							
GO ACCESSION	**GO Term**	**p-value**	**corrected p-value**	**Count in Selection**	**% Count in Selection**	**Count in Total**	**% Count in Total**
GO:0005215|GO:0005478	transporter activity	1.056156E-7	2.630451E-4	9	31.034483	525	11.677046
GO:0005886|GO:0005904	plasma membrane	4.2751494E-6	0.002366143	15	51.724136	315	7.006228
GO:0006810|GO:0015457 |GO:0015460	transport	1.4177001E-5	0.005432168	9	31.034483	774	17.215303
GO:0015075	ion transmembrane transporter activity	5.1712872E-5	0.015152418	1	3.4482758	149	3.3140569
GO:0015082	di-, tri-valent inorganic cation transmembrane transporter activity	3.9102913E-5	0.012173665	1	3.4482758	40	0.88967973
GO:0019184	nonribosomal peptide biosynthetic process	3.1439588E-6	0.001957578	5	17.241379	11	0.24466193
GO:0022857|GO:0005386 |GO:0015646	transmembrane transporter activity	2.428222E-6	0.0017279156	1	3.4482758	354	7.8736653
GO:0022891	substrate-specific transmembrane transporter activity	1.268885E-6	0.001053424	1	3.4482758	317	7.0507116
GO:0022892	substrate-specific transporter activity	7.7334255E-7	9.658953E-4	1	3.4482758	357	7.9403915
GO:0043041	amino acid activation for nonribosomal peptide	2.1239788E-5	0.00705328	4	13.793103	8	0.17793594

	biosynthetic process						
GO:0043042	amino acid adenylylation by nonribosomal peptide synthase	2.1239788E-5	0.00705328	4	13.793103	8	0.17793594
GO:0043043	peptide biosynthetic process	8.424223E-6	0.0038147788	5	17.241379	13	0.28914592
GO:0051179	localisation	1.22373995E-5	0.005079724	9	31.034483	801	17.815836
GO:0051234	establishment of localisation	7.2663747E-6	0.0036195116	9	31.034483	784	17.437723

Table 4.20: Significant GO terms among the down-regulated genes of the ATCC46645 Δ*pacC*/ATCC466645 comparison. p-value represents the probability of obtaining the GO term from a list of random entities, corrected p-value derived from Bonferroni testing of multiple comparisons. Analysis performed using Genespring GX 11.02.

Functional classification of differentially expressed genes (fold change cut off of ±1.5 on a $\log_2$ scale) was also annotated in a non-automated manner by reference to the literature to further identify functional trends within the up-regulated and down-regulated genes. The entire datasets of up-regulated (729 ORFs) and down-regulated (762 ORFs) genes in the ATCC46645 Δ*pacC*/ATCC46645 comparison were analysed and a summary is provided in Tables 4.21 and 4.22. Interestingly, the transcriptional profile of the *A. fumigatus* Δ*pacC* mutant aligns with the acidic-mimicking profile, according to which the prevention or the reduction of growth at alkaline pH corresponds to the increase of GABA transport and acid phosphatase levels and the decrease of alkaline phosphatase, molybdate hypersensitivity and neomycin resistance, is shown by the acidity-mimicking mutations.

Functional classification of selected up-regulated genes in the ATCC46645 Δ*pacC*/ATCC46645 comparison			
Transport		**Metabolism**	
Afu6g13190	H+/nucleoside cotransporter	Afu2g01410	aldo-keto reductase
Afu3g14170	high-affinity hexose transporter	Afu5g14510	beta-lactamase
Afu3g12170	MFS sugar transporter	Afu2g01230	dihydrodipicolinate synthetase family protein
Afu4g01360	MFS transporter of unkown specificity	Afu2g00140	FAD monooxygenase
Afu1g01800	MFS transporter	Afu8g00640	glycosyl transferase
Afu1g03730	MFS transporter	Afu2g04080	GPR/FUN34 family protein
Afu6g12900	mitochondrial carrier protein	Afu7g06380	maltase
Afu6g03060	monosaccharide transporter	Afu3g02640	nucleoside-diphosphate-sugar epimerase family protein
Afu5g02700	multidrug resistant protein	Afu5g11240	oxidoreductase, short chain dehydrogenase/reductase family
Afu7g00910	peptide transporter MTD1	Afu2g14460	oxidoreductase, short-chain dehydrogenase/reductase family
Afu5g01320	phosphate permease	Afu4g13780	polyphenol monooxygenase
Afu1g05170	related to monocarboxylate transporter	Afu7g00150	FAD-dependent monooxygenase
Afu3g13670	siderochrome-iron transporter	Afu8g00680	glycosyl transferase, group 2 family protein
Afu3g03700	Sugar transporter subfamily	Afu5g14340	oxidoreductase, short-chain dehydrogenase/reductase family
Afu8g00720	amino acid transporter	Afu8g04120	carboxypeptidase S1
Afu1g17480	conserved hypothetical protein	Afu4g10140	glucoamylase
Afu8g06580	GABA permease	Afu1g00480	glucosamine-6-phosphate deaminase
Afu3g11790	galactose-proton symport	Afu8g04070	glucosamine-6-phosphate deaminase
Afu2g05320	ion transporter	Afu4g06620	Glutamate/Leucine/Phenylalanine/Valine dehydrogenase
Afu6g02400	MFS drug efflux pump	Afu4g13120	glutamine synthetase
Afu4g00150	MFS maltose transporter	Afu8g02040	glycosyl transferase
Afu6g14440	MFS monosaccharide transporter	Afu1g01430	hypothetical protein
Afu4g13660	MFS multidrug resistance transporter	Afu6g12930	mitochondrial aconitate hydratase
Afu2g17730	MFS multidrug transporter	Afu1g11280	oxidoreductase
Afu3g01940	MFS multidrug transporter	Afu1g10630	S-adenosylmethionine synthetase
Afu1g12240	MFS peptide transporter	Afu4g14800	short chain dehydrogenase
Afu7g01490	MFS peptide transporter	Afu6g00230	isoflavone reductase family protein
Afu2g10690	MFS phosphate transporter	Afu3g14920	LaeA-like methyltransferase
Afu8g06870	MFS sugar transporter	Afu4g11720	phosphatidyl synthase
Afu4g01480	MSF transporter, putative	Afu4g10790	phosphoribosyl diphosphate synthase isoform 4
Afu7g04570	Na/K ATPase alpha 1 subunit	Afu1g10130	adenosylhomocysteinase
Afu8g07200	neutral amino acid permease	Afu5g13090	alpha-1,2-mannosyltransferase
Afu8g00770	sugar transporter family protein	Afu2g11620	alpha-glucosidase
Afu4g09150	ABC multidrug	Afu1g11250	amidohydrolase
Afu5g04260	arginine transporter	Afu8g06970	beta-glucosidase
Afu8g06560	DUF895 domain membrane protein	Afu7g06900	branched-chain amino acid aminotransferase
Afu6g04270	fructose symporter	Afu6g11670	conserved hypothetical protein
Afu8g06760	integral membrane protein	Afu5g07210	homoserine O-acetyltransferase
Afu8g06410	MFS multidrug transporter	Afu2g11920	hypothetical protein
Afu6g07750	MFS phospholipid transporter (Git1)	Afu6g00260	phosphatidylserine decarboxylase family protein
Afu3g04010	MFS transporter	Afu5g14810	pyruvate decarboxylase

Afu2g03860	plasma membrane low affinity zinc ion transporter
Afu5g06670	related to L-fucose permease
Afu7g06570	zinc/cadmium resistance protein
Afu5g11840	protein kinase
Afu7g01720	3-hydroxymethyl-3-methylglutaryl-Coenzyme A lyase
Afu8g05710	autophagy protein Apg6, putative (MFS sugar transporter Stl1)
Afu6g00630	MFS transporter
Afu6g12550	mitochondrial carrier protein
Afu1g10310	RNase L inhibitor of the ABC superfamily
Afu6g13070	UDP-galactose transporter
Afu2g13390	MFS transporter
Afu5g06290	MFS transporter
Afu7g04730	siderochrome-iron transporter
Antigens/cell surface proteins	
Afu3g08990	hypothetical protein
Afu6g00430	IgE-binding protein
Afu7g04930	alkaline serine protease (PR1)
Pathogenesis	
Afu5g00980	multidrug resistant protein
Afu5g00600	NPP1 domain protein
Secondary metabolism	
Afu2g14470	oxidoreductase, FAD-binding
Afu6g12110	salicylate synthetase
Afu3g13240	aldose 1-epimerase
Afu5g13300	aspartic endopeptidase Pep1
Afu3g00470	endo-1,4-beta-xylanase
Afu3g03350	nonribosomal peptide synthase SidE
Afu1g13660	phenol 2-monooxygenase
Afu3g12620	acyl-CoA:6-aminopenicillanic-acid-acyltransferase
Stress	
Afu3g14540	heat shock protein HSP30
Cell wall	
Afu6g10580	antigenic CFEM domain protein
Afu7g05140	class III chitinase
Afu6g14480	alpha-1,3-mannosyltransferase
Afu8g00700	class III chitinase ChiA2
Afu2g09350	endo-beta-1,6-glucanase
Afu2g00680	glycosyl hydrolase
Afu1g05790	GPI anchored serine-rich protein
Afu6g10130	N,O-diacetyl muramidase
Afu2g00430	exo-beta-1,3-glucanase
Lipid metabolism	
Afu3g09960	aureobasidin resistance protein Aur1
Afu4g14150	Diacylglycerol acyltransferase family
Afu3g01950	alcohol dehydrogenase, zinc-containing
Afu1g00420	carboxypeptidase S1
Afu7g04950	lipase
Afu1g11890	serine palmitoyltransferase 2 lysophospholipase
Afu5g01340	oxidoreductase, short-chain dehydrogenase/reductase family
Afu6g03370	Patatin-like serine hydrolase
Afu4g08440	
Protein synthesis/degradation	
Afu6g13180	CECR1 family adenosine deaminase
Afu7g06840	class III aminotransferase
Afu6g06460	fumarylacetoacetate hydrolase family protein
Afu6g00310	serine carboxypeptidase (CpdS)
Afu6g03260	aspartic endopeptidase (AP1), putative
Afu2g09820	conserved hypothetical protein
Afu2g03510	pheromone processing carboxypeptidase (Sxa2),
Afu4g14000	tripeptidyl peptidase A
Afu1g11060	ubiquitin domain protein
Afu5g02400	catabolite degradation protein
RNA processing	
Afu1g06980	mitochondrial small ribosomal subunit protein S4
Afu3g04310	snoRNA binding protein
Afu5g13040	translation initiation factor eif-2b delta subunit
Afu1g15340	polymerase
Afu7g05430	nonsense-mediated mRNA decay factor (Upf2)
Afu3g06010	Nucleolar essential protein 1
Afu4g07580	translation initiation factor EF-2 gamma subunit
Transcription	
Afu1g06900	C2H2 transcription factor (Crz1)
Afu4g12470	bZIP transcription factor CpcA
Afu3g11330	bZIP transcription factor (AtfA)
Afu3g05760	C6 transcription factor (Fcr1)
Afu3g10120	TATA-box binding protein
Afu3g10620	transcription initiation protein
Afu1g01850	hypothetical protein
Afu5g03430	PHD transcription factor (Rum1)
Afu3g11250	C2H2 transcription factor (Swi5)
Afu4g10120	C6 finger domain protein
Afu8g04810	casein kinase
Afu3g08160	eukaryotic translation initiation factor eIF4A

Afu1g01730	glycosyl hydrolase
Afu7g05370	septin AspB
Afu4g10150	alpha-glucosidase
Afu5g08580	alpha-1,6-mannosyltransferase subunit (Och1)
Afu5g02280	endo-1,3(4)-beta-glucanase
Afu4g08960	GPI anchored protein
Afu1g12900	Leucine Rich Repeat domain protein

Development and morphogenesis

Afu7g01930	sexual development protein EsdC
Afu5g06190	sexual development transcription factor SteA

Endo/exocytosis

Afu1g10950	vesicle-mediated transport protein Vid24
Afu3g09360	vacuolar sorting ATPase
Afu6g00640	Vps4 integral membrane protein
Afu5g09020	WSC domain protein

Table 4.21: Functional classification of selected genes having increased abundance in the ATCC46645 Δ*pacC* mutant relative to the parental isolate ATCC46645 during initiation of murine infection. Genes were included if showing a fold change of ±1.5 on a $\log_2$ scale in at least one of the time points.

Functional classification of selected down-regulated genes in the ATCC46645 Δ*pacC*/ATCC46645 comparison

Transport

Afu3g03670	ABC multidrug transporter, putative
Afu3g12220	ABC transporter, putative
Afu7g04970	metalloreductase, putative
Afu8g01310	metalloreductase, putative
Afu3g03640	siderochrome-iron transporter (MirB), putative
Afu7g06060	siderochrome-iron transporter (Sit1), putative
Afu4g00930	CorA family metal ion transporter
Afu6g00470	plasma membrane zinc ion transporter
Afu4g01570	neutral amino acid permease
Afu7g01030	Calcium-transporting ATPase 1 (PMC1)
Afu2g15150	choline transport protein
Afu7g00780	MFS monocarboxylate transporter

Energy production

Afu5g09140	amidase, putative
Afu4g09980	cytochrome P450 monooxygenase
Afu8g00960	cytochrome P450, putative
Afu4g07150	cytochrome-c oxydase chain VIIc-like protein
Afu2g13010	cytochrome c oxidase polypeptide
Afu1g13480	vib ubiquinol-cytochrome C reductase complex subunit
Afu7g02030	UcrQ cytochrome c oxidase assembly protein (Pet117)

Ergosterol biosynthesis

Afu8g02440	C-4 methyl sterol oxidase
Afu1g03150	c-14 sterol reductase
Afu1g05720	c-14 sterol reductase

Metabolism

Afu6g02220	MFS toxin efflux pump
Afu3g01370	MFS transporter
Afu3g03010	phosphate-repressible phosphate permease
Afu8g01850	phosphate-repressible phosphate permease
Afu8g02550	Ptr2-like MFS peptide transporter
Afu4g09440	sodium P-type ATPase
Afu3g12740	copper resistance-associated P-type ATPase
Afu3g07300	ABC multidrug transporter
Afu5g00790	ABC multidrug transporter
Afu8g02660	chromate ion transporter
Afu4g00750	hypothetical protein
Afu6g03140	isp4 protein
Afu4g01560	MFS myo-inositol transporter
Afu7g00710	oxalate/formate antiporter
Afu2g09450	carboxylic acid transport protein
Afu7g00440	GABA permease
Afu2g07910	myo-inositol transporter
Afu4g09990	Nucleoside transporter family
Afu2g03000	nucleoside transporter
Afu2g01320	P-type ATPase
Afu4g09560	ZIP Zinc transporter
Antigens/cell surface proteins	
Afu4g09320	antigenic dipeptidyl-peptidase Dpp4
Afu5g01440	allergen
Afu4g09580	major allergen Asp F2
Afu8g07080	elastinolytic metalloproteinase Mep
Pathogenesis	
Afu2g04570	BNR/Asp-box repeat domain protein
Afu2g12990	cyclophilin
Afu3g00350	hypothetical protein
Secondary metabolism	
Afu6g09640	aminotransferase GliI
Afu6g09670	cytochrome P450 oxidoreductase GliC
Afu6g09730	cytochrome P450 oxidoreductase GliF
Afu6g09700	gliotoxin biosynthesis protein GliK
Afu6g09650	membrane dipeptidase GliJ
Afu6g09720	methyltransferase GliN
Afu6g09710	MFS gliotoxin efflux pump GliA
Afu6g09740	thioredoxin reductase GliT
Afu6g08700	beta glucosidase,
Afu6g14000	Tri7-like toxin biosynthesis protein
Afu2g08500	carboxylesterase
Afu2g05810	dienelactone hydrolase
Afu6g04700	imidazoleglycerol-phosphate dehydratase
Afu1g02890	dUTPase (Dut)
Afu3g07560	enoyl-CoA hydratase/isomerase family protein
Afu6g02960	NADH-ubiquinone oxidoreductase 105 kDa subunit
Afu6g08560	nonribosomal peptide synthase (NRPS)
Afu5g01580	oxidoreductase, short chain dehydrogenase/reductase family
Afu1g15280	polysaccharide deacetylase family protein
Afu5g09130	polysaccharide deacetylase family protein
Afu6g08830	2-oxoisovalerate dehydrogenase complex alpha subunit
Afu4g10370	3-demethylubiquinone-9 3-methyltransferase
Afu5g10090	3-demethylubiquinone-9 3-methyltransferase
Afu7g05840	amidohydrolase family protein
Afu1g05820	isochorismatase family hydrolase,
Afu6g12220	zinc binding dehydrogenase family protein
Afu8g05690	acetyltransferase, GNAT family
Afu7g05010	glyoxalase family protein
Afu6g04620	NADH-ubiquinone oxidoreductase B14 subunit
Afu3g13910	NADH-ubiquinone oxidoreductase B18 subunit
Afu2g07940	NADPH-cytochrome P450 reductase (CprA)
Afu5g02990	aromatic amino acid aminotransferase
Afu2g00540	carboxyphosphonoenolpyruvate phosphonomutase
Afu3g07860	glycosyl transferase
Afu2g00720	aldehyde dehydrogenase
Afu5g00670	glycosyl hydrolase family 35
Afu2g00570	GNAT family acetyltransferase
Lipid metabolism	
Afu8g02270	dihydrodipicolinate synthetase family protein
Afu2g14850	enoyl-CoA hydratase/isomerase family protein
Afu5g09150	oxidoreductase, short-chain dehydrogenase/reductase family
Afu3g01530	phosphatidylglycerol specific phospholipase
Afu6g13280	Fox2 protein
Afu6g12240	Glycerophosphoryl diester phosphodiesterase family
Protein synthesis/degradation	
Afu2g08130	ribosomal protein L41
Afu1g17120	elongation factor-1 gamma
Afu1g01540	Endonuclease/Exonuclease/phosphatase family
Afu2g16880	ribosomal protein L37a
Afu2g02270	ribosomal protein S14p/S29e
RNA processing	
Afu6g04020	peptidyl-tRNA hydrolase domain protein

Afu2g09030	secreted dipeptidyl peptidase
Calcium homeostasis	
Afu1g02930	Ca2+ binding protein (calmodulin)
Afu3g10690	calcium-translocating P-type ATPase(PMCA-type)
Stress	
Afu1g01370	glutathione S-transferase
Afu4g10610	hypothetical protein
Afu3g07930	putative glutathione S-transferase
Afu3g01210	ThiJ/PfpI family protein
Afu1g17370	chaperone/heat shock protein Hsp9
Afu3g14030	alkaline phosphatase
Afu6g13750	ferric-chelate reductase
Afu6g11330	histidine acid phosphatase
Development and morphogenesis	
Afu8g06130	FluG family protein
Cell wall	
Afu2g14630	cell wall glycosyl hydrolase family 88 (YteR)
Afu4g06860	conserved hypothetical protein
Afu1g16250	alpha-glucosidase B
Afu3g03370	cell surface protein
Afu2g05150	cell wall galactomannoprotein Mp2
Afu6g11390	1,3-beta-glucanosyltransferase Gel2
Afu7g00970	GPI-anchored serine-threonine rich protein
Afu8g07060	hydrophobin
Afu2g14540	endoglucanase
Afu7g05610	glucanase
Afu8g06880	pectin methylesterase
Afu7g04280	small nuclear ribonucleoprotein (LSM5)
Afu2g08320	U3 small nucleolar ribonucleoprotein subunit (Imp3)
Afu3g11820	mitochondrial oligoribonuclease
Afu6g13310	26S proteasome non-ATPase regulatory subunit 9
Transcription	
Afu3g11970	C2H2 transcription factor PacC
Afu2g05360	C6 transcription factor
Afu4g06600	hypothetical protein
Afu3g14600	fungal specific transcription factor
Afu2g04260	transcription factor
Afu1g05940	conserved hypothetical protein
Afu1g02860	C2H2 transcription factor
Afu4g06420	fungal specific transcription factor
Afu3g00490	C6 finger domain protein
Afu1g17150	C6 transcription factor
Afu3g13600	C6 transcription factor
DNA organisation	
Afu2g16710	hypothetical protein
Afu2g02090	methylated-DNA-protein-cysteine methyltransferase
Afu3g05360	histone H2A
Afu1g07430	hypothetical protein
Afu2g04140	conserved hypothetical protein
Afu6g13290	SNF2 family helicase/ATPase
Afu2g05180	NF-X1 finger and helicase domain protein
Endo/exocytosis	
Afu7g05950	EF-hand protein
Afu2g01990	Signal recognition particle 14kD protein domain containing protein guanine
Afu4g12490	nucleotide exchange factor VPS9
Afu2g09670	SNARE protein (Ufe1),

Transposition	
Afu2g03570	transposase
Afu3g03770	transposase
Afu4g14370	LINE-1 class reverse transcriptase, RNase H, putative
Afu2g18080	LINE-1 class reverse transcriptase, RNase H, putative
Afu2g18080	LINE-1 class reverse transcriptase, RNase H, putative
Afu3g09430	LINE-1 class reverse transcriptase, RNase H, putative
Afu3g15370	LINE-1 class reverse transcriptase, RNase H, putative
Afu4g14870	LINE-1 class reverse transcriptase, RNase H, putative
Afu4g14870	LINE-1 class reverse transcriptase, RNase H, putative
Afu6g00780	LINE-1 class reverse transcriptase, RNase H, putative
Afu6g00780	LINE-1 class reverse transcriptase, RNase H, putative
Afu8g00310	LINE-1 class reverse transcriptase, RNase H, putative
Afu8g00310	LINE-1 class reverse transcriptase, RNase H, putative
Afu8g06290	revers LINE-1 class reverse transcriptase, RNase H, putative
Afu3g09410	transcriptase
Afu7g08210	reverse transcriptase, putative
Afu4g00820	reverse transcriptase, RNaseH
Afu4g00820	reverse transcriptase, RNaseH
Afu6g14660	reverse transcriptase, RNaseH
Afu6g14660	reverse transcriptase, RNaseH
Afu8g01040	reverse transcriptase, RNaseH
Afu8g01040	reverse transcriptase, RNaseH
Afu6g09470	reverse transcriptase, RNaseH, putative

Table 4.22: Functional classification of selected genes having decreased abundance in the ATCC46645 Δ*pacC* mutant relative to the parental isolate ATCC46645 during initiation of murine infection. Genes were included if showing a fold change of ±1.5 on a $\log_2$ scale in at least one of the time points.

4.4 Discussion

In the past, microarray analyses of *A. fumigatus* transcriptional profiling during host infection have been strictly limited by the difficulty in obtaining RNA in sufficient quantity from the sites of infection. The transcriptional profiling of the *A. fumigatus* ATCC46645 clinical isolate in a temporal window which analyses early, middle and late stages of *A. fumigatus* murine infection in a neutropenic model of IPA identifies genes preferentially expressed during adaptation to the murine niche and provides crucial information about the necessary requirements for establishment of a successful infection. The same experimental approach was used to study the transcriptome of a host-adapting ATCC46645 Δ*pac*C mutant, whose characterisation in terms of phenotype (Fig. 3.2, Chapter III), virulence (Fig. 3.3-3.5, Chapter III) and tissue invasion ability (Fig. 3.6, Chapter III) was presented in Chapter III. This provides significant insight into *A. fumigatus* PacC-mediated adaptation and the mechanisms through which PacC action is accomplished in the murine host.

4.4.1 The *A. fumigatus* ATCC46645 transcriptional profile during initiation of murine infection highlighted crucial trends for the adaptation to the host niche and the establishment of infection

Aiming to identify crucial biological functions *for A. fumigatus* adaptation to the murine host niche transcriptional profiling of the ATCC46645 strain was performed relative to *in vitro*–cultured dormant spores (Fig. 4.2). A total of 1364 and 1299 genes were identified respectively as up-regulated and down-regulated during adaptation to the mammalian host (13.7% and 13.1% of *A. fumigatus* genome, Nierman *et al.*, 2005); among them 617 and 556 remained up- or down-regulated, respectively, across the entire time course of experimentation (Table 4.6). A milestone for DNA microarray analysis of *A. fumigatus* transcriptome analysis was reached when characterisation of the Af293 clinical isolate transcriptome during initiation of murine infection was achieved (McDonagh *et al.*, 2008a). In this previous study only one time point (i.e. 14 hours post-infection) was studied, the authors finding 2180 differentially expressed genes relative to an *in vitro* culture. This dataset is therefore roughly half the size of that reported here for ATCC46645, and though the relative percentages of induced and repressed genes between the two wild-type transcriptional profiles are similar, the overlap between the two datasets is limited to 890 genes. In the present study major transcriptional trends have been identified such as the up-regulation of

transport systems for the uptake and mobilisation of crucial elements, and cell wall functions to counteract the challenging host niche.

Confirming the fundamental role of iron in *A. fumigatus* pathogenicity, at least five genes induced in the ATCC46645 strain during murine infection are involved in iron homeostasis (Afu3g03440, Afu3g03390, Afu7g04730, Afu2g07680, and Afu6g13750). The requirement for iron has been previously studied with respect to *A. fumigatus* virulence (Haas, 2003; Haas *et al.*, 2008; Schrettl *et al.*, 2004; Schrettl *et al.*, 2007). *A. fumigatus* lacks specific uptake systems for host iron sources (Schrettl *et al.*, 2004), but possesses two high-affinity iron uptake mechanisms, namely siderophore-mediated uptake and reductive iron assimilation (RIA) (Schrettl *et al.*, 2004). Both of these systems are induced, at the level of transcription, as a consequence of iron starvation (Schrettl *et al.*, 2004), but whereas RIA is dispensable for *A. fumigatus* virulence, siderophore biosynthesis is essential (Schrettl *et al.*, 2004). In fact, the elimination of both intra- and extracellular siderophores, by deletion of the *SidA*-encoded L-ornithine N5-oxygenase (catalysing the first step of siderophore biosynthesis), completely attenuates *A. fumigatus* virulence in a murine model of invasive aspergillosis (Schrettl *et al.*, 2004). *sidA* (Afu2g07680) can be found among the top 100 up-regulated genes in the ATCC46645 timecourse (Table 4.3) thereby validating the physiological relevance of the dataset with respect to identifying virulence determinants.

In addition to the genes involved in siderophore biosynthesis, other genes commonly associated with *A. fumigatus* pathogenicity are induced in the ATCC46645 strain during infection. Commonly classed as factors facilitating *A. fumigatus* virulence, secreted proteases (Latge, 1999) are proposed to release amino acid nutrients by degradation of murine lung parenchyma. *A. fumigatus* can synthesise a broad range of degradative enzymes, such as elastases and proteases, to assist with invasion of host tissue and nutrient acquisition. Elastin and collagen constitute major components of mammalian lung tissues, and a direct correlation has been demonstrated between elastase production in *A. fumigatus* strains and virulence. Strains not producing elastase showed fewer germinated spores and no destruction of alveoli in murine lungs (Kothary *et al.*, 1984). *A. fumigatus* produces and secretes a series of catabolic enzymes, especially peptidases, to degrade macromolecular complexes and derive nutrients (Alp and Arikan, 2008), however *A. fumigatus* protease mutants have been described as fully virulent (Jaton-Ogay *et al.*, 1994; Latge, 1999), probably because of the redundancy among the many enzymes produced and involved in the degradation of murine lung parenchyma. In this respect the global analysis of peptidase expression during colonisation of the host niche is intriguing and may identify the catalogue of enzymes required to establish infection. The ATCC46645 transcriptional profile does not reveal significant induction of

mechanisms directly involved in nitrogen acquisition, but several secreted peptidase (Afu4g09320, Afu4g11800, Afu6g08640 and Afu5g13300) were strongly upregulated from the earliest stages of infection, relative to dormant spores.

The present study observes significant representation of enzymes and proteins known, and likely, to participate in the extensive cell wall remodelling required to direct cellular morphologensis during developmental growth in the host and also to protect cells from external factors challenging cellular homeostasis (Afu7g05450, Afu1g16250, Afu4g10150 and Afu2g00640 among the top 100 up-regulated genes in the ATCC46645 trascriptional analysis, Table 4.3). In *S. cerevisiae*, tolerance to cell wall stress is mediated by the cell wall integrity (CWI) pathway, a phosphorylative cascade initiated with the activation of protein kinase C (Pkc1p) and acting via various kinases including which Slt2p results in the phosphorylation of several cytosolic and nuclear targets including Rlm1p, Swi4p and Swi6p (Heinisch *et al.*, 1999; Lagorce *et al.*, 2003). A significant overlap has been observed in *S. cerevisiae* between the gene expression modulation as a consequence of the alkalinisation of the environment, and of exposure to cell wall damaging agents (Garcia *et al.*, 2004; Lagorce *et al.*, 2003). Cell wall damage induces genes involved in metabolism, energy production and stress response (such as chaperones), but decreases the expression of transcription factors and of genes involved in protein synthesis and cell growth; this pattern of transcriptional modulation is very similar to that observed as a consequence of other environmental stresses. According to its main function, i.e. to maintain cell morphology and to protect cells from the external factors challenging the cell internal homeostasis, the cell wall is a dynamic structure, which needs to adapt to support cell growth, but also to face environmental changes.

During infection with the ATCC46645 strain, a general repression of transcription is noticeable (Table 4.4) and several ORFs involved in the regulation of transcription, ribosomal biogenesis and assembly, and protein biosynthesis and processing (Afu5g02880, Afu7g02620, Afu5g06140, Afu3g11330, Afu3g10120, Afu1g17360, Afu4g12390, Afu1g14750, Afu2g10550) are down-regulated, relative to the parental strain. This may reflect the poor nutritional value of the host niche, resulting in the slowing of *A. fumigatus* growth. Metabolic repression is a trend which is commonly associated with microbial systems undergoing adaptation to stress, and was previously identified for host-adapting *A. fumigatus* (McDonagh *et al.*, 2008a) where the trend manifested to a much broader extent, involving genes directing ribosomal biogenesis and assembly (rRNA synthesis, RNA polymerase activity) and protein biosynthesis and processing (translation initiation and elongation, tRNA processing and synthesis, intracellular trafficking, secretion and vesicular trafficking). An alternative explanation is that during developmental growth in the murine host niche the

organism experiences a lag phase in growth whereby transcription, relative to dormant spores, is down-regulated temporarily. In support of this hypothesis the trend appears to invert at later stages of infection, where on the contrary several genes encoding transcription regulators are induced (Afu6g12150, Afu1g02860, Afu5g13020 and Afu6g03800). However, of note is the fact that aerobic respiration and oxidative metabolism are concommittantly significantly up-regulated (Tables 4.3) which implies that cell cycle-specific fluctuations in transcriptional activity might be contributing to the observed function profile.

A previously reported finding that, during murine host adaptation, differentially expressed genes are located in contiguous gene clusters and preferentially in subtelomeric regions of the chromosomes was not disputed by this analysis of ATCC46645 transcription (Figs. 4.9 and Fig 4.10 respectively). Where temporal expression profiles were significantly enriched for these terms, temporal expression of such genes increased with time. This finding negates the hypothesis that previous findings were soley attributable to choice of reference sample and further assigns significance to activation of such loci duing murine infection. Subtelomeric genomic regions are predominantly hypoacetylated (Katan-Khaykovich and Struhl, 2005) and are also known to undergo ectopic recombination more often than the rate expected for homologous recombination (Farman, 2007), generating expansion and diversity of chromosome ends. Such gene arrangement has been thought to be advantageous for the fungus, especially in relation to secondary metabolite production (Shwab *et al.*, 2007). The organisation of up-regulated *A. fumigatus* genes into infection clusters, predominantly residing in the telomeric regions of chromosomes suggests additional epigenetic mechanisms of regulation. Epigenetic regulation of gene expression is thought to be mediated by modification in chromatin properties, such as histone acetylation and methylation, which likely modify the interactions of histones with transcriptional regulators (Jenuwein and Allis, 2001). Histone acetylation is probably the best investigated type of histone modification and is controlled by the opposite action of histone acetyltransferases and deacetylases (HDACs). Generally, hypoacetylation of histones is associated with gene silencing, whereas hyperacetylation is associated with gene activation (Robyr *et al.*, 2002; Trojer *et al.*, 2003). Regulation of gene expression has been linked to chromosomal architecture for subtelomeric gene clusters in *A. nidulans* which direct the biosynthesis of penicillin and sterigmatocystin, regulated in opposing fashions by the methyltransferase LeaA (Bok *et al.*, 2005) and the HdaA histone deacteylase (Shwab *et al.*, 2007). In *A. nidulans*, deletion of *hdaA* causes the transcriptional activation of these two gene clusters which are localised in proximity of the telomere. Interestingly, HdaA also regulates a cluster of un-related genes, comprising a variety of genes concomitantly activated as a consequence of challenging environmental

conditions and stresses (Robyr *et al.*, 2002). With respect to the current investigation, it would not appear that subtelomeric regions of the genome are subject to silencing during infection (Fig. 4.10).

Epigenetic regulatory mechanisms are involved in the pathogenicity of other microbes, such as *Plasmodium falciparum* (Freitas-Junior *et al.*, 2005) and *C. glabrata* (De Las Penas *et al.*, 2003). In *P. falciparum*, HDACs are involved in the regulation of the subtelomeric *var* gene cluster which allow the organism to develop antigenic variability, so as to elude the host immune response (Freitas-Junior *et al.*, 2005). In *C. glabrata*, the NAD^+-dependent HDAC Sir2p modulates the expression of the subtelomeric cluster EPA, which is crucial for biofilm formation and therefore pathogenicity (De Las Penas *et al.*, 2003). Epigenetic mechanisms of gene regulation of proximal gene clusters have been identified also in yeast (Bernstein *et al.*, 2000; Hansen *et al.*, 2005; Katan-Khaykovich and Struhl, 2005), where an ever broader and coordinated action for the HDACs has been demonstrated. The *S. cerevisiae* HDACs Hda1, Rpd3, and Sir2 suppress their own unique set of genes, but they also repress numerous shared genes (Bernstein *et al.*, 2000). In *Schizosaccharomyces pombe*, the same scenario is present for the HDACs Clr3, Clr6, Sir2, and Hos2 (homologous to *A. nidulans* HdaA, RpdA, HstA, and HosA, respectively Graessle *et al.*, 2000), which modulate the expression of both unique and shared genes (Hansen *et al.*, 2005; Wiren *et al.*, 2005). An *A. fumigatus* Sir2 homologue is upregulated during ATCC46645 host adaptation (Table AD.1.3 in Appendix D).

A. fumigatus relies upon the production of several toxic secondary metabolites, the biosynthetic pathways for which have evolved to counter hostility in ecological niches (Cui *et al.*, 1996a; Cui *et al.*, 1996b; Frisvad *et al.*, 2009). In the present study the expression of a LaeA-like methyl transferase increased uniquely at 8 hrs post-infection with the ATCC46645 strain. Secondary metabolite production is strongly affected by the disruption of LeaA (Bok *et al.*, 2005), which regulates 10% of the *A. fumigatus* genome and whose deletion results in attenuated virulence in mice (Sugui *et al.*, 2007a; Perrin *et al.*, 2007). Transcriptional profiling of the ATCC46645 strain incorporated differentially expressed genes having predicted roles in secondary metabolite production (Perrin *et al.*, 2007). Gliotoxin is the most extensively studied *A. fumigatus* secondary metabolite and is a metabolite of the epipolythiodioxopiperazine family (Mullbacher and Eichner, 1984; Mullbacher *et al.*, 1985) which is acutely toxic and has immunosuppressive properties, blocking phagocytosis (Waring *et al.*, 1988), release of inflammatory mediators by leukocytes (Pahl *et al.*, 1996), and inducing the apoptosis of neutrophils and monocytes (Frame and Carlton, 1988; Waring *et al.*, 1988; Stanzani *et al.*, 2005). Environmental *A. fumigatus* strains defective in the production of gliotoxin have been demonstrated to be less virulent than strains producing this secondary

metabolite efficiently (Sutton *et al.*, 1996). Deletion of gliotoxin differentially affects *A. fumigatus* virulence depending upon the immunosuppressive regimen of the host; in particular the gliotoxin mutant is characterised by wild type virulence in a neutropenic model, but reduced virulence in a non-neutropenic model (Bok *et al.*, 2006; Spikes *et al.*, 2008; Sugui *et al.*, 2007b). In this study of ATCC46645 temporal gene expression, transcription of genes in the gliotoxin cluster (Afu6g09580–Afu6g09770) (Perrin *et al.*, 2007) strictly follows the expression pattern of the LaeA-like regulator, which is induced at a middle stage of infection.

Pseurotin A is a secondary metabolite which competitively inhibits chitin synthase and acts as an inducer of nerve-cell proliferation (Maiya *et al.*, 2007). The genes required to direct biosynthesis of this compound have been identified and are are localised in a cluster (Afu8g00100-Afu8g00720) on chromosome eight (Perrin *et al.*, 2007). The best characterised of these is the hybrid polyketide synthase-non-ribosomal peptide synthetase (Afu8g00540) (Maiya *et al.*, 2007). Contrary to previous findings differential expression at this secondary metabolite gene cluster is not observed during initiation of ATCC46645 infection, confirming the predictable variability between different *A. fumigatus* strains isolates. Notwithstanding the use of an alternative reference sample, both gliotoxin and pseurotin A are induced during murine infection (McDonagh *et al.*, 2008a) in the Af293 clinical isolate. Of note for the subsequent discussion is the presence of ORFs flanking these gene clusters which are implicated in transposition.

The ATCC46645 transcriptional profiling was also analysed in comparison to the results for *A. fumigatus* shift to alkaline pH *in vitro*. A microarray study performed by our research group to elucidate the transcriptional response to alkaline conditions has recently delineated the temporal response of *A. fumigatus* to an alkaline shift *in vitro* (Loss *et al*., unpublished). For the *in vitro* study the transcriptional profile of *A. fumigatus* mycelia grown for 14 hours in AMM pH 5.0 and subsequently shifted to pH 8.0 was analysed for a window of 60 minutes and samples were taken for RNA extraction after 5, 15, 30, 45 and 60 minutes following alkaline shift. Among a total of 1364 and 433 genes upregulated, respectively, in the *in vivo* time course and in the *in vitro* study, the overlap consists of 127 genes, representing more than 25% of the *in vitro* alkaline-responsive genes, and reinforcing the significance of this adaptation mechanism in host-adaptation. Interestingly, among a total of 1299 and 141 genes downregulated, respectively, in the *in vivo* time course and in the *in vitro* study, the overlap consists of only 30 genes. A plausible explanation for this is the requirement of both alkaline- and acid-regulatable functions during colonisation of the murine host, in support of which hypothesis the induction of both alkaline and acid phosphatases is observable. With respect to temporal expression profiles, high concordance was notable

between up- and down-regulation trends in host and laboratory niches. Some interesting differences were found by STEM analysis, whereby ORFs which were repressed *in vitro* after a shift to alkaline pH, were instead upregulated during infection. Two of these ORFs are predicted to be involved in cell wall organisation (Afu3g08110 and Afu2g144900).

4.4.2 The *A. fumigatus* ATCC46645 Δ*pacC* mutant transcriptional profile during initiation of murine infection reveals possible involvement of epigenetic mechanisms to effect PacC-mediated gene regulation

Elucidating the transcriptional response during initiation of murine infection in the *A. fumigatus* Δ*pacC* mutant and in comparison with the respective parental isolate provided significant insight into *A. fumigatus* PacC-mediated adaptation and the mechanisms through PacC action is accomplished in the murine host. Aiming to analyse biological functions which are crucial for infection at early, middle and late stages transcriptional profiling of the ATCC46645 Δ*pacC* strain was performed relative to isogenic dormant spores (Fig. 4.15). A total of 1198 (12.1% of *A. fumigatus* genome, Nierman *et al.*, 2005) and 1317 (13.3%) were identified respectively as up-regulated and down-regulated during adaptation to the mammalian host (Table 4.9). Within these same categories, 423 and 376 genes were similarly up- or down-regulated, respectively across the entire time course (Fig. 4.19). A direct comparative analysis of ATCC46645 Δ*pacC* relative to the parental isolate ATCC46645 was also performed (Fig. 4.30). This identified a total of 729 (7.3% of *A. fumigatus* genome, Nierman *et al.*, 2005) and 762 (7.8%) genes as being up-regulated or down-regulated respectively, among these 68 and 74 genes were similarly up- or down-regulated, respectively, across the entire temporal comparison (Fig. 4.34 and Table 4.16). This dual approach therefore constituted one focused strategy to analyse differences between ATCC46645 Δ*pacC* and ATCC46645 gene expression in the host and an accompanying set of temporal transcription profiles for both strains which could be selectively probed to identify stage-specific modulation of gene expression. Particularly noteworthy in this respect is the block in developmental growth demonstrated by the mutant strain during infection (Fig. 3.6, Chapter III). Morphological differences were minimal between mutant and parental strain at 4 and 8 hours post-infection, but by 16 hours the ATCC46645 Δ*pacC* mutant was unable to progress beyond primary hyphal morphotypes, whereas ATCC46645 wild type revealed extensively branched invasive growth.

As determined from the ATCC46645 transcriptional profile, nutrient acquisition represents one of the primary fungal requirements, and may be largely attributable to the

alkaline nature of the mammalian lung environment. Proteins often have an optimal pH at which to act and the alkalinisation of the external pH might constitute a challenge for surface or secreted proteins, required for the uptake and mobilisation of crucial nutrients. In addition, most of the transport system across the biological membrane is energised by a proton gradient, which is inevitably affected by the environmental pH. Additionally the solubility itself, of crucial elements can be modified as a function of pH. A conspicuously aberrant regulation of transport was noticeable when comparing the Δ*pacC* mutant transcriptome to that of the parental isolate (Table 4.17-4.18). PacC is known to act as both an activator and a repressor of *Aspergillus* gene expression. Accordingly, there was no bias towards derepression or induction among differential gene expression and moreover, ORFs associated with transport functions are enriched among both up- and down-regulated genes (Table 4.21-4.22). A notable distinction between transporter functionality can be drawn between up- and down-regulated genes whereby those which are down-regulated in the Δ*pacC* genetic background predominantly include those involved in the uptake and mobilisation of metal ions such as copper, zinc, sodium, and calcium, phosphate, amino acids and various nutrients, whereas the up-regulated gene functions are predominantly involved in sugar transport. Given the bifunctional activity of PacC gene regulatory activity this observation might be explained in various ways. An immediately obvious assumption is that genes which are up-regulated in the mutant background, would normally be subject to PacC-mediated repression. Why would a transcription factor mediating alkaline-responsive gene expression negatively regulate such a group of transporters? The answer might lay in the nature of the transport functions supported by these proteins. Often sugars are transported in symport with protons, thereby neutralising the cytoplasm of the cell as carbohydrates are taken up into the cell. Under alkaline conditions such activities would be counterproductive and likely to halt growth. If this hypothesis were correct their upregulated expression in the mutant genetic background might contribute to pH sensitivity of the mutant. On the other hand the range of transporters in which down-regulation is observed in this study might largely represent functions essential for supporting growth at high pH. Given their normally positive regulation by PacC, and their plasma membrane locations they represent an important class of genes for further study as putative virulence modulators and therapeutic targets and would be prime candidates for analysis by split-ubiquitin screening.

The fungal cell wall undergoes extensive remodelling during morphogenesis and in response to stress, including that imposed by alkaline environments. Significant concordance between genes expressed during alkalinisation of the environment and in response to cell wall modulating agents has already been demonstrated (Garcia *et al.*, 2004; Lagorce *et al.*, 2003).

The enrichment of cell wall-related ORFs within the differentially expressed genes in the *A. fumigatus* ATCC46645 Δ*pacC* mutant transcription profile during murine infection and relative to the parental isolate ATCC46645 strengthen the putative connection between maintenance of cell wall integrity and PacC, which has been recently demonstrated for other pathogenic fungi. Using an over-expression rescue screen, Rim101p-dependent functions effecting cell wall alterations, and demonstrated to affect *C. albicans* pathogenic interaction with oral epithelial cells have been identified. Four Rim101p targets, implicated in cell wall organisation, were able to partially restore the pathogenic interactions of a *C. albicans rim101*Δ/Δ mutant with oral epithelial cells (Nobile *et al.*, 2008). Also, in *C. neoformans*, the *rim101*Δ mutant, which is slightly more virulent than the wild-type, suffers major defects in the polysaccharide capsule (O'Meara *et al.*, 2010). Because few capsule biosynthetic genes were transcriptionally regulated by Rim101p, the phenotype observed was attributed to defects in the attachment of the capsule to the cell wall (O'Meara *et al.*, 2010).

Regarding *A. fumigatus* virulence factors which may be affected by *pacC* deletion the analysis of the ATCC46645 transcriptome confirmed the fundamental importance of iron in *A. fumigatus* pathogenicity, showing that at least five genes induced during murine infection are involved in iron homeostasis (Afu3g03440, Afu3g03390, Afu7g04730, Afu2g07680, and Afu6g13750). The elimination of both intra- and extracellular siderophores causes the attenuation of *A. fumigatus* virulence in a murine model of IPA (Schrettl *et al.*, 2004), however, down-regulation of these genes in the ATCC46645 Δ*pacC* mutant was not observed, with the exception of the ferric-chelate reductase (Afu6g13750). Unexpectedly, this disagrees with previous findings which established the PacC-mediated regulation of siderophore biosynthetic genes in *A. nidulans* through the use of acidity- and alkaline-mimicking mutants (Eisendle *et al.*, 2004). Thus the avirulence of Δ*pacC* mutants is unlikely to be simply explained by defective siderophore biosynthesis, although direct physiological support for this hypothesis would require an assessment of siderophore production. In addition to a putative role in the regulation of cation transport, PacC appears to regulate the expression of various other transporters, most notably the MFS gliotoxin efflux pump GliA. Interestingly, PacC may also regulate the expression of putative virulence determinants during infection (e.g. Mep, Afu8g07080, Alp1, Afu4g11800 and Catalase 1, Afu3g02270).

The *A. fumigatus* ATCC46645 Δ*pacC* mutant transcription profile relative to the parental isolate ATCC46645 during initiation of murine infection supports the hypothesis that Δ*pacC* mutant development is specifically deregulated at early stages of infection, given that at least two developmental regulators, the FluG family protein (Afu8g06130) and the sexual development protein EsdC (Afu7g01930) showed altered expression during the initiation of

infection as a consequence of *pacC* deletion. The FluG family protein (Afu8g06130) (D'Souza *et al.*, 2001) and the sexual development protein EsdC (Afu7g01930) (Han *et al.*, 2008) have been only characterised in *A. nidulans*, which differs from *A. fumigatus* for having a well known and characterised sexual cycle. In *A. nidulans*, several factors are able to influence developmental activation through FluG, which has been demonstrated as necessary for the synthesis of a small diffusible factor, required for the induction of asexual sporulation in air-exposed colonies (Lee and Adams, 1994). These stresses include air exposure, carbon or nitrogen starvation, and increased osmolarity. *fluG* and *flbA* are respectively up- and down-regulated during murine infection by a wild-type strain suggesting their potential role in *A. fumigatus* development in the host, which is further strengthened by the strong down-regulation of *fluG* expression in the Δ*pacC* mutant. Given this developmental block, two non-mutually exclusive hypothesis can be applied when interpreting the comparative transcription data. On the one hand, where gene expression (and possibly also function) is limited to a specific developmental phase, differences in gene expression between the wild type ATCC46645 and the ATCC46645 Δ*pacC* mutant would be expected regardless of whether that specific ORF is under PacC regulatory control. In the absence of further experimentation it would not be possible to separate this hypothesis from that of a direct regulatory role for PacC upon expression of the ORF.

A gene cluster on chromosome six, involved in the production of the secondary metabolite gliotoxin, was induced in both the ATCC46645 and Af293 (McDonagh *et al.*, 2008a) datasets. Comparing the transcriptional profiles of *A. fumigatus* ATCC46645 and *A. fumigatus* ATCC46645 Δ*pacC* mutant during initiation of murine infection the impairment of gliotoxin biosynthetic gene expression in the Δ*pacC* mutant relative to the wild-type was revealed (Table 4. 22). At least 8 genes in the gliotoxin cluster are highly down-regulated in the mutant (Afu6g09640, Afu6g09670, Afu6g09730, Afu6g0700, Afu6g0720, Afu6g09650, Afu6g09710, Afu6g09740). In addition, expression of a LeaA-like (Bok *et al.*, 2005) methyltransferase is also affected by *pacC* deletion, suggesting a PacC-dependent mode of LaeA-like regulation for the gliotoxin cluster. The most attractive hypothesis is that gliotoxin biosynthesis is regulated by PacC therefore explaining why, in absence of *pacC*, the gliotoxin cluster is repressed. In support of this hypothesis, the promoter of the MFS gliotoxin efflux transporter GliA (Afu6g09710) contains a recognition site for PacC binding. Alternatively, gliotoxin gene expression is linked to developmental growth blocked and its expression is therefore blocked in the Δ*pacC* mutant.

In addition to the confirmation of the aberrant regulation of many biological functions commonly associated with pH regulation, such as transport, ion homeostasis and cell wall

organisation, the comparison of the transcriptional profiles of *A. fumigatus* ATCC46645 and *A. fumigatus* ATCC46645 Δ*pacC* during initiation of murine infection highlighted the correlation between *pacC* deletion and defects in DNA organisation, whereby at least seven genes involved in this specific function are down-regulated in the ATCC46645 Δ*pacC* transcriptome relative to that of the parental isolate (Afu2g16710, Afu2g02090, Afu3g05360, Afu1g07430, Afu2g04140, Afu6g13290, Afu2g05189). Epigenetic mechanisms act as modulators of gene expression *per se*. The first reports of chromatin-mediated specification of transcriptional factor targets have emerged only recently (Buck and Lieb, 2006). Buck and collaborators demonstrated that the target set of the regulator of yeast metabolism Rap1p is determined by the chromatin regulator Tup1p and associated partners, showing that in this instance, the genome architecture itself is remodelled altering the targeting and therefore the biological effect of the transcription factor.

A striking feature of the mutant transcriptome was the apparent PacC-mediated repression of ORFs involved in transposition, whereby transcriptases and transposable elements (TEs) are down-regulated *in vivo* in the ATCC46645 Δ*pacC* mutant relative to the respective parental isolate (see Table 4.18 and 4.22). TEs are DNA sequences which are able to migrate across the genome, affecting genome size, structure and gene expression, discovered initially by McClintock in the 50s (and discussed in McClintock, 1984). They represent a substantial part of most eukaryotic genomes, e.g. respectively 45% and 3-5% of human and yeast genomes, respectively (Biemont and Vieira, 2006) and can be grouped into two main classes: DNA transposons (class II), acting via a DNA intermediate and using the cell machinery to replicate, and retrotransposons (class I), acting via an RNA intermediate. Retrotransposons include long interspersed nuclear elements (LINEs), short interspersed nuclear elements (SINEs), LTR (long terminal repeats) and non-LTR retrotransposons. LTR retrotransposons encode all the proteins necessary for their migration across the genome. TEs belonging both to class I and class II have been found in the *Aspergillus* species; however, active transposition has been demonstrated only in *A. niger* for the class II elements *Ant1* (Glayzer et al., 1995), *Tan1* (Nyyssonen *et al.*, 1996) and *Vader* (Amutan et al., 1996), whereas for *A. fumigatus* only inactive TEs have currently been identified, i.e. *Afut1* (Neuveglise *et al.*, 1996) and *Afut2* (Paris and Latge, 2001) for class I and *TafI* (Monroy and Sheppard, 2005) for class II. Due to the abundance and distribution of TEs within the genomes of eukaryotes, and analogies with retrovirus genomes, TEs have been for decades at the centre of an ongoing debate to establish whether they are parasitic entities or they actually provide some benefits to the host cell. Supported by increasing experimental evidence, the prevailing common belief is that TEs act as gene regulatory elements (Jordan *et al.*, 2003;

Kashkush *et al.*, 2003; Sehgal *et al.*, 2007 and reviewed in Biemont and Vieira, 2006). Although their impact on gene expression is not well characterised yet, TEs elements have reported to be normally silent, but able to be activated by a variety of stresses (Wessler, 1996). In the fission yeast *Schizosaccharomyces pombe* the Tf2 transposon family has been recently associated with Sre1p oxygen-dependent gene regulation (Sehgal *et al.*, 2007). In *S. pombe*, Sre1p is a transcription factor involved in the response to anaerobic stress. The activation and nuclear entry of Sre1p is determined by proteolytic processing in low-oxygen conditions (Todd *et al.*, 2006). Tf2 LTRs have been demonstrated to act as Sre1-regulated mediators of oxygen-dependent transcription of adjacent genes (Sehgal *et al.*, 2007). A brief examination of the results presented in the current study would reveal that PacC consensus binding sites are not present in all of the differentially expressed genes in the dataset. For example, considering the set of PacC-regulated genes during infection, 87% of these genes lack a PacC consensus sequence in their promoter, suggesting that this transcription factor has a predominantly indirect (i.e. non *cis*-acting) mechanism of gene regulation during infection. Interestingly, the GO Term enrichment analysis of the non *cis*-regulated genes and the genes having at least one PacC consensus sequence in the promoter region (13% of the genes in the same set) highlighted similar processes such as transport, metal-ion transport, pathogenesis, peptide metabolic processes, nonribosomal peptide biosynthetic processes, establishment of localisation and peptide biosynthetic processes. It is likely therefore that differential gene expression in the mutant results from deficits in several distinct regulatory mechanisms, perhaps via the participation of TEs as intermediates. The lack of an evident change in expression of the same set of genes in the ATCC46645 transcriptional profile may exclude a general role for transposition in *A. fumigatus* virulence. The model proposed in *S. pombe* and relating anaerobic stress to Sre1-mediated gene regulation through the Tf2 transposon family (Sehgal *et al.*, 2007) presents an attractive hypothesis against which to test our results. The parallels between the two systems extend to several variables including the action of a proteolytically activated transcription factor (Sre1p or PacC) in response to environmental stress (anaerobic or alkaline) and modulation of expression of several genes, localised in close proximity along the chromosomes. The activity of TEs is under the control of epigenetic regulation, which implies the regulatory instructions relative to the specific element do not depend on the DNA sequence of the element itself, but rather on modification of the DNA or its associated proteins (especially histones). Such modifications consist of methylation of DNA nucleotides and methylation or acetylation of the associated histones (Fedoroff, 1989). Misregulation of genes involved in DNA organisation would therefore corroborate the hypothesis of the involvement of PacC-TE-mediated gene regulation.

The *A. fumigatus* ATCC46645 Δ*pacC* mutant transcription profile relative to the parental isolate ATCC46645 during initiation of murine infection pointed to the indirect way in which PacC might act to regulate the expression of the identified broad set of targets. In particular the results confirmed the possible role of epigenetic mechanisms, which would imply chromatin remodelling and/or transposition, to regulate blocks of adjacent genes. As previously discussed, in a challenging host environment, epigenetic mechanisms might act in a PacC-mediated manner to modulate gene expression *per se* and/or to activate TEs mobilisation. The comparison of *A. fumigatus* ATCC46645 Δ*pacC* and ATCC46645 transcriptional profiles showed ORFs acting in DNA organisation were affected by *pacC* deletion, retrieving the previously mentioned hypothesis that PacC might act through chromatin-mediated specification of its transcriptional targets, as described for the regulator of yeast metabolism Rap1p (Buck and Lieb, 2006). Interestingly, histone modification has been recently identified as crucial for the regulation of secondary metabolite biosynthesis in *A. nidulans*, with the demonstration of a role for COMPASS complex member (complex associated with Set1), Bre1 in the activation of the expression of an otherwise cryptic secondary metabolite cluster (Bok *et al.*, 2009). The conserved eukaryotic COMPASS complex acts to both facilitate and repress chromatin-mediated processes by methylation of lysine 4 of histone 3 (H3K4) (Mueller *et al.*, 2006; Sims and Reinberg, 2006). Independently obtained experimental data to further support the hypothesised role for DNA reorganisation in PacC functionality will also emerge in several subsequent sections of this study.

CHAPTER V

CHARACTERISATION OF AN *A. FUMIGATUS* MEMBRANE PROTEIN COMPLEX INVOLVED IN pH PERCEPTION USING THE SPLIT-UBIQUITIN MEMBRANE YEAST TWO-HYBRID (MYTH) SYSTEM

5.1 Overview

Sensory deprivation could provide a means to inhibit infectious fungal growth, considering protein interactions at the plasma membrane are formative events in *A. fumigatus* environmental sensing. These protein-protein interactions, in particular those occurring in the plasma membrane, are attractive candidates for antimicrobial chemotherapy and are often required during initial adaptations to the host environment. In pathogenic fungi, they could provide a way to interfere with the first stages of infectious fungal growth. For example, in *A. nidulans*, the absence of either of the transmembrane proteins PalH or PalI blocks pH signalling, as PacC is not proteolytically processed (Denison *et al.*, 1995; Negrete-Urtasun *et al.*, 1999). However, it still remains unclear how signalling through the PacC/Rim101 pathway is initiated, particularly regarding the protein-protein interactions required for its activation.

Interactions among fungal proteins involved in pH sensing and adaptation have been described in various studies (Calcagno-Pizarelli *et al.*, 2007; Galindo *et al.*, 2007; Herranz *et al.*, 2005), providing important information about the connections within and between the two complexes involved in the establishment of the ambient pH signal in the model hypothesised for *A. nidulans*. The first of these complexes comprises the two plasma membrane proteins PalH and PalI and an arrestin-like protein PalF (Calcagno-Pizarelli *et al.*, 2007; Herranz *et al.*, 2005; Maccheroni *et al.*, 1997; Negrete-Urtasun *et al.*, 1999). PalH contains seven transmembrane domains and a long, hydrophilic C-terminus located in the cytosol, whose analogies with G-protein coupled receptors have raised the possible involvement in pH signalling of G-protein functionality (Herranz *et al.*, 2005). G-proteins are a group of transmembrane receptors involved in transmitting chemical signals received outside of the

cell and/or causing changes inside the cell. In *A. nidulans*, the hydrophilic C-terminal region of PalH interacts strongly with the arrestin-like protein PalF (Herranz *et al.*, 2005). *palF* and *palH* mutations preventing this interaction prevent pH signalling (Herranz *et al.*, 2005). These findings strongly indicate PalH as one, perhaps the only, essential component of a pH plasma membrane receptor. In *A. nidulans*, PalI contains three putative membrane-spanning domains with an N-terminal signal peptide and the basic C-terminus facing the cytosol (Calcagno-Pizarelli *et al.*, 2007). Unlike the null mutants of other *pal* genes, null *palI* mutants grow, though poorly, at alkaline pH (Denison *et al.*, 1995), suggesting an important, but not essential role for PalI in pH signalling. The function of PalI is suggested as assisting the plasma membrane localisation of PalH (Calcagno-Pizarelli *et al.*, 2007) by three possible mechanisms, which are still under investigation, namely down-regulation of PalH endocytosis, up-regulation of PalH recycling or assistance of PalH exit from the Golgi. Each of the three possibilities could require an interaction between PalH and PalI, either direct or indirect, but this has not been investigated (Peñalva *et al.*, 2008).

Membrane protein-protein interactions are immensely important in the organisation of living cells but they have been among the most difficult aspects of biology to be investigated. In this study, the MYTH (Fig. 5.1), commercially known as the DUALMembrane system, was used to investigate the interactions between component proteins of the *A. fumigatus* pH sensing and signalling pathway. Considering the high similarity between *A. nidulans* and *A. fumigatus* PalH, PalI and PalF (respectively 84.2%, 75.6% and 86.5%), *A. fumigatus* might mimic the model hypothesised for *A. nidulans*. Therefore, establishing the MYTH system utilising the pH sensing proteins PalH, PalI and PalF, not only represents an innovative platform to investigate *A. fumigatus* membrane protein-protein interactions, but will provide novel information about the pH signalling events leading to PacC activation.

Overcoming several limitations of the previous techniques adopted, the split-ubiquitin Membrane Yeast Two-Hybrid (MYTH) system innovatively exploits the functional complementarity of independently co-expressed amino and carboxy terminal portions of yeast ubiquitin (Ub), for characterising membrane protein-protein interactions (Fetchko and Stagljar, 2004; Johnsson and Varshavsky, 1994; Stagljar *et al.*, 1998). Ub is a conserved protein of 76 residues, primarily involved in protein degradation (Hershko and Ciechanover, 1992), whereby it is usually attached to the N-terminus of proteins as a signal for their degradation by the 26S proteosome. While the target protein is degraded by the 26S proteosome, the ubiquitin motifs are saved from degradation by cellular ubiquitin-specific proteases (UBPs), which cleave ubiquitin from the target protein after the C-terminal residue (Gly76), hence recycling the ubiquitin back to the cytoplasm. The two portions of yeast

ubiquitin, called Nub (for N-terminal ubiquitin, amino acids 1-34) and Cub (for C-terminal ubiquitin, amino acids 35-76) have a strong propensity for spontaneous reconstitution. A single amino acid exchange in position 13 of Nub from Ile to Gly (mutated Nub is termed NubG) abolishes the reconstitution of the two domains. However, the reconstitution of the split-ubiquitin can occur also as a consequence of the interaction between two proteins fused to NubG and Cub, which are therefore brought into close proximity within the cell. The bait, a membrane protein of interest which is expressed as a translational fusion to Cub and the hybrid transcription factor LexA-VP16 (Fig. 5.1A), is coexpressed with a second protein of interest, the prey, which is fused to NubG (Fig. 5.1B). The reconstituted split-ubiquitin is immediately recognised by ubiquitin-specific proteases (UBPs) which cleave the polypeptide chain between Cub and LexA-VP16, the latter being translocated to the nucleus of the cell where it binds the LexA operators situated upstream of several reporter genes (Fig. 5.1). The reporter genes used in the system are the two auxotrophic growth markers (*HIS3* and *ADE2*), on which activation depend the yeast to grow on defined minimal medium missing histidine or adenine, and lacZ, which encodes the enzyme b-galactosidase.

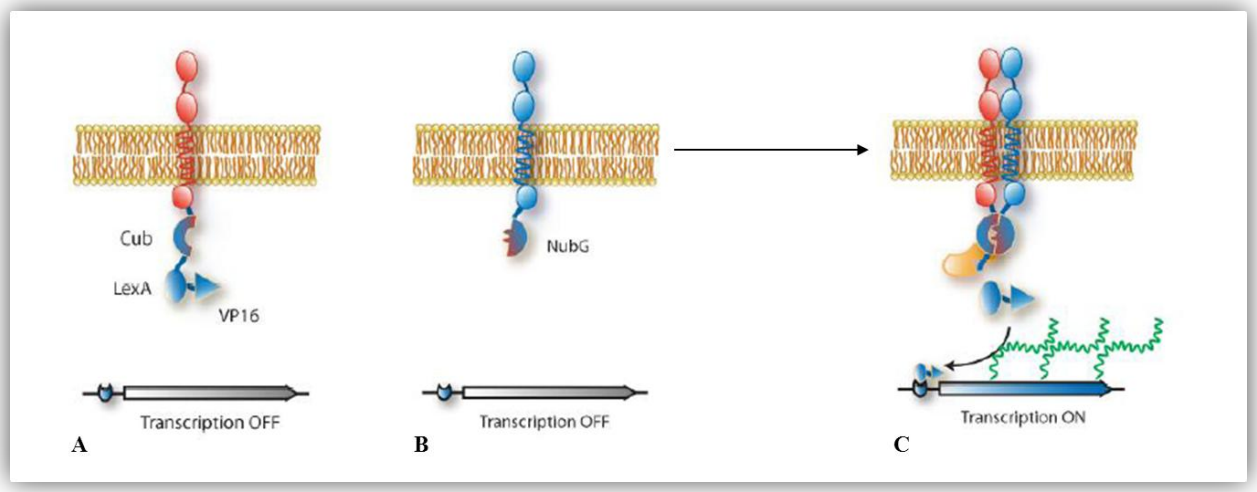


Fig. 5.1: Principle of the split-ubiquitin Membrane Yeast Two-Hybrid (MYTH) system. (A) The bait protein is an integral membrane protein, fused with a C-terminal region (Cub) of ubiquitin and the hybrid transcription factor LexA-VP16. The bait is immobilised at the membrane and unable to reach the nucleus to activate the reporter genes. (B) The prey is constructed by fusing a second protein of interest to a mutated N-terminal region (NubG) of ubiquitin. (C) Interaction between bait and prey places Cub and NubG in close proximity resulting in reconstitution of split-ubiquitin and release, by protease cleavage, of the hybrid transcription factor. LexA-VP16 enters the nucleus and activates the reporter genes. Thus, the interaction between bait and prey results in prototrophy for certain essential nutrients, which is detected on selective media. Modified from www.dualsystems.com.

5.2 Methods

5.2.1 *S. cerevisiae* strains

S. cerevisiae strain NMY51 [MATa *his3delta200 trp1-901 leu2-3,112 ade2 LYS2::(lexAop)4-HIS3 ura3::(lexAop)8-lacZ (lexAop)8-ADE2 GAL4*] was grown in yeast extract peptone adenine dextrose (YPAD) media (1% (w/v) yeast extract, 2% (w/v) peptone, 2% (w/v) glucose, 0.004% adenine sulphate) or in appropriate SD media, as described in Section 2.3.2. Solid YPAD or SD media was produced by addition of 2% (w/v) agar prior to autoclaving. Liquid cultures were agitated by orbital shaking at 180 rpm unless otherwise specified. *S. cerevisiae* strains were cultured for 2-3 days at 30°C. Strains were either stored at 4°C for up to 4 weeks on solid agar plates or for long term storage in 25% (w/v) glycerol at -80°C.

5.2.2 Plasmids

Bait plasmids: pPR3-STE (x-Cub), pPR3-SUC (x-Cub) and pBT3-N (Cub-X)

Three bait plasmids were used in this study. The bait vector pBT3-SUC (Fig. 5.2A) is specifically designed for expression of integral membrane proteins, having a N_{out}/C_{in} topology, whereby the N terminus is extracellular and the C terminus intracellular. The vector supplies a yeast signal sequence derived from the *SUC2* (invertase) gene of *S. cerevisiae*. The Cub-LexA-VP16 cassette is fused to the cytosolic C-terminus of the protein of interest. The vector pBT3-STE (Fig. 5.2B) containing the *STE2* leader sequence derived from the *S. cerevisiae* Ste2 protein (a G protein coupled receptor) is recommended for expressing, as baits, integral membrane proteins having multiple transmembrane domains and a N_{out}/C_{in} topology. The Cub-LexA-VP16 cassette is fused to the C-terminus of the bait. Membrane proteins having luminal C-termini are expressed from vector pBT3-N (Fig. 5.2C), permitting fusion of the LexA-VP16-Cub module to the cytosolic N-terminus of the protein of interest. The properties of these 3 bait vectors in terms of bacterial and fungal origin of replication, auxotrophic and resistance markers are summarised in Table 5.1.

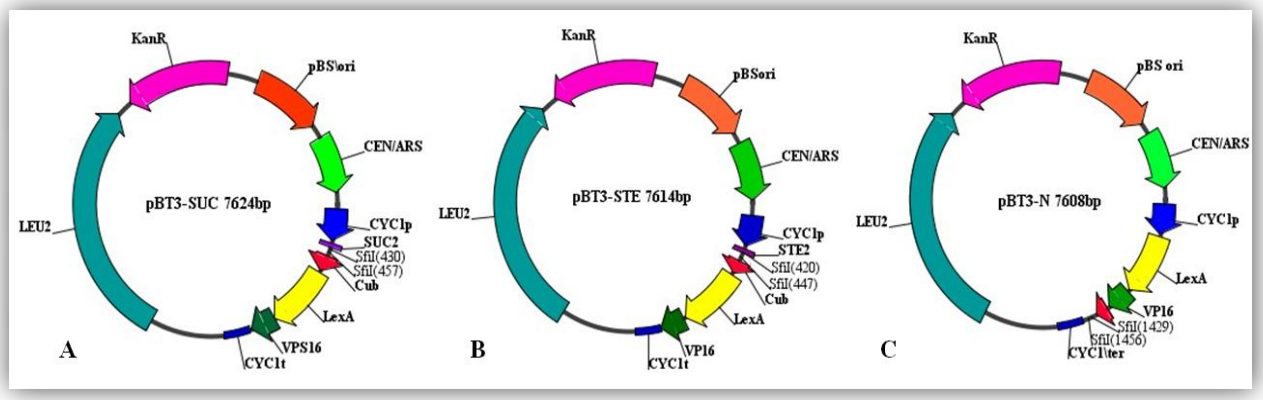


Fig. 5.2: Bait plasmids. (A) pBT3-SUC. This vector contains a yeast signal sequence derived from the *SUC2* (invertase) gene of *S. cerevisiae*. The Cub-LexA-VP16 cassette is fused to the cytosolic C-terminus of the protein of interest. (B) pBT3-STE. The STE2 leader sequence contained in this plasmid derives from the *S. cerevisiae* STE2p, which does not have any targeting function but only serves as a short leader sequence to increase the expression of the protein of interest. The Cub-LexA-VP16 cassette is fused to the C-terminus of the bait. (C) pBT3-N. This vector fuses the LexA-VP16-Cub module to the cytosolic N-terminus of the protein of interest. Maps generated by DNADynamo, www.bluetractorsoftware.co.uk.

Bait vectors				
Vector	Auxotrophic Marker (yeast)	Origin of replication (yeast)	Resistance Marker (*E. coli*)	Origin of replication (*E. coli*)
pBT3-SUC	*LEU2*	CEN/ARS (1-2 copies/ cell)	Kan (select with 30 µg/ml kanamycin)	High copy
pBT3-STE	*LEU2*	CEN/ARS (1-2 copies/cell)	Kan (select with 30 µg/ml kanamycin)	High copy
pBT3-N	*LEU2*	CEN/ARS (1-2 copies/cell)	Kan (select with 30 µg/ml kanamycin)	High copy

Table 5.1: Summary of the bait vectors properties. For each vector is shown the auxotrophic marker in yeast, the origin of replication in yeast, the resistance marker in *E. coli* and the origin of replication in *E. coli*.

Prey plasmids: pPR3-N (x-NubG) and pPR3-STE (NubG-X)

Preys and cDNA libraries can be developed in two orientations expressing fusion proteins with C-terminal NubG (pPR3-STE x-NubG, Fig. 5.3A) or with N-terminal NubG (pPR3-N NubG-X, Fig. 5.3B). The properties of these 2 prey vectors in terms of bacterial and fungal origin of replication, auxotrophic and resistance markers are summarised in Table 5.2.

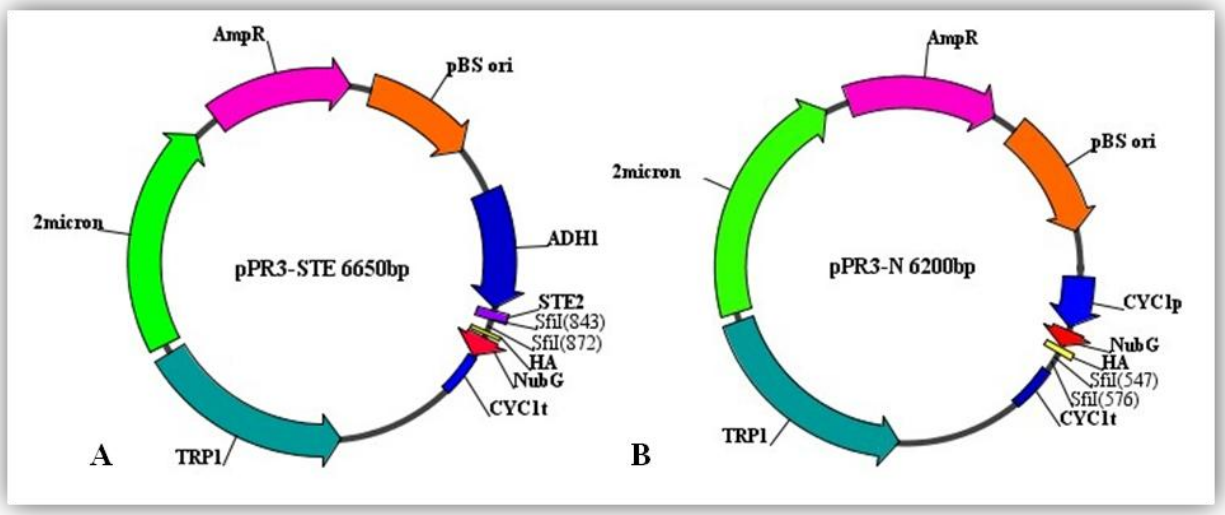


Fig. 5.3: Prey plasmids. (A) pPR3-STE. The NubG domain is fused to the C-terminus of the bait. (B) pPR3-N. This vector fuses the NubG domain to the cytosolic N-terminus of the protein of interest. Maps generated by DNADynamo, www.bluetractorsoftware.co.uk.

Prey vectors				
Vector	Auxotrophic Marker (yeast)	Origin of replication (yeast)	Resistance Marker (*E. coli*)	Origin of replication (*E. coli*)
pPR3-STE	*TRP1*	2 micron (20-50 copies/cell)	Amp (select with 100 µg/ml ampicillin)	High copy
pPR3-N	*TRP1*	2 micron (20-50 copies/cell)	Amp (select with 100 µg/ml ampicillin)	High copy

Table 5.2: Summary of the prey vectors properties. For each vector is shown the auxotrophic marker in yeast, the origin of replication in yeast, the resistance marker in *E. coli* and the origin of replication in *E. coli*.

Control plasmids: pCCW-Alg5, pAL-Alg5 and pDL-Alg5 The plasmid pCCW-Alg5 (Fig. 5.4A) which expresses a fusion of the yeast ER protein Alg5 to the Cub-LexA-Vp16 cassette has been used as control bait, in virtue of the presence of a functional and intracellularly-located Cub-LexA domain. The plasmids pAL-Alg5 (Fig. 5.4B) and pDL-Alg5

(Fig. 5.4C) which express a fusion of the yeast ER protein Alg5 to the wild type Nub portion of the yeast ubiquitin, or to the mutated NubG portion of the yeast ubiquitin, respectively, have been used as control preys. The properties of these control vectors in terms of bacterial and fungal origin of replication, auxotrophic and resistance markers are summarised in Table 5.3.

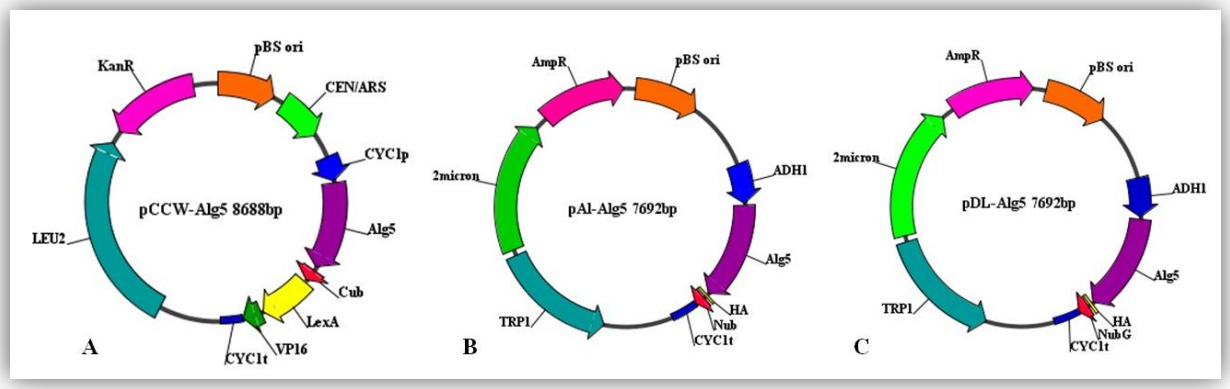


Fig. 5.4: Control plasmids. (A) pCCW-Alg5 for expressing a control bait, a fusion of the yeast ER protein Alg5 to the Cub-LexA-Vp16 cassette. (B) pAL-Alg5 for expression of control prey, a fusion of the yeast ER protein Alg5 to the wild type Nub portion of the yeast ubiquitin. (C) pDL-Alg5 for expressing a control prey, a fusion of the yeast ER protein Alg5 to the mutated NubG portion of the yeast ubiquitin. Maps generated by DNADynamo, www.bluetractorsoftware.co.uk.

Control vectors				
Vector	Auxotrophic Marker (yeast)	Origin of replication (yeast)	Resistance Marker (*E. coli*)	Origin of replication (*E. coli*)
pCCW-Alg5	*LEU2*	CEN/ARS (1-2 copies/ cell)	Kan (select with 30 µg/ml kanamycin)	High copy
pAL-Alg5	*TRP1*	2micron (20-50 copies/cell)	Amp (select with 100 µg/ml ampicillin)	High copy
pDl-Alg5	*TRP1*	2micron (20-50 copies/cell)	Amp (select with 100 µg/ml ampicillin)	High copy

Table 5.3: Summary of the control vectors properties. For each vector is shown the auxotrophic marker in yeast, the origin of replication in yeast, the resistance marker in *E. coli* and the origin of replication in *E. coli*.

Detailed maps of all plasmids can be found in Appendix C.

5.2.3 MYTH system

A. fumigatus membrane protein-protein interactions were tested using the DUALsystems split-ubiquitin MYTH system (DUALsystems Biotech), according to the manufacturer's instructions. All protocols, media and solutions used to perform the DUALmembrane screen are listed in the manufacturer's instructions, unless otherwise stated.

5.3 Results

5.3.1 Construction of a panel of *A. fumigatus* baits and preys to test pH-sensing protein interactions

In *A. nidulans*, PalH contains seven transmembrane domains and a long, hydrophilic C-terminus located in the cytosol, which interacts strongly with the arrestin-like protein PalF (Herranz *et al.*, 2005). PalI contains four highly hydrophobic domains, but *in silico* predictions had revealed the presence of an N-terminal signal peptide, therefore the hypothesised structure for *A. nidulans* PalI consists of three putative membrane-spanning domains and a basic C-terminus facing the cytosol (Calcagno-Pizarelli *et al.*, 2007). Whereas the interaction between PalH and PalF has been demonstrated as crucial for the establishment of pH signalling (Herranz *et al.*, 2005), no published information is available about interaction between PalH and PalI. The function of PalI has been suggested to be as in assisting the plasma membrane localisation of PalH (Calcagno-Pizarelli *et al.*, 2007) by three possible mechanisms, which are still under investigation and could require an interaction between PalH and PalI, either direct or indirect. However, no such demonstration has been provided in the current literature. *A. fumigatus* PalH, PalI and PalF show high similarity with the heterologous ones in *A. nidulans* (respectively 84.2%, 75.6% and 86.5% as shown in Appendix F), therefore suggesting a similar behaviour to that hypothesised for *A. nidulans*. The interaction between PalH and PalF was therefore used as positive control for the correct functioning of the MYTH platform, which was subsequently utilised to test the hypothesis that PalH and PalI directly interact in the plasma membrane.

A fundamental requirement of the MYTH screen is for the Cub-LexA-VP16 module of the bait protein, and for the NubG moiety of the prey protein to be cytosolically located. In order to satisfy these requirements, and to appropriately accommodate the topology of cloned membrane proteins (where it was known), and to overcome problems associated with expression of heterologous proteins (for example expression levels below the limits of

detection or above the limits of cells tolerance) a total of seventeen constructions were made. Fig. 5.5 shows the plasmids constructed to test every possible interaction between the three components of the plasma membrane signalling complex involved in *A. fumigatus* adaptation to environmental pH.

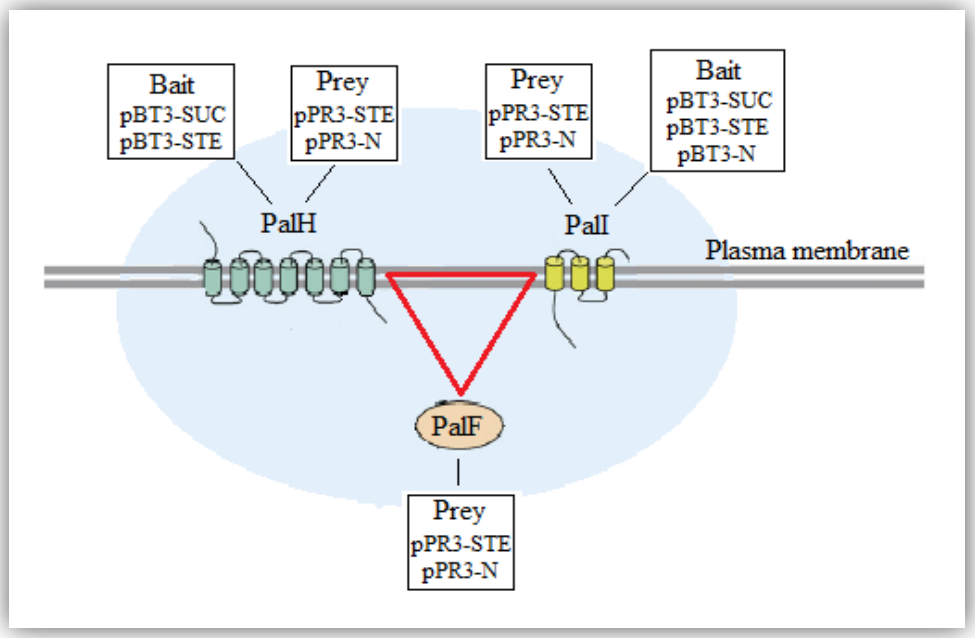


Fig. 5.5: Scheme representing the plasmids constructed to test every possible interaction between the three components of the plasma membrane pH signalling complex of *A. fumigatus*. *A. fumigatus* membrane proteins PalH and PalI were cloned both in bait and prey vectors. Various different vectors were employed for the bait (pBT3-SUC, pBT3-STE and pBT3-N) and prey (pPR3-STE and pPR3-N) expression to accommodate the topology of cloned membrane proteins and overcome problems with heterologous expression.

A. fumigatus membrane proteins PalH and PalI were cloned both in bait and prey vectors. Multiple vectors were employed for bait (pBT3-SUC, pBT3-STE and pBT3-N) and prey (pPR3-STE and pPR3-N) expressions. In particular for PalI, whose *in silico* predicted topology has not been validated by any experimental evidence, was cloned both as bait and prey in two topological orientations, expressing the fusion protein with N-terminal Cub (pBT3-N) or C-terminal Cub (pBT3-STE and pBT3-SUC) for the baits and with N-terminal NubG (pPR3-N) or with C-terminal NubG (pPR3-STE) for the preys. As demonstrated by the physical interaction of its C-terminus with the cytosolic protein PalF in *A. nidulans* (Herranz et al., 2005), *A. fumigatus* transmembrane protein PalH is likely to possess an intracellular C-terminus and was cloned as bait in the vectors pBT3-SUC and pBT3-STE and as prey in the vectors pPR3-N and pPR3-STE. According to its cytosolic location, *A. fumigatus* PalF was cloned uniquely as prey in the vectors pPR3-N and pPR3-STE. In fact, cytosolic proteins can

be tested in the system only as preys to avoid the entrance of the hybrid transcription factor into the nucleus independently of a detected interaction.

A. fumigatus PalH, PalI and PalF cDNAs were obtained by PCR using Platinum HiFi polymerase (Invitrogen) and DNA extracted from a full length *A. fumigatus* cDNA library (Invitrogen, see Chapter VI for details) as template. Inserts were cloned using SfiI sites provided in the multiple cloning sites of the vectors (see Fig. 5.2 and Fig 5.3 and Appendix C for details). The polycloning site of each DUALmembrane system vector is flanked on either side by SfiI sites: GGCCATTA'CGGCC and GGCCGCCT'CGGCC (where the cleavage site is indicated as '), resulting in non-complementary overhangs to allow directional cloning of DNA into the vectors. The absence of SfiI sites in most eukaryotic cDNAs means that most full-length cDNAs could be directionally cloned; nonetheless, every cloned sequence was checked with the software NEBcutter http://tools.neb.com/NEBcutter2/index.php (Biolabs). The oligonucleotides for PCR amplification were carefully designed to remove the native stop codon from the gene of interest and to add appropriate flanking SfiI restriction sites, allowing directional cloning of the insert into the vectors. Oligonucleotides were designed on a case by case basis to maintain an open reading frame in fusions between proteins of interest, and vector-encoded features. In the case of the prey plasmid pPR3-STE, a single nucleotide at the 5' of the sequence was added for each gene, thereby effecting the insertion of a single amino acid at the N-terminus of fusion proteins. To maximise expression levels, and functionality of preys expressed from this vector, three different pPR3-STE preys, for each relevant protein of interest and differing by inserted amino acids, were constructed. The 3 amino acids inserted Leucine (L), Glutamine (G) and Arginine (R) have completely different properties because of their side chain polarity and chain; Leu is non-polar and neutral, Gln is polar and neutral and Arg is polar and positive. According to the amino acid inserted, the plasmids were named with a suffix of L, G, or R for Leu, Gln and Arg respectively. All plasmids were sequence-verified using oligonucleotides specific to the genes of interest, as listed in Appendix B.

Fig 5.6 summarises the experimental procedure to test *A. fumigatus* membrane protein-protein interactions using the split-ubiquitin MYTH system. Once sequence-verified, the plasmids were transformed separately into the yeast reporter strain NMY51 using a modification of the lithium-acetate protocol described by Gietz and Woods (Gietz *et al.*, 1992). The expression of baits and preys was verified by western blotting (Towbin *et al.*, 1979), using proteins extracted from overnight SD cultures. Total protein quantification of the samples was performed using the Bicinchoninic Acid Protein Assay Kit (sigma) according to the manufacturer's instructions. 30 µg of protein samples were run on 8% SDS-PAGE gels as described in Section 2.3.2. In addition, a functional assay was performed to ensure the bait

was properly located within the membrane and was functional by co-transformation with two control preys (D). Finally, the interaction of interest was tested by co-transformation in yeast of the test bait and prey plasmids (E).

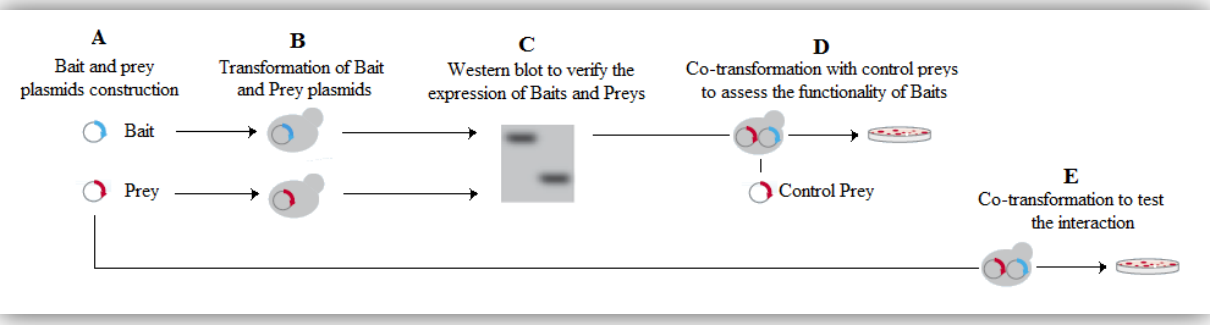


Fig. 5.6: Experimental procedure for testing *A. fumigatus* membrane protein-protein interactions using the split-ubiquitin MYTH system. (A) The cDNAs encoding the proteins of interest were obtained by PCR from DNA extracted from a full length *A. fumigatus* cDNA library and sub-cloned into the appropriate bait and prey vectors. Once sequence-verified, the plasmids were transformed separately into the yeast reporter strain NMY51 (B) and the expression of baits and preys was verified by western blotting (C). For the baits a functional assay was performed to ensure the bait was properly located within the membrane and was functional by co-transformation with control preys (D). Then, the interaction was tested by co-transformation in yeast of the test bait and prey plasmids (E).

5.3.2 Expression of *A. fumigatus* pH-sensing bait and prey fusion proteins

The expression of the proteins of interest was verified by western blotting analysis of total yeast extracts using an antibody directed against the LexA domain of the fusion protein for the baits and an antibody directed against the HA epitope of the fusion protein for the preys. The construct pCCW-Alg5 was used as positive control for the detection of the LexA epitope and expresses a fusion of the yeast ER protein Alg5 to the wild type Cub portion of yeast ubiquitin (expected size, 77.5 KDa). The plasmid pPR3-N was used as positive control for the detection of the HA epitope (expected size, 15 KDa). Due to the vast differences in sizes of controls and test baits and preys, the controls are not visualised in Fig. 5.7.

Panel A in Fig. 5.7 shows the results for the baits. The expression of PalH bait was confirmed from both the pBT3-STE and pBT3-SUC bait vectors (Fig. 5.7.A), where in both cases a recombinant protein of approximately 123.7 KDa is detectable by western blot, this agrees with the size expected following fusion of the PalH protein (85.7 KDa) to the Cub-LexA-VP16 (38 KDa). PalI bait could only be expressed as a C-terminal Cub fusion (pBT3-STE and pBT3-SUC), not as an N-terminal fusion (pBT3-N) (Fig. 5.7A). However, given that

equal amounts of total protein extract were loaded for PalH and PalI baits, it is likely that PalI bait was expressed at comparatively low levels, as a weak signal was visible for the pBT3-STE bait vector, whilst no signal was detectable for pBT3-SUC. Considering the predicted size of PalI protein, (71.6 KDa), and the size of the Cub-LexA-VP16 fusion, the size of the expected product is 109.6 KDa.

Panel B in Fig. 5.7 illustrates the results for the preys. Concordant with the cytoplasmic location for the arrestin-encoding PalF protein, the expression of PalF prey was confirmed from both C and N-terminal fusions (pPR3-STE) and (pPR3-N), respectively, to NubG (Fig. 5.7B). PalH and PalI prey could only be expressed when fusing the NubG domain at the C-termini (pPR3-STE) (Fig. 5.7B). Considering the size of the *A. fumigatus* PalF, PalH and PalI proteins, (respectively 82.1 KDa, 85.8 KDa and 71.6 KDa), and the size of the NubG-HA fusion (7 KDa), the size of the expected products is 89.1 KDa for *A. fumigatus* PalF, 92.8 KDa for *A. fumigatus* PalH and 78.6 KDa for *A. fumigatus* PalI. These experiments confirmed the requirement, when preparing the preys, to construct multiple pPR3-STE preys, with different single amino acid insertions, to secure clones expressing and functioning in the pPR3-STE prey vector. In fact, in the case of PalF pPR3-STE prey, expression was verified when the introduced amino acid was either L or G, but not R.

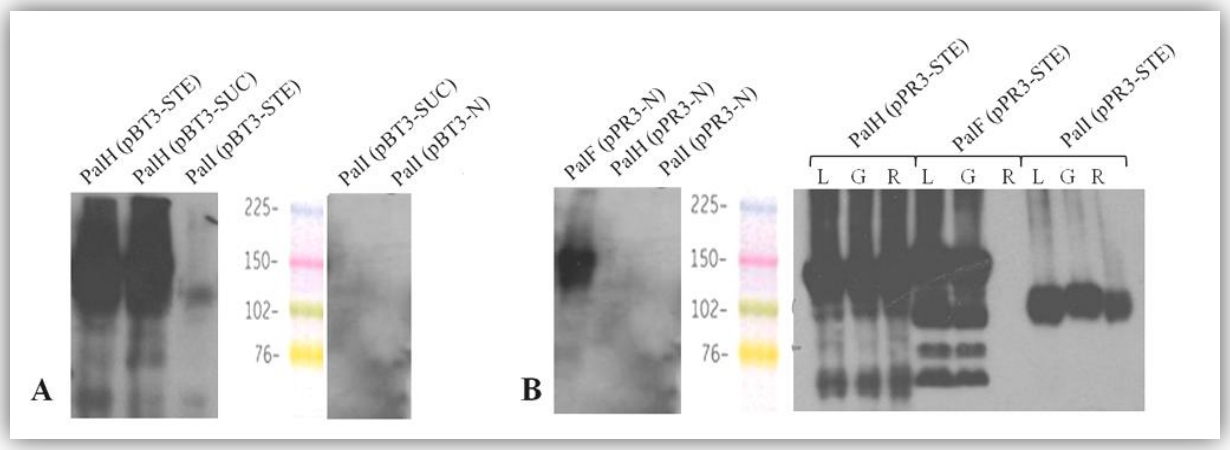


Fig. 5.7: Western blotting analysis to verify the expression of bait and prey proteins. (A) Baits. PalH bait expression (expected size 123.7 KDa) detected from both the pBT3-STE and pBT3-SUC vectors. PalI expression weakly detectable from pBT3-STE (expected size 109.6 KDa), but not from pBT3-SUC or pBT3-N vectors. (B) Preys. In pPR3-N, only PalF (expected size 89.1 KDa), but not PalH (expected size 92.8 KDa) and PalI (expected size 78.6 KDa), was expressed, whereas in pPR3-STE the majority of tested preys were expressed in detectable quantities, the exception being PalF R. To ensure the same loading of 30 µg of protein samples in the 8% SDS-PAGE gels, total protein extracts were quantified using the Bicinchoninic Acid Protein Assay Kit.

5.3.3 Testing of *A. fumigatus* bait functionality for split-ubiquitin reconstitution

Independent verification of PalH and PalI bait was derived by co-transformation with vectors expressing control preys. This control assay is important for determining whether the bait is functional in the split-ubiquitin assay and whether it results in any non-specific background activity. In order to assay the expression of *A. fumigatus* baits in yeast, each of the bait plasmids was co-transformed with the control plasmids pAI-Alg5 and pDL2-Alg5. The construct pAI-Alg5 expresses a fusion of the yeast ER protein Alg5 to the wild type Nub portion of yeast ubiquitin. If the test bait is properly inserted into the membrane of yeast and the Cub-LexAVP16 part is located on the cytosolic side of the membrane, co-expression of the tested bait together with pAI-Alg5 should result in reconstitution of split-ubiquitin through the strong affinity of wild type Nub for Cub and the concurrent activation of reporter genes. pDL2-Alg5 expresses a fusion of the same protein to the mutated Nub portion (NubG); therefore co-expression of the bait of interest together with pDL2-Alg5 should not lead to split-ubiquitin formation, because the mutated NubG has no affinity for Cub, and the bait does not interact with Alg5.

Fig. 5.8 shows the result of the co-transformation experiment for PalH bait in the pBT3-SUC (B) and pBT3-STE (C) vectors and for PalI bait in the pBT3-N (D), pBT3-SUC (E) and pBT3-STE (F) vectors. The functioning prey pCCW-Alg5 (A), expressing a fusion of

the yeast protein Alg5 to the wild type Cub portion of yeast ubiquitin, was used as positive control. For each bait, the total transformants (TT), indicative of the transformation efficiency, and the prototrophic transformants (PT), indicative of a positive interaction and obtained following co-transformation with the tested bait and prey fusion proteins were enumerated. Transformation efficiency was quantified by growth in non selective SD-trp-leu media, and growth of yeast expressing interacting baits and preys in the selective media SD-trp-leu-his-ade. In the case of the latter media, no growth is observed following the co-expression of baits with the negative control prey, as the mutated NubG has no affinity for Cub, and split-ubiquitin is not reconstituted.

From these experiments it was deduced that PalH pBT3-STE and pBT3-SUC, and PalI pBT3-STE and pBT3-SUC baits are appropriately localised in the membrane of yeast with corresponding Cub-LexAVP16 moieties located in the cytoplasm. For PalI pBT3-STE and pBT3-SUC baits, the number of colonies in selective media following co-transformation with the positive prey plasmid pAI-Alg5 was ten times less than that obtained for PalH pBT3-STE and pBT3-SUC baits. This supports a direct link between the expression levels observed in the previous western blotting and the functionality of a specific bait in terms of prototrophic transformants. In addition, whereas no growth is expected in selective media following the co-expression of a test bait with the negative control, a low level of background was visible for all functional baits, likely because of the leaky nature of the *HIS* reporter gene. In light of these findings, and to optimise relative levels of transformation efficiency and of false positives, PalH pBT3-SUC bait was chosen for further analyses.

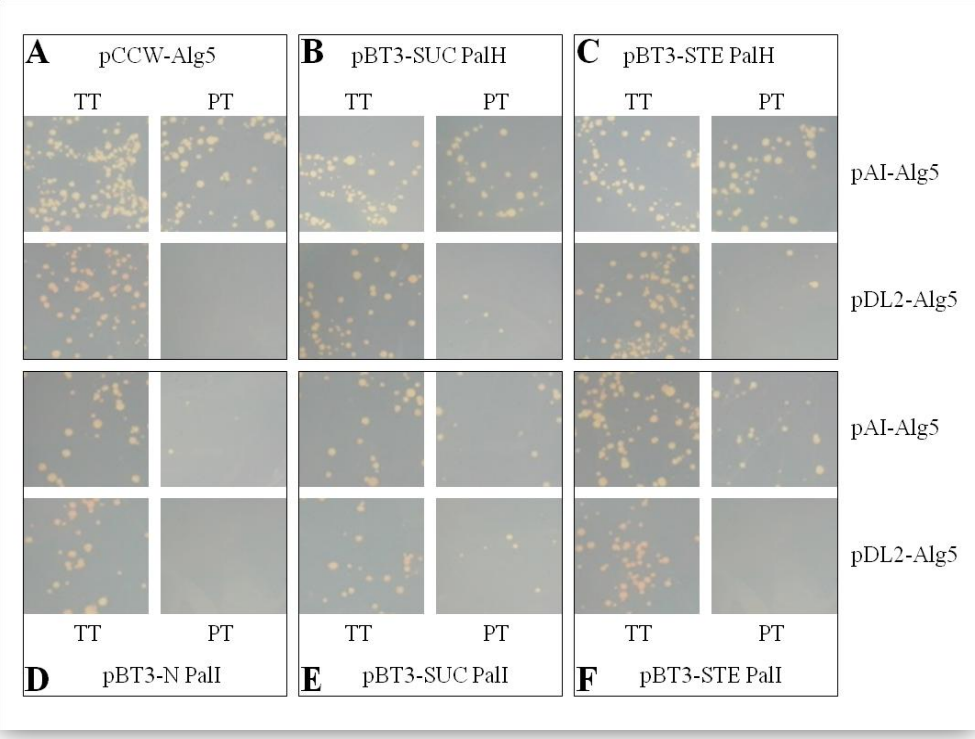


Fig. 5.8: Verification of the expression and functionality of pH-sensing baits constructed by co-transformation with control preys in yeast. The baits tested are (A) the positive control bait pCCW-Alg5, (B) PalH pBT3-SUC, (C) PalH pBT3-STE, (D) PalI pBT3-N, (E) PalI pBT3-SUC and (F) PalI pBT3-STE. Each of these baits was co-transformed with the positive control prey pAI-Alg5 and the negative control prey pDL2-Alg5. For each co-transformation, the total transformants (TT) in SD-leu-trp, indicative of the transformation efficiency, and the prototrophic transformants (PT) in SD-leu-trp-his-ade, indicative of interaction between bait and prey are shown. With lack of interaction, yeast colonies turn pink during the incubation.

NMY51 permits the use of *ADE2* as a reporter gene. In the absence of a protein-protein interaction, this gene is not transcribed and therefore, a red-coloured intermediate accumulates from the adenine metabolic pathway. Activation of the *ADE2* gene by a protein-protein interaction leads to expression of the *ADE2* gene product and unblocks the pathway. For this reason, NMY51 cells expressing an interacting protein pair display a very faint pink to white colour, depending on the strength of the interaction. In the absence of a protein-protein interaction, NMY51 displays a pink colour. When grown in SD-leu, SD-trp or SD-ura, no visible growth occurs after 3 days at 30°C, whereas in SD-his and SD-ade, a background of very small colonies (the colonies are smaller than 1 mm in diameter and do not turn red upon storage) is visible after 3 days at 30°C, because of the slight leakiness respectively of the *HIS3* gene and of the *ADE2* reporter gene.

Due to the *ADE2* reporter gene, the colonies displayed different shades of colour, ranging from dark red to white, depending on whether an interacting protein pair is expressed or not. When the *ADE2* reporter gene is not transcribed (as in the case of the co-

transformation with PalH pBT3-SUC and the negative control prey plasmid, Fig. 5.8B, bottom row), the adenine synthesis pathway is blocked and a red colored intermediate is accumulated, turning the cells red. If a bait and prey interact (as in the case of the co-transformation with PalH pBT3-SUC and the positive control prey plasmid Fig. 5.8B, top row), the *ADE2* reporter gene is activated and the adenine synthesis pathway is unblocked, leading to the disappearance of the red coloured intermediate. Thus, yeast harbouring a protein-protein interaction can exhibit a colour ranging from faintly pink (weak interaction, corresponds with slow growth on SD-trp-leu-his-ade medium) to white (strong interaction, corresponds with strong growth on SD-trp-leu-his-ade medium).

Taken together the results of the western blot and the control assay permitted new conclusions upon the topology for the two plasma membrane proteins PalH and PalI, confirming the literature and the *in silico* predictions and suggesting that both PalH and PalI have their C-terminal domain located intracellularly and their N-terminal domain located extracellularly.

5.3.4 Use of *A. fumigatus* PalH bait to investigate the interaction network between components of the plasma membrane signalling complex

The direct interaction between components of the plasma membrane signalling complex was addressed by co-transformation with PalH pBT3-SUC bait and the *A. fumigatus* preys described above. Fig. 5.9 depicts only a partial subset of the interactions tested to offer an idea of the layout of the experiment and introduce a variety of issues raised at this point of our experimentation. Specifically, the results shown include those from the co-transformation with PalH pBT3-SUC bait and either of PalH, PalI or PalF preys, the latter being expressed as fusions in either of two orientations fusing the NubG at the N-terminus (pPR3-N) or at the C-terminus (pPR3-STE) (B). The functioning prey pCCW-Alg5 (A), expressing a fusion of the yeast protein Alg5 to the wild type Cub portion of yeast ubiquitin, was used as positive control. As before, for every co-transformation the total transformants (TT), indicative of the transformation efficiency, and the prototrophic transformants (PT), indicative of an interaction between the two partners tested were enumerated. As a means for comparison, the results of co-transformation with the positive pAI-Alg5 and the negative pDL-Alg5 control preys, expressing respectively a fusion of the yeast protein Alg5 to the wild type Nub portion of yeast ubiquitin and the mutated Nub portion (NubG) are also shown.

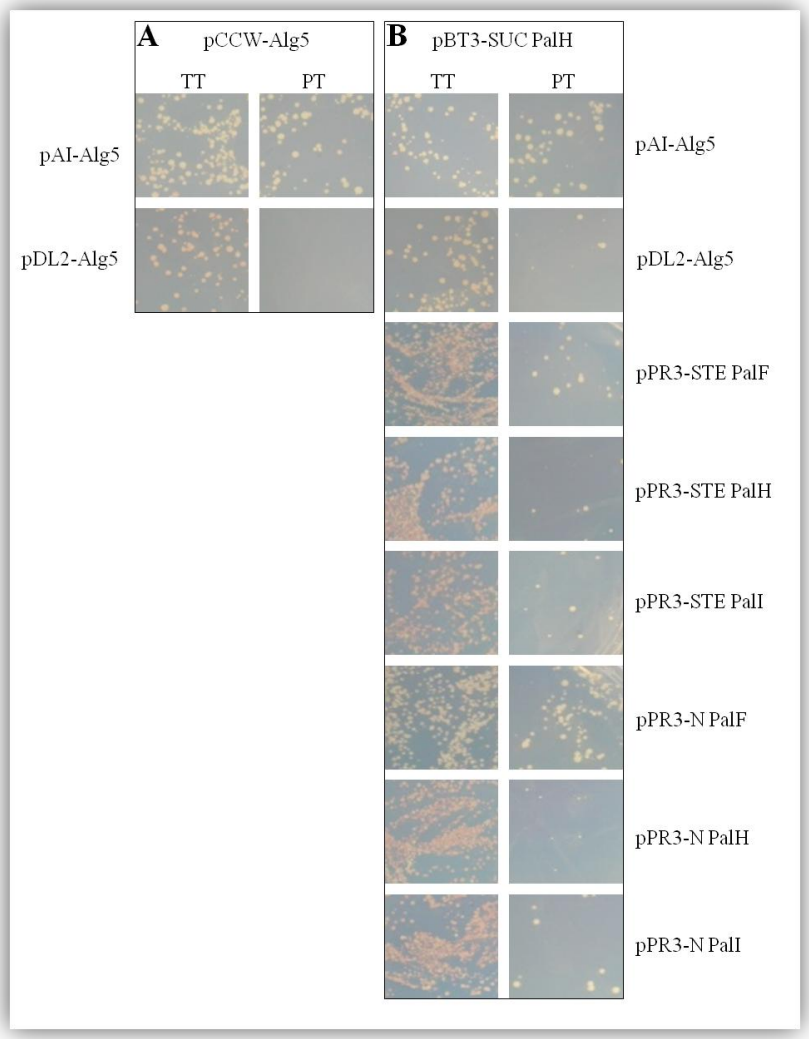


Fig. 5.9: Test to detect interactions between PalH, expressed as bait in the pBT3-SUC vector in the MYTH system, and the members of the membrane signalling complex PalH, PalI and PalF. To define an interaction, growth in selective media is compared with the control co-transformations pCCW-Alg5/pAL-Alg5 (positive control for interaction) and pCCW-Alg5/pDL-Alg5 (negative control for interaction) (A). pBT3-STE PalH has been co-transformed with the positive control prey pAL-Alg5, the negative control prey pDL-Alg5, pPR-STE PalF, pPR-STE PalH, pPR-STE PalI, pPR-N PalF, pPR3-N PalH and pPR3-N PalI (B). For each co-transformation the total transformants (TT) in SD-leu-trp, indicative of the transformation efficiency, and the prototrophic transformants (PT) in SD-leu-trp-his-ade, indicative of interaction between bait and prey are shown. In case of lack of or weak interaction, yeast colonies turn pink during the incubation.

In only one instance (i.e. the co-transformation with PalH pBT3-SUC bait and PalF pPR3-N) did the data support the previous hypothesis (Herranz *et al.*, 2005). For the other preys, a limited number of colonies were present in selective media suggesting a possible limitation of the system in distinguishing between weak and strong interactors, and more importantly between weak interactors and false positive interactions. This was enforced by the fact that no difference in the number of colonies in selective media were observed when

PalH pBT3-SUC bait was co-transformed with the preys PalH pPR3-STE L and PalI pPR3-STE L or with PalH pPR3-N and PalI pPR3-N, whereas western blotting had confirmed the expression of PalH pPR3-STE L and PalI pPR3-STE L, but not of PalH pPR3-N and PalI pPR3-N. The prototrophic transformants observed from the co-transformation with PalH pBT3-SUC bait and PalH pPR3-N or PalI pPR3-N preys therefore surely represent false positives.

Considering the visual examination as too labile a criterion upon which to judge the interaction between two tested partners, attention was therefore focused on further optimisation of the assay by next addressing reproducibility, and limitation of false positive results.

To address the problem of false positivity consistently observed with this bait, 3-aminotriazole (3-AT) was added in varying concentrations to the selective media SD-trp-leu-his-ade. 3-AT is a competitive inhibitor of the *HIS3* gene product. Therefore, the increase in the concentration of 3-AT enhances the stringency of *HIS3* selection. To find an optimal 3-AT concentration, the same volume from three different co-transformation reactions was grown on SD-trp-leu-his-ade plates supplemented with 0, 5, 10, 20, 30, 40 and 50 mM 3-AT. Fig. 5.10 shows the results of one of the three replicates for the three co-transformation reactions, involving PalH pBT3-SUC bait and the empty prey vectors pPR3-STE (A) and pPR3-N (B), and also PalF pPR3-N (C). The prey plasmids pPR3-STE and pPR3-N were chosen because they carry only the NubG domain and therefore no prototrophic transformants are expected in the media selective for the interaction. In addition, these two plasmids represent the vectors for the construction of every *A. fumigatus* prey developed in this study. The prey fusion protein palF pPR3-N was used to exploit its strong positive interaction with PalH pBT3-SUC bait. In the co-transformations with PalH pBT3-SUC bait and the prey vectors pPR3-STE (A) or pPR3-N (B) no colonies are expected, because NubG and Cub have no affinity for each other. However, in the absence of 3-AT a significant number of colonies are visible, so that it is not possible to discriminate between these false positive and the positive interactors obtained from the co-transformation with PalH pBT3-SUC bait and PalF pPR3-N prey (C). Increasing the level of 3-AT up to 20 mM leads to the progressive elimination of false positive results, with minimal impact upon results obtained with the strongly interacting PalF pPR3-N prey. At concentrations of 3-AT exceeding of 20 mM, growth is drastically affected for all the samples, indicating the toxicity threshold for this compound has been reached.

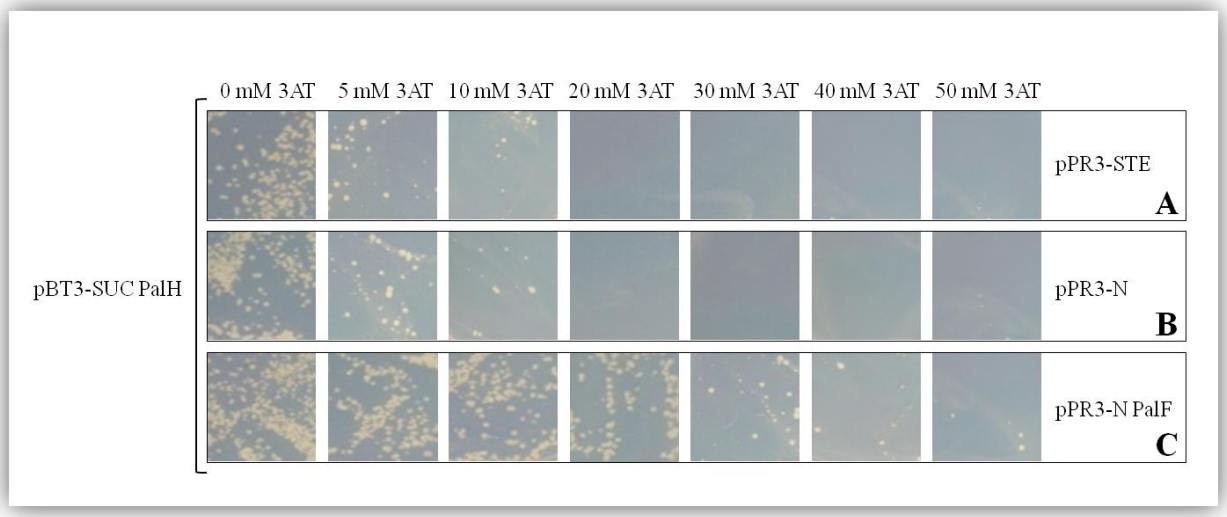


Fig. 5.10: **Panel showing the optimisation of the 3-AT concentration used in SD-leu-trp-his-ade to discriminate between positive interactors and false positives.** The bait plasmid pBT3-SUC PalH is co-transformed in NMY51 together with empty prey vectors pPR3-STE (A) and pPR3-N (B) and the prey pPR3-N PalF (C). Co-transformant cells are plated in SD-leu-trp-his-ade containing increasing concentrations of 3-AT, as indicated at the top of each column.

Based upon these results, a concentration of 20 mM 3-AT was established as optimal for the reduction of the background in co-transformation reactions involving the bait palH pPR3-SUC. The robustness of the system was next tested by repeating, in triplicate, the co-transformations previously shown in Fig. 5.9. Using the new culturing conditions, the direct interaction between PalH, PalI and PalF was addressed by co-transformation with PalH pBT3-SUC bait and the *A. fumigatus* preys as previously described. For each replicate, Table 5.4 shows the results for the co-transformations in terms of number of total transformants (TT) obtained in SD-leu-trp, indicative of the transformation efficiency, and of prototrophic (PT*) transformants in SD-leu-trp-his-ade 20 mM 3-AT (the asterisk signifies the addition of 3-AT to the media), indicative of interaction between bait and prey. In addition, the table illustrates the normalisation process performed upon the data. For each replicate, the ratio between prototrophic and total transformants was calculated and averaged. As control for the experiment, the functioning prey pCCW-Alg5 (A), expressing a fusion of the yeast protein Alg5 to the wild type Cub portion of yeast ubiquitin, was co-transformed with the positive pAI-Alg5 and the negative pDL-Alg5 control preys, expressing respectively a fusion of the yeast protein Alg5 to the wild type Nub portion of yeast ubiquitin and the mutated Nub portion (NubG). To establish the threshold for positive and negative interactions, PalH pBT3-SUC bait was transformed with the positive pAI-Alg5 and the negative pDL-Alg5 control preys.

	1st experiment			2nd experiment			3rd experiment			Normalisation				
Prey	TT	PT*	PT*/ TT	TT	PT*	PT*/ TT	TT	PT*	PT*/ TT	1	2	3	AVG	SD
pAL-Alg5	2000	1000	50	2000	500	25	2000	250	12.5	100	100	100	100	0
pDL-Alg5	1000	0	0	500	2	0.4	500	3	0.6	0	1.6	4.8	2.1	2.4
pPR3-STE PalH L	1000	100	10	1000	100	10	1000	20	2	20	40	16	25.3	12.9
pPR3-STE PalH Q	1000	200	20	1000	100	10	1000	20	2	40	40	16	32.0	13.9
pPR3-STE PalH R	1000	50	5	1000	100	10	1000	20	2	10	40	16	22.0	15.9
pPR3-STE PalF L	1000	100	10	1000	100	10	1000	20	2	20	40	16	25.3	12.9
pPR3-STE PalF Q	1000	100	10	1000	100	10	1000	25	2.5	20	40	20	26.7	11.5
pPR3-STE PalF R	1000	0	0	1000	0	0	1000	0	0	0	0	0	0.0	0.0
pPR3-STE PalI L	1000	20	2	1000	5	0.5	1000	20	2	4	2	16	7.3	7.6
pPR3-STE PalI Q	1000	20	2	2000	0	0	1000	3	0.3	4	0	2.4	2.1	2.0
pPR3-STE PalI R	1000	0	0	1000	0	0	1000	10	1	0	0	8	2.7	4.6
pPR3-N PalH	1000	5	0.5	1000	0	0	1000	0	0	1	0	0	0.3	0.6
pPR3-N PalF	1000	200	20	1000	100	10	1000	20	2	40	40	16	32.0	13.9
pPR3-N PalI	1000	2	0.2	1000	0	0	1000	0	0	0.4	0	0	0.1	0.2

Table 5.4: Results for co-transformations testing the interaction between PalH, expressed as bait in the pBT3-SUC vector in the MYTH system, and the members of the membrane signalling complex PalH, PalI and PalF. Each co-transformation was repeated 3 times and for each replicate the number of total transformants (TT) in SD-leu-trp, indicative of the transformation efficiency, and the prototrophic transformants (PT*) in SD-leu-trp-his-ade 20 mM 3-AT, indicative of interaction between bait and prey, was estimated. The ratio PT*/TT was calculated and averaged (1, 2 and 3 correspond respectively to the first, second and third replicate) fixing the value of the positive control co-transformation PalH pBT3-SUC /pAL-Alg5 to 100. AVG = Average, SD = Standard deviation

Fig. 5.11 shows a graphical representation of the results for the co-transformations to test the interaction between PalH, expressed as bait in the vector pBT3-SUC, and the members of the membrane signalling complex PalH, PalI and PalF, expressed as preys as previously described. For each co-transformation, the ratio between prototrophic and total transformants is plotted, obtained by averaging the three independent experiments and normalizing by fixing the value of the positive control co-transformation with the control prey pAL-Alg5 to 100, reflecting the strong affinity between the two separable domains of the ubiquitin. The standard deviation between replicates is indicated by error bars. As highlighted by the graph, the introduction of the competitive inhibitor of the *HIS3* gene product 3-AT indeed reduced false positives. Following addition of 20 mM 3-AT a clear difference in the number of colonies is visible when PalH pBT3-SUC bait is co-transformed with the preys

PalH pPR3-STE L and PalI pPR3-STE L or with PalH pPR3-N and PalI pPR3-N. Concordant with western blotting results which revealed that the preys PalH pPR3-N, PalI pPR3-N and PalF pPR3-STE R are not expressed, the ratio between prototrophic and total transformants in every co-transformation involving one of these preys is close to a null value, as observed for the negative control co-transformation with PalH pBT3-SUC bait and pDL-Alg5. For a well-expressed bait, such as PalH pPR3-SUC, and in experimental conditions giving at least 1000 total transformants per reaction, the repetition of the co-transformation in triplicate supplied reproducible data from which to infer the interactions between the three components of the membrane signalling complex PalH, PalI and PalF. In particular, by the addition of 20 mM 3-AT to the selective media SD-trp-leu-his-ade, it is also possible to speculate upon the affinity of the interactions. Concordant with its cytosolic location, PalF preys expressed as fusions in either of two possible orientations (pPR3-STE and pPR3-N) interacted with PalH pBT3-SUC bait. This was true with the single exception of PalF pPR3-STE R, whose expression could not be verified by western blotting. A clear interaction, though less detectable than that between PalH pBT3-SUC bait and PalF preys, was also reproducibly demonstrated between PalH pBT3-SUC bait and PalH pBT3-STE preys. No interaction was demonstrated between PalH pBT3-SUC bait and PalI pBT3-STE preys.

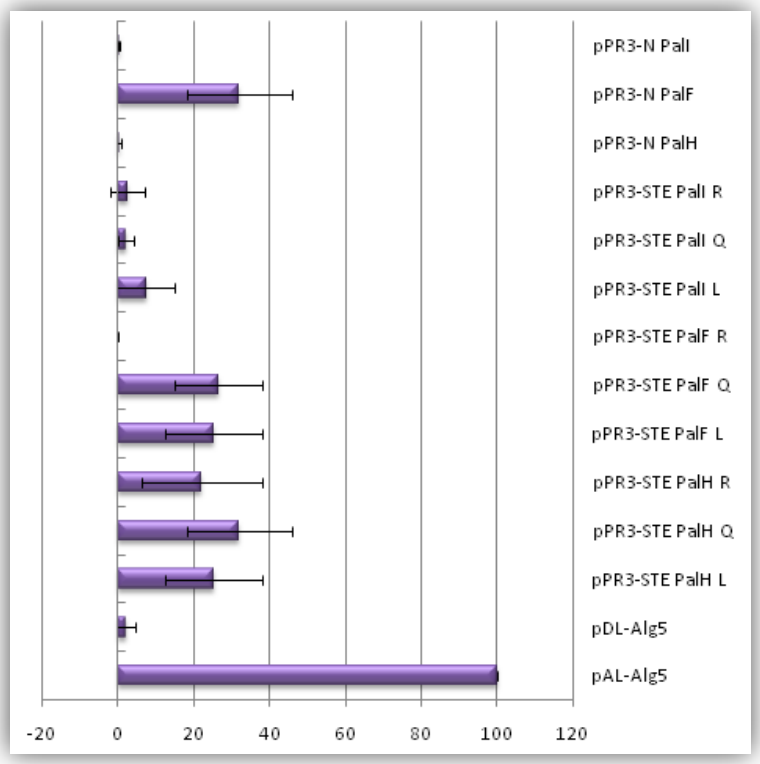


Fig. 5.11: Graphical representation of the results for the co-transformations to test the interaction between PalH, expressed as bait in the pBT3-SUC vector in the MYTH system, and the members of the membrane signalling complex PalH, PalI and PalF. For each co-transformation, the value PT*/TT is shown, obtained by averaging the three independent experiments, and normalised by fixing the value of the positive control co-transformation PalH pBT3-SUC /pAL-Alg5 to 100.

5.4 Discussion

The split-ubiquitin Membrane Yeast Two-Hybrid (MYTH) system is a powerful methodology, for the analysis of heterologous protein-protein interactions in yeast, which overcomes the limitation of the yeast classical two-hybrid assay because it circumvents the requirement for nuclear localisation of interacting proteins. In this study, the split-ubiquitin MYTH system was optimised for *A. fumigatus* protein expression and interaction analysis and used to investigate the interactions between three components (PalH, PalI and PalF) of a plasma membrane signalling complex involved in *A. fumigatus* adaptation to environmental pH.

5.4.1 Split-ubiquitin MYTH analysis confirms *in silico* topological predictions for *A. fumigatus* PalH and PalI

In the model hypothesised for *A. nidulans*, the first complex involved in the activation of the PacC/Rim101p pathway comprises the two plasma membrane proteins PalH and PalI and an arrestin-like protein PalF (Calcagno-Pizarelli *et al.*, 2007; Herranz *et al.*, 2005; Maccheroni *et al.*, 1997; Negrete-Urtasun *et al.*, 1999). PalH contains seven transmembrane domains and a long, hydrophilic C-terminus located in the cytosol (Negrete-Urtasun *et al.*, 1999), whose analogies with G-protein coupled receptors have raised the possible involvement in pH signalling of a G-protein (Herranz *et al.*, 2005). PalI contains four highly hydrophobic domains (Arst *et al.*, 1994), but *in silico* predictions had revealed the presence of an N-terminal signal peptide (Calcagno-Pizarelli *et al.*, 2007) therefore the hypothesised structure for *A. nidulans* PalI consists of three putative membrane-spanning domains and a basic C-terminus facing the cytosol (Calcagno-Pizarelli *et al.*, 2007). *A. fumigatus* PalH, PalI and PalF show high similarity with their homologous in *A. nidulans* (respectively 84.2%, 75.6% and 86.5% as shown in Appendix F), therefore suggesting a similar behaviour to the model hypothesised for *A. nidulans* might be expected in *A. fumigatus*. *In silico* analysis of *A. fumigatus* PalH and PalI proteins by SignalP 3.0 (Bendtsen *et al.*, 2004; Emanuelsson *et al.*, 2007) and TMpred (http://www.ch.embnet.org/software/TMPRED_form.html), which are reported in Appendix F, suggest the two proteins strictly resemble the topology of their homologues in *A. nidulans.*

Taken together, the results of the western blotting and interaction assays permitted some new deductions about the topology (as shown in Fig. 5.12) of the two *A. fumigatus* plasma membrane proteins PalH and PalI. Protein interaction data agreed with reports in the *A. nidulans* literature and also with *in silico* predictions, reported in Appendix F. As suggested by the *in silico* predictions, the hypothesised model of topology for *A. fumigatus* PalH consists of a 7-TMD protein with an extracellular N-terminus and intracellular C-terminus. This prediction is supported by the results presented here (Fig. 5.7 and Fig. 5.8). The expression of PalH as a bait was confirmed by western blotting for fusion proteins expressed from both the pBTR3-STE and pBT3-SUC bait vectors (Fig. 5.7A). In addition, interaction assays demonstrated that PalH baits expressed from pBT3-STE and pBT3-SUC are appropriately localised in the membrane of yeast, and are functional with respect to supporting reconstitution of split-ubiquitin. pBT3-STE PalH and pBT3-SUC PalH baits fuse the Cub domain to the C-terminus of PalH, and their functionality with respect to Alg5 interaction (Fig. 5.8B and C) therefore reflects that the Cub-LexAVP16 reporter is

cytosolically located. If the 7-TMD topology prediction is correct it therefore follows that the PalH N-terminus is extracellular and PalH C-terminus is cytosolic. Accordingly, PalH prey could only be expressed as a C-terminal (pPR3-STE) NubG fusion. As suggested by the *in silico* predictions, the hypothesised model of topology for *A. fumigatus* Pal I (Appendix F) consists of three putative membrane-spanning domains and a basic C-terminus facing the cytosol since SignalP 3.0 (Bendtsen *et al.*, 2004; Emanuelsson *et al.*, 2007) had revealed the presence of an N-terminal signal peptide. In *A. fumigatus*, the predictions by SignalP 3.0 indicate with a probability of 0.99, that the N-terminal hydrophobic domain of PalI is a signal peptide cleaved, with a probability of 0.84, between the residues Ser26 and Thr27. Likewise, in *A. nidulans*, *in silico* analysis with SignalP 3.0 predicted, with a probability of 0.96, that the N-terminal hydrophobic domain is a signal peptide cleaved, with a probability of 0.84, between the residues Ser26 and Thr27 (Calcagno-Pizarelli *et al.*, 2007). Besides, studies in the *S. cerevisiae* homologue Rim9p suggest that the most terminal of the corresponding hydrophobic domains represents a signal peptide (Li and Mitchell, 1997). For *A. nidulans*, the predictions presented in Calcagno-Pizarelli *et al.*, 2007 were indeed confirmed by the results of the present study (see Appendix E "Use of *A. nidulans* PalH for optimisation of MYTH"). *A. fumigatus* PalI bait (Fig. 5.7A) was detectable only when C-terminally fused to the Cub domain (pPR3-STE or pPR3-SUC). In addition, PalI prey (Fig. 5.7B) was only detectably expressed as a C-terminal fusion to NubG (pPR3-STE). In interaction assays, PalI pBT3-STE and pBT3-SUC baits could be demonstrated as appropriately localised in the membrane of yeast, presumably harbouring the Cub-LexAVP16 reporter on the cytosolic side of the membrane (Fig. 5.8D and E), whereas PalI pBT3-N bait was not functional (Fig. 5.8F). Since pBT3-STE PalI and pBT3-SUC PalI baits and pPR3-STE PalI prey fuse ubiquitin domains at the C-termini of the proteins of interest, our data suggest that *A. fumigatus* PalI has an extracellular N-terminus and cytosolic C-terminus (Fig. 5.12).

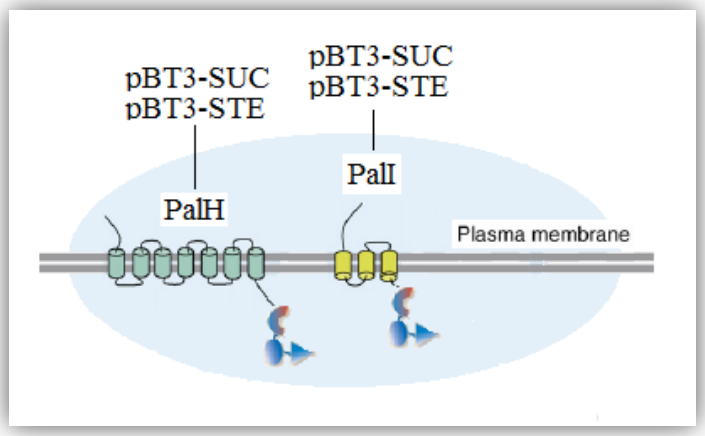


Fig. 5.12: PalH and PalI topology in the *A. fumigatus* plasma membrane, as demonstrated by western blot and interaction assays. The Cub-LexA-VP16 domain is expressed and functional only if fused to the C-termini of PalH and PalI, suggesting that both have intracellular C-termini and extracellular N-terminal domains.

5.4.2 *A. fumigatus* PalH baits are expressed and functional in the MYTH system

As discussed in the previous section, the expression of PalH and PalI as bait was confirmed in both the pBT3-STE and pBT3-SUC bait vectors. The two plasmids pBT3-STE and pBT3-SUC are specifically designed for cloning bait proteins, whose topology includes an extracellular N-terminal domain and an intracellular C-terminal domain. In addition, the bait plasmid pBT3-STE contains the STE2 leader sequence derived from the *S. cerevisiae* Ste2 protein (a G-protein coupled receptor). The short leader sequence has no targeting function but it is intended to optimise the expression of the desired bait, providing a strong ATG sequence for the initiation of the transcription machinery (Romanos *et al.*, 1992). Since its development, the MYTH system has been successfully applied to the study of a variety of membrane proteins from different organisms, as extensively reviewed in Suter *et al.*, 2006. This methodology has permitted the understanding of quaternary structures for sucrose transporters (Reinders *et al.*, 2002), a yeast protein translocation machinery (Scheper *et al.*, 2003a; Stagljar *et al.*, 1998), ErbB3 (a receptor tyrosine kinase) (Thaminy *et al.*, 2003), plant K+ channels (Obrdlik *et al.*, 2004) and the yeast Ycf1p (an ATP-binding cassette transporter) (Paumi *et al.*, 2007). Several of these findings underline, however, that in its current form the system is extremely sensitive to perturbations in the expression levels of baits. The earliest large scale split-ubiquitin screen reported showed that, of a total of 705 integral membrane proteins analysed, 365 were competent for utilisation as baits in the system, whereas many of the remaining 340 were over-expressed from the plasmid chosen and therefore mislocalised

within the cell (Miller *et al.*, 2005). In some instances, ubiquitin fusion can alter irremediably the topology of the membrane protein, which is not directed to the native localisation with unpredictable effects on its functioning and interactions with other proteins. The expression levels for a specific bait in use are therefore crucial for the correct functioning of the MYTH system and several issues had to be considered at this stage of the experimentation. *A. fumigatus* proteins might be detected as heterologous in yeast, and therefore become proteolytically degraded. Also, in an opposing scenario, over-expression could lead to toxicity for the yeast cells. Finally, post-translational modifications in yeast may not reflect the actual post-translational modifications occurring in *A. fumigatus* and affect the localisation of the expressed protein. To overcome these limitations, the system has recently been revised as integrated MYTH (iMYTH) system, where the full-length bait under investigation is expressed under the control of the endogenous promoter (Paumi *et al.*, 2007). Therefore the bait protein is properly expressed within a cell and the stoichiometry is maintained among members of a protein complex, so to drastically reduce inappropriate interactions due to the over-expression via exogenous promoters. In addition bait proteins are expressed in their native context, contributing to their appropriate posttranslational modifications and localisation. Interestingly, another advantage of the revised system is the incorporation of a bait tag, permitting localisation by fluorescence microscopy.

In light of these considerations, in the present study, multiple bait plasmids have been used in parallel to ensure the adequate expression of the proteins of interest. In the western blotting analysis, for both PalH and PalI a difference was visible in expression, depending on the bait vector used for the cloning whereby higher expression levels were always associated with the use of the plasmid pBT3-STE (Fig.5.7A). However, in comparison with the same amount of total protein extract loadings for PalH baits, PalI produced only low protein yields, whereby a weak signal is visible for the pBT3-STE bait vector, and almost no signal is detectable for pBT3-SUC. Interestingly, the interaction assays reflect these results, suggesting a direct link between the expression levels observed in western blotting and the functionality of a specific bait in terms of prototrophic transformants. The baits tested (PalH pBT3-STE and pBT3-SUC and PalI pBT3-STE and pBT3-SUC) were appropriately localised in the membrane of yeast and the Cub-LexAVP16 reporter is located on the cytosolic side of the membrane. However, for PalI pBT3-STE and pBT3-SUC, which were less expressed by western blotting (Fig. 5.7), the number of colonies in selective media after co-transformation with the positive prey plasmid pAI-Alg5 was ten times less than that obtained with PalH pBT3-STE and pBT3-SUC baits. In virtue of all these considerations, to balance between the levels of transformation efficiency and of false positives, PalH pBT3-SUC bait was chosen

for further analysis. Further indications about the choice of this bait and the balance between false positivity and self activation in the MYTH system will be discussed in the Chapter VI.

5.4.3 MYTH analysis identifies *A. fumigatus* PalH and PalF interaction, and PalH homodimerisation

Direct interactions between components of the predicted plasma membrane signalling complex were addressed by yeast co-transformation with pBT3-SUC PalH bait and PalH, PalI and PalF preys expressed as both C- and N-terminal NubG fusions. During this experimentation, a number of technical shortcomings in the manufacturer's protocols became apparent, including extreme subjectivity in using colony counts for identifying interacting partners and a confounding lack of reproducibility, and false positive results. In fact, the initial experiment (Fig. 5.9) identified a single interacting prey for the tested pBT3-SUC PalH bait, resulting from co-transformation with PalF pPR3-N, but nonetheless confirming previous findings (Herranz *et al.*, 2005). For all other preys a paucity of colonies on selective media likely prevented identification of lower affinity, or possibly less frequent interactions, and moreover could not distinguish between weak interactors and false positive results. Titration of 3-aminotriazole (3-AT) in selective media overcame the problem of false positivity (Fig. 5.10) for the PalH pBT3-SUC bait. A detailed discussion on the possible causes of false positive results in MYTH analyses will follow in Chapter VI. The robustness of data acquired with heightened (20 mM 3-AT) selectivity was tested by triplicating the co-transformations with pBT3-SUC PalH bait and all PalH, PalI and PalF preys and counting the number of total and prototrophic transformants (Table. 5.4). For each replicate, the ratio between prototrophic and total transformants was counted and averaged, and the standard deviation was calculated. To establish a lower threshold for positive interactions, PalH pBT3-SUC bait was also transformed with the positive pAI-Alg5 and the negative pDL-Alg5 control preys. For the analysis, the value of the positive control co-transformation with the prey pAL-Alg5 was set to 100, reflecting the strong affinity between the two separable domains of the ubiquitin. These adjustments to the manufacturer's screening protocol permitted the observation of a previously unachievable distinction between positive and negative interaction data for the PalH pBT3-SUC bait with the PalH pPR3-STE and PalI pPR3-STE or PalH pPR3-N and PalI pPR3-N preys (Fig. 5.11). In addition, for well-expressed baits, such as PalH pPR3-SUC, in experiments achieving a minimum of 1000 total transformants, triplicated analyses supplied reproducible data. These experiments inferred interactions between two of the three membrane signalling components, PalH and PalF. It was

also possible to discriminate between the different affinity of these interactors.

Concordant with a predicted cytosolic location for PalF, both C-terminal (pPR3-STE) and N-terminal (pPR3-N) NubG-fused PalF preys interacted with PalH pBT3-SUC bait, with the sole exception of PalF pPR3-STE R, whose expression was not verified by western blotting. The fusion of the NubG domain at the C-terminus (pPR3-STE) or at the N-terminus (pPR3-N) of PalF, does not affect the interaction between *A. fumigatus* PalF and PalH in MYTH analysis. This finding corroborated the importance of constructing three different amino acid insertions for preys of interest. Moreover, an interaction between PalH and PalF was detected, as previously demonstrated for *A. nidulans* (Herranz *et al.*, 2005). In *A. nidulans*, the interaction between PalF and PalH was identified by two-hybrid analysis, using a LexA-PalF fusion protein bait to screen an *A. nidulans* two-hybrid cDNA library. The affinity between the detected interactors was revealed by β-galactosidase assessment, revealing a strong interaction between the hydrophilic PalH C-terminus (amino acids 506-760) and the arrestin-like protein PalF. Besides, two-hybrid mapping demonstrated that two regions in the C-terminus of PalH (residues 349-385 and 657-760) and the arrestin N-terminal domain of PalF plus 63 additional N-terminal residues are crucial for the interaction. In fact, PFAM database searches identify two arrestin-like domains in *A. nidulans* PalF and the yeast homologue Rim8 (Herranz *et al.*, 2005). In mammalian arrestins, through the analysis of truncated and chimeric proteins, it has been established that the N-domain is involved in 7-TMD protein binding, although additional elements in the C-terminus may participate in receptor recognition (Granzin *et al.*, 1998; Gurevich *et al.*, 1995). Mutant phenotype analysis confirmed the importance of this interaction, because *palF* and *palH* mutations, affecting any of the domains involved in the interaction, also prevent pH signalling (Herranz *et al.*, 2005). Among these mutations, PalH truncation of the C-terminal PalF-binding site and PalF substitution of the highly conserved residue Ser86 by Pro, completely prevent fungal growth at pH 8, and the interaction of the respective proteins *in vitro*. On the contrary, PalF substitution of the highly conserved residue Ile133 in the arrestin C-domain, does not affect the interaction *in vitro*, suggesting the associated inability to grow at alkaline pH is due to causes unrelated to the interaction itself (Herranz *et al.*, 2005). This interaction is also required for PalF ubiquitination and phosphorylation, as pH-mediated phosphorylation of PalF was abolished by a *palH*⁻ mutation (Herranz *et al.*, 2005).

An attractive hypothesis places the interaction between the putative pH sensor and the arrestin-like protein as initial step for the internalisation of the 7-TMD protein receptor PalH. *S. cerevisiae* Rim21p and Dfg16p and *A. nidulans* PalH are predicted to be 7-TMD proteins with hydrophilic C-termini and are therefore hypothesised to be G-protein coupled receptors

(Barwell *et al.*, 2005; Herranz *et al.*, 2005). This prediction has been demonstrated in the present study for *A. fumigatus* PalH, whose structure indeed resembles that of G-protein coupled receptors (GPCRs). In association with their classical role in desensitising 7-TMD protein receptor, arrestins are now known to participate in signalling from 7-TMD receptors to downstream regulatory proteins (Lefkowitz and Shenoy, 2005). GPCRs are 7-TMD protein receptors and represent the largest and widespread family of membrane receptors (Fredriksson *et al.*, 2003), also well studied as common targets of therapeutic drugs in mammalians (Gudermann *et al.*, 1995). To participate in signal transduction from a 7-TMD receptor, transducer should be able to interact with the receptor in an activation-dependent way and then undergo conformational changes (Lefkowitz and Shenoy, 2005). Three groups of proteins have this ability: heterotrimeric G proteins, β-arrestin and GRKs. G protein-coupled receptors (GPCRs) are transmembrane receptors, which bind with signal molecules through their extracellular domains and activate a heterotrimetric G protein through their intracellular domain, generating a cascade involving further proteins to ultimately cause a change downstream in the cell. Heterotrimeric G-proteins (guanine nucleotide-binding proteins) are a group of proteins involved in transmitting a remarkable range of stimuli inside the cell regulating various aspects of cell biology, such as metabolism, secretory protein, electrical activity, shape and motility. Receptor-mediated exchange of GTP on the α-subunit of the heterotrimer determines the dissociation of the activated α-subunit from the β-γ subcomplex (Neer, 1995). This subcomplex is able to modulate an array of downstream effectors, whereas the α-subunit contains an intrinsic GTPase activity, to terminate signalling converting the GTP-bound α-subunit into the corresponding GDP-bound form, therefore promoting the reassembly of the heterotrimer. Pioneering studies on the rhodopsin and the β_2AR (adenylyl cyclase-coupled β_2-adrenergic receptor for chatecholamines) indicated G protein-mediated signaling is attenuated by highly conserved mechanisms (Kohout and Lefkowitz, 2003); the active form of the receptors stimulates heterotrimeric G proteins and is phosphorylated by G protein–coupled receptor kinases (GRKs), which leads to β-arrestin recruitment. Arrestins were originally described as proteins that regulate signal transduction by binding activated phosphorylated G-protein-coupled receptors (GPCR). The receptor is thereby desensitised, and the signalling is stalled. However, more recent studies have demonstrated that arrestins also bind a growing list of endocytic and signaling proteins (Shenoy and Lefkowitz, 2003) and act as signal transducers themselves playing an important role in scaffolding receptors to membrane-trafficking machinery, helping receptor internalisation, Mitogen-activated protein kinase (MAPK) activation and regulating gene expression (as reviewed in Jean-Alphonse and Hanyaloglu, 2010 and Lefkowitz and Shenoy, 2005). Endocytosis of the receptors is crucial

for the resensitisation of the receptors by dephosphorylation and for their recycling (Claing *et al.*, 2002) and studies performed in mammalian cells finds that β-arrestins link activated receptors to clathrin-coated pits for endocytosis (Goodman *et al.*, 1996; Moore *et al.*, 2007). Currently, arrestins have been found to regulate inactivation, internalisation, trafficking and signalling of several 7-TMRs (Laporte *et al.*, 1999; McDonald *et al.*, 2000; Shenoy *et al.*, 2001). Upon activation of 7-TMRs, β-arrestins undergo ubiquitination, a process which is now thought to help protein trafficking and signal transduction, other than the classical role of tagging proteins for degradation by the proteasome (Shenoy *et al.*, 2001).

The structural and functional analogies with mammalian arrestins for PalF and with G-protein coupled receptors for PalH raise the possibility of G-protein involvement in fungal pH signalling, particularly given the demonstrated role for arrestins in the stimulation of G-proteins (Lefkowitz and Shenoy, 2005; Shenoy and Lefkowitz, 2005b; Shenoy and Lefkowitz, 2005a). In *A. nidulans*, genetic screens, expressed sequence tags (ESTs), or partial examination of the genome revealed the presence of nine GPCRs (GprA-I) (Han *et al.*, 2004). In addition, heterotrimeric G-protein components have been identified, such as the α-subunits FadA, GanA, and GanB (Chang *et al.*, 2004; Yu *et al.*, 1996), the β subunit SfaD (Rosen *et al.*, 1999), and the γ-subunit GpgA (Seo *et al.*, 2005). FadA/SfaD/GpgA and GanB/SfaD/GpgA are involved in regulation of germination, hyphal growth, and conidiogenesis (Lafon *et al.*, 2005; Rosen *et al.*, 1999; Seo *et al.*, 2005; Yu *et al.*, 1996), but no function has yet been attributed to GanA (Chang *et al.*, 2004; Han *et al.*, 2004). Unfortunately, the components and the roles of G-proteins in *A. fumigatus* are not well investigated, but the publication of the genome (Nierman *et al.*, 2005) permitted analysis in comparison with the genomes of other better studied species, such as *A. nidulans* and *A. oryzae* (Lafon *et al.*, 2006), revealing overlap for most of the GPCRs and G-proteins across the *Aspergillus* species investigated.

An alternative hypothesis raised by this work is that PalH is a G-protein coupled receptor, whose dimerisation is likely involved in pH signalling. This hypothesis was originally suggested for *S. cerevisiae* Rim21p/Dfg16p, which is thought to function as an heterodimeric receptor (Barwell *et al.*, 2005). In the present study, an interaction was also demonstrated between PalH pBT3-SUC bait and PalH pPR3-STE preys (Fig. 5.11). G-protein mutants might present a very pleiotropic phenotype, precluding selection or recognition in pH mutant screens (Herranz *et al.*, 2005). However, mammalian GPCRs have been shown also to activate non-G-protein signaling pathways from endosomes, mostly by interaction with β-arrestins, which create a bridge with MAPK signaling molecules, to establish spatial and temporal control for signalling (Reiter and Lefkowitz, 2006). A range of different approaches

has revealed recently that rather than acting as monomers, GPCRs forms dimers and/or higher-order oligomeric complexes (as reviewed in Milligan *et al.*, 2003; Milligan *et al.*, 2006; Milligan, 2007; Milligan, 2010). The first evidence was provided by the functional GABAb receptor, which is a dimer composed of two distinct GPCR products (Marshall *et al.*, 1999; Mohler and Fritschy, 1999). GABAbR1 does not function on addition of agonist and is trapped intracellularly if expressed in heterologous systems. Its C-terminal domain has been demonstrated by two-hybrid screenings to interact with the C-terminal domain of GABAbR2 (White *et al.*, 2002) and the coexpression of both GABAbR1 and GABAbR2b results in functional GABA activity. Because GABAbR1, when expressed in a heterologous system, is retained in the ER/Golgi, dimerisation is thought to occur, at least for the GABAb receptor in that site, coincidently with protein production. The interaction of the GABAb receptors would provide a mechanism to control delivery of the active GPCRs to the plasma membrane (Milligan, 2001). However, increasing evidence suggests other roles for GPCRs dimerisation beyond that of quality control of protein folding for the plasma membrane delivery, however this topic is just starting to be described in the current literature (as reviewed in Milligan, 2007). Interestingly, however, for Chapter VI, which will describe the use of the MYTH system to identify novel interactors of *A. fumigatus* PalH, the notion has arisen that the early phases of quality control in the ER involve interaction with resident chaperones and possible N-glycosylation, as GPCRs undergo the same processing as proteins trafficked through the secretory pathway (Milligan, 2010).

In *A. nidulans*, null *palI* mutants grow, though poorly, at alkaline pH, unlike the null mutants of other *pal* genes (Denison *et al.*, 1995), suggesting for PalI an important, but not essential role in pH signalling, perhaps in assisting the plasma membrane localisation of PalH (Calcagno-Pizarelli *et al.*, 2007). This suggestion is based upon the observation that co-overexpression of PalI redirects GFP-tagged PalH (PalH-GFP) to the plasma membrane in *A. nidulans*, that otherwise, when over-expressed, is predominantly located in cytosolic punctate structures (Calcagno-Pizarelli *et al.*, 2007). In addition, over-expression of PalH also allows almost wild type growth of *palI* mutants at alkaline pH, as expected if in these mutants the physiological quantity of PalH is unable to sufficiently populate the plasma membrane without the assistance of PalI (Calcagno-Pizarelli *et al.*, 2007). PalI could assist plasma membrane localisation of palH according to three possible mechanisms still under investigation and each of these three possibilities could require an interaction between PalH and PalI, either direct or indirect, but this is still not demonstrated (Peñalva *et al.*, 2008). The first of the hypothesised mechanisms, based on localisation experiments of the GFP-tagged proteins, implies that PalI could assist PalH along the secretory pathway or in its exit from the

Golgi. The abundance of PalI on the plasma membrane suggests PalI exits the Golgi efficiently, so it could mediate or facilitate the sorting of PalH at the Golgi into secretory vesicles destined for the plasma membrane rather than into vesicles destined for endosomes. However, this hypothesis may be ruled out by the demonstration that PalH homodimerises and that this event, as for the GABAb receptors mediates the maturation of the protein. Alternatively, PalI could be involved in the down-regulation of PalH endocytosis, or in the up-regulation of its recycling after PalF-mediated endocytosis. However, in the present study, no interaction was demonstrated between PalH pBT3-SUC bait and any of several PalI pBT3-STE preys.

In this context however, it is important to notice that the MYTH system is developed in the way that the reconstitution of the split-ubiquitin is due to the close proximity of the two proteins tested for the interaction. Hypothesising the participation of PalF in joining the two plasma membrane proteins PalH and PalI, the results of the MYTH test for direct interaction do not completely rule out the participation of PalI in the plasma membrane pH signalling complex.

5.4.5 The MYTH is a versatile and powerful approach to test in yeast *A. fumigatus* protein-protein interactions

The split-ubiquitin Membrane Yeast Two-Hybrid (MYTH) system was here demonstrated to be a versatile and powerful methodology for the analysis of *A. fumigatus* protein-protein interaction in yeast. The current literature reports its broad utilisation, but never regarding its use for *A. fumigatus* proteins. This system has been applied successfully in various studies, for example investigation of mutations affecting the assembly of fragments of presenilin in the development of Alzheimers disease (Cervantes *et al.*, 2001), or the interaction between the two yeast α1,2-mannosidase proteins Mns1p and Rer1p in the endoplasmic reticulum (Massaad and Herscovics, 2001), or the intra- and intermolecular interactions between plant sucrose transporters (Reinders *et al.*, 2002). Of particular importance for the present study is its application to investigate the protein-protein interactions involved in yeast ergosterol biosynthesis (Alcazar-Fuoli *et al.*, 2008; Ferreira *et al.*, 2005); several studies have provided insight on experimental design and optimisation (Mo *et al.*, 2004; Mo and Bard, 2005b; Mo and Bard, 2005a), which will be discussed in Chapter VII.

Summarising the advantages of the system, it does not require the localisation of tested proteins in the nucleus, because the detection of interaction is due to cleavage by UBPs and

not directly to transcriptional activation, therefore, it particularly suits studies involving membrane proteins, such as PalH, PalI and PalF, whose role in pH sensing and virulence has been extensively studied in the *Aspergillus* species. In addition, the fusion of small modules (Cub and NubG) to the proteins of interest generally reduces potential steric influences, as demonstrated when testing the interaction between PalH and PalF in the present study. The fusion of the NubG domain at the C-terminus (pPR3-STE) or at the N-terminus (pPR3-N) of PalF, did not affect the interaction between *A. fumigatus* PalF and PalH in the MYTH system. However, the system requires at least one of the proteins tested to be integral to, or attached to the membrane, because the translocation of a soluble bait to the nucleus would activate the reporter genes independently of a protein interaction. The suitability of a protein of interest for the use as a MYTH bait depends on many variables and therefore has to be tested on a case-by-case basis. This is indeed shown by the results observed for PalH and PalI, whose expression strictly depend upon the vector baits used for the cloning, but also on intrinsic characteristics of the proteins themselves. The orientation in which the domains of the ubiquitin are fused and the expression levels of the bait profoundly affect the types of interactions detected and the level of false positive detection, representing an issue to address in the initial step of the experimentation. Finally, as observed in the case of PalH and PalI, the MYTH system is more appropriate for testing direct binary interactions, because the detection of an interaction between a bait and a prey, which only interact indirectly via a third member, is likely not to be reproduced or detectable in yeast (Snider *et al.*, 2010a; Snider *et al.*, 2010b).

CHAPTER VI

IDENTIFICATION OF NOVEL PROTEIN INTERACTORS FOR *A. FUMIGATUS* PALH

6.1 Overview

The most interesting application of the split-ubiquitin MYTH system is that, by using a membrane-associated protein bait for the screening, it allows the isolation of novel protein interactors from a library of expressed prey proteins. As reported in the current literature, the system has been adapted for large-scale screens using cDNA or gDNA (genomic DNA) libraries for a variety of membrane proteins from various organisms (Snider *et al.*, 2010b; Thaminy *et al.*, 2003; Wang *et al.*, 2004), but never before for *A. fumigatus*. Interestingly, this possibility extends the future use of the system to the screening for potential drugs or inhibitors for a specific membrane-associated protein. In the present study, the MYTH screening system has been optimised and adapted to a high-throughput platform to discover novel protein interactors for *A. fumigatus* PalH from a full-length *A. fumigatus* cDNA prey library.

6.2 Methods

For methods regarding the split-ubiquitin MYTH system and the construction and testing of the pBT3-SUC PalH and the pBT3-STE PalH baits utilised for the screening please refer to Chapter V.

6.2.1 The full length *A. fumigatus* cDNA prey library

The full length *A. fumigatus* cDNA library was constructed by Invitrogen using Invitrogen' proprietary full length technology and a DUALmembrane prey Gateway adapted vector (pPR3N-GW).

The pPR3-N vector (Fig. 6.1.A) was Gateway adapted and used for LR recombination with the cDNA library (pENTR). This allows for a fraction of the cDNAs to be fused and expressed in frame with the N-terminal NubG domain; whereas the presence of native stop codons in the oligodT primed cDNAs precluded the possibility of generating in frame fusion proteins with the C-terminal NubG domain containing vector (pPR3-STE). The pPR3-N vector was adapted at the EcoRI site by insertion of a Gateway cassette for in-frame fusion of the gene of interest, at its N-terminus, with NubG-HA (Fig. 6.1 B). The process typically involves the substitution of the multiple cloning site with a conversion cassette containing *att*R recombination sites, the *ccd*B selection gene and the chloramphenicol resistance gene (CAT). The *att*R1 and *att*R2 sites allow recombinational cloning of the gene of interest from an entry clone, whereas the *ccd*B and CAT genes are used, respectively, for the negative selection and counter-selection of plasmids. The modified vector was validated by restriction analysis using SmaI and DNA sequencing.

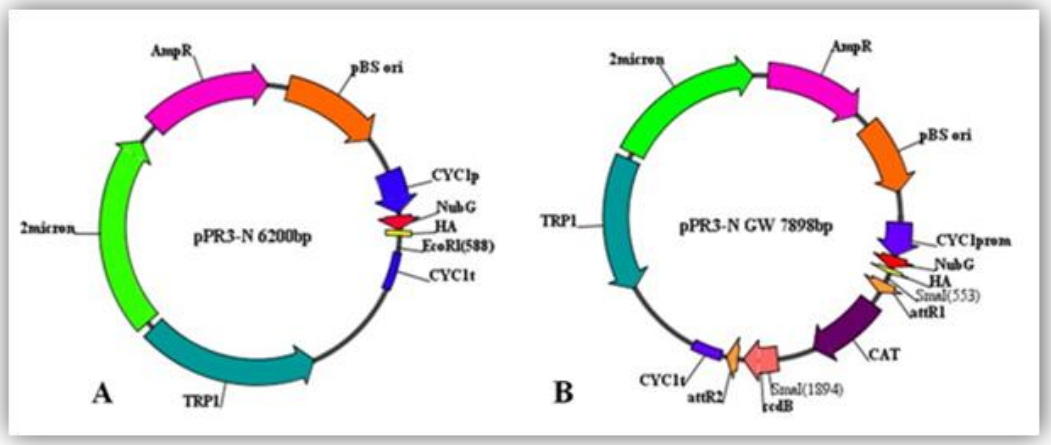


Fig. 6.1: Invitrogen Gateway adaptation of the DUALmembrane vector pPR3-N to generate pPR3-N GW. (A) pPR3-N. The prey vector pPR3-N was adapted by inserting Gateway cassette in frame with NubG-HA via EcoRI digestion. (B) pPR3-N GW. The Gateway adapted prey vector pPR3-N GW carries the cassette containing *att*R recombination sites, the *ccd*B selection gene and the chloramphenicol resistance gene (CAT). The *att*R1 and *att*R2 sites allow recombinational cloning of cDNAs of interest directly from entry clones. The *ccd*B and CAT genes are used for the negative selection and counterselection of plasmids, respectively. The modified vector is validated by restriction analysis using the enzyme SmaI.

RNA was isolated from the *A. fumigatus* clinical isolate 237 under a range of different *A. fumigatus* culture conditions (e.g. minimal and complete media, alkaline and acid conditions, nitrogen starvation, different growth stages from spores to hyphae, oxidative stress) to provide Invitrogen with at least 1 mg of total DNA for library construction. mRNA was isolated by Invitrogen from the total RNA and the library was firstly constructed in the Gateway compatible entry vector pDONR^{TM}222, which can be directionally swapped into any

expression vector, in this study pPR3N-GW, using Invitrogen's SUPERSCRIPT^{TM} III RNase H-RT and ELECTROMAX^{TM} DH10B ton A cells (T1 phage resistant). The proportion of full-length clones was tested by sequencing 24 random clones, representing a minimum of 20 different genes. The clones were defined as full-length if containing the predicted initiating ATG at the 5' end of the gene and a polyA tail in the expected position at the 3' end. As stated by Invitrogen, for unknown clones or clones showing no matches to databases, if the clone contains an ATG with a potential open reading frame downstream, it should be counted as a potential full-length clone. In Table 6.1 the characteristics of the full-length *A. fumigatus* cDNA library are summarised.

Full-length *A. fumigatus* cDNA library	
Number of primary clones (cfu)	1.932×10^7
Average of the insert size (kb)	1.309
Percent of clones containing inserts	> 99
Titre of the full length cDNA library (cfu/ml)	1.61×10^6
Complexity of the full length cDNA library	1.9×10^7

Table 6.1: Summary of the characteristics of the full-length *A. fumigatus* cDNA library. The library was constructed in collaboration with Invitrogen using Invitrogen's proprietary full length technology, the appropriate DUALmembrane prey Gateway adapted vector (pPR3N-GW) and the RNA isolated by our research-group from the *A. fumigatus* clinical isolate 237.

Because the frame of NubG fusions with cDNAs of interest is uncontrolled, only 1/3 of the clones in the library maintain an in-frame translational fusion. It was therefore important to ensure the complexity of the library was high enough to cover the entire genome multiple times (ideally a complexity higher than $2x10^6$ is required). Good quality NubG-x libraries should contain cDNA with an average length of 1.5 kb and complexity ranging from $1x10^6$ to $5x10^6$ (Iyer *et al.*, 2005).

6.2.2 Large scale and high-efficiency lithium acetate transformation protocol for library screenings

The protocol suggested by the manufactures is a variation of the classical lithium acetate protocol for yeast transformation (Gietz *et al.*, 1992), which ensures high efficiency for large scale experiments such library screenings.

NMY51 cells expressing pBT3-SUC PalH bait were initially inoculated into 10 ml of SD-leu and grown for 8 hours at 30°C with shaking. The 10 ml culture was then used to inoculate 100 ml SD-leu and the culture was grown overnight at 30°C with shaking. After measuring the OD_{546} of the sample against a H_2O blank and calculating the amount of culture needed for 30 OD units (30 OD units in 200 ml=OD 0.15), this amount of the overnight culture was centrifuged at 700 g for 5 minutes and the pellet was resuspended in 200 ml 2X YPAD, which was pre-warmed to 30°C, in a 1 litre flask to ensure appropriate aeration of the culture. Cells were grown at 30°C with vigorous shaking to an OD_{546} of 0.6. Single-stranded carrier DNA was prepared by two cycles of boiling and incubation on ice. The LiOAc/TE master mix for 10 ml was prepared with 1.1 ml 1 M LiOAc, 1.1 ml 10 x TE pH 7.5 and 7.8 ml H_2O. The PEG/LiOAc master mix for 12 ml was prepared with 1.2 ml 1 M LiOAc, 1.2 ml 10 x TE pH 7.5 and 9.6 ml 50 % PEG. When the culture was ready, it was divided into four 50 ml Falcon tubes and centrifuged at 700 g for 5 minutes. Each pellet was resuspended in 30 ml of sterile H_2O by vortexing and centrifuged at 700 g for 5 minutes. The supernatant was removed and the pellet was resuspended in 1 ml LiOAc/TE master mix, transferred to an eppendorf tube and centrifuged at 700 g for 5 minutes. The supernatant was removed and each pellet was resuspended in 600 µl of LiOAc/TE master mix. Four 50 ml Falcon tubes were prepared adding 7 µg of the library plasmid, 100 µl of single stranded carrier DNA, 600 µl of cells and 2.5 ml of the PEG/LiOAc mix. The mix was vortexed for 1 minute to thoroughly mix all components and then incubated at 30°C for 45 minutes with mixing briefly every 15 minutes. 160 µl of DMSO were added to each tube, which were mixed immediately by shaking and incubated at 42°C for 20 minutes. Cells were centrifuged at 700 g for 5 minutes and the pellets were resuspend in 3 ml 2X YPAD. The 4 cell suspensions were pooled together and cells were allowed to recover at 30°C for 90 minutes with shaking. Cells were centrifuged at 700 g for 5 minutes and resuspended in 4.8 ml 0.9 % NaCl. The transformation was plated onto sixteen 150 mm SD –leu –trp –his –ade plates, using 300 µl of resuspended cells per 150 mm plate. The remaining resuspended cells were used to prepare 1:100, 1:1000 and 1:10000 dilutions in 0.9% NaCl, 100 µl of which were plated onto a 90

mm SD-trp-leu plate, to calculate the transformation efficiency. Plates were incubated at 30°C for 3-4 days.

The total number of transformants and the transformation efficiency was calculated from the number of colonies on SD-trp-leu plates as follows: Total number of transformants = number of colonies on SD-trp-leu plate x dilution factor x 10 x 4.8. The total number of transformants should be greater than $2x10^6$. Transformation efficiency is calculated as follows: Transformation efficiency (clones/µg DNA) = total number of transformants/28 µg. Transformation efficiency should be greater than $7x10^4$.

6.2.3 Optimisation of *A. fumigatus* cDNA prey library screening

Fig. 6.2 shows the experimental procedure for the screening of the *A. fumigatus* cDNA prey library using the MYTH system. The first step of the library screen involved a pilot screen with the empty library vector pPR3-N, to determine whether the baits PalH pPBT3-SUC and PalH pPBT3-STE display any self-activation and to optimise the screening conditions to minimise false positive results (Fig. 6.2A). The cDNA library was then transformed into PalH bait-expressing *S. cerevisiae* NMY51 and interactors were selected using the stringency conditions determined in the pilot screen (Fig. 6.2B). From this stage, two different approaches can be used to analyse putative interactors, the first of which is suggested by DUALsystems and the second having been developed in this study. In the case of the former strategy, colonies were screened one by one whereby the library plasmids encoding putative positive interactors were isolated from individual positive clones and retransformed into *E. coli* (Fig. 6.2C) for plasmid DNA rescue and sequencing (Fig. 6.2D). However, due to the high numbers of colonies obtained from these primary screens a new method was implemented to facilitate screening in a more high throughput manner. Thus, clones obtained from primary screens were pooled together for a subsequent confirmation assay to collectively identify the putative interactor plasmids of interest. Plasmids encoding putative interactors were passaged in *E.coli* (Fig. 6.2E) and used to transform *S. cerevisiae* a second time with increased stringency of 3-AT titration (Fig. 6.2F). This experimental scheme permitted confirmation of putative interactors before proceeding with sequence analysis, thereby reducing the number of clones to analyse and therefore demanding less resources and manpower.

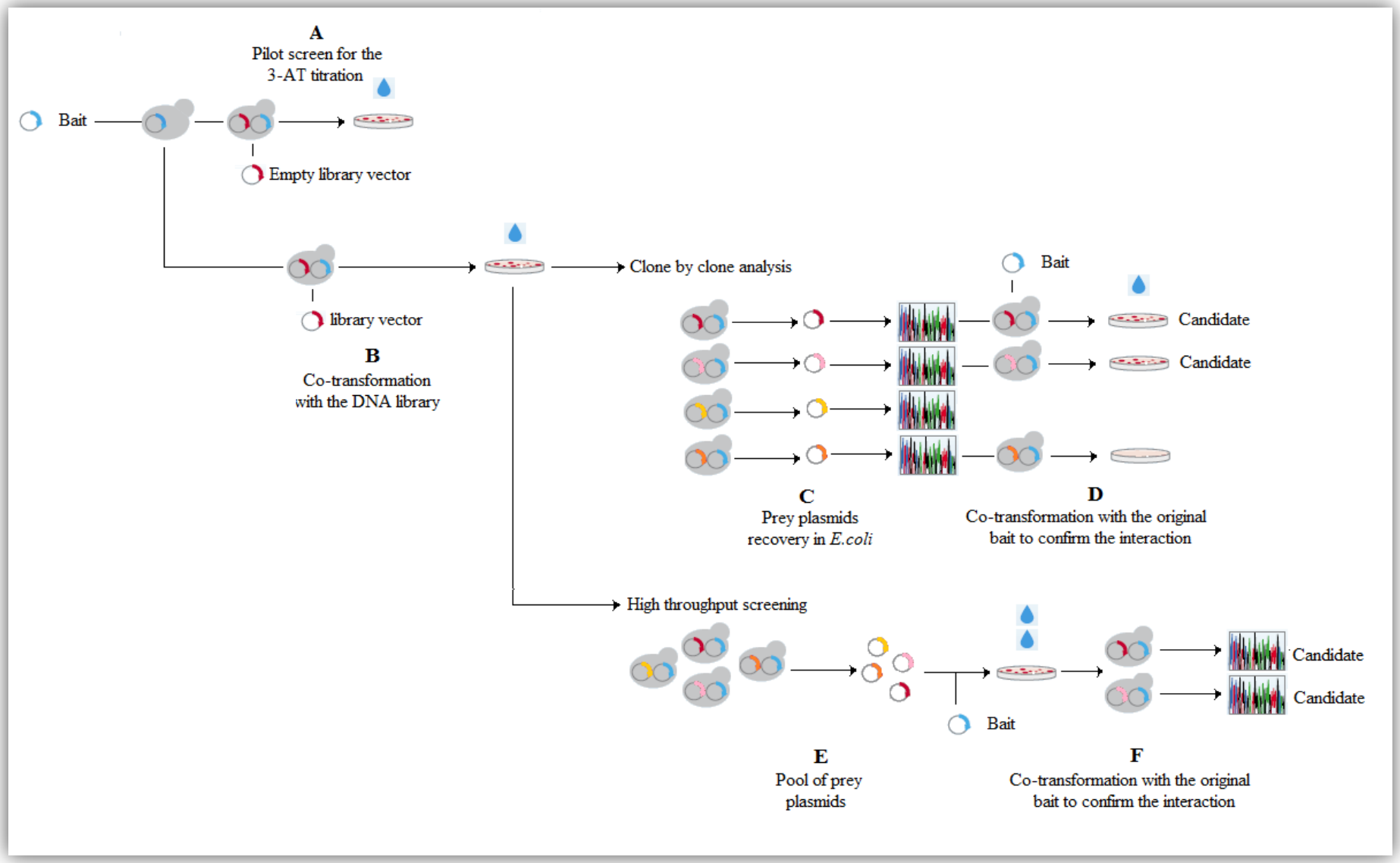

A
Pilot screen for the
3-AT titration
Bait
Empty library vector
B
Co-transformation
with the DNA library
library vector
Clone by clone analysis
Bait
Candidate
Candidate
C
Prey plasmids
recovery in E.coli
D
Co-transformation with the original
bait to confirm the interaction
High throughput screening
Bait
Candidate
Candidate
E
Pool of prey
plasmids
F
Co-transformation with the original
bait to confirm the interaction

Fig. 6.2: Experimental procedure for the screening of the full length *A. fumigatus* cDNA prey library using the MYTH system. Steps A-D represent the recommended protocol (DUALsystems) and Steps A, E, and F represent a modified high-throughput screening protocol optimised in this study. (A) Pilot screen with the empty library vector pPR3-N, to determine whether the baits (pPBT3-SUC PalH and pPBT3-STE PalH) self-activate and to optimise the screening conditions. (B) Transformation of cDNA library into NMY51 expressing *A. fumigatus* PalH bait, and selection of interactors using stringency conditions determined in the pilot screen. (C) Isolation of library plasmids from single positive clones. (D). Sequencing to identify putative interactors. (E) In a modified high-throughput protocol, primary clones obtained from the screening of the library were pooled prior to performing confirmation assay. Following passage in *E. coli* pooled plasmid DNA was transformed into bait-expressing yeast and an increased stringency used for screening. (F) Confirmation of putative interactors before proceeding with sequence analysis.

6.3 Results

6.3.1 Optimisation of library screening conditions for *A. fumigatus* PalH baits

To optimise library screening with *A. fumigatus* PalH bait, a pilot screen was performed to determine whether the baits of interest displayed self-activation when cotransformed, with empty library vector, into NMY51. In split-ubiquitin screens, activation of reporter genes in the absence of a protein-protein interaction may result from over-expression or instability of the bait. Alternatively, some baits contain sequences that are targets for endogenous proteases. In preparation for library screening, the PalH pBT3-STE and PalH pBT3-SUC baits were tested for self-activation.

As explained in Chapter V, sequence-verified constructs were transformed into *S. cerevisiae* NMY51 for expression tests and control assays. The expression of PalH bait in both the pBT3-STE and pBT3-SUC bait vectors was verified by western blotting analysis of total yeast extracts using an antibody directed against the LexA domain of the fusion proteins. The two plasmids differ by presence of a STE2 leader sequence in the pBT3-STE vector, which enhances the expression of encoded bait fusion protein. The level of bait expression was found (Chapter V) to be crucial for optimal functionality of MYTH interaction studies and this must be independently assessed for small- and large-scale experiments since transformation protocols differ between the two. PalH bait expression was found to be consistently higher for plasmid pBT3-STE (Fig. 5.7, Chapter V). Expression and functionality of the two *A. fumigatus* palH baits was validated (Fig. 5.8, Chapter V) by co-transformation with pAI-Alg5 and pDL2-Alg5, respectively expressing a fusion of the yeast ER protein Alg5 to the wild type Nub and to the mutated Nub portion (NubG).

A pilot screen was performed to determine whether PalH pBT3-STE or PalH pBT3-SUC baits self-activate when cotransformed with an empty library vector into NMY51. Following the recommended large-scale lithium-acetate transformation protocol, self-activation was assayed on selective SD-trp-leu-his-ade plates of increasing 3-AT stringency (0-50 mM). Since the bait is co-transformed with un-fused mutated NubG (expressed from the empty library vector pPR3-N), any colonies obtained on these screening plates must be physiologically insignificant, thus the pilot screen aids adjustment of the screening conditions to minimise false positive results. Transformation efficiency was verified by enumeration of the total number of transformants on SD-trp-leu media. For both PalH pBT3-STE and PalH pBT3-SUC baits, transformation efficiency was greater than $7x10^4$ clones/µg of DNA, ensuring meaningful results for the assay. SD-trp-leu-his-ade selective plates were supplemented with 0, 5, 10, 20, 30, 40 and 50 mM 3-AT to fine-tune the selection of positive interactors and reduce the frequency of false positive results. The results of the co-transformation are shown in Fig. 6.3. Growth is expected to be progressively inhibited with increasing 3-AT concentration, as observed for PalH pBT3-SUC where a concentration of 10 mM 3-AT leads to the complete elimination of background. To the contrary, the number of colonies obtained for PalH pBT3-STE was not lessened by the addition of 3-AT, indicating self-activation with this bait. The PalH pBT3-SUC bait was therefore chosen for the screening of the full length *A. fumigatus* cDNA prey library.

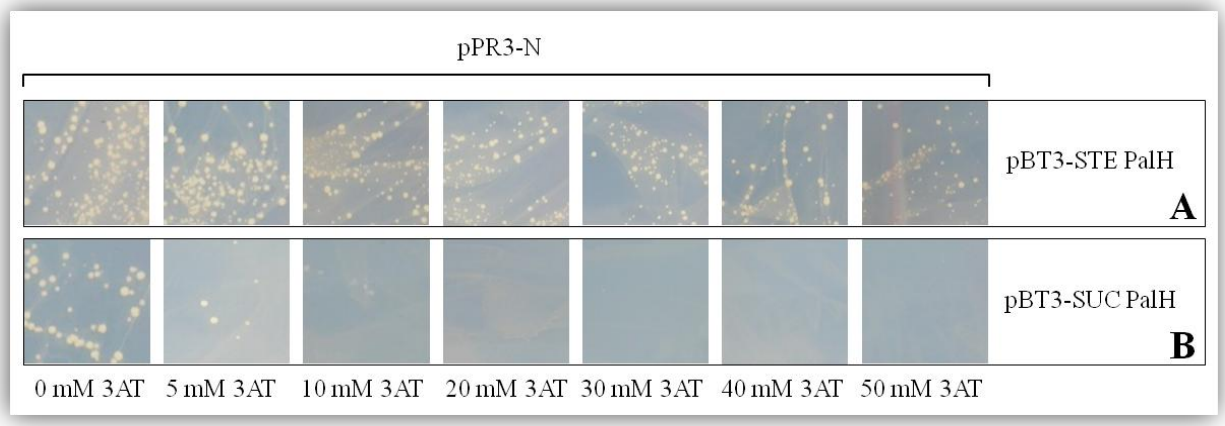


Fig. 6.3: Panel showing the results of the pilot screen for the baits PalH pBT3-STE and PalH pBT3-SUC. Test baits were co-transformed into NMY51 with the empty library vector pPR3-N, to determine whether proteins expressed from PalH pBT3-STE (A) or PalH pBT3-SUC (B) self-activate and to optimise the screening conditions to reduce false positivity. Co-transformant cells were plated in SD-leu-trp-his-ade containing increasing concentrations of 3-AT.

6.3.2 *A. fumigatus* cDNA prey library transformation to select for putative interactors of *A. fumigatus* PalH

The *A. fumigatus* cDNA library was transformed into NMY51 expressing PalH pBT3-SUC bait and prototrophic transformants were selected on SD-trp-leu-his-ade supplemented with 10 mM 3-AT. The recommended high-efficiency transformation protocol yielded transformation efficiencies in the range of $5x10^5$ to $2x10^6$ clones/µg DNA. Table 6.2 summarises two independent screenings of the full-length *A. fumigatus* cDNA prey library with the *A. fumigatus* PalH pBT3-SUC bait. For each screening, the total number of transformants, the transformation efficiency obtained (clones/µg DNA) and the number of colonies are indicated. In order to screen the library comprehensively, it is recommended that one screens 2-3 times the number of independent clones represented in the library ($1.9x10^7$).

Screening of the full-cDNA library with pBT3-SUC PalH		
Complexity of the library (cfu)	1.9×10^7	
Recent titre of the library (cfu/ml)	9×10^8	
	1st screening	**2nd screening**
Total number of transformants	3.7×10^6	5.8×10^6
Transformation efficiency (clones/µg DNA)	1.3×10^5	2.1×10^5
Number of colonies	250	750

Table 6.2: Summary statistics of the two screenings of the full-length *A. fumigatus* cDNA prey library with the *A. fumigatus* PalH pBT3-SUC bait.

Despite performing the screens under identical conditions, transformation efficiency differed significantly between the two screens, which resulted in 250 and 750 transformants for the first and the second screening, respectively.

Initially following the manufacturers' protocol, plasmid DNA was isolated from individual yeast clones obtained from the screening. Plasmid DNA was then transformed into *E. coli*, where it is possible to separate clones expressing bait and prey library vectors by virtue of the differing selective markers contained in prey and bait vectors, *ampR* and *kanR*, respectively. The identity of each cloned prey cDNA is then verified by sequencing. Confirmation of interaction requires reintroduction of each bait and prey partner into NMY51. Prey clones which retain positivity in the second screen are retained for further analysis.

Given the high number of transformants obtained from the primary screens (Table 6.2), a new method was developed to perform the analysis in a high-throughput manner, thereby reducing the number of clones to analyse. Yeast clones obtained from the second screening experiment (Table 6.2) were pooled together prior to performing the confirmation assay. Plasmid DNA isolated from the pool of yeast clones was transformed into *E. coli* to isolate the prey clones by ampicillin selection. Pooled prey clones were retransformed into yeast carrying PalH pBT3-SUC bait. Increasing the selection stringency, prototrophic transformants were selected in SD-trp-leu-his-ade selective plates supplemented with 20 mM 3-AT. This permitted confirmation of positive prey clones prior to sequence analysis. After the confirmation assay, a set of 40 yeast colonies were selected for the extraction of plasmid DNA and sequencing. Table 6.3 shows the identity of the selected putative interactors obtained with this high-throughput screening approach. Validating the robustness of the system, some of the putative interactors were identified multiple times in the set of 40 clones selected, including the phosphate transporter Pho88 (Afu5g01960), the acyl-CoA binding protein (Afu2g11060), the UPF0136 domain protein (Afu1g03720), the MFS glucose transporter (Afu3g13980) and two conserved hypothetical proteins (Afu4g11100 and Afu5g07090). In three instances, however, it was not possible to accurately determine the identity of the putative interactors, because of the poor quality of the sequences obtained.

A.fumigatus ORF	Description	Multiple Id
Afu5g01960	phosphate transporter (Pho88)	4
Afu7g05270	COMPASS complex subunit Sdc1	1
Afu2g12180	lectin family integral membrane protein	1
Afu4g11330	Aha1 domain family	1
Afu3g08380	inorganic diphosphatase	1
Afu2g11060	acyl-CoA binding protein	9
Afu1g02290	conserved hypothetical protein	1
Afu1g03720	UPF0136 domain protein	3
Afu1g04315	integral membrane protein	1
Afu3g13980	MFS glucose transporter	2
Afu5g13040	translation initiation factor eif-2b delta subunit	1
Afu4g09550	conserved hypothetical protein	1
Afu1g06580	high expression lethality protein Hel10	1
Afu8g03905	conserved hypothetical protein	1
Afu4g10350	polyubiquitin UbiD/Ubi4	1
Afu4g11100	conserved hypothetical protein	2
Afu5g07090	conserved hypothetical protein	4
Afu4g09450	hypothetical protein	1
Afu6g02280	allergen Asp F3, identical to peroxisomal-like protein PMP20	1
Afu6g03690	sodium P-type ATPase	maybe 1

Afu6g10300	Thioredoxin	maybe 1
Afu3g03470	conserved hypothetical protein	maybe 1

Table 6.3: Summary of the putative interactors identified from the analysis of 40 random candidates obtained in the high throughput screening of the full-length *A. fumigatus* cDNA prey library with the *A. fumigatus* PalH pBR3-SUC bait.

Methods for testing the relative affinity of the identified interactors were also explored. In addition to the growth reporters *HIS3* and *ADE2,* the strain NMY51 carries a reporter gene *lacZ*, encoding the bacterial enzyme β-galactosidase, which converts the substrate X-gal into a blue compound. In the MYTH system, development of blue colour in yeast cells incubated with X-gal (5-bromo-4-chloro-3-indolyl-β-D-galactopyranoside) is an indication of interaction between the bait and the prey tested. According to Kittanakom and collaborators (Kittanakom *et al.*, 2009), the addition of 0.8 µl/ml X-gal (100 mg/ml in N,N-dimethylformamide) and 0.1X sodium phosphate solution (0.07 g/ml sodium phosphate dibasic and 0.03 g/ml sodium phosphate monobasic) to the SD-trp-leu-his-ade media supplemented with 20 mM 3-AT can eliminate approximately one tenth of the colonies obtained from the screenings. In addition, use of the *lacZ* reporter is recommended by the DUALsystems manufacturer as a means to assess the affinity of the interactors identified from library screens. To date there are no published attempts at using the *lacZ* reporter to quantify the strength of interactions and in our experimentation, the β-galactosidase assay did not provide any reproducible data on the interactions validated by the confirmation assay (data not shown).

Further validation of the detected interactions can be pursued using various techniques, including a bait-dependency test (see below), co-immunoprecipitation, fluorescence microscopy or *in vitro* transport of radiolabeled substrates for transported proteins.

6.3.3 Bait-dependency assay for positive interactors of *A. fumigatus* PalH

As previously described, confirmation of a suspected positive interaction requires that the bait and prey combination retain interaction capability when reintroduced into NMY51. The confirmation assay demonstrates that the activation of the reporter genes is attributable to the actual interaction between two coexpressed protein partners and not to an artefact, as might be expected from, for example, genomic mutations in yeast resulting in the constitutive activation of the reporter genes. A further crucial requirement is establishment of bait-specific

(as opposed to promiscuous) interaction of the prey. This can be tested by co-transformation with an irrelevant bait (in this case pCCW-Alg5) in parallel with a transformation with PalH pBR3-SUC bait. Hence, the plasmid DNA isolated from the 40 putative positive yeast clones was transformed into *E. coli* to amplify the prey protein-encoding plasmids. The prey vectors from the library were co-transformed into the two bait protein-bearing strains. For true interactors, growth on selective media SD-trp-leu-his-ade supplemented with 20 mM 3-AT should be observed only when co-transforming with PalH pBR3-SUC bait, but not with the control pCCW-Alg5 bait. Prey proteins interacting strongly with the PalH pBR3-SUC bait and weakly with the control pCCW-Alg5 bait were chosen for further analysis. The co-transformations were repeated in triplicate, obtaining at least 1000 total transformants per reaction. The results for six putative interactors positive in all three bait dependency replicates is reported in Table 6.4 and summurised in Fig. 6.4. Clones were analyzed by sequencing to determine the identity of the encoding cDNA and to verify if the *A. fumigatus* cDNA was fused in frame with the NubG moiety. Six prey proteins reproducibly interact with PalH bait, these are the phosphate transporter Pho88 (Afu5g01960), the COMPASS complex subunit Sdc1 (Afu7g05270), the lectin family integral membrane protein (Afu2g12180), the MFS glucose transporter (Afu3g13980), the polyubiquitin UbiD/Ubi4 (Afu4g10350) and the acyl-CoA binding protein (Afu2g11060). The *A. fumigatus* cDNA was verified to be in frame with the NubG moiety for all six prey vectors and among them three candidates, the phosphate transporter Pho88, the COMPASS complex subunit Sdc1 and the acyl-CoA binding protein contained full-length cDNA inserts.

PT*/TT						
	1st experiment		2nd experiment		3rd experiment	
	p-BT3-SUC palH	pCCW-ALg5	p-BT3-SUC palH	pCCW-ALg5	p-BT3-SUC palH	pCCW-ALg5
pAl-Alg5	70.0	83.3	40.0	50.0	89.24	56.49
pDL-Alg5	5.0	9.5	5.0	3.3	7.18	9.19
COMPASS complex subunit Sdc1	50.0	2.5	50.0	25.0	11.30	0.97
lectin family integral membrane protein	66.7	3.3	50.0	25.0	17.94	0.90
phosphate transporter (Pho88)	75.0	6.7	66.7	25.0	4.90	2.89
polyubiquitin UbiD/Ubi4	50.0	5.0	50.0	20.0	40.12	2.50
acyl-CoA binding protein	10.0	2.0	50.0	2.0	14.86	0.00
MFS glucose transporter	66.7	7.5	23.3	3.3	32.14	3.23
Normalisation						
	1st experiment		2nd experiment		3rd experiment	
	p-BT3-SUC palH	pCCW-ALg5	p-BT3-SUC palH	pCCW-ALg5	p-BT3-SUC palH	pCCW-ALg5
pAl-Alg5	100	100	100	100	100	100
pDL-Alg5	13	11	6	20	9	16

COMPASS complex subunit Sdc1	125	3	56	17	13	2
lectin family integral membrane protein	167	4	56	17	21	2
phosphate transporter (Pho88)	188	8	75	17	6	15
polyubiquitin UbiD/Ubi4	125	6	56	20	48	4
acyl-CoA binding protein	25	2	56	4	18	0
MFS glucose transporter	167	9	26	3	38	6
	Average		**Standard deviation**			
	p-BT3-SUC palH	pCCW-ALg5	p-BT3-SUC palH	pCCW-ALg5		
pAl-Alg5	100.0	100.0	0.0	0.0		
pDL-Alg5	8.9	15.9	3.5	4.3		
COMPASS complex subunit Sdc1	64.8	7.1	56.3	8.3		
lectin family integral membrane protein	81.4	7.4	75.9	8.1		
phosphate transporter (Pho88)	89.3	13.3	91.7	4.7		
polyubiquitin UbiD/Ubi4	76.3	10.1	42.4	8.6		
acyl-CoA binding protein	32.9	2.1	20.4	2.0		
MFS glucose transporter	77.0	6.0	77.9	2.8		

Table 6.4: Results for co-transformations testing the interaction between PalH, expressed as bait in the pBT3-SUC vector in the MYTH system, and the 6 putative interactors from the screening of the preys *A. fumigatus* library. Each co-transformation was repeated 3 times and for each replicate the number of total transformants (TT) in SD-leu-trp, indicative of the transformation efficiency, and the prototrophic transformants (PT*) in SD-leu-trp-his-ade 20 mM 3-AT, indicative of interaction between bait and prey, was estimated (not shown). The same set of interactors was also tested at the same time by co-trasformation with the unspecific bait pCCW-Alg5. The ratio PT*/TT was calculated and averaged (1, 2 and 3 correspond respectively to the first, second and third replicate) fixing the value of the positive control co-transformation bait /pAL-Alg5 to 100.

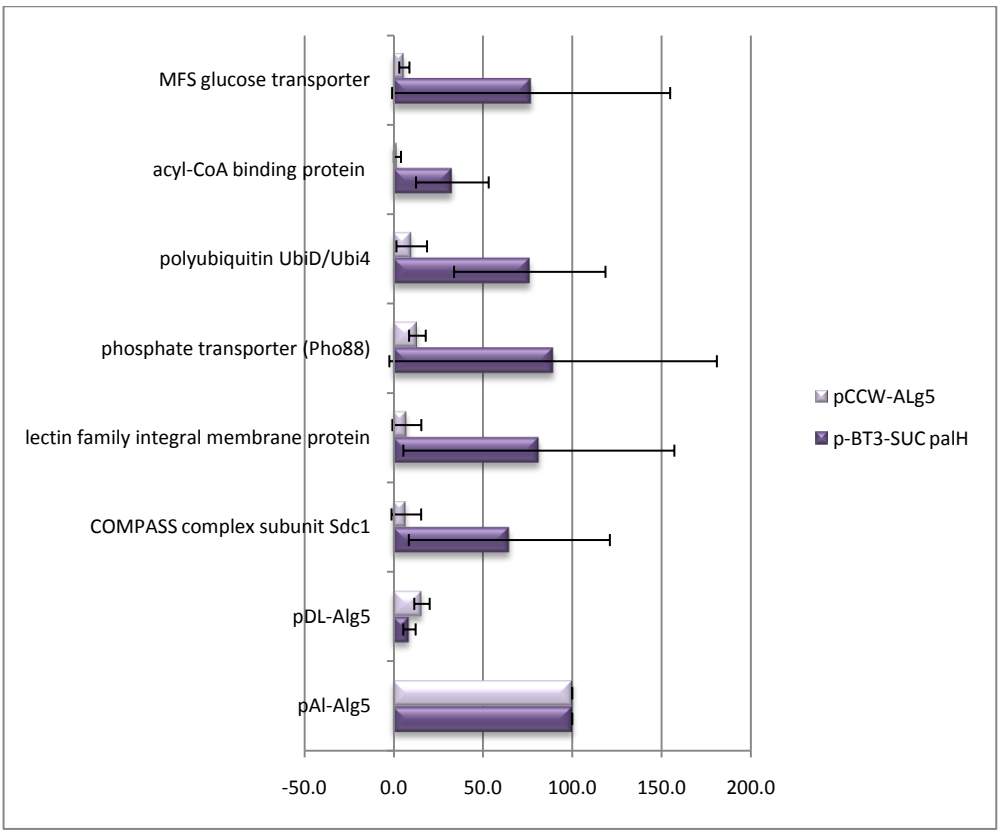


Fig. 6.4: Graphical representation of the results for the co-transformations to test the interaction between PalH, expressed as bait in the pBT3-SUC vector in the MYTH system, and the 6 putative interactors from the screening of the preys *A. fumigatus* library. For each co-transformation with the specific bait pBT3-SUC PalH and the unspecific bait pCCW-Alg5, the value PT*/TT is shown, obtained by averaging the three independent experiments, and normalised by fixing the value of the positive control co-transformation bait/pAL-Alg5 to 100.

6.4 Discussion

In this study the split-ubiquitin MYTH system was used to isolate novel protein interactors of the membrane-associated protein PalH from an *A. fumigatus* prey library, and the MYTH screening methodology was adapted for higher throughput isolation of interactors.

6.4.1 The MYTH system was adapted for the high-throughput screening of the full-length *A. fumigatus* cDNA prey library

Novel protein interactors for *A. fumigatus* PalH were isolated from a full-length *A. fumigatus* cDNA prey library, which was constructed by Invitrogen using their proprietary full length technology (Invitrogen) and a Gateway adapted prey vector (pPR3N-GW).

DUALmembrane prey cDNA was prepared using RNA isolated by our research-group from the *A. fumigatus* clinical isolate 237 under a range of different *A. fumigatus* culture conditions. Notwithstanding a one in three chance of in-frame fusion with N-terminal NubG moieties, the complexity of the library was high enough to cover the entire genome multiple times (ideally a complexity higher than $2x10^6$ is required). Good quality NubG-x libraries should show a complexity ranging from $1x10^6$ to $5x10^6$ (Iyer *et al.*, 2005). Initially, two baits (PalH pBT3-STE and PalH pBT3-SUC) were tested in a pilot screen to determine the extent of associated self-activation when cotransformed into yeast with empty library vector, and thereby optimising the conditions for subsequent library screening. Stringency was titrated with increasing concentrations of 3-AT to fine-tune the selection of positive interactors (Fig 6.3). For PalH pBT3-SUC, 10 mM3-AT led to the complete elimination of false positives. To the contrary, 3-AT titration did not reduce false positive background for PalH pBT3-STE bait, indicating self-activation of this bait. PalH pBT3-SUC bait was therefore chosen for library screening. The full-length *A. fumigatus* cDNA library was subsequently transformed into yeast expressing PalH pBT3-SUC bait and prototrophic transformants were selected in SD-trp-leu-his-ade selective plates supplemented with 10 mM 3-AT. The strategy suggested by the DUALsystems manufacturers was moderated to accommodate the high numbers of colonies obtained from primary screenings (Fig 6.2). Yeast clones expressing putative interactors were pooled together prior to performing the confirmation assay and rescreened in yeast with heightened 3-AT stringency. This permitted confirmation of interacting prey plasmids prior to sequence analysis. A set of 40 yeast colonies were analysed by sequencing to determine the identity of the putative interactors, some of which were identified multiple times (Table 6.3). A bait-dependency test was performed to test promiscuity of prey interactions in the NMY51 reporter strain. Six putative interactors were found to act favourably in three bait dependency replicates and the sequence determined the identity of the encoding cDNA and verified if *A. fumigatus* cDNA is in frame with the NubG moiety. These six proteins, which if expressed as prey interact with PalH bait, are the phosphate transporter Pho88 (Afu5g01960), the COMPASS complex subunit Sdc1 (Afu7g05270), the lectin family integral membrane protein (Afu2g12180), the MFS glucose transporter (Afu3g13980), the polyubiquitin UbiD/Ubi4 (Afu4g10350) and the acyl-CoA binding protein (Afu2g11060) (Table 6.4).

As previously explained in Chapter V, this methodology has permitted the understanding of quaternary structures for various plasma membranes, including sucrose transporters (Reinders *et al.*, 2002), a yeast protein translocation machinery (Scheper *et al.*, 2003a; Stagljar *et al.*, 1998), ErbB3 (a receptor tyrosine kinase) (Thaminy *et al.*, 2003), plant

K+ channels (Obrdlik *et al.*, 2004) and the yeast Ycf1p (an ATP-binding cassette transporter) (Paumi *et al.*, 2007). However, several of these findings underlined a limitation in the MYTH system which is sensitive to perturbations in the expression levels of baits. In one of the earliest large scale split-ubiquitin screens reported, Miller *et al.*, 2005 found that around 340 of the 705 proteins analysed were not suitable for studies in the MYTH system, due to over-expression from the plasmid chosen and consequent mislocalisation. Unpredictably, the ubiquitin fusion can in some instances alter irremediably the topology of the membrane protein, which is not directed to its native localisation and whose functioning and interaction with other proteins is therefore impaired. Adequate bait expression is crucial for the correct functioning of the MYTH system and this must be carefully, and independently, verified for small-scale experiments (to test direct interactions) and in large-scale screening (of cDNA or gDNA libraries) because the transformation protocol differs between the two. DUALmembrane plasmids pBT3-STE and pBT3-SUC are specifically designed for expression of bait proteins like PalH, whose topology involves an extracellular N-terminal domain and an intracellular C-terminal domain. However, the STE2 leader sequence in pBT3-STE was shown to enhance the expression of PalH, as demonstrated by the results of the western blotting analysis of total yeast extracts using an antibody directed against the LexA domain of the fusion protein (Fig. 5.7, Chapter V). For the optimisation of library screening conditions a pilot screen was performed with both PalH pBT3-STE and PalH pBT3-SUC baits to ascertain propensity for self-activation. Self-activation may be the result of several causes, for example, over-expression of the bait protein. Mistargeting of the bait protein can lead to bait instability and degradation and could therefore result in a bait protein that self-activates the transcriptional reporter genes. The straightforward way to address the self-activation issue is to supplement the media with 3-AT. This chemical compound is a competitive inhibitor of the *HIS3* gene product and enhances the stringency of *HIS3* selection when added to the selective media SD-trp-leu-his-ade. As suggested by several studies, which adressed protein-protein interactions involved in yeast ergosterol biosynthesis (Mo *et al.*, 2004; Mo and Bard, 2005b; Mo and Bard, 2005a), to titrate a bait protein under investigation, 3-AT is added in increasing concentrations to the selective media. Whereas for PalH pBT3-SUC growth is progressively inhibited in presence of increasing concentration of 3-AT, the number of colonies obtained for PalH pBT3-SUC is not affected by the progressive addition of 3-AT, indicating self-activation of this bait.

Bait-specific background depends upon multiple variables and false positive clones probably arise from various distinct mechanisms. False positive interactors are proteins that behave as spurious interactors in the MYTH screening and do not interact with the bait

protein in a physiologically meaningful way. Non-specific activation of the NMY51-encoded reporter genes might occur as a result of mutations in their promoter regions or from over-expression of the fusion protein in yeast (Serebriiskii *et al.*, 2000; Thaminy *et al.*, 2003). A list of common false positive interactors is publicly available (Kittanakom *et al.*, 2009). Due to the mechanistic principles of the methodology, ubiquitin is often found as a false positive interactor, especially when using x-NubG prey libraries. In addition, H^+-ATPase is a frequent false positive, likely because most vacuolar ATPases are involved in the sorting of bait proteins to their appropriate intracellular location. Rarely, histone deacetylases (HDAC) are identified as false positive interactors in MYTH screenings, because they are thought to bind to hydrophobic residues on the surface of the Cub domain of the bait. To address the issue of false-positivity, the bait-dependency test investigates if the prey protein under investigation interacts specifically with the bait of interest, or if non-specific interactions occur with other, using irrelevant baits expressed in the NMY51 reporter strain. Putative interactors, positive for interaction with the original bait, but not with the unrelated bait, were considered for further studies. Because MYTH screening is intrinsically prone to a significant level of false positive results, independent approaches are necessary to validate the interactions identified in the screening, such as co-immunoprecipitation or pull-down assay.

6.4.2 Bioinformatic validation of PalH putative interactors

As well as independent experimental verification of interactors there are several *in silico* investigations, addressing functionality of suspected interactors, which can aid deductions. Local (Bignell laboratory) and publicly available bioinformatics resources can be mined to determine, for example, whether bait and interactors follow a common transcriptional expression pattern and whether the associated GO terms support the relevance of the putative interaction in terms of function, process, and/or localisation (Ashburner *et al.*, 2000). For example, if two proteins share the same expression pattern the interaction identified might indeed be physiologically relevant (Ge *et al.*, 2001; Lee *et al.*, 2004). Proteins with different transcription profiles might also interact, but only transiently, so it is necessary to consider carefully the interactions identified case by case. Also, an identified interaction between a plasma membrane and a nuclear protein is likely to be a false positive.

Further validation of the detected interactors of *A. fumigatus* PalH is ideally required and could be pursued using various techniques, such as co-immunoprecipitation, fluorescence microscopy or *in vitro* transport of radiolabeled substrates for transported proteins. The analysis of the results of the screening of the full-length *A. fumigatus* cDNA prey library with

PalH bait using the split-ubiquitin MYTH system support the current theory that in *A. fumigatus*, like in *S. cerevisiae*, adaptation to alkaline stress depends on the integration of simultaneous stress-related signalling pathways other than just PacC/Rim101p (Arino, 2010) and also that the PacC/Rim101p pathway functions in roles other than pH adaptation. Several biological functions are commonly associated with the PacC/Rim101p pathway and with the immediate implications for cells of a sudden alkalinisation of the environment. In the current literature, several pathways are often coupled with PacC/Rim101p to overcome alterations in nutrient homeostasis in alkaline environments. The associated pathways are usually involved in the uptake and mobilisation of essential ions and/or nutrients such as iron/copper, phosphate, zinc, and glucose and in the screening presented in this study, candidates such as the phosphate transporter Pho88 (Afu5g01960) and the MFS glucose transporter (Afu3g13980) fit into these categories. The available understanding for these two candidates comes especially from studies in *S. cerevisiae*, where the PHO pathway (for reviews, see Huang *et al.*, 2002; Lenburg and O'Shea, 1996; Mouillon and Persson, 2005) and the major facilitator superfamily (MFS) (for reviews, see Sa-Correia *et al.*, 2009) have been extensively studied.

The recent characterisation of the *A. fumigatus PHO80* homologue has highlighted the importance of the PHO pathway for *Aspergillus* species, yielding important insight into the contribution of phosphate regulation in other stress-related pathways (de Gouvêa PF, 2008). In *S. cerevisiae*, the PHO pathway regulates genes involved in the uptake and mobilisation of phosphate, whose presence is crucial for the synthesis of nucleic acids, proteins, lipids and sugars (for reviews, see Huang *et al.*, 2002; Lenburg and O'Shea, 1996; Mouillon and Persson, 2005). The PHO pathway is composed of various members, including the transcriptional activators Pho2p and Pho4p, the Pho80p-Pho85p cyclin dependent protein kinase (CDK) complex, the Pho81p CDK inhibitor and the high affinity phosphate transporter Pho84p. The expression of the plasma membrane transporter Pho84p is activated by the PHO pathway itself in phosphate-replete conditions, via Pho81p-mediated inhibition of the Pho80p-Pho85p CDK complex, which is therefore unable to hyperphosphorylate Pho4p (Ogawa *et al.*, 1995a). Hypophosphorylated Pho4p is retained in the nucleus, where in concomitance with Pho2p, it activates gene expression (Kaffman *et al.*, 1998). The *S. cerevisiae* homologue of the phosphate transporter Pho88 is a membrane protein involved in phosphate transport, modulating the function of Pho81p in association with Pho86p, via a mechanism still not characterised (Yompakdee *et al.*, 1996). Yompakdee *et al.*, 1996 used a Gal4 promoter to drive high level constitutive expression of Pho81 and demonstrated that high level expression of Pho81p is not sufficient to promote expression of the acid

phosphatase Pho5p in high phosphate media. This implies that Pho81p activity is limited in high Pi conditions and that over-expression of Pho88p could force Pho81p activity in high phosphate conditions. Phosphate uptake was shown to be deficient in a Δ*pho88* mutant; however, *PHO88* gene expression is not subject to phosphate regulation, as demonstrated by Northern analysis. Hurto *et al.*, 2007 demonstrated using an N-terminal GST-Pho88p fusion protein that the protein localised to the ER. Prediction with TMpred reveals that the protein has an extra luminal N terminus, and since the *A. fumigatus* prey was selected from a library of N-terminal NubG fusions, it follows that the Pho88p protein is likely to be located on an intracellular membrane. Copic *et al.*, 2009 performed a screen for *S. cerevisiae* mutants defective in intracellular retention of the ER chaperone Kar2p, identifying 87 Kar2p secreting strains including the Δ*pho88* mutant. Further analysis of the Δ*pho88* mutant identified synthetic lethality with a *HAC1* deletion, suggesting a role in protein folding through post-translational modification of secretory cargoes. Moreover the study found that the Δ*pho88* mutant was defective for CPY glycosylation indicating that it is defective for processing of secretory proteins. Copic *et al.*, 2009 suggested therefore Pho88p as a prime candidate for participating directly in N-linked glycosylation. Thus, in light of the considerations in Chapter V which suggested PalH is a GPCR homodimer, a plausible hypothesis is that Pho88p facilitates N-glycosylation of the PalH extracellular domain to mediate protein folding and delivery to the cell surface. As previously described in Chapter V, GPCRs activity is modulated by a variety of post-translational modifications, such as phosphorylation, fatty acid acylation and glycosylation. The latter modification is crucial for GPCRs, their intracellular folding, their delivery to the plasma membrane and the protein-protein interactions they are involved in for activation of the specific signal pathways (Lanctot *et al.*, 1999; Ray *et al.*, 1998; Wheatley and Hawtin, 1999). Hence, several GPCRs have been shown to be N-linked glycoproteins, whose activity is mediated by the Asn-X-Ser/Thr domain localised in the extracellular domain. In addition, N-glycosylation has been demonstrated to be involved in the high-affinity binding and signal transduction of several GPCRs (Breitfeld *et al.*, 1984; Rademacher *et al.*, 1988). N-glycosylation has been extensively studied for the family B glucagon-like peptide 1 (GLP-1) receptor, because of the multiple antidiabetic actions of its natural agonist GLP-1 (Chen *et al.*, 2010). Chen *et al.*, 2010 demonstrated that tunicamycin inhibition, which specifically affects N-glycosylation of the GLP-1 receptor, abolishes its binding ability and therefore biological activity. Mutation of all the potential N-linked glycosylation sites, is required to impair binding and biological activity of the GPL-1 receptor, which appears to be expressed at a lower rate on the cell surface, when not properly folded and/or retained in intracellular biosynthetic compartments. The presence of PalH N-

glycosylation sites is predicted *in silico* using NetNGlyc 1.0 (http://www.cbs.dtu.dk/services/NetNGlyc), which reveals with high probability (0.7432) an N-glycosylation site starting from residue 15 of *A. fumigatus* PalH. However, no signal peptide is present in the N-terminal luminal domain of PalH (residues 1-88), therefore indicating this prediction has to be carefully considered, because proteins without signal peptides are unlikely to be exposed to the N-glycosylation machinery. Signal peptides have been thought to be required for the posttranslational translocation of GPCRs across the endoplasmic reticulum membranes, otherwise not possible when stably folded domains are present in the N-terminus. However, Huang *et al.*, 2010 demonstrated for the GLP-1 receptor the cleavage of the signal peptide is not essential for receptor synthesis, but it facilitates processing and trafficking to the cell surface (Huang *et al.*, 2010). Although critical to some extent, the role and indispensability of signal peptides in N-glycosylation of GPCRs remains unclear. The human Na^{+}-Ca^{2+}-exchanger possesses a signal peptide, which is not necessary for plasma membrane localisation or functioning of the receptor itself (Loo *et al.*, 1995). The human family A endothelin ET_b GPCR signal peptide is dispensable for synthesis but essential for delivery to the plasma membrane being otherwise accumulated in the ER (Kochl *et al.*, 2002). The same scenario is observed for the Family B $VPAC_1$ receptors (Couvineau *et al.*, 2004), whereas for the Family B CRF_1 signal peptides enhance the expression of the respective receptors (Alken *et al.*, 2005). A large proportion of GPCRs (around 85%) show no signal peptide in their sequence (Kochl *et al.*, 2002).

Studies in *A. nidulans* have highlighted the significant differences with the PHO pathway as compared to *S. cerevisiae*, suggesting the presence of another component in the Pho80p-Pho85p CDK complex, at least in some *Aspergillus* species, to support the function of *A. nidulans* Pho80p (Wu *et al.*, 2004). *A. nidulans* possesses two *PHO85* homologues, named *phoA* (Bussink and Osmani, 1998) and *phoB* (Dou *et al.*, 2003), but the Pho85-like kinase pair has been demonstrated to likely have an essential function in cell cycle control and morphogenesis, rather than in the PHO pathway (Dou *et al.*, 2003). Within the *Aspergillus* genus, only some species possess two *PHO85* homologues, e.g. *A. fumigatus* only has a single homologue showing 96% homology with the *S. cerevisiae* one. The studies to investigate the role of the PHO pathway in *A. fumigatus* have started only relatively recently with the characterisation of the *PHO80* homologue and the respective null mutant (de Gouvêa PF, 2008). The Δ*pho80* mutant showed over-expression of the *PHO* genes and reduced polar growth, but was not attenuated in a murine low dose model of invasive aspergillosis.

The MFS glucose transporter (Afu3g13980) identified as a PalH putative interactor belongs to the major facilitator superfamily (MFS), a group of multidrug resistance (MDR)

transporters, still poorly characterised in eukaryotes (for reviews, see Sa-Correia *et al.*, 2009) and whose importance has been described in Chapter V. In *S. cerevisiae*, the MFS transporters usually show a 12 or 14 TMD topology and transport physiological substrates, in this case glucose, one of the nutrients whose bioavailability is likely to be modified as a consequence of alkalinisation of the pH and/or during the infection.

As comprehensively described in Chapter VII, the association between the yeast MultiVesicular Bodies (MVB) pathway and Rim101p-mediated regulation has been extensively studied and evidence in the literature links the two pathways. Though the lectin family integral membrane protein (Afu2g12180) and the acyl-CoA binding protein (Afu2g11060) do not belong to the MVB pathway, they may be crucial for the organisation and homeostasis of the biosynthetic and endocytic pathway, whose major coordinator site is the endoplasmic reticulum (ER) (Gruenberg and Maxfield, 1995). The ER has multiple functions within the cell for example participation in the biogenesis of secretory and membrane proteins and lipids. Linear polypeptide chains enter the ER to undergo proper folding, glycosylation and disulphide bond formation, whereas lipids are modified in the ER by several enzymes involved in fatty acid elongation and desaturation, ergosterol synthesis, and glycosylphosphoinositol (GPI) addition. Once modified, proteins and lipids leave the ER via transport vesicles and, as relevant to the present study, intracellular lectins have been extensively associated with N-linked glycoprotein traffic (as reviewed in Hauri *et al.*, 2000; Yamashita *et al.*, 1999). One of the candidates identified by this screen is a lectin family integral membrane protein (Afu2g12180), whose human homologue, vesicular integral-membrane protein VIP36, functions as a sorting receptor by recognising high-mannose type glycans for transport from the Golgi to the cell surface in polarised epithelial cells (Fiedler *et al.*, 1994). The expression of two other animal lectin proteins, ERGIC-53 and VIP36, is up-regulated by ER stress, which causes the accumulation of unfolded proteins in the ER and triggers the signalling response mechanism known as the unfolded protein response (UPR). Interestingly the increase of unfolded proteins in the ER in yeast has been attributed to various type of stresses (Nyfeler *et al.*, 2003), among which the perturbation of calcium homeostasis or redox status, and nutrient deprivation are included. These stresses represent evident links with the PacC/Rim101p pathway as common consequences of the alkalinisation of the media/environment.

The acyl-CoA binding protein (Afu2g11060) belongs to a widely distributed family (as reviewed in Faergeman *et al.*, 2007; Kragelund *et al.*, 1999), whose functions have been extensively characterised in *S. cerevisiae.* Acyl-CoA binding proteins bind to medium and long chain saturated and unsaturated fatty acid acyl-CoA esters and are involved in their

intracellular transport and metabolism (Knudsen *et al.*, 1994; Schjerling *et al.*, 1996). Interestingly, long chain acyl-CoA esters are crucial intermediates in lipid biosynthesis and fatty acid degradation, and have been demonstrated to affect a large number of systems and functions, including ion channels, pumps and transporters (Faergeman and Knudsen, 1997; Knudsen *et al.*, 2000). Besides, as relevant for the purposes of this study, deletion of *ACP1* decreases the levels of very-long-chain fatty acids and of sphingolipid synthesis, and impairs membrane assembly, and organelle organisation and structure, suggesting involvement in vesicular trafficking and cellular integrity maintenance (Gaigg *et al.*, 2001). Accordingly, Δ*acp1* mutants show severe morphological alterations of the vacuole, whose functionality is dramatically impaired, and reduction of ceramide cellular content (Faergeman *et al.*, 2004). Although it is not possible to clearly explain the mechanisms linking the acyl-CoA binding protein and the PacC/Rim101p pathway, at least two non-mutually exclusive hypotheses could be formulated. Regarding the importance of the endocytic system for pH adaptation, the first hypothesis is based on the demonstrated role of this highly-conserved protein family to influence the regulation and coordination of membrane fusion events necessary for endosomal vesicle transport, as demonstrated in yeast (Faergeman *et al.*, 2004; Faergeman and Knudsen, 1997) and recently in *Caenorhabditis elegans* (Larsen *et al.*, 2006). Alternatively, the link between the acyl-CoA binding proteins and the PacC/Rim101p pathway could be attributed to the Acp1p-dependent connection of fatty acid metabolism and transcriptional regulation of phospholipid biosynthesis, as highlighted by the recent DNA microarray study of the Δ*acp1* mutant (Feddersen *et al.*, 2007). Deletion of *ACP1* affects the expression of genes involved in fatty acid and phospholipid synthesis, glycolysis, glycerol metabolism, ion uptake and mobilisation and stress response. Validating the importance of lipid membrane composition, recent experimental evidence in yeast have shown the Rim101p pathway is activated in response to a change in lipid symmetry (Ikeda *et al.*, 2008), composition and shape (Mattiazzi *et al.*, 2010).

A common feature of some of the studies in the current literature trying to explore the links between the PacC/Rim101p pathway and other functionally related pathways is the recurrent and unexplainable presence of members of the functional category chromatin assembly and modification (Copic *et al.*, 2009; Mattiazzi *et al.*, 2010), including components of the SWR1-complex (Korber and Horz, 2004). The functional relationship between the two pathways is still unexplored: however, evidence of the involvement of the SWI1/SNF2 group in pH sensing and regulation are demonstrated in the present study in various instances, as described also in Chapter IV and Chapter VII. Among the candidates of the screening of the full-length *A. fumigatus* cDNA prey library with PalH bait using the split-ubiquitin MYTH

system, *SDC1* encodes the COMPASS complex subunit Sdc1 (Afu7g05270), which methylates lysine 4 of histone H3 and is required in chromatin silencing at telomeres (South *et al.*, 2010). As extensively described in Chapter IV and VII, histone and chromatin remodelling have gained credit as regulators of transcription in the past few years (Buck and Lieb, 2006), with the discovery that these complexes alter nucleosome structure in different ways, such as by covalent modification of the N-terminal histone tails or by ATP-dependent perturbation of histone-DNA interactions (Fyodorov and Kadonaga, 2001).

The remaining putative interactor is the polyubiquitin UbiD/Ubi4 (Afu4g10350). This candidate requires particular attention in the downstream confirmation assay, because it is indicated as a common false positive in screenings, due to the principle of the methodology. However the possibility of an interaction between the polyubiquitin UbiD/Ubi4 and PalH is not to be excluded, considering such an interaction would validate the current model for pH adaptation in *A. nidulans*. Ubiquitination is considered as a signal to sort endosomal cargoes to the MVB pathway (Katzmann *et al.*, 2001) and the current model for pH adaptation in *A. nidulans* hypothesises the involvement of endocytosis for pH-signal transduction; however, it suggests the arrestin-like PalF to be phosphorylated and multi-ubiquitinated depending on alkaline ambient pH in a PalH- and partially PalI- but not PalA-, PalB-, PalC-dependent manner (Herranz *et al.*, 2005).

CHAPTER VII

IDENTIFICATION OF NOVEL *RIM101* REGULATORS BY GENETIC SCREENING IN *S. CEREVISIAE*

7.1 Overview

Previous studies have demonstrated that Rim101p (the yeast homologue of PacC) functionality extends beyond mere pH adaptation to the positive regulation of sporulation, invasive growth, ion tolerance and acquisition, and certain cell wall characteristics (Denison, 2000; Hayashi *et al.*, 1998; Lamb *et al.*, 2001; Lamb and Mitchell, 2003; Li and Mitchell, 1997). In yeast these processes are therefore inextricably linked to environmental pH, which not only influences *S. cerevisiae* growth, but also its differentiation, invasive growth and meiotic sporulation. The main effect of external alkalinity upon cellular physiology is the disruption of the membrane proton gradient, which supplies energy for the transmembrane transport necessary to face consequent nutrient and ion limitation. Rim101p appears to be principally required for ion homeostasis (Lamb *et al.*, 2001; Lamb and Mitchell, 2003) and in alkaline conditions the maintenance of ion and pH homeostasis is ensured by the expression of several pumps including the plasma membrane H^+-ATPase Pma1p, the Na^+-ATPase Ena1p and the vacuolar H^+-ATPase Vma4p (Stevens and Forgac, 1997; Rodriguez-Navarro *et al.*, 1994; van der Rest *et al.*, 1995). The essential role of these transporters at alkaline pH is evidenced by phenotypes of null mutants lacking these pumps, which are unable to grow in alkaline conditions and/or display cation sensitivity (Lamb and Mitchell, 2003). Gene expression is dramatically modified as a consequence of a shift to alkaline pH. Among differentially regulated genes (Lamb *et al.*, 2001), several are involved in zinc, phosphate, iron or copper uptake and utilisation (*CTR3*, *FRE1*, *PHO11*/12, *PHO84*, *ARN4*/*ENB1*, *YOR154W*). *CTR3* and *FRE1* are targets of the copper-responsive transcription factor Mac1p (Jungmann *et al.*, 1993; Pena *et al.*, 1998); *YOR154W* is a target of zinc-responsive transcription factor Zap1p (Lyons *et al.*, 2000); *PHO11/PHO12* and *PHO84* are targets of the phosphate-responsive transcription factor Pho4p (Ogawa *et al.*, 1995a; Ogawa *et al.*, 1995b). Arn4p is involved in iron uptake and in particular imports a bacterial siderophore-iron

complex, facilitating competition with bacteria in alkaline conditions (Heymann *et al.*, 2000; Lamb *et al.*, 2001).

In this study two screening strategies were used to identify novel regulators of *S. cerevisae* Rim101p functionality. Both screens focused upon the 80 mutants identified in the Euroscarf *S. cerevisiae* ORF deletion library as having Δ*rim101*-like cation sensitivity profiles (Bignell, unpublished data). The characteristic cation sensitivity profile associated with Δ*rim101* mutants (which were confirmed in this study also, Fig. 7.3- Fig. 7.9) proved a useful tool to identify mutants having identical phenotypes to a Δ*rim101* strain, which may represent (for example) regulators of Rim101p signalling, processing, nuclear translocation. In this respect, pH sensitivity did not prove a useful phenotypic determinant given a) the poor capacity of *S. cerevisiae* for growth at high pH, and b) the high prevalence of gene deletions which predispose to alkaline sensitivity in a Rim101p-independent manner, such as those impacting *de novo* biosynthesis of nutrients whose uptake from the external medium is pH-dependent. The first of the two screens, (Fig. 7.1) utilised a truncated Rim101p ORF, previously constructed by Castrejon *et al.*, 2006, and used to address how Rim101p contributes to yeast cell wall assembly through the Sltp2 kinase (Castrejon *et al.*, 2006). Where Δ*rim101*-like mutants lack specific regulators of Rim101p processing, introduction of a constitutively processed form of Rim101p would be expected to rescue cation sensitivity. Thus, to identify which of the 80 Δ*rim101*-like mutants lack proteins acting upstream of Rim101p, the mutants were transformed with an activated allele of *RIM101* to attempt to rescue the phenotype. This epistacy screen relied upon the reversal of lithium and sodium toxicity in the presence of activated *RIM101,* thereby identifying PacC regulatory roles for the deleted genes.

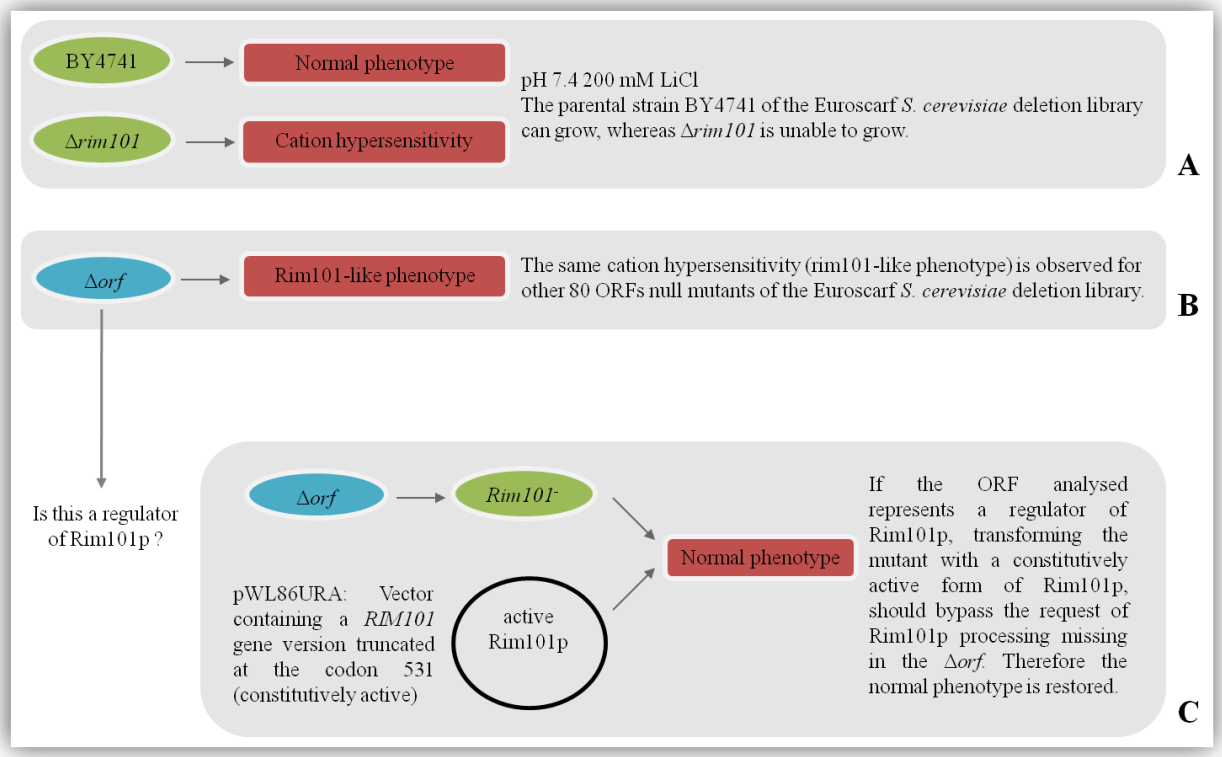


Fig. 7.1: Epistacy screen of 80 *S. cerevisiae* Δ*rim101*-like mutants to identify novel regulators of Rim101p. A global phenotypic screen of the Euroscarf *S. cerevisiae* ORF deletion library had previously revealed that a Δ*rim101* shows cation hypersensitivity compared to the parental strain BY4741 (Bignell, unpublished) (A). This cation hypersensitivity was also observed for 80 other ORF deletions (B). To identify novel regulators of Rim101p, the epistacy screen selected for reversal of lithium and sodium toxicity following transformation with a constitutively active form of Rim101p (C).

The second genetic screen utilised a synthetic Rim101p promoter constructed by Lamb and Mitchell, 2003 and used to study Rim101p-mediated repression of the genes *NRG1* and *SMP1* to direct ion tolerance and cell differentiation (Lamb and Mitchell, 2003). The reporter, consisting of the *lacZ* reporter gene under the control of four Rim101p consensus binding sites, provides a read out of activated Rim101p binding to the synthetic promoter, and consequent transcriptional repression, as measured by β-galactosidase assay (Fig. 7.2). If proteins encoded by deleted ORFs participate in Rim101p processing, DNA binding or nuclear localisation, β-galactosidase activity would become derepressed.

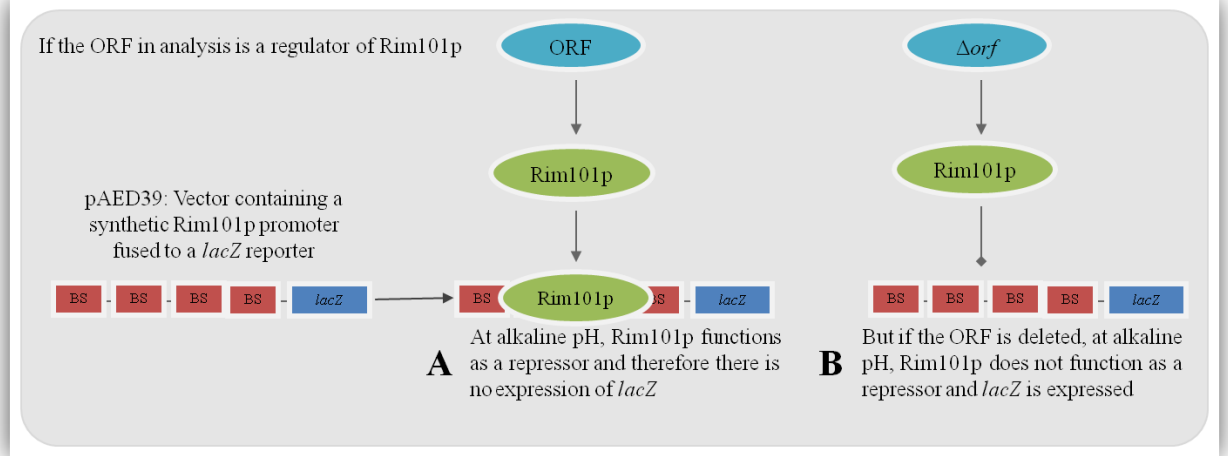


Fig. 7.2: Use of a synthetic Rim101p promoter to identify mutants in Rim101p processing and/or transcriptional activity. Relative to wild type (A) *lacZ* expression is expected to become derepressed in mutants lacking regulators of Rim101p (B).

7.2 Methods

7.2.1 The Euroscarf *S. cerevisiae* ORF deletion library

Yeast strains used in this study come from the YKO library, background BY4741 (MATa *his3_1 leu2_0 met15_0 ura3_0*), which has been developed by the *Saccharomyces* Genome Deletion Project (Open Biosystems, http://www.openbiosystems.com/YKO) (Winzeler *et al.*, 1999; Winzeler *et al.*, 2000). It is a unique collection of non-essential *S. cerevisiae* knockout strains covering 95% of the yeast genome. This collection, which is composed of 4811 gene-disruption mutants for most of the non-essential *S. cerevisiae* genes, was created using a PCR-based gene deletion strategy. This strategy resulted in replacement of each yeast open reading frame (ORF) with a KanMX cassette and a tag.

7.2.2 Plasmids

pWL86URA. pWL86URA was derived from pWL86 (Li and Mitchell, 1997) which was kindly provided by A. P. Mitchell. The plasmid pWL86 was derived from the vector pRS314 and additionally contains the *RIM101* gene truncated at codon 531 (Rim101-531p). pWL86 was constructed by inserting a 2.1-kb PstI-XhoI fragment from plasmid pSS239-CRX (Su and Mitchell, 1993b) between the PstI and XhoI sites of pRS314 (Sikorski and Hieter, 1989). The resulting plasmid includes *RIM101* 5' sequences and coding region through codon

531, whereby the fusion to vector sequences adds C-terminal amino acids RILLEGGPGTSFCSL. For the purposes of this study, the URA auxotrophic marker was amplified by PCR from the plasmid Yep24 (New England Biolabs) using the BD advantage polymerase, and the oligonucleotides UraNot2F and UraNot2R (Appendix B) which added restriction sites for the enzyme NotI to promote cloning in pWL86. The URA auxotrophic marker was subsequently cloned into the single NotI site of pWL86. To facilitate cloning, the vector pWL86 and the NotI-digested URA auxotrophic marker were treated with the enzymes CIP and PNK respectively. After ligation clones were screened by colony-PCR for the presence of the URA auxotrophic marker. Positive clones were verified for the directional cloning of inserts by sequencing (see Appendix B) and for functionality of the URA auxotrophic cassette by transformation into BY4741 (for genotype, please consult Appendix A). The functionally verified plasmid pWL86URA was used to transform BY4741 (the parental strain of the Euroscarf *S. cerevisiae* ORF deletion library), Δ*rim101* and the 80 Δ*rim101*-like mutants. Transformant clones were selected on SD-ura media. For each transformation three independent transformants were isolated for further analysis.

pAED39. The Rim101p repression reporter plasmid pAED39 was kindly provided by A. P. Mitchell (Lamb and Mitchell, 2003). The reporter plasmid pAED39 was constructed by inserting the sequence TCGAGTGCCAAGATGCCAAGACTCGAGTCTTGGCATCTTGG CAC into the *Xho*I site of LGΔ312S.

7.2.3 *S. cerevisiae* phenotypic testing

Δ*rim101-like* mutant phenotypes were confirmed using the test conditions listed in Table 7.1.

Media	Test Condition	Comments
YPD	Control conditions	No buffer
YPD pH 4	Acidic stress	Buffered with 100 mM glycolic acid
YPD pH 8	Alkaline stress	Buffered with 100 mM Tris-HCl
YPD 100 mM LiCl	Cationic stress	Buffered with 100 mM LiCl
YPD 200 mM LiCl	Cationic stress	Buffered with 200 mM LiCl
YPD pH 4 200 mM LiCl	Acidic and cationic stress	Buffered with 100 mM glycolic acid and 200 mM LiCl
YPD pH 4.5 800 mM NaCl	Acidic and cationic stress	Buffered with 100 mM glycolic acid and 800 mM NaCl
YPD pH 7.4 200 mM LiCl	Alkaline and cationic stress	Buffered with 100 mM Tris-HCl and 200 mM LiCl

Table 7.1: Buffers used for pH-buffered media in the *S. cerevisiae* phenotypic screening. The composition of the media is indicated in Section 2.3.2.

7.2.4 Assessment of yeast growth in liquid media

Yeast growth profiling was adapted to 96-well format in liquid media. Mutants and transformants, the latter gridded in triplicate, in 96-well plates were grown overnight in YPD and each was subsequently used to inoculate two further (one with YPD and one with YPD pH 7.4 200 mM LiCl) 96-well plates. OD_{600} was measured using Multiskan EX (Thermo Electron Corporation) at the initiation of 30°C incubation and at subsequent 2, 4, 6, 8, 10, 12 and 24 hour time points.

7.2.5 ß-galactosidase assay

The β-galactosidase activity of *S. cerevisiae* strains was measured using the non-stop protocol recommended by the yeast β-galactosidase assay kit (Pierce) manufacturers, as previously described. The β-galactosidase assay was adapted to the 96-well plate format. Mutants and transformants, the latter gridded in triplicate, in 96-well plates were grown overnight in YPD and each was subsequently used to inoculate three further (YPD pH 6.5, YPD pH 4.5 and YPD pH 8.0) 96-well plates. Overnight YPD broth cultures were diluted (1/10) and grown to OD_{660} approximately of 0.6. The OD_{660} was then recorded and 100 µl of working solution (50 µl 2X ONPG and 50 µl Y-PER Reagent) was added to each well. After

20 minutes, the absorbance at 420 nm was measured and the β-galactosidase activity was calculated applying the following formula: $(1000xA_{420})/(TxVxOD_{660})$=β-galactosidase activity, where T is the reaction time (minutes), V corresponds to the reaction volume (ml) and A_{420} is the absorbance at 420 nm. The experiment was performed in culture conditions of varying pH, as summarised in Table 7.2.

Media	Test Condition	Comments
YPD pH 6.5	Control conditions	No buffer
YPD pH 4.5	Acidic stress	Buffered with 100 mM glycolic acid
YPD pH 8	Alkaline stress	Buffered with 100 mM Tris-HCl

Table 7.2: Buffers used for pH-buffered media. The composition of the media is indicated in Section 2.3.2.

7.3 Results

7.3.1 Confirmation of Δ*rim101*-like phenotypes for 80 mutants from the Euroscarf *S. cerevisiae* ORF deletion library

A global phenotypic screen of the Euroscarf *S. cerevisiae* ORF deletion library performed in our laboratory (Bignell, unpublished) had previously revealed that Δ*rim101* shows cation hypersensitivity compared to the parental strain BY4741. The cation sensitivity profile, termed by us as a Δ*rim101*-like phenotype, was observed for deletions of 80 other ORFs, among which all of the yeast Rim101p signalling components (Rim8p, Rim9p, Rim13p, Rim16p, Rim20p, Rim21p, Dfg16p, Ygr122wp) were included. Phenotypic results are tabulated in Table 7.3. Prior to genetic screening of these mutants cation hypersensitivity was retested to confirm previous observations and also to optimize culture conditions for subsequent epistacy screening. The results of the phenotypic screening are summarised in Figs. 7.3 – 7.9. The media used for phenotype testing were: YPD, YPD pH 8 (100 mM Tris-HCl) (Fig. 7.3), YPD pH 4 (100 mM glycolic acid) (Fig. 7.4), YPD pH 4 (100 mM glycolic acid) 200 mM LiCl (Fig. 7.5), YPD 100 mM LiCl (Fig. 7.6), YPD 200 mM LiCl (Fig. 7.7), YPD pH 4.5 (100 mM glycolic acid) 800 mM NaCl (Fig. 7.8), YPD pH 7.4 (100 mM Tris-HCl) 200 mM LiCl (Fig. 7.9). For each strain, $6.6x10^7$, $3.3x10^7$, $1.65x10^7$ and $8.25x10^6$ cells

were plated and the plates were incubated for 3-5 days. No differences in growth between the wild type and mutant isolates were observed on YPD media (data not shown). Marked growth reduction was observed for all strains at pH 8 (Fig. 7.3), whereas no growth defects were observed at pH 4 (Fig. 7.4). In contrast with the wild type BY4741, reduction or prevention of growth for the mutant yeast strains analysed was observed following the addition of LiCl (Fig. 7.6). In particular, the effect is more pronounced as the concentration of LiCl (Fig. 7.7) and/or pH increased (Fig. 7.9). Coherently with this observation, growth for the yeast null mutants was almost completely prevented in YPD pH 7.4 200 mM LiCl (Fig. 7.9).

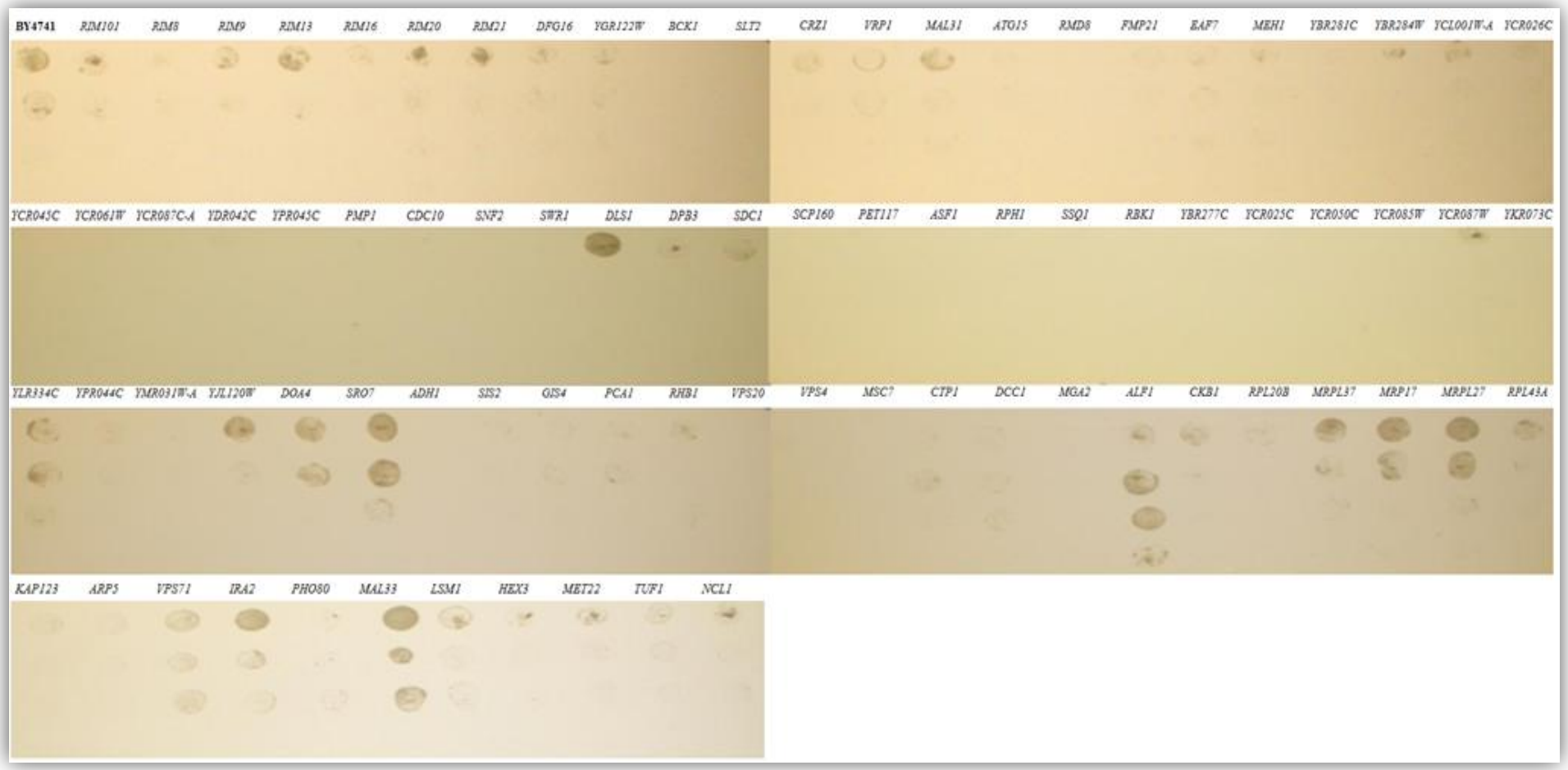


Fig. 7.3: Phenotypes of Δ*rim101* and Δ*rim101*-like mutants on YPD pH 8 (100 mM Tris-HCl). For each null mutant $6.6x10^7$, $3.3x10^7$, $1.65x10^7$ and $8.25x10^6$ c.f.u.s were plated prior to incubation at 30°C for 3-5 days.

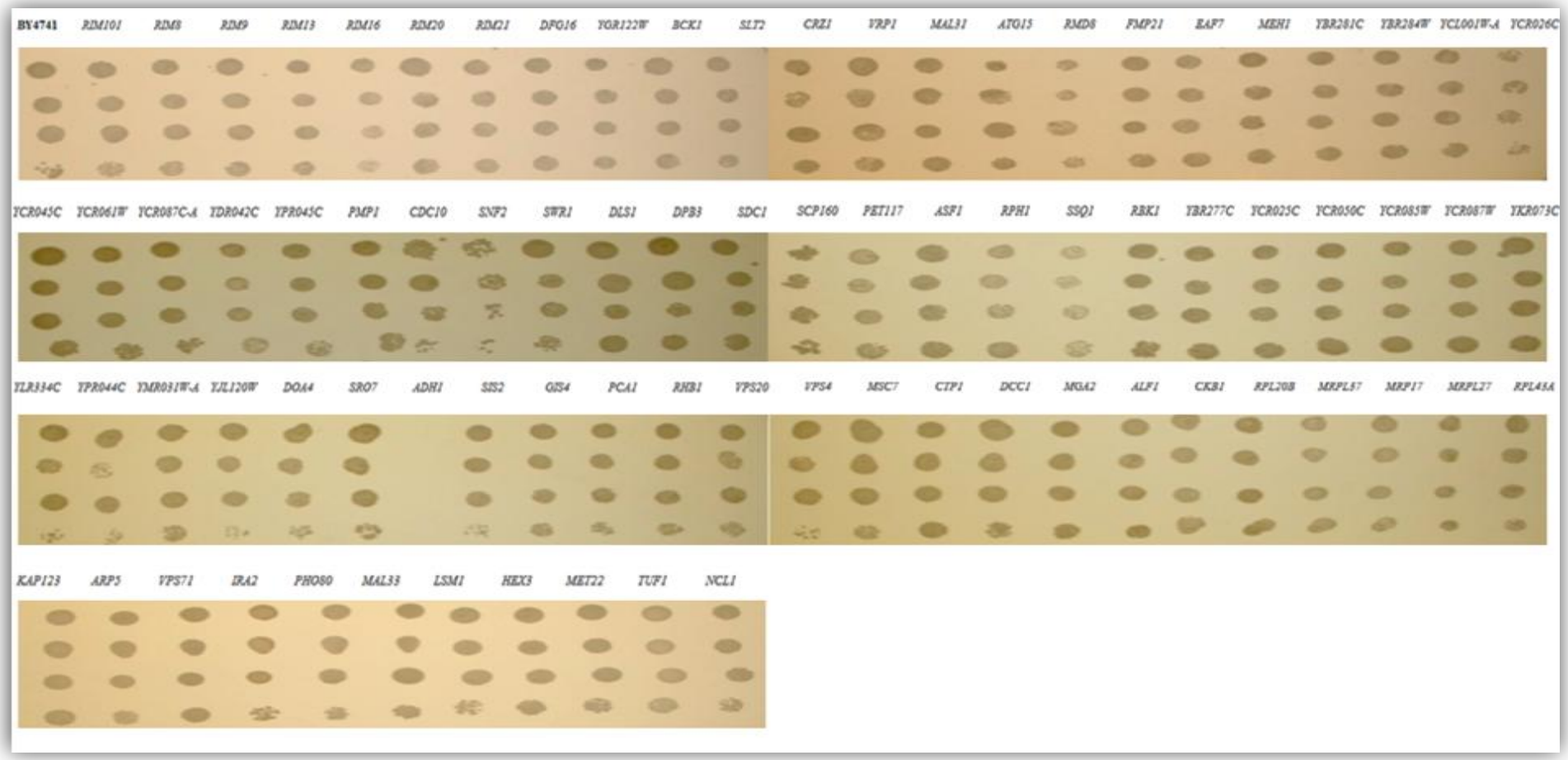


Fig. 7.4: Phenotypes of Δ*rim101* and Δ*rim101*-like mutants on YPD pH 4 (100 mM glycolic acid). For each null mutant $6.6x10^7$, $3.3x10^7$, $1.65x10^7$ and $8.25x10^6$ c.f.u.s were plated prior to incubation at 30°C for 3-5 days.

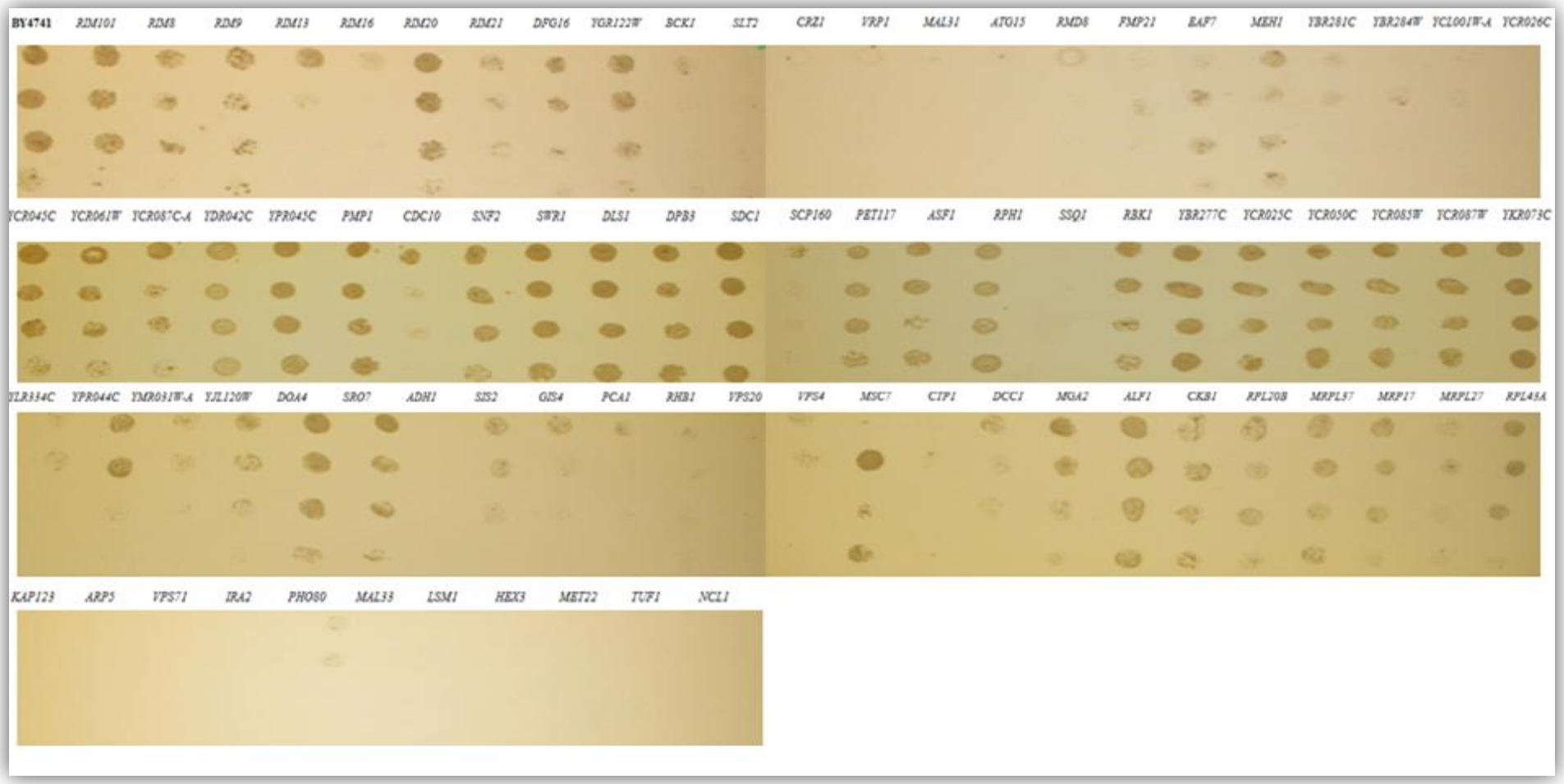


Fig. 7.5: Phenotypes of Δ*rim101* and Δ*rim101*-like mutants on YPD pH 4 (100 mM glycolic acid) 200 mM LiCl. For each null mutant $6.6x10^7$, $3.3x10^7$, $1.65x10^7$ and $8.25x10^6$ c.f.u.s were plated prior to incubation at 30°C for 3-5 days.

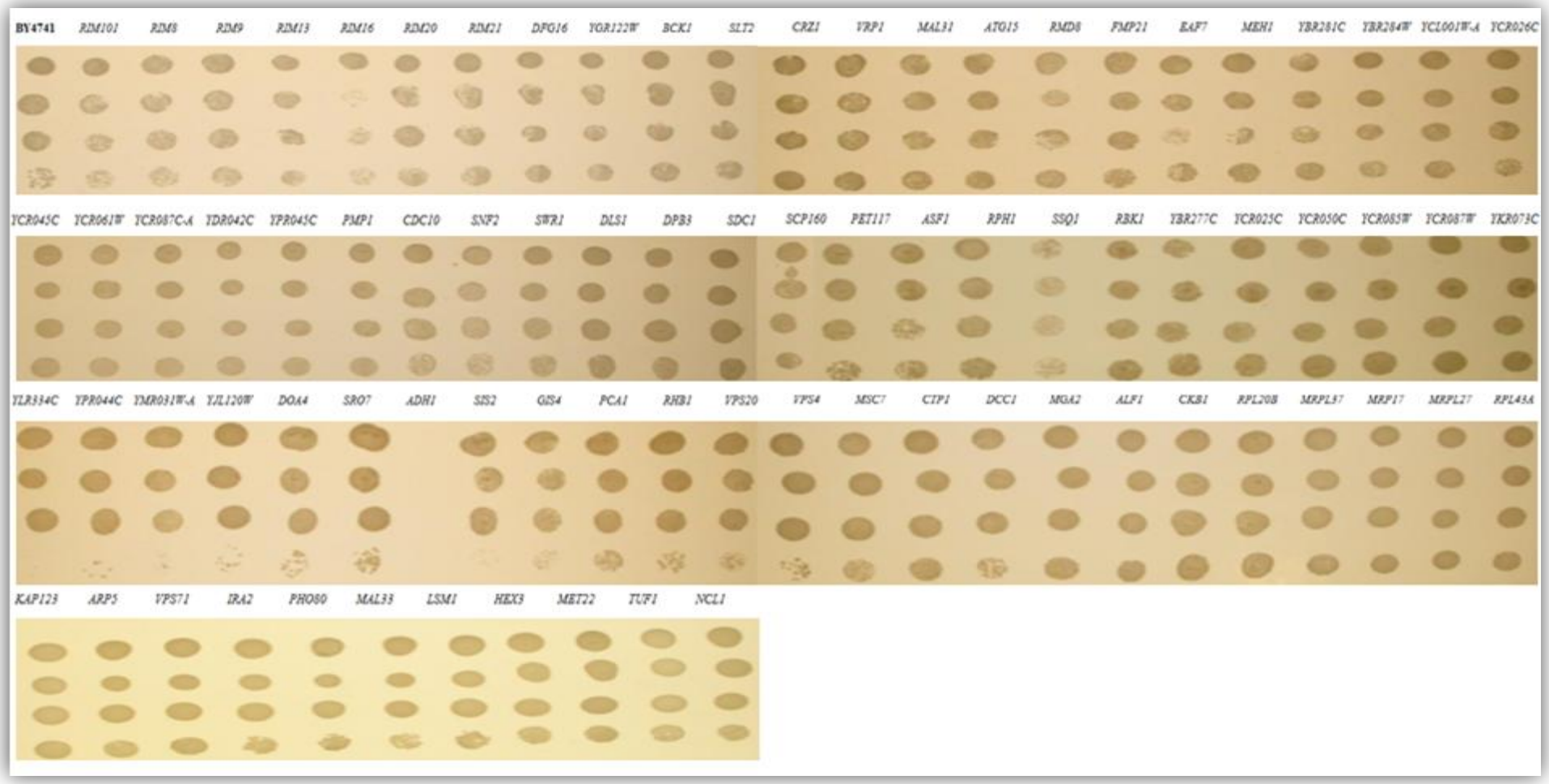


Fig. 7.6: Phenotypes of Δ*rim101* and Δ*rim101*-like mutants on YPD 100 mM LiCl. For each null mutant $6.6x10^7$, $3.3x10^7$, $1.65x10^7$ and $8.25x10^6$ c.f.u.s were plated prior to incubation at 30°C for 3-5 days.

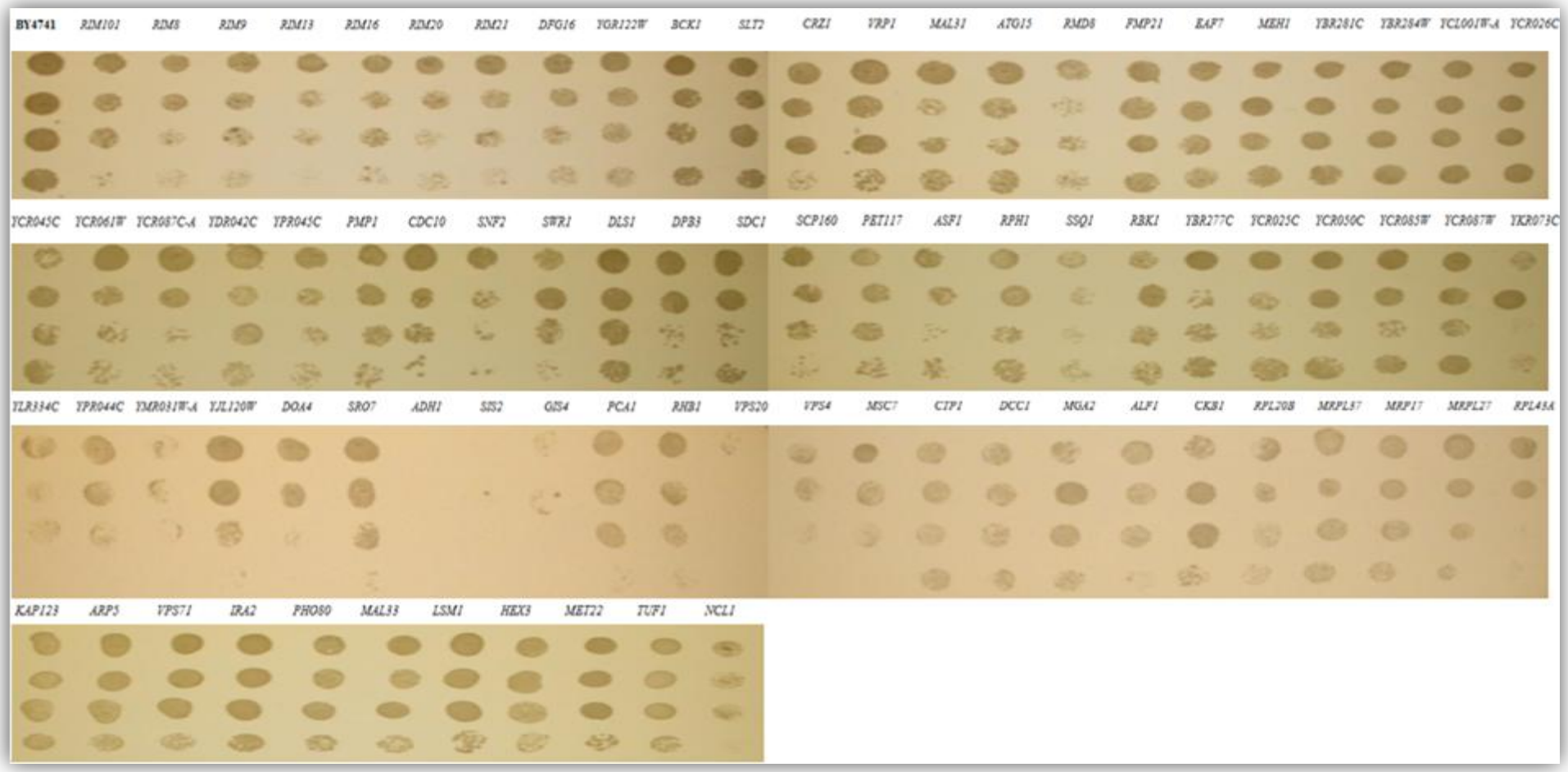


Fig. 7.7: Phenotypes of Δ*rim101* and Δ*rim101*-like mutants on YPD 200 mM LiCl. For each null mutant $6.6x10^7$, $3.3x10^7$, $1.65x10^7$ and $8.25x10^6$ c.f.u.s were plated prior to incubation at 30°C for 3-5 days.

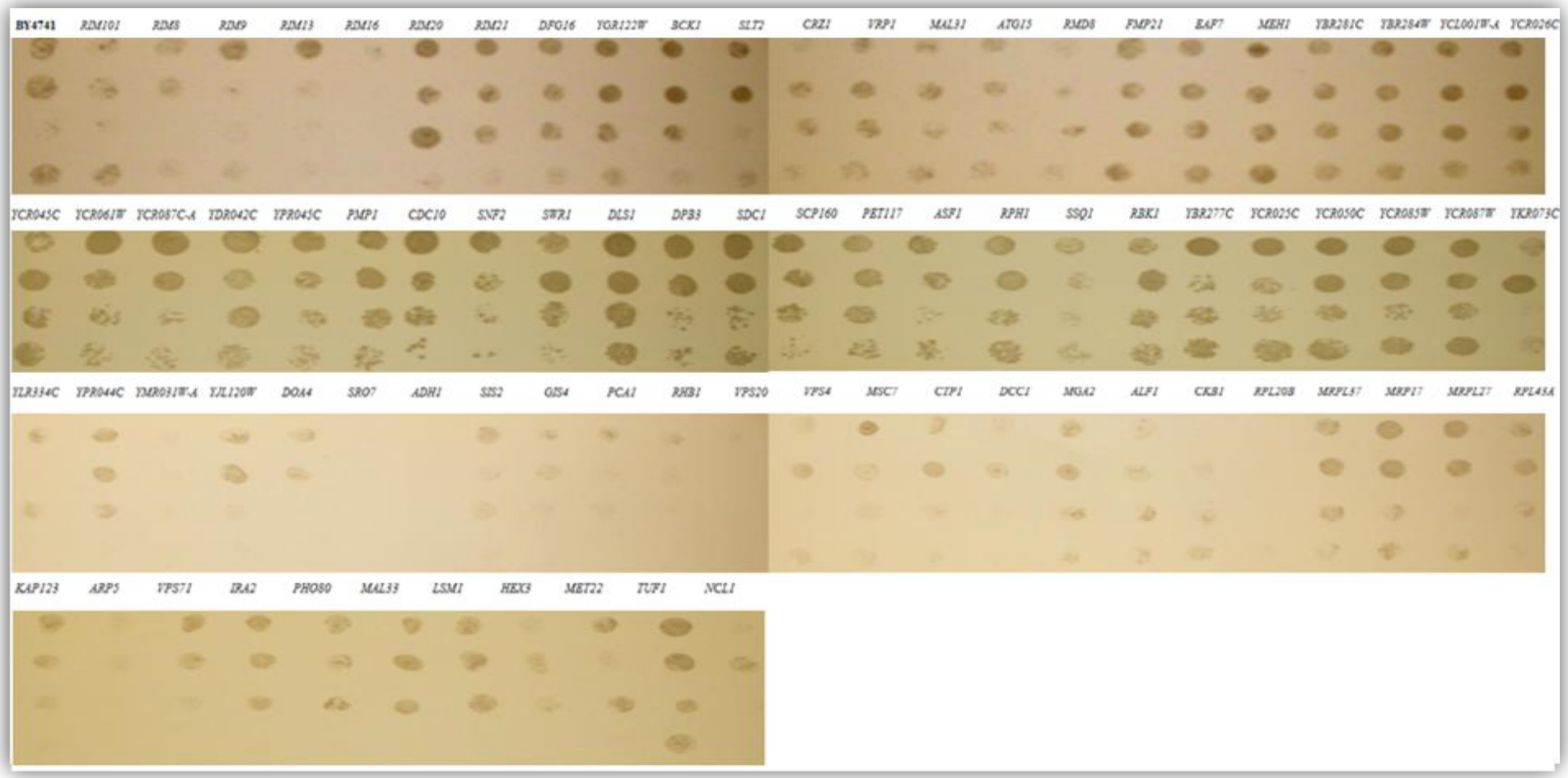


Fig. 7.8: Phenotypes of Δ*rim101* and Δ*rim101*-like mutants on YPD pH 4.5 (100 mM glycolic acid) 800 mM NaCl. For each null mutant $6.6x10^7$, $3.3x10^7$, $1.65x10^7$ and $8.25x10^6$ c.f.u.s were plated prior to incubation at 30°C for 3-5 days.

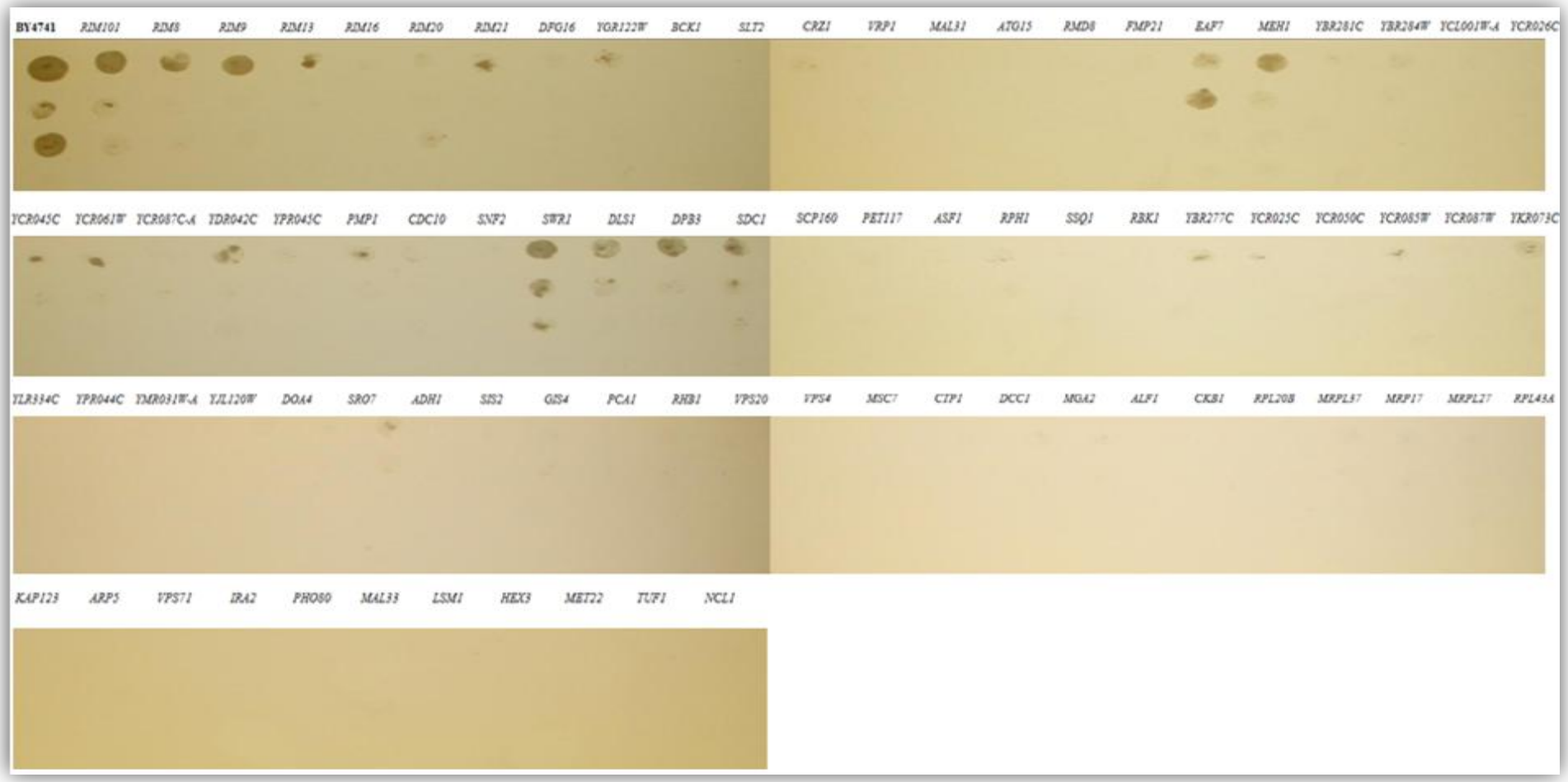


Fig. 7.9: Phenotypes of Δ*rim101* and Δ*rim101*-like mutants on YPD pH 7.4 (100 mM Tris-HCl) 200 mM LiCl. For each null mutant $6.6x10^7$, $3.3x10^7$, $1.65x10^7$ and $8.25x10^6$ c.f.u.s were plated prior to incubation at 30°C for 3-5 days.

Gene name	Biological process	pH 8	pH 4	pH 4 200 mM LiCl	100 mM LiCl	200 mM LiCl	pH 4.5 800 mM NaCl	pH 7.4 200 mM LiCl
BY4741		S	G	G	G	G	S	S
RIM101	**sporulation (sensu Fungi)**	SS	G	S	S	S	SS	SS
ADH1	fermentation	SS	G	NG	S	SS	SS	NG
ALF1	post-chaperonin tubulin folding pathway	SS	G	SS	S	SS	SS	NG
ARP5	protein-vacuolar targeting	NG	G	NG	S	S	S	NG
ASF1	DNA damage response, signal transduction resulting in induction of apoptosis	NG	G	S	S	S	S	NG
ATG15	autophagy	NG	G	NG	S	S	SS	NG
BCK1	protein kinase C signaling pathway	SS	G	NG	S	SS	SS	NG
CDC10	cell wall organisation and biogenesis	NG	G	S	S	S	S	NG
CKB1	protein amino acid phosphorylation	S	G	S	S	SS	SS	NG
CRZ1	regulation of transcription, DNA-dependent	NG	G	NG	S	S	SS	NG
CTP1	mitochondrial citrate transport	NG	G	NG	S	SS	SS	NG
DCC1	mitotic sister chromatid cohesion	NG	G	SS	S	SS	SS	NG
DFG16	pseudohyphal growth	SS	G	NG	S	SS	SS	NG
DLS1	chromatin silencing at telomere	SS	G	S	S	S	G	SS
DOA4	endocytosis	SS	G	S	S	SS	SS	NG
DPB3	chromatin silencing at telomere	NG	G	S	S	S	S	SS
EAF7	biological process NK	NG	G	S	S	S	S	SS
FMP21	biological process NK	NG	G	NG	S	S	S	NG
GIS4	intracellular signaling cascade	NG	G	SS	S	NG	SS	NG
HEX3	sporulation (sensu Fungi)	SS	G	NG	S	S	SS	NG
IRA2	Ras protein signal transduction	SS	G	NG	S	S	SS	NG
KAP123	Protein-nucleus import	NG	G	NG	S	S	S	NG
LSM1	rRNA processing	SS	G	NG	S	S	SS	NG
MAL31	alpha-glucoside transport	SS	G	NG	S	S	SS	NG
MAL33	regulation of transcription, DNA-dependent	S	G	NG	S	S	SS	NG
MEH1	biological process NK	NG	G	S	S	S	S	SS
MET22	sulphate assimilation	SS	G	NG	S	S	SS	NG
MGA2	positive regulation of transcription from Pol II promoter	NG	G	SS	S	SS	SS	NG
MRP17	protein biosynthesis	S	G	SS	S	SS	SS	NG
MRPL27	protein biosynthesis	S	G	SS	S	SS	SS	NG
MRPL37	protein biosynthesis	SS	G	SS	S	SS	SS	NG
MSC7	meiotic recombination	NG	G	S	S	SS	SS	NG
NCL1	tRNA methylation	SS	G	NG	S	SS	SS	NG
PCA1	iron ion homeostasis	NG	G	SS	S	SS	SS	NG
PET117	cytochrome c oxidase biogenesis	NG	G	S	S	S	S	NG
PHO80	regulation of phosphate metabolism	NG	G	SS	S	S	SS	NG
PMP1	cation transport	NG	G	S	S	S	S	SS
RBK1	D-ribose metabolism	NG	G	S	S	S	S	NG
RHB1	L-arginine transport	NG	G	NG	S	SS	SS	NG
RIM13	protein processing	SS	G	SS	S	S	SS	SS
RIM20	proteolysis and peptidolysis	SS	G	S	S	S	SS	NG
RIM21	sporulation (sensu Fungi)	SS	G	SS	S	S	G	SS
RIM8	meiosis	NG	G	SS	S	S	SS	SS
RIM9	sporulation (sensu Fungi)	SS	G	SS	S	S	SS	SS
RMD8	biological process NK	NG	G	NG	S	S	SS	NG

RPH1	DNA repair	NG	G	S	S	S	S	NG
RPL20B	protein biosynthesis	NG	G	SS	S	SS	NG	NG
RPL43A	protein biosynthesis	SS	G	SS	S	SS	SS	NG
SCP160	chromosome segregation	NG	G	SS	S	S	S	NG
SDC1	chromatin silencing at telomere	NG	G	S	S	S	S	SS
SIS2	G1/S transition of mitotic cell cycle	NG	G	SS	S	NG	SS	NG
SLT2	cell wall organisation and biogenesis	SS	G	NG	S	SS	SS	NG
SNF2	chromatin remodelling	NG	G	S	S	S	S	NG
SRO7	exocytosis	S	G	S	S	SS	NG	SS
SSQ1	DNA-dependent DNA replication	NG	G	SS	S	S	S	NG
SWR1	chromatin remodelling	NG	G	S	S	S	S	SS
TUF1	translational elongation	SS	G	NG	S	S	S	NG
VPS20	late endosome to vacuole transport	NG	G	NG	S	NG	NG	NG
VPS4	late endosome to vacuole transport	NG	G	SS	S	SS	SS	NG
VPS71	protein-vacuolar targeting	NG	G	NG	S	S	NG	NG
VRP1	actin filament organisation	NG	G	NG	S	S	SS	NG
YBR277C	dubious ORF	NG	G	S	S	S	S	SS
YBR281C	biological process NK	NG	G	S	S	S	S	NG
YBR284W	biological process NK	NG	G	NG	S	S	S	NG
YCL001W-A	biological process NK	NG	G	NG	S	S	S	NG
YCR025C	dubious ORF	NG	G	S	S	S	S	SS
YCR026C	biological process NK	NG	S	NG	S	S	S	NG
YCR045C	biological process NK	NG	G	S	S	S	S	SS
YCR050C	dubious ORF	NG	G	S	S	S	S	NG
YCR061W	biological process NK	NG	G	S	S	S	S	SS
YCR085W	dubious ORF	NG	G	S	S	S	S	SS
YCR087C-A	biological process NK	NG	G	S	S	S	S	NG
YCR087W	dubious ORF	SS	G	S	S	S	S	NG
YDR042C	biological process NK	NG	G	S	S	S	S	SS
YGR122W	biological process NK	NG	G	S	S	S	G	SS
YJL120W	dubious ORF	SS	G	SS	S	SS	SS	NG
YKR073C	dubious ORF	NG	G	S	S	S	S	SS
YLR334C	dubious ORF	SS	G	SS	S	SS	SS	NG
YMR031W-A	dubious ORF	NG	G	SS	S	SS	NG	NG
YPR044C	dubious ORF	NG	G	S	S	SS	SS	NG
YPR045C	biological process NK	NG	G	S	S	S	S	NG

Table 7.3: Phenotypes of Δ*rim101* and Δ*rim101*-like mutants. For each null mutant $6.6x10^7$, $3.3x10^7$, $1.65x10^7$ and $8.25x10^6$ c.f.u.s were plated prior to incubation at 30°C for 3-5 days. G=growth, S=sensitive, SS=super sensitive, and NG=not growing, based on two independent observations.

7.3.2 Epistacy screen of the *S. cerevisiae* Δ*rim101*-like mutants

The parental strain BY4741 of the Euroscarf *S. cerevisiae* ORF deletion library, Δ*rim101* and the other 80 Δ*rim101*-like mutants were transformed with the plasmid pWL86URA. Three independent transformants were selected from each transformation for further analysis. In the first instance phenotypes were screened on solid YPD pH 7.4 mM 200 LiCl medium. For each of the strains analysed, serial dilutions of 10^6, 10^5, 10^4 and 10^3 cells

were plated in parallel on YPD and on YPD pH 7.4 200 mM LiCl and plates were incubated for 3 and 5 days respectively. Phenotypes were scored by two independent observers. Despite the ease with which cation-sensitive Δ*rim101*-like mutants were initially identified among Euroscarf *S. cerevisiae* ORF deletants (Fig. 7.3-7.9 and Table 7.3) transformation with pWL86 expressing constitutively active Rim101p could not reproducibly rescue cation sensitivity in plate tests (Fig. 7.10). Attempts to resolve the problem included serial dilutions as well as technical and biological triplication but without success. An alternative, quantitative approach was therefore developed.

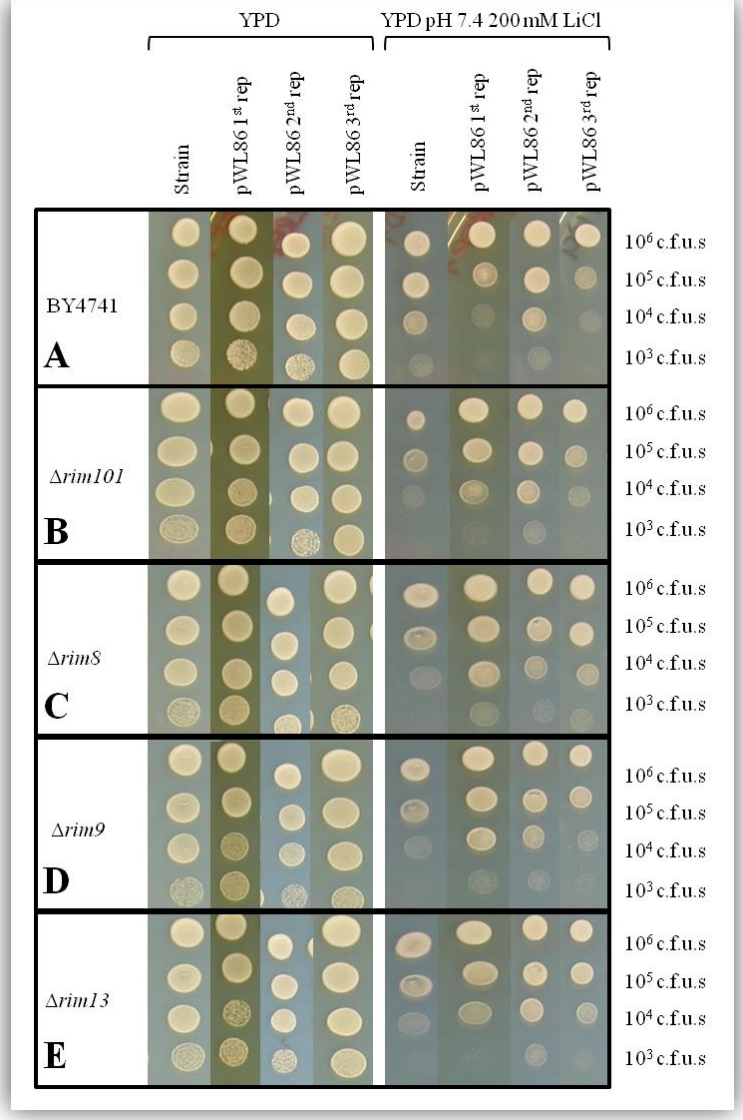


Fig. 7.10: Lithium sensitivity phenotype on solid media for BY4741, (A) Δ*rim101* (B), Δ*rim8* (C), Δ*rim9* (D) and Δ*rim13* (E) and resulting pWL86URA transformants. All strains are plated in serial dilutions representing inocula of 10^6, 10^5, 10^4 and 10^3 c.f.u.s.

Quantitative assessments of yeast growth were subsequently performed in liquid media. BY4741, Δ*rim101*, 80 Δ*rim101*-like mutants and three independent pWL86URA transformants (resulting from transformation of Δ*rim101*-like mutants with the plasmid pWL86URA: 1 rep, 2 rep and 3 rep) were arrayed in 96-well plates and yeast growth profiling was adapted to 96-well format in liquid media (Fig. 7.11). Mutants and transformants, the latter gridded in triplicate, in 96-well plates were grown overnight in YPD and each was subsequently used to inoculate two further (one with YPD and one with YPD pH 7.4 200 mM LiCl) 96-well plates. OD_{600} was measured at the initiation of 30°C incubation and at subsequent 2, 4, 6, 8, 10, 12 and 24 hour time points.

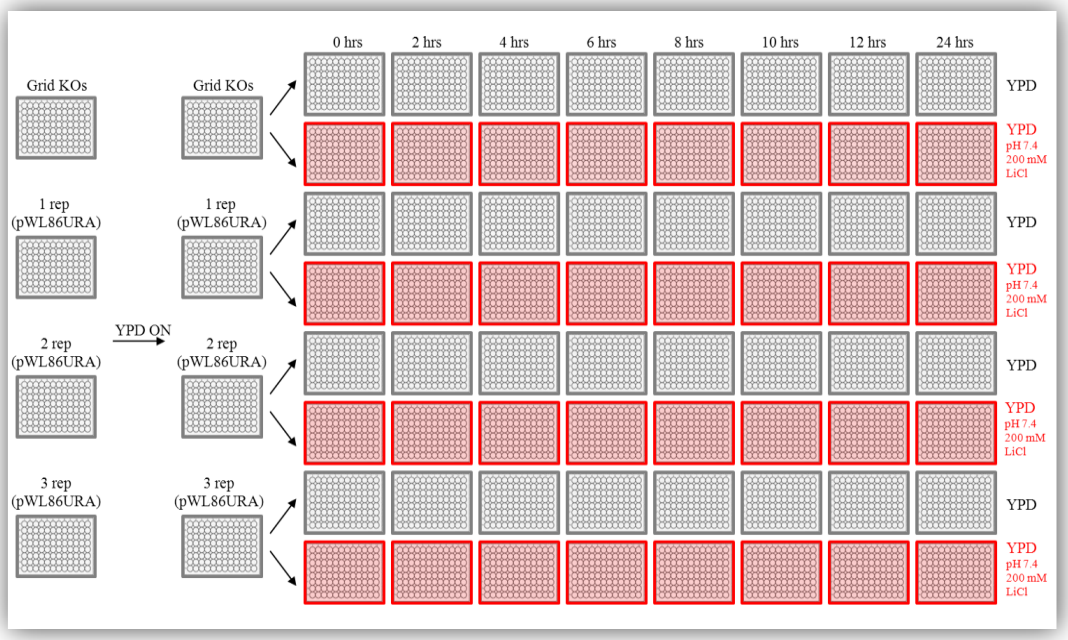


Fig. 7.11: Experimental scheme for assessment of cation sensitivity in liquid media. BY4741, Δ*rim101*, 80 Δ*rim101*-like mutants (Grid KOs) and three independent pWL86URA transformants (resulting from transformation of Δ*rim101*-like mutants with the plasmid pWL86URA: 1 rep, 2 rep and 3 rep), were arrayed in 96-well plates. Following overnight culture in YPD these were each used to inoculate two further plates, one containing YPD and one containing YPD pH 7.4 200 mM LiCl. OD_{600} was measured at the initiation of 30°C incubation and at subsequent 2, 4, 6, 8, 10, 12 and 24 hour time points.

The assay was calibrated using BY4741 and Δ*rim101*, comparing growth of the two strains in YPD and YPD pH 7.4 200 mM LiCl. To facilitate direct comparisons of media- and strain-specific growth profiles, sequential normalisations to OD_{600} of BY4741 at time-zero [$BY4741_{(T0)}$] and time-zero OD_{600} on a strain-specific basis [$\Delta_{(T0)}$] were performed (Fig. 7.12A and B). To adjust for strain-specific differences in growth rates a further correction was made, using a growth coefficient [g] defined as the fractional OD_{600} in YPD relative to

the wild type, for each strain and time point of the analysis (Fig. 7.12C). Following this protocol, clear cation hypersensitivity was discernable for Δ*rim101* in YPD pH 7.4 200 mM LiCl relative to the parental strain BY4741.

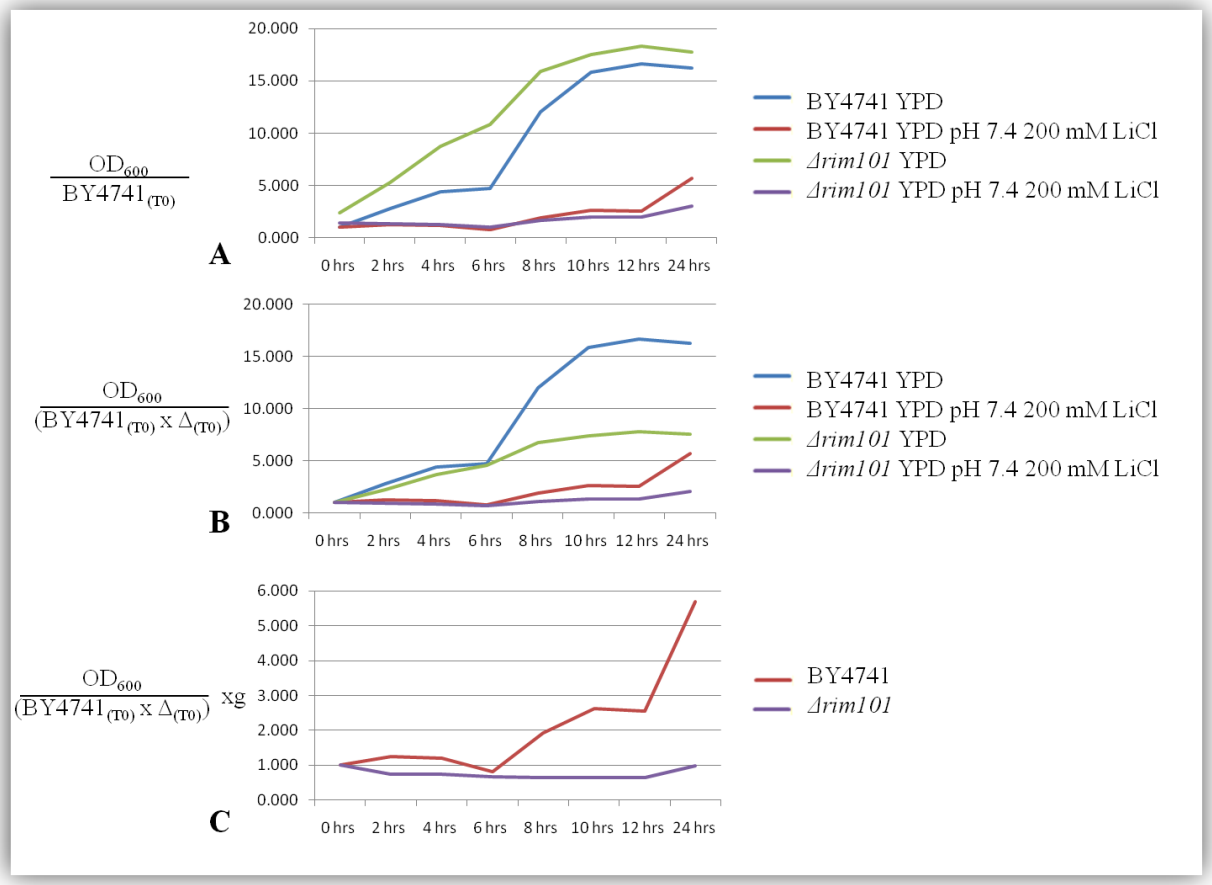


Fig. 7.12: OD_{600} adjustments for comparative cation sensitivity analysis of BY4741 and Δ*rim101* in liquid culture. To facilitate direct comparisons of media- and strain-specific growth profiles sequential normalisations to OD_{600} of BY4741 at time-zero [$BY4741_{(T0)}$] and OD_{600}, at time-zero, on a strain-specific basis [$\Delta_{(T0)}$] were performed (A and B). To adjust for strain-specific differences in growth rates a further correction was made, using a growth coefficient [g] defined as the fractional OD_{600} in YPD relative to the wild type, for each strain and time point of the analysis (C).

Following optimisation of experimental and normalisation protocols the screen was repeated, this time including all previously characterised Δ*rim* mutants and respective pWL86URA clones (Fig. 7.13). The Δ*rim101*-like phenotype, in comparison with the parental strain BY4741 in YPD pH 7.4 200 mM LiCl, clearly emerged for all of the Δ*rim* mutants (Fig. 7.13A). In addition, rescue of cation hypersensitivity was reproducibly quantificable in each of three biological replicates (1st rep, 2nd rep and 3rd rep, respectively Fig. 7.13B.1, B.2 and B.3) as well for averaged data (Fig. 7.13C). Thus, in support of the

phenotypic screening performed on solid media for mutant library screening (Fig. 7.3-7.9 and Table 7.3) cation sensitivity is measurable in liquid media, and moreover, expression of constitutively active Rim101p rescues cation hypersensitivity in YPD pH 7.4 200 mM LiCl selective media.

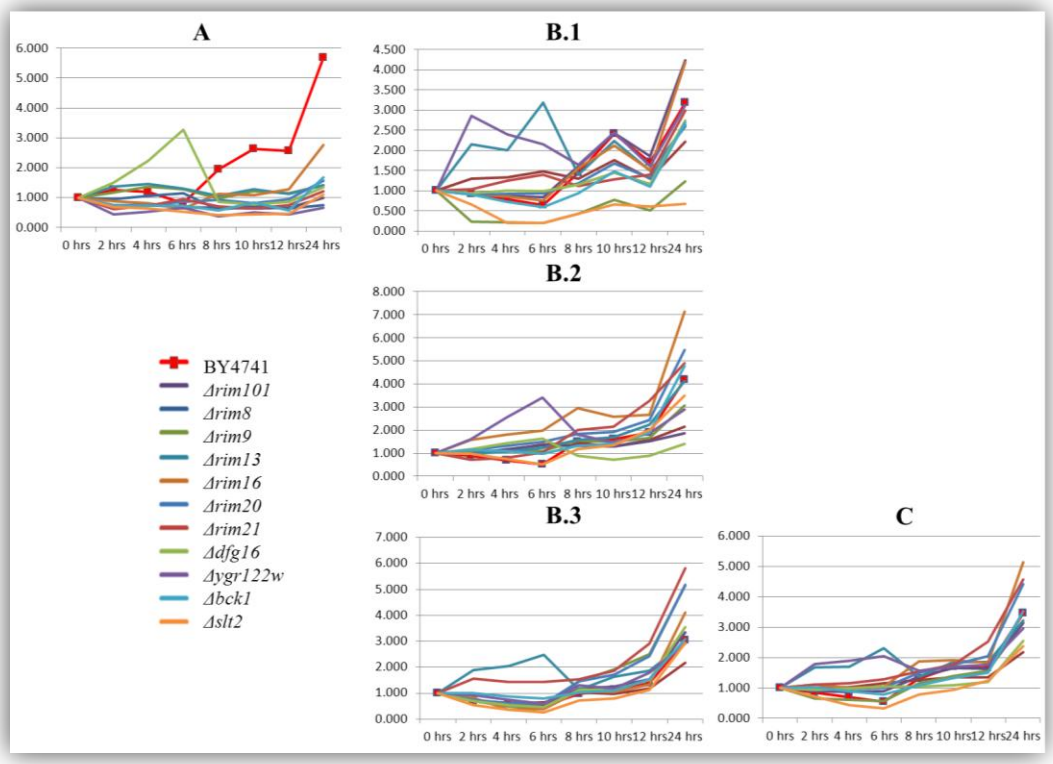


Fig. 7.13: Cation sensitivity profiles of Δ*rim101* and other previously characterised Rim pathway mutants in YPD pH 7.4 200 mM LiCl. To facilitate direct comparisons of media- and strain-specific growth profiles sequential normalisations to OD_{600} of BY4741 at time-zero [$BY4741_{(T0)}$] and OD_{600}, at time-zero, on a strain-specific basis [$\Delta_{(T0)}$] were performed. To adjust for strain-specific differences in growth rates a further correction was made, using a growth coefficient [g] defined as the fractional OD_{600} in YPD relative to the wild type. The resulting value ([OD_{600}/($BY4741_{(T0)}$x$\Delta_{(T0)}$]xg) is plotted on the Y-axis. Cation sensitivity was measured in YPD pH 7.4 200 mM LiCl liquid culture, relative to YPD, for each mutant (A) and three respective pWL86URA clones (B.1, B.2 and B.3) at eight independent time points (0, 2, 4, 6, 8, 10, 12, 24 hrs) (X-axis). Panel (C) shows data averages for the 3 biological replicates B.1, B.2 and B.3).

In all instances, and as indicated in Fig. 7.13, the greatest detectable divergences of Δ*rim101*-like and wild type phenotypes were measurable at 24 hours. Onward data representations therefore considered only this time point of the analyses. Adopting this procedure Fig. 7.14A depicts background subtracted, normalised values for three replications of the epistacy screen using Δ*rim101* and all other characterised Rim pathway mutants.

Having averaged the data for three biological replicates (B), Δ*rim101*-like phenotypes clearly emerge from this analysis for all of the mutants tested (blue bars). Rescue of the cation hypersensitive phenotype was visible to different extents for each of the three replicates of each mutant (red, green and purple line in A respectively for 1st, 2nd and 3rd replicate) but undoubtedly evident for the average of the three replicates (red line in B).

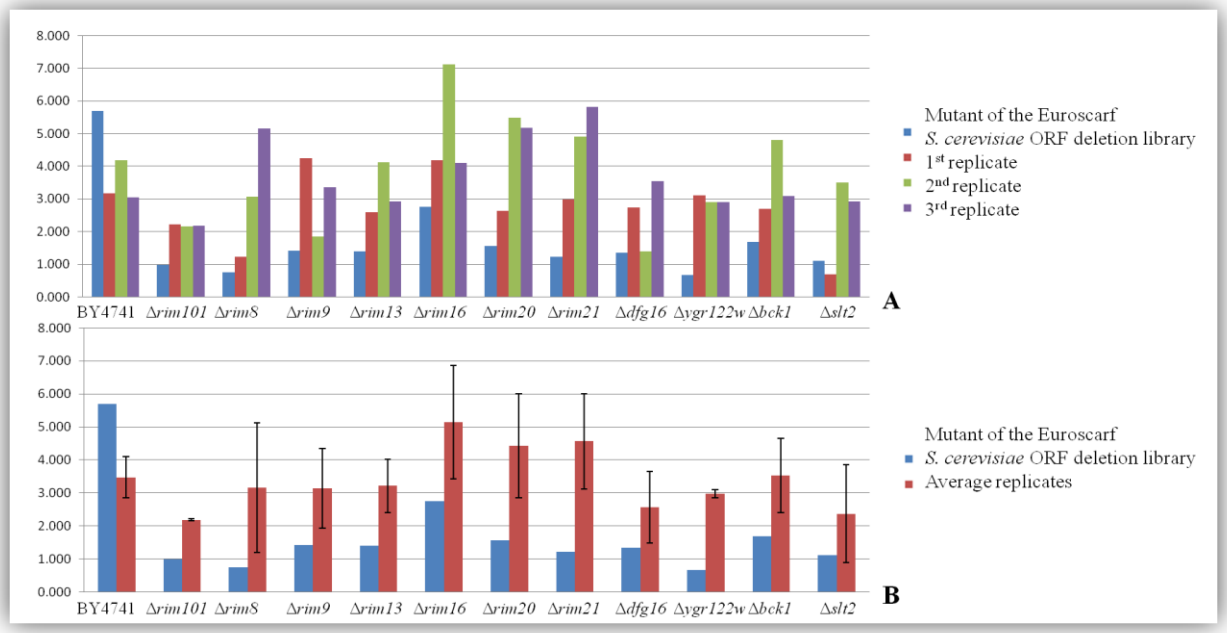


Fig. 7.14: Relative cation hypersensitivity of BY4741 and Rim pathway mutants following pWL86URA transformation. ([OD_{600}/($BY4741_{(T0)}$x$\Delta_{(T0)}$]xg) values (on the Y-axis) were calculated following 24 hours growth in YPD and YPD pH 7.4 200 mM LiCl. 1st rep, 2nd rep and 3rd rep biological replicate values for each transformants were compared to the respective KO (A) and average values for the 3 replicates were calculated (B).

Fig. 7.15 shows the complete panel of results from the epistacy screening of Δ*rim101* and the 80 Δ*rim101*-like mutants. The data are also summarised in Table 7.4 which lists normalised, corrected OD_{600} values for each mutant, plus corresponding, averaged values for pWL86URA transformants. Values in the table are colorimetrically graded whereby darker red or blue represents higher or lower adjusted OD_{600} value, relative to BY4741. On face value a closer examination of the behaviour of the 80 mutants confirmed cation hypersensitivity (normalised, corrected OD_{600} values in the range 0.0-2.6), relative to the wild type, for only 42 of the mutants. 15 of the mutants showed a weak (normalised, corrected OD_{600} values in the range 2.6-4.6) Δ*rim101*-like phenotype and 24 displayed no cation sensitivity phenotype in YPD pH 7.4 200 mM LiCl. The Δ*rim101*-like phenotype was

considered as rescued for cation hypersensitivity where an OD_{600} increment of at least +1.0, relative to the mutant phenotype was observed in averaged values obtained from three independent pWL86URA transformants. According to these criteria, among the 57 mutants retaining a Δ*rim101*-like phenotype in liquid media, rescue of cation hypersensitivity was measurable in 40 mutants following pWL86URA transformation. 15 Δ*rim101*-like mutant phenotypes were unaltered following transformation with WL86URA, whereas in two cases (Δ*crz1* and Δ*dls1*) an extreme value was registered. In particular, for Δ*crz1* a weak Δ*rim101*-like phenotype was detected which, after transformation, led to increase of cation hypersensitivity. In contrast, for Δ*dls1* a strong Δ*rim101*-like phenotype was observed and as a consequence of the transformation with pWL86URA, cation tolerance was increased. 24 of the Euroscarf *S. cerevisiae* deletion mutants contradicted the Δ*rim101*-like phenotype previously observed on solid media. For 21 of these mutants, no major phenotypic changes were detectable after the introduction of a constitutively active form of Rim101p. However, the transformation with pWL86URA increased cation sensitivity for Δ*scp160* and Δ*pet117* or cation tolerance for Δ*ssq1*.

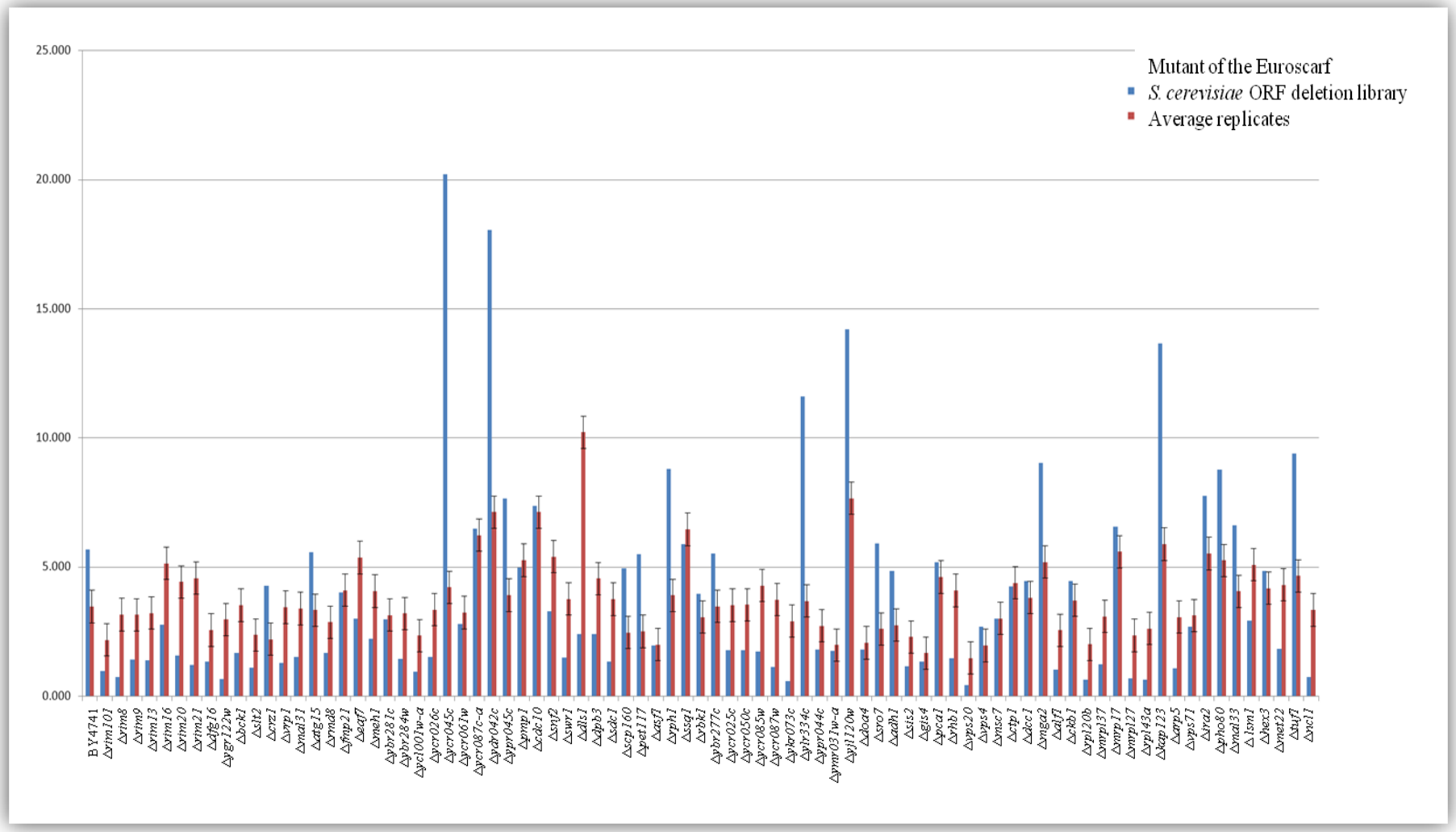


Fig. 7.15: Relative cation hypersensitivity of BY4741 and Δ*rim101*-like mutants following pWL86URA transformation. Values were calculated following 24 hours growth in YPD and YPD pH 7.4 200 mM LiCl.

Gene name	Euroscarf *S. cerevisiae* mutant	pWL86URA Euroscarf *S. cerevisiae* mutant	Rescue of the cation hypersensitivity
BY4741	5.686	3.471	no Δ*rim101*-like phenotype
RIM101	0.983	2.179	rescue of cation hypersensitivity
ADH1	4.860	2.756	no Δ*rim101*-like phenotype
ALF1	1.027	2.552	rescue of cation hypersensitivity
ARP5	1.085	3.069	rescue of cation hypersensitivity
ASF1	1.961	1.997	no effects on cation hypersensitivity
ATG15	5.581	3.337	no Δ*rim101*-like phenotype
BCK1	1.685	3.527	rescue of cation hypersensitivity
CDC10	7.361	7.130	no Δ*rim101*-like phenotype
CKB1	4.469	3.715	no effects on cation hypersensitivity
CRZ1	4.270	2.207	increased cation sensitivity *
CTP1	4.240	4.392	no effects on cation hypersensitivity
DCC1	4.460	3.821	no effects on cation hypersensitivity
DFG16	1.347	2.561	rescue of cation hypersensitivity
DLS1	2.412	10.222	increased cation tolerance*
DOA4	1.801	2.069	no effects on cation hypersensitivity
DPB3	2.406	4.558	rescue of cation hypersensitivity
EAF7	3.009	5.371	rescue of cation hypersensitivity
FMP21	4.026	4.108	no effects on cation hypersensitivity
GIS4	1.342	1.675	no effects on cation hypersensitivity
HEX3	4.862	4.182	no effects on cation hypersensitivity
IRA2	7.750	5.523	no Δ*rim101*-like phenotype
KAP123	13.648	5.889	no Δ*rim101*-like phenotype
LSM1	2.918	5.089	rescue of cation hypersensitivity
MAL31	1.522	3.397	rescue of cation hypersensitivity
MAL33	6.610	4.059	no Δ*rim101*-like phenotype
MEH1	2.234	4.069	rescue of cation hypersensitivity
MET22	1.844	4.313	rescue of cation hypersensitivity
MGA2	9.025	5.196	no Δ*rim101*-like phenotype
MRP17	6.564	5.591	no Δ*rim101*-like phenotype
MRPL27	0.701	2.353	rescue of cation hypersensitivity
MRPL37	1.234	3.086	rescue of cation hypersensitivity
MSC7	2.999	3.009	no effects on cation hypersensitivity
NCL1	0.742	3.340	rescue of cation hypersensitivity
PCA1	5.197	4.617	no Δ*rim101*-like phenotype
PET117	5.505	2.514	increased cation sensitivity*
PHO80	8.765	5.255	no Δ*rim101*-like phenotype
PMP1	4.977	5.264	no Δ*rim101*-like phenotype
RBK1	3.961	3.069	no effects on cation hypersensitivity
RHB1	1.483	4.095	rescue of cation hypersensitivity
RIM13	1.403	3.216	rescue of cation hypersensitivity
RIM16	2.761	5.140	rescue of cation hypersensitivity
RIM20	1.564	4.429	rescue of cation hypersensitivity
RIM21	1.221	4.569	rescue of cation hypersensitivity
RIM8	0.753	3.157	rescue of cation hypersensitivity
RIM9	1.420	3.149	rescue of cation hypersensitivity
RMD8	1.688	2.869	rescue of cation hypersensitivity
RPH1	8.808	3.908	no Δ*rim101*-like phenotype
RPL20B	0.640	2.008	rescue of cation hypersensitivity
RPL43A	0.647	2.620	rescue of cation hypersensitivity
SCP160	4.957	2.464	increased cation sensitivity*
SDC1	1.352	3.756	rescue of cation hypersensitivity
SIS2	1.152	2.295	rescue of cation hypersensitivity
SLT2	1.109	2.369	rescue of cation hypersensitivity
SNF2	3.299	5.400	rescue of cation hypersensitivity
SRO7	5.903	2.604	no Δ*rim101*-like phenotype
SSQ1	5.890	6.464	increased cation tolerance*
SWR1	1.486	3.767	rescue of cation hypersensitivity
TUF1	9.405	4.658	no Δ*rim101*-like phenotype
VPS20	0.427	1.475	no effects on cation hypersensitivity
VPS4	2.694	1.965	no effects on cation hypersensitivity
VPS71	2.698	3.122	no effects on cation hypersensitivity

VRP1	1.282	3.448	rescue of cation hypersensitivity
YBR277C	5.533	3.482	no Δ*rim101*-like phenotype
YBR281C	2.967	3.138	no effects on cation hypersensitivity
YBR284W	1.450	3.207	rescue of cation hypersensitivity
YCL001W-A	0.951	2.351	rescue of cation hypersensitivity
YCR025C	1.778	3.522	rescue of cation hypersensitivity
YCR026C	1.535	3.352	rescue of cation hypersensitivity
YCR045C	20.350	4.216	no Δ*rim101*-like phenotype
YCR050C	1.795	3.545	rescue of cation hypersensitivity
YCR061W	2.794	3.240	rescue of cation hypersensitivity
YCR085W	1.737	4.282	rescue of cation hypersensitivity
YCR087C-A	6.484	6.239	no Δ*rim101*-like phenotype
YCR087W	1.124	3.744	rescue of cation hypersensitivity
YDR042C	18.045	7.124	no Δ*rim101*-like phenotype
YGR122W	0.668	2.975	rescue of cation hypersensitivity
YJL120W	14.198	7.667	no Δ*rim101*-like phenotype
YKR073C	0.596	2.906	rescue of cation hypersensitivity
YLR334C	11.601	3.686	no Δ*rim101*-like phenotype
YMR031W-A	1.744	1.981	no effects on cation hypersensitivity
YPR044C	1.797	2.724	rescue of cation hypersensitivity
YPR045C	7.646	3.912	no Δ*rim101*-like phenotype

Table 7.4: Summary of cation sensitivity data from epistacy screen of Δ*rim101*-like mutants. Table lists normalised, corrected OD_{600} values for each mutant, plus corresponding, averaged values for pWL86URA transformants. Values in the table are colorimetrically graded whereby darker red or blue represents higher or lower adjusted OD_{600} value, relative to BY4741.

7.3.3 Use of a synthetic Rim101p promoter to identify novel regulators of Rim101p processing and/or transcriptional activity

Phenotypic screening of the Euroscarf *S. cerevisiae* ORF deletion library identified 80 Δ*rim101*-like mutants. To identify which of these Δ*rim101*-like mutants suffer aberrant Rim101p processing and transcriptional activity, they were transformed with the plasmid pAED39, containing a synthetic Rim101p promoter fused to a *lacZ* reporter. For the purpose of the study, the β-galactosidase assay was adapted to a 96-well plate format as graphically represented in Fig. 7.16. The parental strain BY4741, Δ*rim101* and 80 other Δ*rim101*-like mutants were transferred in 96-well plate format (Grid KOs), together with three replicates for each strain, obtained after the transformation with the plasmid pAED39 (1 rep, 2 rep and 3 rep). The four plates were grown overnight in YPD and subsequently used to inoculate three plates each, one with YPD pH 6.5, one with YPD pH 4.5 and one with YPD pH 8.0. As before, the cultures were grown to an OD_{660} approximately of 0.6 and the measurements of the OD_{660} were recorded. 100 µL of working solution (50 µl 2X ONPG and 50 µl Y-PER Reagent) was added to each well. After 20 minutes, the absorbance at 420 nm was measured and the β-galactosidase activity (in Millers units) was calculated applying the appropriate

formula: $(1000xA_{420})/(TxVxOD_{660})$=β-galactosidase activity, where T is the reaction time (minutes), V corresponds to the reaction volume (ml) and A_{420} is the absorbance at 420 nm.

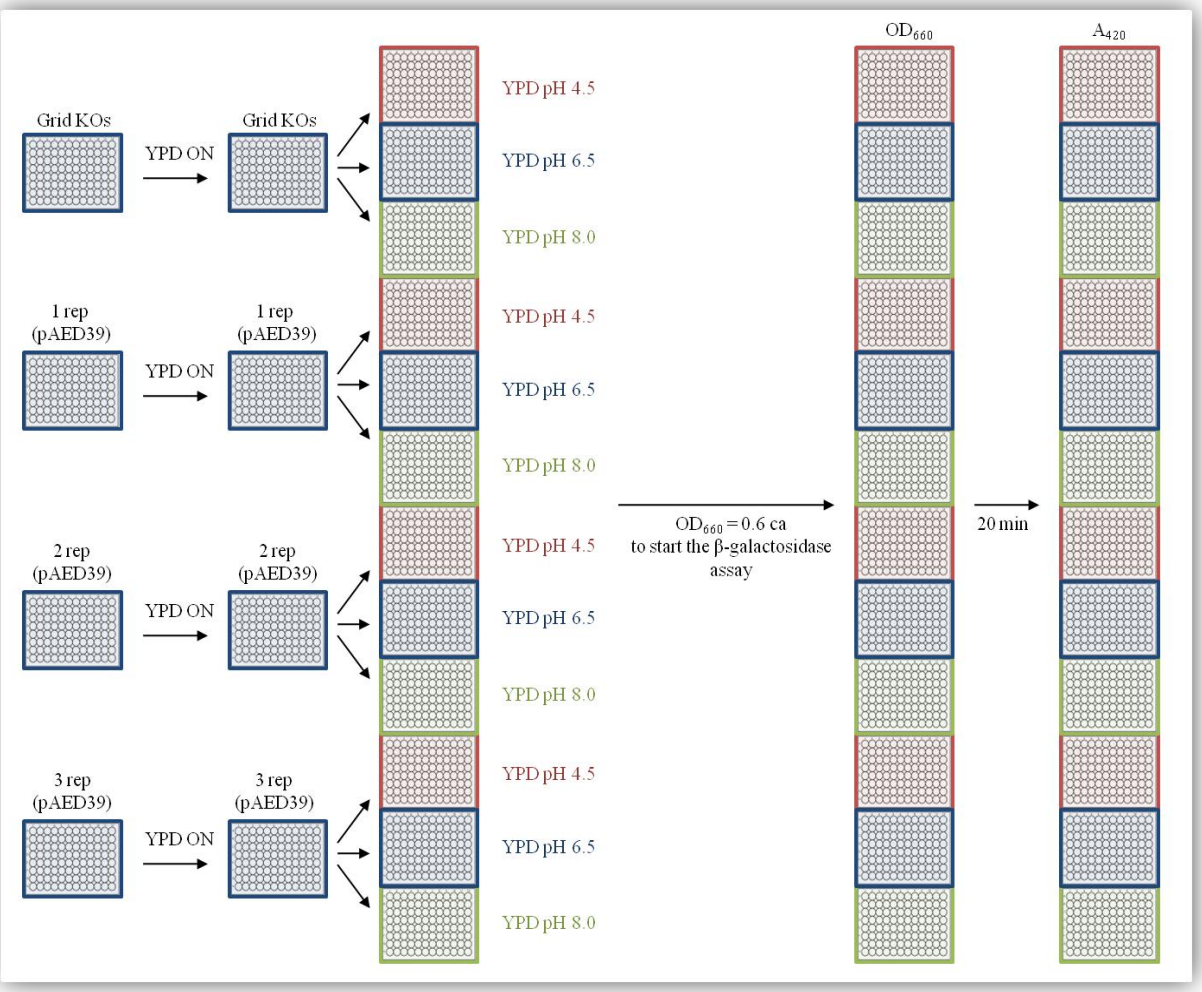


Fig. 7.16: Experimental scheme for assessment of β-galactosidase activity in a 96-well plate format. BY4741, Δ*rim101*, 80 Δ*rim101*-like mutants (Grid KOs) and three independent pAED39 transformants (resulting from transformation of Δ*rim101*-like mutants with the plasmid pAED39: 1 rep, 2 rep and 3 rep), were arrayed in 96-well plates. Following overnight culture in YPD three further plates (YPD pH 6.5, YPD pH 4.5 and YPD pH 8.0) were inoculated. The 96-well plates were grown to OD_{660} of 0.6 prior to β-galactosidase assay.

A pilot screen was initially performed using the parental BY4741, and Δ*rim101* strains. The two strains were transformed with the plasmid pAED39, carrying the synthetic Rim101p promoter fused to a *lacZ* reporter. Two colonies obtained from these transformations were analysed. The overnight inoculum in YPD of each of these cultures was diluted (1/10) to prepare three cultures in different media, to approximate neutral (YPD pH 6.5), acidic (YPD pH 4.5) and alkaline conditions (YPD pH 8.0). Following growth to OD_{660}

of approximately 0.6, β-galactosidase assay was performed. For the β-galactosidase assay, 100 µl of working solution was added to 100 µl of culture. After 20 minutes, the absorbance at 420 nm was measured. Values of OD_{660} and A_{420} were background subtracted for the OD_{660} and A_{420} of the respective media and the β-galactosidase activity (in Millers units) was calculated by applying the following formula: $(1000xA_{420})/(TxVxOD_{660})$=β-galactosidase activity, where T is the reaction time (minutes), V corresponds to the reaction volume (ml) and A_{420} is the absorbance at 420 nm. Values for the two replicates were averaged. The results are shown in Fig. 7.17, plotting the β-galactosidase activity for the strains (BY4741 and Δ*rim101*) in the three different growth conditions (pH 4.5, 6.5 and 8.0). In the parental strain BY4741, β-galactosidase activity is unaltered under all tested conditions. This is as expected, given that processed Rim101p, which functions as a repressor, is appropriately represented in the wild type genetic background and sets a baseline for the assay. When *RIM101* is deleted, however, derepression of *lac*Z expression is observed with increasing pH, reflecting defective Rim101p-mediated repression of the synthetic promoter at alkaline pH, and revealing pH-dependent repressor activity for Rim101p at promoters having Rim101p binding sites.

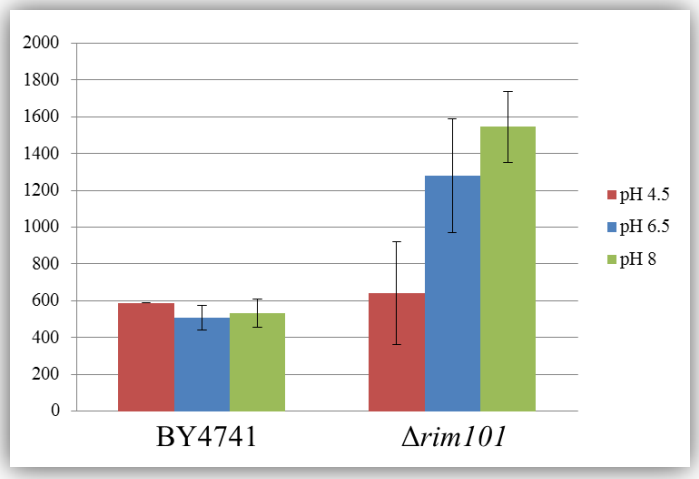


Fig. 7.17: β-galactosidase activity in BY4741 and Δ*rim101* strains expressing a synthetic Rim101p-regulated promoter. Strains expressed a synthetic Rim101p-regulated promoter (fused to a *lac*Z reporter). The β-galactosidase activity (in Millers units) has been calculated on the basis of OD_{600} and A_{420} measurements and averaged for two biological replicates.

7.3.4 Analysis of the Δ*rim101*-like null mutants using a synthetic Rim101p-regulated promoter

In order to identify which of the Δ*rim101*-like mutants suffer aberrant Rim101p processing and/or transcriptional activity, the parental strain BY4741 of the Euroscarf *S. cerevisiae* ORF deletion library, Δ*rim101* and 80 other Δ*rim101*-like mutants were transformed with the plasmid pAED39. In each case three independent clones were selected and β-galactosidase activity was measured. In this analysis, if the ORF in question is a regulator of Rim101p, depression of *lac*Z gene expression is expected. For genetic screening the optimised protocol was performed in 96 well-plate format. The results are shown in Fig. 7.18, which plots β-galactosidase activity, measured at three pHs for all of the Δ*rim101*-like null mutants. Fig. 7.19 summarises those showing derepression of *lac*Z gene expression, presumably occurring as a consequence of aberrant Rim101p processing and/or transcriptional activity at alkaline pH.

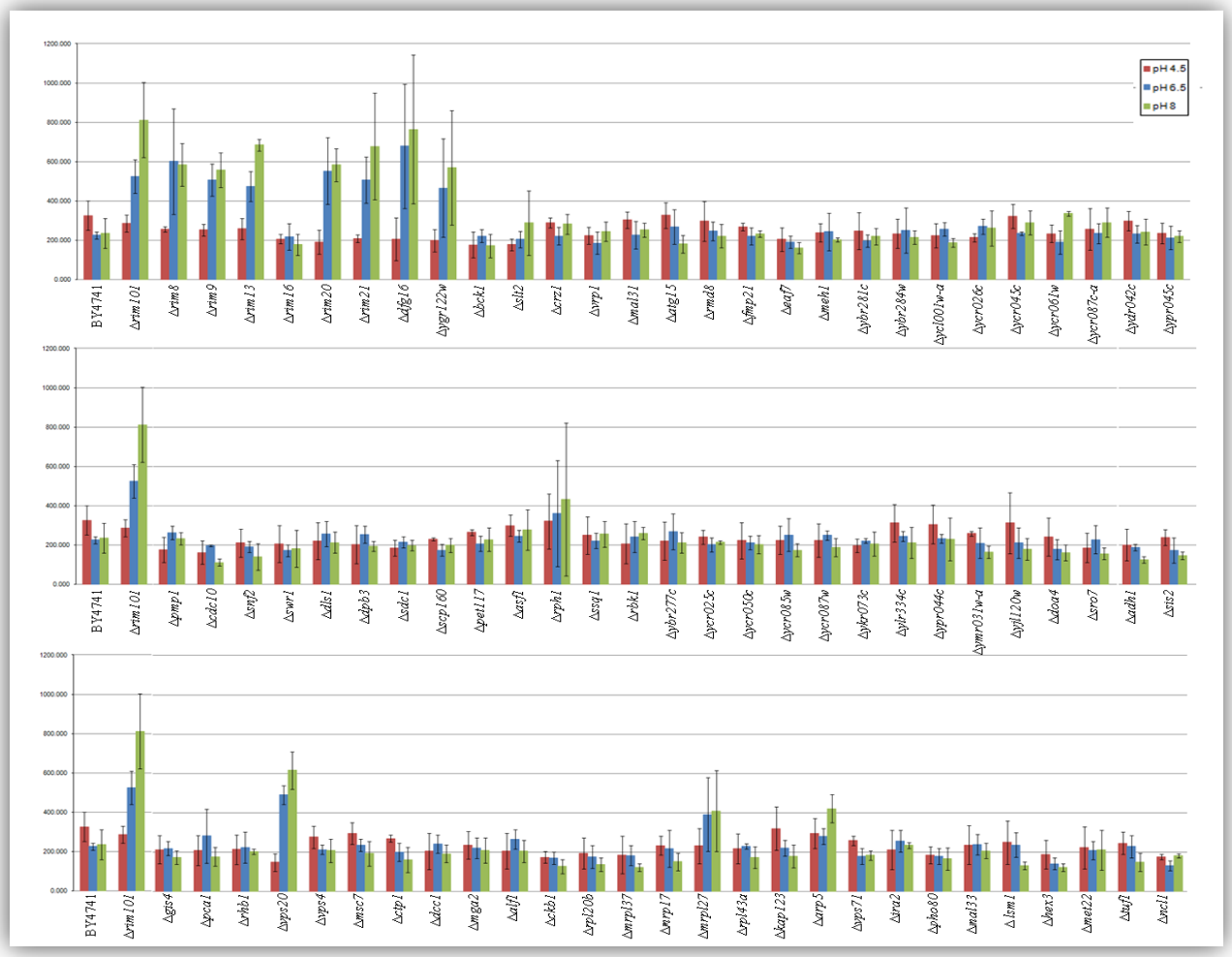


Fig. 7.18: β-galactosidase activity in BY4741 and Δ*rim101*-like mutants expressing a synthetic Rim101p-regulated promoter. Strains expressed a synthetic Rim101p-regulated promoter (fused to a *lac*Z reporter). The β-galactosidase activity (in Millers units) has been calculated on the basis of OD_{660} and A_{420} measurements and averaged for three replicates.

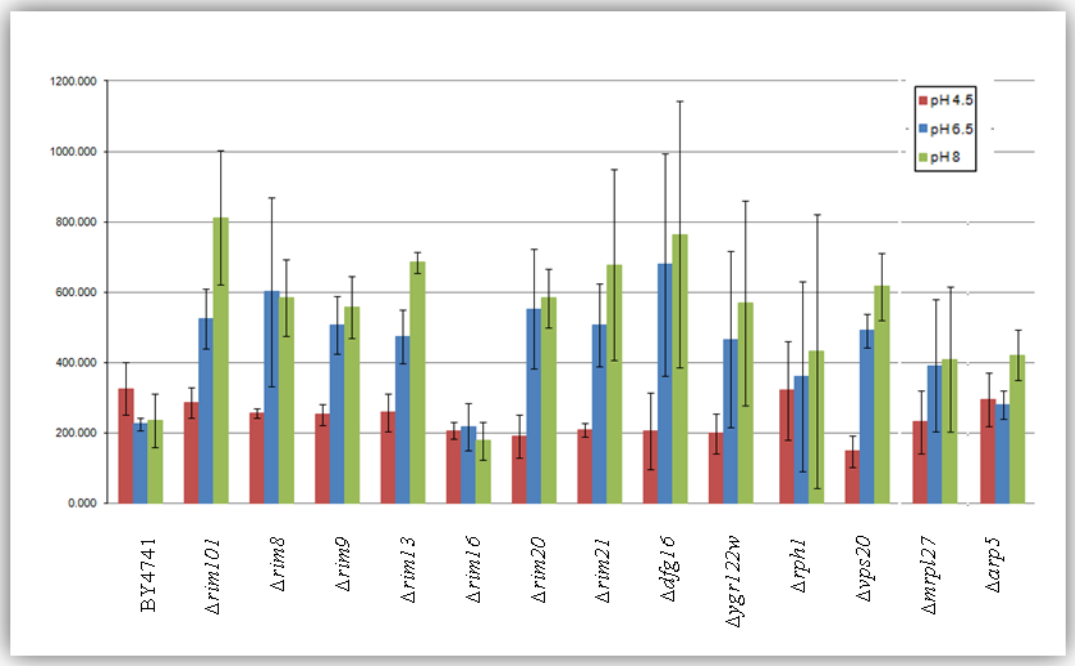


Fig. 7.19: Summary of β-galactosidase activity in BY4741 and Δ*rim101*-like mutants highlighting mutants showing derepression of *lacZ* gene expression. Strains expressed a synthetic Rim101p-regulated promoter (fused to a *lacZ* reporter). The β-galactosidase activity (in Millers units) has been calculated on the basis of OD_{660} and A_{420} measurements and averaged for three replicates.

7.4 Discussion

In a neutropenic model of IPA, virulence of *A. nidulans* is acutely attenuated when the PacC transcription factor is deleted or unprocessed (Bignell *et al.*, 2005). Attenuation of *pacC* null mutants is also observed in the major pathogen *A. fumigatus* (Chapter III); it therefore follows that proteins regulating *A. fumigatus* PacC activity will impact upon virulence and may represent novel therapeutic targets. Rim101p, the *S. cerevisiae* homologue of *Aspergillus* PacC transcription factors participates, not only in environmental pH adaptation but also in the positive regulation of sporulation, invasive growth, ion tolerance and acquisition, and certain cell wall-related activities (Denison, 2000; Hayashi *et al.*, 1998; Lamb *et al.*, 2001; Lamb and Mitchell, 2003; Li and Mitchell, 1997). Considering the wide spectrum of actions demonstrated for Rim101p and the documented overlaps in functionality of the Rim101p/PacC regulatory systems in *S. cerevisiae* and in the *Aspergillus* species, *S. cerevisiae* presents an ideal, and methodologically advanced, model platform upon which to base assays for identification of novel upstream components of the Rim101p/PacC pathway.

7.4.1 Δ*rim101*-like phenotypes

A global phenotypic screen of the Euroscarf *S. cerevisiae* ORF deletion library had revealed that a Δ*rim101* mutant shows cation hypersensitivity compared to the parental strain BY4741 (Bignell, unpublished). This cation hypersensitivity profile was also observed for 80 other ORF deletions including all of the *S. cerevisiae* homologues of *A. fumigatus* Pal pH signalling proteins. To identify which of the 80 Δ*rim101*-like proteins act upstream of Rim101p, an epistacy screen was performed to identify mutants having cation sensitivity profiles which could be complemented by the introduction of an activated *RIM101* allele, thereby strongly suggesting a Rim101p-regulating role for the protein products of these genes. The initial phenotypic screen was repeated (Figs. 7.3-7.9 and Table 7.3) to verify cation-sensitive phenotypes and optimise the culturing conditions for the subsequent epistacy screen. The growth of the null mutants in comparison to the parental isolate BY4741 was analysed in different conditions, including YPD pH 8 (100 mM Tris-HCl), YPD pH 4 (100 mM glycolic acid), YPD pH 4 (100 mM glycolic acid) 200 mM LiCl, YPD 100 mM LiCl, YPD 200 mM LiCl, YPD pH 4.5 (100 mM glycolic acid) 800 mM NaCl, and YPD pH 7.4 (100 mM Tris-HCl) 200 mM LiCl. At this stage of the experimentation, no significant differences were visually discerned between any of the strains when grown on YPD. Alkalinisation of the media to pH 8 resulted in a reduction of growth for all strains tested, including the wild type strain BY4741 (Fig 7.3), whereas no effect was noted upon acidification of the media to pH 4 (Fig. 7.4). This confirmed the previously noted observation that yeast cells grow faster at acidic than neutral or alkaline pH (Lamb *et al.*, 2001). In contrast with the wild type BY4741, addition of LiCl reduced or prevented growth of the Δ*rim101*-like strains analysed; in particular, the effect was observed as more pronounced with increasing concentration of LiCl and/or increased pH. Coherent with this observation, growth for the yeast null mutants was almost completely prevented in YPD pH 7.4 mM 200 LiCl (Fig. 7.9). Previous screenings of the *S. cerevisiae* deletion library (Giaever *et al.*, 2002; Serrano *et al.*, 2004) have identified 216 mutants with defective growth at alkaline pH, highlighting the widespread effect of environmental alkalinisation on yeast physiology. In comparison to the parental isolate BY4741, a reduction or a complete inhibition of growth were here demonstrated for the Δ*rim101*, other Δ*rim* mutants and many Δ*rim101*-like mutants of the Euroscarf *S. cerevisiae* ORF deletion library in the presence of lithium chloride at pH 7.4. This cation hypersensitivity profile offered a powerful tool to investigate functions acting upstream of the transcription factor Rim101p to cooperate in its

activation. The compound phenotype exhibited by these strains is likely attributable to the heightened requirement for tight ionic homeostatic control in alkalinised media which is supported by Rim101p pathway control. Alkaline conditions impact dramatically upon membrane proton gradients, which supply energy for transmembrane transport of nutrients and ions. Accordingly, among the principal targets of Rim101p regulatory control are *PMA1*, *ENA1* and *VMA1* (Lamb *et al.*, 2001). *PMA1* encodes the plasma membrane H^+-ATPase, which hydrolyses ATP to provide energy for proton extrusion, thereby neutralizing the cytoplasm (van der Rest *et al.*, 1995). This protein represents the most abundant plasma membrane protein and is responsible for generating the proton gradient necessary for all secondarily active symporters and antiporters acquiring solutes from the extracellular environment, in particular those transporting amino acids, nucleotide bases, phosphate and other molecules. *ENA1* encodes a Na^+-ATPase which extrudes Na^+ generating a gradient utilised for the uptake of other cations (Rodriguez-Navarro *et al.*, 1994). A further contributor to cytosolic pH homeostasis is encoded by *VMA1*, a vacuolar H^+-ATPase (Stevens and Forgac, 1997). The importance of these transporters for cellular homeostasis at high pH is affirmed by the inability of corresponding null mutants to grow in alkaline conditions and/or in the presence of a high concentration of extracellular cations (Lamb and Mitchell, 2003).

Mutants having Δ*rim101*-like phenotypes might represent functions which impact upon Rim101p processing. This hypothesis is indeed supported by the observation that in all cases lack of a Rim pathway component results in a Δ*rim101*-like phenotype and that this phenotype can be rescued in the epistacy screen (Figs. 7.13 and 7.14). The functional classification of genes in which deletions resulted in Δ*rim101*-like phenotypes reveals many ORFs involved in vacuolar organisation and biogenesis (*ARP5, VPS20, VPS4, VPS71*), vesicle transport (*DOA4, SRO7*), transmembrane transport (*MAL31, RHB1*), intra organelle transport (*CTP1, KAP123*), cell polarity and cell wall biogenesis (*CDC10, SLT2*), stress response and cation homeostasis (*BCK1, DFG16, GIS4, IRA2, MET22, PCA1, PHO80, PMP1, YGR122W*). Interestingly, several ORFs are likely to participate in chromatin modification (*ASF1, DCC1, DLS1, DPB3, MSC7, RPH1, SCP160, SDC1, SNF2, SWR1*). Other represented functions include metabolism and energy (*ADH1, PET117, RBK1*), protein degradation, synthesis and modification (*ALF1, HEX3, MRP17, MRPL27, MRPL37, RPL20B, RPL43A*) and transcription and RNA processing (*CRZ1, LSM1, MAL33, MGA2, NCL1, SSQ1, TUF1*). The genes *ATG15, VRP1, CKB1* and *SIS2* are involved respectively in autophagy (*ATG15*), structure (*VRP1*) and cell cycle (*CKB1* and *SIS2*). Numerous genes are thus far of unknown biological function (*EAF7, FMP21, MEH1, RMD8, YBR277C,*

YBR281C, YBR284W, YCL001W-A, YCR025C, YCR026C, YCR045C, YCR050C, YCR061W, YCR085W, YCR087C-A, YCR087W, YDR042C, YJL120W, YKR073C, YLR334C, YMR031W-A, YPR044C, YPR045C). However, it is important to underline the fact that the Euroscarf *S. cerevisiae* ORF deletion library used for this study covers only 95% of the non-essential yeast genome. Some exclusions are particularly relevant to this study. For example, none of the *ENA* gene deletants (*ENA1*, *ENA2* and *ENA5*) is present in the library, because of the technical limitations involved in designing unique primers due to high similarity between the members (Giaever *et al.*, 2002).

7.4.2 For several null mutants, the Δ*rim101*-like phenotype depends on whether the assessment is performed on solid media or in liquid culture

In a time course analysis comprising nine time points (0, 2, 4, 6, 8, 10, 12 and 24 hours), the parental strain BY4741, Δ*rim101*, 80 Δ*rim101*-like mutants, and respective pWL86URA transformants were screened for cation sensitivity in a 96-wells plate format. The normalised, corrected OD_{600} [OD_{600}^{NC}] values for growth in liquid YPD and YPD pH 7.4 200 mM LiCl reproducibly detected differential cation sensitivity among Δ*rim101*-like and wild type strains, most specifically at the 24 hour time point. In subsequent liquid culture assays Δ*rim101*-like phenotypes were assigned according to baseline values obtained for the parental strain BY4741 (OD_{600}^{NC} = 5.686) and for Δ*rim101* (OD_{600}^{NC} = 0.983). In agreement with the Δ*rim101*phenotype all other Δ*rim* mutants displayed equivalent cation sensitive phenotypes (Fig. 7.14 and Table 7.4) in the range OD_{600}^{NC} = 0.0-2.6, this included deletions in genes encoding more recently identified components of the Rim101p pathway, *DFG16* and *YGR122W* (Barwell *et al.*, 2005; Rothfels *et al.*, 2005). Although the Δ*rim101*-like phenotype was initially identified on solid media adaptation of the screening protocol to 96-wells plate format created some discrepancy of phenotype among the 81 mutants screened, whereby cation hypersensitivity was retained for only 57 of the 81 mutants. Referring to the previous classification according to biological functions, the ORFs resulting in a strong Δ*rim101*-like phenotype retain functions such as vacuole organisation and biogenesis (*ARP5, DOA4, VPS20*), transport (*MAL31, RHB1*), cell polarity, cell wall biogenesis (*SLT2*), stress response and cation homeostasis (*BCK1, DFG16, GIS4, MET22, YGR122W*), protein degradation, synthesis and modification (*ALF1, MRPL27, MRPL37, RPL20B, RPL43A*), transcription and RNA processing (*NCL1*), chromatin modification, architecture and transcription (*ASF1,*

DLS1, *DPB3*, *SDC1*, *SNF2*, *SWR1*), cell cycle (*SIS2*), and structure (*VRP1*). Strong Δ*rim101*-like phenotype ORFs also include candidates with an unknown function i.e. *MEH1*, *RMD8*, *YBR284W*, *YCL001W-A*, *YCR025C*, *YCR026C*, *YCR050C*, *YCR085W*, *YCR087W*, *YKR073C*, *YMR031W-A*, *YPR044C*. 24 ORF deletants grew normally in YPD pH 7.4 200 mM LiCl. These ORFs include members of all the categories previously introduced, such as vacuole organisation and biogenesis (*SRO7*), metabolism and energy (*ADH1*, *PET117*), transport to other organelles (*KAP123*), cell polarity and cell wall biogenesis (*CDC10*), stress response and cation homeostasis (*IRA2*, *PCA1*, *PHO80*), protein degradation, synthesis and modification (*HEX3*, *MRP17*), transcription and RNA processing (*MAL33*, *MGA2*, *SSQ1*, *TUF1*), chromatin modification, architecture and transcription (*RPH1*, *SCP160*), and autophagy (*ATG15*). It seems therefore that cation sensitivity of the mutants becomes exacerbated on solid medium likely reflecting the difficulty associated with colony counts and/or colony measurements, and also demonstrating the partial lack of sensitivity it introduces when screening phenotypes of gene knockouts lacking proteins only partially contributing to the specific pathway or phenotype investigated (Toussaint *et al.*, 2006). Phenotypic analyses in liquid culture are expected to be more accurate and sensitive, and permit temporal analyses to be conducted. The differences observed between solid media and liquid culture screens are likely due to various factors such as heightened availability of nutrients, ion and oxygen in liquid culture which are of limited availability on the surface of a solid agar plate.

7.4.3 Identification of putative novel regulators of Rim101p

Among the 57 mutants retaining Δ*rim101*-like phenotypes, the cation hypersensitivity was rescued by expression of a constitutively active form of Rim101p in 40 mutants. Importantly, this included all of the null mutants for known components of the Rim101p pathway (including *RIM16*, *DFG16* and *YGR122W*), as well as the following mutants: *ARP5* (vacuole organisation and biogenesis), *MAL31*, *RHB1* (transport), *SLT2* (cell polarity, cell wall organisation and biogenesis), *BCK1*, *MET22* (stress response and cation homeostasis), *ALF1*, *MRPL27*, *MRPL37*, *RPL20B*, *RPL43A* (protein degradation, synthesis and modification), *LSM1*, *NCL1* (transcription and RNA processing), *DPB3*, *SDC1*, *SNF2*, *SWR1* (chromatin modification, architecture and transcription), *SIS2* (cell cycle) and *VRP1* (structure). For 15 Δ*rim101*-like mutants cation sensitivity was unaltered, whereas in two cases (Δ*crz1* and *Δdls1*) extreme values were registered whereby for *Δcrz1* a weak Δ*rim101*-

like phenotype became increased for cation hypersensitivity, and for *Δdls1* a strong Δ*rim101*-like phenotype became cation tolerant following expression of activated Rim101p. Of the 24 Euroscarf *S. cerevisiae* deletion library mutants showing contradictory phenotypes to those detected upon solid media, 21 were unchanged by introduction of a constitutively active form of Rim101p. However, transformation with pWL86URA increased cation sensitivity for Δ*scp160* and Δ*pet117* and cation tolerance for *Δssq1*.

7.4.4 Diverse functional classes of proteins govern Rim101p functionality

The diverse functional categories contributing to Rim101p activation may reflect the extreme demands high pH stress places upon cellular physiology. Alkalinisation promotes dramatic remodelling of gene expression, through simultaneous activation, of various stress-related signalling pathways (including but not limited to Rim101p signalling) such as that regulating cell wall integrity (CWI) (Levin, 2005), Wsc1-Pkc1-Slt2 MAP kinase signalling (Castrejon *et al.*, 2006), and the calcium-activated calcineurin pathway (Serrano *et al.*, 2002). These, and other regulatory mechanisms contribute to nutrient and ion acquisition in alkaline environments by moderating iron/copper, phosphate, zinc, and glucose uptake and mobilisation (Arino, 2010). Global modulation of gene expression in response to alkaline stress shows a different timing according to the specific pathway(s) involved in the regulation of specific subsets of genes. Accordingly Arino, 2010 documented the observation that of about 400 genes whose expression is induced by exposing yeast cells to high pH (7.6-8.2) in a variety of DNA microarray experiments (Causton *et al.*, 2001; Lamb *et al.*, 2001; Lamb and Mitchell, 2003; Serrano *et al.*, 2002; Viladevall *et al.*, 2004) the expression of some subsets of genes varies very quickly (10–15 minutes), whereas others varies at later stages (after 30–45 min).

The multivesicular body (MVB) pathway. The three protein complexes ESCRT-I, -II, and –III, composed of "class E" vacuolar protein sorting (*VPS*) gene products are components of the endosomal trafficking machinery, involved in the formation of, and trafficking through multivesicular bodies (MVBs) (Katzmann *et al.*, 2002). MVB sorting requires a pH gradient across the endosomal membranes and efficient functioning of vacuolar protein sorting is affected in alkaline conditions (Klionsky *et al.*, 1992). Recent work in *S. cerevisiae* has shown an unexpected role in pH signal transduction for most, but not all, the ESCRT components. The function of receptor endocytosis was initially attributed to down-regulation of plasma membrane receptors. However, plasma membrane receptors do not

always reach the vacuole, instead remaining in the endosome and thereby suggesting that endocytosis could promote, rather than prevent, signalling, as shown by a growing number of examples. Among these, there is the Rim101p/PacC pH-signalling pathway, where the positive-acting association between endocytosis and signalling putatively connects two spatially separated complexes, located at the plasma membrane and on endosomal membranes (Di Fiore PP, 2001; Katzmann *et al.*, 2002). The proposed endosomal membrane complex comprises Rim101p/PacC, a cysteine protease of the calpain family Rim13p/PalB (Denison *et al.*, 1995), a scaffold Rim20p/PalA (Peñalva and Arst Jr, 2004) and endosomal components. PalC, the last component of the ambient pH signalling pathway to be characterised in *A. nidulans* (Galindo *et al.*, 2007), is distantly related to *Saccharomyces cerevisiae* pheripheral endosomal sorting complexes required for transport III (ESCRT-III) protein Bro1p. As shown by two-hybrid interaction assays, PalC contains a Bro1-like domain supporting its interaction with Vps32 and this interaction has been demonstrated to be essential for pH signalling (Tilburn *et al.*, 1995; Galindo *et al.*, 2007). From its ability to localise in cortical puntate structures and to bind to Vps32, PalC has the expected requisites to link the two complexes involved in pH regulation. As demonstrated by PalC-GFP localisation experiments, in alkaline conditions PalC is recruited and assembled in punctate structures associated with the plasma membrane; these cortical punctate structures have been shown to be dependent on the presence of PalH but not of PalA and therefore hypothesised to be the sites of PalH-PalF signal-dependent interactions (Galindo *et al.*, 2007). PalC is therefore likely to act later in the pH signalling pathway than PalH but earlier, or in concomitance, with PalA action. As recently suggested in Peñalva *et al*., 2008, an attractive hypothesis is that, after PalF-mediated internalisation, the plasma membrane complex recruits PalC, which functions as a guide to the endosomal membranes containing PalA and PalB. The other Bro1-like domain is Rim20p/PalA (Davis *et al.*, 2000b; Xu and Mitchell, 2001; Xu *et al.*, 2004), like its mammalian homologue AIP1/Alix, interacts also with Vps4p and Vps32p/Snf7p (Bowers *et al.*, 2004; Ito *et al.*, 2001; Vincent *et al.*, 2003), the latter of which is a component of the endosomal complex required at a late stage in the multivesicular body pathway (Vincent *et al.*, 2003). Work with *S. cerevisiae* suggests a role for this protein in the pH signal transduction pathway. PalA might serve as an adapter to link PacC to a multiprotein complex on the cytosolic side of the endosomal membrane (Xu and Mitchell, 2001; Xu *et al.*, 2004). Rim13p/PalB is a cysteine protease of the calpain family, most likely the signalling protease, which removes the negatively acting C-terminus to form PacC^{53} (Denison *et al.*, 1995) (Mingot *et al.*, 1999). In *S. cerevisiae*, a demonstrated interaction

between Vps32p and the yeast PalB homologue Rim13p (Ito *et al.*, 2001) suggests that Vps32p might act like a scaffold in the protein complex in which Rim20p/PalA recruit the protease Rim13p/PalB to its Rim101/PacC substrate (Ito *et al.*, 2001). Several null mutants for components of the MVB pathway show the same sensitivity to alkaline pH and LiCl as the null mutants for members of the Rim101p pathway (Bowers *et al.*, 2004; Giaever *et al.*, 2002; Lamb *et al.*, 2001). In this study, the null mutants for the genes *VPS20* and *VPS4* demonstrated cation hypersensitivity which was not rescued by constitutive activation of Rim101p. Genetic analysis of the respective mutants has indicated that Vps20p but not Vps4p is required for Rim101p processing (Xu *et al.*, 2004). Vps20 is a myristoylated subunit of ESCRT-III and in collaboration with Vps32p recruits various proteins, including Rim20p, Bro1p, and Vps2-24 (Bowers *et al.*, 2004). Vps4p is an AAA-ATPase involved in multivesicular body (MVB) protein sorting, localised to endosomes and catalyzing ESCRT-III disassembly and membrane release. The role of Vps4 in Rim101p processing is controversial, because, despite its indispensability for Rim101p processing (Xu *et al.*, 2004), two-hybrid analyses have demonstrated its interaction with Rim20p (Bowers *et al.*, 2004; Ito *et al.*, 2001). Nonetheless, the Δ*rim101*-like phenotype for the Δ*vps20* and Δ*vps4* mutants validates the involvement of the MVB pathway in the response to alkaline stress. Moreover, the failure to rescue cation hypersensitivity after transformation with a constitutively active form of Rim101p highlights, in the case of *VPS20*, the diversity of MVB pathway functions and, in the case of *VPS4*, the differentiation of functions for the different components within the pathway itself. Hence, screening for suppressors of Δ*rim9* and Δ*rim21* mutations, Hayashi *et al.*, 2005 found that mutations in *DID4/VPS2*, *VPS24*, and *VPS4p*, suppress LiCl sensitivity of Δ*rim8*, Δ*rim9*, and Δ*rim21* but not Δ*rim13* or Δ*rim20*, indicating that Rim8, Rim9, and Rim21 act upstream of Rim13 and Rim20 in the pathway. The deletion of *VPS4*, *DID4* and *VPS24* causes the constitutive activation of Rim101p (Hayashi *et al.*, 2005), and uncouples pH sensing from Rim101 processing, leading to constitutive Rim101 activation. This scenario is the opposite of that observed for other mutants of the MVB pathway (except *SRN2*), which are acidic-mimicking (Xu *et al.*, 2004). Defects in Vps20p and Snf7p and in other components of the ESCRT-I and -II prevent their loading onto the endosomal membranes (Babst *et al.*, 2002); therefore, the model from Hayashi *et al.*, 2005 proposes that either formation or loading onto the endosomal membranes of the Vps20/Snf7 subcomplex is responsible for the activation of Rim101p processing, whereby a Rim20p-Snf7p-Rim13p complex catalyses the processing. Rim20p and Rim13 are both recruited by an interaction with Snf7, therefore doubting the degree of involvement of Vps20

in Rim101p processing, which has been mostly argued by two-hybrid analysis (Bowers *et al.*, 2004), which as extensively discussed in Chapter V and VI, identify close proximity rather than actual direct interaction. Vps4p function is instead to catalyse ESCRT-III disassembly and membrane release. It therefore acts consequently to Rim101p processing, explaining the failure to rescue cation hypersensitivity after transformation with a constitutively active form of Rim101p. The Vps20p/Snf7 subcomplex is not released from the endosomal membrane, therefore *vps4* mutants likely exhibit constitutive processing of Rim101 (Hayashi *et al.*, 2005).

The cell wall integrity (CWI) pathway. Tolerance to cell wall stress is mediated by the cell wall integrity (CWI) pathway, a phosphorylative cascade initiated with the activation of the protein kinase C Pkc1p. This kinase activates three other protein kinases Bck1p, and the redundant couple of MAPK kinases, Mkk1p and Mkk2p, and Slt2p MAPK kinase (Heinisch *et al.*, 1999; Lagorce *et al.*, 2003). Activation of Slt2p results in the phosphorylation of several cytosolic and nuclear targets, which modulates functions essential for growth and tolerance to cell wall damaging agents, including the transcription factors Rlm1p, Swi4p and Swi6p. Interestingly, previous publications indicate a significant overlap between gene expression modulation as a consequence of the alkalinisation of the environment, and resulting from exposure to cell wall damaging agents (Garcia *et al.*, 2004; Lagorce *et al.*, 2003) whereby cell wall damage induces genes involved in metabolism, energy production and stress response (such as chaperones), but decreases the expression of transcription factors and of genes involved in protein synthesis and cell growth. In this study both the Δ*bck1* and Δ*slt2* mutants from the Euroscarf *S. cerevisiae* ORF deletion library display strong cation hypersensitivity, which is rescued by complementation with a plasmid expressing a constitutively active form of Rim101p. In addition, on the basis of genetic manipulation and phenotypic analysis of the Δ*rim101* and Δ*slt2* in response to cell wall damaging compounds, it has been demonstrated that the Rim101p pathway contributes to cell wall remodelling in parallel with the CWI pathway or if the latter pathway is impaired (Castrejon *et al.*, 2006). Based on the phenotypic analysis of the Δ*slt2* mutant in response to various types of stresses, various conditions have been identified as activators of the CWI pathway, among which is alkaline pH, likely to effect cell wall damage. According to its main function, i.e. to maintain cell morphology and to protect cells from the external factors challenging the cell internal homeostasis, the cell wall is a dynamic structure, which needs to adapt to support cell growth, but also to face environmental changes. The importance of cell wall adaptation to alkaline pH has been indeed demonstrated in the present study (Chapter

IV) by the abundance of *A. fumigatus* PacC targets, which are involved in cell wall organisation and biogenesis. The convergence between the CWI and the Rim101 pathway in *S. cerevisiae* is underlined by the observation that the Slt2p-mediated transcriptional response is crucial for the yeast tolerance to alkaline pH (Giaever *et al.*, 2002). Studying the effect of osmotic stress in *S. cerevisiae* mutants by addition of 1M NaCl, which disturbs ion homeostasis and is toxic to yeast cells, Giaever *et al.*, 2002 highlighted that several genes critical for growth under ionic stress are also sensitive to high pH, indicating an overlap in the cellular response to these conditions. Interestingly, this overlap includes the calcineurin-dependent transcription factor Crz1p, the proteins involved in ion transport Npr1p and Sat4p, Rim101p and Rim13p from the Rim101p pathway and Sro7p. The impairment of the Rim101p pathway results in cell wall defects (Castrejon *et al.*, 2006). Δ*rim21* and Δ*rim101* are in fact synthetically lethal with Δ*slt2* and this synthetic lethality decreases by osmotic stabilisation of the media. The double mutants however, when growing in media, which was osmotically stabilised, still remain extremely hypersensitive to the cell wall damaging agent zymolyase and possess thicker cell walls, with decreased abundance of mannoproteins. On the basis that mutations in members of the CWI pathway confer sensitivity to alkaline conditions, Serrano *et al.*, 2006 indicated by DNA microarray analysis that several genes involved in cell wall organisation and biogenesis are induced by alkaline pH, at least partially, in a Slt2-dependent manner (Serrano *et al.*, 2006), proposing an essential role for the Slt2-mediated MAPK pathway in alkaline adaptation. However, recent studies on the Δ*rim101* Δ*slt2* double synthetic mutant have suggested Slt2p and Rim101p may act in an independent way, in particular in the context of the assembly of the chitin ring at *S. cerevisiae* bud necks (Gomez *et al.*, 2009). According to Gomez *et al.*, 2009, deletion of *SLT2* would impact its iteraction with Glc7p (Andrews and Stark, 2000; Garcia-Gimeno *et al.*, 2003), which functions with Bni4p at the bud neck (Kozubowski *et al.*, 2003; Larson *et al.*, 2008). Defects in *BNI4* are associated with altered septin assembly (Gladfelter *et al.*, 2005). Deletion of *RIM101* would instead act on *RSB1*, which has been demonstrated to be downregulated in the Δ*rim101* mutant (Lamb and Mitchell, 2003), and is required for maintainance of lipid symmetry (Ikeda *et al.*, 2008). Both Δ*rim101* and Δ*rsb1* mutants show delocalised chitin deposition, whereas the Δ*rim101* Δ*slt2* double mutant displays a significant degree of lysis, therefore suggesting the effect may be due to misregulation of *RSB1* (Gomez *et al.*, 2009). Showing the direct involvement in the Rim101p pathway for Bck1p and Slt2p, the rescue of the cation-sensitive phenotype for the Δ*bck1* and Δ*slt2* mutants after the transformation with

a constitutively active form of Rim101p in this study suggest a rather integrated model of action between the Slt2-mediated MAPK pathway and the Rim101p pathway.

The calcineurin pathway. In *S. cerevisiae* several distinct stresses, including alkaline pH prompt the rapid cytoplasmic entry of calcium from the extracellular media or from internal stores, such as the vacuole. Initially using an aequorin luminescence reporter to monitor the rise of intracellular calcium within the cell as a consequence of the alkalinisation of the media, and then by DNA microarray analysis in *S. cerevisiae*, calcium-mediated signalling has been demonstrated as involved in gene expression remodelling in the context of responses to alkalinisation of the media (Viladevall *et al.*, 2004). Increase of cytosolic calcium activates the protein phosphatase calcineurin, a heterodimer composed of a catalytic and a regulatory subunit, respectively encoded by *CNA1* and *CNA2* (Cyert, 2003), and *CNB1* (Kuno et al., 1991). Activated calcineurin dephosphorylates the transcription factor Crz1p, permitting its entrance to the nucleus to activate target gene expression through binding to calcineurin-dependent responsive elements (CDREs) in their promoters. By DNA microarray analysis of the transcriptional response to the alkalinisation of the media in calcineurin-deficient (Δ*cnb1*) and Δ*crz1* mutants, two transcription factors, Crz1p and Rim101p, have been demonstrated to regulate a distinct, but partially overlapping set of target genes involved in the response to alkaline stress (Viladevall *et al.*, 2004). Serrano *et al.*, 2002 also showed that the calcineurin pathway mediates, at least in part, the activation of ENA1, crucial for adaptation to alkaline pH (Serrano *et al.*, 2002). From the cited studies, it has been inferred that the calcineurin-mediated transcriptional response has a relatively minor role for survival at high pH, which it integrates with several other regulatory pathways, including that of Rim101p. Accordingly, in the epistacy screen performed in this study, a Δ*crz1* mutant showed only a weak Δ*rim101*-like phenotype, reflecting a likely partial requirement for the calcineurin pathway in adaptation to alkaline conditions, and moreover, uncoupling from the Rim101p pathway. Furthermore, growth of *crz1* mutants has previously been reported to be unaffected (Stathopoulos and Cyert, 1997) or only marginally affected by alkaline conditions (Arino, 2010). After transformation with a constitutively active Rim101p, a Δ*crz1* mutant shows increased cation-sensitivity, thereby strengthening the hypothesis that calcineurin and Rim101p pathways are uncoupled in the response to alkalinisation of the media. According to the repressor role of Rim101p in *S. cerevisiae*, the introduction of a constitutively active Rim101p would lead to a scenario where the repressive action of Rim101p on the *nrg1* gene is restored, therefore exacerbating the cation hypersensitivity phenotype, if the deleted ORF is involved in Rim101p processing. However, if the two pathways function independently to

mediate adaptation to alkaline conditions, the introduction of a constitutively active Rim101p may lead to the unbalancing of the equilibrium between the two cooperative pathways, resulting in increased cation hypersensitivity. A crucial point of convergence between the calcineurin and the Rim101p pathways is the independent modulation of the expression of *ENA1* (Mendoza *et al.*, 1994), which represents a major element in alkaline adaptation and detoxification of sodium and lithium and whose expression is dramatically induced by alkaline, saline and osmotic stress. Deleting both *CRZ1* and *RIM101,* does not completely abolish the expression of *ENA1*, suggesting the participation of additional signalling pathways for the adaptation to alkaline pH (Serrano *et al.*, 2002). Besides, at alkaline pH, the induction of the *ENA1* gene is completely abolished in a *snf1 rim101* double mutant in the presence of FK506, which is an inhibitor of the calcineurin pathway (Platara *et al.*, 2006). Demonstrating the integration of different signalling pathways to integrate alkaline adaptation response, *ENA1* has been described as modulated in response to alkaline stress by three main pathways (Platara *et al.*, 2006).

7.4.5 Novel regulators of Rim101p functionality

Functional categorisation of the null mutants of the Euroscarf *S. cerevisiae* ORF deletion library, whose cation sensitive phenotype is rescued after the transformation with a constitutively active form of Rim101p, retrieves several biological functions commonly associated with the Rim101p pathway and likely related to dealing with the physiological implication of a sudden alkalinisation of the environment.

Transport. As extensively discussed in the introduction to the present study and supported by evidence in Chapter IV and VI, the ability to regulate transport systems under alkaline pH is crucial to maintain pH homeostasis and ensure the supply of nutrients, otherwise limited by the environment. In the present assay, two transporter null mutants exhibited a Δ*rim101*-like phenotype and the rescue of cation hypersensitivity when transformed with a constitutively active form of Rim101p. These gene deletants are *MAL31*, a high-affinity maltose transporter, belonging to the 12-TMD superfamily of sugar transporters driven by the electrochemical gradient across the plasma membrane, and *RHB1*, a putative Rheb-related GTPase involved in regulating canavanine resistance and arginine uptake and a member of the Ras superfamily of G-proteins.

Chromatin modification, architecture and transcription. This category, including *ARP5*, represents the most highly populated functional category amongst mutants whose

cation hypersensitivity was rescued by constitutively active Rim101p. *DPB3* encodes for the third-largest subunit of the DNA polymerase II (DNA polymerase ε), required to maintain fidelity of chromosomal replication and for inheritance of telomeric silencing. *SDC1* encodes for a subunit of the COMPASS (Set1C) complex, which methylates lysine 4 of histone H3 and is required for chromatin silencing at telomeres. As described extensively in Chapter IV and VI, histone and chromatin remodelling have gained credit as contributing to the regulation of transcription in the past few years (Buck and Lieb, 2006), with the discovery that these complexes alter nucleosome structure in different ways, such as by covalent modification of N-terminal histone tails or by ATP-dependent perturbation of histone-DNA interactions (Fyodorov and Kadonaga, 2001). The latter mechanism in particular is executed by the SWI/SNF family of protein complexes, interestingly representing two of the genes in the present study, whose deletion resulted in a Δ*rim101*-like phenotype and whose cation hypersensitivity was rescued by the introduction of an active Rim101p. These two genes are *SWR1*, a Swi2/Snf2-related ATPase, exchanging histone variant H2AZ (Htz1p) for chromatin-bound histone H2A, and *SNF2*, the catalytic subunit of the SWI/SNF chromatin remodelling complex. In addition, Arp5 has been demonstrated to be part of numerous chromatin-modifying enzyme complexes, not only structural, but also enzymatic functions (Shen *et al.*, 2003; Vignali *et al.*, 2000). The experimental evidence presented in this study supports the involvement of the SWI1/SNF2 group in pH sensing and regulation.

Cell cycle. Two genes belonging to this category have been demonstrated as having a Δ*rim101*-like phenotype when deleted i.e. *CKB1* and *SIS2*, but only for the latter one cation hypersensitivity was rescued after transformation with a constitutively active form of Rim101p. *CKB1* is an highly conserved Ser/Thr protein kinase involved in cell polarity and cell cycle proliferation (Bidwai *et al.*, 1995; Glover, 1998), whose role in salt tolerance in *S. cerevisiae* has been has been extensively studied as part of the Trk1-Trk2 transport system (de Nadal *et al.*, 1999). The TRK system controls the uptake of K^+ and Na^+; in particular it prevents the entry of Na^+ when the cation is present in high concentrations in the media (Arino *et al.*, 2010b). However, the role of Cbk1p in salt tolerance has been shown to be independent from the regulation of Ena1p. Indeed, high salinity stress induces the transition from mitosis to the G1 stage (Melamed *et al.*, 2008; Reiser *et al.*, 2006). The link between cell cycle control and ion homeostasis is validated by the involvement in both pathways of Hal3p, otherwise called Sis2p (Ferrando et al., 1995). When over-expressed this gene confers resistance to high concentrations of NaCl and rescues the salt sensitivity of a calcineurin null mutant. In addition to its function in yeast growth arrest, *HAL3* is therefore thought to be

involved in the regulation of expression of *ENA1*, in concert with the calcineurin pathway. In the current literature, however there is no indication of the possible involvement of *HAL3* and/or *CBK1* in other environmental stresses such as alkalinisation of the pH.

Structure. The Δ*rim101*-like phenotype of the Δ*vrp1* mutant was rescued for cation sensitivity in the epistacy screen. The gene *VRP1* encodes a proline-rich actin-associated protein involved in cytoskeleton organisation and cytokinesis and related to mammalian Wiskott-Aldrich syndrome protein (WASP)-interacting protein (WIP). In addition, this gene has been demonstrated to be essential for endocytosis (Thanabalu *et al.*, 2007), although the relationship between actin organisation and endocytosis is still not well understood. However, the link of *VRP1* with pH signalling might correspond to the crucial role the endocytic pathway has in Rim101p processing and activation.

7.4.6 Use of a synthetic Rim101p-regulated promoter for identification of null mutants suffering aberrant Rim101p processing and/or transcriptional activity

Using the same set of 80 Δ*rim101*-like mutants from the Euroscarf *S. cerevisiae* ORF deletion library, the use of a synthetic Rim101p-regulated promoter fused to a *lacZ* reporter permitted identification of mutants likely suffering aberrant Rim101p processing and/or transcriptional activity. The synthetic Rim101p promoter, constructed by Lamb and Mitchell, 2003 was initially used to study Rim101p-mediated repression of the genes *NRG1* and *SMP1* to direct ion tolerance and cell differentiation (Lamb and Mitchell, 2003). In fact, in a wild-type scenario, as in the case of the parental strain BY4741, Rim101p functions as a repressor of the general repressor functions Nrg1 and Smp1. Deletion of *NRG1* and *SMP1* suppresses the defects in ion tolerance, haploid invasive growth and sporulation of a Δ*rim101* mutant, therefore indicating the two proteins Nrg1p and Smp1p function as Rim101p-mediated repressors of alkaline pH responses. Interestingly, one of the targets of Rim101p via Nrg1p is the Na^+ pump gene *ENA1*. This study finds that, following transformation with a synthetic Rim101p promoter fused to a *lacZ* reporter, β-galactosidase activity is repressed, under all environmental pH conditions studied. However, when *RIM101* is deleted, thereby removing processed Rim101p from the cell, β-galactosidase activity becomes derepressed at high pH (Fig. 7.16) as a consequence of removing Rim101p-mediated repression, according to the functioning as a repressor demonstrated by Lamb and Mitchell, 2003. According to this model, if the ORF deletants studied regulate Rim101p promoter binding, derepression of β-galactosidase activity is expected. β-galactosidase activity for the various transformed strains

was assayed and compared in normal, alkaline and acidic conditions, to identify, among all the Δ*rim101*-like null mutants of the Euroscarf *S. cerevisiae* ORF deletion library, those showing derepression of the *lacZ* gene occurring as a consequence of aberrant Rim101p processing and/or transcriptional activity at alkaline pH. As in the case of the previous epistacy screen, all of the previously identified Δ*rim* mutants showed the expected phenotype. Agreeing with the results of the epistacy screen, among all Δ*rim101*-like mutants screened, derepression of the *lacZ* gene indicates a regulatory role for Arp5p and Mrpl27p. *ARP5* is involved in chromatin modification, architecture and transcription, one of the most highly populated functional category amongst mutants whose cation hypersensitivity was rescued by constitutively active Rim101p (see above). This protein has been demonstrated to be part of numerous chromatin-modifying enzyme complexes, having not only structural but also enzymatic functions (Shen *et al.*, 2003; Vignali *et al.*, 2000). Also the Δ*vps20* mutant, whose cation sensitivity was not rescued by transformation with a constitutively active form of Rim101p in the prior experiment, was positive in this second assay, confirming the association between the yeast MVB pathway and Rim101p-mediated regulation to environmental pH, as discussed above. Surprisingly, the gene *RPH1*, whose deletion mutant did not exhibit a Δ*rim101*-like phenotype, was also identified. This gene is a histone demethylase which can specifically demethylate H3K36 tri- and dimethyl modification states; and is involved in damaged DNA repair. This supports the hypothesised role of histone and chromatin remodelling as regulators of pH-responsive gene expression.

CHAPTER VIII

CONSTRUCTION OF *A. FUMIGATUS* STRAINS EXPRESSING LUCIFERASE FOR BIOLUMINESCENCE DETECTION

8.1 Overview

Bioluminescence imaging (BLI) of microorganisms allows the study of establishment, manifestation and progression of infection in real time. This technique has already been successfully applied to a multitude of microorganisms, such as bacteria (Glomski *et al.*, 2007; Karsi and Lawrence, 2007; Sjolinder and Jonsson, 2007), viruses (Hutchens and Luker, 2007) and eukaryotic parasites like *Toxoplasma*, *Leishmania*, and *Plasmodium* species (Dellacasa-Lindberg *et al.*, 2007; Franke-Fayard *et al.*, 2006; Hutchens and Luker, 2007; Saeij *et al.*, 2005); it would indeed represent a significant innovation for the imaging of *Aspergillus* species during infection, providing real time data on location and distribution of infectious particles, which is currently unobtainable. In addition, repetitive imaging of single mice would dramatically reduce the number of animals required for certain experiments.

For the ultimate purpose of transposing protein interaction assays into tissue culture and murine models of infection, an *A. fumigatus* strain expressing firefly luciferase under the control of the glyceraldehde-3-phosphate dehydrogenase gene (*gpdA*) promoter was constructed and characterised. Firefly luciferase (FLuc) is a single polypeptide (550 aa; 62 kDa), derived from *Photinus pyralis*, one of the most famous bioluminescent organisms which utilises bioluminescence as a way to attract potential mates (Wood *et al.*, 1989). In this chapter the development and initial characterisation of *A. fumigatus* strains expressing firefly luciferase is reported. *A. fumigatus* bioluminescence imaging would facilitate understanding of the dynamics of infection and ultimately the development of protein interactions assays *in vivo*.

8.2 Methods

8.2.1 *A. fumigatus* strains

A. fumigatus strains used in this study are the wild type strain CEA10, and the PyrG Δ*ku80,* which has a non-homologous end joining deficiency (da Silva Ferreira *et al.*, 2006), as listed in Appendix A. Recipes for solid and liquid media are described in Chapter II. To select and propagate the transformant strains, AMM (- aneurin) was supplemented with 0.5 μg/ml Pyrithiamine (Takara).

8.2.2 Plasmid pSK379 for the construction of the bioluminescent *A. fumigatus* CEA10 and Δ*ku80* strains

To construct the *A. fumigatus* strains expressing firefly luciferase the plasmid pSK379 from Sven Krappman (Julius-Maximilians-University Würzburg, Germany), shown in Fig. 8.1, was utilised. pSK379 contains a pyrithiamine resistance cassette (*ptrA*) for selection in *A. fumigatus*. A unique restriction site for the enzyme PmeI is positioned between the sequence of the constitutively-expressed promoter of *A. fumigatus* gene (*gpdA*) and the sequence *his2A* which drives targeted insertion of the plasmid in the *A. fumigatus* genome. For selection and maintenance in bacterial cells, the plasmid carries the ampicillin resistance marker (*amp*) and a bacterial origin of replication.

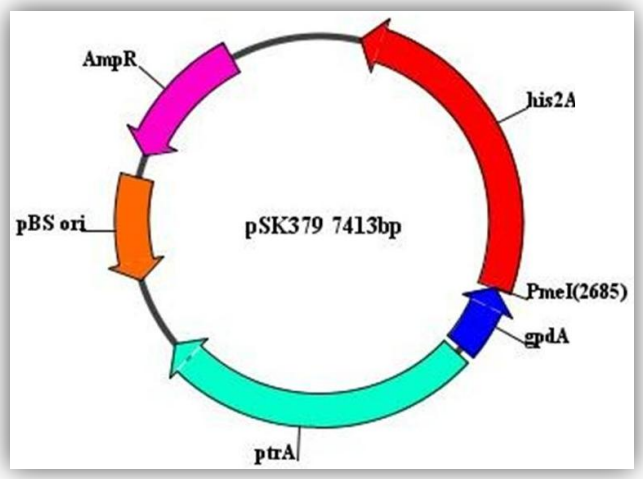


Fig. 8.1: pSK379. The plasmid contains a pyrithiamine resistance marker (*ptrA*). A PmeI restriction, positioned between the *gpdA* promoter, and the sequence *his2A* facilitates fusion of the bioluminescence cassette to the constitutive promoter. In addition, the plasmid carries the ampicillin resistance marker (*amp*) and a bacterial origin of replication.

To generate the plasmid pSK379Luc (Fig. 8.2) the firefly luciferase open reading frame was fused to the promoter of a constitutively-expressed *A. fumigatus* gene (*gpdA*) in the plasmid pSK379, designed to be specifically integrated into the histone 2A locus of the *A. fumigatus* genome. The vector pSK379 was digested with the restriction enzyme PmeI, a restriction enzyme that produces blunt ends, and dephosphorylated using the enzyme Calf Intestinal Alkaline Phosphatase to avoid self-ligation. The luciferase (*Photinus pyralis*, gene accession: BAF91092) was kindly supplied by Siouxsie Wiles (Imperial College London) in the vector, pUC19, and obtained by PCR using the Platinum Taq DNA Polymerase High Fidelity (Invitrogen). The firefly luciferase gene (LucF) was amplified by PCR using the oligonucleotides FireflyF1 and FireflyR1 (Appendix B) and treated to blunt and phosphorylate its ends. This involved the treatment of PCR products sequentially with two enzymes: DNA Polymerase I, Large (Klenow) Fragment to fill-in 5' overhangs and T4 Polynucleotide Kinase (PNK) for the addition of 5´-phosphates. The ligation was performed using T4 DNA Ligase and plasmids purified from 20 selected colonies was checked by PCR with the BIO-X-ACT-Long polymerase (Bioline) and using the oligonucleotides FireflyF1 and FireflyR2 to confirm the presence of the LucF gene. Because blunt ended ligation was used, the insert could have integrated in either the forward or the reverse orientations and in order to establish which clones had the correct orientation, 10 of the PCR-positive clones were checked using the oligonucleotides FireflyF1, FireflyF2, FireflyR1, FireflyR2 and FireflyR3 (Appendix B).

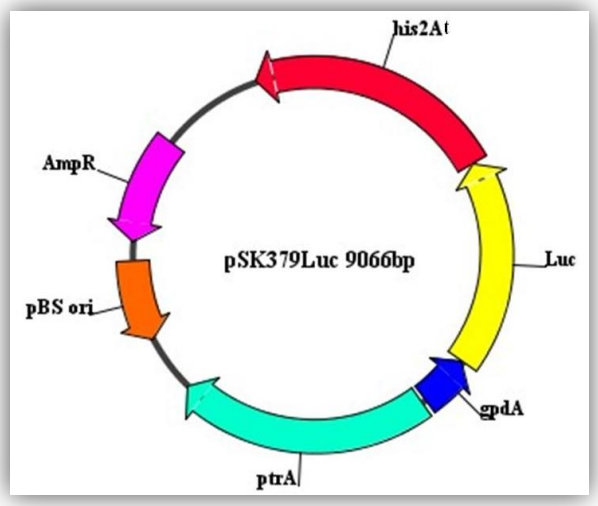


Fig. 8.2: pSK379Luc. The plasmid is a pSK379 derivative having the luciferase open reading frame fused to the promoter of the constitutively-expressed *A. fumigatus* gene (*gpdA*).

8.2.3 Verification of the bioluminescent *A. fumigatus* CEA10 strains

Following *A. fumigatus* transformation, the correct and single insertion of the firefly luciferase gene was verified by Southern blotting. In the case of Δ*ku80* mutants this was performed by our collaborator Sven Krappman and in the case of CEA10 mutants as part of this study. For transformants in the CEA10 genetic background, Southern Blotting was performed by digesting the genomic DNA extracted from the mycelia with the enzyme EcoRI and using two different probes. Probe 1 was designed to verify the correct insertion of the plasmid carrying the luciferase gene in the genomic DNA and constructed using the oligonucleotides LucSBF and LucSBR, which amplify a region of 580 bp, flanking the region of *his2A*. Probe 2 was designed to verify the single insertion of the PTR cassette in the genome and was constructed using the oligonucleotides LucPtrAF and LucPtrAR, amplifying a region of 580 bp in the *ptrA* gene. For details about the oligonucleotides see Appendix B.

8.2.4 *In vitro* bioluminescence imaging of *A. fumigatus* CEA10 strains

In vitro bioluminescence imaging of selected *A. fumigatus* strains producing firefly luciferase was performed by inducing light emission following the addition of D-luciferin (50 µg/ml, Promega) to the medium. Bioluminescence (photons s^{-1} cm^{-2} sr^{-1}) was measured using the IVIS100 camera system (Xenogen, now part of Caliper Life Sciences). The sample shelf was set to position D (field of view 21.2 cm). A photograph (reference image) was taken

under low illumination prior to quantification of photons emitted from *Aspergillus* transformants at a binning of 8 over 1 minute (or if the signal was very weak, of 16 over 2 or 3 minutes) using the software program Living Image (Xenogen) as an overlay on Igor (Wavemetrics, Seattle, WA). Bioluminescence from specific transformants was also quantified using the region of interest (ROI) tool in the Living Image software program (given as photons s^{-1}).

8.3 Results

8.3.1 Development of the bioluminescent *A. fumigatus* CEA10 strains

To generate the *A. fumigatus* strain expressing firefly luciferase, the plasmid pSK379Luc was constructed, fusing the firefly luciferase open reading frame to the promoter of a constitutively-expressed *A. fumigatus* gene (*gpdA*) in the plasmid pSK379. Once verified by sequencing, the plasmid was transformed into the sequenced *A. fumigatus* isolate CEA10 by electroporation (see Chapter II) with selection for pyrithiamine resistance (Kubodera *et al.*, 2000; Kubodera *et al.*, 2002).

In order to optimise the concentration of pyrithiamine and the electroporation protocol conditions that were varied on transferring the spores to selective plates included the concentration of spores plated (neat or a 1/50 dilution), the concentration of pyrithiamine in the media (from 0.1 μg/ml to 1 μg/ml), and spores were either plated directly on selective media, or alternatively overlaid with selective media following overnight incubation on plates without selection. For this genetic background and selective drug, the following conditions were established to be optimal: plating the transformed spores directly after the electroporation, without dilution, on AMM (-aneurin) supplemented with 0.5 μg/ml Pyrithiamine (Takara). To increase the probability of the correct insertion of the LucF gene in the appropriate genomic location (his2A) the transformation was performed using the undigested constructs (pSK379 was used as positive control to calculate the transformation efficiency), requiring therefore only one single event of homologous recombination with the homologous genomic locus for insertion of the entire vector.

Having optimised the conditions, many transformants were obtained (around 150) and 20 colonies were purified growing them in the same selective media used for the transformation to extract the genomic DNA from spores. The clones were checked by PCR

using the oligonucleotides FireflyF1 and FireflyR2 and six of them presented a PCR product of 1.1 Kb, corresponding to the LucF size, and were therefore considered for further analysis. An immediate screen was performed to judge functionality of the luciferase cassette and assesses detection ability. These transformants were grown in the same selective media used for the transformation adding 50 µg/ml luciferin (Doyle *et al.*, 2004) to induce light emission and assess the bioluminescence using the IVIS100 camera system. Fig. 8.3 shows the results obtained. Two of the transformants (11 and 19) negative for bioluminescence, whereas the other four were positive to different extents.

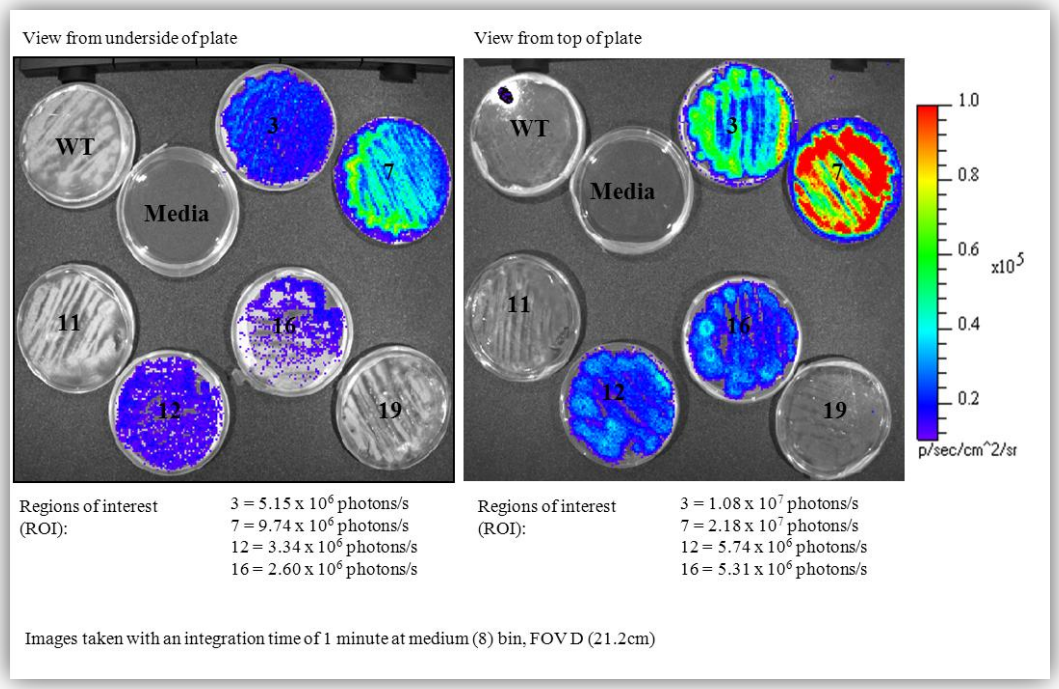


Fig. 8.3: *In vitro* bioluminescence imaging of purified *A. fumigatus* CEA10 strains producing firefly luciferase. Six clones obtained from the transformation of *A. fumigatus* CEA10 with pSK379 containing Luc and resulted positive by PCR were tested for light emission (Clone 3, Clone 7, Clone 11, Clone 12, Clone 16 and Clone 19) compared to the wild type CEA10.

These six transformants (Luc strains) were further investigated to verify the correct and single insertion by Southern Blotting with two different probes, designed according to the predicted mode of integration of pSK379Luc in the targeted genomic locus as shown in Figure 8.4. The plasmid pSK379Luc is designed to specifically integrate after the histone 2A locus of the *A. fumigatus* genome because of the presence *his2A* 3' flanking region, called *his2At*. The predicted mode of integration involves the recombination of pSK379Luc and the *his2A* region in the *A. fumigatus* genome via single crossing over. The genomic DNA was

extracted from the mycelia and digested with the enzyme EcoRI. Probe 1 was designed to verify the correct insertion of the plasmid carrying the luciferase gene into the genome and was obtained by PCR using the oligonucleotides LucSBF and LucSBR (Fig. 8.4, orange square). The expected signal is 3.6 Kb for the wild type. Following single homologous integration the size expected would be 4.7 Kb. Probe 2 was designed to verify the single insertion of the pyrithiamine cassette in the genomic DNA and constructed using the oligonucleotides LucPtrAF and LucPtrAR (Fig. 8.4, red square), amplifying a region of 580 bp in the *ptrA* gene. No signal is expected for the wild type CEA10 while for the Luc strains the expected signal is 4.7 Kb.

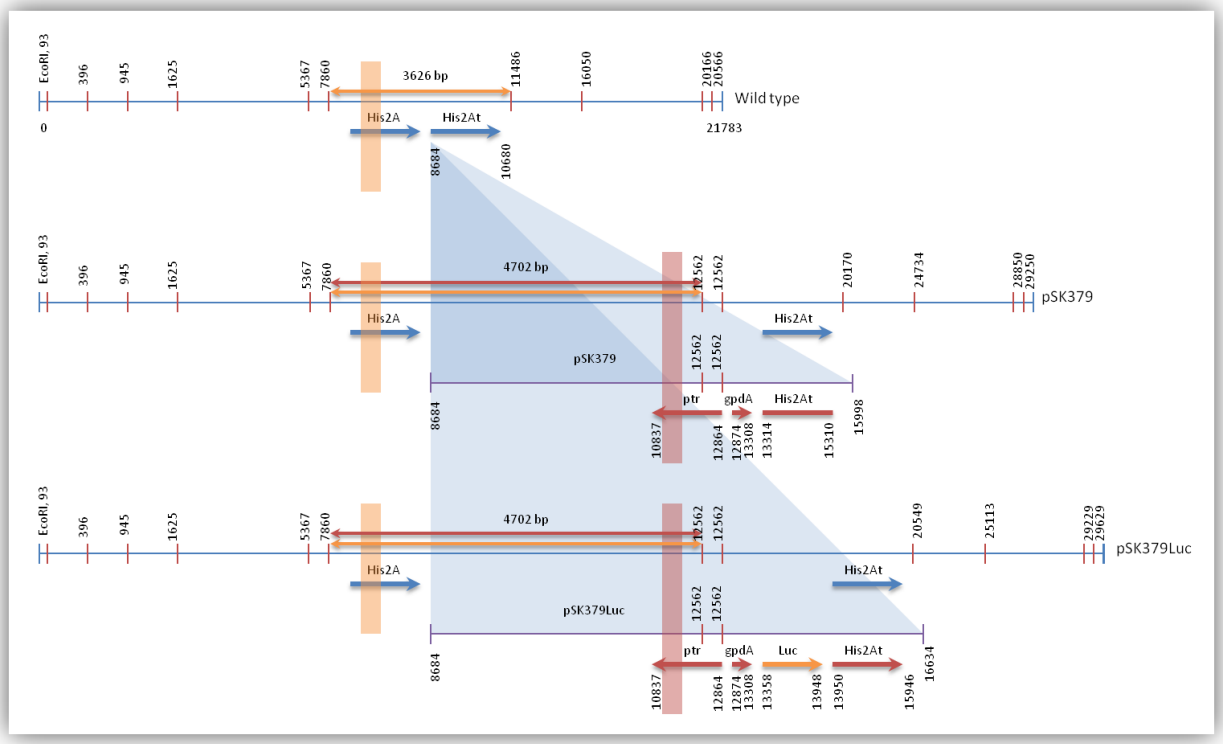


Fig. 8.4: Scheme representing the predicted mode of integration of pSK379Luc in the targeted genomic locus and the adopted Southern bloting strategy. The plasmid pSK379, used for construction of pSK379Luc, is designed to specifically integrate into the histone 2A locus of the *A. fumigatus* genome because of the presence *his2A* 3' flanking region, called *his2At*. The predicted mode of integration involves the insertion of pSK379Luc and the his2A region in the *A. fumigatus* genome via single crossing over.

The CEA10 Luc strains were also screened using the BD-advantage polymerase and two sets of oligonucleotides (Appendix B) However, as indicated by the previous experiments, the six Luc strains screened were positive for the integration of the Luc gene, but the recombination event appeared not to have occurred in the appropriate genetic locus.

The plasmid pSK379, used as a basis for these experiments, is designed to specifically integrate into the histone 2A locus of the *A. fumigatus* genome. It would therefore be necessary to repeat the transformation to achieve insertion of the construct into the appropriate *A. fumigatus* genomic locus.

The transformation was repeated, this time using the same plasmid pSK379Luc and the same conditions, and a non-homologous end rejoining mutant Δ*ku80* strain (da Silva Ferreira *et al.*, 2006). As before, among the many transformants obtained (around 150), 20 colonies were purified by growing them in the same selective media used for the transformation prior to extracting the genomic DNA from spores. The clones were checked by PCR using the oligonucleotides FireflyF1 and FireflyR2 and eleven of them produced a PCR product of 1.1 Kb, corresponding to the LucF size. For these strains, the correct and single insertion of the firefly luciferase gene and the pyrithiamine marker in the genomic DNA to gene was verified by Southern blotting (by our collaborator Sven Krappman). Two clones were revealed positive for the correct insertion of the Luc gene in the appropriate *A. fumigatus* genomic locus.

8.3.2 Preliminary testing of the bioluminescent *A. fumigatus* CEA10 strains

Various *in vitro* experiments were performed to evaluate experimental parameters relating to detection of bioluminescence in *A. fumigatus*. Questions to be addressed included whether the strains would be detectable in mice, at which stage of growth the bioluminescence would become detectable and whether the light emission correlated with the concentration of spores inoculated, giving a quantitative measurement for the fungal biomass. Initially the luminescence of all available Luc Strains was tested. 1 x 10^4 conidia of each one were plated in AMM (-aneurin) adding 50 µg/ml luciferin to induce light emission and the bioluminescence was measured after 2 days of incubation using the IVIS100 camera system. Fig. 8.5 shows the comparison between the different transformants in analysis and the wild type CEA10.

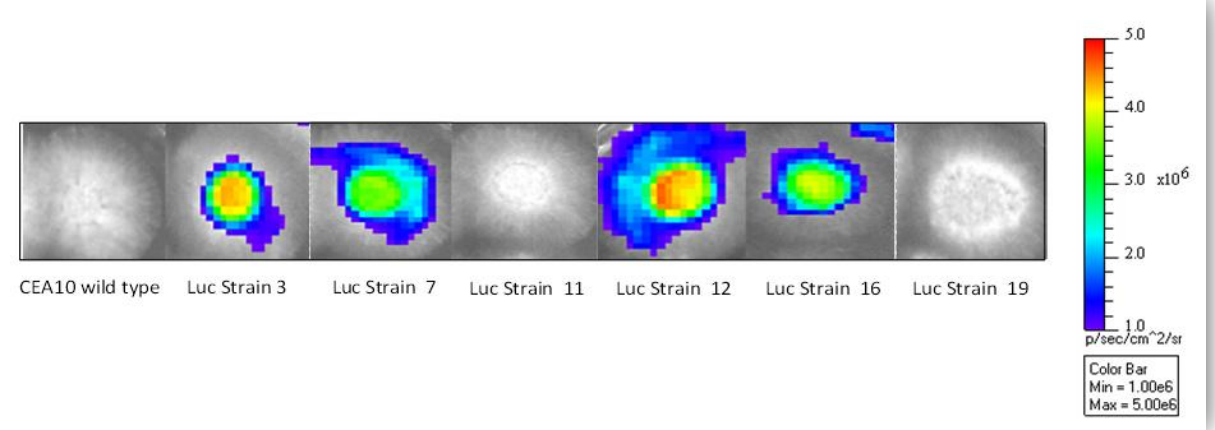


Fig. 8.5: *In vitro* bioluminescence imaging of purified *A. fumigatus* CEA10 strains producing firefly luciferase. 1 x 10^4 conidia of each Luc strain obtained from the transformation of *A. fumigatus* CEA10 with pSK379 containing the luciferase gene (Clone 3, Clone 7, Clone 11, Clone 12, Clone 16 and Clone 19) compared to the wild type CEA10.

To determine the effect of spore number, growth stage of the fungus and the quantity of D-luciferin required for successful detection, several concentrations of conidia, for both the wild type CEA10 and the Luc strains ($1x10^4$, $1x10^5$ and $1x10^6$) were grown in AMM (-aneurin), as shown in Fig. 8.6. The serial dilutions were incubated at 37°C for different times aiming to obtain a representation of conidia (0h), germlings (8h) and hyphae (16h) for each sample (A). Growth did not appear to be affected by the density of conidia inoculated in the media. For each sample, 10 µl of D-luciferin (20 mM) was added to induce light emission and measure the bioluminescence (B). The bioluminescent signal started to become visible after 8 hours in the $1x10^5$ and $1x10^6$ inocula, and was weakly detectable also after 16 hours in the $1x10^4$ inoculum. To determine if a delay in measuring bioluminescence would impact upon light emitted, luminescence was measured 20 minutes after the D-luciferin was added. No significant decrease of the signal was detectable (data not shown). To test the effect of an increasing dose of substrate, the luminescence was assessed after the addition of a single and a double extra dose of D-luciferin. The signal doubled in response to the single extra dose of D-luciferin, but no significant improvement in the detection of the fungi was recorded when a double extra dose was added (data not shown).

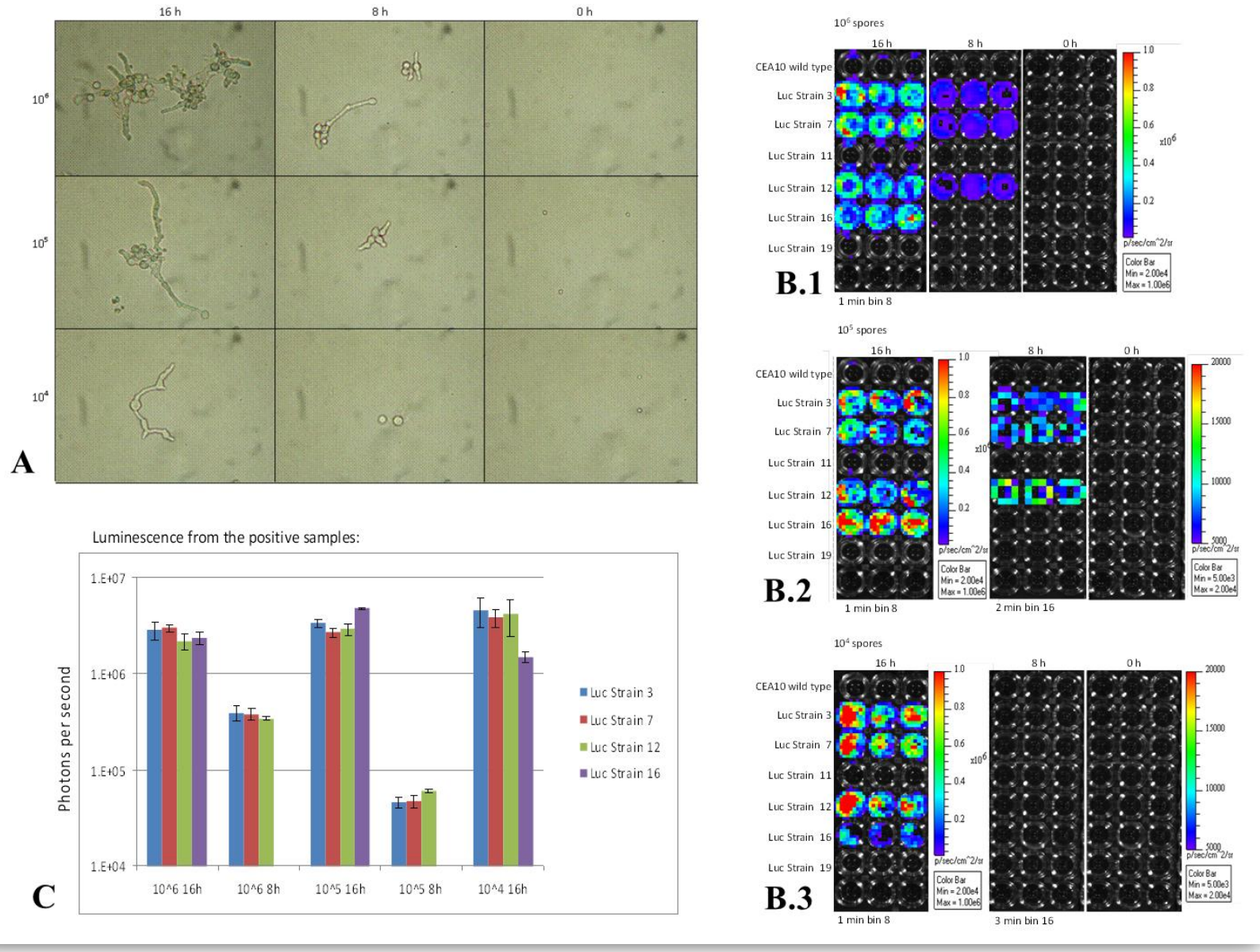

16 h
8 h
0 h
10^6
10^5
10^4
A
Luminescence from the positive samples:
Photons per second
1.E+07
1.E+06
1.E+05
1.E+04
10^6 16h
10^6 8h
10^5 16h
10^5 8h
10^4 16h
Luc Strain 3
Luc Strain 7
Luc Strain 12
Luc Strain 16
C
10^6 spores
CEA10 wild type
Luc Strain 3
Luc Strain 7
Luc Strain 11
Luc Strain 12
Luc Strain 16
Luc Strain 19
B.1
1 min bin 8
10^5 spores
B.2
1 min bin 8
2 min bin 16
10^4 spores
B.3
1 min bin 8
3 min bin 16

Fig. 8.6: *In vitro* bioluminescence imaging of purified *A. fumigatus* strains producing firefly luciferase. $1x10^4$, $1x10^5$ and $1x10^6$ conidia for the wild type CEA10 and the Luc strains (Clone 3, Clone 7, Clone 11, Clone 12, Clone 16 and Clone 19) were grown in AMM (-aneurin). Each serial dilution was plated 3 times and they were incubated at 37°C. Developmental growth (conidia, 0h; germlings, 8h; hyphae, 16h) was assessed by light microscopy (A). For each sample, 10 µl of D-luciferin (20 mM) was added to induce light emission and measure the bioluminescence for varying spore concentrations (B.1 to B.3) in triplicate for each strain. Quantification of light emission (photons per second) for the luminescent clones identified (C).

8.4 Discussion

Successful imaging of fungal species during infection provides real time data on location and distribution of infectious particles, which is currently unobtainable for *A. fumigatus*. In addition, repetitive imaging of single mice will dramatically reduce the number of animals required for the experiments. The use of an internal biological source of light, called luciferase, to tag cells or pathogens or genes represents a versatile approach to supply *in vivo* indicators that can be detected externally. This technique for the study of animal models of infectious disease provides not only insights into disease processes but also reveals new methods used by the pathogens to avoid host defences during the infection. Bioluminescence (Doyle *et al.*, 2004; Tannous *et al.*, 2005; Verhaegent and Christopoulos, 2002; Wiles *et al.*, 2006) is a naturally occurring enzyme reaction whereby light is produced by enzyme-mediated chemical conversion of a substrate usually through an intermediate highly energised state. This process occurs in a number of organisms from a variety of different genera, to facilitate location of food or for identifying mates. Independent evolution has originated different luciferases and substrates with different colours of emission but in general, these enzymes require energy, oxygen and a specific substrate (commonly known as luciferin) and may also require cofactors for light production.

For the ultimate purpose of transposing protein interaction assays into tissue culture and murine models of infection, an *A. fumigatus* strain expressing firefly luciferase under the control of the glyceraldehde-3-phosphate dehydrogenase gene (*gpdA*) promoter has been constructed and preliminarily characterised for its use in future infection assays. The *A. fumigatus* strain expressing firefly luciferase will aid understanding of the dynamics of infection and possibly fungal protein interactions during murine infection in real time, and permit analysis of disease parameters such as levels of tissue colonisation and invasion.

8.4.1 The *A. fumigatus* strain expressing firefly luciferase represents a promising tool for *A. fumigatus* bioluminescence detection purposes

A plasmid to drive luciferase gene expression within *A. fumigatus* was constructed, fusing the promoter of a constitutively-expressed *A. fumigatus* gene (*gpdA*) to the luciferase open reading frame of the well-characterised bioluminescent organism *Photinus pyralis* (Firefly). The *gpdA* promoter was chosen because it is constitutively active, with some variations depending on the carbon source, but is actively expressed when the mycelium is growing invasively in the host tissue. The firefly luciferase (FLuc) is a single polypeptide (550 aa; 62 kDa) which uses a benzothiazole, luciferin, as substrate along with ATP and oxygen to generate light and Mg^{2+} as cofactor. Cells expressing this enzyme, when provided with luciferin, will emit a yellow-green light with an emission peak at 560 nm ca using cellular ATP as the energy source (Doyle *et al.*, 2004; Wiles *et al.*, 2006).

Once a suitable plasmid had been constructed and verified, it was fundamental to optimize the concentration of the selective drug pyrithiamine and the protocol for the transformation using the clinical isolate *A. fumigatus* CEA10. The transformation of *A. fumigatus* by electroporation has the advantage of being quick and simple but suffers from growth of background colonies with certain selective agents, particularly pyrithiamine, due to the extremely high numbers of colony forming units electroporated. Once the selection conditions had been optimised, transformants were screened to verify functional, targeted and single insertion of the *Luc* gene by PCR, by the assessment of bioluminescence and by Southern Blotting. Taken together, the results of these experiments indicate the six Luc strains screened are positive for the integration of the *Luc* gene, but the recombination event had not occurred in the appropriate genetic locus. The integration site of the plasmid into the *A. fumigatus* genome is very important because it directs the stable expression of the luciferase gene while ensuring that the integration does not disrupt any other important gene. Thus, for the CEA10 genetic background repetition of the transformation will be required to target the insertion of the gene of interest in the appropriate *A. fumigatus* genomic locus. In the meantime, use of the Δ*ku80* mutant, which has a non-homologous end joining deficiency (da Silva Ferreira *et al.*, 2006) provided a single, targeted, integrant which could be used, alongside the CEA10 ectopic integrants, to optimise certain aspects of onward experimentation.

In this respect the strains were comparatively analysed for bioluminescent signal, its dependency upon spore concentration and kinetics of expression during developmental growth. These preliminary results validated the suitability of the *Luc* gene as a reporter for

subsequent murine experiments, given that the bioluminescent signal is visible within the range of infectious doses normally given to mice (Fig. 8.5).

In parallel with our study, another group has developed and recently published the use of BLI for *A. fumigatus*, using the firefly luciferase under the control of the *gpdA* promoter (Brock *et al.*, 2008), providing additional information on the potential use of the methodology in murine models of pulmonary aspergillosis (Ibrahim-Granet *et al.*, 2010). As shown by our results, the study confirmed a good correlation between the bioluminescent signal generated by the *A. fumigatus* engineered strain during infection, and fungal biomass. This correlation is fundamental for permitting the evaluation of fungal burden in infected tissues and for providing a means of testing antifungal treatments for efficacy. In addition, light emission can be directly correlated with the copies of luciferase gene present in the engineered strain (Brock *et al.*, 2008). The same study demonstrated that the *A. fumigatus* strain expressing firefly luciferase is a powerful tool for drug efficacy testing and *in vivo* monitoring of IPA, allowing the assessment of infection parameters such as the levels of tissue colonisation and invasion (Brock *et al.*, 2008). In addition, the *A. fumigatus* strain expressing firefly luciferase has been used to monitor fungal progression and location during the infection in mice with different types of immunosuppressive regimens, affecting either macrophages or neutrophils functions. In particular bioluminescent imaging of infected mice and histopathological analysis have correlated light emission and fungal invasion for the cyclophosphamide-treated murine model, where neutrophils function is depleted (Ibrahim-Granet *et al.*, 2010). This murine model is currently in use in our laboratory, and indeed formed the basis of experimentation described in Chapters III and IV).

8.4.2 Future perspectives and applications for BLI

Engineering *A. fumigatus* to express luciferase has been demonstrated as a very powerful option for tracking *A. fumigatus* murine infection in real time with bioluminescence assays and to assess infection parameters such as tissue colonisation and invasion. Besides, repetitive imaging of single mice will dramatically reduce the number of animals required for the experiments. Interestingly it would also represent an innovative tool for the ultimate purpose of studying *Aspergillus* protein-protein interactions during infection. Many attractive possibilities for the use of the *Luc* marker gene are reported in the literature. For example, adaptation of methodology such as Bioluminescence Resonance Energy Transfer (BRET) or similar approaches could permit the discovery and monitoring of protein-protein interactions not only at the cell level, but in the living model animal.

Chemioluminescence Resonance Energy Transfer (CRET), also known as Bioluminescent Resonance Energy Transfer (BRET) or Luminescence Resonance Energy Transfer (LRET) requires the transfer of emitted energy from a luciferase to the GFP in the same species. The luciferase emits light in a broad but low-intensity spectrum; part or all of the energy is absorbed by the GFP, which consequently emits in a narrow bandwidth peak but with higher intensity and higher wavelength. Thus, if two interacting partners are fused, the emitted light shifts from the luciferase to that of the GFP. Gene fusions between GFP and *Renilla* luciferase have been successfully performed in a variety of studies, showing that cells expressing this fusion can similarly be detected in animals after administration of the coelenterazine substrate (Wang *et al.,* 2001; Wang *et al.,* 2002; Xu *et al.,* 1999; Xu *et al.,* 2002; Xu *et al.,* 2003; Yu and Szalay, 2002). However, the wavelengths of emission of these fusions remain a limiting factor for this potentially powerful approach to study protein–protein interactions. Alternatively, the firefly luciferase has been expressed under the control of a modified NF-kappaB promoter to detect eventual protein-protein interactions resulting in transcriptional activation (Ray *et al.,* 2002).

The most promising applications reported in the literature for the use of the *Luc* marker for *in vivo* protein-protein assays are represented by the use of the split-luciferase in an intein-mediated reporter gene assay (Kanno *et al.,* 2006; Ozawa *et al.,* 2000; Ozawa *et al.,* 2001a; Ozawa *et al.,* 2001b). This methodology represents an improvement of the recent systems utilising the split GFPs and the split firefly luciferase as reporter to investigate protein-protein interactions (Ozawa *et al.,* 2000; Ozawa *et al.,* 2001a; Ozawa *et al.,* 2001b). For example, Ozawa and collaborators tested the ability of the split-luciferase to report *in vivo* protein-protein interactions, using the known insulin-induced interaction of the insulin receptor substrate 1 (IRS-1) and the N-terminal SH2 domain of the PI 3-kinase and demonstrated a direct correlation between the addition of insulin and luciferin, and light emission (Ozawa *et al.,* 2001a). The intein-mediated reporter gene assay has been applied by Kanno and his collaborators to monitor the epidermal growth factor (EGF)-induced interactions between the two known partners, the oncogenic product Ras and its target Raf-1 (Kanno *et al.,* 2006). The intein-mediated reporter gene assay has the advantage compared to the split-ubiquitin that it can assess interactions between membrane and/or cytoplasmic proteins and or nuclear proteins. This methodology is based on the protein splicing of transcription factors with DnaE inteins, where DnaE stands for the catalytic α subunit of DNA polymerase III and inteins represent segments of the protein. Protein splicing is a posttranslational autocatalytic processing in which an intein is excised out with the concomitant ligation of the flanking exteins. DnaE are connected with mLexA and VP16AD

and the proteins tested for interaction are linked to the ends of DnaEs. When the two proteins tested interact, the DnaEs are brought into proximity and undergo correct folding, which induces protein splicing and the connection of the DNA-binding protein (mLexA) with the transcription activation domain of a *Herpes simplex* protein (VP16AD) by a peptide bond. Until mLexA is ligated with VP16AD, the firefly luciferase reporter gene is not transcribed. As a result, the protein-protein interaction is measured by the luminescence intensity originating from firefly luciferase translated from the mRNA.

CHAPTER IX

SUMMARY AND CONCLUSIONS

In all circumstances where metabolism is active, a steady flux of protons enters and leaves the cytoplasm of cells, which have therefore evolved multiple mechanisms to maintain ion balance and guarantee optimal activity of major metabolic pathways, whose functionality would be damaged by large deviations of intracellular pH. Clear benefits are associated with having a means with which to modulate gene expression according to the ambient environment, and thereby secure rapid adaptations to environmental change. Such adaptation is particularly important for pathogenic microorganisms in withstanding multiple stresses exerted by the host niche.

Due to the existence of sexual and parasexual stages in the *A. nidulans* life cycle, this *Aspergillus* species has long been exploited as a model organism for the genus. The importance of the *A. nidulans* PacC-mediated pH response in the pathogenesis of murine pulmonary aspergillosis was first shown using mutational analysis which demonstrated that murine virulence is acutely attenuated if the *A. nidulans* transcription factor PacC is deleted, becomes (mutationally) resistant to processing or does not receive the pH signal (Bignell *et al.*, 2005).

This study describes the characterisation of *A. fumigatus* Δ*PacC* mutants in terms of phenotype, virulence and histopathology, and infection-related, genome-wide transcriptional defects, assigning roles for PacC in mammalian virulence (Chapter III) and infection-related gene expression (Chapter IV).

In each of two, genetically distinct, *A. fumigatus pacC* null mutants, aberrant conidiation and inability to adapt to alkaline pH *in vitro* was demonstrated (Fig. 3.2). Survival analyses in a neutropenic murine model of infection (Figs. 3.3-3.5) confirmed that this growth defect manifests also in murine lungs where a Δ*pacC* mutant is unable to progress beyond primary hyphal morphotypes during early stages of infection (Fig 3.6). Relative to the parental isolate, therefore, the mutant appears to be blocked in development and is unable to invade host tissues.

Although the phenotypes are likely to be due to the combinatorial impairment of several functions involved in *A. fumigatus* growth, on the basis of transcriptional profiling of *A. fumigatus* ATCC46645 and the isogenic Δ*pacC* mutant during initiation of murine infection (Chapter IV), several hypotheses may be formulated to explain the apparent developmental block of the Δ*pacC* mutant and its attenuation of virulence.

In *A. nidulans* a protein, believed to be necessary for synthesis of a small diffusible factor, and encoded by the *fluG* gene has been demonstrated as necessary for the induction of asexual sporulation in air-exposed colonies (Lee and Adams, 1994). *A. nidulans* FluG is constantly produced and when a specific quantity threshold is surpassed development is induced. Mutations in *fluG*, therefore, impair fungal ability to transit from a vegetative state to one in which conidiophores develop. The *fluG* mutant phenotype is rescued by over-expression of *flbA*, which is therefore believed to act downstream of FluG. Thus far however, in the context of *A. nidulans* developmental regulation, FluG has been studied soley for its role in controlling conidiophore development whereas, on the basis of the aconidial phenotype associated with an *flbA* mutant, FlbA has been hypothesised to act to a broader extent upon colony development. The observation that *fluG* and *flbA* are respectively up- and down-regulated during murine infection by a wild-type strain represents therefore an interesting finding, and points towards a role for this developmental pathway in *A. fumigatus* development in the host. The relevance of this observation, with respect to virulence, is strengthened by finding that *fluG* expression is highly down regulated in the Δ*pacC* mutant, during initiation of infection (Table 4.3).

During infection, *A. fumigatus* satisfies its requirement for proteinaceous substrates by destructing host tissues by means of several proteases (Ibrahim-Granet *et al.*, 2008; Kogan *et al.*, 2004; Rementeria *et al.*, 2005). Proteases appear to have a crucial role among the multitude of hydrolytic enzymes secreted by *A. fumigatus*, given the huge number of genes encoded by its genome, which is estimated to be over 100 (Nierman *et al.*, 2005). In terms of the relevance of this category of secreted enzymes during virulence, particular difficulty is associated with identifying pathologically significant enzymes due the redundancy of function among them. A recent example is provided by the transcription factor *ptrT*, which represents a conserved regulator of the expression of several secreted proteases. Although *ptrT* null mutants are defective, relative to the wild type in protease secretion, deletion of *ptrT* appears not to affect virulence (Bergmann *et al.*, 2009), indicating the likely compensatory action of other secreted proteases. Three major *A. fumigatus* proteases have been previously demonstrated to be secreted during infection (Monod *et al.*, 1999), namely the Alp alkaline serine protease (Afu4g11800), the Mep metalloprotease (Afu8g07080), and the Pep aspartic

protease (Afu5g13300). The induction of several other proteases has been reported from infection studies (Markaryan *et al.*, 1994; Moutaouakil *et al.*, 1993; Reichard *et al.*, 1990; Reichard *et al.*, 1994). Scrutiny of the ATCC46645 data, and comparative analysis of *pacC* null transcription during initiation of murine infection, permits unprecedented insight with respect to the temporal programming of transcription of such enzymes during early infection. Relative to the wild type, *pacC* deletion impacts heavily upon protease expression, as indicated by the down-regulation of at least six proteases (Afu4g11800, Afu6g12420, Afu3g00650, afu2g15950, Afu6g09650, Afu8g07080), among which Alp1 (Afu4g11800) and Mep (Afu8g07080) are included. An impairment of secreted protease secretion may, therefore be one of the impediments suffered by the Δ*pacC* mutant, possibly exacerbated by secretory defects given the stunted growth of the mutant in the host, and its non-invasive phenotype.

The cellular function, most significantly impaired by *pacC* deletion is transport. Down-regulated genes in the Δ*pacC* mutant predominantly include those involved in the uptake and mobilisation of metal ions such copper, zinc, sodium, and calcium, phosphate, amino acids and various nutrients (Table 4.18). These transporters are likely essential for supporting growth at alkaline pH, and given their normally positive regulation by PacC and their plasma membrane locations, they represent potential targets for further study, both of their role in *A. fumigatus* virulence, and their use as therapeutic targets, an aim which could be facilitated using the, now optimised, split-ubiquitin MYTH system (Chapter V). In the absence of PacC, upregulated transport functions are predominantly involved in sugar transport (Table 4.17). This might be explained in different ways. Considering the bilateral regulatory activity of PacC (which can function to activate and repress transcription) an immediate assumption is that genes which are up-regulated in the mutant should normally be subject to PacC-mediated repression. Given that sugars are commonly transported in symport with protons, carbohydrate uptake might simply represent a compensatory mechanism mounted by the mutant in an attempt to neutralise the cytoplasm of the cell. *A. nidulans* PacC null mutants have been frequently described as acidity-mimicking, implying that the cells (regardless of extracellular pH) are locked in an acid-responsive state, thus under acidic conditions such a hypothesis would make physiological sense, however, in the alkaline environment of the murine lung such activities would be counterproductive and therefore contribute to pH sensitivity of the Δ*pacC* mutant. Whether this response is under the direct regulatory control of PacC remains unclear but might be addressed by ChIP-Chip analysis. ChIP-chip combines chromatin immunoprecipitation with microarray technology, to investigate interactions between proteins and DNA *in vivo*. This would allow the identification, on a genome-wide basis (Aparicio *et al.*, 2004), of PacC binding, but would

still be subject to sample size limitation in disease settings. In particular, according the hypothesised role of epigenetic mechanisms in PacC regulatory action, such techniques would serve a multiple function.

Differentially-regulated genes did not exclusively contain PacC binding sites in fact, 87% of the genes less abundantly expressed in the Δ*pacC* mutant during the infection do not have a PacC consensus sequence. This may suggest a predominantly indirect (i.e. non *cis*-acting) mechanism(s) of gene regulation during infection. It is certainly likely that PacC regulation of gene expression is achieved via multiple mechanisms, and the down-regulation of genes likely to be involved in transposition might be significant in this respect.

Recent work in the Bignell laboratory has demonstrated developmentally-linked mobilisation of LINE-1 retrotransposable elements on the basis of such transcriptional profiles in a LaeA methylase-deficient mutant (Bignell, unpublished). Taken together, the regulatory impact of TEs upon gene cluster regulation (Shaaban *et al.*, 2010) and non-expression of the entire gliotoxin gene cluster in the PacC null mutant (Table 4.22) lend support to the hypothesis that PacC operates, at least partially through an epigenetic mechanism. Furthermore, in addition to their role in the activation of TEs, epigenetic mechanisms might however act in this instance as modulators of gene expression *per se*, according to recent evidence showing the chromatin-mediated specification of transcriptional factor targets (Buck and Lieb, 2006). In *S. cerevisiae*, targets of the regulator of yeast metabolism, Rap1p, are modulated by the chromatin regulator Tup1p and associated partners, which modify genome architecture itself, altering the targeting of the transcription factor and ultimately biological responses. In *A. nidulans,* the COMPASS complex member Bre1, which acts by modulating chromatin-mediated processes by methylation of lysine 4 of histone 3 (H3K4) (Mueller *et al.*, 2006; Sims and Reinberg, 2006), has been demonstrated to be involved in the activation of the expression of an otherwise cryptic secondary metabolite cluster (Bok *et al.*, 2009).

Membrane protein-protein interactions play key roles in the organisation of living cells, yet they have been among the most difficult aspects of biology to be studied (Ozawa *et al.*, 2000; Ozawa *et al.*, 2001a; Ozawa *et al.*, 2001b). The specificity of these interactions could be exploited to interfere and block specific sensory pathways, such as the protein interactions (studied here for pH sensing) in the plasma membrane which are formative in *A. fumigatus* environmental sensing and may provide a means to prevent host-adaptation. Sensory deprivation might provide a valid means of inhibiting infectious fungal growth, since in the absence of either PalH or PalI pH signalling is blocked and PacC is not proteolytically processed (Denison, 2000; Negrete-Urtasun *et al.*, 1999). Environmental-sensing proteins are

particularly interesting from a therapeutic perspective because they act at the interface between host and pathogen and they are more accessible to inhibitory agents due to their membrane localisation.

During pH signalling in *Aspergillus nidulans* a protein complex, hypothesised to initiate the ambient pH signal, is composed of: the 7-TMD protein PalH, the arrestin PalF and, very likely, the 3-TMD protein PalI (Calcagno-Pizarelli *et al.*, 2007; Herranz *et al.*, 2005; Negrete-Urtasun *et al.*, 1999). PalH has been identified as one, perhaps the only, pH plasma membrane receptor and interacts with the arrestin-like protein PalF. *palF* and *palH* mutations preventing this interaction also prevent pH signalling (Herranz *et al.*, 2005). Based upon the observation that, unlike null mutants of other *pal* genes, null *palI* mutants grow, though poorly, at alkaline pH (Denison *et al.*, 1995), PalI function has been hypothesised as assisting the plasma membrane localisation of PalH (Calcagno-Pizarelli *et al.*, 2007). This would require an interaction, either direct or indirect, and has not yet been demonstrated between PalH and PalI. To overcome difficulties in studying membrane proteins several methods have been reported, including the split-ubiquitin MYTH system (Fetchko and Stagljar, 2004; Johnsson and Varshavsky, 1994; Stagljar *et al.*, 1998). The MYTH system has here been demonstrated as a useful methodology for the analysis of *A. fumigatus* protein-protein interactions in yeast.

In this study (Chapter V), the MYTH system was used to test the interaction network for the three components of the *A. fumigatus* plasma membrane pH signalling complex, PalH, PalI and PalF, whose role in pH signalling has been extensively studied. Initial investigations confirmed topology of the two plasma membrane proteins PalH and PalI (Fig. 5.12), confirming previous reports and also *in silico* predictions by SignalP 3.0 and TMpred (Appendix F). The hypothesised model of topology implies that PalH and PalI are respectively a 7-TMD protein and a 3-TMD protein with extracellular N-termini and intracellular C-termini. PalF was demonstrated to interact with PalH, confirming that findings in *A. nidulans* (Herranz *et al*., 2005) remain relevant in the pathogen. In *A. nidulans*, the hydrophilic C-terminus of PalH interacts with the arrestin-like protein PalF and this interaction is required for PalF ubiquitination and phosphorylation, leading to the internalisation of PalF and its 7-TMD protein receptor associate, PalH. Additionally a novel finding (Fig 5.11) was the identification of PalH-PalH interaction, suggesting that PalH pH reception has further parallels with G-protein coupled receptor signalling, whereby homodimerisation of PalH is likely involved in pH signalling. *S. cerevisiae* Rim21p and Dfg16p and *A. nidulans* PalH have been predicted to be seven transmembrane domain

proteins with hydrophilic C-termini and therefore they have been hypothesised to form a G-protein coupled receptor (Barwell *et al.*, 2005; Herranz *et al.*, 2005).

The structure, topology and interaction partners for PalH resemble findings for GPCR proteins. Novel parallels identified in this study include PalH dimerisation (Chapter V) and possible N-glycosylation, requiring Pho88p and/or a lectin-like protein (Chapter VI). N-glycosylation is crucial for the proper folding of GPCRs, their intracellular folding, their delivery to the plasma membrane and appropriate protein-protein interactions (Lanctot *et al.*, 1999; Ray *et al.*, 1998; Wheatley and Hawtin, 1999). Moreover, GPCRs are now known to form dimers and/or higher-order oligomeric complexes (as reviewed in Milligan *et al.*, 2003; Milligan *et al.*, 2006; Milligan, 2007; Milligan, 2010) and such oligomerisation is associated with various functions, including quality control of protein folding for plasma membrane delivery (as reviewed in Milligan, 2007). Taken together this evidence supports a model in which appropriate targeting of the GPCR-like protein PalH requires homodimer formation, possibly in a glycosylation-dependent manner. Although no direct involvement of G-protein has been demonstrated in PacC-mediated pH signalling, mammalian GPCRs have been shown to activate non-G-protein signaling pathways from endosomes, mostly by interaction with β-arrestins, which create a bridge with MAPK signaling molecules, thereby establishing spatial and temporal control for signalling (Reiter and Lefkowitz, 2006).

No interaction was demonstrated in the present study (Chapter V) between PalH and PalI. PalI has been hypothesised to assist plasma membrane localisation of PalH which would require interaction between PalH and PalI, either direct or indirect in manner, but this has not been demonstrated (Peñalva *et al.*, 2008). The results presented here do not definitively rule out the participation of PalI in the plasma membrane signalling complex but do cast doubt upon a direct mode of interaction between the two proteins.

The most interesting application of the DUAL membrane system is that, using a membrane-associated protein for the screening, it allows the isolation of novel protein interactors from expression libraries (Chapter VI). The *A. fumigatus* cDNA library constructed for this study used Invitrogen proprietary technology, a Gateway-adapted DUALmembrane prey vector (pPR3N-GW) and *A. fumigatus* RNA isolated from a range of growth conditions. The MYTH system was adapted, and optimised for high-throughput identification of novel PalH interaction partners. Implementation of the system for large-scale screening involved the evaluation of expression level achieved from PalH bait plasmids, which was crucial for optimal functioning of the MYTH system. To limit bait self-activation, media was supplemented with 3-AT, competitive inhibitor of the *HIS3* gene product, which enhances the stringency of *HIS3* selection. The candidates for PalH putative interactors

identified using the high-throughput MYTH system are the phosphate transporter Pho88 (Afu5g01960), the COMPASS complex subunit Sdc1 (Afu7g05270), the lectin family integral membrane protein (Afu2g12180), the MFS glucose transporter (Afu3g13980), the polyubiquitin UbiD/Ubi4 (Afu4g10350) and the acyl-CoA binding protein (Afu2g11060). Further validation of the putative interactions is absolutely required, and could be pursued using co-immunoprecipitation or fluorescence microscopy.

In *S. cerevisiae*, Rim101p, the yeast homologue of *Aspergillus* species PacC, has been associated with various biological functions, not simply in environmental pH adaptation, but also in positive regulation of sporulation, invasive growth, ion tolerance and acquisition, and certain cell wall activates (Denison, 2000; Hayashi *et al.*, 1998; Lamb *et al.*, 2001; Lamb and Mitchell, 2003; Li and Mitchell, 1997). Considering the wide spectrum of actions demonstrated for Rim101p and the overlap between the functioning of the regulatory system in *S. cerevisiae* and in the *Aspergillus* species, the budding yeast represented an ideal platform in which to screen for novel upstream components of the Rim101p/PacC pathway. A global phenotypic screen of the Euroscarf *S. cerevisiae* ORF deletion library had previously revealed a highly characteristic Δ*rim101* cation hypersensitivity phenotype which was identified in the case of 80 other ORF deletants. To identify which of these might act upstream of Rim101p, reversal of lithium toxicity in the presence of an activated *RIM101* was tested (Chapter VII). Those mutants where cation sensitivity could be rescued in this manner are lacking gene functions having plausible significance for alkaline stress resistance, such as cell wall maintenance and vesicle transport. In addition, the data suggest the novel involvement of histone modifications and/or chromatin remodelling in pH sensing and regulation. This was further supported by the findings of a second screen (Chapter VII) which used a synthetic Rim101p-regulated promoter to identify *rim101*-like mutants suffering Rim101p-dependent defects.

The two reporter assays identified overlapping cohorts of deletion mutants which varied markedly in size. This difference might be attributable to the different nature of the experiments performed. In Chapter VII, a constitutively active form of Rim101p (Castrejon *et al.*, 2006) was transformed into the Δ*rim101*-like mutants to rescue cation hypersensitivity, most likely via up-regulation of transcription of the Na^+-ATPase Ena1p (Rodriguez-Navarro *et al.*, 1994). Given that Rim101p is thought to achieve Ena1 activation, at high pH, by lifting Nrg1-mediated repression (Lamb and Mitchell, 2003) which requires Rim101p processing, mutants deficient in Rim101 processing, nuclear localisation, or perhaps Nrg1 promoter accessibility might be among those identified. The functional variety among those identified as having Rim101p-rescuable phenotypes is pleasing but requires further scrutiny given the

indirect nature of the reporter assay and possible contribution of other ion transporters in restoring cation tolerance. Regulation of *ENA1* has been demonstrated to integrate at least three different signalling pathways in alkaline adaptation response (Platara *et al.*, 2006). It would therefore be interesting to repeat the epistacy screen on the same *rim101*-like mutants but in a Δ*nrg1* background.

The use of a synthetic Rim101p-regulated promoter provided a more restricted result. Having shown that Rim101p represses reporter activity exclusively in alkaline conditions a small number of mutants were identified where activated Rim101p could not derepress promoter activity. Although likely to be a more direct route for finding Rim101p-specific regulators a necessary next step of investigation for these mutants requires that the role of Nrg1p or Smp1p be addressed. It would be interesting, for example, to repeat the experiment on the same *rim101*-like mutants but in a Δ*nrg1* or Δ*smp1* background, to identify those mutants in which the Rim101-regulated gene activation is mediated by the repression of the two repressors Nrg1p or Smp1p.

The Split-ubiquitin MYTH assay cannot provide information on the dynamics of protein interactions in the native organism *A. fumigatus*, or on the relevance of tested interactions during infection. In this respect, bioluminescence imaging (BLI) might ultimately prove invaluable. BLI allows the study of establishment, manifestation and progression infection in real time. An *A. fumigatus* strain expressing firefly luciferase, under the control of the *gpdA* promoter, was constructed and preliminarily tested (Chapter VIII), for the ultimate purpose of transposing protein interaction assays into tissue cultures and murine models of infection. The CEA10 Luc strains developed in this study have answered several questions regarding the potential use of the firefly luciferase in tissue culture and murine models of infection. The luminescence of the Luc Strains available was compared and was analysed to determine the effect on the bioluminescent signal of the concentration of spores inoculated, of the growth stage of the fungus considered and of the quantity of D-luciferin added. These preliminary results have indicated the suitability of the *Luc* gene as a reporter for subsequent murine experiments, considering the bioluminescent signal is already visible with the concentration of *A. fumigatus* spores usually injected in mice. Engineering *A. fumigatus* to express the luciferase has been demonstrated to be a very powerful option to follow *A. fumigatus* murine infection in real time with bioluminescence assays and to assess infection parameters such as tissue colonisation and invasion (Doyle *et al.*, 2004). Besides, repetitive imaging of single mice will dramatically reduce the number of animals required for the experiments. Interestingly it would also represent an innovative tool for the ultimate purpose of studying *Aspergillus* protein-protein interactions during infection. Many attractive

possibilities for the use of the *Luc* marker gene are reported in the literature, such as the use of the split-luciferase in an intein-mediated reporter gene assay (Kanno *et al.*, 2006; Ozawa *et al.*, 2000; Ozawa *et al.*, 2001a; Ozawa *et al.*, 2001b).

APPENDIX A

STRAINS

Name	Genotype	Phenotype	Organism	Application
XL-10	F- *mcr*A Δ(*mrr-hsd*RMS-*mcr*BC) Φ80*lac*ZΔM15 Δ*lac*X74 *rec*A1 *ara*D139 Δ(*araleu*) 7697 *gal*U *gal*K *rps*L (StrR) *end*A1 *nup*G		*E. coli*	For general molecular cloning techniques
CEA10	Wild type clinical isolate		*A. fumigatus*	Chapter III
ATCC46645	Wild type clinical isolate		*A. fumigatus*	Chapter III, IV
ATCC46645 Δ*pacC*	Δ*pacC*::*ptr*^{R}	Alkaline pH sensitive	*A. fumigatus*	Chapter III, IV
CEA10 Δ*pacC*	Δ*pacC*::*ptr*^{R}	Alkaline pH sensitive	*A. fumigatus*	Chapter III
PyrG Δ*ku80*	Δ*ku80*::*pyrG*$^{+}$		*A. fumigatus*	Chapter IX
NMY51	*MATa his3delta200 trp1-901 leu2-3,112 ade2 LYS2::(lexAop)4-HIS3 ura3::(lexAop)8-lacZ (lexAop)8-ADE2 GAL4)*		*S. cerevisiae*	Chapter V, VI
BY4741	MATa *his3_1 leu2_0 met15_0 ura3_0*		*S. cerevisiae*	Chapter VII

Table AA.1: Strains used for this study.

APPENDIX B

OLIGONUCLEOTIDE PRIMER SEQUENCES

Name	Sequence	Reference
pF-PacCint1	acgttcctctgaagcctcata	Chapter III
pR-PacCint1	tcggccatcgtggttgat	Chapter III
PacCSB1	cttggtctttcctgtcgg	Chapter III
PacCSB2	cttttcttgggagcagcg	Chapter III
LucPtrAF	cttcctgttgatggaatgg	Chapter III
LucPtrAR	gacggcgcatgaccatag	Chapter III
SHF	nnnnnnnnggccattacggccatgggggatgatgctcgtct	Chapter V, pBT3-STE PalH, pBT3-SUC – PalH
SHR	nnnnnnnnggccgaggcggccgtgtcgtctcgactggg	Chapter V, pBT3-STE PalH, pBT3-SUC – PalH, pPR3-STE – PalH, pPR3-N – PalH
SIF	nnnnnnnnggccattacggccatgttactcaagcctgcaa	Chapter V, pBT3-STE – PalI, pBT3-SUC – PalI, pPR3-N – PalI
SIR	nnnnnnnnggccgaggcggccggcaaagggtatcgtgag	Chapter V, pBT3-STE – PalI, pBT3-SUC – PalI
PSHLEUF	nnnnnnnnggccattacggcctgatgggggatgatgctcgtct	Chapter V, pPR3-STE – PalH
PSHGLNF	nnnnnnnnggccattacggccagatgggggatgatgctcgtct	Chapter V, pPR3-STE – PalH
PSHARGF	nnnnnnnnggccattacggccgaatgggggatgatgctcgtct	Chapter V, pPR3-STE – PalH
PSFLEUF	nnnnnnnnggccattacggcctgatgtccgtcaattcctttac	Chapter V, pPR3-STE – PalF
PSFGLNF	nnnnnnnnggccattacggccagatgtccgtcaattcctttac	Chapter V, pPR3-STE – PalF
PSFARGF	nnnnnnnnggccattacggccgaatgtccgtcaattcctttac	Chapter V, pPR3-STE – PalF
SFR	nnnnnnnnggccgaggcggcccgctggtaacgcggtaatga	Chapter V, pPR3-STE – PalF
PSILEUF	nnnnnnnnggccattacggcctgatgttactcaagcctgcaa	Chapter V, pPR3-STE – PalI
PSI GLNF	nnnnnnnnggccattacggccagatgttactcaagcctgcaa	Chapter V, pPR3-STE – PalI
PSI ARGF	nnnnnnnnggccattacggccgaatgttactcaagcctgcaa	Chapter V, pPR3-STE – PalI
NHR	nnnnnnnnggccgaggcggccgtgtgtcgtctcgactg	Chapter V, pPR3-N – PalH
NFF	nnnnnnnnggccattacggccatgtccgtcaattcctttac	Chapter V, pPR3-N – PalF
NFR	nnnnnnnnggccgaggcggccgtcgctggtaacgcggtaat	Chapter V, pPR3-N – PalF
NIR	nnnnnnnnggccgaggcggccgtggcaaagggtatcgtg	Chapter V, pPR3-N – PalI
PalHF1	atgggggatgatgctcgt	Chapter V
PalHF2	tcattccgggtcgctgag	Chapter V
PalHF3	tacctacatacgatgggt	Chapter V
PalHF4	tatgagacaggtcagctg	Chapter V
PalHF5	gccgctccgtggagcata	Chapter V
PalHR1	tcatgtgtcgtctcgact	Chapter V

PalHR2	aagcatctgcgtcgcgtt	Chapter V
PalHR3	gacgtcgcacatcggaac	Chapter V
PalHR4	gaacagcacacaaggata	Chapter V
PalHR5	acggccttccacccaacgc	Chapter V
PalIF1	atgttactcaagcctgca	Chapter V
PalIF2	ttccctccttgccttctt	Chapter V
PalIF3	tgatattcctgcgccaga	Chapter V
PalIF4	tctacaggcctcaatcct	Chapter V
PalIF5	catgctcttggagaaaat	Chapter V
PalIR1	tcatggcaaagggtatcg	Chapter V
PalIR2	agcatgcgaggctgtatg	Chapter V
PalIR3	cgtagttgtaggcatcat	Chapter V
PalIR4	gtggccgcgtgcagcata	Chapter V
PalIR5	aaaagaagaatgtccacc	Chapter V
PalFF1	atgtccgtcaattccttt	Chapter V
PalFF2	atccacactcaccaaacc	Chapter V
PalFF3	ttatcgtcacgttatacc	Chapter V
PalFF4	gaaaagggagttgtagct	Chapter V
PalFF5	gagtcggtgcagactgta	Chapter V
PalFR1	ccgcgttaccagcgataa	Chapter V
PalFR2	ccgctcagcactaccaat	Chapter V
PalFR3	tgtctttcctacgattac	Chapter V
PalFR4	tagtccggcccccagtaat	Chapter V
PalFR4	agaacacagtgccttcgg	Chapter V
pPR3-NF	gtcgaaaattcaagacaagg	Chapter VI
pPR3-NR	aagcgtgacataactaattac	Chapter VI
UraNot2F	nnnnnngcggccgcagcttttcaattcaatt	Chapter VII
UraNot2R	nnnnnngcggccgcagctttttctttcc	Chapter VII
UraF1	ttccatggagggcacag	Chapter VII
UraF2	ctgacattattattgttgg	Chapter VII
UraR1	gcttttcgtgcatgatat	Chapter VII
UraR2	aaaggcctctaggttcct	Chapter VII
FireflyF1	atggaagacgccaaaaaca	Chapter VIII
FireflyR1	gcaggttacaatttgg	Chapter VIII
FireflyR2	ggttacaatttggactttccgc	Chapter VIII
FireflyF2	cccgcgaacgacatttataa	Chapter VIII
FireflyR3	aatatcgattccaattcagcg	Chapter VIII
pSK379F1	catattttcctgctctcccca	Chapter VIII
pSK379R1	aaccgtctagccgttgcaca	Chapter VIII

LucSBF	gtaactacgctcaacgtgtt	Chapter VIII
LucSBR	gaaagctgtcggtatcattc	Chapter VIII

Table AB.1: Oligonucleotides used in this study.

APPENDIX C

PLASMIDS FOR THE SPLIT-UBIQUITIN MYTH SYSTEM

Vector	Auxotrophic Marker (yeast)	Origin of replication (yeast)	Resistance Marker (*E. coli*)	Origin of replication (*E. coli*)	Reference
pBT3-SUC	*LEU2*	CEN/ARS (1-2 copies/ cell)	Kan (select with 30 µg/ml kanamycin)	High copy	Chapter V,VI
pBT3-STE	*LEU2*	CEN/ARS (1-2 copies/cell)	Kan (select with 30 µg/ml kanamycin)	High copy	Chapter V,VI
pBT3-N	*LEU2*	CEN/ARS (1-2 copies/cell)	Kan (select with 30 µg/ml kanamycin)	High copy	Chapter V,VI
pPR3-SUC	*TRP1*	2micron (20-50 copies/cell)	Amp (select with 100 µg/ml ampicillin)	High copy	Chapter V,VI
pPR3-STE	*TRP1*	2micron (20-50 copies/cell)	Amp (select with 100 µg/ml ampicillin)	High copy	Chapter V,VI
pCCW-Alg5	*LEU2*	CEN/ARS (1-2 copies/ cell)	Kan (select with 30 µg/ml kanamycin)	High copy	Chapter V,VI
pAL-Alg5	*TRP1*	2micron (20-50 copies/cell)	Amp (select with 100 µg/ml ampicillin)	High copy	Chapter V,VI
pDl-Alg5	*TRP1*	2micron (20-50 copies/cell)	Amp (select with 100 µg/ml ampicillin)	High copy	Chapter V,VI

Table AC.1: Plasmids used in this study for the split-ubiquitin MYTH system.

pBT3-SUC. The bait vector pBT3-SUC (Figure AC.1) is specifically designed for type I integral membrane proteins, which have a single TMD, an N-terminal cleavable signal sequence and topology with $N_{out}/C_{in.}$ The vector supplies a yeast signal sequence derived from the SUC2 (invertase) gene of *S. cerevisiae*. The Cub-LexA-VP16 cassette is fused to the cytosolic C-terminus of the protein of interest.

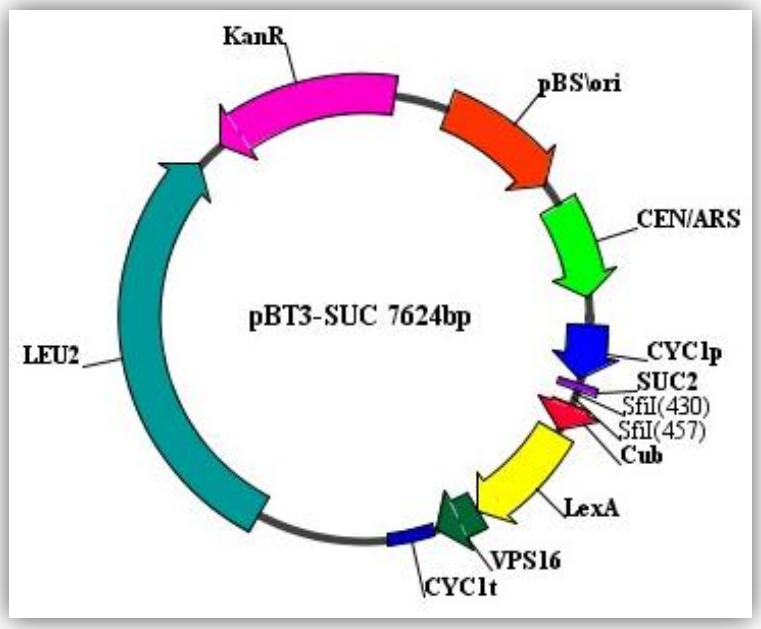


Fig. AC.1: pBT3-SUC. This vector contains a yeast signal sequence derived from the *SUC2* (invertase) gene of *S. cerevisiae*. The Cub-LexA-VP16 cassette is fused to the cytosolic C-terminus of the protein of interest. Map generated by DNADynamo, www.bluetractorsoftware.co.uk.

pBT3-STE. The vector pBT3-STE (Figure AC.2) is recommended for multispan integral membrane proteins (i.e. those having multiple transmembrane domains) with a N_{out}/C_{in} topology, because it contains the STE2 leader sequence derived from the *S. cerevisiae* Ste2 protein (a G protein coupled receptor). It does not have any targeting function but only serves as a short leader sequence to optimize expression of the desired bait. The Cub-LexA-VP16 cassette is fused to the C-terminus of the bait.

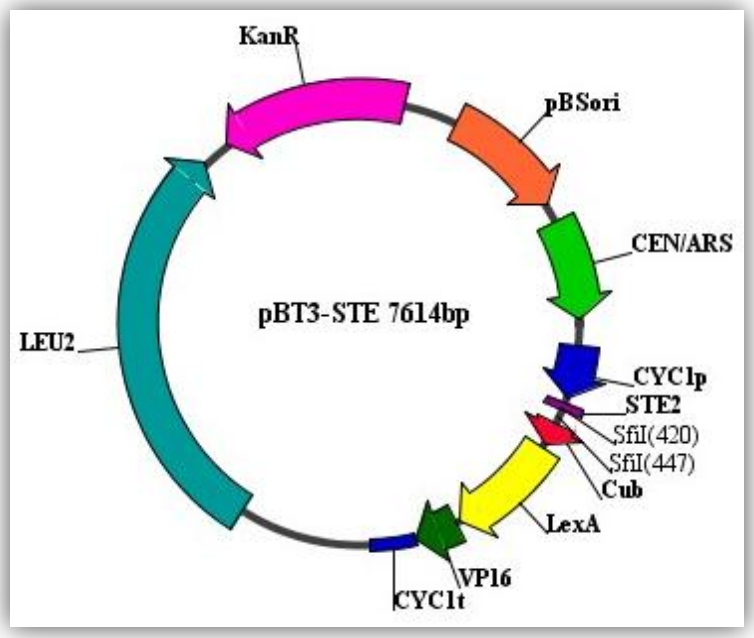


Fig. AC.2 pBT3-STE. The STE2 leader sequence contained in this plasmid derives from the *S. cerevisiae* STE2p. It does not have any targeting function but only serves as a short leader sequence to increase the expression of the protein of interest. The Cub-LexA-VP16 cassette is fused to the C-terminus of the bait. Map generated by DNADynamo, www.bluetractorsoftware.co.uk.

pBT3-N. On the other hand, if the protein has a lumenal C-terminus, the use of pBT3-N (Figure AC.3) is recommended to fuse the LexA-VP16-Cub module to the cytosolic N-terminus of the protein of interest.

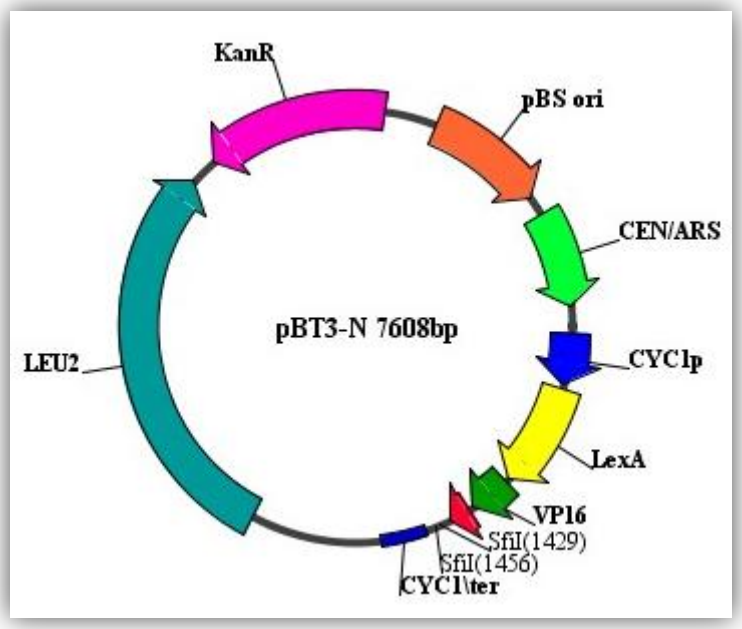


Fig. AC.3: pBT3-N. This vector fuses the LexA-VP16-Cub module to the cytosolic N-terminus of the protein of interest. Maps generated by DNADynamo, www.bluetractorsoftware.co.uk.

pPR3-N. Preys and cDNA libraries can be constructed in an orientation expressing fusion proteins with N-terminal NubG using the vector pPR3-N (Figure AC.4).

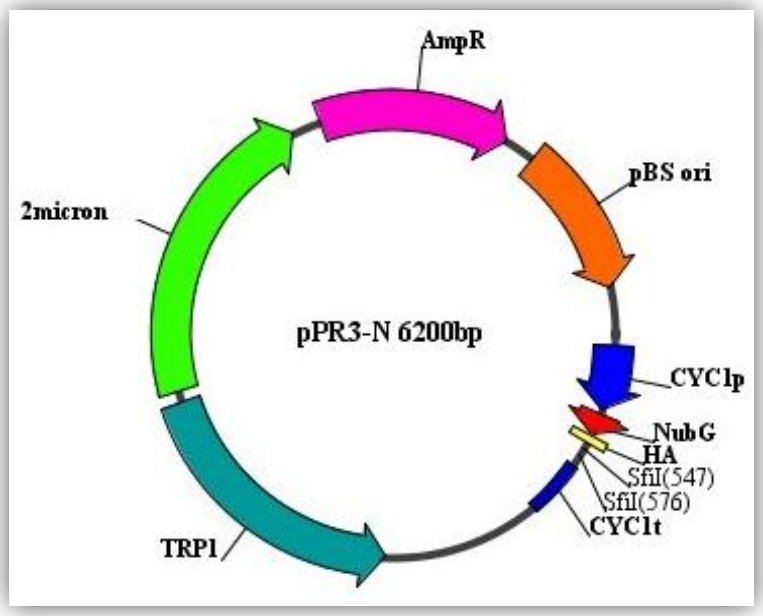


Fig. AC.4: pPR3-N. This vector fuses the NubG domain to the cytosolic N-terminus of the protein of interest. Map generated by DNADynamo, www.bluetractorsoftware.co.uk**.**

pPR3-STE. Preys and cDNA libraries can be constructed in an orientation expressing fusion proteins with C-terminal NubG using the vector pPR3-STE (Figure AC.5).

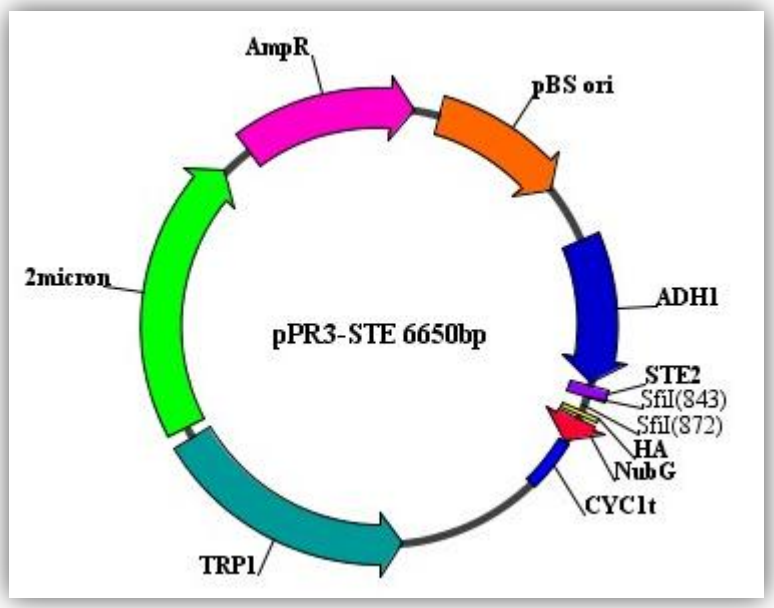


Fig. AC.5: pPR3-STE. As previously described the STE2 leader sequence from the *S. cerevisiae* STE2p does not have any targeting function but only serves to increase the expression of the protein of interest. The NubG domain is fused to the C-terminus of the bait. Map generated by DNADynamo, www.bluetractorsoftware.co.uk.

pCCW-Alg5. The plasmid pCCW-Alg5 (Figure AC.6) has been used as a control bait and expresses a fusion of the yeast ER protein Alg5 to the Cub-LexA-Vp16 cassette.

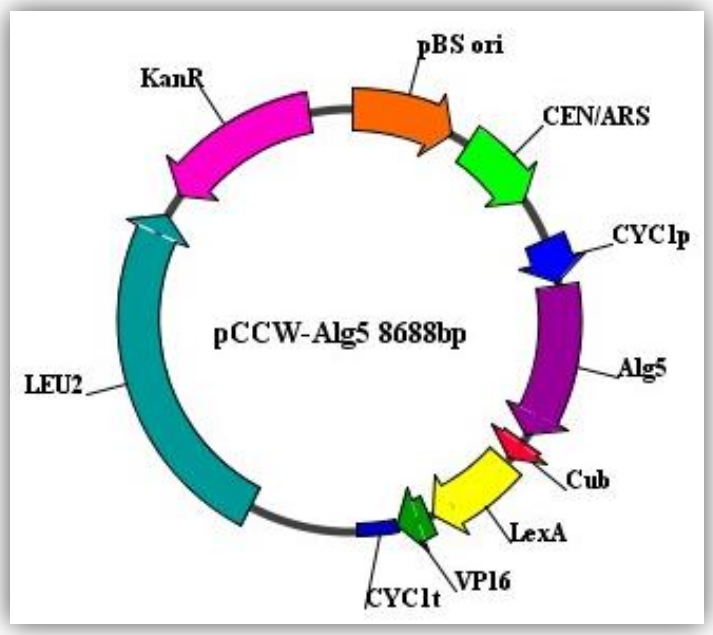


Fig. AC.6: pCCW-Alg5. The plasmid is the control bait expressing a fusion of the yeast ER protein Alg5 to the Cub-LexA-Vp16 cassette. Map generated by DNADynamo, www.bluetractorsoftware.co.uk.

pAL-Alg5. The plasmid pAL-Alg5 (Figure AC.7) has been used as a control prey and expresses a fusion of the yeast ER protein Alg5 to the wild type Nub portion of the yeast ubiquitin.

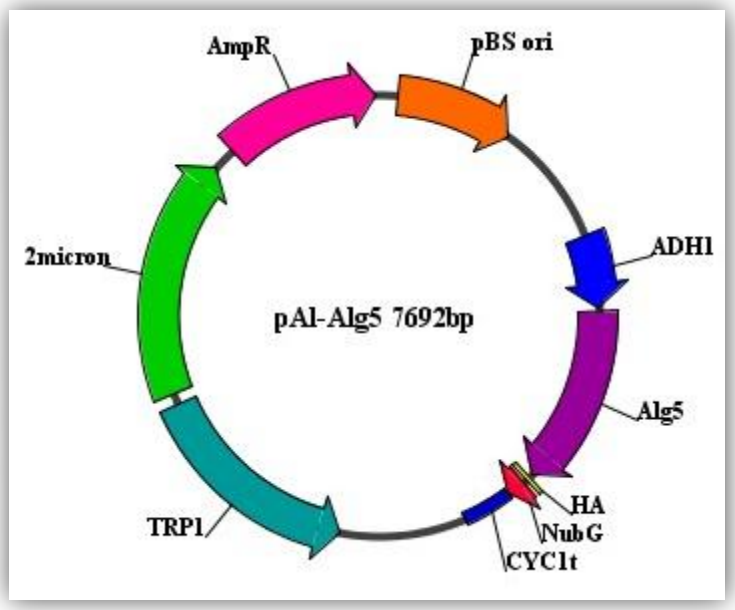


Fig. AC.7: pAL-Alg5. The plasmid is one of the control preys and expresses a fusion of the yeast ER protein Alg5 to the wild type Nub portion of the yeast ubiquitin. Map generated by DNADynamo, www.bluetractorsoftware.co.uk.

pDL-Alg5. The plasmid pDL-Alg5 (Figure AC.8) has been used as a control prey and expresses a fusion of the yeast ER protein Alg5 to the mutated Nub portion of the yeast ubiquitin.

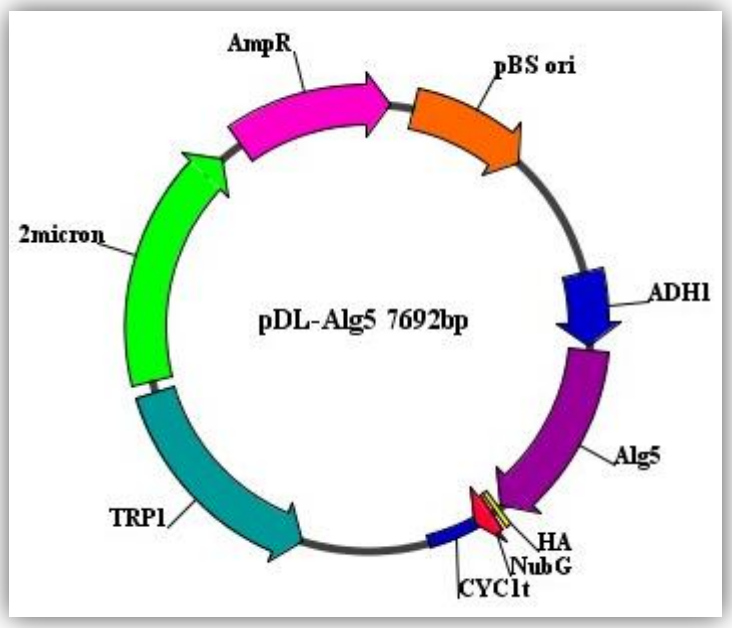


Fig. AC.8: pDL-Alg5. The plasmid is one of the control preys and expresses a fusion of the yeast ER protein Alg5 to the mutated Nub portion of the yeast ubiquitin. Map generated by DNADynamo, www.bluetractorsoftware.co.uk.

APPENDIX D

LIST OF GENES DIFFERENTIALLY EXPRESSED IN THE MICROARRAY DATASETS

The tables listed in this appendix are contained on the Supplementary Data CD attached, which also include the complete heat maps for the differentially expressed genes in the ATCC46645 time course, in the ATCC46645 Δ*pacC* time course and in the ATCC46645 Δ*pacC*/ATCC46645 dataset. Genes shown in red were up-regulated; genes shown in green were down-regulated. Black boxes represent the cases where the gene is not differentially expressed or has not been detected. Each column corresponds to a time point versus the reference. Analysis was performed using Genespring GX 11.02. The Supplementary Data CD also includes the file reporting the extended GO annotation for STEM analysis described in Chapter IV.

AD.1 *A. fumigatus* ATCC46645 transcript profile during initiation of murine infection

Table AD.1.1: List of up-regulated genes in the ATCC46645 time course. Genes significantly up-regulated were included if showing a fold change of +2 on a $\log_2$ scale at least in one of the time point datasets. T0 vs T4 = 4 hrs, T0 vs T8 hrs = 8 hrs, T0 vs T16 = 16 hrs.

Table AD.1.2: 30 ORFs with the highest $\log_2$ values between the up-regulated genes unique to the 4 hrs time point of the ATCC46645 time course.

Table AD.1.3: 30 ORFs with the highest $\log_2$ values between the up-regulated genes unique to the 8 hrs time point of the ATCC46645 time course.

Table AD.1.4: 30 ORFs with the highest $\log_2$ values between the up-regulated genes unique to the 16 hrs time point of the ATCC46645 time course.

Table AD.1.5: List of down-regulated genes in the ATCC46645 time course. Genes significantly down-regulated were included if showing a fold change of -2 on a $\log_2$ scale at least in one of the time point datasets. T0 vs T4 = 4 hrs, T0 vs T8 hrs = 8 hrs, T0 vs T16 = 16 hrs.

Table AD.1.6: 30 ORFs with the lowest $\log_2$ values between the down-regulated genes unique to the 4 hrs time point of the ATCC46645 time course.

Table AD.1.7: 30 ORFs with the lowest log_2 values between the down-regulated genes unique to the 8 hrs time point of the ATCC46645 time course.

Table AD.1.8: 30 ORFs with the lowest log_2 values between the down-regulated genes unique to the 16 hrs time point of the ATCC46645 time course.

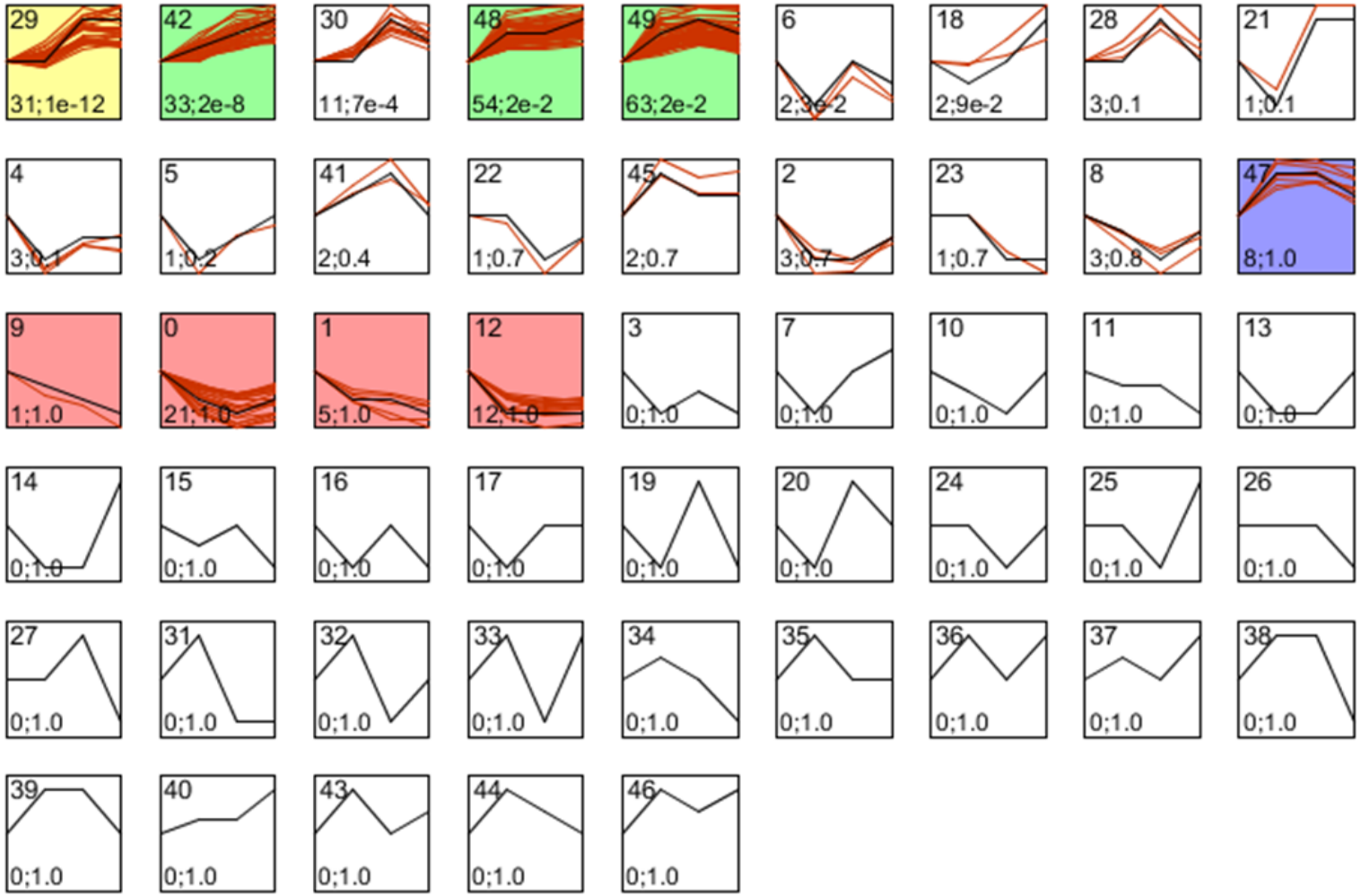


Fig. AD.1.1: STEM clustering analysis of the differentially expressed genes in the ATCC46645 time course during initiation of murine infection ordered on the basis of the Af293 infection clusters (McDonagh *et al.*, 2008a). The two values at the bottom of each profile indicate the number of specific genes (in this case genes previously identified in the Af293 infection clusters) present in the profile and the significance of the intersect size, based upon the hypergeometric distribution of dataset genes in the respective model profiles.

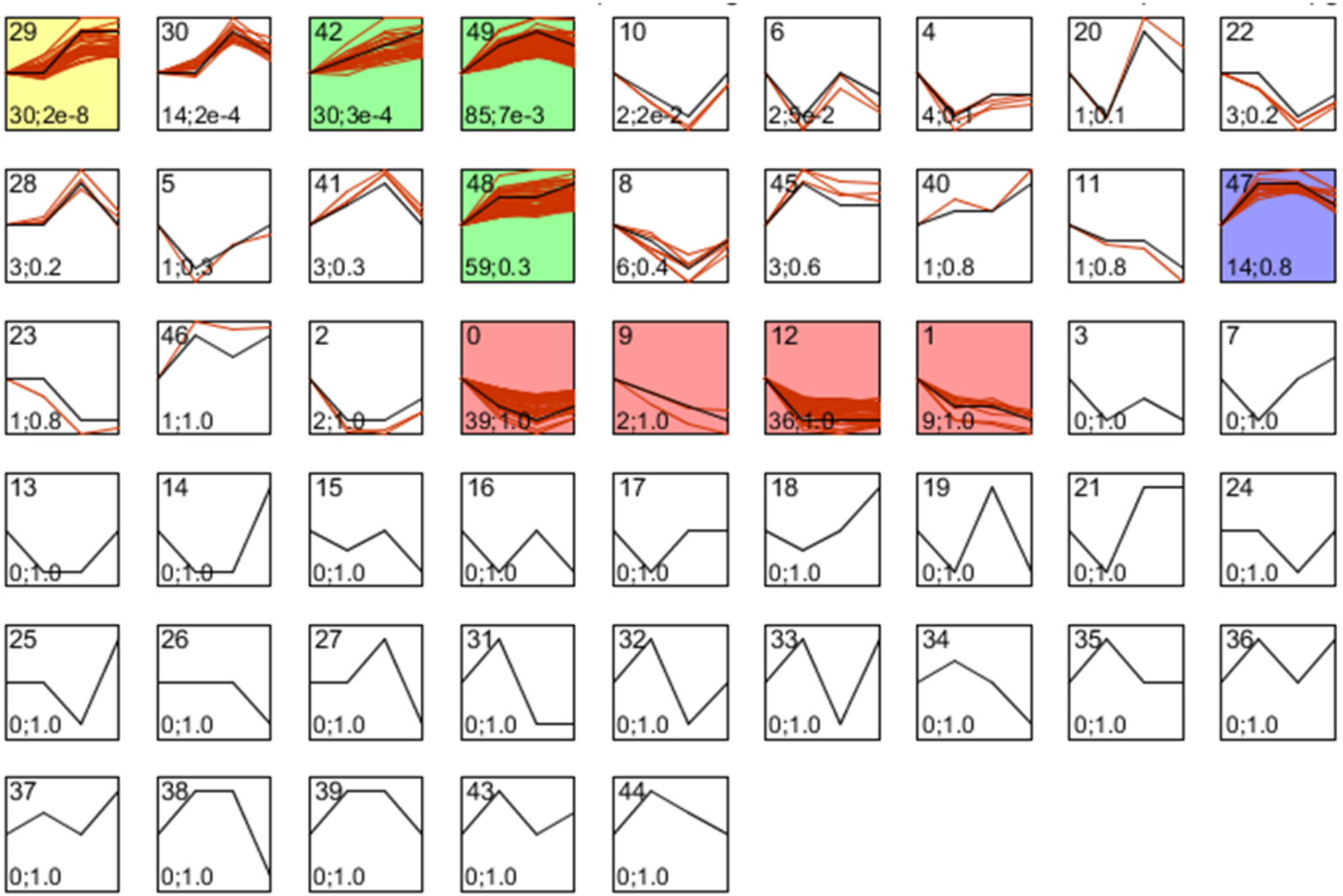


Fig. AD.1.2: STEM clustering analysis of the differentially expressed genes in the ATCC46645 time course during initiation of murine infection ordered on the basis of the subtelomeric location (McDonagh *et al.*, 2008a). The two values at the bottom of each profile indicate how many specific genes (in this case genes with subtelomeric location) are present in the profile and the significance of the intersect size, based upon the hypergeometric distribution of dataset genes in the respective model profiles.

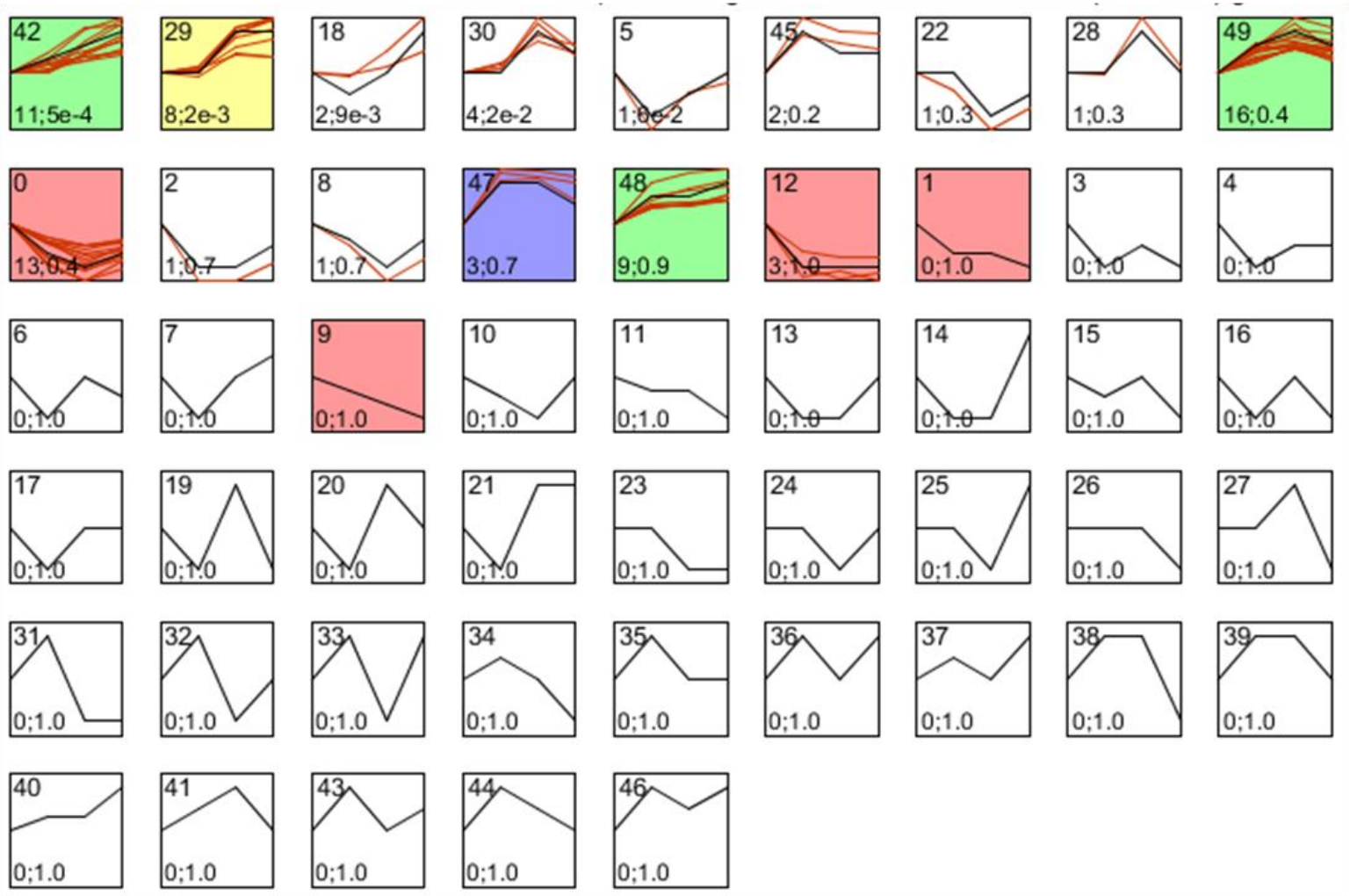


Fig. AD.1.3: STEM clustering analysis of the differentially expressed genes in the ATCC46645 time course during initiation of murine infection ordered on the basis of the involvement on secondary metabolite production (Perrin *et al.*, 2007). The two values at the bottom of each profile indicate how many specific genes (in this case genes involved on secondary metabolite production) are present in the profile and the significance of the intersect size, based upon the hypergeometric distribution of dataset genes in the respective model profiles.

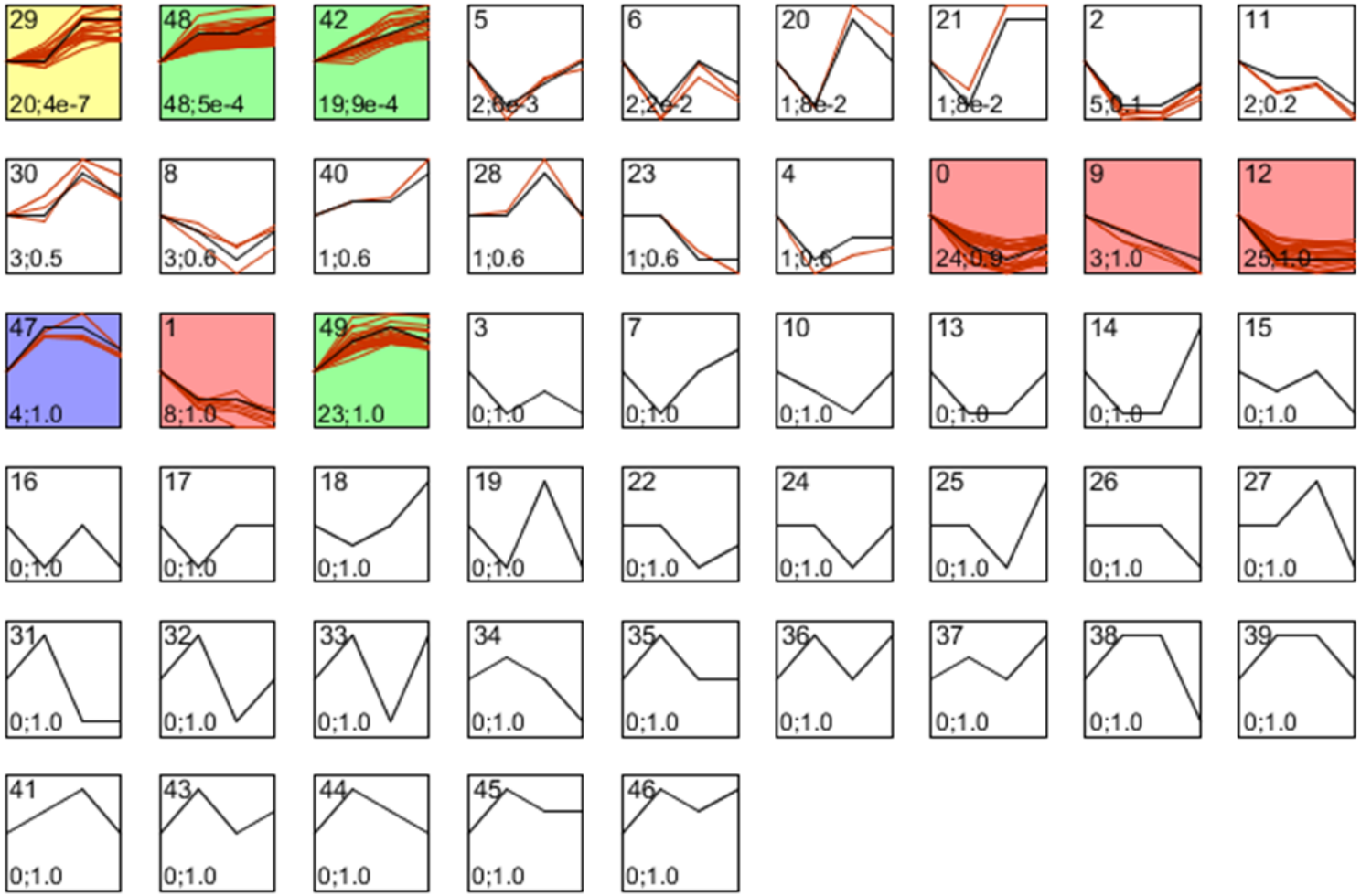


Fig. AD.1.4: STEM clustering analysis of the differentially expressed genes in the ATCC46645 time course during initiation of murine infection ordered on the basis of the *in vitro* up-regulated genes in response to an alkaline pH shift (Loss, unpublished). The two values at the bottom of each profile indicate how many specific genes (in this case up-regulated genes in response to an alkaline pH shift) are present in the profile and the significance of the intersect size, based upon the hypergeometric distribution of dataset genes in the respective model profiles.

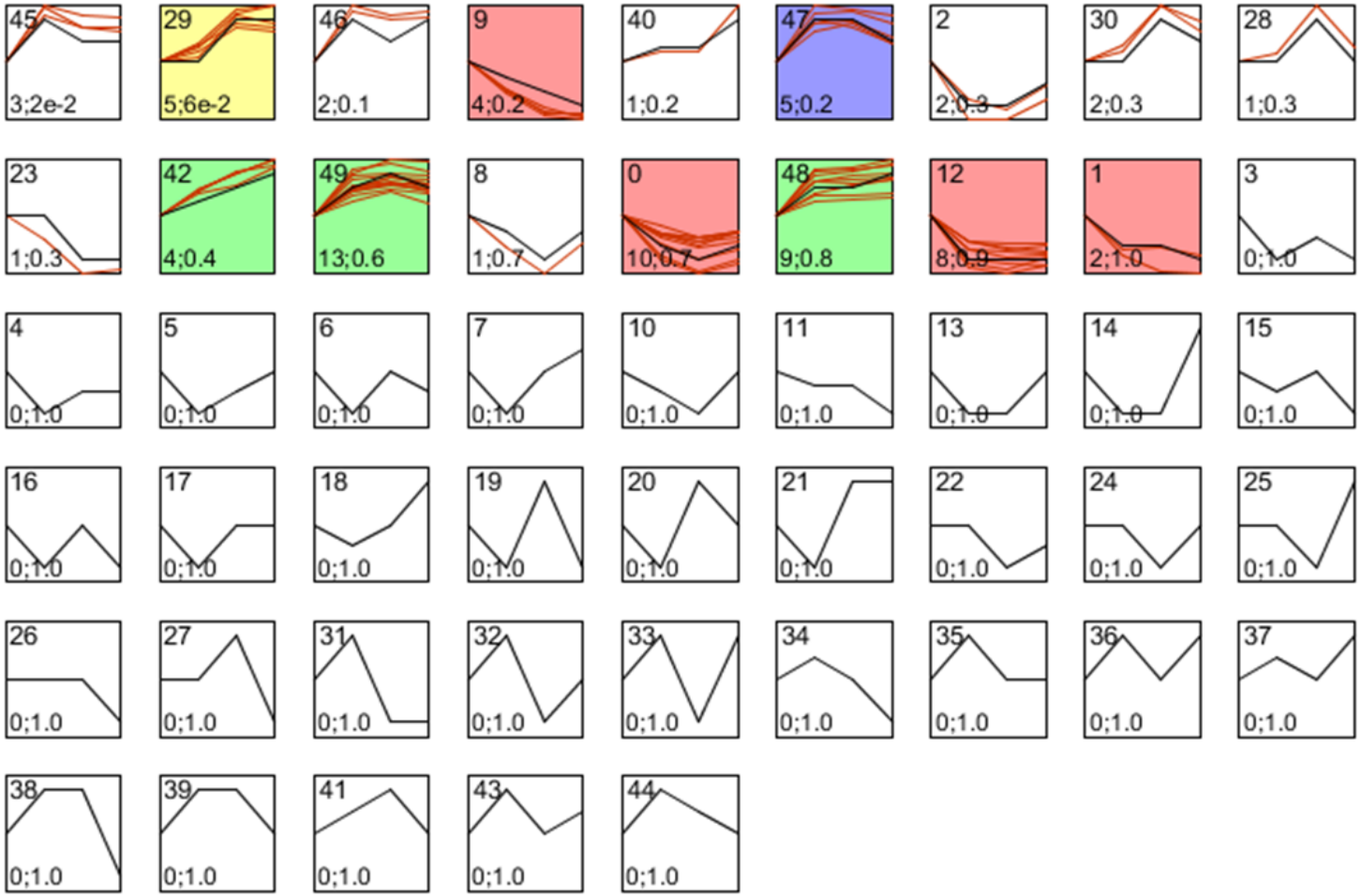


Fig. AD.1.5: STEM clustering analysis of the differentially expressed genes in the ATCC46645 time course during initiation of murine infection ordered on the basis of the *in vitro* down-regulated genes in response to an alkaline pH shift (Loss, unpublished). The two values at the bottom of each profile indicate how many specific genes (in this case down-regulated genes in response to an alkaline pH shift) are present in the profile and the significance of the intersect size, based upon the hypergeometric distribution of dataset genes in the respective model profiles.

AD.2 *A. fumigatus* ATCC46645 Δ*pacC* mutant transcript profile during initiation of murine infection

Table AD.2.1: List of up-regulated genes in the ATCC46645 Δ*pacC* time course. Genes significantly up-regulated were included if showing a fold change of +2 on a $\log_2$ scale at least in one of the time point datasets. T0 vs T4 = 4 hrs, T0 vs T8 hrs = 8 hrs, T0 vs T16 = 16 hrs.

Table AD.2.2 30 ORFs having the highest $\log_2$ among up-regulated genes unique to the 4 hrs time point of the ATCC46645 Δ*pacC* time course.

Table AD.2.3: 30 ORFs with the highest $\log_2$ values between the up-regulated genes unique to the 8 hrs time point of the ATCC46645 Δ*pacC* time course.

Table AD.2.4: 30 ORFs with the highest $\log_2$ values among up-regulated genes unique to the 16 hrs time point of the ATCC46645 Δ*pacC* time course.

Table AD.2.5: List of down-regulated genes in the ATCC46645 Δ*pacC* time course. Genes significantly down-regulated were included if showing a fold change of -2 on a $\log_2$ scale at least in one of the time point datasets. T0 vs T4 = 4 hrs, T0 vs T8 hrs = 8 hrs, T0 vs T16 = 16 hrs.

Table AD.2.6: 30 ORFs with the lowest $\log_2$ values among down-regulated genes unique to the 4 hrs time point of the ATCC46645 Δ*pacC* time course.

Table AD.2.7: 30 ORFs with the lowest $\log_2$ values among down-regulated genes unique to the 8 hrs time point of the ATCC46645 Δ*pacC* time course.

Table AD.2.8: 30 ORFs with the lowest $\log_2$ values between the down-regulated genes unique to the 16 hrs time point of the ATCC46645 Δ*pacC* time course.

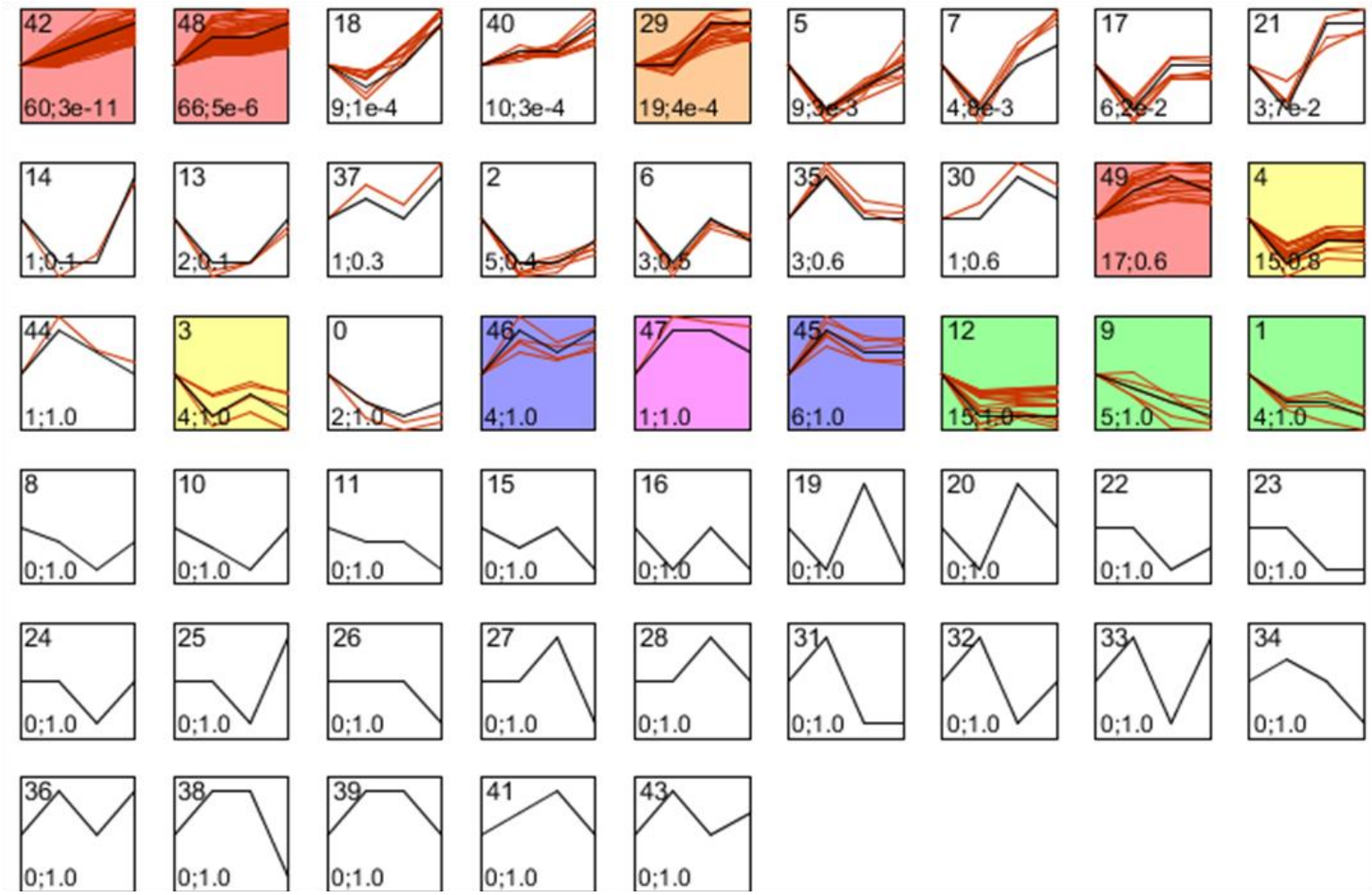


Fig. AD.2.1: STEM clustering analysis of the differentially expressed genes in the ATCC46645 Δ*pacC* time course during initiation of murine infection ordered on the basis of the Af293 infection clusters (McDonagh *et al.*, 2008a). The two values at the bottom of each profile indicate the number of specific genes (in this case genes previously identified in the Af293 infection clusters) present in the profile and the significance of the intersect size, based upon the hypergeometric distribution of dataset genes in the respective model profiles.

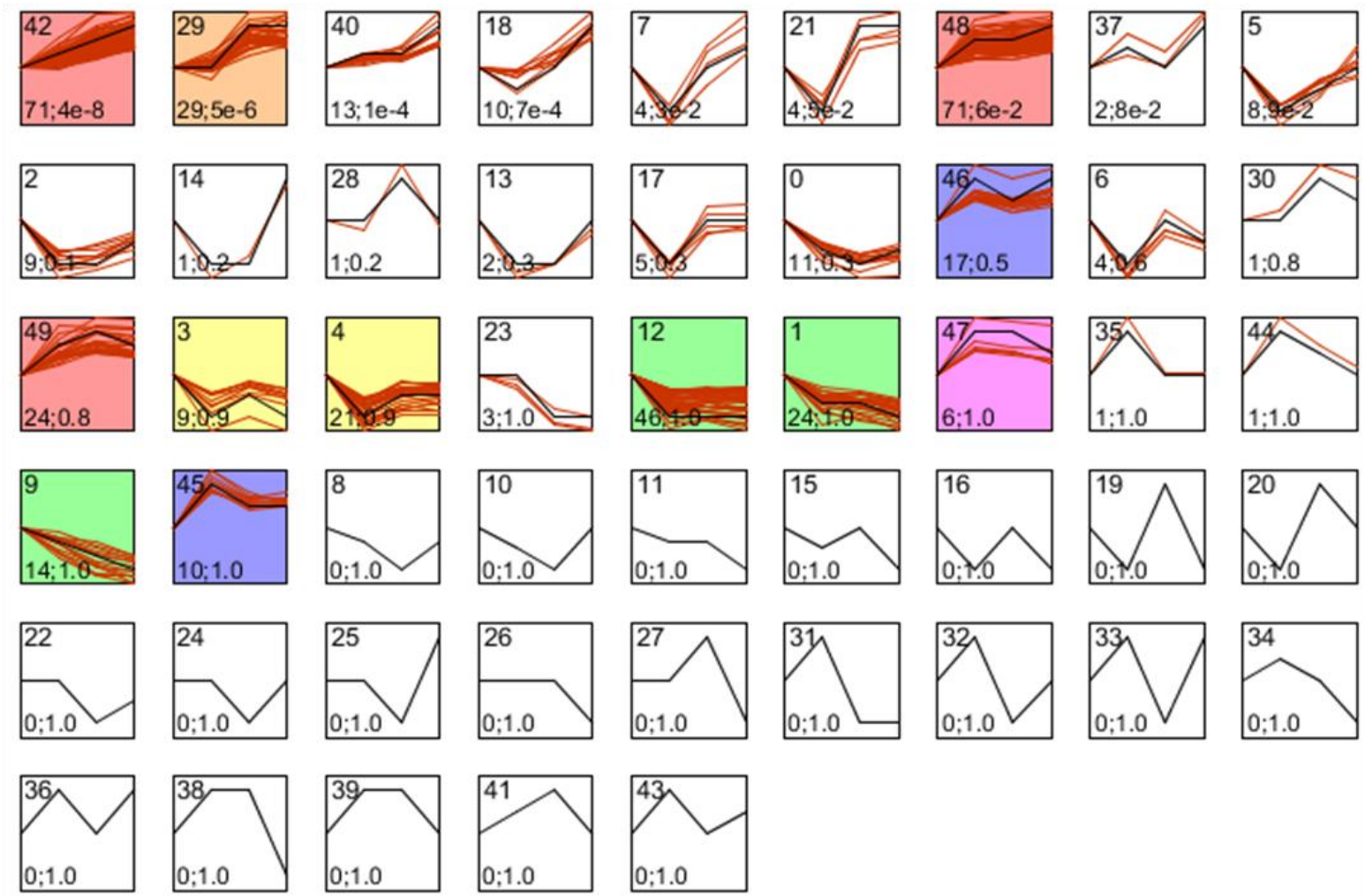


Fig. AD.2.2: STEM clustering analysis of the differentially expressed genes in the ATCC46645 Δ*pacC* time course during initiation of murine infection ordered on the basis of the subtelomeric location (McDonagh *et al.*, 2008a). The two values at the bottom of each profile indicate how many specific genes (in this case genes with subtelomeric location) are present in the profile and the significance of the intersect size, based upon the hypergeometric distribution of dataset genes in the respective model profiles.

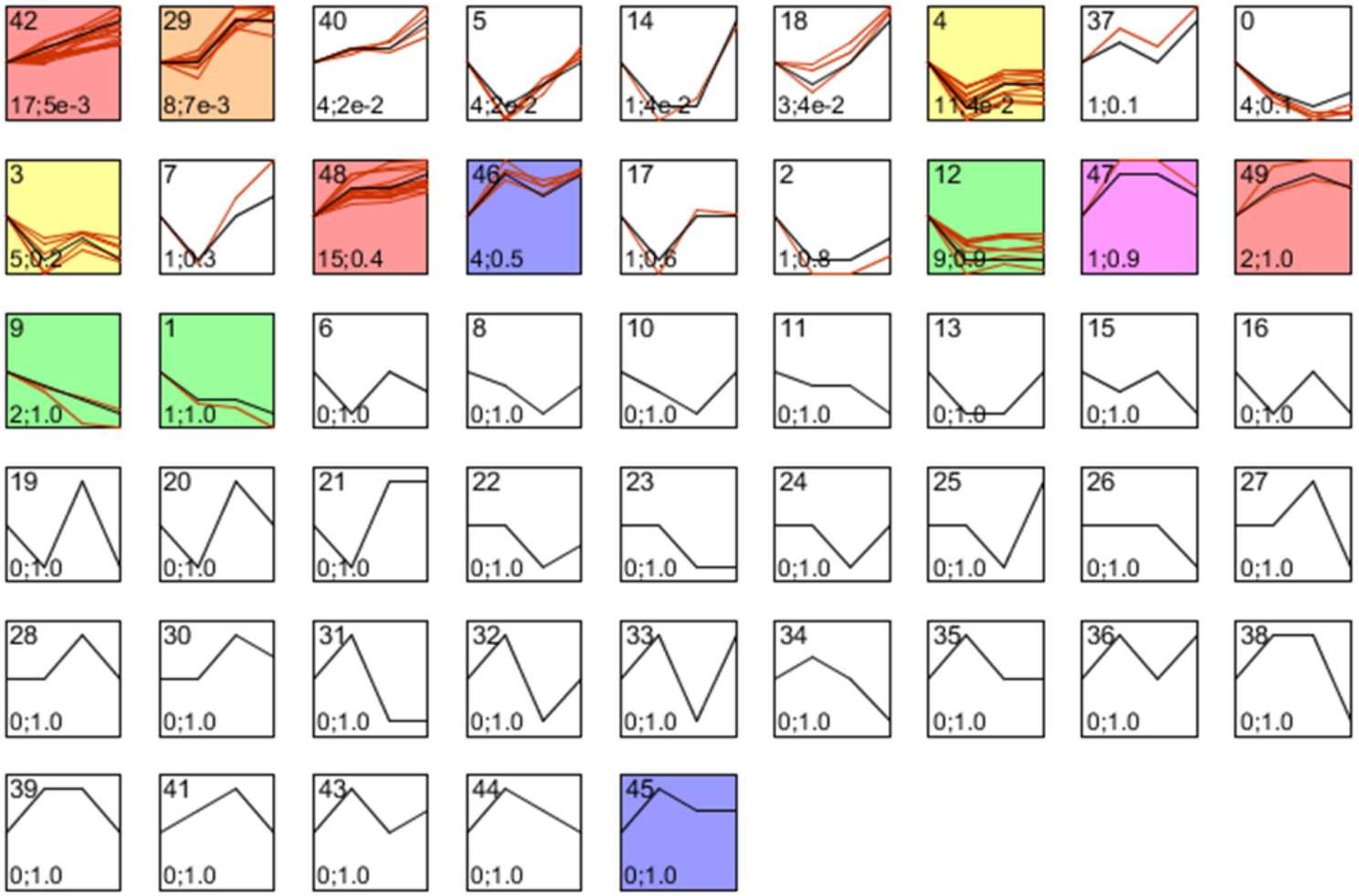


Fig. AD.2.3: STEM clustering analysis of the differentially expressed genes in the ATCC46645 Δ*pacC* time course during initiation of murine infection ordered on the basis of the involvement on secondary metabolite production (Perrin *et al.*, 2007). The two values at the bottom of each profile indicate how many specific genes (in this case genes involved on secondary metabolite production) are present in the profile and the significance of the intersect size, based upon the hypergeometric distribution of dataset genes in the respective model profiles.

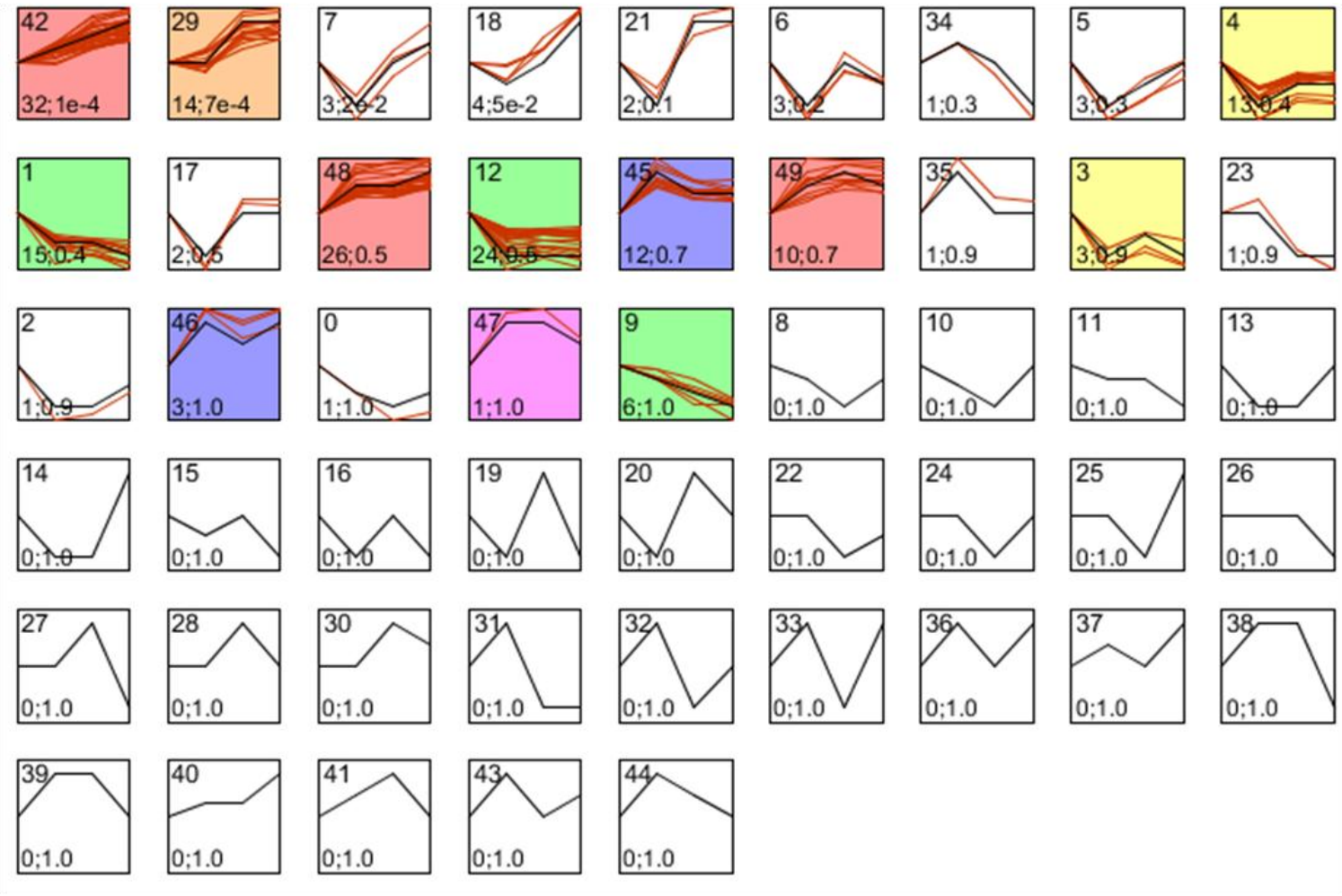


Fig. AD.2.4: STEM clustering analysis of the differentially expressed genes in the ATCC46645 Δ*pacC* time course during initiation of murine infection ordered on the basis of the *in vitro* up-regulated genes in response to an alkaline pH shift (Loss, unpublished). The two values at the bottom of each profile indicate how many specific genes (in this case up-regulated genes in response to an alkaline pH shift) are present in the profile and the significance of the intersect size, based upon the hypergeometric distribution of dataset genes in the respective model profiles.

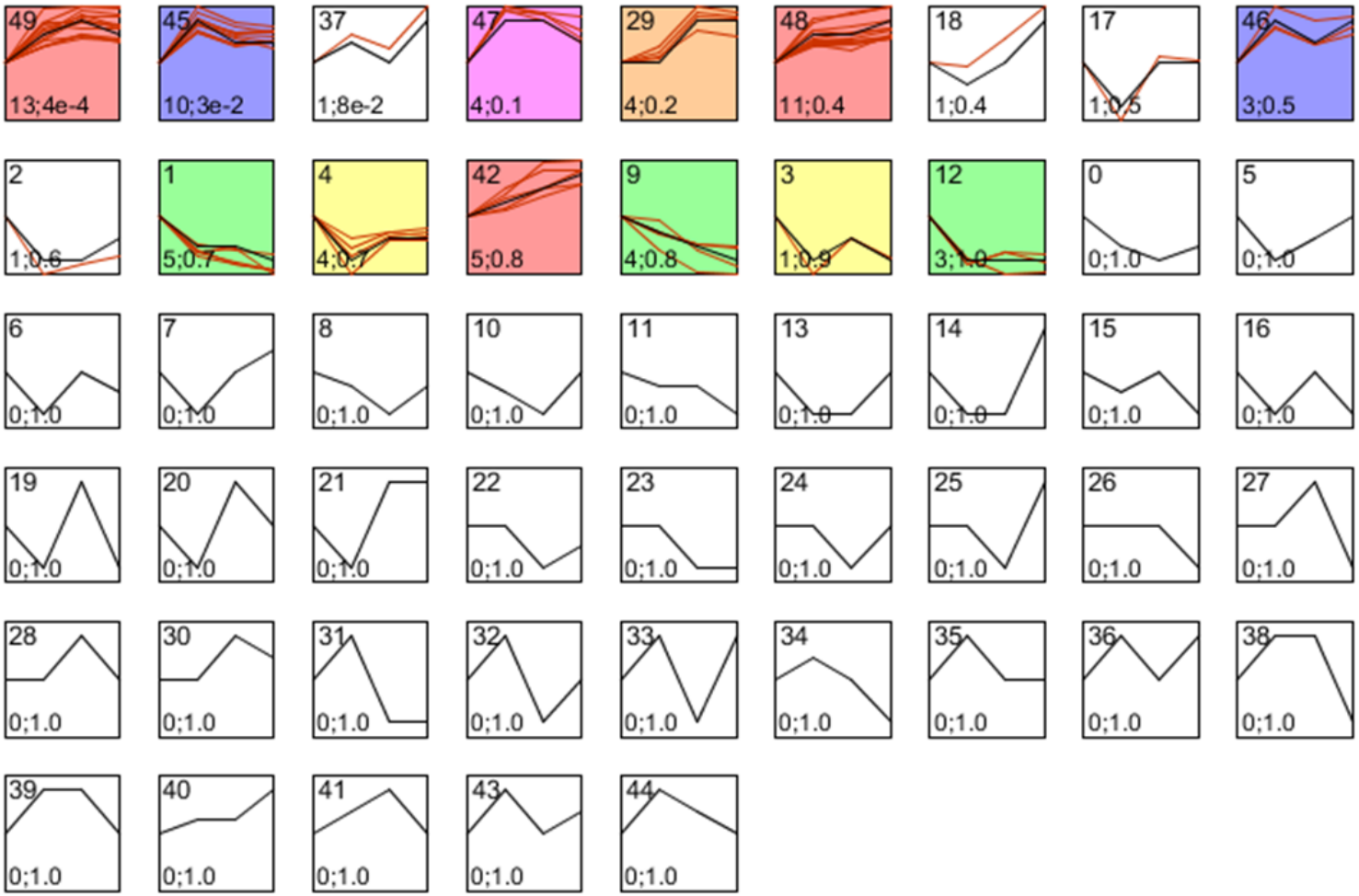


Fig. AD.2.5: STEM clustering analysis of the differentially expressed genes in the ATCC46645 Δ*pacC* time course during initiation of murine infection ordered on the basis of the *in vitro* down-regulated genes in response to an alkaline pH shift (Loss, unpublished). The two values at the bottom of each profile indicate how many specific genes (in this case down-regulated genes in response to an alkaline pH shift) are present in the profile and the significance of the intersect size, based upon the hypergeometric distribution of dataset genes in the respective model profiles.

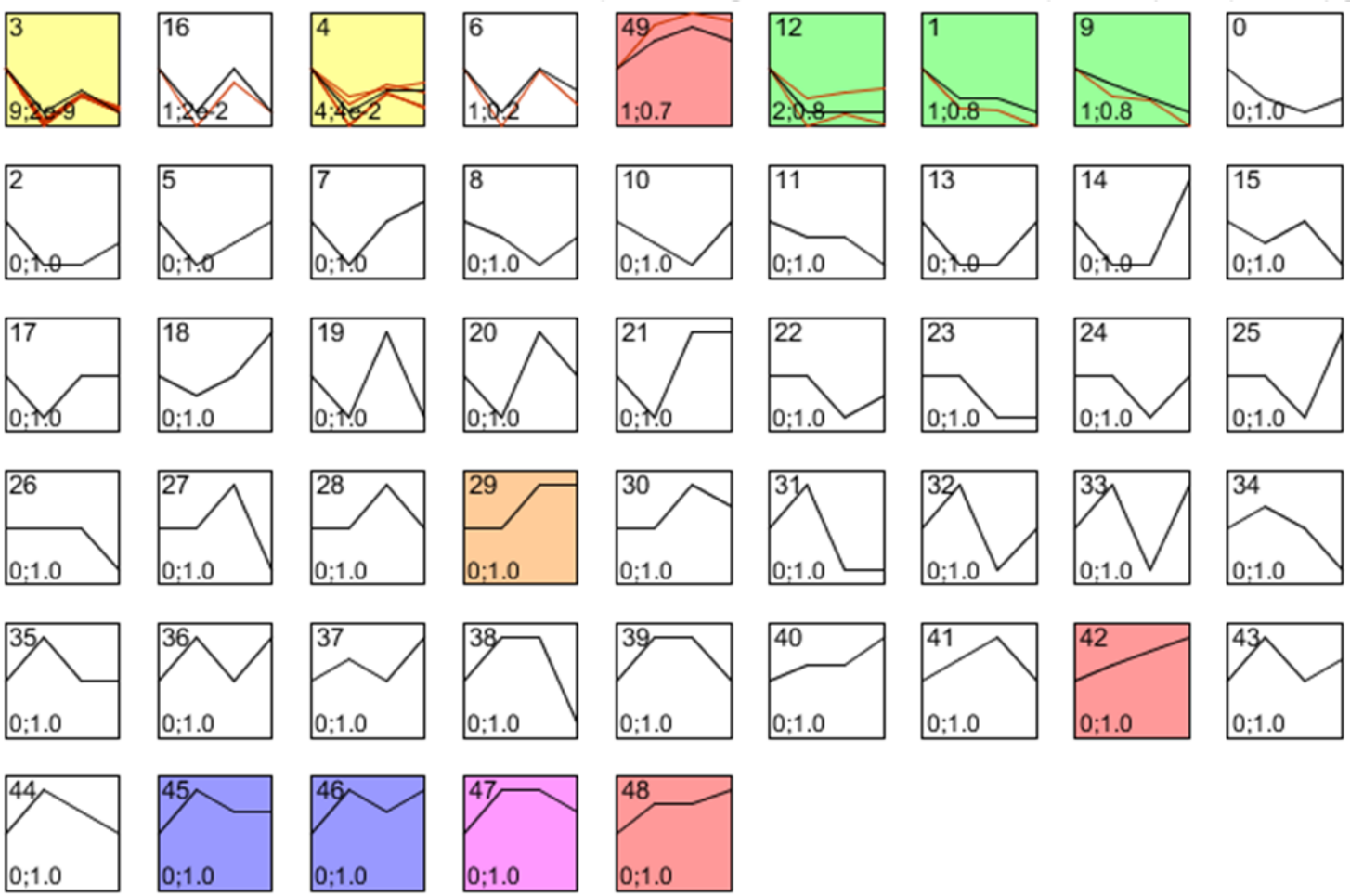


Fig. AD.2.6: STEM clustering analysis of the differentially expressed genes in the ATCC46645 Δ*pacC* time course during initiation of murine infection ordered on the basis of the involvement in transposition. The two values at the bottom of each profile indicate how many specific genes (in this case genes involved in transposition) are present in the profile and the significance of the intersect size, based upon the hypergeometric distribution of dataset genes in the respective model profiles.

AD.3 *A. fumigatus* ATCC46645 Δ*pacC*/ATCC46645 log_2 ratio comparison during initiation of murine infection

Table AD.3.1: List of up-regulated genes in the ATCC46645 Δ*pacC*/ATCC46645 dataset. Genes significantly up-regulated were included if showing a fold change of +1.5 on a log_2 scale at least in one of the time point datasets. T0 vs T4 = 4 hrs, T0 vs T8 hrs = 8 hrs, T0 vs T16 = 16 hrs.

Table AD.3.2: 30 ORFs with the highest log_2 values between the up-regulated genes unique to the 4 hrs time point of the ATCC46645 Δ*pacC*/ATCC46645 comparison.

Table AD.3.3: 23 up-regulated ORFs unique to the 8 hrs time point of the ATCC46645 Δ*pacC*/ATCC46645 comparison.

Table AD.3.4: 30 ORFs with the highest log_2 values between the up-regulated genes unique to the 16 hrs time point of the ATCC46645 Δ*pacC*/ATCC46645 comparison.

Table AD.3.5: List of down-regulated genes in the ATCC46645 Δ*pacC*/ATCC46645 dataset. Genes significantly down-regulated were included if showing a fold change of -1.5 on a log_2 scale at least in one of the time point datasets. T0 vs T4 = 4 hrs, T0 vs T8 hrs = 8 hrs, T0 vs T16 = 16 hrs.

Table AD.3.6: 30 ORFs with the lowest log_2 values between the down-regulated genes unique to the 4 hrs time point of the ATCC46645 Δ*pacC*/ATCC46645 comparison.

Table AD.3.7: 11 down-regulated ORFs unique to the 8 hrs time point of the ATCC46645 Δ*pacC*/ATCC46645 comparison.

Table AD.3.8 30 ORFs with the lowest log_2 values between the down-regulated genes unique to the 16 hrs time point of the ATCC46645 Δ*pacC*/ATCC46645 comparison.

APPENDIX E

OPTIMISATION OF THE SPLIT-UBIQUITIN MYTH SYSTEM USING PBT3-STE *A. NIDULANS* PALH BAIT

Initially, the optimisation of the split-ubiquitin MYTH system was performed using *A. nidulans* PalH as bait in the vector pBT3-STE and *A. nidulans* PalI as prey in the vectors pPR3-N and pPR3-STE. These vectors were kindly provided by Ana Maria Calcagno-Pizarelli (Herb Arst's Laboratory, Imperial College London).

As explained in the experimental procedure in CHAPTER V and VI, the sequence-verified constructs were transformed into the yeast strain provided, NMY51, for expression tests and control assays. The expression of the genes of interest was verified by western blotting analysis of total yeast extracts using an antibody directed against the LexA domain of the fusion protein for the baits and an antibody directed against the HA epitope of the fusion protein for the preys. As shown in Fig. AE.1, the expression of *A. nidulans* PalH as bait in the vector pBT3-STE was confirmed. Considering the size of *A. nidulans* PalH protein (83.7 KDa) and the size of the Cub-LexA-VP16 fusion (38 KDa) the size of the expected product was 121.7 KDa, whereas the positive control's size, derived from the yeast transformed with the plasmid pCCW-Alg5, was 77.5 KDa. The construct pCCW-Alg5, used as positive control for the detection of the LexA epitope, expresses a fusion of the yeast ER protein Alg5 to the wild type Cub portion of yeast ubiquitin. *A. nidulans* PalI was expressed as prey only when cloned in the orientation fusing the NubG domain at the C-terminal (pPR3-STE). The plasmid pPR3-N was used as positive control for the detection of the HA epitope. Considering the size of *A. nidulans* PalI protein (44.3 KDa) and the size of the NubG-HA fusion (7 KDa) the size of the expected product was 52.3 KDa, whereas the positive control size, derived from the yeast transformed with the plasmid pPR3-N, was 15 KDa.

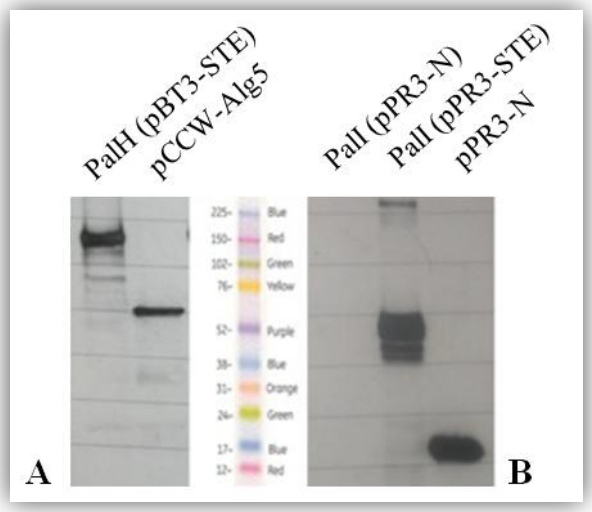


Fig. AE.1: Western blotting analysis to verify the expression of *A. nidulans* bait and preys. *A. nidulans* PalH bait (A) was expressed. (B) *A. nidulans* PalI as a prey was properly expressed only in the orientation fusing the NubG domain at the C-terminal (pPR3-STE).

According to the structure of the two prey vectors used for the expression of *A. nidulans* PalI as prey, the verification of preys expression by western blotting provided additional evidence of the presence in *A. nidulans* PalI of a signal peptide, as previously predicted (Calcagno-Pizarelli *et al.*, 2007) by SignalP 3.0 (Bendtsen *et al.*, 2004). Expression of *A. nidulans* bait was also verified using the control preys supplied with the kit. The control assay is an important step to determine whether the bait is functional in the assay and whether it displays any non-specific background. In order to assay the expression of *A. nidulans* PalH bait protein in yeast, the bait plasmid was co-transformed with the control plasmids pAI-Alg5 and pDL2-Alg5. The construct pAI-Alg5 expresses a fusion of the yeast ER protein Alg5 to the wild type Nub portion of yeast ubiquitin, whereas pDL2-Alg5 expresses a fusion of the same protein to the mutated Nub portion (NubG). Co-expression of the bait together with pAI-Alg5 should result in reconstitution of split-ubiquitin through the strong affinity of wild type Nub for Cub and the concurrent activation of the reporter genes, if the bait tested is properly inserted into the membrane of yeast and the Cub-LexAVP16 part is located on the cytosolic side of the membrane. Co-expression of the bait of interest together with pDL2-Alg5 should instead not lead to split-ubiquitin formation, because the mutated Nub has no affinity for Cub. Fig. AE.2 shows the result of this experiment for *A. nidulans* PalH bait indicating that this bait is appropriately localised in the membrane of yeast and the Cub-LexAVP16 part is located on the cytosolic side of the membrane. Transformation efficiency

is confirmed by the growth in SD-trp-leu media. Growth of yeast expressing the tested bait and the Alg5-NubI control in the selective media SD-trp-leu-his-ade signifies that *A. nidulans* PalH bait is functional in the DUALmembrane system. Co-expression of the baits together with pDL2-Alg5 should not activate the reporter genes, as the mutated NubG moiety has no affinity for Cub. In addition, if a bait and prey interact, as in the case of the co-transformation with *A. nidulans* with the positive control prey plasmid pAI-Alg5, the *ade2* reporter gene is activated and the adenine synthesis pathway is unblocked, leading to the disappearance of the red colour.

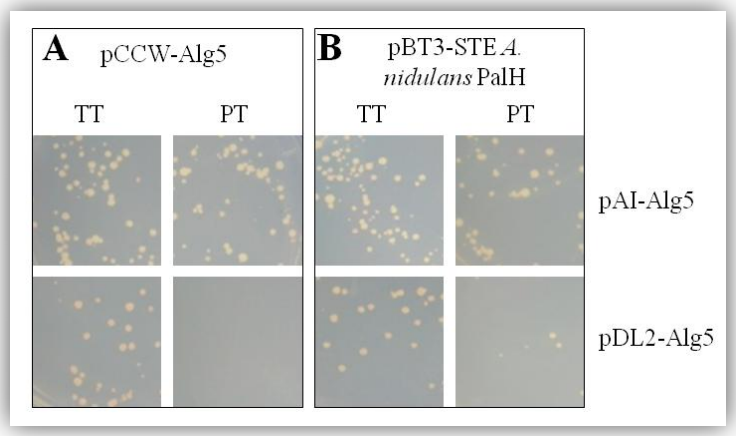


Fig. AE.2: Verification of the expression and functionality of *A. nidulans* PalH bait (pBT3-STE) by co-transformation with the control preys in yeast. The baits tested are (A) the positive control bait pCCW-Alg5 and (B) pBT3-STE *A. nidulans* PalH. Each of these baits was co-transformed with the positive control prey pAI-Alg5 and the negative control prey pDL2-Alg5 and for each co-transformation the total transformants (TT) in SD-leu-trp (indicative of the transformation efficiency) and the prototrophic transformants (PT) in SD-leu-trp-his-ade (indicative of interaction between bait and prey) are shown. With lack of interaction, yeast colonies turn pink during the incubation.

Appropriate expression of *A. nidulans* PalH bait and *A. nidulans* PalI and *A. fumigatus* PalF (see Chapter V) preys, as confirmed by the previous western blotting, provided an opportunity to further optimize the split-ubiquitin methodology. Having demonstrated the functionality of *A. nidulans* PalH bait, the direct interaction of *A. nidulans* PalI and *A. fumigatus* PalF preys was addressed by co-expression with *A. nidulans* PalH bait, using the same method described above, as shown in Fig. AE.3.

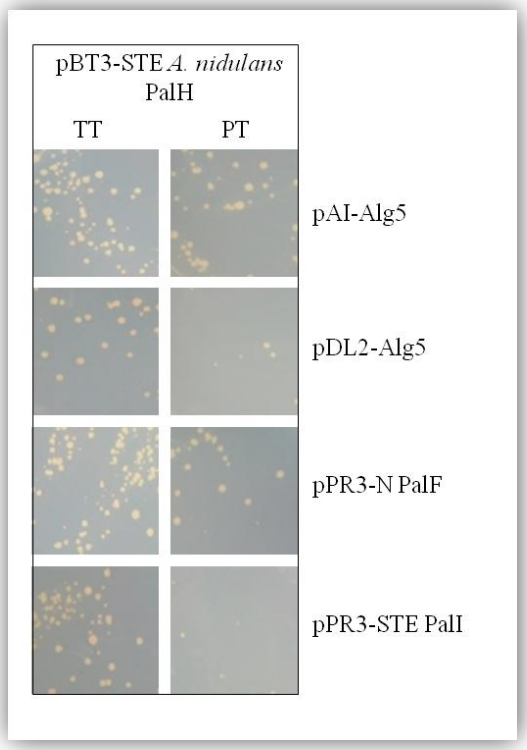


Fig. AE.3: Co-transformation of the expression-verified *A. nidulans* PalH pBT3-STE bait with *A. fumigatus* PalI pPR3-STE (A) and *A. fumigatus* PalF pPR3-N (B) preys to test direct interactions. For each co-transformation the total transformants (TT) in SD-leu-trp (indicative of the transformation efficiency) and the prototrophic transformants (PT) in SD-leu-trp-his-ade (indicative of interaction between bait and prey) are shown. With lack of interaction, yeast colonies turn pink during the incubation.

As demonstrated by the degree of growth on SD-trp-leu-his-ade media and by the colour of the transformant colonies, an interaction was detectable between *A. nidulans* PalH and *A. nidulans* PalI and between *A. nidulans* PalH and *A. fumigatus* PalF. However, only few colonies were obtained from the co-transformation with *A. nidulans* PalH and *A. nidulans* PalI and this might indicate the proteins are localised in close proximity in the plasma membrane signalling complex, but do not directly interact. Although the interaction between PalH and PalF has already been demonstrated in *A. nidulans* (Herranz *et al.*, 2005), this co-transformation experiment confirmed interaction, even if the two proteins were heterologous in species origin, suggesting the potential use of *A. nidulans* PalH bait to screen the full length *A. fumigatus* cDNA library for possible interactors.

The first step for the screening of the full-length *A. fumigatus* cDNA library with *A. nidulans* PalH bait was a pilot screen to determine whether the bait displays any self-activation when transformed together with empty library vector. For this, the bait construct was co-transformed with an aliquot of the empty library vector pPR3-N and assayed on

selective SD-trp-leu-his-ade plates of increasing stringency, supplemented with different amounts of 3-AT. Since the bait is co-expressed with unfused mutated Nub (expressed from an the empty library vector), any colonies obtained from the screening plates must be background and the pilot screen helps to adjust the screening conditions to obtain in the following library screen the absolute minimum of false positives possible. The efficiency of the pilot screen was verified calculating the total number of transformants and the transformation efficiency from the number of colonies on SD-trp-leu media. The total number of transformants should be greater than $8x10^5$ for the assay to deliver meaningful results (the background on selection plates is directly proportional to the total number of transformants, i.e. the total number of yeast transformants containing a bait and prey plasmid). In this case, the total number of transformants was $3.85x10^6$ with a transformation efficiency of $1.8x10^5$ clones/μg_{DNA}. SD-trp-leu-his-ade media was supplemented with 0, 1, 2.5, 5, 7.5 and 10 mM 3-AT and the optimal conditions for the screening resulted as be SD-trp-leu-his-ade supplemented with 10 mM 3-AT.

The full-length *A. fumigatus* cDNA library was transformed into NMY51 expressing *A. nidulans* PalH bait and interactors were selected using the stringency conditions determined in the pilot screen. The high-efficiency protocol described should yield transformation efficiencies in the range of $5x10^5$ to $2x10^6$ clones/μg_{DNA}, in this case $2.7x10^6$ clones/μg_{DNA}.

200 possible interactions were detected with this screening and positive colonies were purified on the same selective media used in the library screen. Library plasmids encoding putative interactors were isolated from yeast, culturing each interactor strain in liquid media, lysing the yeast cells and purifying the bait and library plasmids. The plasmid mix was subsequently transformed into *E. coli* and the library plasmid was selectively propagated, since the library plasmids carry an ampicillin marker, whereas the bait plasmid carries a kanamycin marker. As yeast can take up several plasmids during the transformation procedure, two *E. coli* colonies were analysed from each transformation.

To assess the composition of the putative interactors, a set of 85 putative interactors was analysed by sequencing using the oligonucleotides pPR3-NF and pPR3-NR (Appendix B). Among these 85, 10 were represented by a single colony in *E. coli*, so the total set of *E. coli* clones analysed was composed of 160 samples. All the sequences were examined using the software BLAST (http://blast.ncbi.nlm.nih.gov/) for the research of similarity in the available sequence databases. Among the samples, 29 had no similarity with any *A. fumigatus*

genes, but with *S. cerevisiae* genes, probably representing false positives. 12 of the putative interactors with two available clones out of 75 contained more than one library plasmid.

All the clones showing similarity with an *A. fumigatus* gene were further analysed to determine if the *A. fumigatus* gene was in frame with the mutated Nub domain of the library vector and if its sequence was complete. The results, summarised in Figs. AE.4 and AE.5, excluded from subsequent screening another 24 clones: 9 of them where the *A. fumigatus* gene was not in frame with the NubG, 6 because the *A. fumigatus* gene carried by the library plasmid was inverted, and another 9 containing only a partial sequence of the *A. fumigatus* gene (less than 100 nucleotides). The remaining 107 E. *coli* clones were in frame, 35 of these clones contained the complete sequence of the *A. fumigatus* gene whereas 72 contained only a part of the *A. fumigatus* gene (more than 100 nucleotides).

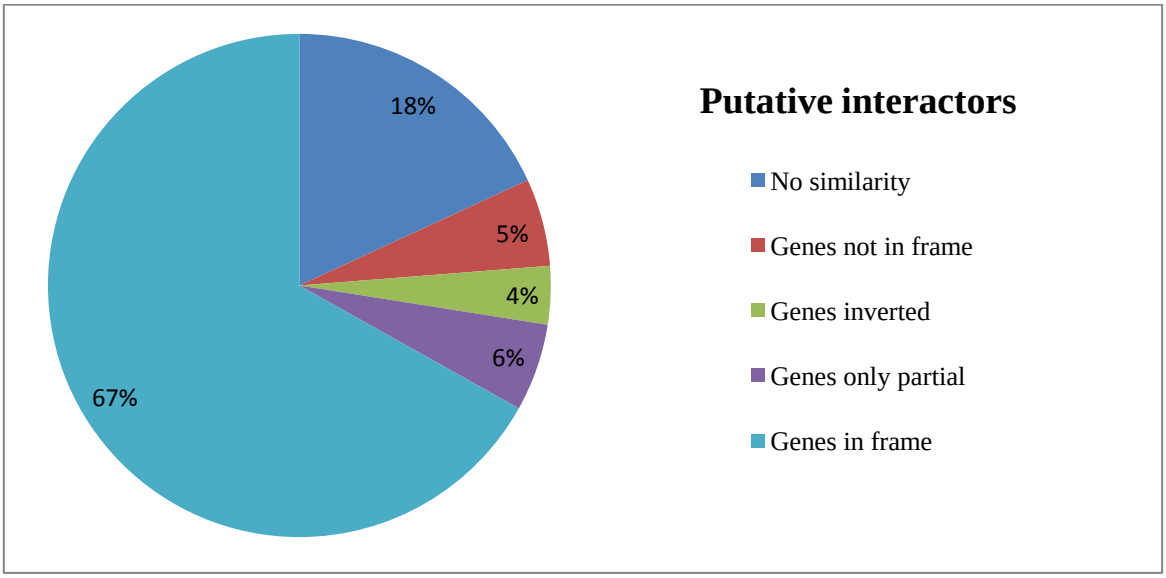


Fig. AE.4: Scheme showing the preliminary analysis of 85 of the 200 putative interactors identified by the screening of the full length *A. fumigatus* cDNA library with *A. nidulans* PalH bait. The total set of *E. coli* clones analysed was composed of 160 samples: samples showing no similarity with any *A. fumigatus* genes (blue), samples where the *A. fumigatus* gene was not in frame with the NubG (red), samples carrying an inverted *A. fumigatus* gene (green), samples with a partial sequence of the *A. fumigatus* gene (purple), samples in frame (light blue).

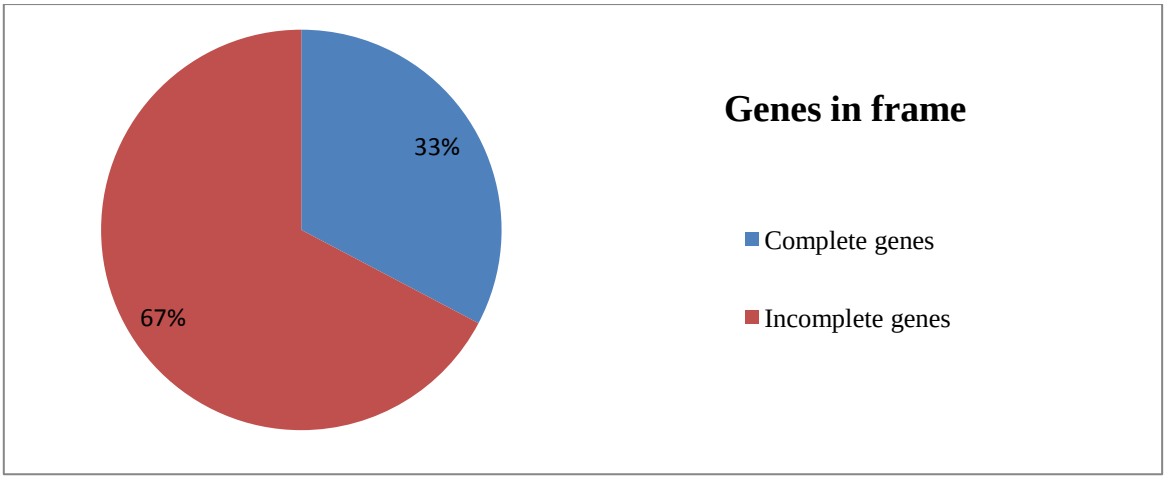


Fig. AE.5: Scheme showing the composition of the 107 E. *coli* clones containing an *A. fumigatus* gene in frame with the NubG of the library vector identified by the preliminary analysis of 85 of the 200 putative interactors obtained by the screening of the full-length *A. fumigatus* cDNA library with *A. nidulans* PalH bait. Clones containing the complete sequence of the *A. fumigatus* gene (light blue) and clones containing only a part of the *A. fumigatus* gene (red) (more than 100 nucleotides).

Table AE.1 summarises the clones identified as putative interactors and where the *A. fumigatus* gene identified is in frame with the NubG domain of the library vector to allow the expression of a functional fusion protein. As annotated in the last column, 10 *A. fumigatus* genes were identified in more than one sample and significantly, in most of the cases each sample encoding the same *A. fumigatus* gene carries a different sub-terminal fragment of the gene itself. This could inform upon which part of the confirmed interactor is fundamental for the interaction with *A. nidulans* PalH. One example is the *A. fumigatus* gene encoding the UPF0136 domain protein (Afu1g03720) identified 8 times among the clones analysed and belonging to the poorly characterised UPF0136 family of short transmembrane proteins. The portion of this gene present in these 8 clones is in a range between 93% and 57% of the entire ORF, calculating the lengths from the 3' end. Interestingly, *A. fumigatus* PalF was not identified among the clones analysed, suggesting the possibility that *palF* is poorly represented in the full length *A. fumigatus* cDNA library.

A. fumigatus ORF	Description	Complete	Multiple Id
Afu6g09740	thioredoxin reductase GliT	no	
Afu1g03720	UPF0136 domain protein	no	8 (93%)
Afu4g09360	ATP synthase subunit ATP9	yes	
Afu5g07450	conserved hypothetical protein	no	

Afu1g03720	UPF0136 domain protein	no	8 (90%)
Afu1g14240	Golgi membrane protein (Coy1)	yes	
Afu3g07570	conserved hypothetical protein	no	
Afu1g03720	UPF0136 domain protein	no	8 (74%)
Afu2g11060	Acyl CoA binding protein family	no	2 (93%)
Afu5g09330	CipC-like antibiotic response protein	yes	2 (100%)
Afu6g04110	CLPTM1 domain protein	no	
Afu1g03720	UPF0136 domain protein	no	8 (83%)
Afu1g04315	integral membrane protein	yes	2 (100%)
Afu6g11270	synaptobrevin-like protein Sybl1	no	
Afu1g09100	60S ribosomal protein L9	yes	
Afu1g03720	UPF0136 domain protein	no	8 (82%)
Afu2g00180	neutral amino acid permease	no	2 (30%)
Afu2g11550	ergosterol biosynthesis protein Erg28	no	3 (97%)
Afu2g11550	ergosterol biosynthesis protein Erg28	no	3 (96%)
Afu2g09870	eukaryotic translation initiation factor 3	no	2 (70%)
Afu7g05730	conserved hypothetical protein	no	
Afu4g03595	conserved hypothetical protein	no	
Afu6g10700	chaperonin	no	2 (78%)
Afu3g06597	conserved hypothetical protein	yes	
Afu4g07435	60S ribosomal protein L36	no	
Afu1g17350	CP2 transcription factor	no	
Afu1g02290	conserved hypothetical protein	yes	
Afu4g03630	sterol 24-c-methyltransferase	no	
Afu2g01010	myo-inositol-phosphate synthase	no	
Afu1g04315	integral membrane protein	yes	2 (100%)
Afu2g11550	ergosterol biosynthesis protein Erg28	yes	3 (100%)
Afu5g07340	DnaJ domain protein Psi	no	
Afu2g00180	neutral amino acid permease	no	2 (28%)
Afu3g11710	saccharopine dehydrogenase Lys1	yes	
Afu7g00280	conserved hypothetical protein	no	
Afu2g11060	Acyl CoA binding protein family	no	2 (94%)
Afu1g15820	fatty acid hydroxylase	yes	
Afu3g01900	conserved hypothetical protein	no	2 (90%)
Afu1g03720	UPF0136 domain protein	no	8 (82%)
Afu6g10700	chaperonin	no	2 (89%)
Afu5g10560	cytochrome c oxidase subunit V	no	
Afu1g05720	c-14 sterol reductase	yes	

Afu1g01870	presequence translocase-associated motor	yes	
Afu2g05060	alternative oxidase AlxA	yes	
Afu1g13430	conserved hypothetical protein	no	
Afu5g01960	phosphate transporter (Pho88)	yes	2 (100%)
Afu1g14200	mitochondrial processing peptidase beta	no	
Afu2g04610	DUF967 domain protein	yes	
Afu2g09870	eukaryotic translation initiation factor 3	no	2 (77%)
Afu5g09330	CipC-like antibiotic response protein	no	2 (96%)
Afu5g08100	conserved hypothetical protein	yes	
Afu5g01960	phosphate transporter (Pho88)	yes	2 (100%)
Afu1g03720	UPF0136 domain protein	no	8 (83%)
Afu3g01900	conserved hypothetical protein	yes	2 (100%)
Afu7g00540	integral membrane protein	no	
Afu5g02700	MFS multidrug transporter	no	
Afu2g04710	cytochrome b5	no	
Afu1g03720	UPF0136 domain protein	no	8 (57%)

Table AE.1: Summary of the clones identified as putative interactors of *A. nidulans* PalH because containing an *A. fumigatus* gene in frame with the NubG domain of the library vector to allow the expression of a functional fusion protein. For each putative interactors are reported the *A. fumigatus* ORF, a general description and the number of times it has been identified in the analysis.

APPENDIX F

IN SILICO STUDIES OF *A. FUMIGATUS* PACC/RIM101P PATHWAY MEMBERS

AF.1 Alignments of *A. nidulans* and *A. fumigatus* PacC/Rim101p pathway members

Alignments were performed using the *A. fumigatus* protein sequence of interest as query for the FASTA alignment tools available at www.ebi.ac.uk with the default settings. In each alignment therefore the top sequence represents the *A. fumigatus* protein sequence, whereas the bottom sequence the *A. nidulans* one.

```
Smith-Waterman score: 3013; 69.1% identity (83.0% similar) in 689 aa overlap

               10        20        30        40        50        60
Sequen MSEHQDTATNNNTTASPSATAAPMPAPISQEQPSSQPAATTPAPVSTSTPPASVTATAAA
                          ::. .: .::::.::::::   : :.: : : ::::::::
UNIPRO            MLGAMAEEAVAPVAVPTTQEQPTSQPAA---AQVTTVTSP-SVTATAAA
                         10        20           30         40

               70                  80        90       100
Sequen ATAAVSAPQANGT------PPSD-----EQLSCLWQGCSEKCPSAEALYDHICERHVGRK
       ::::::..::::::.      : :.     :.:.:.:::::::: :. :.:::.:.:::::::::
UNIPRO ATAAVASPQANGNAASPVAPASSTSRPAEELTCMWQGCSEKLPTPESLYEHVCERHVGRK
          50        60        70        80        90       100

     110       120       130       140       150       160
Sequen STNNLNLTCQWGSCRTTTVKRDHITSHIRVHVPLKPHKCEFCGKAFKRPQDLKKHVKTHA
       ::::::::::::::::::::::::::::::::::::::::.::::::::::::::::::
UNIPRO STNNLNLTCQWGSCRTTTVKRDHITSHIRVHVPLKPHKCDFCGKAFKRPQDLKKHVKTHA
         110       120       130       140       150       160

     170       180       190       200       210       220
Sequen DDSVLVRSPEPGARNPDMMFHGAGKGYAAAAHYFEPSLNAVPSQGYAHGAPQYYSSHPPH
       ::::::::::::.:::::::: : ::::::: ::::::.:: ::::::::: :::::..:
UNIPRO DDSVLVRSPEPGSRNPDMMFGGNGKGYAAA-HYFEPALNPVPSQGYAHGPPQYYQAHHAP
         170       180       190       200       210       220

     230       240       250       260       270       280
Sequen QPSNPSYGNVYYALNHGHDGH-ASYESKKRGYDALNEFFGDLKRRQFDLHSYAAVGQRLL
       :::::::::::::: : . : :::::::::::::::::::::::::: .::::::::::
UNIPRO QPSNPSYGNVYYALNTGPEPHQASYESKKRGYDALNEFFGDLKRRQFDPNSYAAVGQRLL
          230       240       250       260       270       280

      290       300       310       320       330       340
Sequen GLQNLSLPILTGGPLPEYQPMPAPVAVGGG-YGPGGHGAPVYHLPPMSNIRTKNDLINID
       .::::::::.::..:::::: ::::::::.: :: : : ::.:::::::::.::::::::::
UNIPRO SLQNLSLPVLTAAPLPEYQAMPAPVAVASGPYGGGPHPAPAYHLPPMSNVRTKNDLINID
          290       300       310       320       330       340

       350       360       370       380       390       400
Sequen QFLQQMQDTIYENDDHVAAAGVAQPGAHYVHGGMSYRTTHSPPTQLPPSHAVATTSASTS
       :::::::::::::::.:::::::::::::.:.:.:::::::::::::: .::.. :.:.
```

```
UNIPRO QFLQQMQDTIYENDDNVAAAGVAQPGAHYIHNGISYRTTHSPPTQLPSAHATTQTTAGPI
          350       360       370       380       390       400

       410       420       430       440       450       460
Sequen MSNPATHSPPTGTPALTPPSSAQSYTSARSPISISSAHRVSPPHHDGGSGMYPRLPSTTM
       .:: ..::: ..:::::::::::::::::.:::::. ::::::::: ..::.::::::::.:
UNIPRO ISNTSAHSPSSSTPALTPPSSAQSYTSGRSPISLPSAHRVSPPH-ESGSSMYPRLPSAT-
          410       420       430       440        450       460

       470       480       490        500       510       520
Sequen ADSLAGGYPTASSAAPPSTLSGIFDDD-RRRYTGGTLQRARPEERRPSIQMDTSHDGKED
        :....:: .:::::::::::.::::.: ::::::::::::::  :  : .:: : : ::.
UNIPRO -DGMTSGYTAASSAAPPSTLGGIFDNDERRRYTGGTLQRARPASRAASESMDLSSDDKES
             470       480       490       500       510       520

        530       540       550       560       570       580
Sequen GERTPTGKARSSGSDSPVRISANLIDPALHSSSPSDAEAALRTAQAATEVADRAD--SQW
       :::::             .:::.:::::::::.::.. ... :::.::::::.:.:  :.:
UNIPRO GERTPK------------QISASLIDPALHSGSPGEDDVT-RTAKAATEVAERSDVQSEW
                         530       540       550       560

          590       600       610                           620
Sequen VEKVRLLEYLRSYIASRLERGEYDSDSDDHAS-------------------AAASPVIKH
       :::::::.::::.:::.:::::::...::... .                   .. ::: :
UNIPRO VEKVRLIEYLRNYIANRLERGEFSDDSEQEQDQEQEQDQEQEQDQEQGQDRVSRSPVSKA
      570       580       590       600       610       620

         630       640       650       660       670
Sequen DGHMDGVESSHKPITAEETSAPPAAKAESNH-GVMYPTLHGLDGDEDTKMHH
       :  :.::: .  : . .  ..:  . .:: . .::::::.::: : :.::
UNIPRO DVDMEGVERDSLPRSPR--TVPIKTDGESAEDSVMYPTLRGLDEDGDSKMPS
                            630    640    650    660    670
```

Fig. AF.1: Alignment between *A. nidulans* PacC (AN2855) and *A. fumigatus* PacC (Afu3g11970).

```
Smith-Waterman score: 3374; 67.1% identity (84.2% similar) in 767 aa overlap

               10        20        30        40        50        60
Sequen MGDDARLTPRQIWANPTTTTSKSYSPGCTPFLLPSDGYVYFNRSFAITLTENAVFEPVCT
       : ::.::.:::::: ::.::..:: ::::::::::::::::.::...:.: :::...:.::
UNIPRO MEDDGRLAPRQIWARPTSTTTRSYVPGCTPFLLPSDGYVYLNRTYSISLGENAIYDPACT
               10        20        30        40        50        60

               70        80        90       100       110       120
Sequen SQPTDTRQPSPLLDTRDPFYSSVTPQLYAIGCATVVSYLLVIILLITPRTFYVGGPGGGA
       : :: :.. .  :: .::::.:::: :::.:::::::::::::::::::::::::::::
UNIPRO STPTTTEHAGAALDIHDPFYASVTPLLYAMGCATVVSYLLVIILLITPRTFYVGGPGGGA
               70        80        90       100       110       120

              130       140       150       160       170       180
Sequen NFLGRHGMISGSYSGNSSVVGVGGRPWLQKVAAILVAVSLTIASADSFRVAERQYNYGYS
       :::::::::.::::::.:::::::::::::::::::.:::.::::::.:::::::::.::..:::
UNIPRO NFLGRHGMVSGSYSNNSSVVGVGGRPWLQKVAALLVAISLTIATADSFRVAEKQYDHGYS
              130       140       150       160       170       180

              190       200       210       220       230       240
Sequen DAEALTEEVIDGTEIRVVRVISSTFLWLAQVQTLIRLFPRHKEKIMIKWAGFALIVLDTI
       :::::: ::::::::.:::.:::::::::::::::::::::::::.:::::::::::::::
UNIPRO DAEALTSEVIDGTEIKVVRIISSTFLWLAQVQTLIRLFPRHKEKVMIKWAGFALIVLDTI
              190       200       210       220       230       240

              250       260       270       280       290       300
Sequen FSILDKFLVKTNTTRPRLYDDAIPALSYLFELALNLLYAAWVIFYSLSKHRYAFFHPKMR
       :.:::::::::::::::.:::::::::::::::::::::::::::::::.::::::::
UNIPRO FAILDKFLVKTNTTRPRLYEDAIPALSYLFELALNLLYAAWVIFYSLSKHRFAFFHPKMR
```

```
              250       260       270       280       290       300

              310       320       330       340       350       360
Sequen NICLVALLSLCAVLIPVIFFVLDIAKEEIAGWGTYIRWVGSAAASVVVWEWVERIEALER
       ::::::::::::::::.:::::::: :::::::::::::::::::::::::::::::::::
UNIPRO NICLVALLSLCAVLIPVVFFVLDIAKPEIAGWGTYIRWVGSAAASVVVWEWVERIEALER
              310       320       330       340       350       360

              370       380       390       400       410       420
Sequen DERKDGILGRELFDGDEMLEVTPSEEVDWPRQTYGGGDRDGGSGTSSGWGGVMGLANRPL
       ::::::::::.::::::.::::::::::: . : :: ::.: ::.:::::::::.:::
UNIPRO DERKDGILGREVFDGDEMIEVTPSEEVDWPRQQFHGHDRGGGTGMSSAWGGVMGLAHRPL
              370       380       390       400       410       420

              430          440       450       460       470
Sequen RTRVGLPRGNRKPDKQRKT---VSSDVRRHGAGRPTPPPAATTPVSRADTTSAASTVYNV
       :     :::.:  . ::..   ...  :.. ..:::::::::.::::::::::::::::::
UNIPRO R-----PRGGRITQTQREAEGATAAKSRKRRSARPTPPPAAVTPVSRADTTSAASTVYNV
                  430       440       450       460       470

       480       490       500       510       520       530
Sequen HYHPVSSPTPPVVMPHMEEEDEYETGQLKEMTMRTEDGGGDVGQPRLSAQQTREESPQIV
       ::.::::::::.:: ::::::   :. ..    ...  ...      ..  :..:::::
UNIPRO HYYPVSSPTPPVAMPFMEEEDEGSDGDGEKELAVVQNQQSSLPTQDTYTEPRRQNSPQIV
         480       490       500       510       520       530

       540       550       560       570       580         590
Sequen NMDGRWRTLLNPFRKRRASLPREVASAQADEDPSTAQEDLYGDEGDR--PRAACSKQGYL
       :.:.::: .::::..:.:.:::::::::::.:.   . .:    .:::  :. .  ..: :
UNIPRO NVDNRWRFILNPFKNRHAALPREVASAQAEEEGFLSPDDQAPRQGDEENPHYTPRHRG-L
         540       550       560       570       580       590

         600       610         620       630       640       650
Sequen FPFNFRIRPGSDKRD--ADASLPVTVIPARRRGQNTWSPQWLNDANILEPTPNRVVRSNR
       : :.  .  :...:.  ::  :::::::::::::.:::::::...:... . .: . :
UNIPRO FSFH-PMSDGASRRQSGADQPLPVTVIPARRRGQDTWSPQWFTNSNLVDRSSSRRTASRP
           600       610       620       630       640       650

           660       670       680       690          700       710
Sequen SNLPVRVIQPQTRTAAPWSIPEGDTILGNGNYELRYDPETAALI---VPDGHQAQQRTAA
        .  ..:::::...::::.  . .. ... .:::::::::.:::.   .:: :.  : : :
UNIPRO RDQRMKVIQPQVQSAAPWTAADMEASFSSMDYELRYDPEAAALVSEDIPDHHS--QPTQA
           660       670       680       690       700         710

                720        730       740       750       760
Sequen SSTAH----NGDGQPVDEA-TAGPAGHDAPDMLRESQISAPPEQPPSSTPSRQDGQRSPT
       .: ::    .:.:    :. .:  .:      . :...   ::.  :
UNIPRO DSPAHPTMSGGNGPSGGETQSALDTGPGIEGSVNEGSVIEGPEESHSQR
             720       730       740       750       760

         770
Sequen HPSLGGDPSRDDT
```

Fig. AF.2: Alignment between *A. nidulans* PalH (AN6886) and *A. fumigatus* PalH (Afu5g13270).

```
Smith-Waterman score: 2184; 59.9% identity (75.6% similar) in 594 aa overlap

               10        20        30        40        50        60
Sequen MLLKPATPLTILLLAAFVLLLLSVLSTPIIQGIPLATFNHVDYGVFGFCKAGQCTNIHIG
       :::::::::::::: ::::::::::.::::...::::::..:.:::::.:::: :: ::::
UNIPRO MLLKPATPLTILLLIAFVLLLLSVISTPIVKSIPLATFDNVEYGVFGYCKAGTCTAIHIG
               10        20        30        40        50        60

               70          80        90       100       110
Sequen YTTDEISNTD--NSEFDLPSSTRRSLSSILIVHPVAAFLTLVCLCLAAAAHLHAPSHSPR
```

```
       :::.:: ::   .:.:.:::..:::::::::::::.::::::.:::::::::::::::::
UNIPRO YTTEEIENTGSTDSDFNLPSDARRSLSSILIVHPIAAFLTLICLCLAAAAHLHAPSHSPR
               70        80        90       100       110       120

      120       130       140       150       160       170
Sequen YLLALLILLLPTLLVSLLAFLVDILLFVPHLGWGGWIVLGATILLVISGVVTCAMRRTLV
       :::::::::::::::::::::::::::::::.::::::.:::.::  ::::::::::::
UNIPRO YLLALLILLLPTLLVSLLAFLVDILLFVPHLSWGGWIVLAATIILVTCGVVTCAMRRTLV
              130       140       150       160       170       180

      180       190       200       210       220       230
Sequen SRKARKRRIAENAEMSGENYYNRQNAAVPVVASGFTGPRSAALNAETKEAIITTSPNSES
       :::::::::::::::::.:::::::::. ..       .:  .  :.::..... .:::
UNIPRO SRKARKRRIAENAEMSGQNYYNRQNAAAAALN------ESKPIAPEAKETFVAATQSSES
              190       200       210             220       230

      240       250       260       270       280       290
Sequen GPMFATFRTTTHSSDDDQTPLNTQGAPTDIPAPDSQYAARGHGDRMPSGAPFDESRNHPY
       :: ::::::.:.:::::.:::::.. :.   : :. : .:  :: .: .:: :.  :
UNIPRO GPTFATFRTNTRSSDDDRTPLNNHSDPS---AQDAGYQSRIPGDPVPYNAPRDDFGNPLP
          240       250       260          270       280       290

      300        310            320       330       340       350
Sequen AGSYGPGPRMR-PGPGDP-----RLRPQYSDGSMGSRRGPPPPGFAPRGRGGYPPRGGYG
        :.:. .:::: :::  :     :.: ::::     :::::  :::::::::::::::::
UNIPRO PGAYNSAPRMRTPGPPGPPPPDSRVRDQYSD----PRRGPPT-GFAPRGRGGYPPRGGYG
             300       310       320            330       340

            360           370       380       390       400
Sequen RGGPYGGPRGP----PPNGRGGPMGPMRGAPSGMMGRGQRGPNPAGYGYGPVSTGLNPGY
       :::::::: ::    : .:::: :::::::.:.: :.::   :.::. :::
UNIPRO RGGPYGGPYGPNSRAPLTGRGGYMGPMRGGPAGPMARGGYRPQPAAGGYGN---------
        350       360       370       380       390

      410       420       430       440       450       460
Sequen DAYNYGPGPRPSQRFGENGIDYHGPSPVETARRPSPGPIGMAVSPPETAPIGQAIEMTSQ
                .. .::.   :.:::    .:. .::::.  ..:   .: ::::::  :
UNIPRO -----------ARAMGEDEYGYRGPS----SRQRTPGPMAAPAAP---GPAGQAIEMMPQ
                400       410           420          430

      470       480       490       500       510       520
Sequen PRHTDSAVELGPNAVPEEEQPHAVSNDGHPEPVSPSSLYSRSASYIPPRAGWTPADLRVG
       :::  .:     . ::::.: ::.: :.. :::::.:::::. ::.::: .: :   ..
UNIPRO PRHEPDA----QDEVPEQQQLHAISIDNQHEPVSPTSLYSRTQSYVPPRRNWGP---QAY
     440           450       460       470       480          490

      530       540       550       560       570       580
Sequen HSPSPVHALGENHTASHARSNSGDSYYEDVDPRFAEPHQPPAGNRALPSALTPGAGELKL
       .:  :      :.   ::::.::. :::: :: ..  ..  .:: ..::.::::
UNIPRO QSSEPNLPYQPNQP-RHARSQSGSMYYEDEDPVYTSRNESAVGNSGVPSVLTPGNSAK
            500       510       520       530       540

      590       600       610       620       630       640
Sequen TDDLAETPGSPTTSEISHFTSISERPINPRWRPPPPPALPAQQRQNVLLENNPDFDLRAG
```

Fig. AF.3: Alignment between *A. nidulans* PalI (AN4853) and *A. fumigatus* PalI (Afu3g07530).

```
Smith-Waterman score: 3538; 70.6% identity (86.5% similar) in 769 aa overlap

                       10        20        30        40        50
Sequen          MSVNSFTSPSAPSPLGRNRSSLLSKFRAPFGHRNRSIADFYIEPDDPWRSY
                :::: ... .. :::.:::::::::::. .:.::::.:.:::::::::::::
UNIPRO MVRATCSCVMSVNPLSAQTSASPLSRNRSSLLSKFRTQLGQRNRAITDFYIEPDDPWRSY
               10        20        30        40        50        60
```

```
              60        70        80        90       100       110
Sequen FPGDVVKGTVALTVVRPVRITHLVVCLHGYVKVFKNTVPSGETDPDLGFLGPGRGRRGPE
       :::::.::::.:::::::::::::. ::: :::::::.::.::: ::.: ::::::::: :
UNIPRO FPGDVIKGTVSLTVVRPVRITHLVISLHGIVKVFKNNVPAGETPPDVGSLGPGRGRRGAE
               70        80        90       100       110       120

             120       130       140       150       160       170
Sequen YLGNGLATLFEDEVVLCGEGRLKEGIYKFRFEMCFPPYALPSSISFERGTISYMLTSTLT
       :::::.:::::::::::::::::::::::::: :::: ::::::::::::::::::::
UNIPRO YLGNGVATLFEDEVVLCGEGRLKEGIYKFRFEMSFPPYPLPSSISFERGTISYMLTSTLT
             130       140       150       160       170       180

             180       190       200       210       220       230
Sequen KPTTMNPTVSCRRRVNFLENIDIAPFPAPKARIVTLEPVTRRSKPKGKAKSVESDAAADV
       ::::::::.:::::.:.:::::::: ::::: :.::::::..::::::::.:..  ::  :.
UNIPRO KPTTMNPTLSCRRRINLLENIDIAAFPAPKPRVVTLEPISKRSKPKGKTKAAGFDAP-DT
             190       200       210       220       230

             240       250       260       270       280
Sequen QSREPSLNGSGAVGDNRPPLSPAPSNVSSSSRLSNSSQSFQLASDPSSSAGTGVRNG---
        : ::: .:. .: ..:::::::::::::::::::::::...::.:.:..::::.
UNIPRO ASLEPSASGGITVPEHRPPLSPAPSNVSSSSRLSNSSQSFQIVTDPGSTASSGVRNSEAR
     240       250       260       270       280       290

      290       300       310       320       330       340
Sequen SITPSIADKTITAKTELLRAGVLPGETLPIVITINHCKQVRSAHGIIVTLYRQGRIDLHP
       : :::..:  ::::.:.:::::::::.:::: ::::: ::::::::::.::::.:::::::
UNIPRO SNTPSVTDGIITAKAEVLRAGVLPGDTLPIKITINHTKQVRSAHGIIITLYRSGRIDLHP
     300       310       320       330       340       350

      350       360       370       380       390       400
Sequen AIPIGTTANGKKPVYEDYYPRSRTGLGGLTLGTSRTSSVFRKDLAQTFAPLVVDPATMTA
       :::.:.::::::::.:::::::::::::::::::::.:::::::.::::.:.::
UNIPRO AIPMGSTANGKKPIYEDYYPRSRTGLGGLTLGTSRASSVFRKDLSQTFAPLIVDPTTLTA
     360       370       380       390       400       410

      410       420       430       440       450       460
Sequen VVKTSIRIPEDVFPTITRTPGSMINFRYYVEVVVDLRGKLTSPERFLPRFNMVSSGSNFS
        .:::::::::.:::::::::::::::::::::::::::::::::::.:::: :::
UNIPRO DIKTSIRIPEDAFPTITRTPGSMINFRYYVEVVVDLRGKLTSPERFLPRFNLVSSGRNFS
     420       430       440       450       460       470

      470       480       490       500       510       520
Sequen PSGQVLNPSDANGNSITTNWAGNILDTAQIRREKGVVAVAFEVVIGTRDSQRHKEKTERT
        .:....:.:.::..::.::. ::::: :::::::::::: ::::::::.:.::.: ...:
UNIPRO SNGKIVHPADTNGSAITANWGDNILDTDQIRREKGVVAVIFEVVIGTQDTQRRKSEARRM
     480       490       500       510       520       530

      530       540          550       560       570       580
Sequen HSVAAVSDISPPQAHPAAESD---HWQNGYSPMPTTNSEYLPQTDYGFPEESQWPMYEDE
        :.:  .... : .. ....:   :  .:    :  .   : .: :: :.. .:: : ..
UNIPRO SSTAEEAEFQQP-VENSVDGDYAGHDYQGSMAGPEPGYAPLENTAYG-PDQIRWPDYPEQ
     540       550         560       570       580         590

         590       600       610       620       630        640
Sequen TA-QHYQSLGGMVATPQVEEPTDEKARLRHAEQTLLPSRPPDDSEPGPSAG-HLAMPTAP
       .  .::    : . .:: .:: ::::::::.::::::::.:: : : ::::. . ::::::
UNIPRO SEHEHYPFQPGTLPSPQPDEPMDEKARLRRAEQTLLPSQPPCDPEAGPSSAVEAAMPTAP
       600       610       620       630       640       650

           650       660          670       680       690       700
Sequen VLPEDDHINGYHHLPSPVENCLPH---TLGSAESVQTVVASSSVAEPNGSTAPPGEDKQE
       ::::::::.: :::::: . : .     .: ::::::::.:.:: :  .. . :  :::::
UNIPRO VLPEDDHLNDYHHLPSTTVNGMTGMAPALMSAESVQTVIAGSSSAPLTSPSRPSEEDKQE
       660       670       680       690       700       710

             710       720       730       740        750
```

```
Sequen LERRRLMMEASAPEDMDAHTDNSAMDGPSAPVFHDDHDEQ-LVGGAAHGDESLPRYQR
       :::.:::::::::: : ::. .. : :::::::.:::: :.: :::::::.::: ::::::
UNIPRO LERQRLMMEASAPGDPDARHNDRADDGPSAPIFHDDDDDQQLVGGAANGDELLPRYQR
       720       730       740       750       760       770
```

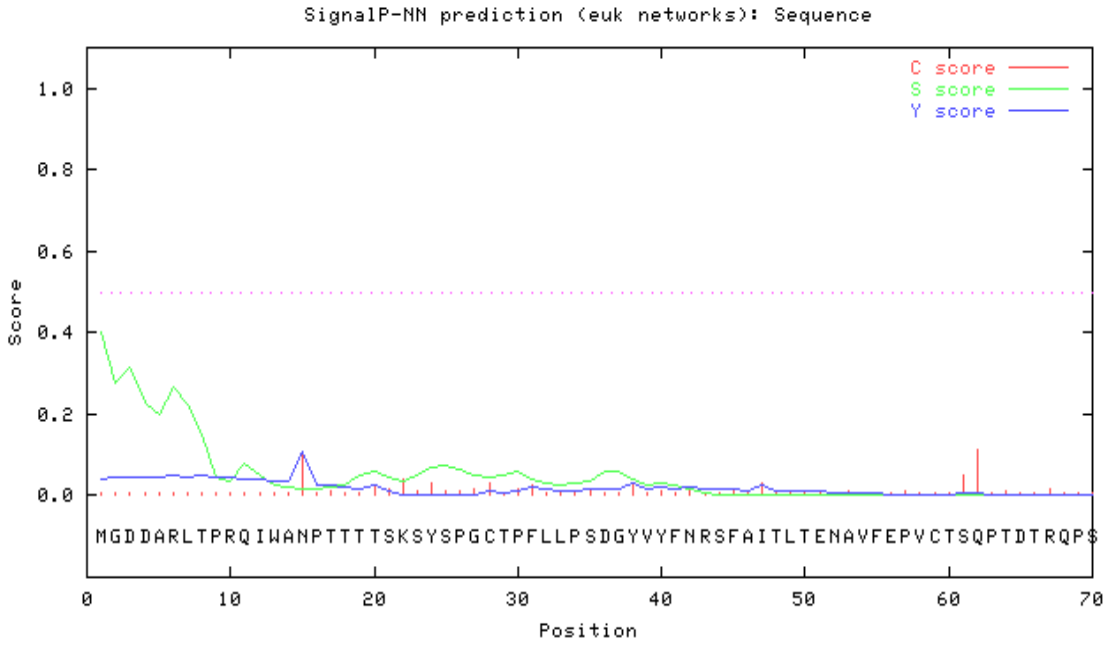
Fig. AF.4: Alignment between *A. nidulans* PalF (AN1844) and *A. fumigatus* PalF (Afu4g09650).

AF.2 *In silico* prediction topology for *A. fumigatus* PalH and PalI

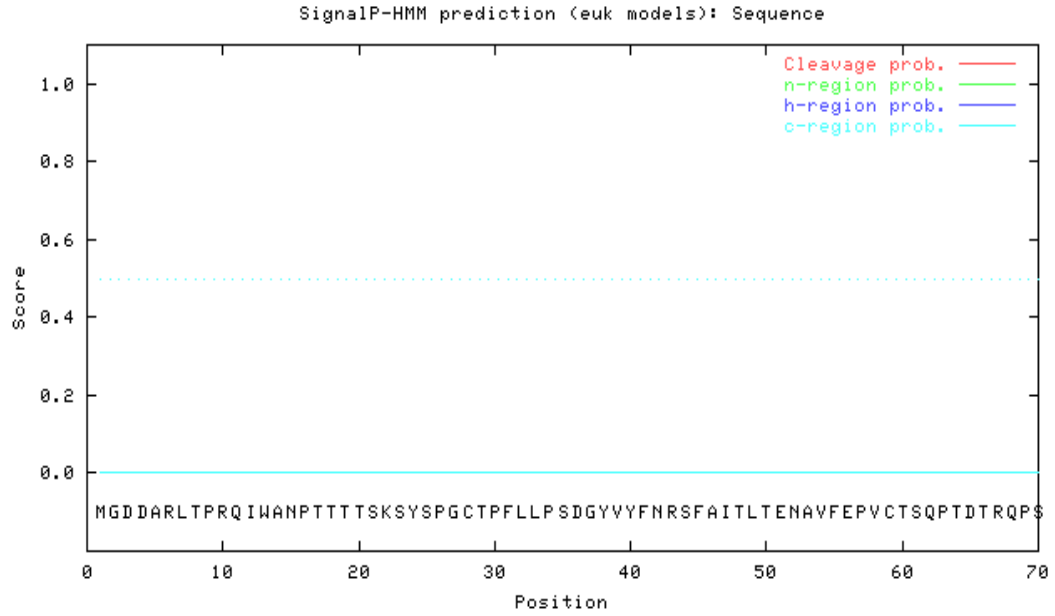
```
-----> STRONGLY prefered model: N-terminus outside
 7 strong transmembrane helices, total score : 10996
 # from   to length score orientation
 1   88  105 (18)    2291 o-i
 2  150  168 (19)    1215 i-o
 3  197  219 (23)     614 o-i
 4  225  244 (20)    1520 i-o
 5  268  287 (20)    1520 o-i
 6  301  322 (22)    2692 i-o
 7  333  352 (20)    1144 o-i

------> alternative model
 7 strong transmembrane helices, total score : 9974
 # from   to length score orientation
 1   89  108 (20)    1989 i-o
 2  147  165 (19)    1252 o-i
 3  200  218 (19)    1032 i-o
 4  225  244 (20)    1135 o-i
 5  270  287 (18)    1324 i-o
 6  302  322 (21)    2528 o-i
 7  334  352 (19)     714 i-o
```

Fig. AF.5: TMpred prediction for the topology of the *A. fumigatus* plasma membrane PalH (Afu5g13270).



```
>Sequence                 length = 70
# Measure   Position  Value  Cutoff  signal peptide?
  max. C     62       0.114   0.32   NO
  max. Y     15       0.109   0.33   NO
  max. S      1       0.402   0.87   NO
  mean S     1-14     0.166   0.48   NO
       D     1-14     0.138   0.43   NO
```



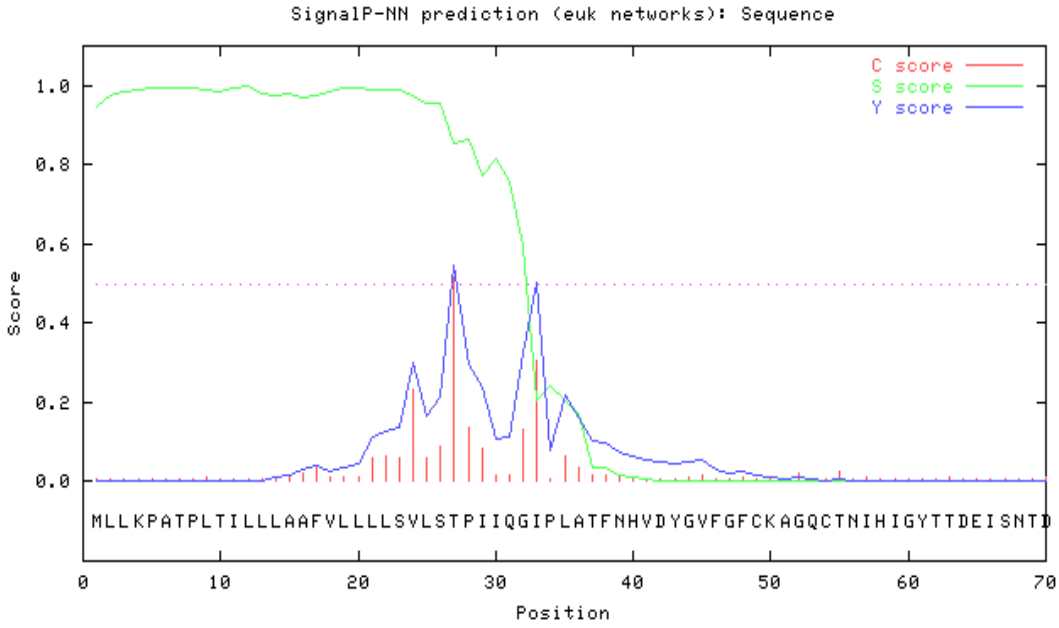

```
>Sequence
Prediction: Non-secretory protein
Signal peptide probability: 0.000
Signal anchor probability: 0.000
Max cleavage site probability: 0.000 between pos. 37 and 38
```

Fig. AF.6: Signal P3.0 prediction for the presence of a signal peptide in the *A. fumigatus* plasma membrane PalH (Afu5g13270).

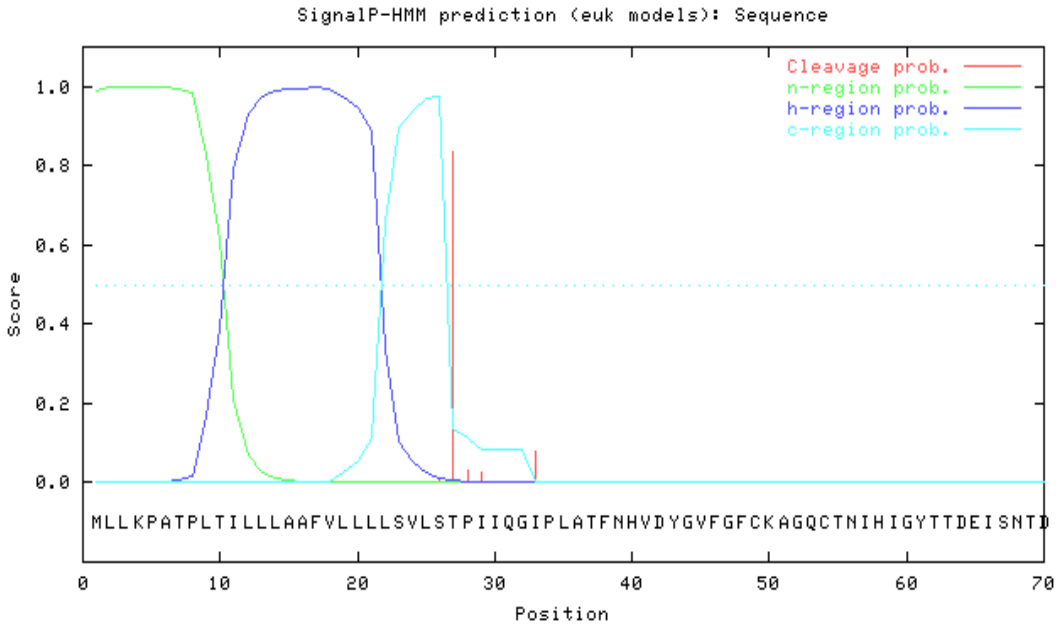
```
-----> STRONGLY prefered model: N-terminus inside
 4 strong transmembrane helices, total score : 9856
 # from   to length score orientation
 1    8   26 (19)    2427 i-o
 2   87  108 (22)    2263 o-i
 3  119  146 (28)    2493 i-o
 4  153  170 (18)    2673 o-i

------> alternative model
 4 strong transmembrane helices, total score : 9032
 # from   to length score orientation
 1    9   25 (17)    2502 o-i
 2   86  110 (25)    1897 i-o
 3  119  140 (22)    2494 o-i
 4  151  168 (18)    2139 i-o
```

Fig. AF.7: TMpred prediction for the topology of the *A. fumigatus* plasma membrane PalI (Afu3g07530).




```
>Sequence                length = 70
# Measure  Position  Value  Cutoff  signal peptide?
  max. C    27        0.516   0.32   YES
  max. Y    27        0.547   0.33   YES
  max. S    12        0.997   0.87   YES
  mean S     1-26     0.982   0.48   YES
       D     1-26     0.765   0.43   YES
# Most likely cleavage site between pos. 26 and 27: VLS-TP
```




```
>Sequence
Prediction: Signal peptide
Signal peptide probability: 0.991
Signal anchor probability: 0.009
Max cleavage site probability: 0.836 between pos. 26 and 27
```

Fig. AF.8: Signal P3.0 prediction for the presence of a signal peptide in the *A. fumigatus* plasma membrane PalI (Afu3g07530).

REFERENCES

Addrizzo-Harris, D. J., Harkin, T. J., McGuinness, G., Naidich, D. P. &Rom, W. N. (1997). Pulmonary aspergilloma and AIDS. A comparison of HIV-infected and HIV-negative individuals. *Chest* 111(3): 612-618.

Alcazar-Fuoli, L., Mellado, E., Garcia-Effron, G., Lopez, J. F., Grimalt, J. O., Cuenca-Estrella, J. M. &Rodriguez-Tudela, J. L. (2008). Ergosterol biosynthesis pathway in *Aspergillus fumigatus*. *Steroids* 73(3): 339-347.

Alken, M., Rutz, C., Kochl, R., Donalies, U., Oueslati, M., Furkert, J., Wietfeld, D., Hermosilla, R., Scholz, A., Beyermann, M., Rosenthal, W. &Schulein, R. (2005). The signal peptide of the rat corticotropin-releasing factor receptor 1 promotes receptor expression but is not essential for establishing a functional receptor. *Biochem J* 390(Pt 2): 455-464.

Alp, S. &Arikan, S. (2008). Investigation of extracellular elastase, acid proteinase and phospholipase activities as putative virulence factors in clinical isolates of *Aspergillus* species. *Journal of Basic Microbiology* 48(5): 331-337.

Amich, J., Leal, F. &Calera, J. A. (2009). Repression of the acid ZrfA/ZrfB zinc-uptake system of *Aspergillus fumigatus* mediated by PacC under neutral, zinc-limiting conditions. *Int Microbiol* 12(1): 39-47.

Amich, J., Vicentefranqueira, R., Leal, F. &Calera, J. A. (2010). *Aspergillus fumigatus* survival in alkaline and extreme zinc-limiting environments relies on the induction of a zinc homeostasis system encoded by the *zrfC* and *aspf2* genes. *Eukaryot Cell* 9(3): 424-437.

Amitani, R., Murayama, T., Nawada, R., Lee, W. J., Niimi, A., Suzuki, K., Tanaka, E. &Kuze, F. (1995a). *Aspergillus* culture filtrates and sputum sols from patients with pulmonary aspergillosis cause damage to human respiratory ciliated epithelium *in vitro*. *Eur Respir J* 8(10): 1681-1687.

Amitani, R., Taylor, G., Elezis, E. N., Llewellyn-Jones, C., Mitchell, J., Kuze, F., Cole, P. J. &Wilson, R. (1995b). Purification and characterization of factors produced by *Aspergillus fumigatus* which affect human ciliated respiratory epithelium. *Infect Immun* 63(9): 3266-3271.

Amutan, M., Nyyssonen, E., Stubbs, J., Diaz-Torres, M. R. &Dunn-Coleman, N. (1996). Identification and cloning of a mobile transposon from *Aspergillus niger* var. *awamori*. *Curr Genet* 29(5): 468-473.

Andrews, P. D. &Stark, M. J. (2000). Type 1 protein phosphatase is required for maintenance of cell wall integrity, morphogenesis and cell cycle progression in *Saccharomyces cerevisiae*. *J Cell Sci* 113 (Pt 3): 507-520.

Aparicio, O., Geisberg, J. V. &Struhl, K. (2004). Chromatin immunoprecipitation for determining the association of proteins with specific genomic sequences *in vivo*. *Curr Protoc Cell Biol* Chapter 17: Unit 17 17.

Arechiga-Carvajal, E. T. &Ruiz-Herrera, J. (2005). The RIM101/pacC homologue from the basidiomycete *Ustilago maydis i*s functional in multiple pH-sensitive phenomena. *Eukaryot Cell* 4(6): 999-1008.

Arino, J. (2010). Integrative Responses to High pH Stress in *S. cerevisiae*. *OMICS*.

Arino, J., Ramos, J. &Sychrova, H. (2010a). Alkali Metal Cation Transport and Homeostasis in Yeasts. *Microbiol. Mol. Biol. Rev.* 74(1): 95-120.

Arino, J., Ramos, J. &Sychrova, H. (2010b). Alkali metal cation transport and homeostasis in yeasts. *Microbiol Mol Biol Rev* 74(1): 95-120.

Arst, H. (2003). pH regulation in *Aspergillus* and parallels with higher eukaryotic regulatory systems. *TRENDS in Genetics* 19(4): 224-231.
Arst, H. N., Jr. (1967). Studies on metabolic control and uptake in *Aspergillus*. *Ph.D thesis* University of Cambridge(Cambridge, United Kingdom).
Arst, H. N., Jr., Bailey, C. R. &Penfold, H. A. (1980). A possible role for acid phosphatase in gamma-amino-n-butyrate uptake in *Aspergillus nidulans*. *Arch Microbiol* 125(1-2): 153-158.
Arst, H. N., Jr., Bignell, E. &Tilburn, J. (1994). Two new genes involved in signalling ambient pH in *Aspergillus nidulans*. *Mol Gen Genet* 245(6): 787-790.
Arst Jr, H. &Peñalva, M. (2003). Recognizing gene regulation by ambient pH. *Fungal genetics and biology: FG & B* 40(1): 1.
Ashburner, M., Ball, C. A., Blake, J. A., Botstein, D., Butler, H., Cherry, J. M., Davis, A. P., Dolinski, K., Dwight, S. S., Eppig, J. T., Harris, M. A., Hill, D. P., Issel-Tarver, L., Kasarskis, A., Lewis, S., Matese, J. C., Richardson, J. E., Ringwald, M., Rubin, G. M. &Sherlock, G. (2000). Gene ontology: tool for the unification of biology. The Gene Ontology Consortium. *Nat Genet* 25(1): 25-29.
Askew, D. S. (2008). *Aspergillus fumigatus*: virulence genes in a street-smart mold. *Curr Opin Microbiol* 11(4): 331-337.
Auerbach, D., Thaminy, S., Hottiger, M. O. &Stagljar, I. (2002). The post-genomic era of interactive proteomics: facts and perspectives. *Proteomics* 2(6): 611-623.
Babst, M., Katzmann, D. J., Estepa-Sabal, E. J., Meerloo, T. &Emr, S. D. (2002). Escrt-III: an endosome-associated heterooligomeric protein complex required for mvb sorting. *Dev Cell* 3(2): 271-282.
Baddley, J. W. (2010). Clinical risk factors for invasive aspergillosis. *Med Mycol*.
Baker, S. E. (2006). *Aspergillus niger* genomics: past, present and into the future. *Med Mycol* 44 Suppl 1: S17-21.
Balloy, V., Huerre, M., Latge, J. P. &Chignard, M. (2005). Differences in patterns of infection and inflammation for corticosteroid treatment and chemotherapy in experimental invasive pulmonary aspergillosis. *Infect Immun* 73(1): 494-503.
Barwell, K., Boysen, J., Xu, W. &Mitchell, A. (2005). Relationship of DFG16 to the Rim101p pH response pathway in *Saccharomyces cerevisiae* and *Candida albicans*. *Eukaryotic cell* 4(5): 890.
Basich, J. E., Graves, T. S., Baz, M. N., Scanlon, G., Hoffmann, R. G., Patterson, R. &Fink, J. N. (1981). Allergic bronchopulmonary aspergillosis in corticosteroid-dependent asthmatics. *J Allergy Clin Immunol* 68(2): 98-102.
Beauvais, A., Maubon, D., Park, S., Morelle, W., Tanguy, M., Huerre, M., Perlin, D. S. &Latge, J. P. (2005). Two alpha(1-3) glucan synthases with different functions in *Aspergillus fumigatus*. *Appl Environ Microbiol* 71(3): 1531-1538.
Becker, A., Hessenius, C., Licha, K., Ebert, B., Sukowski, U., Semmler, W., Wiedenmann, B. &Grotzinger, C. (2001). Receptor-targeted optical imaging of tumors with near-infrared fluorescent ligands. *Nat Biotechnol* 19(4): 327-331.
Bendtsen, J. D., Nielsen, H., von Heijne, G. &Brunak, S. (2004). Improved prediction of signal peptides: SignalP 3.0. *J Mol Biol* 340(4): 783-795.
Bensen, E., Martin, S., Li, M., Berman, J. &Davis, D. (2004). Transcriptional profiling in *Candida albicans* reveals new adaptive responses to extracellular pH and functions for Rim101p. *Molecular microbiology* 54(5): 1335-1351.
Bergmann, A., Hartmann, T., Cairns, T., Bignell, E. M. &Krappmann, S. (2009). A regulator of *Aspergillus fumigatus* extracellular proteolytic activity is dispensable for virulence. *Infect Immun* 77(9): 4041-4050.

Bernstein, B. E., Tong, J. K. &Schreiber, S. L. (2000). Genomewide studies of histone deacetylase function in yeast. *Proc Natl Acad Sci U S A* 97(25): 13708-13713.
Bhabhra, R., Miley, M. D., Mylonakis, E., Boettner, D., Fortwendel, J., Panepinto, J. C., Postow, M., Rhodes, J. C. &Askew, D. S. (2004). Disruption of the Aspergillus fumigatus gene encoding nucleolar protein CgrA impairs thermotolerant growth and reduces virulence. *Infect Immun* 72(8): 4731-4740.
Bhaumik, S. &Gambhir, S. S. (2002). Optical imaging of *Renilla* luciferase reporter gene expression in living mice. *Proc Natl Acad Sci U S A* 99(1): 377-382.
Bidwai, A. P., Reed, J. C. &Glover, C. V. C. (1995). Cloning and Disruption of CKB1, the Gene Encoding the 38-kDa Subunit of *Saccharomyces cerevisiae* Casein Kinase II (CKII). *Journal of Biological Chemistry* 270(18): 10395-10404.
Biemont, C. &Vieira, C. (2006). Genetics: junk DNA as an evolutionary force. *Nature* 443(7111): 521-524.
Bignell, E., Negrete-Urtasun, S., Calcagno, A., Haynes, K., Arst Jr, H. &Rogers, T. (2005). The *Aspergillus* pH-responsive transcription factor PacC regulates virulence. *Molecular microbiology* 55(4): 1072-1084.
Bodey, G. P. &Vartivarian, S. (1989). Aspergillosis. *Eur J Clin Microbiol Infect Dis* 8(5): 413-437.
Bok, J. W., Balajee, S. A., Marr, K. A., Andes, D., Nielsen, K. F., Frisvad, J. C. &Keller, N. P. (2005). LaeA, a regulator of morphogenetic fungal virulence factors. *Eukaryot Cell* 4(9): 1574-1582.
Bok, J. W., Chiang, Y. M., Szewczyk, E., Reyes-Dominguez, Y., Davidson, A. D., Sanchez, J. F., Lo, H. C., Watanabe, K., Strauss, J., Oakley, B. R., Wang, C. C. &Keller, N. P. (2009). Chromatin-level regulation of biosynthetic gene clusters. *Nat Chem Biol* 5(7): 462-464.
Bok, J. W., Chung, D., Balajee, S. A., Marr, K. A., Andes, D., Nielsen, K. F., Frisvad, J. C., Kirby, K. A. &Keller, N. P. (2006). GliZ, a transcriptional regulator of gliotoxin biosynthesis, contributes to *Aspergillus fumigatus* virulence. *Infect Immun* 74(12): 6761-6768.
Bolard, J. (1986). How do the polyene macrolide antibiotics affect the cellular membrane properties? *Biochim Biophys Acta* 864(3-4): 257-304.
Botterel, F., Cordonnier, C., Barbier, V., Wingerstmann, L., Liance, M., Coste, A., Escudier, E. &Bretagne, S. (2002). *Aspergillus fumigatus* causes *in vitro* electrophysiological and morphological modifications in human nasal epithelial cells. *Histol Histopathol* 17(4): 1095-1101.
Bowers, K., Lottridge, J., Helliwell, S. B., Goldthwaite, L. M., Luzio, J. P. &Stevens, T. H. (2004). Protein-protein interactions of ESCRT complexes in the yeast *Saccharomyces cerevisiae*. *Traffic* 5(3): 194-210.
Boysen, J. &Mitchell, A. (2006). Control of Bro1-domain protein Rim20 localization by external pH, ESCRT machinery, and the *Saccharomyces cerevisiae* Rim101 pathway. *Molecular biology of the cell* 17(3): 1344.
Brajtburg, J. &Bolard, J. (1996). Carrier effects on biological activity of amphotericin B. *Clin Microbiol Rev* 9(4): 512-531.
Brajtburg, J., Elberg, S., Schwartz, D. R., Vertut-Croquin, A., Schlessinger, D., Kobayashi, G. S. &Medoff, G. (1985). Involvement of oxidative damage in erythrocyte lysis induced by amphotericin B. *Antimicrob Agents Chemother* 27(2): 172-176.
Brakhage, A. A. &Langfelder, K. (2002). Menacing mold: the molecular biology of *Aspergillus fumigatus*. *Annu Rev Microbiol* 56: 433-455.
Brakhage, A. A. &Liebmann, B. (2005). *Aspergillus fumigatus* conidial pigment and cAMP signal transduction: significance for virulence. *Med Mycol* 43 Suppl 1: S75-82.

Breakspear, A. &Momany, M. (2007). The first fifty microarray studies in filamentous fungi. *Microbiology* 153(1): 7-15.
Breitfeld, P. P., Rup, D. &Schwartz, A. L. (1984). Influence of the N-linked oligosaccharides on the biosynthesis, intracellular routing, and function of the human asialoglycoprotein receptor. *J Biol Chem* 259(16): 10414-10421.
Brock, M., Jouvion, G., Droin-Bergere, S., Dussurget, O., Nicola, M. A. &Ibrahim-Granet, O. (2008). Bioluminescent *Aspergillus fumigatus*, a new tool for drug efficiency testing and in vivo monitoring of invasive aspergillosis. *Appl Environ Microbiol* 74(22): 7023-7035.
Buck, M. J. &Lieb, J. D. (2006). A chromatin-mediated mechanism for specification of conditional transcription factor targets. *Nat Genet* 38(12): 1446-1451.
Bussink, H. J. &Osmani, S. A. (1998). A cyclin-dependent kinase family member (PHOA) is required to link developmental fate to environmental conditions in *Aspergillus nidulans*. *EMBO J* 17(14): 3990-4003.
Caddick, M. X. &Arst, H. N., Jr. (1986). Structural genes for phosphatases in *Aspergillus nidulans*. *Genet Res* 47(2): 83-91.
Caddick, M. X., Arst, H. N., Jr., Taylor, L. H., Johnson, R. I. &Brownlee, A. G. (1986a). Cloning of the regulatory gene areA mediating nitrogen metabolite repression in *Aspergillus nidulans*. *EMBO J* 5(5): 1087-1090.
Caddick, M. X., Brownlee, A. G. &Arst, H. N., Jr. (1986b). Phosphatase regulation in *Aspergillus nidulans*: responses to nutritional starvation. *Genet Res* 47(2): 93-102.
Caddick, M. X., Brownlee, A. G. &Arst, H. N., Jr. (1986c). Regulation of gene expression by pH of the growth medium in *Aspergillus nidulans*. *Mol Gen Genet* 203(2): 346-353.
Calcagno-Pizarelli, A., Negrete-Urtasun, S., Denison, S., Rudnicka, J., Bussink, H., Munera-Huertas, T., Stanton, L., Hervas-Aguilar, A., Espeso, E. &Tilburn, J. (2007). Establishment of the ambient pH signaling complex in *Aspergillus nidulans*: PalI assists plasma membrane localization of PalH. *Eukaryotic cell* 6(12): 2365.
Calera, J. A., Paris, S., Monod, M., Hamilton, A. J., Debeaupuis, J. P., Diaquin, M., Lopez-Medrano, R., Leal, F. &Latge, J. P. (1997). Cloning and disruption of the antigenic catalase gene of *Aspergillus fumigatus*. *Infect Immun* 65(11): 4718-4724.
Caracuel, Z., Casanova, C., Roncero, M. I., Di Pietro, A. &Ramos, J. (2003a). pH response transcription factor PacC controls salt stress tolerance and expression of the P-Type Na^+ -ATPase Ena1 in *Fusarium oxysporum*. *Eukaryot Cell* 2(6): 1246-1252.
Caracuel, Z., Roncero, M. I., Espeso, E. A., Gonzalez-Verdejo, C. I., Garcia-Maceira, F. I. &Di Pietro, A. (2003b). The pH signalling transcription factor PacC controls virulence in the plant pathogen *Fusarium oxysporum*. *Mol Microbiol* 48(3): 765-779.
Carafoli, E. (2005). Calcium--a universal carrier of biological signals. Delivered on 3 July 2003 at the Special FEBS Meeting in Brussels. *FEBS J* 272(5): 1073-1089.
Casadevall, A. &Pirofski, L. A. (1999). Host-pathogen interactions: redefining the basic concepts of virulence and pathogenicity. *Infect Immun* 67(8): 3703-3713.
Casselton, L. A. (2002). Mate recognition in fungi. *Heredity* 88(2): 142-147.
Castrejon, F., Gomez, A., Sanz, M., Duran, A. &Roncero, C. (2006). The RIM101 pathway contributes to yeast cell wall assembly and its function becomes essential in the absence of mitogen-activated protein kinase Slt2p. *Eukaryotic cell* 5(3): 507.
Causton, H. C., Ren, B., Koh, S. S., Harbison, C. T., Kanin, E., Jennings, E. G., Lee, T. I., True, H. L., Lander, E. S. &Young, R. A. (2001). Remodeling of yeast genome expression in response to environmental changes. *Mol Biol Cell* 12(2): 323-337.
Cervantes, S., Gonzalez-Duarte, R. &Marfany, G. (2001). Homodimerization of presenilin N-terminal fragments is affected by mutations linked to Alzheimer's disease. *FEBS Lett* 505(1): 81-86.

Chabane, S., Sarfati, J., Ibrahim-Granet, O., Du, C., Schmidt, C., Mouyna, I., Prevost, M. C., Calderone, R. &Latge, J. P. (2006). Glycosylphosphatidylinositol-anchored Ecm33p influences conidial cell wall biosynthesis in *Aspergillus fumigatus*. *Appl Environ Microbiol* 72(5): 3259-3267.

Chang, M. H., Chae, K. S., Han, D. M. &Jahng, K. Y. (2004). The GanB Galpha-protein negatively regulates asexual sporulation and plays a positive role in conidial germination in *Aspergillus nidulans*. *Genetics* 167(3): 1305-1315.

Chazalet, V., Debeaupuis, J. P., Sarfati, J., Lortholary, J., Ribaud, P., Shah, P., Cornet, M., Vu Thien, H., Gluckman, E., Brucker, G. &Latge, J. P. (1998). Molecular typing of environmental and patient isolates of *Aspergillus fumigatus* from various hospital settings. *J Clin Microbiol* 36(6): 1494-1500.

Chen, Q., Miller, L. J. &Dong, M. (2010). Role of N-linked glycosylation in biosynthesis, trafficking, and function of the human glucagon-like peptide 1 receptor. *Am J Physiol Endocrinol Metab* 299(1): E62-68.

Chiang, L. Y., Sheppard, D. C., Gravelat, F. N., Patterson, T. F. &Filler, S. G. (2008). *Aspergillus fumigatus* stimulates leukocyte adhesion molecules and cytokine production by endothelial cells in vitro and during invasive pulmonary disease. *Infect Immun* 76(8): 3429-3438.

Chishima, T., Miyagi, Y., Wang, X., Baranov, E., Tan, Y., Shimada, H., Moossa, A. R. &Hoffman, R. M. (1997). Metastatic patterns of lung cancer visualized live and in process by green fluorescence protein expression. *Clin Exp Metastasis* 15(5): 547-552.

Chryssanthou, E. (1997). *In vitro* susceptibility of respiratory isolates of *Aspergillus* species to itraconazole and amphotericin B. acquired resistance to itraconazole. *Scand J Infect Dis* 29(5): 509-512.

Claing, A., Laporte, S. A., Caron, M. G. &Lefkowitz, R. J. (2002). Endocytosis of G protein-coupled receptors: roles of G protein-coupled receptor kinases and beta-arrestin proteins. *Prog Neurobiol* 66(2): 61-79.

Clements, J. S., Jr. &Peacock, J. E., Jr. (1990). Amphotericin B revisited: reassessment of toxicity. *Am J Med* 88(5N): 22N-27N.

Cody, D. T., 2nd, McCaffrey, T. V., Roberts, G. &Kern, E. B. (1997). Effects of *Aspergillus fumigatus* and *Alternaria alternata* on human ciliated epithelium in vitro. *Laryngoscope* 107(11 Pt 1): 1511-1514.

Contag, C. H. &Bachmann, M. H. (2002). Advances in *in vivo* bioluminescence imaging of gene expression. *Annu Rev Biomed Eng* 4: 235-260.

Contag, C. H., Contag, P. R., Mullins, J. I., Spilman, S. D., Stevenson, D. K. &Benaron, D. A. (1995). Photonic detection of bacterial pathogens in living hosts. *Mol Microbiol* 18(4): 593-603.

Contag, C. H., Jenkins, D., Contag, P. R. &Negrin, R. S. (2000). Use of reporter genes for optical measurements of neoplastic disease *in vivo*. *Neoplasia* 2(1-2): 41-52.

Contag, C. H., Spilman, S. D., Contag, P. R., Oshiro, M., Eames, B., Dennery, P., Stevenson, D. K. &Benaron, D. A. (1997). Visualizing gene expression in living mammals using a bioluminescent reporter. *Photochem Photobiol* 66(4): 523-531.

Contag, C. H. &Stevenson, D. K. (2001). *In vivo* patterns of heme oxygenase-1 transcription. *J Perinatol* 21 Suppl 1: S119-124; discussion S125-117.

Cooney, N. M. &Klein, B. S. (2008). Fungal adaptation to the mammalian host: it is a new world, after all. *Curr Opin Microbiol* 11(6): 511-516.

Copic, A., Dorrington, M., Pagant, S., Barry, J., Lee, M. C., Singh, I., Hartman, J. L. t. &Miller, E. A. (2009). Genomewide analysis reveals novel pathways affecting

endoplasmic reticulum homeostasis, protein modification and quality control. *Genetics* 182(3): 757-769.
Cormack, B. P., Bertram, G., Egerton, M., Gow, N. A., Falkow, S. &Brown, A. J. (1997). Yeast-enhanced green fluorescent protein (yEGFP)a reporter of gene expression in *Candida albicans*. *Microbiology* 143 (Pt 2): 303-311.
Couvineau, A., Rouyer-Fessard, C. &Laburthe, M. (2004). Presence of a N-terminal signal peptide in class II G protein-coupled receptors: crucial role for expression of the human VPAC1 receptor. *Regul Pept* 123(1-3): 181-185.
Cui, C. B., Kakeya, H., Okada, G., Onose, R. &Osada, H. (1996a). Novel mammalian cell cycle inhibitors, tryprostatins A, B and other diketopiperazines produced by *Aspergillus fumigatus*. I. Taxonomy, fermentation, isolation and biological properties. *J Antibiot (Tokyo)* 49(6): 527-533.
Cui, C. B., Kakeya, H. &Osada, H. (1996b). Novel mammalian cell cycle inhibitors, tryprostatins A, B and other diketopiperazines produced by *Aspergillus fumigatus*. II. Physico-chemical properties and structures. *J Antibiot (Tokyo)* 49(6): 534-540.
Cyert, M. S. (2003). Calcineurin signaling in *Saccharomyces cerevisiae*: how yeast go crazy in response to stress. *Biochem Biophys Res Commun* 311(4): 1143-1150.
D'Enfert, C., Diaquin, M., Delit, A., Wuscher, N., Debeaupuis, J., Huerre, M. &Latge, J. (1996). Attenuated virulence of uridine-uracil auxotrophs of *Aspergillus fumigatus*. *Infect. Immun.* 64(10): 4401-4405.
D'Souza, C. A., Lee, B. N. &Adams, T. H. (2001). Characterization of the role of the FluG protein in asexual development of *Aspergillus nidulans*. *Genetics* 158(3): 1027-1036.
da Silva Ferreira, M. E., Heinekamp, T., Hartl, A., Brakhage, A. A., Semighini, C. P., Harris, S. D., Savoldi, M., de Gouvea, P. F., de Souza Goldman, M. H. &Goldman, G. H. (2007). Functional characterization of the *Aspergillus fumigatus* calcineurin. *Fungal Genet Biol* 44(3): 219-230.
da Silva Ferreira, M. E., Kress, M. R., Savoldi, M., Goldman, M. H., Hartl, A., Heinekamp, T., Brakhage, A. A. &Goldman, G. H. (2006). The akuB(KU80) mutant deficient for nonhomologous end joining is a powerful tool for analyzing pathogenicity in *Aspergillus fumigatus*. *Eukaryot Cell* 5(1): 207-211.
Dagenais, T. R. &Keller, N. P. (2009). Pathogenesis of *Aspergillus fumigatus* in Invasive Aspergillosis. *Clin Microbiol Rev* 22(3): 447-465.
Davis, D. (2003). Adaptation to environmental pH in *Candida albicans* and its relation to pathogenesis. *Current genetics* 44(1): 1-7.
Davis, D., Edwards, J. E., Jr., Mitchell, A. P. &Ibrahim, A. S. (2000a). *Candida albicans RIM101* pH response pathway is required for host-pathogen interactions. *Infect Immun* 68(10): 5953-5959.
Davis, D., Wilson, R. B. &Mitchell, A. P. (2000b). RIM101-dependent and-independent pathways govern pH responses in *Candida albicans*. *Mol Cell Biol* 20(3): 971-978.
Davis, D. A. (2009). How human pathogenic fungi sense and adapt to pH: the link to virulence. *Curr Opin Microbiol* 12(4): 365-370.
De Bernardis, F., Muhlschlegel, F. A., Cassone, A. &Fonzi, W. A. (1998). The pH of the host niche controls gene expression in and virulence of *Candida albicans*. *Infect Immun* 66(7): 3317-3325.
De Beule, K. (1996). Itraconazole: pharmacology, clinical experience and future development. *Int J Antimicrob Agents* 6(3): 175-181.
de Gouvêa PF, S. F., Malavazi I, Savoldi M, Goldman MH, Loss O, Bignell E, da Silva Ferreira ME, Goldman GH (2008). Functional characterization of the *Aspergillus fumigatus* PHO80 homologue. *Fungal Genet Biol* 45(7): 1135-1146.

De Las Penas, A., Pan, S. J., Castano, I., Alder, J., Cregg, R. &Cormack, B. P. (2003). Virulence-related surface glycoproteins in the yeast pathogen *Candida glabrata* are encoded in subtelomeric clusters and subject to RAP1- and SIR-dependent transcriptional silencing. *Genes Dev* 17(18): 2245-2258.

de Nadal, E., Calero, F., Ramos, J. &Arino, J. (1999). Biochemical and Genetic Analyses of the Role of Yeast Casein Kinase 2 in Salt Tolerance. *J. Bacteriol.* 181(20): 6456-6462.

De Pauw, B. E. (1997). Practical modalities for prevention of fungal infections in cancer patients. *Eur J Clin Microbiol Infect Dis* 16(1): 32-41.

De Sarro, A., La Camera, E. &Fera, M. T. (2008). New and investigational triazole agents for the treatment of invasive fungal infections. *J Chemother* 20(6): 661-671.

de Wet, J. R., Wood, K. V., DeLuca, M., Helinski, D. R. &Subramani, S. (1987). Firefly luciferase gene: structure and expression in mammalian cells. *Mol Cell Biol* 7(2): 725-737.

de Wet, J. R., Wood, K. V., Helinski, D. R. &DeLuca, M. (1985). Cloning of firefly luciferase cDNA and the expression of active luciferase in *Escherichia coli*. *Proc Natl Acad Sci U S A* 82(23): 7870-7873.

Dellacasa-Lindberg, I., Hitziger, N. &Barragan, A. (2007). Localized recrudescence of *Toxoplasma infections* in the central nervous system of immunocompromised mice assessed by in vivo bioluminescence imaging. *Microbes Infect* 9(11): 1291-1298.

Denison, S. (2000). pH regulation of gene expression in fungi. *Fungal Genetics and Biology* 29(2): 61-71.

Denison, S., Orejas, M. &Arst, H. (1995). Signaling of ambient pH in *Aspergillus* involves a cysteine protease. *Journal of Biological Chemistry* 270(48): 28519.

Denison, S. H., Negrete-Urtasun, S., Mingot, J. M., Tilburn, J., Mayer, W. A., Goel, A., Espeso, E. A., Penalva, M. A. &Arst, H. N., Jr. (1998). Putative membrane components of signal transduction pathways for ambient pH regulation in Aspergillus and meiosis in saccharomyces are homologous. *Mol Microbiol* 30(2): 259-264.

Denning, D. W. (1995). Issues in the management of invasive aspergillosis. *Ann Med Interne (Paris)* 146(2): 106-110.

Denning, D. W. (1996a). Aspergillosis: diagnosis and treatment. *Int J Antimicrob Agents* 6(3): 161-168.

Denning, D. W. (1996b). Therapeutic outcome in invasive aspergillosis. *Clin Infect Dis* 23(3): 608-615.

Denning, D. W. (1998). Invasive aspergillosis. *Clin Infect Dis* 26(4): 781-803; quiz 804-785.

Denning, D. W., Baily, G. G. &Hood, S. V. (1997a). Azole resistance in Candida. *Eur J Clin Microbiol Infect Dis* 16(4): 261-280.

Denning, D. W., Venkateswarlu, K., Oakley, K. L., Anderson, M. J., Manning, N. J., Stevens, D. A., Warnock, D. W. &Kelly, S. L. (1997b). Itraconazole resistance in *Aspergillus fumigatus*. *Antimicrob Agents Chemother* 41(6): 1364-1368.

DeRisi, J. L., Iyer, V. R. &Brown, P. O. (1997). Exploring the metabolic and genetic control of gene expression on a genomic scale. *Science* 278(5338): 680-686.

Di Fiore PP, D. C. P. (2001). Endocytosis and signaling. an inseparable partnership. *Cell* 13(106(1)): 1-4.

Diez, E., Alvaro, J., Espeso, E. A., Rainbow, L., Suarez, T., Tilburn, J., Arst, H. N., Jr. &Penalva, M. A. (2002). Activation of the *Aspergillus* PacC zinc finger transcription factor requires two proteolytic steps. *EMBO J* 21(6): 1350-1359.

Dixon, D. M., Polak, A. &Walsh, T. J. (1989). Fungus dose-dependent primary pulmonary aspergillosis in immunosuppressed mice. *Infect Immun* 57(5): 1452-1456.

Dixon, D. M. &Walsh, T. J. (1992). Human pathogenesis. *Biotechnology* 23: 249-267.

Do, J. H., Yamaguchi, R. &Miyano, S. (2009). Exploring temporal transcription regulation structure of *Aspergillus fumigatus* in heat shock by state space model. *BMC Genomics* 10: 306.
Dorn, G. (1965a). Genetic Analysis of the Phosphatases in Aspergillus Nidulans. *Genet Res* 10: 13-26.
Dorn, G. (1965b). Phosphatase mutants in Aspergillus nidulans. *Science* 150(700): 1183-1184.
Dotis, J., Panagopoulou, P., Filioti, J., Winn, R., Toptsis, C., Panteliadis, C. &Roilides, E. (2003). Femoral osteomyelitis due to *Aspergillus nidulans* in a patient with chronic granulomatous disease. *Infection* 31(2): 121-124.
Dotis, J. &Roilides, E. (2004). Osteomyelitis due to *Aspergillus* spp. in patients with chronic granulomatous disease: comparison of *Aspergillus nidulans* and *Aspergillus fumigatus*. *Int J Infect Dis* 8(2): 103-110.
Dou, X., Wu, D., An, W., Davies, J., Hashmi, S. B., Ukil, L. &Osmani, S. A. (2003). The PHOA and PHOB cyclin-dependent kinases perform an essential function in *Aspergillus nidulans*. *Genetics* 165(3): 1105-1115.
Doyle, T. C., Burns, S. M. &Contag, C. H. (2004). *In vivo* bioluminescence imaging for integrated studies of infection. *Cell Microbiol* 6(4): 303-317.
Doyle, T. C., Nawotka, K. A., Kawahara, C. B., Francis, K. P. &Contag, P. R. (2006). Visualizing fungal infections in living mice using bioluminescent pathogenic *Candida albicans* strains transformed with the firefly luciferase gene. *Microb Pathog* 40(2): 82-90.
Dyer, P. S. &Paoletti, M. (2005). Reproduction in *Aspergillus fumigatus*: sexuality in a supposedly asexual species? *Med Mycol* 43 Suppl 1: S7-14.
Eisendle, M., Oberegger, H., Buttinger, R., Illmer, P. &Haas, H. (2004). Biosynthesis and uptake of siderophores is controlled by the PacC-mediated ambient-pH regulatory system in *Aspergillus nidulans*. *Eukaryotic cell* 3(2): 561.
Emanuelsson, O., Brunak, S., von Heijne, G. &Nielsen, H. (2007). Locating proteins in the cell using TargetP, SignalP and related tools. *Nat Protoc* 2(4): 953-971.
Ernst, J. &Bar-Joseph, Z. (2006). STEM: a tool for the analysis of short time series gene expression data. *BMC Bioinformatics* 7: 191.
Espeso, E. &Arst Jr, H. (2000). On the mechanism by which alkaline pH prevents expression of an acid-expressed gene. *Molecular and Cellular Biology* 20(10): 3355.
Espeso, E., Roncal, T., Díez, E., Rainbow, L., Bignell, E., Álvaro, J., Suárez, T., Denison, S., Tilburn, J. &Arst, H. (2000). On how a transcription factor can avoid its proteolytic activation in the absence of signal transduction. *The EMBO Journal* 19(4): 719-728.
Espeso, E. A. &Penalva, M. A. (1996). Three binding sites for the *Aspergillus nidulans* PacC zinc-finger transcription factor are necessary and sufficient for regulation by ambient pH of the isopenicillin N synthase gene promoter. *J Biol Chem* 271(46): 28825-28830.
Espeso, E. A., Tilburn, J., Sanchez-Pulido, L., Brown, C. V., Valencia, A., Arst, H. N., Jr. &Penalva, M. A. (1997). Specific DNA recognition by the *Aspergillus nidulans* three zinc finger transcription factor PacC. *J Mol Biol* 274(4): 466-480.
Faergeman, N. J., Feddersen, S., Christiansen, J. K., Larsen, M. K., Schneiter, R., Ungermann, C., Mutenda, K., Roepstorff, P. &Knudsen, J. (2004). Acyl-CoA-binding protein, Acb1p, is required for normal vacuole function and ceramide synthesis in *Saccharomyces cerevisiae*. *Biochem J* 380(Pt 3): 907-918.
Faergeman, N. J. &Knudsen, J. (1997). Role of long-chain fatty acyl-CoA esters in the regulation of metabolism and in cell signalling. *Biochem J* 323 (Pt 1): 1-12.

Faergeman, N. J., Wadum, M., Feddersen, S., Burton, M., Kragelund, B. B. &Knudsen, J. (2007). Acyl-CoA binding proteins; structural and functional conservation over 2000 MYA. *Mol Cell Biochem* 299(1-2): 55-65.

Farman, M. L. (2007). Telomeres in the rice blast fungus *Magnaporthe oryzae*: the world of the end as we know it. *FEMS Microbiol Lett* 273(2): 125-132.

Feddersen, S., Neergaard, T. B., Knudsen, J. &Faergeman, N. J. (2007). Transcriptional regulation of phospholipid biosynthesis is linked to fatty acid metabolism by an acyl-CoA-binding-protein-dependent mechanism in *Saccharomyces cerevisiae*. *Biochem J* 407(2): 219-230.

Fedoroff, N. V. (1989). About maize transposable elements and development. *Cell* 56(2): 181-191.

Fedorova, N. D., Khaldi, N., Joardar, V. S., Maiti, R., Amedeo, P., Anderson, M. J., Crabtree, J., Silva, J. C., Badger, J. H., Albarraq, A., Angiuoli, S., Bussey, H., Bowyer, P., Cotty, P. J., Dyer, P. S., Egan, A., Galens, K., Fraser-Liggett, C. M., Haas, B. J., Inman, J. M., Kent, R., Lemieux, S., Malavazi, I., Orvis, J., Roemer, T., Ronning, C. M., Sundaram, J. P., Sutton, G., Turner, G., Venter, J. C., White, O. R., Whitty, B. R., Youngman, P., Wolfe, K. H., Goldman, G. H., Wortman, J. R., Jiang, B., Denning, D. W. &Nierman, W. C. (2008). Genomic islands in the pathogenic filamentous fungus *Aspergillus fumigatus*. *PLoS Genet* 4(4): e1000046.

Fernández-Martinez, J., Brown, C., DI ez, E., Tilburn, J., Arst Jr, H., Peñalva, M. &Espeso, E. (2003). Overlap of nuclear localisation signal and specific DNA-binding residues within the zinc finger domain of PacC. *Journal of molecular biology* 334(4): 667-684.

Ferrando, A., Kron, S. J., Rios, G., Fink, G. R. &Serrano, R. (1995). Regulation of cation transport in *Saccharomyces cerevisiae* by the salt tolerance gene *HAL3*. *Mol Cell Biol* 15(10): 5470-5481.

Ferreira, M. E., Colombo, A. L., Paulsen, I., Ren, Q., Wortman, J., Huang, J., Goldman, M. H. &Goldman, G. H. (2005). The ergosterol biosynthesis pathway, transporter genes, and azole resistance in *Aspergillus fumigatus*. *Med Mycol* 43 Suppl 1: S313-319.

Fetchko, M. &Stagljar, I. (2004). Application of the split-ubiquitin membrane yeast two-hybrid system to investigate membrane protein interactions. *Methods* 32(4): 349-362.

Fiedler, K., Parton, R. G., Kellner, R., Etzold, T. &Simons, K. (1994). VIP36, a novel component of glycolipid rafts and exocytic carrier vesicles in epithelial cells. *EMBO J* 13(7): 1729-1740.

Fields, S. &Song, O. (1989). A novel genetic system to detect protein-protein interactions. *Nature* 340(6230): 245-246.

Fortwendel, J. R., Panepinto, J. C., Seitz, A. E., Askew, D. S. &Rhodes, J. C. (2004). *Aspergillus fumigatus rasA* and *rasB* regulate the timing and morphology of asexual development. *Fungal Genet Biol* 41(2): 129-139.

Fox, D. S. &Heitman, J. (2002). Good fungi gone bad: the corruption of calcineurin. *Bioessays* 24(10): 894-903.

Frame, R. &Carlton, W. W. (1988). Acute toxicity of gliotoxin in hamsters. *Toxicol Lett* 40(3): 269-273.

Franke-Fayard, B., Waters, A. P. &Janse, C. J. (2006). Real-time *in vivo* imaging of transgenic bioluminescent blood stages of rodent malaria parasites in mice. *Nat Protoc* 1(1): 476-485.

Fredriksson, R., Lagerstrom, M. C., Lundin, L. G. &Schioth, H. B. (2003). The G-protein-coupled receptors in the human genome form five main families. Phylogenetic analysis, paralogon groups, and fingerprints. *Mol Pharmacol* 63(6): 1256-1272.

Freitas-Junior, L. H., Hernandez-Rivas, R., Ralph, S. A., Montiel-Condado, D., Ruvalcaba-Salazar, O. K., Rojas-Meza, A. P., Mancio-Silva, L., Leal-Silvestre, R. J., Gontijo, A.

M., Shorte, S. &Scherf, A. (2005). Telomeric heterochromatin propagation and histone acetylation control mutually exclusive expression of antigenic variation genes in malaria parasites. *Cell* 121(1): 25-36.

Frisvad, J. C., Rank, C., Nielsen, K. F. &Larsen, T. O. (2009). Metabolomics of *Aspergillus fumigatus*. *Med Mycol* 47 Suppl 1: S53-71.

Futai, E., Maeda, T., Sorimachi, H., Kitamoto, K., Ishiura, S. &Suzuki, K. (1999). The protease activity of a calpain-like cysteine protease in Saccharomyces cerevisiae is required for alkaline adaptation and sporulation. *Mol Gen Genet* 260(6): 559-568.

Fyodorov, D. V. &Kadonaga, J. T. (2001). The many faces of chromatin remodeling: SWItching beyond transcription. *Cell* 106(5): 523-525.

Gaigg, B., Neergaard, T. B., Schneiter, R., Hansen, J. K., Faergeman, N. J., Jensen, N. A., Andersen, J. R., Friis, J., Sandhoff, R., Schroder, H. D. &Knudsen, J. (2001). Depletion of acyl-coenzyme A-binding protein affects sphingolipid synthesis and causes vesicle accumulation and membrane defects in *Saccharomyces cerevisiae*. *Mol Biol Cell* 12(4): 1147-1160.

Galagan, J. E., Calvo, S. E., Cuomo, C., Ma, L. J., Wortman, J. R., Batzoglou, S., Lee, S. I., Basturkmen, M., Spevak, C. C., Clutterbuck, J., Kapitonov, V., Jurka, J., Scazzocchio, C., Farman, M., Butler, J., Purcell, S., Harris, S., Braus, G. H., Draht, O., Busch, S., D'Enfert, C., Bouchier, C., Goldman, G. H., Bell-Pedersen, D., Griffiths-Jones, S., Doonan, J. H., Yu, J., Vienken, K., Pain, A., Freitag, M., Selker, E. U., Archer, D. B., Penalva, M. A., Oakley, B. R., Momany, M., Tanaka, T., Kumagai, T., Asai, K., Machida, M., Nierman, W. C., Denning, D. W., Caddick, M., Hynes, M., Paoletti, M., Fischer, R., Miller, B., Dyer, P., Sachs, M. S., Osmani, S. A. &Birren, B. W. (2005). Sequencing of *Aspergillus nidulans* and comparative analysis with *A. fumigatus* and *A. oryzae*. *Nature* 438(7071): 1105-1115.

Galarneau, A., Primeau, M., Trudeau, L. E. &Michnick, S. W. (2002). Beta-lactamase protein fragment complementation assays as *in vivo* and *in vitro* sensors of protein protein interactions. *Nat Biotechnol* 20(6): 619-622.

Galindo, A., Hervás-Aguilar, A., Rodríguez-Galán, O., Vincent, O., Arst Jr, H., Tilburn, J. &Peñalva, M. (2007). PalC, one of two Bro1 domain proteins in the fungal pH signalling pathway, localizes to cortical structures and binds Vps32. *Traffic (Copenhagen, Denmark)* 8(10): 1346.

Gallis, H. A., Drew, R. H. &Pickard, W. W. (1990). Amphotericin B: 30 years of clinical experience. *Rev Infect Dis* 12(2): 308-329.

Garcia-Gimeno, M. A., Munoz, I., Arino, J. &Sanz, P. (2003). Molecular characterization of Ypi1, a novel *Saccharomyces cerevisiae* type 1 protein phosphatase inhibitor. *J Biol Chem* 278(48): 47744-47752.

Garcia, R., Bermejo, C., Grau, C., Perez, R., Rodriguez-Pena, J. M., Francois, J., Nombela, C. &Arroyo, J. (2004). The global transcriptional response to transient cell wall damage in *Saccharomyces cerevisiae* and its regulation by the cell integrity signaling pathway. *J Biol Chem* 279(15): 15183-15195.

Garciadeblas, B., Rubio, F., Quintero, F. J., Banuelos, M. A., Haro, R. &Rodriguez-Navarro, A. (1993). Differential expression of two genes encoding isoforms of the ATPase involved in sodium efflux in *Saccharomyces cerevisiae*. *Mol Gen Genet* 236(2-3): 363-368.

Gavin, A. C., Bosche, M., Krause, R., Grandi, P., Marzioch, M., Bauer, A., Schultz, J., Rick, J. M., Michon, A. M., Cruciat, C. M., Remor, M., Hofert, C., Schelder, M., Brajenovic, M., Ruffner, H., Merino, A., Klein, K., Hudak, M., Dickson, D., Rudi, T., Gnau, V., Bauch, A., Bastuck, S., Huhse, B., Leutwein, C., Heurtier, M. A., Copley, R. R., Edelmann, A., Querfurth, E., Rybin, V., Drewes, G., Raida, M., Bouwmeester,

T., Bork, P., Seraphin, B., Kuster, B., Neubauer, G. &Superti-Furga, G. (2002). Functional organization of the yeast proteome by systematic analysis of protein complexes. *Nature* 415(6868): 141-147.

Ge, H., Liu, Z., Church, G. M. &Vidal, M. (2001). Correlation between transcriptome and interactome mapping data from *Saccharomyces cerevisiae*. *Nat Genet* 29(4): 482-486.

Ghannoum, M. A. &Rice, L. B. (1999). Antifungal agents: mode of action, mechanisms of resistance, and correlation of these mechanisms with bacterial resistance. *Clin Microbiol Rev* 12(4): 501-517.

Giaever, G., Chu, A. M., Ni, L., Connelly, C., Riles, L., Veronneau, S., Dow, S., Lucau-Danila, A., Anderson, K., Andre, B., Arkin, A. P., Astromoff, A., El Bakkoury, M., Bangham, R., Benito, R., Brachat, S., Campanaro, S., Curtiss, M., Davis, K., Deutschbauer, A., Entian, K.-D., Flaherty, P., Foury, F., Garfinkel, D. J., Gerstein, M., Gotte, D., Guldener, U., Hegemann, J. H., Hempel, S., Herman, Z., Jaramillo, D. F., Kelly, D. E., Kelly, S. L., Kotter, P., LaBonte, D., Lamb, D. C., Lan, N., Liang, H., Liao, H., Liu, L., Luo, C., Lussier, M., Mao, R., Menard, P., Ooi, S. L., Revuelta, J. L., Roberts, C. J., Rose, M., Ross-Macdonald, P., Scherens, B., Schimmack, G., Shafer, B., Shoemaker, D. D., Sookhai-Mahadeo, S., Storms, R. K., Strathern, J. N., Valle, G., Voet, M., Volckaert, G., Wang, C.-y., Ward, T. R., Wilhelmy, J., Winzeler, E. A., Yang, Y., Yen, G., Youngman, E., Yu, K., Bussey, H., Boeke, J. D., Snyder, M., Philippsen, P., Davis, R. W. &Johnston, M. (2002). Functional profiling of the *Saccharomyces cerevisiae* genome. *Nature* 418(6896): 387-391.

Gietz, D., St Jean, A., Woods, R. &Schiestl, R. (1992). Improved method for high efficiency transformation of intact yeast cells. *Nucleic acids research* 20(6): 1425.

Gisler, S. M., Kittanakom, S., Fuster, D., Wong, V., Bertic, M., Radanovic, T., Hall, R. A., Murer, H., Biber, J., Markovich, D., Moe, O. W. &Stagljar, I. (2008). Monitoring Protein-Protein Interactions between the Mammalian Integral Membrane Transporters and PDZ-interacting Partners Using a Modified Split-ubiquitin Membrane Yeast Two-hybrid System. *Molecular & Cellular Proteomics* 7(7): 1362-1377.

Gladfelter, A. S., Kozubowski, L., Zyla, T. R. &Lew, D. J. (2005). Interplay between septin organization, cell cycle and cell shape in yeast. *J Cell Sci* 118(Pt 8): 1617-1628.

Glayzer, D. C., Roberts, I. N., Archer, D. B. &Oliver, R. P. (1995). The isolation of Ant1, a transposable element from *Aspergillus niger*. *Mol Gen Genet* 249(4): 432-438.

Glomski, I. J., Piris-Gimenez, A., Huerre, M., Mock, M. &Goossens, P. L. (2007). Primary involvement of pharynx and peyer's patch in inhalational and intestinal anthrax. *PLoS Pathog* 3(6): e76.

Glover, C. V., 3rd (1998). On the physiological role of casein kinase II in *Saccharomyces cerevisiae*. *Prog Nucleic Acid Res Mol Biol* 59: 95-133.

Goffeau, A., Barrell, B. G., Bussey, H., Davis, R. W., Dujon, B., Feldmann, H., Galibert, F., Hoheisel, J. D., Jacq, C., Johnston, M., Louis, E. J., Mewes, H. W., Murakami, Y., Philippsen, P., Tettelin, H. &Oliver, S. G. (1996). Life with 6000 genes. *Science* 274(5287): 546, 563-547.

Gomez, A., Perez, J., Reyes, A., Duran, A. &Roncero, C. (2009). Slt2 and Rim101 contribute independently to the correct assembly of the chitin ring at the budding yeast neck in *Saccharomyces cerevisiae*. *Eukaryot Cell* 8(9): 1449-1459.

Goodman, O. B., Jr., Krupnick, J. G., Santini, F., Gurevich, V. V., Penn, R. B., Gagnon, A. W., Keen, J. H. &Benovic, J. L. (1996). Beta-arrestin acts as a clathrin adaptor in endocytosis of the beta2-adrenergic receptor. *Nature* 383(6599): 447-450.

Graessle, S., Dangl, M., Haas, H., Mair, K., Trojer, P., Brandtner, E. M., Walton, J. D., Loidl, P. &Brosch, G. (2000). Characterization of two putative histone deacetylase genes from *Aspergillus nidulans*. *Biochim Biophys Acta* 1492(1): 120-126.

Granger, D. L., Perfect, J. R. &Durack, D. T. (1985). Virulence of *Cryptococcus neoformans*. Regulation of capsule synthesis by carbon dioxide. *J Clin Invest* 76(2): 508-516.
Granzin, J., Wilden, U., Choe, H. W., Labahn, J., Krafft, B. &Buldt, G. (1998). X-ray crystal structure of arrestin from bovine rod outer segments. *Nature* 391(6670): 918-921.
Greenberger, P. A. &Patterson, R. (1987). Allergic bronchopulmonary aspergillosis. Model of bronchopulmonary disease with defined serologic, radiologic, pathologic and clinical findings from asthma to fatal destructive lung disease. *Chest* 91(6 Suppl): 165S-171S.
Grentzmann, G., Ingram, J. A., Kelly, P. J., Gesteland, R. F. &Atkins, J. F. (1998). A dual-luciferase reporter system for studying recoding signals. *RNA* 4(4): 479-486.
Gruenberg, J. &Maxfield, F. R. (1995). Membrane transport in the endocytic pathway. *Curr Opin Cell Biol* 7(4): 552-563.
Gudermann, T., Nurnberg, B. &Schultz, G. (1995). Receptors and G proteins as primary components of transmembrane signal transduction. Part 1. G-protein-coupled receptors: structure and function. *J Mol Med* 73(2): 51-63.
Gurevich, V. V., Dion, S. B., Onorato, J. J., Ptasienski, J., Kim, C. M., Sterne-Marr, R., Hosey, M. M. &Benovic, J. L. (1995). Arrestin interactions with G protein-coupled receptors. Direct binding studies of wild type and mutant arrestins with rhodopsin, beta 2-adrenergic, and m2 muscarinic cholinergic receptors. *J Biol Chem* 270(2): 720-731.
Haas, H. (2003). Molecular genetics of fungal siderophore biosynthesis and uptake: the role of siderophores in iron uptake and storage. *Appl Microbiol Biotechnol* 62(4): 316-330.
Haas, H., Eisendle, M. &Turgeon, B. G. (2008). Siderophores in fungal physiology and virulence. *Annu Rev Phytopathol* 46: 149-187.
Han, K. H., Kim, J. H., Moon, H., Kim, S., Lee, S. S., Han, D. M., Jahng, K. Y. &Chae, K. S. (2008). The *Aspergillus nidulans esdC* (early sexual development) gene is necessary for sexual development and is controlled by veA and a heterotrimeric G protein. *Fungal Genet Biol* 45(3): 310-318.
Han, K. H., Seo, J. A. &Yu, J. H. (2004). A putative G protein-coupled receptor negatively controls sexual development in *Aspergillus nidulans*. *Mol Microbiol* 51(5): 1333-1345.
Hansen, K. R., Burns, G., Mata, J., Volpe, T. A., Martienssen, R. A., Bahler, J. &Thon, G. (2005). Global effects on gene expression in fission yeast by silencing and RNA interference machineries. *Mol Cell Biol* 25(2): 590-601.
Haro, R., Garciadeblas, B. &Rodriguez-Navarro, A. (1991). A novel P-type ATPase from yeast involved in sodium transport. *FEBS Lett* 291(2): 189-191.
Hastings, J. W. (1996). Chemistries and colors of bioluminescent reactions: a review. *Gene* 173(1 Spec No): 5-11.
Hauri, H., Appenzeller, C., Kuhn, F. &Nufer, O. (2000). Lectins and traffic in the secretory pathway. *FEBS Lett* 476(1-2): 32-37.
Hayashi, M., Fukuzawa, T., Sorimachi, H. &Maeda, T. (2005). Constitutive activation of the pH-responsive Rim101 pathway in yeast mutants defective in late steps of the MVB/ESCRT pathway. *Mol Cell Biol* 25(21): 9478-9490.
Hayashi, M., Ohkuni, K. &Yamashita, I. (1998). Control of division arrest and entry into meiosis by extracellular alkalisation in *Saccharomyces cerevisiae*. *Yeast* 14(10): 905-913.
Hearn, V. M. &Mackenzie, D. W. (1980). Mycelial antigens from two strains of *Aspergillus fumigatus*: an analysis by two-dimensional immunoelectrophoresis. *Mykosen* 23(10): 549-562.

Heinisch, J. J., Lorberg, A., Schmitz, H. P. &Jacoby, J. J. (1999). The protein kinase C-mediated MAP kinase pathway involved in the maintenance of cellular integrity in *Saccharomyces cerevisiae*. *Mol Microbiol* 32(4): 671-680.

Henrici, A. T. (1939). An Endotoxin from *Aspergillus Fumigatus*. *The Journal of Immunology* 36(319 -338).

Hensel, M., Arst, H. N., Jr., Aufauvre-Brown, A. &Holden, D. W. (1998). The role of the *Aspergillus fumigatus areA* gene in invasive pulmonary aspergillosis. *Mol Gen Genet* 258(5): 553-557.

Herbrecht, R. (2002). Improving the outcome of invasive aspergillosis: new diagnostic tools and new therapeutic strategies. *Ann Hematol* 81 Suppl 2: S52-53.

Herbrecht, R., Denning, D. W., Patterson, T. F., Bennett, J. E., Greene, R. E., Oestmann, J. W., Kern, W. V., Marr, K. A., Ribaud, P., Lortholary, O., Sylvester, R., Rubin, R. H., Wingard, J. R., Stark, P., Durand, C., Caillot, D., Thiel, E., Chandrasekar, P. H., Hodges, M. R., Schlamm, H. T., Troke, P. F. &de Pauw, B. (2002). Voriconazole versus amphotericin B for primary therapy of invasive aspergillosis. *N Engl J Med* 347(6): 408-415.

Herranz, S., Rodríguez, J., Bussink, H., Sánchez-Ferrero, J., Arst, H., Peñalva, M. &Vincent, O. (2005). Arrestin-related proteins mediate pH signaling in fungi. *Proceedings of the National Academy of Sciences of the United States of America* 102(34): 12141.

Hershko, A. &Ciechanover, A. (1992). The ubiquitin system for protein degradation. *Annu Rev Biochem* 61: 761-807.

Hervas-Aguilar, A., Rodriguez, J. M., Tilburn, J., Arst, H. N., Jr. &Penalva, M. A. (2007). Evidence for the direct involvement of the proteasome in the proteolytic processing of the *Aspergillus nidulans* zinc finger transcription factor PacC. *J Biol Chem* 282(48): 34735-34747.

Heymann, P., Ernst, J. F. &Winkelmann, G. (2000). A gene of the major facilitator superfamily encodes a transporter for enterobactin (Enb1p) in *Saccharomyces cerevisiae*. *Biometals* 13(1): 65-72.

Hirai, S., Kawasaki, H., Yaniv, M. &Suzuki, K. (1991). Degradation of transcription factors, c-Jun and c-Fos, by calpain. *FEBS Lett* 287(1-2): 57-61.

Hissen, A. H., Wan, A. N., Warwas, M. L., Pinto, L. J. &Moore, M. M. (2005). The *Aspergillus fumigatus* siderophore biosynthetic gene *sidA*, encoding L-ornithine N^5-oxygenase, is required for virulence. *Infect Immun* 73(9): 5493-5503.

Ho, Y., Gruhler, A., Heilbut, A., Bader, G. D., Moore, L., Adams, S. L., Millar, A., Taylor, P., Bennett, K., Boutilier, K., Yang, L., Wolting, C., Donaldson, I., Schandorff, S., Shewnarane, J., Vo, M., Taggart, J., Goudreault, M., Muskat, B., Alfarano, C., Dewar, D., Lin, Z., Michalickova, K., Willems, A. R., Sassi, H., Nielsen, P. A., Rasmussen, K. J., Andersen, J. R., Johansen, L. E., Hansen, L. H., Jespersen, H., Podtelejnikov, A., Nielsen, E., Crawford, J., Poulsen, V., Sorensen, B. D., Matthiesen, J., Hendrickson, R. C., Gleeson, F., Pawson, T., Moran, M. F., Durocher, D., Mann, M., Hogue, C. W., Figeys, D. &Tyers, M. (2002). Systematic identification of protein complexes in *Saccharomyces cerevisiae* by mass spectrometry. *Nature* 415(6868): 180-183.

Hohl, T. M. &Feldmesser, M. (2007). *Aspergillus fumigatus*: principles of pathogenesis and host defense. *Eukaryot Cell* 6(11): 1953-1963.

Hospenthal, D. R., Kwon-Chung, K. J. &Bennett, J. E. (1998). Concentrations of airborne *Aspergillus* compared to the incidence of invasive aspergillosis: lack of correlation. *Med Mycol* 36(3): 165-168.

Huang, D., Moffat, J. &Andrews, B. (2002). Dissection of a complex phenotype by functional genomics reveals roles for the yeast cyclin-dependent protein kinase Pho85 in stress adaptation and cell integrity. *Mol Cell Biol* 22(14): 5076-5088.
Huang, Y., Wilkinson, G. F. &Willars, G. B. (2010). Role of the signal peptide in the synthesis and processing of the glucagon-like peptide-1 receptor. *Br J Pharmacol* 159(1): 237-251.
Hurto, R. L., Tong, A. H., Boone, C. &Hopper, A. K. (2007). Inorganic phosphate deprivation causes tRNA nuclear accumulation via retrograde transport in *Saccharomyces cerevisiae*. *Genetics* 176(2): 841-852.
Hutchens, M. &Luker, G. D. (2007). Applications of bioluminescence imaging to the study of infectious diseases. *Cell Microbiol* 9(10): 2315-2322.
Ibrahim-Granet, O., Dubourdeau, M., Latge, J. P., Ave, P., Huerre, M., Brakhage, A. A. &Brock, M. (2008). Methylcitrate synthase from *Aspergillus fumigatus* is essential for manifestation of invasive aspergillosis. *Cell Microbiol* 10(1): 134-148.
Ibrahim-Granet, O., Jouvion, G., Hohl, T. M., Droin-Bergere, S., Philippart, F., Kim, O. Y., Adib-Conquy, M., Schwendener, R., Cavaillon, J. M. &Brock, M. (2010). *In vivo* bioluminescence imaging and histopathopathologic analysis reveal distinct roles for resident and recruited immune effector cells in defense against invasive aspergillosis. *BMC Microbiol* 10: 105.
Ibrahim-Granet, O., Philippe, B., Boleti, H., Boisvieux-Ulrich, E., Grenet, D., Stern, M. &Latge, J. P. (2003). Phagocytosis and intracellular fate of *Aspergillus fumigatus* conidia in alveolar macrophages. *Infect Immun* 71(2): 891-903.
Ikeda, M., Kihara, A., Denpoh, A. &Igarashi, Y. (2008). The Rim101 pathway is involved in Rsb1 expression induced by altered lipid asymmetry. *Mol Biol Cell* 19(5): 1922-1931.
Israel, H. L., Lenchner, G. S. &Atkinson, G. W. (1982). Sarcoidosis and aspergilloma. The role of surgery. *Chest* 82(4): 430-432.
Ito, T., Chiba, T., Ozawa, R., Yoshida, M., Hattori, M. &Sakaki, Y. (2001). A comprehensive two-hybrid analysis to explore the yeast protein interactome. *Proc Natl Acad Sci U S A* 98(8): 4569-4574.
Iyer, K., Burkle, L., Auerbach, D., Thaminy, S., Dinkel, M., Engels, K. &Stagljar, I. (2005). Utilizing the split-ubiquitin membrane yeast two-hybrid system to identify protein-protein interactions of integral membrane proteins. *Science Signaling* 2005(275).
Jaton-Ogay, K., Paris, S., Huerre, M., Quadroni, M., Falchetto, R., Togni, G., Latge, J. P. &Monod, M. (1994). Cloning and disruption of the gene encoding an extracellular metalloprotease of *Aspergillus fumigatus*. *Mol Microbiol* 14(5): 917-928.
Jean-Alphonse, F. &Hanyaloglu, A. C. (2010). Regulation of GPCR signal networks via membrane trafficking. *Mol Cell Endocrinol*.
Jenuwein, T. &Allis, C. D. (2001). Translating the histone code. *Science* 293(5532): 1074-1080.
Johnsson, N. &Varshavsky, A. (1994). Split ubiquitin as a sensor of protein interactions *in vivo*. *Proceedings of the National Academy of Sciences* 91(22): 10340.
Johnston, R. B., Jr. (2001). Clinical aspects of chronic granulomatous disease. *Curr Opin Hematol* 8(1): 17-22.
Jordan, I. K., Rogozin, I. B., Glazko, G. V. &Koonin, E. V. (2003). Origin of a substantial fraction of human regulatory sequences from transposable elements. *Trends Genet* 19(2): 68-72.
Juliano, R. L., Grant, C. W., Barber, K. R. &Kalp, M. A. (1987). Mechanism of the selective toxicity of amphotericin B incorporated into liposomes. *Mol Pharmacol* 31(1): 1-11.
Jungmann, J., Reins, H. A., Lee, J., Romeo, A., Hassett, R., Kosman, D. &Jentsch, S. (1993). MAC1, a nuclear regulatory protein related to Cu-dependent transcription factors is

involved in Cu/Fe utilization and stress resistance in yeast. *EMBO J* 12(13): 5051-5056.
Kaffman, A., Rank, N. M., O'Neill, E. M., Huang, L. S. &O'Shea, E. K. (1998). The receptor Msn5 exports the phosphorylated transcription factor Pho4 out of the nucleus. *Nature* 396(6710): 482-486.
Kanno, A., Ozawa, T. &Umezawa, Y. (2006). Intein-mediated reporter gene assay for detecting protein-protein interactions in living mammalian cells. *Anal Chem* 78(2): 556-560.
Karsi, A. &Lawrence, M. L. (2007). Broad host range fluorescence and bioluminescence expression vectors for Gram-negative bacteria. *Plasmid* 57(3): 286-295.
Kashkush, K., Feldman, M. &Levy, A. A. (2003). Transcriptional activation of retrotransposons alters the expression of adjacent genes in wheat. *Nat Genet* 33(1): 102-106.
Katan-Khaykovich, Y. &Struhl, K. (2005). Heterochromatin formation involves changes in histone modifications over multiple cell generations. *EMBO J* 24(12): 2138-2149.
Katzmann, D. J., Babst, M. &Emr, S. D. (2001). Ubiquitin-dependent sorting into the multivesicular body pathway requires the function of a conserved endosomal protein sorting complex, ESCRT-I. *Cell* 106(2): 145-155.
Katzmann, D. J., Odorizzi, G. &Emr, S. D. (2002). Receptor downregulation and multivesicular-body sorting. *Nat Rev Mol Cell Biol* 3(12): 893-905.
Kauffman, C. A. (2006). Fungal infections. *Proc Am Thorac Soc* 3(1): 35-40.
Khoufache, K., Puel, O., Loiseau, N., Delaforge, M., Rivollet, D., Coste, A., Cordonnier, C., Escudier, E., Botterel, F. &Bretagne, S. (2007). Verruculogen associated with *Aspergillus fumigatus* hyphae and conidia modifies the electrophysiological properties of human nasal epithelial cells. *BMC Microbiol* 7: 5.
Kirsten, D., Rieger, U., Amthor, M. &Magnussen, H. (1992). Invasive aspergillosis in cavitary lung sarcoidosis. *Pneumologie* 46(6): 239-242.
Kittanakom, S., Chuk, M., Wong, V., Snyder, J., Edmonds, D., Lydakis, A., Zhang, Z., Auerbach, D. &Stagljar, I. (2009). Analysis of membrane protein complexes using the split-ubiquitin membrane yeast two-hybrid (MYTH) system. *Methods Mol Biol* 548: 247-271.
Klionsky, D. J., Nelson, H. &Nelson, N. (1992). Compartment acidification is required for efficient sorting of proteins to the vacuole in *Saccharomyces cerevisiae*. *J Biol Chem* 267(5): 3416-3422.
Knudsen, J., Faergeman, N. J., Skott, H., Hummel, R., Borsting, C., Rose, T. M., Andersen, J. S., Hojrup, P., Roepstorff, P. &Kristiansen, K. (1994). Yeast acyl-CoA-binding protein: acyl-CoA-binding affinity and effect on intracellular acyl-CoA pool size. *Biochem J* 302 (Pt 2): 479-485.
Knudsen, J., Neergaard, T. B., Gaigg, B., Jensen, M. V. &Hansen, J. K. (2000). Role of acyl-CoA binding protein in acyl-CoA metabolism and acyl-CoA-mediated cell signaling. *J Nutr* 130(2S Suppl): 294S-298S.
Knutsen, A. &Slavin, R. G. (1992). Allergic bronchopulmonary mycosis complicating cystic fibrosis. *Semin Respir Infect* 7(3): 179-192.
Knutsen, A. P. &Slavin, R. G. (1991). Allergic bronchopulmonary aspergillosis in patients with cystic fibrosis. *Clin Rev Allergy* 9(1-2): 103-118.
Kochl, R., Alken, M., Rutz, C., Krause, G., Oksche, A., Rosenthal, W. &Schulein, R. (2002). The signal peptide of the G protein-coupled human endothelin B receptor is necessary for translocation of the N-terminal tail across the endoplasmic reticulum membrane. *J Biol Chem* 277(18): 16131-16138.

Kogan, T. V., Jadoun, J., Mittelman, L., Hirschberg, K. &Osherov, N. (2004). Involvement of secreted *Aspergillus fumigatus* proteases in disruption of the actin fiber cytoskeleton and loss of focal adhesion sites in infected A549 lung pneumocytes. *J Infect Dis* 189(11): 1965-1973.

Kohout, T. A. &Lefkowitz, R. J. (2003). Regulation of G protein-coupled receptor kinases and arrestins during receptor desensitization. *Mol Pharmacol* 63(1): 9-18.

Korber, P. &Horz, W. (2004). SWRred not shaken; mixing the histones. *Cell* 117(1): 5-7.

Kothary, M. H., Chase, T., Jr. &Macmillan, J. D. (1984). Correlation of elastase production by some strains of *Aspergillus fumigatus* with ability to cause pulmonary invasive aspergillosis in mice. *Infect Immun* 43(1): 320-325.

Kozubowski, L., Panek, H., Rosenthal, A., Bloecher, A., DeMarini, D. J. &Tatchell, K. (2003). A Bni4-Glc7 phosphatase complex that recruits chitin synthase to the site of bud emergence. *Mol Biol Cell* 14(1): 26-39.

Kragelund, B. B., Knudsen, J. &Poulsen, F. M. (1999). Acyl-coenzyme A binding protein (ACBP). *Biochim Biophys Acta* 1441(2-3): 150-161.

Krappmann, S., Bignell, E. M., Reichard, U., Rogers, T., Haynes, K. &Braus, G. H. (2004). The *Aspergillus fumigatus* transcriptional activator CpcA contributes significantly to the virulence of this fungal pathogen. *Mol Microbiol* 52(3): 785-799.

Krappmann, S. &Braus, G. H. (2005). Nitrogen metabolism of *Aspergillus* and its role in pathogenicity. *Med Mycol* 43 Suppl 1: S31-40.

Krasnick, J., Patterson, R. &Roberts, M. (1995). Allergic bronchopulmonary aspergillosis presenting with cough variant asthma and identifiable source of *Aspergillus fumigatus*. *Ann Allergy Asthma Immunol* 75(4): 344-346.

Kubodera, T., Yamashita, N. &Nishimura, A. (2000). Pyrithiamine resistance gene (*ptrA*) of *Aspergillus oryzae*: cloning, characterization and application as a dominant selectable marker for transformation. *Biosci Biotechnol Biochem* 64(7): 1416-1421.

Kubodera, T., Yamashita, N. &Nishimura, A. (2002). Transformation of *Aspergillus* sp. and *Trichoderma reesei* using the pyrithiamine resistance gene (ptrA) of *Aspergillus oryzae*. *Biosci Biotechnol Biochem* 66(2): 404-406.

Kuno, T., Tanaka, H., Mukai, H., Chang, C. D., Hiraga, K., Miyakawa, T. &Tanaka, C. (1991). cDNA cloning of a calcineurin B homolog in Saccharomyces cerevisiae. *Biochem Biophys Res Commun* 180(2): 1159-1163.

Lafon, A., Han, K. H., Seo, J. A., Yu, J. H. &d'Enfert, C. (2006). G-protein and cAMP-mediated signaling in aspergilli: a genomic perspective. *Fungal Genet Biol* 43(7): 490-502.

Lafon, A., Seo, J. A., Han, K. H., Yu, J. H. &d'Enfert, C. (2005). The heterotrimeric G-protein GanB(α)-SfaD(β)-GpgA(γ) is a carbon source sensor involved in early cAMP-dependent germination in *Aspergillus nidulans*. *Genetics* 171(1): 71-80.

Lagorce, A., Hauser, N. C., Labourdette, D., Rodriguez, C., Martin-Yken, H., Arroyo, J., Hoheisel, J. D. &Francois, J. (2003). Genome-wide analysis of the response to cell wall mutations in the yeast *Saccharomyces cerevisiae*. *J Biol Chem* 278(22): 20345-20357.

Lamarre, C., Sokol, S., Debeaupuis, J. P., Henry, C., Lacroix, C., Glaser, P., Coppee, J. Y., Francois, J. M. &Latge, J. P. (2008). Transcriptomic analysis of the exit from dormancy of *Aspergillus fumigatus* conidia. *BMC Genomics* 9: 417.

Lamb, T. &Mitchell, A. (2003). The transcription factor Rim101p governs ion tolerance and cell differentiation by direct repression of the regulatory genes NRG1 and SMP1 in *Saccharomyces cerevisiae*. *Mol Cell Biol* 23((2)): 677-686.

Lamb, T., Xu, W., Diamond, A. &Mitchell, A. (2001). Alkaline Response Genes of *Saccharomyces cerevisiae* and their relationship to the RIM101 Pathway. *Journal of Biological Chemistry* 276(3): 1850.

Lambert, M., Blanchin-Roland, S., Le Louedec, F., Lepingle, A. &Gaillardin, C. (1997). Genetic analysis of regulatory mutants affecting synthesis of extracellular proteinases in the yeast *Yarrowia lipolytica*: identification of a RIM101/pacC homolog. *Mol. Cell. Biol.* 17(7): 3966-3976.

Lanctot, P. M., Leclerc, P. C., Escher, E., Leduc, R. &Guillemette, G. (1999). Role of N-glycosylation in the expression and functional properties of human AT1 receptor. *Biochemistry* 38(27): 8621-8627.

Laporte, S. A., Oakley, R. H., Zhang, J., Holt, J. A., Ferguson, S. S., Caron, M. G. &Barak, L. S. (1999). The beta2-adrenergic receptor/betaarrestin complex recruits the clathrin adaptor AP-2 during endocytosis. *Proc Natl Acad Sci U S A* 96(7): 3712-3717.

Larsen, M. K., Tuck, S., Faergeman, N. J. &Knudsen, J. (2006). MAA-1, a novel acyl-CoA-binding protein involved in endosomal vesicle transport in *Caenorhabditis elegans*. *Mol Biol Cell* 17(10): 4318-4329.

Larson, J. R., Bharucha, J. P., Ceaser, S., Salamon, J., Richardson, C. J., Rivera, S. M. &Tatchell, K. (2008). Protein phosphatase type 1 directs chitin synthesis at the bud neck in *Saccharomyces cerevisiae*. *Mol Biol Cell* 19(7): 3040-3051.

Lashkari, D. A., DeRisi, J. L., McCusker, J. H., Namath, A. F., Gentile, C., Hwang, S. Y., Brown, P. O. &Davis, R. W. (1997). Yeast microarrays for genome wide parallel genetic and gene expression analysis. *Proc Natl Acad Sci U S A* 94(24): 13057-13062.

Latge, J. P. (1999). *Aspergillus fumigatus* and aspergillosis. *Clin Microbiol Rev* 12(2): 310-350.

Latge, J. P., Mouyna, I., Tekaia, F., Beauvais, A., Debeaupuis, J. P. &Nierman, W. (2005). Specific molecular features in the organization and biosynthesis of the cell wall of Aspergillus fumigatus. *Med Mycol* 43 Suppl 1: S15-22.

Lazarus, A. A., Thilagar, B. &McKay, S. A. (2008). Allergic bronchopulmonary aspergillosis. *Dis Mon* 54(8): 547-564.

Lee, B. N. &Adams, T. H. (1994). The Aspergillus nidulans *fluG* gene is required for production of an extracellular developmental signal and is related to prokaryotic glutamine synthetase I. *Genes Dev* 8(6): 641-651.

Lee, H. K., Hsu, A. K., Sajdak, J., Qin, J. &Pavlidis, P. (2004). Coexpression analysis of human genes across many microarray data sets. *Genome Res* 14(6): 1085-1094.

Lefkowitz, R. J. &Shenoy, S. K. (2005). Transduction of receptor signals by β-arrestins. *Science* 308(5721): 512-517.

Lenburg, M. E. &O'Shea, E. K. (1996). Signaling phosphate starvation. *Trends Biochem Sci* 21(10): 383-387.

Leslie, C. E., Flannigan, B. &Milne, L. J. (1988). Morphological studies on clinical isolates of *Aspergillus fumigatus*. *J Med Vet Mycol* 26(6): 335-341.

Lessing, F., Kniemeyer, O., Wozniok, I., Loeffler, J., Kurzai, O., Haertl, A. &Brakhage, A. A. (2007). The *Aspergillus fumigatus* transcriptional regulator AfYap1 represents the major regulator for defense against reactive oxygen intermediates but is dispensable for pathogenicity in an intranasal mouse infection model. *Eukaryot Cell* 6(12): 2290-2302.

Letscher-Bru, V. &Herbrecht, R. (2003). Caspofungin: the first representative of a new antifungal class. *J Antimicrob Chemother* 51(3): 513-521.

Levin, D. E. (2005). Cell wall integrity signaling in *Saccharomyces cerevisiae*. *Microbiol Mol Biol Rev* 69(2): 262-291.

Levitz, S. M., Nong, S. H., Seetoo, K. F., Harrison, T. S., Speizer, R. A. &Simons, E. R. (1999). *Cryptococcus neoformans* resides in an acidic phagolysosome of human macrophages. *Infect Immun* 67(2): 885-890.

Li, W. &Mitchell, A. (1997). Proteolytic activation of Rim1p, a positive regulator of yeast sporulation and invasive growth. *Genetics* 145(1): 63.

Lin, S. J., Schranz, J. &Teutsch, S. M. (2001). Aspergillosis case-fatality rate: systematic review of the literature. *Clin Infect Dis* 32(3): 358-366.

Lionakis, M. S. &Kontoyiannis, D. P. (2003). Glucocorticoids and invasive fungal infections. *Lancet* 362(9398): 1828-1838.

Lipshutz, G. S., Gruber, C. A., Cao, Y., Hardy, J., Contag, C. H. &Gaensler, K. M. (2001). *In utero* delivery of adeno-associated viral vectors: intraperitoneal gene transfer produces long-term expression. *Mol Ther* 3(3): 284-292.

Lissanu Deribe, Y., Wild, P., Chandrashaker, A., Curak, J., Schmidt, M. H. H., Kalaidzidis, Y., Milutinovic, N., Kratchmarova, I., Buerkle, L., Fetchko, M. J., Schmidt, P., Kittanakom, S., Brown, K. R., Jurisica, I., Blagoev, B., Zerial, M., Stagljar, I. &Dikic, I. (2009). Regulation of Epidermal Growth Factor Receptor Trafficking by Lysine Deacetylase HDAC6. *Sci. Signal.* 2(102): ra84-.

Liu, J. Y., Timm, D. E. &Hurley, T. D. (2006). Pyrithiamine as a substrate for thiamine pyrophosphokinase. *J Biol Chem* 281(10): 6601-6607.

Loo, T. W., Ho, C. &Clarke, D. M. (1995). Expression of a functionally active human renal sodium-calcium exchanger lacking a signal sequence. *J Biol Chem* 270(33): 19345-19350.

Lorenz, W. W., Cormier, M. J., O'Kane, D. J., Hua, D., Escher, A. A. &Szalay, A. A. (1996). Expression of the *Renilla reniformis* luciferase gene in mammalian cells. *J Biolumin Chemilumin* 11(1): 31-37.

Lyons, T. J., Gasch, A. P., Gaither, L. A., Botstein, D., Brown, P. O. &Eide, D. J. (2000). Genome-wide characterization of the Zap1p zinc-responsive regulon in yeast. *Proc Natl Acad Sci U S A* 97(14): 7957-7962.

Ma, Y., Qiao, J., Liu, W., Wan, Z., Wang, X., Calderone, R. &Li, R. (2008). The Sho1 sensor regulates growth, morphology, and oxidant adaptation in *Aspergillus fumigatus* but is not essential for development of invasive pulmonary aspergillosis. *Infect Immun* 76(4): 1695-1701.

MacCabe, A. P., Van den Hombergh, J. P., Tilburn, J., Arst, H. N., Jr. &Visser, J. (1996). Identification, cloning and analysis of the *Aspergillus niger* gene *pacC*, a wide domain regulatory gene responsive to ambient pH. *Mol Gen Genet* 250(3): 367-374.

Maccheroni, W., Jr., May, G. S., Martinez-Rossi, N. M. &Rossi, A. (1997). The sequence of palF, an environmental pH response gene in *Aspergillus nidulans*. *Gene* 194(2): 163-167.

Machida, M., Asai, K., Sano, M., Tanaka, T., Kumagai, T., Terai, G., Kusumoto, K., Arima, T., Akita, O., Kashiwagi, Y., Abe, K., Gomi, K., Horiuchi, H., Kitamoto, K., Kobayashi, T., Takeuchi, M., Denning, D. W., Galagan, J. E., Nierman, W. C., Yu, J., Archer, D. B., Bennett, J. W., Bhatnagar, D., Cleveland, T. E., Fedorova, N. D., Gotoh, O., Horikawa, H., Hosoyama, A., Ichinomiya, M., Igarashi, R., Iwashita, K., Juvvadi, P. R., Kato, M., Kato, Y., Kin, T., Kokubun, A., Maeda, H., Maeyama, N., Maruyama, J., Nagasaki, H., Nakajima, T., Oda, K., Okada, K., Paulsen, I., Sakamoto, K., Sawano, T., Takahashi, M., Takase, K., Terabayashi, Y., Wortman, J. R., Yamada, O., Yamagata, Y., Anazawa, H., Hata, Y., Koide, Y., Komori, T., Koyama, Y., Minetoki, T., Suharnan, S., Tanaka, A., Isono, K., Kuhara, S., Ogasawara, N. &Kikuchi, H. (2005). Genome sequencing and analysis of *Aspergillus oryzae*. *Nature* 438(7071): 1157-1161.

Maertens, J., Raad, I., Petrikkos, G., Boogaerts, M., Selleslag, D., Petersen, F. B., Sable, C. A., Kartsonis, N. A., Ngai, A., Taylor, A., Patterson, T. F., Denning, D. W. &Walsh, T. J. (2004). Efficacy and safety of caspofungin for treatment of invasive aspergillosis in patients refractory to or intolerant of conventional antifungal therapy. *Clin Infect Dis* 39(11): 1563-1571.

Maiya, S., Grundmann, A., Li, X., Li, S. M. &Turner, G. (2007). Identification of a Hybrid PKS/NRPS Required for Pseurotin A Biosynthesis in the Human Pathogen *Aspergillus fumigatus*. *ChemBioChem* 8(14): 1736-1743.

Mandel, M. &Higa, A. (1970). Calcium-dependent bacteriophage DNA infection. *Journal of molecular biology* 53(1): 159-162.

Markaryan, A., Morozova, I., Yu, H. &Kolattukudy, P. E. (1994). Purification and characterization of an elastinolytic metalloprotease from *Aspergillus fumigatus* and immunoelectron microscopic evidence of secretion of this enzyme by the fungus invading the murine lung. *Infect Immun* 62(6): 2149-2157.

Marr, K. A., Carter, R. A., Boeckh, M., Martin, P. &Corey, L. (2002). Invasive aspergillosis in allogeneic stem cell transplant recipients: changes in epidemiology and risk factors. *Blood* 100(13): 4358-4366.

Marshall, F. H., White, J., Main, M., Green, A. &Wise, A. (1999). GABA(B) receptors function as heterodimers. *Biochem Soc Trans* 27(4): 530-535.

Massaad, M. J. &Herscovics, A. (2001). Interaction of the endoplasmic reticulum alpha 1,2-mannosidase Mns1p with Rer1p using the split-ubiquitin system. *J Cell Sci* 114(Pt 24): 4629-4635.

Mattiazzi, M., Jambhekar, A., Kaferle, P., Derisi, J. L., Krizaj, I. &Petrovic, U. (2010). Genetic interactions between a phospholipase A2 and the Rim101 pathway components in *S. cerevisiae* reveal a role for this pathway in response to changes in membrane composition and shape. *Mol Genet Genomics* 283(6): 519-530.

Maubon, D., Park, S., Tanguy, M., Huerre, M., Schmitt, C., Prevost, M. C., Perlin, D. S., Latge, J. P. &Beauvais, A. (2006). AGS3, an alpha(1-3)glucan synthase gene family member of *Aspergillus fumigatus*, modulates mycelium growth in the lung of experimentally infected mice. *Fungal Genet Biol* 43(5): 366-375.

McClintock, B. (1984). The significance of responses of the genome to challenge. *Science* 226(4676): 792-801.

McDonagh, A., Fedorova, N. D., Crabtree, J., Yu, Y., Kim, S., Chen, D., Loss, O., Cairns, T., Goldman, G., Armstrong-James, D., Haynes, K., Haas, H., Schrettl, M., May, G., Nierman, W. C. &Bignell, E. (2008a). Sub-Telomere Directed Gene Expression during Initiation of Invasive Aspergillosis. *PLoS Pathog* 4(9): e1000154.

McDonald, P. H., Chow, C. W., Miller, W. E., Laporte, S. A., Field, M. E., Lin, F. T., Davis, R. J. &Lefkowitz, R. J. (2000). Beta-arrestin 2: a receptor-regulated MAPK scaffold for the activation of JNK3. *Science* 290(5496): 1574-1577.

Melamed, D., Pnueli, L. &Arava, Y. (2008). Yeast translational response to high salinity: global analysis reveals regulation at multiple levels. *RNA* 14(7): 1337-1351.

Mendoza, I., Rubio, F., Rodriguez-Navarro, A. &Pardo, J. M. (1994). The protein phosphatase calcineurin is essential for NaCl tolerance of *Saccharomyces cerevisiae*. *J Biol Chem* 269(12): 8792-8796.

Mikulska, M., Raiola, A. M., Bruno, B., Furfaro, E., Van Lint, M. T., Bregante, S., Ibatici, A., Del Bono, V., Bacigalupo, A. &Viscoli, C. (2009). Risk factors for invasive aspergillosis and related mortality in recipients of allogeneic SCT from alternative donors: an analysis of 306 patients. *Bone Marrow Transplant* 44(6): 361-370.

Miller, J. P., Lo, R. S., Ben-Hur, A., Desmarais, C., Stagljar, I., Noble, W. S. &Fields, S. (2005). Large-scale identification of yeast integral membrane protein interactions. *Proc Natl Acad Sci U S A* 102(34): 12123-12128.
Miller, M. B. &Tang, Y.-W. (2009). Basic Concepts of Microarrays and Potential Applications in Clinical Microbiology. *Clin. Microbiol. Rev.* 22(4): 611-633.
Milligan, G. (2001). Oligomerisation of G-protein-coupled receptors. *J Cell Sci* 114(Pt 7): 1265-1271.
Milligan, G. (2007). G protein-coupled receptor dimerisation: molecular basis and relevance to function. *Biochim Biophys Acta* 1768(4): 825-835.
Milligan, G. (2010). The role of dimerisation in the cellular trafficking of G-protein-coupled receptors. *Curr Opin Pharmacol* 10(1): 23-29.
Milligan, G., Canals, M., Pediani, J. D., Ellis, J. &Lopez-Gimenez, J. F. (2006). The role of GPCR dimerisation/oligomerisation in receptor signalling. *Ernst Schering Found Symp Proc* (2): 145-161.
Milligan, G., Ramsay, D., Pascal, G. &Carrillo, J. J. (2003). GPCR dimerisation. *Life Sci* 74(2-3): 181-188.
Mingot, J. M., Tilburn, J., Diez, E., Bignell, E., Orejas, M., Widdick, D. A., Sarkar, S., Brown, C. V., Caddick, M. X., Espeso, E. A., Arst, H. N., Jr. &Penalva, M. A. (1999). Specificity determinants of proteolytic processing of *Aspergillus* PacC transcription factor are remote from the processing site, and processing occurs in yeast if pH signalling is bypassed. *Mol Cell Biol* 19(2): 1390-1400.
Mira, N., Lourenço, A., Fernandes, A., Becker, J. &Sá-Correia, I. (2008). The RIM101 pathway has a role in *Saccharomyces cerevisiae* adaptive response and resistance to propionic acid and other weak acids. *FEMS yeast research* 9(2): 202-216.
Miyawaki, A., Llopis, J., Heim, R., McCaffery, J. M., Adams, J. A., Ikura, M. &Tsien, R. Y. (1997). Fluorescent indicators for Ca2+ based on green fluorescent proteins and calmodulin. *Nature* 388(6645): 882-887.
Mo, C. &Bard, M. (2005a). Erg28p is a key protein in the yeast sterol biosynthetic enzyme complex. *The Journal of Lipid Research* 46(9): 1991.
Mo, C. &Bard, M. (2005b). A systematic study of yeast sterol biosynthetic protein-protein interactions using the split-ubiquitin system. *Biochimica et Biophysica Acta (BBA)-Molecular and Cell Biology of Lipids* 1737(2-3): 152-160.
Mo, C., Valachovic, M. &Bard, M. (2004). The ERG28-encoded protein, Erg28p, interacts with both the sterol C-4 demethylation enzyme complex as well as the late biosynthetic protein, the C-24 sterol methyltransferase (Erg6p). *Biochimica et Biophysica Acta (BBA)-Molecular and Cell Biology of Lipids* 1686(1-2): 30-36.
Mohler, H. &Fritschy, J. M. (1999). GABAB receptors make it to the top--as dimers. *Trends Pharmacol Sci* 20(3): 87-89.
Momany, M. &Taylor, I. (2000). Landmarks in the early duplication cycles of *Aspergillus fumigatus* and *Aspergillus nidulans*: polarity, germ tube emergence and septation. *Microbiology* 146 Pt 12: 3279-3284.
Monod, M., Jaton-Ogay, K. &Reichard, U. (1999). *Aspergillus fumigatus*-secreted proteases as antigenic molecules and virulence factors. *Contrib Microbiol* 2: 182-192.
Monroy, F. &Sheppard, D. C. (2005). *Taf1*: a class II transposon of *Aspergillus fumigatus*. *Fungal Genet Biol* 42(7): 638-645.
Moore, C. A., Milano, S. K. &Benovic, J. L. (2007). Regulation of receptor trafficking by GRKs and arrestins. *Annu Rev Physiol* 69: 451-482.
Moreno, M. A., Ibrahim-Granet, O., Vicentefranqueira, R., Amich, J., Ave, P., Leal, F., Latge, J. P. &Calera, J. A. (2007). The regulation of zinc homeostasis by the ZafA

transcriptional activator is essential for *Aspergillus fumigatus* virulence. *Mol Microbiol* 64(5): 1182-1197.

Morgan, J., Wannemuehler, K. A., Marr, K. A., Hadley, S., Kontoyiannis, D. P., Walsh, T. J., Fridkin, S. K., Pappas, P. G. &Warnock, D. W. (2005). Incidence of invasive aspergillosis following hematopoietic stem cell and solid organ transplantation: interim results of a prospective multicenter surveillance program. *Med Mycol* 43 Suppl 1: S49-58.

Mouillon, J. M. &Persson, B. L. (2005). Inhibition of the protein kinase A alters the degradation of the high-affinity phosphate transporter Pho84 in *Saccharomyces cerevisiae*. *Curr Genet* 48(4): 226-234.

Moutaouakil, M., Monod, M., Prevost, M. C., Bouchara, J. P., Paris, S. &Latge, J. P. (1993). Identification of the 33-kDa alkaline protease of *Aspergillus fumigatus in vitro* and *in vivo*. *J Med Microbiol* 39(5): 393-399.

Mueller, J. E., Canze, M. &Bryk, M. (2006). The requirements for COMPASS and *Paf1* in transcriptional silencing and methylation of histone H3 in *Saccharomyces cerevisiae*. *Genetics* 173(2): 557-567.

Mullbacher, A. &Eichner, R. D. (1984). Immunosuppression *in vitro* by a metabolite of a human pathogenic fungus. *Proc Natl Acad Sci U S A* 81(12): 3835-3837.

Mullbacher, A., Waring, P. &Eichner, R. D. (1985). Identification of an agent in cultures of *Aspergillus fumigatus* displaying anti-phagocytic and immunomodulating activity *in vitro*. *J Gen Microbiol* 131(5): 1251-1258.

Neer, E. J. (1995). Heterotrimeric C proteins: Organizers of transmembrane signals. *Cell* 80(2): 249-257.

Negrete-Urtasun, S., Denison, S. H. &Arst, H. N., Jr. (1997). Characterization of the pH signal transduction pathway gene *palA* of *Aspergillus nidulans* and identification of possible homologs. *J Bacteriol* 179(5): 1832-1835.

Negrete-Urtasun, S., Reiter, W., Diez, E., Denison, S. H., Tilburn, J., Espeso, E. A., Penalva, M. A. &Arst, H. N., Jr. (1999). Ambient pH signal transduction in *Aspergillus*: completion of gene characterization. *Mol Microbiol* 33(5): 994-1003.

Neuveglise, C., Sarfati, J., Latge, J. P. &Paris, S. (1996). Afut1, a retrotransposon-like element from *Aspergillus fumigatus*. *Nucleic Acids Res* 24(8): 1428-1434.

Newman, S. L. (1999). Macrophages in host defense against *Histoplasma capsulatum*. *Trends Microbiol* 7(2): 67-71.

Nierman, W. C., Pain, A., Anderson, M. J., Wortman, J. R., Kim, H. S., Arroyo, J., Berriman, M., Abe, K., Archer, D. B., Bermejo, C., Bennett, J., Bowyer, P., Chen, D., Collins, M., Coulsen, R., Davies, R., Dyer, P. S., Farman, M., Fedorova, N., Feldblyum, T. V., Fischer, R., Fosker, N., Fraser, A., Garcia, J. L., Garcia, M. J., Goble, A., Goldman, G. H., Gomi, K., Griffith-Jones, S., Gwilliam, R., Haas, B., Haas, H., Harris, D., Horiuchi, H., Huang, J., Humphray, S., Jimenez, J., Keller, N., Khouri, H., Kitamoto, K., Kobayashi, T., Konzack, S., Kulkarni, R., Kumagai, T., Lafon, A., Latge, J. P., Li, W., Lord, A., Lu, C., Majoros, W. H., May, G. S., Miller, B. L., Mohamoud, Y., Molina, M., Monod, M., Mouyna, I., Mulligan, S., Murphy, L., O'Neil, S., Paulsen, I., Penalva, M. A., Pertea, M., Price, C., Pritchard, B. L., Quail, M. A., Rabbinowitsch, E., Rawlins, N., Rajandream, M. A., Reichard, U., Renauld, H., Robson, G. D., Rodriguez de Cordoba, S., Rodriguez-Pena, J. M., Ronning, C. M., Rutter, S., Salzberg, S. L., Sanchez, M., Sanchez-Ferrero, J. C., Saunders, D., Seeger, K., Squares, R., Squares, S., Takeuchi, M., Tekaia, F., Turner, G., Vazquez de Aldana, C. R., Weidman, J., White, O., Woodward, J., Yu, J. H., Fraser, C., Galagan, J. E., Asai, K., Machida, M., Hall, N., Barrell, B. &Denning, D. W. (2005). Genomic sequence of

the pathogenic and allergenic filamentous fungus *Aspergillus fumigatus*. *Nature* 438(7071): 1151-1156.
Nobile, C. J., Solis, N., Myers, C. L., Fay, A. J., Deneault, J. S., Nantel, A., Mitchell, A. P. &Filler, S. G. (2008). *Candida albicans* transcription factor Rim101 mediates pathogenic interactions through cell wall functions. *Cell Microbiol* 10(11): 2180-2196.
Nyfeler, B., Nufer, O., Matsui, T., Mori, K. &Hauri, H. P. (2003). The cargo receptor ERGIC-53 is a target of the unfolded protein response. *Biochem Biophys Res Commun* 304(4): 599-604.
Nyyssonen, E., Amutan, M., Enfield, L., Stubbs, J. &Dunn-Coleman, N. S. (1996). The transposable element Tan1 of *Aspergillus niger* var. *awamori*, a new member of the Fot1 family. *Mol Gen Genet* 253(1-2): 50-56.
O'Gorman, C. M., Fuller, H. T. &Dyer, P. S. (2009). Discovery of a sexual cycle in the opportunistic fungal pathogen *Aspergillus fumigatus*. *Nature* 457(7228): 471-474.
O'Meara, T. R., Norton, D., Price, M. S., Hay, C., Clements, M. F., Nichols, C. B. &Alspaugh, J. A. (2010). Interaction of *Cryptococcus neoformans* Rim101 and Protein Kinase A Regulates Capsule. *PLoS Pathog* 6(2): e1000776.
Obrdlik, P., El-Bakkoury, M., Hamacher, T., Cappellaro, C., Vilarino, C., Fleischer, C., Ellerbrok, H., Kamuzinzi, R., Ledent, V., Blaudez, D., Sanders, D., Revuelta, J. L., Boles, E., Andre, B. &Frommer, W. B. (2004). K+ channel interactions detected by a genetic system optimized for systematic studies of membrane protein interactions. *Proc Natl Acad Sci U S A* 101(33): 12242-12247.
Ogawa, N., Noguchi, K., Sawai, H., Yamashita, Y., Yompakdee, C. &Oshima, Y. (1995a). Functional domains of Pho81p, an inhibitor of Pho85p protein kinase, in the transduction pathway of Pi signals in *Saccharomyces cerevisiae*. *Mol Cell Biol* 15(2): 997-1004.
Ogawa, N., Saitoh, H., Miura, K., Magbanua, J. P., Bun-ya, M., Harashima, S. &Oshima, Y. (1995b). Structure and distribution of specific cis-elements for transcriptional regulation of PHO84 in *Saccharomyces cerevisiae*. *Mol Gen Genet* 249(4): 406-416.
Orejas, M., Espeso, E. A., Tilburn, J., Sarkar, S., Arst, H. N., Jr. &Penalva, M. A. (1995). Activation of the *Aspergillus* PacC transcription factor in response to alkaline ambient pH requires proteolysis of the carboxy-terminal moiety. *Genes Dev* 9(13): 1622-1632.
Ostrosky-Zeichner, L., Casadevall, A., Galgiani, J. N., Odds, F. C. &Rex, J. H. (2010). An insight into the antifungal pipeline: selected new molecules and beyond. *Nat Rev Drug Discov* 9(9): 719-727.
Ozawa, T., Kaihara, A., Sato, M., Tachihara, K. &Umezawa, Y. (2001a). Split luciferase as an optical probe for detecting protein-protein interactions in mammalian cells based on protein splicing. *Anal Chem* 73(11): 2516-2521.
Ozawa, T., Nogami, S., Sato, M., Ohya, Y. &Umezawa, Y. (2000). A fluorescent indicator for detecting protein-protein interactions *in vivo* based on protein splicing. *Anal Chem* 72(21): 5151-5157.
Ozawa, T., Takeuchi, T. M., Kaihara, A., Sato, M. &Umezawa, Y. (2001b). Protein splicing-based reconstitution of split green fluorescent protein for monitoring protein-protein interactions in bacteria: improved sensitivity and reduced screening time. *Anal Chem* 73(24): 5866-5874.
Pagano, L., Girmenia, C., Mele, L., Ricci, P., Tosti, M. E., Nosari, A., Buelli, M., Picardi, M., Allione, B., Corvatta, L., D'Antonio, D., Montillo, M., Melillo, L., Chierichini, A., Cenacchi, A., Tonso, A., Cudillo, L., Candoni, A., Savignano, C., Bonini, A., Martino, P. &Del Favero, A. (2001). Infections caused by filamentous fungi in

patients with hematologic malignancies. A report of 391 cases by GIMEMA Infection Program. *Haematologica* 86(8): 862-870.
Pahl, H. L., Krauss, B., Schulze-Osthoff, K., Decker, T., Traenckner, E. B., Vogt, M., Myers, C., Parks, T., Warring, P., Muhlbacher, A., Czernilofsky, A. P. &Baeuerle, P. A. (1996). The immunosuppressive fungal metabolite gliotoxin specifically inhibits transcription factor NF-kappaB. *J Exp Med* 183(4): 1829-1840.
Paoletti, M., Rydholm, C., Schwier, E. U., Anderson, M. J., Szakacs, G., Lutzoni, F., Debeaupuis, J. P., Latge, J. P., Denning, D. W. &Dyer, P. S. (2005). Evidence for sexuality in the opportunistic fungal pathogen *Aspergillus fumigatus*. *Curr Biol* 15(13): 1242-1248.
Paris, S. &Latge, J. P. (2001). *Afut2*, a new family of degenerate gypsy-like retrotransposon from *Aspergillus fumigatus*. *Med Mycol* 39(2): 195-198.
Paris, S., Wysong, D., Debeaupuis, J. P., Shibuya, K., Philippe, B., Diamond, R. D. &Latge, J. P. (2003). Catalases of *Aspergillus fumigatus*. *Infect Immun* 71(6): 3551-3562.
Parsons, A. B., Brost, R. L., Ding, H., Li, Z., Zhang, C., Sheikh, B., Brown, G. W., Kane, P. M., Hughes, T. R. &Boone, C. (2004). Integration of chemical-genetic and genetic interaction data links bioactive compounds to cellular target pathways. *Nat Biotechnol* 22(1): 62-69.
Pathak, A., Pien, F. D. &Carvalho, L. (1998). Amphotericin B use in a community hospital, with special emphasis on side effects. *Clin Infect Dis* 26(2): 334-338.
Patterson, T. F. (1998). Approaches to therapy for invasive mycoses. The role of amphotericin B. *Clin Infect Dis* 26(2): 339-340.
Patterson, T. F. (2005). Advances and challenges in management of invasive mycoses. *Lancet* 366(9490): 1013-1025.
Paumi, C. M., Menendez, J., Arnoldo, A., Engels, K., Iyer, K. R., Thaminy, S., Georgiev, O., Barral, Y., Michaelis, S. &Stagljar, I. (2007). Mapping Protein-Protein Interactions for the Yeast ABC Transporter Ycf1p by Integrated Split-Ubiquitin Membrane Yeast Two-Hybrid Analysis. *Molecular Cell* 26(1): 15-25.
Payne, G. A., Nierman, W. C., Wortman, J. R., Pritchard, B. L., Brown, D., Dean, R. A., Bhatnagar, D., Cleveland, T. E., Machida, M. &Yu, J. (2006). Whole genome comparison of *Aspergillus flavus* and *A. oryzae*. *Medical Mycology* 44(s1): 9-11.
Payne, N. I., Cosgrove, R. F., Green, A. P. &Liu, L. (1987). *In vivo* studies of amphotericin B liposomes derived from proliposomes: effect of formulation on toxicity and tissue disposition of the drug in mice. *J Pharm Pharmacol* 39(1): 24-28.
Pena, M. M., Koch, K. A. &Thiele, D. J. (1998). Dynamic regulation of copper uptake and detoxification genes in *Saccharomyces cerevisiae*. *Mol Cell Biol* 18(5): 2514-2523.
Penalva, M. &Arst Jr, H. (2002). Regulation of gene expression by ambient pH in filamentous fungi and yeasts. *Microbiology and molecular biology reviews* 66(3): 426.
Peñalva, M. &Arst Jr, H. (2004). Recent advances in the characterization of ambient pH regulation of gene expression in filamentous fungi and yeasts.
Peñalva, M., Tilburn, J., Bignell, E. &Arst Jr, H. (2008). Ambient pH gene regulation in fungi: making connections. *Trends in microbiology* 16(6): 291-300.
Perrin, R. M., Fedorova, N. D., Bok, J. W., Cramer, R. A., Jr., Wortman, J. R., Kim, H. S., Nierman, W. C. &Keller, N. P. (2007). Transcriptional Regulation of Chemical Diversity in *Aspergillus fumigatus* by LaeA. *PLoS Pathog* 3(4): e50.
Philippe, B., Ibrahim-Granet, O., Prevost, M. C., Gougerot-Pocidalo, M. A., Sanchez Perez, M., Van der Meeren, A. &Latge, J. P. (2003). Killing of *Aspergillus fumigatus* by alveolar macrophages is mediated by reactive oxidant intermediates. *Infect Immun* 71(6): 3034-3042.

Platara, M., Ruiz, A., Serrano, R., Palomino, A., Moreno, F. &Arino, J. (2006). The transcriptional response of the yeast Na^+-ATPase ENA1 gene to alkaline stress involves three main signaling pathways. *J Biol Chem* 281(48): 36632-36642.

Pontecorvo, G., Roper, J. A., Hemmons, L. M., Macdonald, K. D. &Bufton, A. W. (1953). The genetics of *Aspergillus nidulans*. *Adv Genet* 5: 141-238.

Post, M. J., Lass-Floerl, C., Gastl, G. &Nachbaur, D. (2007). Invasive fungal infections in allogeneic and autologous stem cell transplant recipients: a single-center study of 166 transplanted patients. *Transpl Infect Dis* 9(3): 189-195.

Pringle, A., Baker, D. M., Platt, J. L., Wares, J. P., Latge, J. P. &Taylor, J. W. (2005). Cryptic speciation in the cosmopolitan and clonal human pathogenic fungus *Aspergillus fumigatus*. *Evolution* 59(9): 1886-1899.

Purnell, D. M. &Martin, G. M. (1971). *Aspergillus nidulans*: association of certain alkaline phosphatase mutations with decreased virulence for mice. *J Infect Dis* 123(3): 305-306.

Rademacher, T. W., Parekh, R. B. &Dwek, R. A. (1988). Glycobiology. *Annu Rev Biochem* 57: 785-838.

Raeder, U. &Broda, P. (2008). Rapid preparation of DNA from filamentous fungi. *Letters in Applied Microbiology* 1(1): 17-20.

Ramos, H., Attias de Murciano, A., Cohen, B. E. &Bolard, J. (1989). The polyene antibiotic amphotericin B acts as a Ca2+ ionophore in sterol-containing liposomes. *Biochim Biophys Acta* 982(2): 303-306.

Raper, K. B. F., D.I. (1965). *Aspergillus fumigatus* group. *In K.B.Raper and D.I.Fennel (ed.),the genus Aspergillus* The William & Wilkins Co., Baltimore, Md.: 238-268.

Ray, K., Clapp, P., Goldsmith, P. K. &Spiegel, A. M. (1998). Identification of the sites of N-linked glycosylation on the human calcium receptor and assessment of their role in cell surface expression and signal transduction. *J Biol Chem* 273(51): 34558-34567.

Ray, P., Pimenta, H., Paulmurugan, R., Berger, F., Phelps, M. E., Iyer, M. &Gambhir, S. S. (2002). Noninvasive quantitative imaging of protein-protein interactions in living subjects. *Proc Natl Acad Sci U S A* 99(5): 3105-3110.

Reeves, E. P., Lu, H., Jacobs, H. L., Messina, C. G., Bolsover, S., Gabella, G., Potma, E. O., Warley, A., Roes, J. &Segal, A. W. (2002). Killing activity of neutrophils is mediated through activation of proteases by K^+ flux. *Nature* 416(6878): 291-297.

Rehemtulla, A., Hall, D. E., Stegman, L. D., Prasad, U., Chen, G., Bhojani, M. S., Chenevert, T. L. &Ross, B. D. (2002). Molecular imaging of gene expression and efficacy following adenoviral-mediated brain tumor gene therapy. *Mol Imaging* 1(1): 43-55.

Rehemtulla, A., Stegman, L. D., Cardozo, S. J., Gupta, S., Hall, D. E., Contag, C. H. &Ross, B. D. (2000). Rapid and quantitative assessment of cancer treatment response using *in vivo* bioluminescence imaging. *Neoplasia* 2(6): 491-495.

Reichard, U., Buttner, S., Eiffert, H., Staib, F. &Ruchel, R. (1990). Purification and characterisation of an extracellular serine proteinase from *Aspergillus fumigatus* and its detection in tissue. *J Med Microbiol* 33(4): 243-251.

Reichard, U., Eiffert, H. &Ruchel, R. (1994). Purification and characterization of an extracellular aspartic proteinase from *Aspergillus fumigatus*. *J Med Vet Mycol* 32(6): 427-436.

Reinders, A., Schulze, W., Thaminy, S., Stagljar, I., Frommer, W. B. &Ward, J. M. (2002). Intra- and intermolecular interactions in sucrose transporters at the plasma membrane detected by the split-ubiquitin system and functional assays. *Structure* 10(6): 763-772.

Reiser, V., D'Aquino, K. E., Ee, L. S. &Amon, A. (2006). The stress-activated mitogen-activated protein kinase signaling cascade promotes exit from mitosis. *Mol Biol Cell* 17(7): 3136-3146.

Reiss, T. (2001). Drug discovery of the future: the implications of the human genome project. *Trends Biotechnol* 19(12): 496-499.
Reiter, E. &Lefkowitz, R. J. (2006). GRKs and beta-arrestins: roles in receptor silencing, trafficking and signaling. *Trends Endocrinol Metab* 17(4): 159-165.
Rementeria, A., Lopez-Molina, N., Ludwig, A., Vivanco, A. B., Bikandi, J., Ponton, J. &Garaizar, J. (2005). Genes and molecules involved in *Aspergillus fumigatus* virulence. *Rev Iberoam Micol* 22(1): 1-23.
Rice, B. W., Cable, M. D. &Nelson, M. B. (2001). *In vivo* imaging of light-emitting probes. *J Biomed Opt* 6(4): 432-440.
Rinyu, E., Varga, J. &Ferenczy, L. (1995). Phenotypic and genotypic analysis of variability in *Aspergillus fumigatus*. *J Clin Microbiol* 33(10): 2567-2575.
Robertson, J. B., Stowers, C. C., Boczko, E. &Johnson, C. H. (2008). Real-time luminescence monitoring of cell-cycle and respiratory oscillations in yeast. *Proc Natl Acad Sci U S A* 105(46): 17988-17993.
Robyr, D., Suka, Y., Xenarios, I., Kurdistani, S. K., Wang, A., Suka, N. &Grunstein, M. (2002). Microarray deacetylation maps determine genome-wide functions for yeast histone deacetylases. *Cell* 109(4): 437-446.
Rodriguez-Navarro, A., Quintero, F. J. &Garciadeblas, B. (1994). Na^+-ATPases and Na^+/H^+ antiporters in fungi. *Biochim Biophys Acta* 1187(2): 203-205.
Rollins, J. A. (2003). The *Sclerotinia sclerotiorum pac1* gene is required for sclerotial development and virulence. *Mol Plant Microbe Interact* 16(9): 785-795.
Rollins, J. A. &Dickman, M. B. (2001). pH signaling in *Sclerotinia sclerotiorum*: identification of a *pacC/RIM1* homolog. *Appl Environ Microbiol* 67(1): 75-81.
Romano, J., Nimrod, G., Ben-Tal, N., Shadkchan, Y., Baruch, K., Sharon, H. &Osherov, N. (2006). Disruption of the *Aspergillus fumigatus* ECM33 homologue results in rapid conidial germination, antifungal resistance and hypervirulence. *Microbiology* 152(Pt 7): 1919-1928.
Romanos, M. A., Scorer, C. A. &Clare, J. J. (1992). Foreign gene expression in yeast: a review. *Yeast* 8(6): 423-488.
Ronning, C. M., Fedorova, N. D., Bowyer, P., Coulson, R., Goldman, G., Kim, H. S., Turner, G., Wortman, J. R., Yu, J., Anderson, M. J., Denning, D. W. &Nierman, W. C. (2005). Genomics of *Aspergillus fumigatus*. *Rev Iberoam Micol* 22(4): 223-228.
Rosen, S., Yu, J. H. &Adams, T. H. (1999). The *Aspergillus nidulans sfaD* gene encodes a G protein β subunit that is required for normal growth and repression of sporulation. *EMBO J* 18(20): 5592-5600.
Rossi, F., Charlton, C. A. &Blau, H. M. (1997). Monitoring protein-protein interactions in intact eukaryotic cells by β-galactosidase complementation. *Proc Natl Acad Sci U S A* 94(16): 8405-8410.
Rothfels, K., Tanny, J. C., Molnar, E., Friesen, H., Commisso, C. &Segall, J. (2005). Components of the ESCRT pathway, DFG16, and YGR122w are required for Rim101 to act as a corepressor with Nrg1 at the negative regulatory element of the DIT1 gene of *Saccharomyces cerevisiae*. *Mol Cell Biol* 25(15): 6772-6788.
Rudin, M. &Weissleder, R. (2003). Molecular imaging in drug discovery and development. *Nat Rev Drug Discov* 2(2): 123-131.
Ruiz, A. &Arino, J. (2007). Function and regulation of the Saccharomyces cerevisiae ENA sodium ATPase system. *Eukaryot Cell* 6(12): 2175-2183.
Rydholm, C., Szakacs, G. &Lutzoni, F. (2006). Low genetic variation and no detectable population structure in *Aspergillus fumigatus* compared to closely related *Neosartorya* species. *Eukaryot Cell* 5(4): 650-657.

Sa-Correia, I., dos Santos, S. C., Teixeira, M. C., Cabrito, T. R. &Mira, N. P. (2009). Drug:H+ antiporters in chemical stress response in yeast. *Trends Microbiol* 17(1): 22-31.

Saeed, A. I., Sharov, V., White, J., Li, J., Liang, W., Bhagabati, N., Braisted, J., Klapa, M., Currier, T., Thiagarajan, M., Sturn, A., Snuffin, M., Rezantsev, A., Popov, D., Ryltsov, A., Kostukovich, E., Borisovsky, I., Liu, Z., Vinsavich, A., Trush, V. &Quackenbush, J. (2003). TM4: a free, open-source system for microarray data management and analysis. *Biotechniques* 34(2): 374-378.

Saeij, J. P., Boyle, J. P., Grigg, M. E., Arrizabalaga, G. &Boothroyd, J. C. (2005). Bioluminescence imaging of *Toxoplasma gondi*i infection in living mice reveals dramatic differences between strains. *Infect Immun* 73(2): 695-702.

Sambrook, J. &Russell, D. (2001). *Molecular cloning: a laboratory manual.* CSHL press.

Samson, R. A. (1994). Current systematics of the genus *Aspergillus*. *In K.A.Powell, A. Renwick & J.F.Peberdy (ed.), The genus Aspergillus: from taxonomy and genetics to industrial application. Plenum Press, London, United Kingdom*: 261-276.

Samson, R. A. &Varga, J. (2009). What is a species in *Aspergillus*? *Med Mycol* 47 Suppl 1: S13-20.

Sanchez, O. &Aguirre, J. (1996). Efficient transformation of *Aspergillus nidulans* by electroporation of germinated conidia. *Fungal Genetics Newsletter*: 48-51.

Schena, M., Shalon, D., Davis, R. W. &Brown, P. O. (1995). Quantitative Monitoring of Gene Expression Patterns with a Complementary DNA Microarray. *Science* 270(5235): 467-470.

Scheper, W., Thaminy, S., Kais, S., Stagljar, I. &Romisch, K. (2003a). Coordination of N-glycosylation and protein translocation across the endoplasmic reticulum membrane by Sss1 protein. *J Biol Chem* 278(39): 37998-38003.

Scheper, W., Thaminy, S., Kais, S., Stagljar, I. &Römisch, K. (2003b). Coordination of N-Glycosylation and Protein Translocation across the Endoplasmic Reticulum Membrane by Sss1 Protein. *Journal of Biological Chemistry* 278(39): 37998-38003.

Schjerling, C. K., Hummel, R., Hansen, J. K., Borsting, C., Mikkelsen, J. M., Kristiansen, K. &Knudsen, J. (1996). Disruption of the gene encoding the acyl-CoA-binding protein (ACB1) perturbs acyl-CoA metabolism in *Saccharomyces cerevisiae*. *J Biol Chem* 271(37): 22514-22521.

Schmitt, E. K., Kempken, R. &Kuck, U. (2001). Functional analysis of promoter sequences of cephalosporin C biosynthesis genes from *Acremonium chrysogenum*: specific DNA-protein interactions and characterization of the transcription factor PACC. *Mol Genet Genomics* 265(3): 508-518.

Schrettl, M., Bignell, E., Kragl, C., Joechl, C., Rogers, T., Arst, H. N., Jr., Haynes, K. &Haas, H. (2004). Siderophore biosynthesis but not reductive iron assimilation is essential for *Aspergillus fumigatus* virulence. *J Exp Med* 200(9): 1213-1219.

Schrettl, M., Bignell, E., Kragl, C., Sabiha, Y., Loss, O., Eisendle, M., Wallner, A., Arst, H. N., Jr., Haynes, K. &Haas, H. (2007). Distinct roles for intra- and extracellular siderophores during *Aspergillus fumigatus* infection. *PLoS Pathog* 3(9): 1195-1207.

Schrettl, M., Kim, H. S., Eisendle, M., Kragl, C., Nierman, W. C., Heinekamp, T., Werner, E. R., Jacobsen, I., Illmer, P., Yi, H., Brakhage, A. A. &Haas, H. (2008). SreA-mediated iron regulation in *Aspergillus fumigatus*. *Mol Microbiol* 70(1): 27-43.

Segal, B. H., DeCarlo, E. S., Kwon-Chung, K. J., Malech, H. L., Gallin, J. I. &Holland, S. M. (1998). *Aspergillus nidulans* infection in chronic granulomatous disease. *Medicine (Baltimore)* 77(5): 345-354.

Sehgal, A., Lee, C. Y. &Espenshade, P. J. (2007). SREBP controls oxygen-dependent mobilization of retrotransposons in fission yeast. *PLoS Genet* 3(8): e131.

Seo, J. A., Han, K. H. &Yu, J. H. (2005). Multiple roles of a heterotrimeric G-protein γ-subunit in governing growth and development of *Aspergillus nidulans*. *Genetics* 171(1): 81-89.
Serebriiskii, I., Estojak, J., Berman, M. &Golemis, E. A. (2000). Approaches to detecting false positives in yeast two-hybrid systems. *Biotechniques* 28(2): 328-330, 332-326.
Serrano, R., Bernal, D., Simón, E. &Ariño, J. (2004). Copper and Iron Are the Limiting Factors for Growth of the Yeast *Saccharomyces cerevisiae* in an Alkaline Environment. *Journal of Biological Chemistry* 279(19): 19698-19704.
Serrano, R., Martin, H., Casamayor, A. &Arino, J. (2006). Signaling alkaline pH stress in the yeast *Saccharomyces cerevisiae* through the Wsc1 cell surface sensor and the Slt2 MAPK pathway. *J Biol Chem* 281(52): 39785-39795.
Serrano, R., Ruiz, A., Bernal, D., Chambers, J. R. &Arino, J. (2002). The transcriptional response to alkaline pH in *Saccharomyces cerevisiae*: evidence for calcium-mediated signalling. *Mol Microbiol* 46(5): 1319-1333.
Shaaban, M., Palmer, J. M., El-Naggar, W. A., El-Sokkary, M. A., Habib el, S. E. &Keller, N. P. (2010). Involvement of transposon-like elements in penicillin gene cluster regulation. *Fungal Genet Biol* 47(5): 423-432.
Shalon, D., Smith, S. J. &Brown, P. O. (1996). A DNA microarray system for analyzing complex DNA samples using two-color fluorescent probe hybridization. *Genome Research* 6(7): 639-645.
Shen, X., Ranallo, R., Choi, E. &Wu, C. (2003). Involvement of actin-related proteins in ATP-dependent chromatin remodeling. *Mol Cell* 12(1): 147-155.
Shenoy, S. K. &Lefkowitz, R. J. (2003). Multifaceted roles of beta-arrestins in the regulation of seven-membrane-spanning receptor trafficking and signalling. *Biochem J* 375(Pt 3): 503-515.
Shenoy, S. K. &Lefkowitz, R. J. (2005a). Receptor regulation: β-arrestin moves up a notch. *Nat Cell Biol* 7(12): 1159-1161.
Shenoy, S. K. &Lefkowitz, R. J. (2005b). Seven-transmembrane receptor signaling through beta-arrestin. *Sci STKE* 2005(308): cm10.
Shenoy, S. K., McDonald, P. H., Kohout, T. A. &Lefkowitz, R. J. (2001). Regulation of receptor fate by ubiquitination of activated beta 2-adrenergic receptor and beta-arrestin. *Science* 294(5545): 1307-1313.
Sheppard, D. C., Rieg, G., Chiang, L. Y., Filler, S. G., Edwards, J. E., Jr. &Ibrahim, A. S. (2004). Novel inhalational murine model of invasive pulmonary aspergillosis. *Antimicrob Agents Chemother* 48(5): 1908-1911.
Shwab, E. K., Bok, J. W., Tribus, M., Galehr, J., Graessle, S. &Keller, N. P. (2007). Histone deacetylase activity regulates chemical diversity in *Aspergillus*. *Eukaryot Cell* 6(9): 1656-1664.
Sikorski, R. S. &Hieter, P. (1989). A system of shuttle vectors and yeast host strains designed for efficient manipulation of DNA in *Saccharomyces cerevisiae*. *Genetics* 122(1): 19-27.
Sims, R. J., 3rd &Reinberg, D. (2006). Histone H3 Lys 4 methylation: caught in a bind? *Genes Dev* 20(20): 2779-2786.
Sjolinder, H. &Jonsson, A. B. (2007). Imaging of disease dynamics during meningococcal sepsis. *PLoS One* 2(2): e241.
Smith, J. M., Tang, C. M., Van Noorden, S. &Holden, D. W. (1994). Virulence of *Aspergillus fumigatus* double mutants lacking restriction and an alkaline protease in a low-dose model of invasive pulmonary aspergillosis. *Infect Immun* 62(12): 5247-5254.

Snider, J., Kittanakom, S., Curak, J. &Stagljar, I. (2010a). Split-ubiquitin based membrane yeast two-hybrid (MYTH) system: a powerful tool for identifying protein-protein interactions. *J Vis Exp* (36).

Snider, J., Kittanakom, S., Damjanovic, D., Curak, J., Wong, V. &Stagljar, I. (2010b). Detecting interactions with membrane proteins using a membrane two-hybrid assay in yeast. *Nat Protoc* 5(7): 1281-1293.

Song, Y., Thiagarajah, J. &Verkman, A. S. (2003). Sodium and chloride concentrations, pH, and depth of airway surface liquid in distal airways. *J Gen Physiol* 122(5): 511-519.

Sörensen, O. E. (1909). Ergänzung zu der Abhandlung: Enzymstudien II: Über die Messung und die Bedeutung der Wasserstoff-ionenkonzentration bei enzymatischen Prozessen. *Biochem. Zeitsch.*: 131-304.

Soriani, F. M., Malavazi, I., da Silva Ferreira, M. E., Savoldi, M., Von Zeska Kress, M. R., de Souza Goldman, M. H., Loss, O., Bignell, E. &Goldman, G. H. (2008). Functional characterization of the *Aspergillus fumigatus* CRZ1 homologue, CrzA. *Mol Microbiol* 67(6): 1274-1291.

Sorimachi, H., Ishiura, S. &Suzuki, K. (1997). Structure and physiological function of calpains. *Biochem J* 328 (Pt 3): 721-732.

South, P. F., Fingerman, I. M., Mersman, D. P., Du, H. N. &Briggs, S. D. (2010). A conserved interaction between the SDI domain of Bre2 and the Dpy-30 domain of Sdc1 is required for histone methylation and gene expression. *J Biol Chem* 285(1): 595-607.

Southern, E. (1975). Detection of specific sequences among DNA fragments separated by gel electrophoresis. *Journal of molecular biology* 98(3): 503-517.

Spikes, S., Xu, R., Nguyen, C. K., Chamilos, G., Kontoyiannis, D. P., Jacobson, R. H., Ejzykowicz, D. E., Chiang, L. Y., Filler, S. G. &May, G. S. (2008). Gliotoxin production in *Aspergillus fumigatus* contributes to host-specific differences in virulence. *J Infect Dis* 197(3): 479-486.

Stables, J., Scott, S., Brown, S., Roelant, C., Burns, D., Lee, M. G. &Rees, S. (1999). Development of a dual glow-signal firefly and Renilla luciferase assay reagent for the analysis of G-protein coupled receptor signalling. *J Recept Signal Transduct Res* 19(1-4): 395-410.

Stagljar, I., Korostensky, C., Johnsson, N. &Te Heesen, S. (1998). A genetic system based on split-ubiquitin for the analysis of interactions between membrane proteins *in vivo*. *Proceedings of the National Academy of Sciences of the United States of America* 95(9): 5187.

Stanzani, M., Orciuolo, E., Lewis, R., Kontoyiannis, D. P., Martins, S. L., St John, L. S. &Komanduri, K. V. (2005). *Aspergillus fumigatus* suppresses the human cellular immune response via gliotoxin-mediated apoptosis of monocytes. *Blood* 105(6): 2258-2265.

Stathopoulos, A. M. &Cyert, M. S. (1997). Calcineurin acts through the CRZ1/TCN1-encoded transcription factor to regulate gene expression in yeast. *Genes Dev* 11(24): 3432-3444.

Steinbach, W. J., Benjamin, D. K., Jr., Trasi, S. A., Miller, J. L., Schell, W. A., Zaas, A. K., Foster, W. M. &Perfect, J. R. (2004). Value of an inhalational model of invasive aspergillosis. *Med Mycol* 42(5): 417-425.

Steinbach, W. J., Cramer, R. A., Jr., Perfect, B. Z., Asfaw, Y. G., Sauer, T. C., Najvar, L. K., Kirkpatrick, W. R., Patterson, T. F., Benjamin, D. K., Jr., Heitman, J. &Perfect, J. R. (2006). Calcineurin controls growth, morphology, and pathogenicity in *Aspergillus fumigatus*. *Eukaryot Cell* 5(7): 1091-1103.

Stephens-Romero, S. D., Mednick, A. J. &Feldmesser, M. (2005). The pathogenesis of fatal outcome in murine pulmonary aspergillosis depends on the neutrophil depletion strategy. *Infect Immun* 73(1): 114-125.

Stergiopoulou, T., Meletiadis, J., Roilides, E., Kleiner, D. E., Schaufele, R., Roden, M., Harrington, S., Dad, L., Segal, B. &Walsh, T. J. (2007). Host-dependent patterns of tissue injury in invasive pulmonary aspergillosis. *Am J Clin Pathol* 127(3): 349-355.

Stevens, T. H. &Forgac, M. (1997). Structure, function and regulation of the vacuolar H^+-ATPase. *Annu Rev Cell Dev Biol* 13: 779-808.

Su, S. &Mitchell, A. (1993a). Identification of functionally related genes that stimulate early meiotic gene expression in yeast. *Genetics* 133(1): 67.

Su, S. &Mitchell, A. (1993b). Molecular characterization of the yeast meiotic regulatory gene *RIM1*. *Nucleic acids research* 21(16): 3789.

Suarez, T. &Penalva, M. A. (1996). Characterization of a *Penicillium chrysogenum* gene encoding a *PacC* transcription factor and its binding sites in the divergent pcbAB-pcbC promoter of the penicillin biosynthetic cluster. *Mol Microbiol* 20(3): 529-540.

Sugui, J. A., Kim, H. S., Zarember, K. A., Chang, Y. C., Gallin, J. I., Nierman, W. C. &Kwon-Chung, K. J. (2008). Genes differentially expressed in conidia and hyphae of *Aspergillus fumigatus* upon exposure to human neutrophils. *PLoS One* 3(7): e2655.

Sugui, J. A., Pardo, J., Chang, Y. C., Mullbacher, A., Zarember, K. A., Galvez, E. M., Brinster, L., Zerfas, P., Gallin, J. I., Simon, M. M. &Kwon-Chung, K. J. (2007a). Role of laeA in the Regulation of alb1, gliP, Conidial Morphology, and Virulence in *Aspergillus fumigatus*. *Eukaryot Cell* 6(9): 1552-1561.

Sugui, J. A., Pardo, J., Chang, Y. C., Zarember, K. A., Nardone, G., Galvez, E. M., Mullbacher, A., Gallin, J. I., Simon, M. M. &Kwon-Chung, K. J. (2007b). Gliotoxin is a virulence factor of *Aspergillus fumigatus*: gliP deletion attenuates virulence in mice immunosuppressed with hydrocortisone. *Eukaryot Cell* 6(9): 1562-1569.

Surarit, R. &Shepherd, M. G. (1987). The effects of azole and polyene antifungals on the plasma membrane enzymes of *Candida albicans*. *J Med Vet Mycol* 25(6): 403-413.

Suter, B., Auerbach, D. &Stagljar, I. (2006). Yeast-based functional genomics and proteomics technologies: the first 15 years and beyond. *Biotechniques* 40(5): 625-644.

Sutton, P., Waring, P. &Mullbacher, A. (1996). Exacerbation of invasive aspergillosis by the immunosuppressive fungal metabolite, gliotoxin. *Immunol Cell Biol* 74(4): 318-322.

Tannous, B. A., Kim, D. E., Fernandez, J. L., Weissleder, R. &Breakefield, X. O. (2005). Codon-optimized Gaussia luciferase cDNA for mammalian gene expression in culture and *in vivo*. *Mol Ther* 11(3): 435-443.

Taubitz, A., Bauer, B., Heesemann, J. &Ebel, F. (2007). Role of respiration in the germination process of the pathogenic mold *Aspergillus fumigatus*. *Curr Microbiol* 54(5): 354-360.

Tenney, K. A. &Glover, C. V. (1999). Transcriptional regulation of the *S. cerevisiae* ENA1 gene by casein kinase II. *Mol Cell Biochem* 191(1-2): 161-167.

Thaminy, S., Auerbach, D., Arnoldo, A. &Stagljar, I. (2003). Identification of Novel ErbB3-Interacting Factors Using the Split-Ubiquitin Membrane Yeast Two-Hybrid System. *Genome Research* 13(7): 1744-1753.

Thanabalu, T., Rajmohan, R., Meng, L., Ren, G., Vajjhala, P. R. &Munn, A. L. (2007). Verprolin function in endocytosis and actin organization. *FEBS Journal* 274(16): 4103-4125.

Thau, N., Monod, M., Crestani, B., Rolland, C., Tronchin, G., Latge, J. P. &Paris, S. (1994). *rodletless* mutants of *Aspergillus fumigatus*. *Infect Immun* 62(10): 4380-4388.

Tilburn, J., Sarkar, S., Widdick, D. A., Espeso, E. A., Orejas, M., Mungroo, J., Penalva, M. A. &Arst, H. N., Jr. (1995). The *Aspergillus* PacC zinc finger transcription factor

mediates regulation of both acid- and alkaline-expressed genes by ambient pH. *EMBO J* 14(4): 779-790.
Todd, B. L., Stewart, E. V., Burg, J. S., Hughes, A. L. &Espenshade, P. J. (2006). Sterol regulatory element binding protein is a principal regulator of anaerobic gene expression in fission yeast. *Mol Cell Biol* 26(7): 2817-2831.
Toussaint, M., Levasseur, G., Gervais-Bird, J., Wellinger, R. J., Elela, S. A. &Conconi, A. (2006). A high-throughput method to measure the sensitivity of yeast cells to genotoxic agents in liquid cultures. *Mutation Research/Genetic Toxicology and Environmental Mutagenesis* 606(1-2): 92-105.
Towbin, H., Staehelin, T. &Gordon, J. (1979). Electrophoretic transfer of proteins from polyacrylamide gels to nitrocellulose sheets: procedure and some applications. *Proc Natl Acad Sci U S A* 76(9): 4350-4354.
Trojer, P., Brandtner, E. M., Brosch, G., Loidl, P., Galehr, J., Linzmaier, R., Haas, H., Mair, K., Tribus, M. &Graessle, S. (2003). Histone deacetylases in fungi: novel members, new facts. *Nucleic Acids Res* 31(14): 3971-3981.
Valiante, V., Heinekamp, T., Jain, R., Hartl, A. &Brakhage, A. A. (2008). The mitogen-activated protein kinase MpkA of *Aspergillus fumigatus* regulates cell wall signaling and oxidative stress response. *Fungal Genet Biol* 45(5): 618-627.
van der Rest, M. E., Kamminga, A. H., Nakano, A., Anraku, Y., Poolman, B. &Konings, W. N. (1995). The plasma membrane of *Saccharomyces cerevisiae*: structure, function, and biogenesis. *Microbiol Rev* 59(2): 304-322.
Vanden Bossche, H., Marichal, P., Gorrens, J., Coene, M. C., Willemsens, G., Bellens, D., Roels, I., Moereels, H. &Janssen, P. A. (1989). Biochemical approaches to selective antifungal activity. Focus on azole antifungals. *Mycoses* 32 Suppl 1: 35-52.
Vanden Bossche, H., Marichal, P., Gorrens, J., Geerts, H. &Janssen, P. A. (1988). Mode of action studies. Basis for the search of new antifungal drugs. *Ann N Y Acad Sci* 544: 191-207.
Vanden Bossche, H., Marichal, P., Willemsens, G., Bellens, D., Gorrens, J., Roels, I., Coene, M. C., Le Jeune, L. &Janssen, P. A. (1990). Saperconazole: a selective inhibitor of the cytochrome P-450-dependent ergosterol synthesis in *Candida albicans, Aspergillus fumigatus* and *Trichophyton mentagrophytes*. *Mycoses* 33(7-8): 335-352.
Vanden Bossche, H., Willemsens, G., Cools, W., Cornelissen, F., Lauwers, W. F. &van Cutsem, J. M. (1980). In vitro and in vivo effects of the antimycotic drug ketoconazole on sterol synthesis. *Antimicrob Agents Chemother* 17(6): 922-928.
Vanden Bossche, H., Willemsens, G., Cools, W., Marichal, P. &Lauwers, W. (1983). Hypothesis on the molecular basis of the antifungal activity of N-substituted imidazoles and triazoles. *Biochem Soc Trans* 11(6): 665-667.
Verhaegent, M. &Christopoulos, T. K. (2002). Recombinant Gaussia luciferase. Overexpression, purification, and analytical application of a bioluminescent reporter for DNA hybridization. *Anal Chem* 74(17): 4378-4385.
Verweij, P. E., Oakley, K. L., Morrissey, J., Morrissey, G. &Denning, D. W. (1998). Efficacy of LY303366 against amphotericin B-susceptible and -resistant *Aspergillus fumigatus* in a murine model of invasive aspergillosis. *Antimicrob Agents Chemother* 42(4): 873-878.
Vicentefranqueira, R., Moreno, M. A., Leal, F. &Calera, J. A. (2005). The *zrfA* and *zrfB* genes of *Aspergillus fumigatus* encode the zinc transporter proteins of a zinc uptake system induced in an acid, zinc-depleted environment. *Eukaryot Cell* 4(5): 837-848.
Vignali, M., Hassan, A. H., Neely, K. E. &Workman, J. L. (2000). ATP-Dependent Chromatin-Remodeling Complexes. *Mol. Cell. Biol.* 20(6): 1899-1910.

Viladevall, L., Serrano, R., Ruiz, A., Domenech, G., Giraldo, J., Barcelo, A. &Arino, J. (2004). Characterization of the calcium-mediated response to alkaline stress in *Saccharomyces cerevisiae*. *J Biol Chem* 279(42): 43614-43624.

Villar, C. C., Kashleva, H., Nobile, C. J., Mitchell, A. P. &Dongari-Bagtzoglou, A. (2007). Mucosal tissue invasion by *Candida albicans* is associated with E-cadherin degradation, mediated by transcription factor Rim101p and protease Sap5p. *Infect Immun* 75(5): 2126-2135.

Vincent, O., Rainbow, L., Tilburn, J., Arst, H. N., Jr. &Penalva, M. A. (2003). YPXL/I is a protein interaction motif recognized by *aspergillus* PalA and its human homologue, AIP1/Alix. *Mol Cell Biol* 23(5): 1647-1655.

Vyas, V. K., Berkey, C. D., Miyao, T. &Carlson, M. (2005). Repressors Nrg1 and Nrg2 regulate a set of stress-responsive genes in *Saccharomyces cerevisiae*. *Eukaryot Cell* 4(11): 1882-1891.

Walsh, T. J., Teppler, H., Donowitz, G. R., Maertens, J. A., Baden, L. R., Dmoszynska, A., Cornely, O. A., Bourque, M. R., Lupinacci, R. J., Sable, C. A. &dePauw, B. E. (2004). Caspofungin versus liposomal amphotericin B for empirical antifungal therapy in patients with persistent fever and neutropenia. *N Engl J Med* 351(14): 1391-1402.

Wang, B., Pelletier, J., Massaad, M. J., Herscovics, A. &Shore, G. C. (2004). The yeast split-ubiquitin membrane protein two-hybrid screen identifies BAP31 as a regulator of the turnover of endoplasmic reticulum-associated protein tyrosine phosphatase-like B. *Mol Cell Biol* 24(7): 2767-2778.

Wang, Y., Wang, G., O'Kane, D. J. &Szalay, A. A. (2001). A study of protein-protein interactions in living cells using luminescence resonance energy transfer (LRET) from Renilla luciferase to Aequorea GFP. *Mol Gen Genet* 264(5): 578-587.

Wang, Y., Yu, Y. A., Shabahang, S., Wang, G. &Szalay, A. A. (2002). Renilla luciferase-Aequorea GFP (Ruc-GFP) fusion protein, a novel dual reporter for real-time imaging of gene expression in cell cultures and in live animals. *Mol Genet Genomics* 268(2): 160-168.

Wardlaw, A. &Geddes, D. M. (1992). Allergic bronchopulmonary aspergillosis: a review. *J R Soc Med* 85(12): 747-751.

Waring, P., Eichner, R. D., Mullbacher, A. &Sjaarda, A. (1988). Gliotoxin induces apoptosis in macrophages unrelated to its antiphagocytic properties. *J Biol Chem* 263(34): 18493-18499.

Warwas, M. L., Watson, J. N., Bennet, A. J. &Moore, M. M. (2007). Structure and role of sialic acids on the surface of *Aspergillus fumigatus* conidiospores. *Glycobiology* 17(4): 401-410.

Wasylnka, J. A. &Moore, M. M. (2000). Adhesion of *Aspergillus* Species to Extracellular Matrix Proteins: Evidence for Involvement of Negatively Charged Carbohydrates on the Conidial Surface. *Infect. Immun.* 68(6): 3377-3384.

Weissleder, R., Tung, C. H., Mahmood, U. &Bogdanov, A., Jr. (1999). *In vivo* imaging of tumors with protease-activated near-infrared fluorescent probes. *Nat Biotechnol* 17(4): 375-378.

Wessler, S. R. (1996). Turned on by stress. Plant retrotransposons. *Curr Biol* 6(8): 959-961.

Wheatley, M. &Hawtin, S. R. (1999). Glycosylation of G-protein-coupled receptors for hormones central to normal reproductive functioning: its occurrence and role. *Hum Reprod Update* 5(4): 356-364.

White, J. H., Wise, A. &Marshall, F. H. (2002). Heterodimerization of γ-aminobutyric acid B receptor subunits as revealed by the yeast two-hybrid system. *Methods* 27(4): 301-310.

Wiederhold, N. P., Lewis, R. E. &Kontoyiannis, D. P. (2003). Invasive aspergillosis in patients with hematologic malignancies. *Pharmacotherapy* 23(12): 1592-1610.
Wild, C. P. (2007). Aflatoxin exposure in developing countries: the critical interface of agriculture and health. *Food Nutr Bull* 28(2 Suppl): S372-380.
Wiles, S., Hanage, W. P., Frankel, G. &Robertson, B. (2006). Modelling infectious disease - time to think outside the box? *Nat Rev Microbiol* 4(4): 307-312.
Winzeler, E. A., Liang, H., Shoemaker, D. D. &Davis, R. W. (2000). Functional analysis of the yeast genome by precise deletion and parallel phenotypic characterization. *Novartis Found Symp* 229: 105-109; discussion 109-111.
Winzeler, E. A., Shoemaker, D. D., Astromoff, A., Liang, H., Anderson, K., Andre, B., Bangham, R., Benito, R., Boeke, J. D., Bussey, H., Chu, A. M., Connelly, C., Davis, K., Dietrich, F., Dow, S. W., El Bakkoury, M., Foury, F., Friend, S. H., Gentalen, E., Giaever, G., Hegemann, J. H., Jones, T., Laub, M., Liao, H., Liebundguth, N., Lockhart, D. J., Lucau-Danila, A., Lussier, M., M'Rabet, N., Menard, P., Mittmann, M., Pai, C., Rebischung, C., Revuelta, J. L., Riles, L., Roberts, C. J., Ross-MacDonald, P., Scherens, B., Snyder, M., Sookhai-Mahadeo, S., Storms, R. K., Veronneau, S., Voet, M., Volckaert, G., Ward, T. R., Wysocki, R., Yen, G. S., Yu, K., Zimmermann, K., Philippsen, P., Johnston, M. &Davis, R. W. (1999). Functional characterization of the *S. cerevisiae* genome by gene deletion and parallel analysis. *Science* 285(5429): 901-906.
Wiren, M., Silverstein, R. A., Sinha, I., Walfridsson, J., Lee, H. M., Laurenson, P., Pillus, L., Robyr, D., Grunstein, M. &Ekwall, K. (2005). Genomewide analysis of nucleosome density histone acetylation and HDAC function in fission yeast. *EMBO J* 24(16): 2906-2918.
Wollschlager, C. &Khan, F. (1984). Aspergillomas complicating sarcoidosis. A prospective study in 100 patients. *Chest* 86(4): 585-588.
Wood, K. V., Lam, Y. A., Seliger, H. H. &McElroy, W. D. (1989). Complementary DNA coding click beetle luciferases can elicit bioluminescence of different colors. *Science* 244(4905): 700-702.
Wu, D., Dou, X., Hashmi, S. B. &Osmani, S. A. (2004). The Pho80-like cyclin of *Aspergillus nidulans* regulates development independently of its role in phosphate acquisition. *J Biol Chem* 279(36): 37693-37703.
Xu, W. &Mitchell, A. P. (2001). Yeast PalA/AIP1/Alix homolog Rim20p associates with a PEST-like region and is required for its proteolytic cleavage. *J Bacteriol* 183(23): 6917-6923.
Xu, W., Smith, F. J., Jr., Subaran, R. &Mitchell, A. P. (2004). Multivesicular body-ESCRT components function in pH response regulation in *Saccharomyces cerevisiae* and *Candida albicans*. *Mol Biol Cell* 15(12): 5528-5537.
Xu, Y., Johnson, C. H. &Piston, D. (2002). Bioluminescence resonance energy transfer assays for protein-protein interactions in living cells. *Methods Mol Biol* 183: 121-133.
Xu, Y., Kanauchi, A., von Arnim, A. G., Piston, D. W. &Johnson, C. H. (2003). Bioluminescence resonance energy transfer: monitoring protein-protein interactions in living cells. *Methods Enzymol* 360: 289-301.
Xu, Y., Piston, D. W. &Johnson, C. H. (1999). A bioluminescence resonance energy transfer (BRET) system: application to interacting circadian clock proteins. *Proc Natl Acad Sci U S A* 96(1): 151-156.
Yamashita, K., Hara-Kuge, S. &Ohkura, T. (1999). Intracellular lectins associated with N-linked glycoprotein traffic. *Biochim Biophys Acta* 1473(1): 147-160.
Yang, M., Baranov, E., Jiang, P., Sun, F. X., Li, X. M., Li, L., Hasegawa, S., Bouvet, M., Al-Tuwaijri, M., Chishima, T., Shimada, H., Moossa, A. R., Penman, S. &Hoffman, R.

M. (2000). Whole-body optical imaging of green fluorescent protein-expressing tumors and metastases. *Proc Natl Acad Sci U S A* 97(3): 1206-1211.

Yasmin, S., Abt, B., Schrettl, M., Moussa, T. A., Werner, E. R. &Haas, H. (2009). The interplay between iron and zinc metabolism in *Aspergillus fumigatus*. *Fungal Genet Biol* 46(9): 707-713.

Yompakdee, C., Ogawa, N., Harashima, S. &Oshima, Y. (1996). A putative membrane protein, Pho88p, involved in inorganic phosphate transport in *Saccharomyces cerevisiae*. *Mol Gen Genet* 251(5): 580-590.

You, B. J., Choquer, M. &Chung, K. R. (2007). The *Colletotrichum acutatum* gene encoding a putative pH-responsive transcription regulator is a key virulence determinant during fungal pathogenesis on citrus. *Mol Plant Microbe Interact* 20(9): 1149-1160.

Yu, J. H., Wieser, J. &Adams, T. H. (1996). The *Aspergillus* FlbA RGS domain protein antagonizes G protein signaling to block proliferation and allow development. *EMBO J* 15(19): 5184-5190.

Yu, Y. A. &Szalay, A. A. (2002). A Renilla luciferase-Aequorea GFP (ruc-gfp) fusion gene construct permits real-time detection of promoter activation by exogenously administered mifepristone *in vivo*. *Mol Genet Genomics* 268(2): 169-178.

Zhang, W., Feng, J. Q., Harris, S. E., Contag, P. R., Stevenson, D. K. &Contag, C. H. (2001). Rapid *in vivo* functional analysis of transgenes in mice using whole body imaging of luciferase expression. *Transgenic Res* 10(5): 423-434.

Zhao, W., Panepinto, J. C., Fortwendel, J. R., Fox, L., Oliver, B. G., Askew, D. S. &Rhodes, J. C. (2006). Deletion of the regulatory subunit of protein kinase A in *Aspergillus fumigatus* alters morphology, sensitivity to oxidative damage, and virulence. *Infect Immun* 74(8): 4865-4874.

Zmeili, O. S. &Soubani, A. O. (2007). Pulmonary aspergillosis: a clinical update. *QJM* 100(6): 317-334.